



U.S. Department of Transportation
Federal Highway Administration

Publication No. FHWA-NHI-11-032
GEC No. 3
August 2011 (Rev. 1)

NHI Course No. 130094

LRFD Seismic Analysis and Design of Transportation Geotechnical Features and Structural Foundations

Reference Manual

Developed following:

AASHTO LRFD Bridge Design Specifications 4th Ed., 2007, and 2008 and 2009 Interims
AASHTO Guide Specifications for LRFD Seismic Bridge Design, 2009



NATIONAL HIGHWAY INSTITUTE

Training Solutions for Transportation Excellence



AUTHORIZED
IACET
PROVIDER

NOTICE

The contents of this report reflect the views of the authors, who are responsible for the facts and accuracy of the data presented herein. The contents do not necessarily reflect policy of the Department of Transportation. This report does not constitute a standard, specification, or regulation. The United States Government does not endorse products or manufacturers. Trade or manufacturer's names appear herein only because they are considered essential to the object of this document.

Technical Report Documentation Page

1. Report No. FHWA-NHI-11-032		2. Government Accession No.		3. Recipient's Catalog No.	
4. Title and Subtitle LRFD SEISMIC ANALYSIS AND DESIGN OF TRANSPORTATION GEOTECHNICAL FEATURES AND STRUCTURAL FOUNDATIONS NHI COURSE NO. 130094 REFERENCE MANUAL GEOTECHNICAL ENGINEERING CIRCULAR NO. 3				5. Report Date August 2011 (Rev. 1)	
				6. Performing Organization Code	
7. Author(s) Edward Kavazanjian, Jr. ¹ , PhD, PE, Jaw-Nan Joe Wang, PhD, PE, Geoffrey R. Martin ² , PhD, Anoosh Shamsabadi ³ , PhD, PE, Ignatius (Po) Lam ² , PhD, PE, Stephen E. Dickenson ⁴ , PhD, PE, and C. Jeremy Hung, PE.				8. Performing Organization Report No.	
9. Performing Organization Name and Address Parsons Brinckerhoff, Inc. One Penn Plaza, New York, NY 10119 ¹ Arizona State University, Tempe, AZ 85287 ² Earth Mechanics Inc., Fountain Valley, CA 92708 ³ California Department of Transportation, Sacramento, CA 95816 ⁴ New Albion Geotechnical, Inc., Corvallis, OR 97333				10. Work Unit No. (TRAIS)	
				11. Contract or Grant No. DTFH-61-D-00011/T-07-004	
12. Sponsoring Agency Name and Address National Highway Institute (NHI) U.S. Department of Transportation Federal Highway Administration, Washington, D.C. 20590				13. Type of Report and Period Covered	
				14. Sponsoring Agency Code	
15. Supplementary Notes <i>FHWA COTR: Louisa Ward</i> <i>FHWA Task Manager: Firas I. S. Ibrahim, PhD, PE</i> <i>FHWA Technical Reviewers: Silas Nichols, PE; Justice Maswoswe, PhD, PE; Thomas K. Saad, PE; and Jerry A. DiMaggio, P.E.</i>					
16. Abstract This manual serves as a reference manual for use with the 5-day NHI training course 130094 "LRFD Seismic Analysis and Design of Transportation Geotechnical Features and Structural Foundations." Additionally it replaces the previous version of Geotechnical Engineering Circular No.3 "Design Guidance: Geotechnical Earthquake Engineering for Highways" published in May 1997. This manual is intended to provide a technical resource for bridge and geotechnical engineers responsible for seismic analysis and design of transportation geotechnical features and structures such as soil and rock slopes, earth embankments, retaining structures and buried structures; and structural foundations including shallow and deep foundations and abutments. Topics include earthquake fundamentals and engineering seismology, seismic hazard analysis, ground motion characterization, site characterization, site-specific seismic site response analysis, geotechnical hazards including liquefaction, slope instability, and seismic settlement, and soil-foundation-structure interaction are included. This manual also addresses LRFD analysis and design requirements and recommendations of the seismic provisions in AASHTO LRFD Bridge Design Specifications, AASHTO Guide Specifications for LRFD Seismic Bridge Design, and the NCHRP Report 611 from NCHRP Project 12-70 "Seismic Analysis and Design of Retaining Walls, Buried Structures, Slopes, and Embankments."					
17. Key Words Seismic design, earthquakes, geotechnical hazard, seismic hazard analysis, ground motion characterization, liquefaction, soil slopes, rock slopes, slope stability, earth embankments, earth retaining structures, soil structure interaction, bridge structural foundations, seismic settlement.				18. Distribution Statement No restrictions.	
19. Security Classif. (of this report) UNCLASSIFIED		20. Security Classif. (of this page) UNCLASSIFIED		21. No. of Pages 592	
22. Price					

CONVERSION FACTORS

Approximate Conversions to SI Units		Approximate Conversions from SI Units			
When you know	Multiply by	To find	When you know	Multiply by	To find
(a) Length					
inch	25.4	millimeter	millimeter	0.039	inch
foot	0.305	meter	meter	3.28	foot
yard	0.914	meter	meter	1.09	yard
mile	1.61	kilometer	kilometer	0.621	mile
(b) Area					
square inches	645.2	square millimeters	square millimeters	0.0016	square inches
square feet	0.093	square meters	square meters	10.764	square feet
acres	0.405	hectares	hectares	2.47	acres
square miles	2.59	square kilometers	square kilometers	0.386	square miles
(c) Volume					
fluid ounces	29.57	milliliters	milliliters	0.034	fluid ounces
gallons	3.785	liters	liters	0.264	gallons
cubic feet	0.028	cubic meters	cubic meters	35.32	cubic feet
cubic yards	0.765	cubic meters	cubic meters	1.308	cubic yards
(d) Mass					
ounces	28.35	grams	grams	0.035	ounces
pounds	0.454	kilograms	kilograms	2.205	pounds
short tons (2000 lb)	0.907	megagrams (tonne)	megagrams (tonne)	1.102	short tons (2000 lb)
(e) Force					
pound	4.448	Newton	Newton	0.2248	pound
(f) Pressure, Stress, Modulus of Elasticity					
pounds per square foot	47.88	Pascals	Pascals	0.021	pounds per square foot
pounds per square inch	6.895	kiloPascals	kiloPascals	0.145	pounds per square inch
(g) Density					
pounds per cubic foot	16.019	kilograms per cubic meter	kilograms per cubic meter	0.0624	pounds per cubic foot
(h) Temperature					
Fahrenheit temperature(°F)	5/9(°F- 32)	Celsius temperature(°C)	Celsius temperature(°C)	9/5(°C)+ 32	Fahrenheit temperature(°F)

Notes: 1) The primary metric (SI) units used in civil engineering are meter (m), kilogram (kg), second(s), newton (N) and pascal (Pa=N/m²).
 2) In a "soft" conversion, an English measurement is mathematically converted to its exact metric equivalent.
 3) In a "hard" conversion, a new rounded metric number is created that is convenient to work with and remember.

PREFACE

This manual is intended to provide a technical resource for bridge and geotechnical engineers responsible for seismic analysis and design of transportation geotechnical features and structures such as soil and rock slopes, earth embankments, retaining structures and buried structures; and structural foundations including shallow and deep foundations and abutments. This manual includes topics such as earthquake fundamentals and engineering seismology, seismic hazard analysis, ground motion characterization, site characterization, site-specific seismic site response analysis, geotechnical hazards including liquefaction, slope instability, and seismic settlement, and soil-foundation-structure interaction, and addresses the requirements and recommendations of the seismic provisions in *AASHTO LRFD Bridge Design Specifications (2007, 2008, and 2009)*, *AASHTO Guide Specifications for LRFD Seismic Bridge Design (2009)*, and the NCHRP Report 611 (2008) from NCHRP Project 12-70 “*Seismic Analysis and Design of Retaining Walls, Buried Structures, Slopes, and Embankment.*”

Chapters 1 and 2 present LRFD seismic analysis and design principles, and basic concepts of seismic geology and engineering seismology. This information is essential background information for subsequent discussions of seismic hazard analysis, ground motion characterization and structural foundation design.

Chapter 3 presents the details of both probabilistic and deterministic seismic hazard analysis. Development of the Uniform Hazard Spectrum for a specified probability and exposure period using either the National Seismic Hazard maps developed by the USGS or the ground motion maps developed by USGS specifically for AASHTO is presented. Development of the AASHTO truncated acceleration response spectra for use in structural analysis from the Uniform Hazard Spectrum is illustrated. The process of deaggregation by which a probabilistically-derived uniform hazard spectrum is decomposed into magnitude and distance combinations in order to determine a representative magnitude and distance for the design earthquake is described. Guidelines for selecting a suite of representative time histories for the representative design event are presented.

Chapter 4 described site characterization for seismic analysis. The use of the Standard Penetration Test (SPT) and the Cone Penetration Test (CPT) to evaluate site stratigraphy and geotechnical properties is explained in detail. Geophysical techniques for site investigation are also addressed. Characterization of rock mass behavior and quantification of rock mass strength is described. Correlations between important geotechnical properties, including relative density, shear strength, and shear wave velocity, from both in situ test results and soil classification and index test data are presented.

In Chapter 5, the process of site specific seismic response analysis is described. Methods addressed in this chapter include simplified chart-based methods to adjust the peak ground acceleration for local site conditions, equivalent linear one-dimensional site response analysis, non-linear one-dimensional site response analysis with pore pressure generation, and advanced two-dimensional site response analysis. The development of input parameters for equivalent-linear one-dimensional site response analyses, the most common type of advanced analysis performed in practice, are described in detail.

Chapter 6 describes earthquake-induced damage due to the geotechnical seismic hazards of slope instability, liquefaction, and seismic settlement. Methods to evaluate seismic slope deformation, liquefaction potential, liquefaction-induced ground displacements, and seismic settlement are described in detail in this chapter. A method to evaluate the appropriate value of the seismic coefficient for pseudo-static slope stability analyses that accounts for spatial incoherence of ground motions, the local seismic environment, local site conditions, and acceptable displacement levels is presented.

Chapter 7 addresses design of earthwork features for transportation facilities, including soil and rock slopes and embankments. A performance-based seismic design philosophy that employs the concept of allowable displacement is described. Soil and site improvement techniques that can be used when the seismic displacement are unacceptable are presented with an emphasis on remediation of slope stability and liquefaction.

Chapter 8 describes the seismic design process and the AASHTO seismic design methodology, including capacity design of bridge foundations, the concept of the earthquake resisting system for a bridge, guidelines for what types of earthquake resisting elements are allowable and not recommended, and basic principles of soil-foundation-structure interaction. The principles of both kinematic and inertial interaction are described.

Chapter 9 describes the seismic design of shallow foundations, including techniques to assess both foundation stiffness and foundation capacity. Equations for calculating the stiffness coefficients for the six modes of foundation displacement for use in an inertial interaction analysis are presented. Foundation capacity analyses discussed in the chapter include bearing, overturning, and sliding.

Chapter 10 addresses deep foundation design. Both p-y/t-z analyses and simple elastic solutions to evaluate the stiffness of an individual pile are discussed along with methods to account for group effects and to assemble individual pile and pile cap stiffness into a group stiffness. Sophisticated methods and a simple approximate method to account for kinematic interaction at soft soil sites are described. Analyses to evaluate the response of pile foundations to ground displacement demand from laterally spreading induced by liquefaction are discussed.

Chapter 11 presents methods for seismic design of free standing retaining walls. A variety of methods for predicting seismic active earth pressures, including the Mononobe-Okabe method, design charts that include the influence of a cohesion component to the shear strength, the Coulomb wedge method, and the general equilibrium method, are described along with a displacement-based method for evaluating the appropriate seismic coefficient for use in design. Charts for evaluating the passive earth pressure coefficient, including the effect of cohesion, are also presented in this chapter. Design of gravity and semi-gravity retaining walls for sliding, overturning, and bearing modes is discussed in detail. Earth pressure diagrams for non-gravity cantilever walls, anchored walls, and MSE walls are described along with recommendations for the seismic coefficient for use in design.

Chapter 12 describes bridge abutment design. The characterization of the stiffness of both conventional seat-type and integral abutments for inclusion in the global bridge model is presented. The effect of skewed abutments on the seismic performance of the bridge is discussed.

Lastly, Chapter 13 presents design considerations for buried structures, including culverts and pipelines. Simple closed form solutions are presented for the displacement demand on buried structures subject to seismic loading.

ACKNOWLEDGMENTS

This document serves as a reference manual for use with the National Highway Institute (NHI) Course 130094 titled *LRFD Seismic Analysis and Design of Transportation Geotechnical Features and Structural Foundations* developed in March 2011 by Parsons Brinckerhoff Inc. (PB) and authored by E. Kavazanjian, Jr., J. Wang, G.R. Martin, A. Shamsabadi, I.P. Lam, S.E. Dickenson, and C.J. Hung. It also replaces the 1997 version of FHWA Geotechnical Engineering Circular No.3 “Design Guidance: Geotechnical Earthquake Engineering for Highways” (FHWA-SA-97-076) developed by GeoSyntec Consultants and authored by E. Kavazanjian, Jr., N. Matasovic, T. Hadj-Hamou, and P.J. Sabatini.

This manual addresses in general the requirements and recommendations of the seismic provisions in *AASHTO LRFD Bridge Design Specifications (2007, 2008 and 2009)*, *AASHTO Guide Specifications for LRFD Seismic Bridge Design (2009)*, and the NCHRP Report 611 from NCHRP Project 12-70 “*Seismic Analysis and Design of Retaining Walls, Buried Structures, Slopes, and Embankments*” (2009). Permission by the FHWA to include some original manuscripts and graphics from the FHWA Reference Manual “*Geotechnical Earthquake Engineering*” (FHWA-HI-99-012) developed by Parsons Brinckerhoff Inc. and authored by E. Kavazanjian, Jr., N. Matasovic, T. Hadj-Hamou, and J. Wang, is gratefully appreciated.

The authors would like to especially acknowledge the continuing support of Louisa Ward, NHI Program Manager, and Firas Ibrahim, FHWA Task Manger, and the reviews and recommendations provided by the following individuals who served on the Technical Working Group for this project:

- Firas I. S. Ibrahim, PhD, P.E. FHWA
- Silas Nichols, P.E. FHWA
- Justice Maswoswe, PhD, P.E. FHWA
- Thomas K. Saad, P.E. FHWA, and
- Jerry A. DiMaggio, P.E. Strategic Highway Research Program/the National Academies

In addition, the authors are grateful for the generous contributions and reviews from Lee Marsh of BergerABAM, and from the representatives at South Carolina DOT, Washington DOT, and Illinois DOT.

Lastly, the authors wish to extend their gratitude for the supports provided by a number of professionals from Parsons Brinckerhoff (PB), Arizona State University, Tempe, and Earth Mechanics Inc. including Matteo Montesi, Vinnie Hung, Lauren Chu and Amy Mengert at PB, and David (Zbigniew) Czupak and Simon Ghanat at Arizona State University for their support and assistance.

This page is intentionally left blank.

TABLE OF CONTENTS

LIST OF FIGURES	xiii
LIST OF TABLES	xxi
CHAPTER 1 - INTRODUCTION.....	1-1
1.1 BACKGROUND	1-1
1.2 EARTHQUAKE DAMAGE CATEGORIES.....	1-3
1.2.1 Primary Damage	1-4
1.2.2 Secondary Damage	1-5
1.2.3 Indirect Damage.....	1-6
1.3 DAMAGE TO HIGHWAY FACILITIES IN EARTHQUAKES	1-7
1.4 AASHTO SEISMIC DESIGN PHILOSOPHY	1-12
1.5 LOAD AND RESISTANCE FACTOR DESIGN	1-14
1.5.1 Basic Principles of LRFD	1-14
1.5.2 LRFD versus ASD	1-15
1.5.3 AASHTO Specifications for Seismic LRFD	1-15
1.5.4 AASHTO Limit States and Load and Resistance Factors.....	1-16
1.6 ORGANIZATION OF THE DOCUMENT	1-19
CHAPTER 2 - EARTHQUAKE FUNDAMENTALS AND ENGINEERING SEISMOLOGY.....	2-1
2.1 INTRODUCTION	2-1
2.2 EARTHQUAKE SOURCES	2-1
2.2.1 General.....	2-1
2.2.2 Plate Tectonics	2-2
2.2.3 Fault Movements	2-6
2.2.4 Fault Activity	2-8
2.3 SEISMIC WAVES	2-11
2.4 STRONG MOTION RECORDS (TIME HISTORIES).....	2-12
2.5 PARAMETERS DESCRIBING EARTHQUAKE SIZE AND LOCATION	2-14
2.5.1 Earthquake Magnitude	2-14
2.5.2 Earthquake Location	2-15
2.5.3 Earthquake Recurrence	2-17
2.6 PARAMETERS DESCRIBING FAULTING	2-19
2.7 PARAMETERS DESCRIBING GROUND SHAKING.....	2-21
2.7.1 Intensity.....	2-21
2.7.2 Peak Ground Motions	2-23
2.7.3 Energy Content	2-23
2.7.4 Duration	2-24
2.7.5 Response Spectrum	2-27
2.7.6 Smoothed Uniform Hazard Spectra	2-29

2.7.7	Ground Motion Attenuation Relationships	2-31
2.7.8	Predominant Period of the Strong Ground Motions	2-31
2.7.9	Magnitude-Distance Deaggregation	2-32
2.8	SUMMARY	2-33

CHAPTER 3 – SEISMIC HAZARD ANALYSIS AND GROUND MOTION CHARACTERIZATION 3-1

3.1	GENERAL	3-1
3.2	SEISMIC HAZARD ANALYSIS	3-3
3.2.1	Seismic Source Identification	3-3
3.2.2	Magnitude-Recurrence Relationships	3-4
3.2.3	Strong Motion Attenuation Relationships.....	3-9
3.2.4	Uniform Hazard Spectra	3-19
3.2.5	Return Period and Seismic Risk.....	3-21
3.2.6	De-aggregation of Design Earthquake, Magnitude and Distance	3-23
3.2.7	Deterministic Maximum Magnitude and Ground Motion Evaluation	3-25
3.2.8	Probabilistic versus Deterministic Analysis Method	3-26
3.3	HAZARD LEVELS AND RETURN PERIODS FOR FUNCTIONAL AND LIFE SAFETY DESIGN	3-28
3.3.1	Performance Levels for Seismi Design.....	3-28
3.3.2	Return Period for Use in Design	3-31
3.3.3	Site Specific Analysis versus USGS National Seismic Hazard Maps	3-32
3.3.4	Ground Motion Characterization	3-33
3.3.5	Correlation for Peak Ground Velocity	3-36
3.3.6	Acceleration Response Spectra versus Displacement Spectra.....	3-37
3.3.7	Near-Fault (Near-Field) Directivity Effects	3-37
3.3.8	Local Site Effects	3-39
3.3.9	Representative Ground Motion Time Histories	3-43
3.3.10	Adjusting Time Histories to a Target Spectrum.....	3-47
3.3.11	Spatially Varying Ground Motions	3-49
3.3.12	Vertical Ground Motions	3-52
3.4	DEVELOPMENT OF AASHTO ACCELERATION RESPONSE SPECTRUM.....	3-53
3.4.1	Use of the USGS Website.....	3-54
3.4.2	Use of the USGS/AASHTO CD	3-60
3.4.3	Magnitude Deaggregation.....	3-67
3.5	RECENT ADVANCES IN ENGINEERING SEISMOLOGY AND GROUND MOTION CHARACTERIZATION.....	3-72
3.6	SUMMARY	3-74

CHAPTER 4 - SITE CHARACTERIZATION..... 4-1

4.1	INTRODUCTION.....	4-1
4.2	SUBSURFACE PROFILE DEVELOPMENT.....	4-2
4.2.1	General	4-2
4.2.2	Water Level.....	4-2
4.2.3	Soil Stratigraphy.....	4-3

4.2.4	Depth to Bedrock	4-4
4.2.5	Rock Mass Characterization	4-5
4.3	REQUIRED SOIL AND ROCK PARAMETERS	4-5
4.3.1	General	4-5
4.3.2	Unit Weight and Relative Density	4-6
4.3.3	Shear Wave Velocity.....	4-7
4.3.4	Cyclic Stress-Strain Behavior	4-8
4.3.5	Peak and Residual Shear Strength.....	4-11
4.4	EVALUATION OF SOIL AND ROCK PROPERTIES FOR SEISMIC ANALYSIS	4-12
4.4.1	General	4-12
4.4.2	In Situ Testing	4-13
4.4.3	Unit Weight and Relative Density	4-21
4.4.4	Shear Wave Velocity.....	4-25
4.4.5	Cyclic Stress-Strain Parameters	4-28
4.4.6	Peak and Residual Shear Strength.....	4-38
4.5	ROCK MASS PROPERTIES.....	4-43
4.5.1	Rock Mass Categories.....	4-43
4.5.2	Highly Fractured Rock Masses	4-44
4.5.3	Rock Masses with Discrete Discontinuities	4-51
4.6	SUMMARY	4-53
 CHAPTER 5 - SEISMIC SITE RESPONSE ANALYSIS.....		5-1
5.1	GENERAL	5-1
5.2	SITE-SPECIFIC SEISMIC RESPONSE ANALYSES	5-3
5.2.1	Types of Site-Specific Analysis	5-3
5.2.2	Simple Empirical Relationships	5-5
5.3	ONE-DIMENSIONAL SITE RESPONSE ANALYSES	5-11
5.3.1	Equivalent Linear One-Dimensional Response Analyses.....	5-11
5.3.2	Advanced One-Dimensional Site Response Analysis.....	5-16
5.3.3	Analyses Including Pore Pressure Generation	5-19
5.4	TWO- AND THREE-DIMENSIONAL SEISMIC SITE RESPONSE ANALYSIS	5-21
5.5	SUMMARY	5-23
 CHAPTER 6 - GEOTECHNICAL HAZARDS		6-1
6.1	GENERAL	6-1
6.2	SEISMIC SLOPE INSTABILITY HAZARD	6-2
6.2.1	Modes of Slope Instability	6-2
6.2.2	Limit Equilibrium Pseudo Static Stability Analysis	6-4
6.2.3	Displacement-Based Seismic Stability Analysis	6-10
6.2.4	Rock Slope Stability Analyses.....	6-15
6.3	SOIL LIQUEFACTION HAZARD	6-18
6.3.1	Hazard Description and Initial Screening	6-18
6.3.2	Liquefaction Strengths: Laboratory and In-situ Tests.....	6-23

6.3.3	Empirical and Numerical Evaluation Procedures for Liquefaction Potential	6-26
6.3.4	Evaluation of Liquefaction Potential	6-28
6.3.5	Use of Site-Specific response Analyses	6-37
6.4	LIQUEFACTION INDUCED GROUND DEFORMATIONS	6-38
6.4.1	Post Liquefaction Residual Strength	6-38
6.4.2	Flow Failures	6-39
6.4.3	Lateral Spread Displacement Evaluations	6-40
6.5	SOIL SETTLEMENT HAZARD	6-41
6.5.1	Settlement of Unsaturated Cohesionless Soils	6-41
6.5.2	Post Earthquake Settlement of Liquefied Soils	6-46
6.6	SURFACE FAULT RUPTURE HAZARD	6-47
6.6.1	Fault Types and Field Identification	6-47
6.6.2	Fault Rupture Characteristics and Displacement Estimates	6-51
6.7	SUMMARY	6-54
CHAPTER 7 - GEOTECHNICAL DESIGN OF EARTHWORK FEATURES		7-1
7.1	GENERAL	7-1
7.2	SEISMIC PERFORMANCE OF SLOPES AND EMBANKMENTS	7-2
7.2.1	Natural Slopes	7-2
7.2.2	Embankment Fills	7-5
7.2.3	Liquefaction Induced Deformations and Lateral Spreads	7-8
7.3	SLOPE STABILITY DESIGN APPROACHES	7-18
7.3.1	Constructed Fill Slopes and Embankments	7-18
7.3.2	Natural Slopes	7-25
7.3.3	Screening Criteria	7-26
7.3.4	Strategies for Developing Acceptable Displacement	7-28
7.3.5	Approach for Defining Acceptable Displacements	7-30
7.4	SLOPE STABILITY MITIGATION MEASURES	7-31
7.4.1	Introduction	7-31
7.4.2	Soil Slopes	7-31
7.4.3	Rock Slopes	7-35
7.5	LIQUEFACTION INDUCED LATERAL SPREADS: DESIGN APPROACH AND REMEDICATION	7-42
7.5.1	Background	7-42
7.5.2	Structural Design to Accommodate Liquefaction-Induced Deformations	7-44
7.5.3	Liquefaction Mitigation Ground Improvement Methods	7-56
7.6	SUMMARY	7-66
CHAPTER 8 - GEOTECHNICAL SEISMIC DESIGN FOR TRANSPORTATION STRUCTURES AND SOIL-FOUNDATION-STRUCTURE INTERACTION		8-1
8.1	GENERAL	8-1
8.2	INTERACTION BETWEEN STRUCTURAL DESIGNERS AND GEOTECHNICAL SPECIALISTS IN THE SEISMIC DESIGN PROCESS	8-1

8.3	GLOBAL DYNAMIC RESPONSE MODEL.....	8-2
8.4	MEASURES FOR SEISMIC DEMAND IN DESIGN	8-4
8.5	CAPACITY PROTECTED DESIGN FOR FOUNDATIONS	8-8
8.6	FORCE VERSUS DISPLACEMENT BASED SEISMIC DESIGN	8-11
8.7	THE EARTHQUAKE RESISTING SYSTEM.....	8-12
8.8	SOIL-FOUNDATION-STRUCTURE INTERACTION ANALYSIS.....	8-14
8.9	AASHTO SEISMIC DESIGN REQUIREMENTS.....	8-19
8.9.1	Interim Revisions	8-19
8.9.2	Guide Specifications	8-20
8.10	COORDINATION BETWEEN STRUCTURAL DESIGNERS AND GEOTECHNICAL SPECIALISTS.....	8-22
8.11	TREATMENT OF UNCERTAINTY IN SEISMIC DESIGN.....	8-23
8.12	FOUNDATION DESIGN STRATEGY FOR GOOD SEISMIC PERFORMANCE.....	8-25
8.13	SUMMARY	8-27
CHAPTER 9 - SHALLOW FOUNDATIONS.....		9-1
9.1	GENERAL TYPES OF SHALLOW FOUNDATIONS	9-1
9.2	SEISMIC PERFORMANCE AND VULNERABILITY OF SHALLOW FOUNDATIONS.....	9-2
9.3	STATIC VERSUS SEISMIC LOADS ON SHALLOW FOUNDATIONS	9-3
9.4	SOIL-FOUNDATION-STRUCTURE INTERACTION	9-4
9.4.1	Foundation Substructuring	9-4
9.4.2	Kinematic and Inertial Interaction	9-5
9.5	FOUNDATION STIFFNESS FORMULATION.....	9-8
9.5.1	Spring Constants	9-8
9.5.2	Equivalent Stiffness Matrix for Shallow Footing	9-8
9.5.3	Footing Embedment Effects.....	9-10
9.5.4	Soil Modulus for Foundation Stiffness	9-12
9.5.5	Effects of Limited Depth to Hard Layer	9-13
9.5.6	Advanced Numerical Analysis.....	9-13
9.5.7	Incorporation of Foundation Model into Bridge Response Model	9-14
9.6	GEOTECHNICAL CAPACITY	9-15
9.6.1	Pseudo-Static Seismic Loads	9-15
9.6.2	Effective Footing Dimensions	9-16
9.6.3	Overturning.....	9-17
9.6.4	Bearing Capacity.....	9-17
9.6.5	Sliding Capacity.....	9-18
9.7	STRUCTURAL CAPACITY	9-19
9.8	PERMANENT FOUNDATION DISPLACEMENT	9-20
9.8.1	Liquefaction-Induced Lateral Spreading and Settlement.....	9-21
9.9	SUMMARY	9-21

CHAPTER 10 - DEEP FOUNDATIONS	10-1
10.1 TYPES OF DEEP FOUNDATIONS	10-1
10.2 SEISMIC VULNERABILITY OF DEEP FOUNDATIONS	10-1
10.3 SEISMIC LOADS ON DEEP FOUNDATIONS	10-8
10.3.1 Soil-Foundation-Structure Interaction	10-8
10.3.2 Kinematic Loading.....	10-10
10.4 EFFECTIVE SUPPORT MOTIONS FOR DEEP FOUNDATIONS AT SOFT SOIL SITES	10-10
10.5 SOIL-FOUNDATION INTERACTION SPRINGS.....	10-13
10.5.1 Two-Springs-in-Series Model.....	10-13
10.5.2 p-y and t-z Curves for Soil-Pile Interaction Analyses.....	10-14
10.6 FOUNDATION STIFFNESS EVALUATION.....	10-15
10.6.1 Pile Head Stiffness for Lateral Loading.....	10-16
10.6.2 Pile Head Stiffness for Axial Loading	10-25
10.6.3 Lateral Stiffness of Pile Cap	10-27
10.6.4 Group Effects for Typical Pile Footings	10-28
10.6.5 Group Effects for Very Large Pile Groups	10-30
10.6.6 p-y Curves for Liquefied Sand.....	10-31
10.6.7 Stiffness Matrix of a Pile Group	10-32
10.6.8 Pile Head Rotational Stiffness	10-32
10.7 MOMENT CAPACITY OF PILE GROUPS	10-34
10.8 DESIGNING FOR UNCERTAINTY	10-36
10.9 DESIGNING FOR KINEMATIC DISPLACEMENT DEMAND IN LIQUEFIED SOILS	10-38
10.10 DESIGN PROCEDURES FOR LARGE DIAMETER DRILLED SHAFTS	10-43
10.11 CAISSONS DESIGN	10-43
10.12 SUMMARY	10-46
 CHAPTER 11- EARTH RETAINING STRUCTURES.....	 11-1
11.1 INTRODUCTION.....	11-1
11.1.1 Design Criteria	11-1
11.1.2 Types of Earth Retaining Structures	11-2
11.1.3 Gravity and Semi-Gravity Walls.....	11-2
11.1.4 Non-Gravity Cantilevered Walls	11-4
11.1.5 Non-Gravity Anchored Walls	11-5
11.1.6 Mechanically Stabilized Earth Walls.....	11-6
11.1.7 Soil Nail Wall	11-7
11.1.8 Prefabricated Modular Walls	11-8
11.2 SEISMIC FORCES ON EARTH RETAINING STRUCTURES	11-9
11.2.1 Seismic Load and Resistance.....	11-9
11.2.2 No Analysis Provisions.....	11-10
11.3 SEISMIC LATERAL EARTH PRESSURES	11-11

11.3.1	Mononobe-Okabe Seismic Earth Pressure Theory	11-11
11.3.1.1	Limitations of Mononobe-Okabe Theory	11-12
11.3.2	Trial Wedge Method	11-13
11.3.2.1	Influence of Cohesion on Seismic Active Earth Pressure	11-15
11.3.3	Log Spiral Earth Pressure Theory	11-17
11.3.4	General Limit Equilibrium Method	11-19
11.4	SEISMIC EARTH PRESSURE COEFFICIENT	11-20
11.4.1	Maximum Seismic Coefficients for Design	11-20
11.4.1.1	Wall Height Adjustment Factor	11-21
11.4.2	Displacement-Based Seismic Coefficient	11-22
11.4.2.1	Displacement Ductility Adjustment Factor	11-23
11.4.3	Walls with Backfill of Limited Extent	11-25
11.5	GRAVITY AND SEMI-GRAVITY EARTH RETAINING STRUCTURE DESIGN	11-25
11.5.1	External Stability for Walls Supported on a Shallow Foundation	11-27
11.5.2	Internal Stability Assessment of Semi-Gravity Cantilever Retaining Walls	11-30
11.5.3	Gravity and Semi-Gravity Retaining Walls on Piles	11-32
11.6	DESIGN OF CANTILEVER AND ANCHORED EARTH RETAINING STRUCTURES	11-34
11.6.1	Non-Gravity Cantilevered Earth Retaining System	11-34
11.6.2	Anchored Walls	11-37
11.7	MECHANICALLY STABILIZED WALLS	11-42
11.8	SUMMARY	11-46
CHAPTER 12 - BRIDGE ABUTMENT		12-1
12.1	INTRODUCTION	12-1
12.1.1	Types of Abutment	12-2
12.1.2	Seat Type Abutment	12-2
12.1.3	Monolithic Abutment	12-4
12.1.4	Mechanism of the Abutment Backfill Failure	12-5
12.1.5	Typical Backfill Soil Behavior	12-8
12.1.6	Full Scale Abutment Loading Tests	12-9
12.1.6.1	UCLA Abutment Experiment	12-9
12.1.6.2	UCD Abutment Experiment	12-10
12.2	MODELING OF REGULAR (NON-SKEWED) ABUTMENTS	12-13
12.2.1	Bi-linear Model	12-13
12.2.2	Non-Linear Hyperbolic Abutment Stiffness Relationship	12-15
12.2.3	Advanced Numerical Analysis	12-17
12.2.4	Global Backwall-Backfill Longitudinal Response	12-18
12.3	MODELING OF SKEWED ABUTMENTS	12-20
12.3.1	3-D Finite Element Model of the Abutment Backfill	12-22
12.3.2	Load-Deformation Relationship	12-23
12.3.3	Effects of Skew Angles on the Bridge Abutment Global Response	12-25
12.4	SUMMARY	12-26

CHAPTER 13 - BURIED STRUCTURES	13-1
13.1 GENERAL	13-1
13.2 SEISMIC PERFORMANCE OF CULVERTS AND PIPELINES	13-1
13.3 CULVERT/PIPE CHARACTERISTICS	13-2
13.3.1 Flexible Culverts and Pipes.....	13-2
13.3.2 Rigid Culverts and Pipes.....	13-4
13.4 GENERAL EFFECTS OF EARTHQUAKES AND POTENTIAL FAILURE MODES	13-4
13.4.1 Ground Shaking	13-5
13.4.2 Ground Failure	13-8
13.5 CURRENT SEISMIC DESIGN PRACTICE FOR BURIED STRUCTURES	13-8
13.6 GENERAL METHODOLOGY AND RECOMMENDED PROCEDURES.....	13-11
13.6.1 Ovaling of Circular Conduits.....	13-11
13.6.2 Lining-Ground Interaction Solutions for Ovaling Response of Circular Lining	13-17
13.6.3 Lining-Ground Interaction Solutions for Racking Response of Rectangular Lining.....	13-21
13.7 NUMERICAL MODELING METHODS.....	13-27
13.8 GENERAL DESIGN METHODOLOGY FOR PERMANENT GROUND	
DISPLACEMENT.....	13-29
13.9 SUMMARY	13-30

LIST OF FIGURES

Figure 1-1	Peak Ground Acceleration with a 10% Probability of Being Exceeded in a 50 year Period	1-2
Figure 1-2	Areas Impacted by Historic Earthquakes in the United States	1-2
Figure 1-3	Collapse of the Cypress Viaduct in the 1989 Loma Prieta Earthquake	1-3
Figure 1-4	Collapse of the I-5, SR-14 Overpass in the 1971 San Fernando Earthquake	1-4
Figure 1-5	Collapse of the Showa Bridge in the 1964 Niigata, Japan Earthquake.....	1-5
Figure 1-6	Fire Following the 1994 Northridge Earthquake due to a Rupture Gas Main	1-6
Figure 1-7	Damage to the San Francisco-Oakland Bay Bridge East Span due to the 1989 Loma Prieta Earthquake.....	1-7
Figure 1-8	Failure of the Wingwall at the Roxford Street Undercrossing in the 1971 San Fernando Earthquake	1-8
Figure 1-9	Settlement of Abutment Embankment Fill in the 1971 San Fernando Earthquake	1-9
Figure 1-10	Collapse of the Bridge over Struve Slough in the 1989 Loma Prieta Earthquake	1-10
Figure 1-11	Shear Failure of the Head of a Pile at the Struve Slough Bridge.....	1-10
Figure 1-12	Landsliding Along SR-17 in the 1989 Loma Prieta Earthquake	1-11
Figure 1-13	Collapse of the I-5, SR-14 Interchange in the 1994 Northridge Earthquake	1-12
Figure 1-14	Failure of a Bridge Column – Foundation Connection.....	1-13
Figure 2-1	Major Tectonic Plates and Their Approximate Direction of Movement	2-3
Figure 2-2	Worldwide Seismic Activity and Plate Boundaries	2-4
Figure 2-3	Cross-Section Through a Subduction Zone.	2-4
Figure 2-4	Southeastern US Seismic Zones and Instrumental Seismicity.....	2-7
Figure 2-5	Blind Thrust Faulting.....	2-8
Figure 2-6	Deformations Produced by Body Waves: (a) P-waves; (b) SV-Waves.....	2-11
Figure 2-7	Deformations Produced by Rayleigh Waves	2-12
Figure 2-8	Acceleration, Velocity, and Displacement Strong Ground Motion Time Histories	2-13
Figure 2-9	Comparison of Earthquake Magnitude Scales	2-15
Figure 2-10	Basic Fault Geometry and Definition	2-16
Figure 2-11	Various Site-to-Source Distance Measures Used in Earthquake Engineering.....	2-17
Figure 2-12	Truncated Gutenberg Richter and Characteristic Magnitude-Recurrence Models	2-18
Figure 2-13	Types of Fault Movement.....	2-20
Figure 2-14	Bracketed Duration of Strong Shaking	2-25
Figure 2-15	Significant Duration of Strong Shaking.....	2-26
Figure 2-16	Schematic Representation of Acceleration Response Spectra.....	2-28
Figure 2-17	Tripartite Representation of Acceleration, Velocity, and Displacement Response Spectra.	2-29
Figure 2-18	Uniform Hazard Acceleration Response Spectra for Memphis, Tennessee, with a 5% Probability of Exceedance 50-years.....	2-30
Figure 2-19	Magnitude-Distance Deaggregation for Oceano, California	2-33
Figure 3-1	Steps in Probabilistic Seismic Hazard Analysis	3-2
Figure 3-2	Geometry of Seismic Sources in Seismic Hazard Analysis.....	3-3
Figure 3-3	Truncated Gutenberg Richter and Characteristic Magnitude-Recurrence Models	3-4
Figure 3-4	Example of Peak Horizontal Ground Acceleration Attenuation Relationship for Strike Slip Earthquake and Soil Sites.....	3-9
Figure 3-5	Variation in Definitions on Distance (site to seismic source) in Commonly Used Attenuation Relationships; (a) Strike Slip Faulting; (b) Reverse or Normal Faulting, Hanging-wall Site; (c) Reverse or Normal Faulting, Foot-wall Site	3-10
Figure 3-6	Boundary Defining WUS and CEUS Seismic Hazard Regions Based on Change in Attenuation Relationship	3-11

Figure 3-7	Comparison between Spectral Curve Shapes for the WUS and CEUS Hazard Regions (NUREG, 2001); (a) Acceleration Spectra for M=6.5, and R=20 km; (b) Displacement Spectra for M=6.5, and R=20 km	3-13
Figure 3-8	Acceleration Response Spectra from Abrahamson and Silva (1997)	3-19
Figure 3-9	Seismic Hazard Curves for Site in Southern California: Total Hazard and Individual Contributions and Total Hazard from Three Faults	3-20
Figure 3-10	Magnitude Deaggregation for Augusta, GA, at 1.0 sec Period for a 2500-year Return Period: Predominant Hazard is Charleston M7.3 Characteristic Earthquake	3-25
Figure 3-11	Design Response Spectrum Constructed with the Three-Point Method	3-34
Figure 3-12	Comparison of USGS Spectra to AASHTO Spectra for a Rock Site in Memphis, Tennessee (1,000-yr Return Period)	3-35
Figure 3-13	Influence of Rupture Directivity on Velocity Time Histories Recorded at the Lucerne and Joshua Tree Sites During the 1992 Landers Earthquake	3-38
Figure 3-14	Representative Scaled versus Spectrum-Compatible Adjusted Motion	3-48
Figure 3-15	Coherency Function for Horizontal Component Motion	3-50
Figure 3-16	Coherency Function for Vertical Component Motion	3-51
Figure 3-17	Initiation Screen for the Seismic Design Values for Buildings option	3-54
Figure 3-18	Initial Screen for Seismic Hazard Curves and Uniform Hazard Response Spectra	3-55
Figure 3-19	Input Screen for Seismic Hazard Curves, Response Parameters, and Design Parameters	3-56
Figure 3-20	Input Screen for Probabilistic Hazard Curves	3-57
Figure 3-21	Screen for PGA for 1000-yr Return Period	3-57
Figure 3-22	Screen for 0.2 sec Spectral Acceleration for 1000-yr Return Period	3-58
Figure 3-23	Screen for 1.0 sec Spectral Acceleration for 1000-yr Return Period	3-58
Figure 3-24	Bay Bridge Site AASHTO Design Spectrum for Site Class C Conditions	3-60
Figure 3-25	Initiation Screen in the USGS/AASHTO Ground Motion CD	3-61
Figure 3-26	Screen No. 2: Site Location and Design Hazard Level	3-61
Figure 3-27	Screen No. 3: Site Factor Table.	3-62
Figure 3-28	Screen No. 4: Site Class Adjusted Anchoring Points for Design Spectrum.	3-63
Figure 3-29	Screen No. 5: Reference Site Spectrum Values	3-64
Figure 3-30	Screen No. 6: Site Class D Spectrum Values	3-64
Figure 3-31	Screen No. 7: Options for Viewing Various Spectra	3-66
Figure 3-32	Screen No. 8: Example of “All S_a vs. T Spectra” Option	3-66
Figure 3-33	Screen No. 9: Example of “All S_a vs. S_d Spectra” Option	3-67
Figure 3-34	Initial Screen from the USGS Web Site for Interactive Deaggregation	3-68
Figure 3-35	Screen for Specifying Location and PSHA Return Period	3-69
Figure 3-36	Available Interactive Deaggregation Results	3-70
Figure 3-37	Hazard Deaggregation for Combinations of Magnitude and Distance	3-71
Figure 3-38	Geographic Hazard Deaggregation	3-71
Figure 4-1	Stresses Induced in a Soil Element by Vertically Propagating Shear Wave	4-9
Figure 4-2	Hysteretic Stress-Strain Response of Soil Subjected to Cyclic Loading	4-10
Figure 4-3	Shear Modulus Reduction and Equivalent Viscous Damping Ratio Curves	4-11
Figure 4-4	Correction Factor for the Effective Overburden Pressure, C_N	4-18
Figure 4-5	Soil Classification Chart Based on the CPT	4-20
Figure 4-6	CPT-SPT Correlation Chart	4-20
Figure 4-7	Correlation between Dry Unit Weight and Normalized Cone Tip Resistance	4-21
Figure 4-8	Correlation among Saturated Weight, Shear Wave Velocity, and Depth	4-22
Figure 4-9	Correlation among Saturated Weight, CPT Sleeve Friction, and Specific Gravity	4-22
Figure 4-10	Correlation among CPT Tip Resistance, Relative Density, and Compressibility for Clean Sands	4-24
Figure 4-11	Field and Laboratory Methods for Evaluating Shear Wave Velocity	4-26

Figure 4-12	CPT – Shear Wave Velocity Correlation for Clean Quartz Sands	4-33
Figure 4-13	CPT – Shear Wave Velocity Correlation for Clay Soils	4-34
Figure 4-14	Shear Modulus Reduction Curves for Sands	4-35
Figure 4-15	Comparison of Seed et al. (1985) Modulus Reduction and Damping Curves for Sand with Darendeli (2001) Curves for $PI = 0$	4-36
Figure 4-16	Darendeli (2001) Confining Pressure Dependent Curves for $PI = 30$	4-37
Figure 4-17	Comparison of Hashash and Park (2001) Modulus Reduction and Damping Curves for the Mississippi Embayment with EPRI (1993) curves	4-38
Figure 4-18	Correlation between the Undrained Residual Strength Ratio, S_r/σ'_{vo} and a) Standardized Normalized SPT Blow Count, $(N_1)_{60}$ and b) Normalized CPT Tip Resistance, q_{c1}	4-41
Figure 4-19	Correlation between the Residual Undrained Strength Ratio, S_r/σ'_{vo} and Equivalent Clean Sand SPT Blow Count, $(N_1)_{60-CS}$	4-42
Figure 4-20	Void Ratio Redistribution Due to an Overlying Confining Layer	4-43
Figure 4-21	Classes of Rock Mass Discontinuities	4-46
Figure 4-22	Relationship between Friction Angles and Cohesive Strength Mobilized at Failure for Slopes	4-46
Figure 4-23	Relationships between Major and Minor Principal Stresses for Hoek-Brown and equivalent Mohr-Coulomb Criteria	4-50
Figure 4-24	Definition of Joint Roughness Coefficient, JRC	4-52
Figure 4-25	Definition of Instantaneous Cohesion c_i and Instantaneous Friction Angle ϕ_i for a Non-Linear Failure Criterion	4-53
Figure 5-1	Refraction of Shear Waves Approaching the Ground Surface	5-4
Figure 5-2	Relationship between PGA on Rock and on Other Local Site Conditions	5-6
Figure 5-3	PGA Amplification Based Upon NEHRP Site Class	5-7
Figure 5-4	Relationship between PHGA on Rock and on Soft Soil Sites	5-8
Figure 5-5	Base and Crest Peak Accelerations Recorded at the Earth Dams	5-9
Figure 5-6	1-Dimensional Column for SHAKE Equivalent Linear Seismic Site Response Analysis	5-13
Figure 5-7	Influence of Pressure Dependent Soil Behavior on the Seismic Response of a 3,300 ft (1,000 m) Thick Soil Column in the Mississippi Embayment	5-14
Figure 5-8	Equivalent Linear Response Analysis for a Shallow Impedance Contrast Site in Columbia, South Carolina	5-16
Figure 5-9	Non-Linear Soil Model for Time-Domain Site Response Analysis	5-17
Figure 5-10	Comparison of Total Stress Site Response Analysis to Effective Stress Site Response Analyses with Pore Pressure Softening	5-20
Figure 5-11	Quasi Two-Dimensional Site Response Analysis Using One-Dimensional Column	5-21
Figure 6-1	Newmark Sliding Block Concept for Slopes	6-3
Figure 6-2	Pseudo-Static Limit Equilibrium Analysis	6-5
Figure 6-3	Simplified Height-Dependent Scaling Factor Recommended for Design	6-9
Figure 6-4	Permanent Seismic Deformation Chart	6-11
Figure 6-5	Comparison between AASHTO (2004) and Recommended Displacement Equation 6-5 for $PGV = 30k_{max}$ (in/sec)	6-13
Figure 6-6	Problem Definition	6-16
Figure 6-7	Representative Analysis Results	6-16
Figure 6-8	Main Types of Slope Failure and Stereoplots of Structural Conditions Likely to Give Rise to these Failures	6-17
Figure 6-9	Strength Degradation in Cyclic Torsional Shear tests	6-24
Figure 6-10	Undrained Cyclic Simple Shear Test Results Nevada Sand, $Dr = 40\%$	6-24
Figure 6-11	Shear Stress Strain History at the Wildlife Refuge Site during Liquefaction	6-25

Figure 6-12	The CSR Required to Reach Initial Liquefaction ($r_u=100\%$) , from Shaking Table Tests by De Alba et al. (1976)	6-25
Figure 6-13	Simplified Base Curve Recommended for Determination of CRR from SPT Data for Magnitude 7.5 Along with Empirical Liquefaction Data	6-30
Figure 6-14	Magnitude Scaling Factors Derived by Various Investigators	6-31
Figure 6-15	CPT-Liquefaction Resistance Correlation Chart	6-32
Figure 6-16	CPT Grain Size Characteristic Correction Factor.....	6-34
Figure 6-17	Shear Wave Velocity – Liquefaction Resistance Correlation Chart.....	6-35
Figure 6-18	Soil Flexibility Factor (r_d) Versus Depth Curves Developed by Seed and Idriss	6-36
Figure 6-19	Example of a Liquefaction Triggering Analysis for a Single SPT Boring	6-37
Figure 6-20	Newmark Sliding Block Analysis in Liquefied Soil.....	6-41
Figure 6-21	Plot for Determination of Earthquake-induced Shear Strain in Sand Deposits	6-43
Figure 6-22	Relationship between Volumetric Strain, Cyclic Shear Strain, and Penetration Resistance for Unsaturated Sands.....	6-44
Figure 6-23	Computation of Settlement for 50-ft Deep Sand Layer	6-45
Figure 6-24	Curves for Estimation of Post-liquefaction Volumetric Strain Using SPT Data and Cyclic Stress Ratio for M_w 7.5 Earthquakes	6-46
Figure 6-25	Types of Earthquake Faults	6-49
Figure 6-26	Relationship between Maximum Surface Fault Displacement and Earthquake Moment.....	6-53
Figure 7-1	Ditullio Landslide, Loma Prieta Earthquake.....	7-3
Figure 7-2	Route 17 landslide, Loma Prieta Earthquake.....	7-4
Figure 7-3	Planar Rock Slide in Volcanic Tuff 1989 Armenia Earthquake	7-4
Figure 7-4	Slope Failure with Ground Cracking along Mulholland Drive, 1994 Northridge Earthquake	7-5
Figure 7-5	Differential Settlement Induced by Seismic Compaction at the Easterly Approach to Bridge 53-1991R in I-5 to I-210 Interchange During 1971 San Fernando Earthquake...	7-6
Figure 7-6	Differential Settlement across Pavement Joints Near Cut-fill Boundary on I-5 north of I-405 Separation. The Settlement is due to Seismic Compaction of Fill during the 1971 San Fernando Earthquake.	7-7
Figure 7-7	Wavy Pavement due to Differential Settlement Enhanced by Liquefaction during the 1993 Hokkaido-Nansei-Oki, Japan Earthquake.....	7-8
Figure 7-8	Failure Mechanism for an Embankment Founded Upon Liquefied Soil	7-9
Figure 7-9	Segment of Highway 36 Near Carribean Coast in Costa Rica that Split Longitudinally, Settled and Spread Laterally during 1991 Earthquake by Mechanism	7-9
Figure 7-10	Disrupted Fill and Pavement due to Liquefaction at the Approach to the Highway 36 bridge Over Rio Estrella, Costa Rica, during 1991 Earthquake.	7-10
Figure 7-11	Rigid pavement on I-5 south of I-5/I-210 interchange that sheared and buckled at two localities during the 1971 San Fernando earthquake due to 6.5 ft (2 m) of lateral spread displacement.	7-11
Figure 7-12	Extensional Fissures in Flexible Pavement Caused by Lateral Spread of Floodplain Deposits Toward Rio Viscaya during the 1991 Costa Rica Earthquake.....	7-11
Figure 7-13	Liquefaction-induced Flow Failure of Roadway Embankment into Lake Merced During 1957 Daly City, California Earthquake	7-12
Figure 7-14	Damage to the Abutments and Piers of Yachiyo Bridge on the Left Bank	7-13
Figure 7-15	Showa Bridge Collapse.....	7-14
Figure 7-16	Deformation of a Steel Pipe pile for the Showa Bridge.....	7-14
Figure 7-17	Landing Road Bridge, Whakatane, New Zealand.....	7-15
Figure 7-18	Schematic of the Raked-pile Foundation at the Landing Road Bridge.....	7-16
Figure 7-19	Potential Collapse Mechanism for Landing Load Bridge.....	7-16

Figure 7-20	Site and Damage Characteristics for a Precast Concrete Pile Subjected to Lateral Spread in the Kobe Earthquake	7-17
Figure 7-21	Slope Geometry	7-20
Figure 7-22	Procedure to Establish Acceptable Slope Movement	7-32
Figure 7-23	Rock Buttress Used to Increase Forces Resisting Slope Failure.....	7-33
Figure 7-24	Classification Scheme for Earth Retention Systems.....	7-34
Figure 7-25	Examples of Externally and Internally Stabilized Earth Retention Systems	7-34
Figure 7-26	Types of Vertical and Horizontal Drains used to Lower the Groundwater in Natural Slopes.....	7-35
Figure 7-27	Categories of Rock Slope Stabilization Measures	7-36
Figure 7-28	Rock Slope Reinforcement Methods	7-37
Figure 7-29	Rock-removal Methods for Slope Stabilization.....	7-38
Figure 7-30	Side View of Rock Fall Restraint Net System with Fully Embedded Posts and Anchor Support.....	7-39
Figure 7-31	Example of Rock Shed	7-40
Figure 7-32	Rock Slope Mitigation Methods Used by Selected States.....	7-41
Figure 7-33	Elevation View of a Representative Bridge on a Liquefiable Stratum	7-42
Figure 7-34	Pseudo-static Stability Analysis.....	7-43
Figure 7-35	Design Flowchart.....	7-48
Figure 7-36	Deformation Models for Piles at Lateral Spreading Sites.....	7-49
Figure 7-37	Site profile, Washington Bridge	7-52
Figure 7-38	Typical Sliding Mechanism for Flow Failure.....	7-53
Figure 7-39	Forces Provided by Bridge and Foundation Piles for Resisting Lateral Spread	7-54
Figure 7-40	Dynamic Deep Compaction.....	7-58
Figure 7-41	The Vibro Compaction Process	7-59
Figure 7-42	Vibro-replacement Equipment and Process.....	7-60
Figure 7-43	Vibro-system (stone column) Treatment at Toe of Approach Embankment.....	7-61
Figure 7-44	Vibro-system (stone column) Treatment Around a Pile-supported Bridge Pier.....	7-61
Figure 7-45	Compaction Grout Bulb Construction	7-63
Figure 7-46	Dry Method Column Installation	7-63
Figure 7-47	Deep Mixing Column Patterns.....	7-64
Figure 7-48	Deep Mixing Applications in Japan.....	7-65
Figure 7-49	Kobe Hotel Foundation Plan in Japan	7-65
Figure 8-1	Global Structural Model for Seismic Design.....	8-3
Figure 8-2	Acceleration and Displacement Design Spectra	8-5
Figure 8-3	Elastic and Inelastic Force and Displacement Demand and the Ductility Ratio.....	8-6
Figure 8-4	Pushover Analysis for Displacement Demand Distribution	8-8
Figure 8-5	Concept for Capacity Protecting the Foundation	8-9
Figure 8-6	Typical Structural Forms for Bridge Foundation Systems	8-10
Figure 8-7	Inertial Interaction Models; a) Shallow Foundation Model and b) Deep Foundation Model.....	8-15
Figure 8-8	Direct (or Total) Soil-Structure Kinematic Interaction Model	8-16
Figure 8-9	Foundation Substructuring Model for Kinematic Analysis	8-17
Figure 8-10	Comparison of Kinematic Motion from SSI to Free field Depth Varying Motions	8-18
Figure 8-11	Effect of Soil Stiffness on Performance of 24-inch Reinforced Concrete Pile.....	8-24
Figure 9-1	Types of Shallow Foundations.....	9-2
Figure 9-2	Two Step Rigorous Inertial Response Solution Incorporating Frequency Dependent Foundation Impedance.....	9-6
Figure 9-3	Frequency Dependent Dynamic Stiffness Factor for a Surface Footing.....	9-7
Figure 9-4	Form of the Shallow Foundation Stiffness Matrix.....	9-9
Figure 9-5	Stiffnesses for a Rigid Surface Footing on a Semi-Infinite Half Space.....	9-10

Figure 9-6	Embedment Factors for a Rigid Footing on a Semi-Infinite Half Space	9-11
Figure 9-7	Embedment Factor in Graphical Format from Lam and Martin (1986)	9-12
Figure 9-8	Footing Stiffness for a Finite Soil Layer above Rigid Base	9-13
Figure 9-9	Implementation of Foundation Submodel in the Global Structural Model.....	9-14
Figure 9-10	Equivalent Footing Dimensions.....	9-16
Figure 10-1	Damage to the Head of Battered Piles at the Port of Oakland.....	10-2
Figure 10-2	Shear Failure in the Cap Beam Connection of the Struve Slough Pile Bent	10-3
Figure 10-3	Piles Punched-Through the Deck Slab in the Collapsed Struve Slough Bridge	10-3
Figure 10-4	Large Lateral Displacements Imposed on Adjacent Piles, Struve Slough Bridge	10-3
Figure 10-5	Damage to Excavated Pile from the Niigata Court House.....	10-5
Figure 10-6	Pile Damage Observed from S Building; (a) Damage to Foundation Pile; (b) SPT Value; (c) Photos of Damage	10-5
Figure 10-7	Pile Damage Observed from NHK Building	10-6
Figure 10-8	Pile Damage Observed from Hotel Niigata	10-7
Figure 10-9	Pile Layout of Hokuriku Building	10-7
Figure 10-10	Seismic Design of Pile Foundations	10-9
Figure 10-11	Modeling Approaches to Solve for the Kinematic Interaction	10-11
Figure 10-12	Pile Group Layout and Kinematic Interaction Model, San Francisco East Bay Bridge Replacement Structure Skyway	10-12
Figure 10-13	Comparison of Ground Motions from 1-D Site Response Analysis to Kinematic Motion.....	10-13
Figure 10-14	Two-Springs-in Series Soil-Pile Interaction Model.....	10-14
Figure 10-15	Lateral Translational Diagonal Stiffness Coefficient.....	10-17
Figure 10-16	Rotational Diagonal Stiffness Coefficient	10-18
Figure 10-17	Cross Coupling of Diagonal Stiffness Coefficient.....	10-19
Figure 10-18	Lateral Free Head Stiffness Coefficient.....	10-20
Figure 10-19	Lateral Translational Diagonal Stiffness Coefficient for Embedded Pile Head	10-21
Figure 10-20	Rotational Diagonal Stiffness Coefficient for Embedded Pile Head.....	10-22
Figure 10-21	Cross Coupling of Diagonal Stiffness Coefficient for Embedded Pile Head	10-23
Figure 10-22	Recommended Coefficient of Variation in Subgrade Stiffness with Depth for Sands	10-24
Figure 10-23	Recommended Coefficient of Variation in Subgrade Stiffness with Depth for Clays.	10-24
Figure 10-24	Graphical Solution for Developing Axial Pile Stiffness	10-26
Figure 10-25	Method for Passive Pressure Capacity of Pile Cap.....	10-28
Figure 10-26	P-Multipliers for Two-Way Seismic Loading	10-30
Figure 10-27	Scaling Factor to Reese's static p-y Curves from the 1995 Liu and Dobry Centrifuge Test	10-31
Figure 10-28	Measured versus Predicted Pile Head Rotation	10-33
Figure 10-29	Shear vs. Moment Load Solution.....	10-34
Figure 10-30	Moment Capacity of a Pile Group	10-35
Figure 10-31	Sensitivity of a 16-inch Drilled Shaft to Variations in p-y Curve Stiffness.....	10-37
Figure 10-32	The Two Cases for Pile Design in Lateral Spreading Liquefied Soils	10-39
Figure 10-33	p-y Curves Back calculated from Soil Liquefied by Blasting	10-40
Figure 10-34	3-D Finite Element Model of a Pile in Laterally Spreading Ground with a Nonliquefied Crust.....	10-41
Figure 10-35	Maximum Pile Moment Location.....	10-42
Figure 10-36	Maximum Pile Moment Solution.....	10-42
Figure 10-37	Maximum Pile Shear Solution	10-43
Figure 10-38	Various SSI Modeling Approaches for Caissons.....	10-45
Figure 11-1	Mass Concrete Gravity Wall.....	11-2

Figure 11-2	Semi-Gravity Cantilever Retaining Walls.....	11-3
Figure 11-3	Counterfort Retaining Walls	11-3
Figure 11-4	Buttressed Retaining Walls	11-4
Figure 11-5	Non-Gravity Cantilever Wall.....	11-4
Figure 11-6	Single Tieback System.....	11-5
Figure 11-7	MSE Wall with Precast Concrete Face Panels	11-6
Figure 11-8	Soil Nail Wall.....	11-7
Figure 11-9	Precast Concrete Crib Walls	11-8
Figure 11-10	Seismic Forces on a Semi-gravity Retaining Wall	11-10
Figure 11-11	Free Body Diagram for Mononobe-Okabe Active Earth Pressure Theory.....	11-11
Figure 11-12	Inclination of the Seismic Active Wedge for $\phi = 35^\circ$	11-13
Figure 11-13	Active Trial Wedge.....	11-14
Figure 11-14	Effect of cohesion on the seismic active earth pressure coefficient for $\phi = 35^\circ$	11-16
Figure 11-15	Critical Log Spiral Surfaces Compared to Planar Critical Surfaces	11-17
Figure 11-16	Passive Seismic Earth Pressure Coefficient from the Log Spiral Method for Cohesionless Soil and $\delta = 0.67\phi$	11-18
Figure 11-17	General Limit Equilibrium Method for Evaluating the Seismic Active Earth Pressure.....	11-19
Figure 11-18	Wall height adjustment factor, α , vs. wall height	11-21
Figure 11-19	Modes of Failure for a Semi-Gravity Earth Retaining Structure	11-26
Figure 11-20	Combined Thrust Loads and Deformed Shape of Cantilever Wall	11-31
Figure 11-21	Forces Acting at the Critical Sections of the Wall.....	11-32
Figure 11-22	Pile Supported Retaining Wall.....	11-33
Figure 11-23	Cantilevered and Anchored Earth Retaining Systems	11-34
Figure 11-24	Seismic Load Distribution for Non-Gravity Cantilever Retaining Walls.....	11-35
Figure 11-25	Lateral Earth Pressure for Anchored/Braced Walls.....	11-37
Figure 11-26	Single Tieback System.....	11-39
Figure 11-27	General Pressure Distribution for Tieback Retaining Walls.....	11-40
Figure 11-28	Simple Seismic Pressure Distribution for a Multiple Tieback System	11-41
Figure 11-29	Hinge Method for Tieback Design	11-42
Figure 11-30	Potential External Failure Mechanisms for MSE Walls	11-43
Figure 11-31	Pressure Diagram for MSE Wall with Seismic Force.....	11-44
Figure 11-32	Pressure Diagram for MSE Walls with Sloping Backslope.....	11-45
Figure 12-1	Seat-Type Abutment and Foundation System	12-3
Figure 12-2	Seat Type Abutments; a) Short Seat and b) High Cantilever.....	12-3
Figure 12-3	Monolithic Abutment and Foundation System	12-4
Figure 12-4	Monolithic Abutment Types; (a) Short Stem and (b) High Stem	12-5
Figure 12-5	Mobilization of Passive Resistance (Shamsabadi, 2007).....	12-6
Figure 12-6	Formations of Mobilized Passive Wedges (Kosa et al., 2001)	12-7
Figure 12-7	Puente Los Banos Bridge.....	12-8
Figure 12-8	Full Scale Abutment Experiment with Silty Sand Backfill	12-10
Figure 12-9	UCD Abutment Field Test.....	12-11
Figure 12-10	UCD Abutment Test Loading Setup.....	12-11
Figure 12-11	Failure Mechanism of the UCD Abutment Test	12-12
Figure 12-12	Bridge Model for Seat-Type Abutment with an Expansion Gap.....	12-13
Figure 12-13	Bi-Linear Abutment Force-Deformation Relationship	12-14
Figure 12-14	Closed-Form Solution.....	12-16
Figure 12-15	2-D finite Element Mesh of Bridge Abutment.....	12-17
Figure 12-16	Deformed Shape of Abutment Backfill in Simulation by the 2-D FEM Model	12-18
Figure 12-17	Bridge and Abutment Model	12-19

Figure 12-18	Near-field Ground Motion with High Velocity Pulse.....	12-19
Figure 12-19	Longitudinal Hysteretic Behavior of a Single-Span Bridge Abutment	12-20
Figure 12-20	Deck Rotation in a Bridge with Skewed Abutments During a Seismic Event	12-21
Figure 12-21	Non-Uniform Passive Wedge behind a Skewed Abutment	12-21
Figure 12-22	Passive Soil Wedge in a Non-Skewed Abutment	12-22
Figure 12-23	3-D FE Model of Passive Wedge Formation behind a Skewed Abutment.....	12-23
Figure 12-24	Nonlinear Normal and Tangential Components of Abutment-Backfill Resistance for a 30° Skew	12-24
Figure 12-25	Impact of Skew Angles on Nonlinear Abutment Force-Deformation Relationship	12-24
Figure 12-26	Single Span Bridge 45° Skew Angles	12-25
Figure 12-27	Hysteretic Abutment Response Obtuse and Acute Corner of the Single-Span Bridge with 45° Skew Angle	12-26
Figure 13-1	Longitudinal Axial and Curvature Response to Traveling Waves.....	13-5
Figure 13-2	Transverse Ovaling and Racking Response to Vertically Propagating Shear Waves....	13-6
Figure 13-3	Shear Distortion of Ground – Free-Field Condition vs Cavity In-Place Condition.....	13-14
Figure 13-4	Lining Response Coefficient, K_1	13-18
Figure 13-5	Lining Response Coefficient, K_2 , for Poisson’s Ratio = 0.2.....	13-19
Figure 13-6	Lining Response Coefficient, K_2 , for Poisson’s Ratio = 0.35.....	13-19
Figure 13-7	Lining Response Coefficient, K_2 , for Poisson’s Ratio = 0.5.....	13-20
Figure 13-8	Soil Deformation Profile and Racking Deformation of a Box Structure	13-22
Figure 13-9	Racking Coefficient R_r for Rectangular Structures.....	13-26
Figure 13-10	Simplified Racking Frame Analysis of a Rectangular Structure	13-26

LIST OF TABLES

Table 1-1	AASHTO Limit States for Bridge Design	1-16
Table 1-2	Load Combinations and Load Factors for AASHTO Limit States	1-17
Table 1-3	AASHTO Permanent Load Factors	1-18
Table 1-4	Resistance Factors for Deep Foundations	1-19
Table 2-1	Modified Mercalli Intensity Scale.....	2-22
Table 3-1	Selected Attenuation Relationships Used to Develop USGS Seismic Hazards Maps...	3-15
Table 3-2	Coefficients for the Abrahamson and Silva (1997) Attenuation Model	3-17
Table 3-3	Magnitude Deaggregation for Bakersfield, California, for a 2500 YR Return Period ..	3-24
Table 3-4	Performance Based Seismic Design Criteria for Transportation Facilities	3-29
Table 3-5	NEHRP Site Classification System	3-40
Table 3-6	Values of F_{pga} as a Function of Site Class and the Site Class B Peak Ground Acceleration	3-41
Table 3-7	Values of F_a as Function of Site Class and the Site Class B Short Periods (0.2 Seconds) Spectral Acceleration	3-42
Table 3-8	Values of F_v as a Function of Site Class and the Site Class B Long Periods (1 Second) Spectral Acceleration	3-42
Table 4-1	Recommended "Standardized" SPT Equipment	4-16
Table 4-2	Correction Factors for Non-Standard SPT Procedure and Equipment	4-17
Table 4-3	Relative Density of Sandy Soils	4-24
Table 4-4	Typical Values of Initial Shear Modulus	4-31
Table 4-5	Index Property Correlations for Estimating the Initial (Small Strain) Shear Modulus, G_{max}	4-33
Table 4-6	Blow Count Correction, N_{corr} for the Equivalent Clean Sand Blow Count, $(N_1)_{60-cs}$	4-42
Table 4-7	Field Estimates of Uniaxial Compressive Strength of Intact Rock.....	4-45
Table 4-8	Geological Strength Index (GSI) for Jointed Rock Masses	4-47
Table 4-9	Values of m_i for Intact Rock by Rock Group.....	4-48
Table 4-10	Estimation of Disturbance Factor, D	4-49
Table 5-1	Uses of Site Response Analysis in Seismic Design of Transportation Facilities	5-3
Table 6-1	Seismic Hazard Level	6-20
Table 6-2	Estimated Susceptibility of Sedimentary Deposits to Liquefaction During Strong Ground Motion	6-22
Table 6-3	Influence of Earthquake Magnitude on Volumetric Strain Ratio for Dry Sands	6-44
Table 6-4	Computation of Settlement for Deposit of Dry Sand.....	6-45
Table 7-1	Site Coordinates and Seismicity Data	7-21
Table 7-2	Height-Adjusted Seismic Coefficients for Site Class D, Compacted Fill Slope Example	7-22
Table 7-3	Pseudo-Static Stability Analyses Capacity to Demand Ratio (Factor of Safety) for a Seismic Coefficient Equal to $0.5k_{AV}$, Compacted Fill Slope Example.....	7-23
Table 7-4	Yield Acceleration, k_Y , for Compacted Fill Slope Example.....	7-23
Table 7-5	Newmark Displacements for Compacted Fill Slope Example	7-24
Table 7-6	Seismic Displacement Estimates, Natural Slope Examples.....	7-27
Table 7-7	No Seismic Analysis Screening Criterion for Stability of Slopes not Suceptible to Liquefaction	7-27
Table 7-8	Ground Improvement Methods.....	7-57

Table 8-1	Force Reduction Factors, R, for Bridge Substructures	8-6
Table 8-2	AASHTO Seismic Design Categories	8-19
Table 8-3	Seismic Analysis Requirements for Bridges from the Interim Revisions.....	8-20
Table 8-4	Seismic Design Requirements for Bridges from the Interim Revisions	8-20
Table 8-5	Seismic Design Requirements from the 2009 AASHTO Guide Specifications	8-21
Table 8-6	Foundation Modeling Requirements from the 2009 AASHTO Guide Specifications...	8-21
Table 10-1	p-Multipliers for Piles in a 3 x 3 Group at 3 Diameter Spacing Subject to Monotonic Loading	10-29
Table 10-2	Influence of Pile Spacing on p-Multipliers for Pile Subject to Monotonic Loading ...	10-29
Table 10-3	p-Multipliers for Large Pile Groups	10-30
Table 11-1	Conditions Under which Seismic Analysis is Not Required for a Free Standing Earth Retaining Wall	11-10
Table 11-2	Maximum Amount of Apparent Cohesion that should be Assumed for Backfill Soils	11-16
Table 12-1	Presumptive Displacement Factors, F_w	12-15

CHAPTER 1

INTRODUCTION

1.1 BACKGROUND

While earthquakes are sometimes considered primarily a California or west coast problem in the continental United States (US), damaging earthquakes are not limited to the western US. In fact, some of the strongest earthquakes in historical time in the United States occurred in the central and eastern US. The Charleston, South Carolina earthquake of 1886 is believed to have been as strong, if not stronger, than the 1971 San Fernando and 1994 Northridge earthquakes, and there were three large magnitude earthquakes, including at least one believed to have been as strong as the 1906 San Francisco earthquake, in the New Madrid seismic zone in the central United States in 1811 and 1812. Furthermore, in many areas of the United States bridges and other transportation structures are inadequately designed to resist even moderate levels of ground shaking without collapse.

Figure 1-1 shows the United States Geological Survey (USGS) National Seismic Hazard Map for the peak ground acceleration with a 10% probability of being exceeded in 50 Years. The probability level for the map in Figure 1-1 corresponds to an annual probability of occurrence of 0.2%, or a return period of approximately 500 years, i.e. ground motions that are roughly twice as likely to occur as the design level specified in the current AASHTO (American Association of State Highway and Transportation Officials) seismic design provisions for bridges in the United States. Data produced by the USGS National Seismic Hazard Mapping Program indicates that at least 40 percent of the United States is subject to damaging ground shaking levels with 7 percent probability of occurrence in a 75 year period (the AASHTO bridge design criterion (corresponding to an approximately 0.1% annual probability of occurrence , or a 1000 year return period).

A factor that contributes the seismic hazard in the central and eastern US is that earthquake ground motions do not appear to attenuate as rapidly as they do in the western US. Thus, earthquake motions are felt over a much larger area in the western US compared to the central and eastern US for similar size earthquakes. Figure 1-2 compares the felt areas from the Charleston and New Madrid earthquakes to the San Fernando and San Francisco earthquakes.

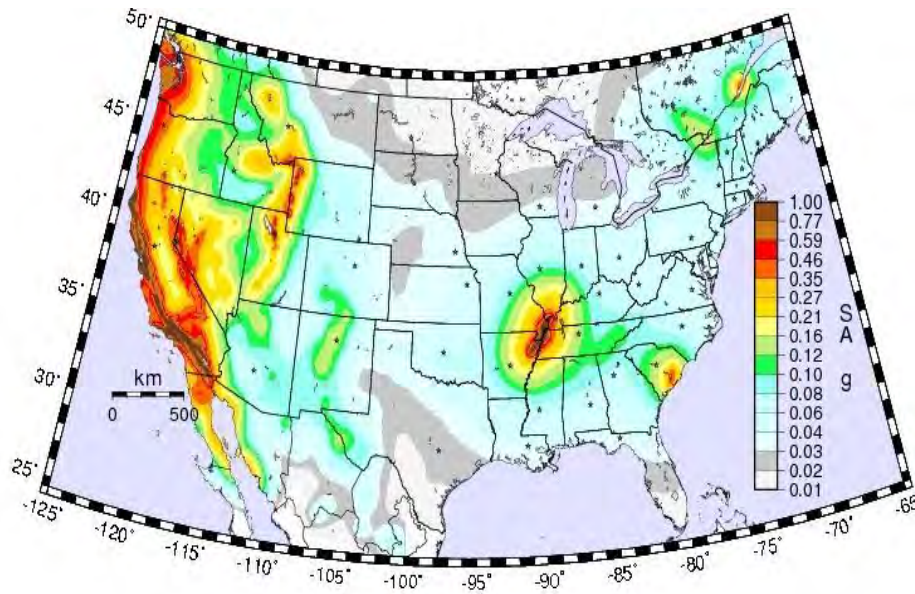


Figure 1-1 Peak Ground Acceleration with a 10% Probability of Being Exceeded in a 50 year Period
<http://earthquake.usgs.gov/hazards/products/conterminous/2008/maps/>

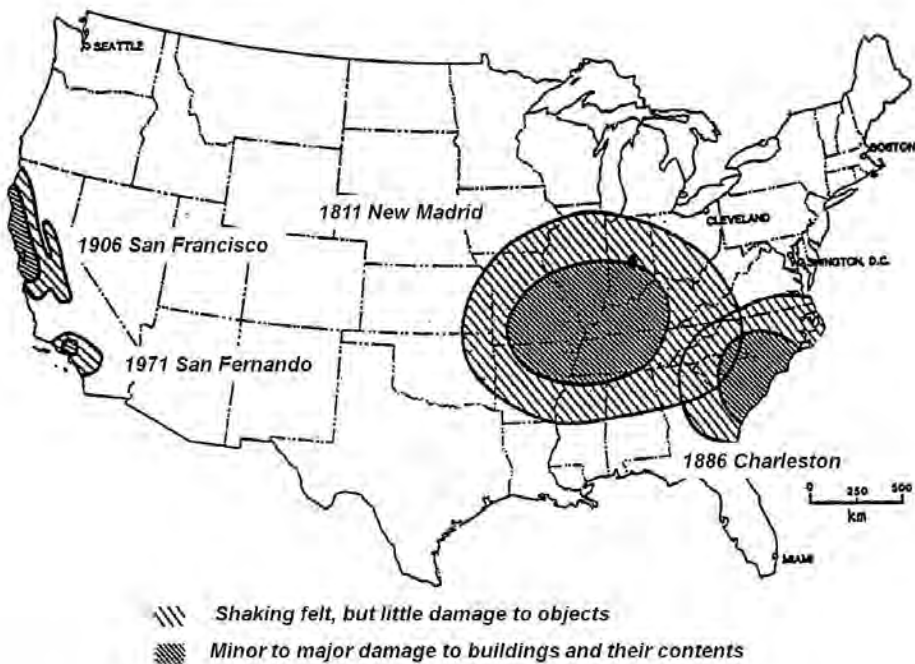


Figure 1-2 Areas Impacted by Historic Earthquakes in the United States (ASCE)

The susceptibility of older bridges and highway structures commonly found in the central and eastern US to earthquake shaking also contributes to the seismic risk in these areas. The photo in Figure 1-3 shows the collapse of the Cypress viaduct in Oakland in the 1989 Loma Prieta earthquake. This type of non-ductile concrete construction is common in some parts of the central and eastern US and the level of earthquake shaking at the Cypress viaduct was similar to the AASHTO design levels in the many of these areas. Essentially, any of the pale green or darker areas on the National Seismic Hazard Map shown in Figure 1-1 are subject to ground motions of similar intensity to those experiences by the Cypress structure.



Figure 1-3 Collapse of the Cypress Viaduct in the 1989 Loma Prieta Earthquake (USGS)

1.2 EARTHQUAKE DAMAGE CATEGORIES

Damage from earthquakes can be subdivided into direct damage and indirect damage. Direct damage is the physical damage due to the earthquake. Direct damage includes primary damage due to strong shaking and fault rupture and secondary damage due to the effects of strong shaking or fault rupture. Indirect damage refers to the socio-economic impacts of an earthquake. The economic component of indirect damage often exceeds the economic consequences of direct damage from a major earthquake.

1.2.1 Primary Damage

Primary damage includes damage due to fault rupture and strong shaking. While fault rupture can cause significant damage to facilities built on or across the fault, the extent of the area impacted by fault rupture is relatively small as it is limited to the immediate vicinity of the rupture zone. Furthermore, areas susceptible to fault rupture in the western United States are often well-defined on geologic maps and construction in these areas may be restricted (e.g. Alquist-Priolo special study zones in California). Fault rupture is usually not a concern east of the Rocky Mountains, as faults east of the Rocky Mountains tend not to have surface expressions when they rupture.

Primary damage due to strong shaking includes partial or total collapse of structures, landslides, and liquefaction. Figure 1-4 shows an example of direct damage to a highway structure due to strong shaking in the 1971 San Fernando earthquake. Factors influencing primary damage due to strong shaking include the intensity, duration, and frequency characteristics of the strong ground motion. These factors are related to distance between the site and the earthquake, the magnitude of the earthquake, and other characteristics of the earthquake as well as local site conditions. Primary damage also includes ground displacement phenomenon such as landslides and liquefaction induced by strong ground motions



Figure 1-4 Collapse of the I-5, SR-14 Overpass in the 1971 San Fernando Earthquake (USGS)

1.2.2 Secondary Damage

Secondary damage is damage due to impact of primary damage, i.e., to phenomena induced by strong shaking or ground displacement. Secondary damage includes the impacts of landslides (e.g. disrupted roadways) and liquefaction (e.g. bearing capacity failure, lateral spreading, and slope instability) as well as damage due to seismically-induced settlement and impacts to constructed facilities from seiches and tsunamis. Figure 1-5 shows the collapse of the Showa Bridge in the 1964 Niigata, Japan earthquake due to liquefaction induced lateral spreading of the bridge piers. Case history data indicates that lateral spreading of liquefied soils is one of the major sources of damage to bridge foundations in earthquakes.



Figure 1-5 Collapse of the Showa Bridge in the 1964 Niigata, Japan Earthquake (NGDC)

Other types of secondary damage include fire following earthquakes and hazardous material spills. Much of the damage in San Francisco in 1906 was due to fire following the earthquake. The fire damage was exacerbated by ruptures to the water distribution due to earthquake-induced ground failure (e.g. liquefaction), which hindered attempts to suppress the fires. More recently, fires following the Coalinga (1984) earthquake were a significant source of secondary damage. Figure 1-6 shows fire due to a ruptured gas main in the 1994 Northridge earthquake. Gas and oil pipelines and storage facilities are often located within or adjacent to highway right-of-ways, creating fire and other secondary earthquake hazards (e.g. hazardous material spills) that may impact transportation facilities.

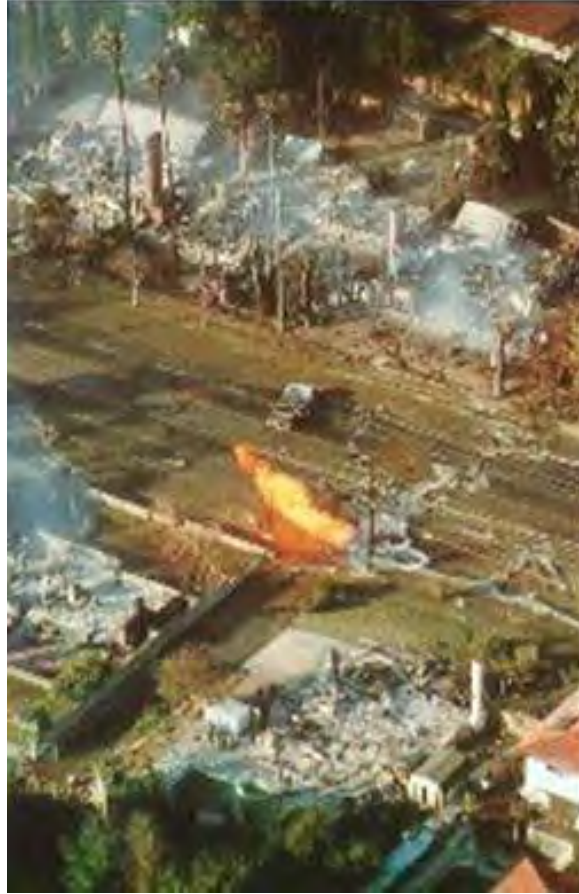


Figure 1-6 Fire Following the 1994 Northridge Earthquake due to a Rupture Gas Main

1.2.3 Indirect Damage

There are many sources of indirect damage following an earthquake. Besides the more obvious losses due to disruption of business and commerce, disruption of essential services, and decline of property values, environmental impacts and mental stress are significant sources of indirect damage. Environmental effects can include not only hazardous material spills but also increased air pollution due to increased travel distances and congestion from disrupted highways. Mental stress in the aftermath of earthquakes often leads to an increase in divorce and suicide rates and other types of emotional problems. Indirect damage following the 1989 Loma Prieta earthquake due to closure of the San Francisco-Oakland Bay Bridge east span, shown in Figure 1-7, is estimated to have totaled hundreds of millions of dollars of economic loss. In total, the economic component of secondary damage due to the Loma Prieta event is estimated to have been well over \$5 billion dollars.



Figure 1-7 Damage to the San Francisco-Oakland Bay Bridge East Span due to the 1989 Loma Prieta Earthquake (USGS)

1.3 DAMAGE TO HIGHWAY FACILITIES IN EARTHQUAKES

The record of damage to highway facilities from earthquakes starts with the 1933 Long Beach earthquake – primarily because there were few highways before 1933 in areas subject to strong earthquake shaking, e.g. in the vicinity of the 1906 San Francisco earthquake. The first scientific studies of bridge damage, and liquefaction, commenced after the 1964 earthquakes in Niigata, Japan and Alaska. However, most of the bridges damaged in Alaska were railway bridges. The first major study of earthquake-induced highway bridge damage in the US followed the 1971 San Fernando earthquake. There have been numerous studies of damage to highway facilities in the US and abroad since 1971. Today, almost essentially every major earthquake is followed by reconnaissance studies that document both the damage to and successful performance of constructed facilities, including transportation systems.

The 1971 San Fernando event was the first earthquake in the US which caused extensive damage to modern highway facilities. The strong motion records collected in the San Fernando event also facilitated the first statistical studies of strong ground motions. Observed damage on the San Fernando event included structural damage to bridges and retaining walls, cracking and lateral spreading of roadways, and slope instability.

Figure 1-4 showed damage to the Interstate 5, State Route 14 interchange in the San Fernando earthquake, under construction at the time of the earthquake. These spans fell off their bearings due to inadequate seat width. Figure 1-8 shows the failure of an abutment wingwall at the Roxford Street undercrossing for SR-101 in the San Fernando event. The wall in Figure 1-8 had inadequate capacity to resist the seismically-induced lateral earth pressures.



Figure 1-8 Failure of the Wingwall at the Roxford Street Undercrossing in the 1971 San Fernando Earthquake

Backfill placed against bridge abutments may be vulnerable to seismic settlement, particularly if the fill is cohesionless and poorly compacted. Figure 1-9 shows settlement of an approach fill at an abutment in the 1971 San Fernando event. The damage shown in Figure 1-8 and Figure 1-9 may be considered acceptable under the current AASHTO performance standard for ordinary bridges, as AASHTO allows for damage in the design earthquake, even to the point of requiring complete replacement of the structure, as long it is not likely to result in structural collapse or loss of life.



Figure 1-9 Settlement of Abutment Embankment Fill in the 1971 San Fernando Earthquake (FHWA, 2004)

Several recent earthquakes provide dramatic examples of the types of damage that can occur to highway facilities in an earthquake. In addition to the collapse of the Cypress viaduct (Figure 1-3) and the east span of the San Francisco-Oakland Bay Bridge (Figure 1-7), another 91 bridges suffered significant damage in the 1989 Loma Prieta event. Furthermore, State Route 17, the main highway from the Bay Area to Santa Cruz, was blocked by a landslide, hindering emergency response and recovery. Figure 1-10 shows the Struve Slough Bridge following the Loma Prieta event. The pile – cap beam connection failed due to strong shaking and ground displacement, the cap beam shifted off the piles, the bridge sat down in the slough, and the piles punched through the bridge deck. Figure 1-11 shows the shear failure at the head of the piles for the Struve Slough Bridge. Failure at the head of a pile due to inadequate confinement or poor connection detailing is one of the most common types of damage to piles in earthquakes.



Figure 1-10 Collapse of the Bridge over Struve Slough in the 1989 Loma Prieta Earthquake (USGS)



Figure 1-11 Shear Failure of the Head of a Pile at the Struve Slough Bridge

Landslides along the route of SR-17, including the one shown in Figure 1-12, closed 12 miles of this the highway, the main route between the epicentral region of the Loma Prieta event, including the city of Santa Cruz, and the San Francisco Bay Area, for 32 days. Besides hindering emergency response and recovery, this closure resulted in substantial economic losses due to loss of commerce, increased traffic congestion on alternate routes, and other secondary effects.



Figure 1-12 Landsliding Along SR-17 in the 1989 Loma Prieta Earthquake (USGS)

Figure 1-13 shows the collapse of the I-5 / SR-14 overpass in the 1994 Northridge earthquake. This is the same overpass that collapsed in the 1971 earthquake (Figure 1-4). The overpass was rebuilt after San Fernando earthquake as originally designed, before lessons learned from that earthquake were incorporated into practice. The overpass was recognized as being seismically inadequate and was on the list of bridges to be seismically retrofit, but funds had not yet been allocated for the retrofit project. About 10% of the approximately 12,000 miles of the state highway system were impacted by the Northridge earthquake, and several major interchanges in the Los Angeles area failed.



Figure 1-13 Collapse of the I-5, SR-14 Interchange in the 1994 Northridge Earthquake (USGS)

1.4 AASHTO SEISMIC DESIGN PHILOSOPHY

The seismic design philosophy adopted by AASHTO for ordinary bridges is that they should be able to withstand large rare earthquakes without collapse or loss of life (though they may suffer damage that requires complete replacement of the structure) and that they should withstand smaller, more frequent earthquakes without significant damage. However, only performance in the large, rare earthquake is actually analyzed. “Acceptable” performance in smaller events is implicitly assumed, but not quantified, and may range from repairable damage to no significant damage.

The 2009 AASHTO Guide Specifications for LRFD Seismic Bridge Design note that more stringent performance requirements are appropriate for critical and essential structures. Bridges are classified by the Owner as Critical, Essential, and Other (sometimes called Ordinary) Bridges (in descending order of importance), depending on their function. A critical bridge is a bridge that is expected to remain open to all traffic, including emergency vehicles, and for defense and security purposes after the design

earthquake. Essential bridges are bridges that are expected to be useable by emergency vehicles and for security and defense purposes after the design earthquake. Bridges that don't fall into either the Critical or Essential categories are designated as Other Bridges. Most bridges are classified as Other (or Ordinary) Bridges and are designed for significant damage in the design event – the large rare earthquake with a 1000-year return period.

The 2009 AASHTO Guide Specifications define significant damage as conditions that may require closure to repair the bridge and/or partial or complete replacement of the structure. Figure 1-8 and Figure 1-9 provided examples of acceptable damage to bridge abutments in the 1971 San Fernando earthquake. After the 1971 San Fernando earthquake, it was evident that many bridge abutments had been subjected to large forces and had actually helped dissipate energy by absorbing these forces at the cost of damage to the abutment. This type of abutment performance is now recognized as beneficial to the overall seismic performance of the bridge. Longitudinal movement of the bridge deck beyond the point at which the abutment wall engages the soil takes energy out of the system. While the thrust of the bridge deck on the abutment wall may result in damage to the wall, under the AASHTO design philosophy abutment walls may be considered sacrificial elements for seismic design of ordinary bridges.

Figure 1-3, Figure 1-4, Figure 1-7, Figure 1-10, Figure 1-11, and Figure 1-13 show unacceptable damage to bridges in earthquakes. Figure 1-14 is another example of unacceptable damage. In this figure, the bridge columns have failed at their connection to the foundation.



Figure 1-14 Failure of a Bridge Column – Foundation Connection

1.5 LOAD AND RESISTANCE FACTOR DESIGN

1.5.1 Basic Principles of LRFD

AASHTO has recently moved to a new design philosophy, Load and Resistance Factor Design (LRFD) LRFD, from the old Allowable Stress Design (ASD) approach. Ideally, LRFD provides a balanced, reliability based design that includes consideration of the various sources of uncertainties that impact structural performance. Equation 1-1 shows the basic LRFD design equation:

$$\sum \eta_i \gamma_i Q_i \leq \sum \phi_i R_i \quad 1-1$$

where:

η_i	=	a load modifier to account for ductility, redundancy, and operational importance of the bridge or other structure (dimensionless)
γ_i	=	load factor; a multiplier applied to force effect i
Q_i	=	force effect i
ϕ_i	=	resistance factor for resistance component i
R_i	=	nominal value of resistance component i

In plain language, Equation 1-1 says that the sum of the factored loads must be less than or equal to the sum of the factored resistances. Load combinations and values for load and resistance factors specified in AASHTO are discussed below.

One complication for the geotechnical specialist is that LRFD notation uses several common soil mechanics symbols. In standard LRFD notation, load factors are designated by the symbol γ and resistance factors are represented by the symbol ϕ . In soil mechanics, we use these symbols for unit weight and the Mohr-Coulomb friction angle, respectively. We therefore need to pay attention to the context in which these symbols are used to know which meaning they have in the equations we are using. An LRFD related term that will be used in this document is the capacity/demand (C/D) ratio. This is not an AASHTO term. The C/D ratio can be calculated using factored or unfactored (nominal) values. In accordance with Equation 1-1, the LRFD design criterion is that the $(C/D)_{\text{factored}}$ must be equal to or greater than 1.0:

$$(C/D)_{\text{factored}} = \sum \phi_i R_i / \sum \eta_i \gamma_i Q_i \quad 1-2a$$

$$(C/D)_{\text{factored}} \geq 1.0 \quad 1-2b$$

The unfactored capacity/demand ratio is analogous to the factor of safety (FS).

$$(C/D)_{\text{unfactored}} = \sum R_i / \sum Q_i \quad 1-3a$$

$$(C/D)_{\text{unfactored}} = \text{FS} \quad 1-3b$$

The unfactored C/D, like the factor of safety, must exceed 1, often times by a significant margin, for a design to be acceptable.

1.5.2 LRFD versus ASD

There is a basic difference how uncertainties in design are accounted for between LRFD and ASD. In the ASD approach for geotechnical design, uncertainties are generally lumped together into a single safety factor. In the LRFD approach, load and resistance factors are used to account for varying levels of uncertainty in the components of the load and the resistance. In LRFD we do not use terms such as allowable capacity, allowable load, and ultimate capacity. Instead, we talk about the factored capacity, factored load, and nominal resistance

1.5.3 AASHTO Specifications for Seismic LRFD

AASHTO specifications for seismic design of bridges using LRFD include the 2007 LRFD Bridge Design Specifications (including the 2008 Interim Revisions) and the 2009 Guide Specifications for LRFD Seismic Bridge Design. These two sets of specifications use two different approaches to seismic design. The LRFD Bridge Design Specifications employ a force-based design approach while the LRFD Seismic Bridge Design specifications employ a displacement based design approach. This document addresses both approaches for design of foundations and earth retaining structures. Neither of these LRFD-based specifications addresses geotechnical aspects of seismic design beyond the design of foundations and earth retaining structures. However, NCHRP Project 12-70 (described in NCHRP Report 611) produced recommendations for LRFD seismic design of free standing retaining walls, slopes, embankments, and buried structures. Recommendations from the NCHRP 12-70 project for seismic design of these features are included in this document, as appropriate.

1.5.4 AASHTO Limit States and Load and Resistance Factors

In AASHTO, LRFD design is based upon four different limit states, including the strength, serviceability, extreme loading, and fatigue limit states. The limit state for each of the cases defines the boundary between acceptable and unacceptable performance. Table 1-1 defines the limit states considered by AASHTO in LRFD for bridges.

TABLE 1-1 AASHTO LIMIT STATES FOR BRIDGE DESIGN

Limit State Type	Case	Load Combination
Strength	I	Normal vehicular use of the bridge without wind
	II	Use of the bridge by Owner-specified special vehicles, evaluation permit vehicles, or both, without wind
	III	Bridge exposed to wind velocity exceeding 55 mph
	IV	Very high dead load to live load force effect ratios
	V	Normal vehicular use of the bridge with wind of 55 mph
Extreme Event	I	Load combination including earthquake
	II	Ice load, collision by vessels and vehicles, and certain hydraulic events with a reduced live load other than that which is part of the vehicular collision load, <i>CT</i>
Service	I	Normal operational use of the bridge with a 55 mph wind and all loads taken at their nominal values
	II	Intended to control yielding of steel structures and slip of slip-critical connections due to vehicular live load
	III	Longitudinal analysis relating to tension in prestressed concrete superstructures with the objective of crack control and to principal tension in the webs of segmental concrete girders
	IV	Tension in prestressed concrete columns with the objective of crack control
Fatigue		Repetitive gravitational vehicular live load and dynamic responses under the effects of a single design truck

The AASHTO specifications define the load combinations and load factors that must be considered for each limit state. More than one load combination may be evaluated for a given limit state. In this document, we are only concerned with the Extreme Event I limit state, earthquake loading.

Table 1-2 shows the load combinations prescribed in AASHTO for each limit state. For Extreme Event 1 limit state design (earthquake loading) there is only one load combination. Included in the load combination for the Extreme Event 1 limit state are the permanent (dead) loads, earthquake live loads,

water and friction loads, and the earthquake load itself. Note that we use a load factor of 1 on the earthquake load.

TABLE 1-2 LOAD COMBINATIONS AND LOAD FACTORS FOR AASHTO LIMIT STATES (After AASHTO 2007, Table 3.4.1-1)

Load Combination Limit State	PL	LL	WA	WS	WL	FR	TCS	TG	SE	Use one of these at a time			
										EQ	IC	CT	CV
Strength I	γ_p	1.75	1.00	-	-	1.00	0.50/1.20	γ_{TG}	γ_{SE}	-	-	-	-
Strength II	γ_p	1.35	1.00	-	-	1.00	0.50/1.20	γ_{TG}	γ_{SE}	-	-	-	-
Strength III	γ_p	-	1.00	1.40	-	1.00	0.50/1.20	γ_{TG}	γ_{SE}	-	-	-	-
Strength IV	γ_p	-	1.00	-	-	1.00	0.50/1.20	-	-	-	-	-	-
Strength V	γ_p	1.35	1.00	0.40	1.00	1.00	0.50/1.20	γ_{TG}	γ_{SE}	-	-	-	-
Extreme Event I	γ_p	γ_{EQ}	1.00	-	-	1.00	-	-	-	1.00	-	-	-
Extreme Event II	γ_p	0.50	1.00	-	-	1.00	-	-	-	-	1.00	1.00	1.00
Service I	1.00	1.00	1.00	0.30	1.00	1.00	1.00/1.20	γ_{TG}	γ_{SE}	-	-	-	-
Service II	1.00	1.30	1.00	-	-	1.00	1.00/1.20	-	-	-	-	-	-
Service III	1.00	0.80	1.00	-	-	1.00	1.00/1.20	γ_{TG}	γ_{SE}	-	-	-	-
Service IV	1.00	-	1.00	0.70	-	1.00	1.00/1.20	-	1.00	-	-	-	-
Fatigue	-	0.75	-	-	-	-	-	-	-	-	-	-	-

PL permanent load

WL wind on live load

EQ earthquake

LL live load

FR friction

IC ice load

WA water load and stream pressure

TG temperature gradient

CT vehicular collision force

WS wind load on structure

SE settlement

CV vessel collision force

TCS uniform temperature, creep, and shrinkage

γ_p load factor for permanent loads (see Table 1-3)

γ_{TG} load factor for temperature gradient (see AASHTO 2007 Article 3.4.1)

γ_{SE} load factor for settlement (see AASHTO 2007 Article 3.4.1)

Table 1-3 defines the permanent loads and associated load factors considered by AASHTO in LRFD. Note that there are maximum and minimum values for each load factor, and the minimum values are less than 1. We have maximum and minimum load factors because in some cases loads increase stability and in other cases they decrease stability. Both maximum and minimum load combinations need to be considered, with the more (or most) critical combination used for design, i.e. when increased load increases stability, we use the minimum load factor for design. Furthermore, we generally use load factors less than 1 for minimum loads.

TABLE 1-3 AASHTO PERMANENT LOAD FACTORS

Type of Load	Load Factor, γ_p		
	Maximum	Minimum	
DC: Components and Attachments	1.25	0.90	
DC: Strength IV Only	1.50	0.90	
DD: Downdrag	1.25	0.35	
DW: Wearing surfaces and utilities	1.50	0.65	
EH: Horizontal earth pressure			
	Active	1.50	0.90
	At-Rest	1.35	0.90
EL: Locked-in stresses	1.00	1.00	
EV: Vertical earth pressure			
	Overall Stability	1.00	N/A
	Retaining walls and abutments	1.35	1.00
	Rigid buried structure	1.30	0.90
	Rigid frames	1.35	0.90
	Flexible buried structures other than metal box culverts	1.95	0.90
	Flexible metal box culverts	1.50	0.90
	ES: Earth Surcharge	1.50	0.75

The live load factor for seismic loading, γ_{EQ} , is not explicitly defined in AASHTO. In the old AASHTO ASD specifications, a value of zero was used. The AASHTO LRFD specifications notes that some engineers recommend using the average daily truck traffic (ADTT) load for γ_{EQ} , but suggests that 0.5 ADTT is a reasonable value. A value of 0.5 ADTT for the maximum load case and 0 for the minimum load would thus be consistent with these recommendations. However, for earthquake loads the live load is often ignored. Another alternative is to use the HL-93 load as γ_{EQ} for the maximum load case.

At present, the AASHTO Guide Specifications for LRFD Seismic Bridge Design recommends that a resistance factor of 1 be used for seismic design for all resistance components of foundation design except for deep foundation axial uplift and lateral resistance., wherein a resistance factor of 0.8 is recommended. Furthermore, the recommendation in NCHRP 12-70 for the bearing resistance of retaining walls on spread footings founded upon soil calls for a resistance factor of 0.67 to be applied to the nominal bearing capacity. In other words, except for these cases, we should use a resistance factor of 1, reflecting use of our best (but reasonably prudent) estimate of resistance parameters. This is described in AASHTO as an interim recommendation until more data is available. This, however, does not mean that we are not incorporating uncertainty into the seismic resistance parameters. Many geotechnical resistance parameters have a reserve capacity for seismic loading that is not quantified (e.g. an increase in the shear strength of sand subject to rapid loading).

Table 1-4 presents the resistance factors recommended in the NHI training course on LRFD Design for Deep Foundations. As noted previously, a resistance factor of 0.8 is recommended for axial uplift and lateral resistance.

TABLE 1-4 RESISTANCE FACTORS FOR DEEP FOUNDATIONS

Limit State	Component of Resistance	Geomaterial	Method	Resistance Factor, ϕ
Extreme Event I and II	Axial geotechnical uplift resistance	All Geomaterials	Methods cited for strength Limit states	0.80
	Geotechnical lateral resistance	All Geomaterials	p-y methods pushover analysis	0.80
	All other cases	All Geomaterials	Methods cited for strength Limit states	1.00

1.6 ORGANIZATION OF THE DOCUMENT

Chapter 2 presents basic concepts of seismic geology and engineering seismology. This information is essential background information for subsequent discussions of seismic hazard analysis and ground motion characterization.

Chapter 3 presents the details of both probabilistic and deterministic seismic hazard analysis, including seismic source characterization and ground motion attenuation, and the development of design ground motions. The advantages and disadvantages of both probabilistic and deterministic seismic hazard analysis are discussed. Development of the Uniform Hazard Spectrum for a specified probability and exposure period using either the National Seismic Hazard maps developed by the USGS or the ground motion maps developed by USGS specifically for AASHTO is presented. Development of the AASHTO truncated acceleration response spectra for use in structural analysis from the Uniform Hazard Spectrum, including the use of the shear wave velocity in the top 100 ft of the site to account for the influence of local site conditions, is illustrated. The process of deaggregation by which a probabilistically-derived uniform hazard spectrum is decomposed into magnitude and distance combinations in order to determine a representative magnitude and distance for the design earthquake is described. Guidelines for selecting a suite of representative time histories for the representative design event are presented. Special topics,

including near field ground motions, spatially varying ground motions, and vertical ground motions, are briefly addressed.

Chapter 4 described site characterization for seismic analysis. The use of the Standard Penetration Test (SPT) and the Cone Penetration Test (CPT) to evaluate site stratigraphy and geotechnical properties is explained in detail. Geophysical techniques for site investigation are also addressed. Characterization of rock mass behavior and quantification of rock mass strength is described. Correlations between important geotechnical properties, including relative density, shear strength, and shear wave velocity, from both in situ test results and soil classification and index test data are presented.

In Chapter 5, the process of site specific seismic response analysis is described. Methods addressed in this chapter include simplified chart-based methods to adjust the peak ground acceleration for local site conditions, equivalent linear one-dimensional site response analysis, non-linear one-dimensional site response analysis with pore pressure generation, and advanced two-dimensional site response analysis. The development of input parameters for equivalent-linear one-dimensional site response analyses, the most common type of advanced analysis performed in practice, are described in detail.

Chapter 6 describes earthquake-induced damage due to the geotechnical seismic hazards of slope instability, liquefaction, and seismic settlement. Methods to evaluate seismic slope deformation, liquefaction potential, liquefaction-induced ground displacements, and seismic settlement are described in detail in this chapter. A method to evaluate the appropriate value of the seismic coefficient for pseudo-static slope stability analyses that accounts for spatial incoherence of ground motions, the local seismic environment, local site conditions, and acceptable displacement levels is presented.

Chapter 7 addresses design of earthwork features for transportation facilities, including soil and rock slopes and embankments. A performance-based seismic design philosophy that employs the concept of allowable displacement is described. Soil and site improvement techniques that can be used when the seismic displacement are unacceptable are presented with an emphasis on remediation of slope stability and liquefaction.

Chapter 8 describes the seismic design process and the AASHTO seismic design methodology, including capacity design of bridge foundations, the concept of the earthquake resisting system for a bridge, guidelines for what types of earthquake resisting elements are allowable and not recommended, and basic

principles of soil-foundation-structure interaction. The principles of both kinematic and inertial interaction are described.

Chapter 9 describes the seismic design of shallow foundations, including techniques to assess both foundation stiffness and foundation capacity. Equations for calculating the stiffness coefficients for the six modes of foundation displacement for use in an inertial interaction analysis are presented. Foundation capacity analyses discussed in the chapter include bearing, overturning, and sliding.

Chapter 10 addresses deep foundation design. Both p-y/t-z analyses and simple elastic solutions to evaluate the stiffness of an individual pile are discussed along with methods to account for group effects and to assemble individual pile and pile cap stiffness into a group stiffness. Sophisticated methods and a simple approximate method to account for kinematic interaction at soft soil sites are described. Analyses to evaluate the response of pile foundations to ground displacement demand from laterally spreading induced by liquefaction are discussed.

Chapter 11 presents methods for seismic design of free standing retaining walls. A variety of methods for predicting seismic active earth pressures, including the Mononobe-Okabe method, design charts that include the influence of a cohesion component to the shear strength, the Coulomb wedge method, and the general equilibrium method, are described along with a displacement-based method for evaluating the appropriate seismic coefficient for use in design. Charts for evaluating the passive earth pressure coefficient, including the effect of cohesion, are also presented in this chapter. Design of gravity and semi-gravity retaining walls for sliding, overturning, and bearing modes is discussed in detail. Earth pressure diagrams for non-gravity cantilever walls, anchored walls, and MSE walls are described along with recommendations for the seismic coefficient for use in design.

Chapter 12 describes bridge abutment design. The characterization of the stiffness of both conventional seat-type and integral abutments for inclusion in the global bridge model is presented. The effect of skewed abutments on the seismic performance of the bridge is discussed.

Chapter 13 presents design considerations for buried structures, including culverts and pipelines. Simple closed form solutions are presented for the displacement demand on buried structures subject to seismic loading.

CHAPTER 2

EARTHQUAKE FUNDAMENTALS AND ENGINEERING SEISMOLOGY

2.1 INTRODUCTION

Earthquakes are produced by abrupt relative movements on fractures or fracture zones in the earth's crust. These fractures or fracture zones are termed *earthquake faults*. The mechanism of fault movement is the sudden release of built-up stress along the fault. The primary source of this built-up stress is the accumulated relative movement of large, essentially intact pieces of the earth's crust called *tectonic plates*. This relative movement is restrained by frictional and other forces (e.g. interlocking) along the fault, leading to a buildup of stress along the fault and strain (or strain energy) in the rocks adjacent to the fault. When the built up stress exceeds the strength of the rock along the fault, relative movement between the rocks on either side of the fault, commonly called *fault rupture*, takes place along the *rupture zone*. When fault rupture occurs, the built up strain energy in the rocks on either side of the fault is released as the strained rock rebounds elastically on both sides of the fault. This rebound produces vibrations that pass through the earth's crust and along the earth's surface, generating the ground motions that are the source of most damage attributable to earthquakes. If the displacement associated with the fault rupture propagates upward to the ground surface, the relative movement may manifest itself as *surface rupture*. Surface ruptures are also a source of earthquake damage to constructed facilities. Fault rupture may also cause secondary ground deformations and regional ground deformations (e.g. uplift or subsidence) that can be damaging to engineered facilities. Volcanism constitutes a secondary source of stress and strain energy accumulation in the earth's crust. The release of the strain energy associated with volcanism may also result in damaging earthquake ground motions.

2.2 EARTHQUAKE SOURCES

2.2.1 General

Faults are ubiquitous in the earth's crust. They exist both at the contacts between tectonic plates (large intact pieces of the earth's crust that tend to move as a coherent unit) and within the tectonic plates themselves. In some areas of the western United States, it is practically impossible to perform a site investigation and not encounter a fault. However, not all faults are *seismogenic* (i.e., not all faults are capable of producing earthquakes at the present time). Faults that are known to be capable of producing

earthquakes are termed *active faults*. Faults for which the potential for producing earthquakes is uncertain are termed *potentially active faults*. Faults that at one time produced earthquakes but are now considered dormant are sometimes referred to as inactive faults. However, the term inactive fault is no longer in widespread use, as dormant faults can be reactivated under some circumstances. Thus faults that are considered to be dormant may also be considered potentially active.

When a fault is encountered in an area known or suspected to be a source of earthquakes, a careful analysis and understanding of the fault is needed to evaluate its potential for generating earthquakes. One of the most common means of investigating the potential for a fault to produce earthquakes is through the study of surface manifestations of faulting. However, not all active faults have surface manifestations. In some cases, faults may be too deep to produce obvious surface manifestations. In other cases, the earthquakes generated by a fault may occur so infrequently, or surface geologic processes may be so rapid, that surface manifestations of the faulting have been erased. Careful study of geomorphic and seismologic information by qualified geo-professionals is required to identify the earthquake faults (or seismogenic sources) capable of damaging engineered facilities in a region.

2.2.2 Plate Tectonics

Plate tectonics theory has established beyond a reasonable doubt that the earth's crust is a mosaic of tectonic plates. These tectonic plates are composed of either oceanic or continental crust and “float” on top of a molten rock layer referred to as the upper mantle. Tectonic plates move as relatively intact bodies on top of the upper mantle except at their margins, where they may grow due to upwelling of molten rock from the mantle or be consumed by crust being drawn down, or subducted, into the mantle. The motions of the tectonic plates are driven by convection currents in the molten rock in the earth's upper mantle, which cause the upwelling of molten rock at the plate margins where the crust is growing. These convection currents are generated by heat sources within the earth (e.g. radioactive decay). The zones where tectonic plates grow in size, i.e. where the convection currents send plumes of material from the upper mantle to the earth's surface, are referred to as spreading zones. The zones where tectonic plates are consumed, i.e. are drawn downwards back into the mantle, are referred to as subduction zones. Tectonic plates may also override one another and slide past each other. Plate boundaries where two tectonic plates slide past each other are referred to as transform boundaries.

The major tectonic plates of the earth's crust are shown in Figure 2-1. There are also numerous smaller, minor tectonic plates not shown in this figure. The motions of these plates are related to the activation of

faults, the generation of earthquakes, and the presence of volcanism. Most earthquakes occur on or near plate boundaries, as illustrated in Figure 2-2. Earthquakes also occur in the interior of the plates, although generally with a much lower frequency of occurrence than at plate boundaries. For the continental United States, the principal tectonic plate boundary is along the western coast of the continent, where the North American Plate and the Pacific Plate are in contact (see Figure 2-1). In California, the boundary between these plates is a transform boundary wherein the relative movement is generally (though not exclusively) one of lateral (horizontal) slippage of one plate past the other.

In Washington and Oregon, a smaller plate, the Juan de Fuca plate, is interposed between the North American and Pacific plates. The boundary between the North American plate and the Juan de Fuca plate is a subduction zone, as is the boundary between the North American plate and the Pacific plate along the Aleutian Islands in Alaska. Subduction zones, wherein one plate dives (subducts) beneath the other plate (as illustrated in Figure 2-3), are considered capable of very large magnitude earthquakes. Furthermore, volcanic activity is generally also associated with subduction, as magma generated by the subducting plate rises to the earth's surface in a zone above the subducting plate (as illustrated in Figure 2-3).

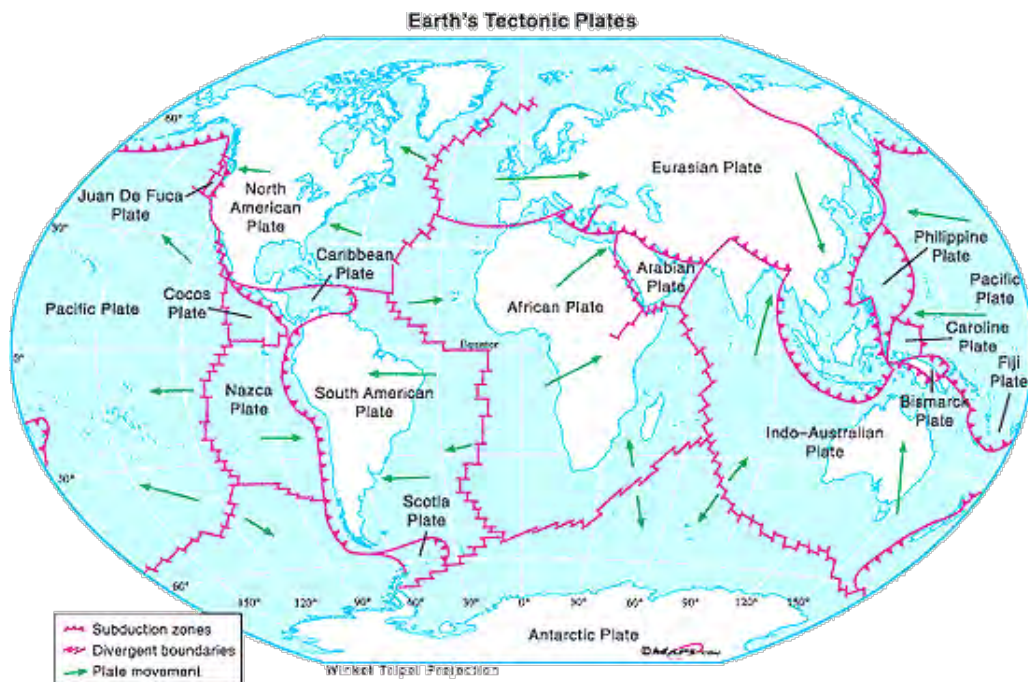


Figure 2-1 Major Tectonic Plates and Their Approximate Direction of Movement (Source: www.maps.com)

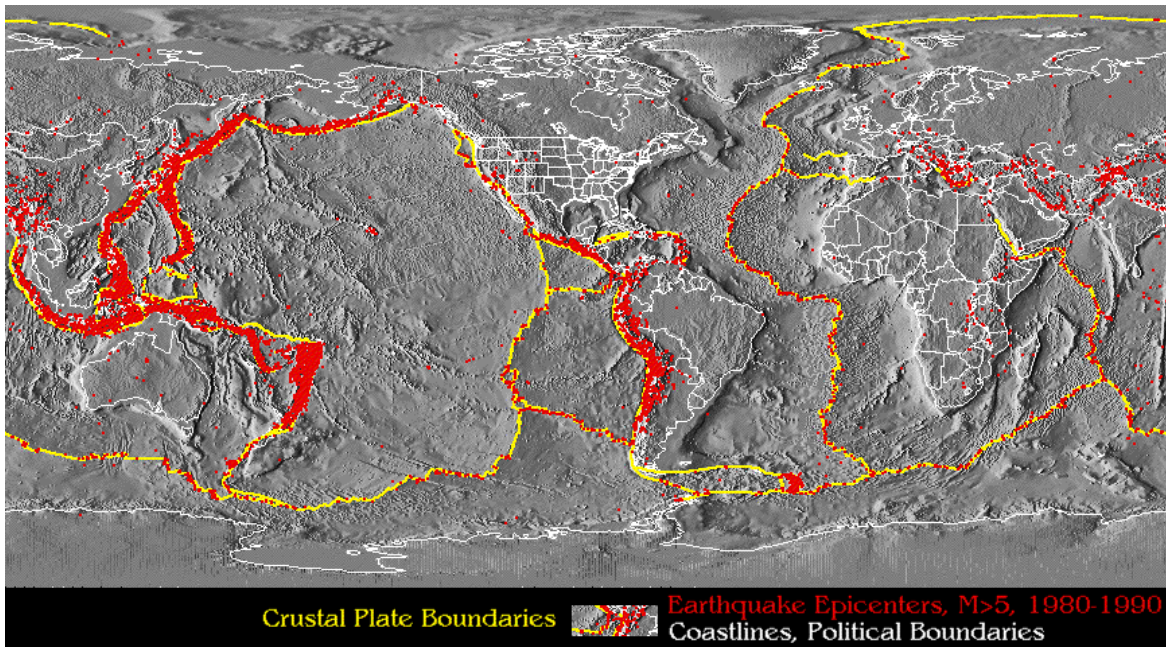


Figure 2-2 Worldwide Seismic Activity and Plate Boundaries (U.C. Berkeley Museum of Paleontology (www.ucmp.berkeley.edu/))

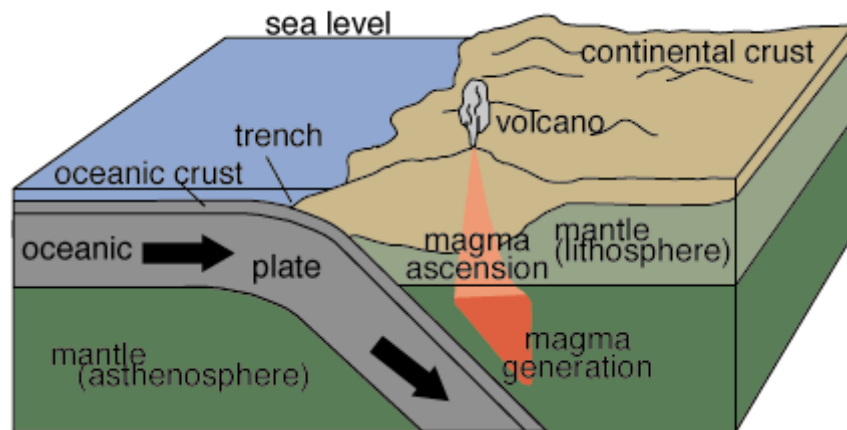


Figure 2-3 Cross-Section Through a Subduction Zone. (Source: www.platetectonics.com)

In the western interior of the United States, adjacent to the western edge of the North American plate (e.g. in Montana, Utah, Nevada), stresses induced by the complex movements of the North American plate (i.e., spreading, translating, and rotating on the surface of the earth) may also result in normal (extensional) and thrust (compressional) faulting as well as transform faulting.

Earthquake source areas in the central and eastern United States are termed *intraplate* source zones, as they lie in the interior of a tectonic plate (the North American plate). The mechanisms generating earthquakes in intraplate source zones are poorly understood. Potential mechanisms for intraplate earthquakes include relief of locked-in stresses from ancient tectonic movements, crustal rebound from the ice ages, and re-adjustment of stress in the interior of the plate due to loads imposed at plate boundaries. Earthquakes associated with intraplate volcanism, e.g. earthquakes in Hawaii, are believed to be associated with isolated plumes of molten rock rising to the surface from the mantle. These isolated plumes of molten rock are sometimes referred to as hot spots.

The intensity of the ground motions produced by an earthquake at a given site depends upon a variety of factors. Primary factors influencing earthquake ground motion intensity include the amount of strain energy released by the event (generally quantified as earthquake magnitude), the distance from the earthquake to the site in question, the depth of the earthquake, the geologic conditions between the earthquake fault and the site, and local ground conditions (e.g. topography and local soil conditions, including soil profile and soil properties). Due to significant differences in geologic conditions between the source and the site, the intensity of the ground motions from an earthquake of a given magnitude and distance may be greater in plate interiors (i.e. an intraplate event) than at active plate boundaries. Therefore, while earthquake activity is much greater along the plate boundaries than in the plate interior, intraplate events appear to impact a larger area than plate boundary events of the same magnitude because the intensity of ground motions (e.g. peak ground acceleration) from intraplate earthquakes appears to attenuate, or dissipate, much more slowly than from plate boundary events.

The depth at which fault rupture occurs is also an important factor influencing the intensity of ground motions at a site. This is particularly true for sites close to the surface projection of a fault rupture, where the depth of the rupture can contribute significantly to the distance the earthquake waves have to travel before arriving at the site. In a subduction zone, such as that along the coast of Oregon and Washington, there are both faults that are shallow and located within the over-riding crust (fault depth <12 miles), referred to as shallow crustal faults, and faults that are deep within the subducting plate (fault depth >12 miles). Intraplate faults in the plate interior may also vary from shallow to deep and may be covered by a thick mantle of sediments. However, faults along transform boundaries such as along the California coast line, where the plates slide laterally past each other are generally relatively shallow (< 12 miles depth) crustal faults.

2.2.3 Fault Movements

Faults are created when the built up stresses within geologic materials exceed the ability of those materials to withstand the stresses. Most faults that exist today are the result of tectonic activity that occurred in earlier geological times. These faults are usually non-seismogenic (i.e. incapable of generating earthquakes, or inactive). However, faults related to past tectonism may be reactivated by present-day tectonism in seismically active areas and can also be activated by anthropogenic (man-made) activities such as impoundment of a reservoir by a dam or injection of fluids deep into the subsurface (e.g. for geothermal energy development). The maximum size of an earthquake on an anthropogenically reactivated fault is a subject of some controversy, but earthquakes as large as moment magnitude 6.5 have been attributed to reservoir impoundment.

Not all faults along which relative movement is occurring are a source of damaging earthquakes. Some faults may be surfaces along which relative movement is occurring at a slow, relatively continuous rate, with an insufficient stress drop to cause a damaging earthquake. Such movement is called *fault creep*. Fault creep may occur along a shallow fault, where the low overburden stress on the fault results in a relatively low threshold stress for initiating displacement along the fault. Alternatively, a creeping fault may be at depth in soft and/or ductile materials that deform plastically. Also, there may be a lack of frictional resistance or asperities (non-uniformities) along the fault plane, allowing steady creep and the associated relatively slow release of the strain energy along the fault. Fault creep may also prevail where phenomena such as magma intrusion or growing salt domes activate small shallow faults in soft sediments. Faults generated by extraction of fluids (e.g., oil or water in southern California) may cause ground settlement and activate faults near the surface, resulting in fault creep. Faults activated by other non-tectonic mechanisms, e.g. faults generated by gravity slides that take place in thick, unconsolidated sediments, could also produce fault creep.

Active faults that extend into crystalline bedrock are generally capable of building up the strain energy needed to produce, upon rupture, strong ground motions, i.e. ground motions strong enough to damage transportation facilities. Fault ruptures in crystalline rock may also propagate from the crystalline bedrock to the ground surface and produce ground rupture. Fault ruptures which propagate to the surface in a relatively narrow zone of deformation that can be traced back to the causative fault in crystalline rock are sometimes referred to as primary fault ruptures. Fault ruptures may also propagate to the surface in diffuse, distributed zones of deformation which cannot be traced directly back to the basement rock. In this case, the surface deformation may be referred to as secondary fault rupture.

In some instances, fault rupture may be confined to the subsurface with no relative displacement at the ground surface due to the fault movement. Absence of primary fault rupture at the ground surface is believed to be characteristic of all but the largest magnitude earthquakes in the central and eastern United States. Furthermore, geological processes may erase surface manifestations of faulting in some areas, particularly when the interval between earthquakes with surface manifestations is large. Therefore, intraplate seismic source zones often must be evaluated using instrumental seismicity and paleoseismicity studies. This is particularly true if the intraplate sources are covered by a thick mantle of sediments, as in the New Madrid, Tennessee, and Charleston, South Carolina, intraplate seismic zones. Instrumental recording of small magnitude events can be particularly effective in defining seismic source zones. Figure 2-4 shows seismic zones in the southeastern US identified using both instrumental seismicity for events as small as magnitude 3 and historical records of larger (> M 5) events.

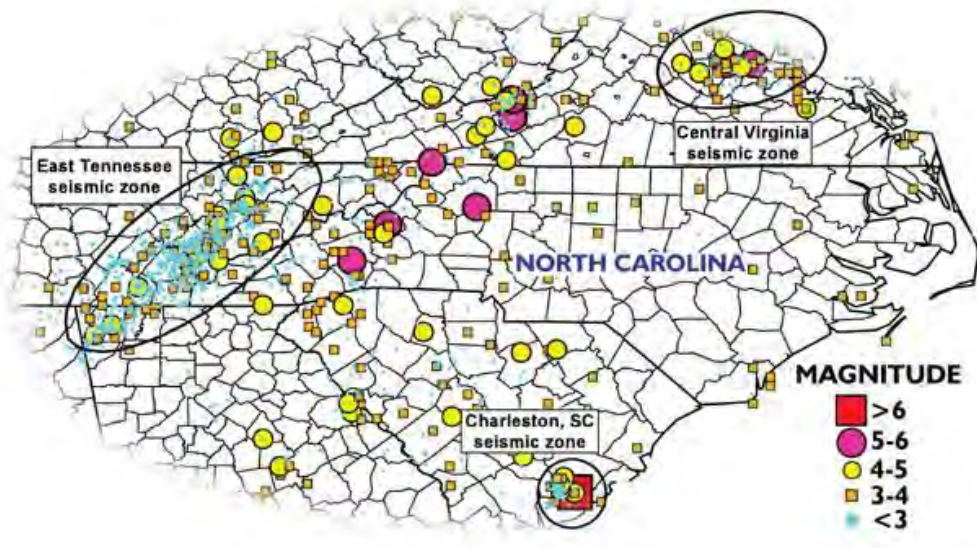


Figure 2-4 Southeastern US Seismic Zones and Instrumental Seismicity

Essentially all of the active faults with surface fault traces (i.e. where fault rupture propagates to the ground surface) in the United States are shallow crustal faults west of the Rocky Mountains. However, not all shallow crustal faults west of the Rocky Mountains have surface fault traces. Several recent significant earthquakes along the Pacific Coast plate boundary (e.g., the 1987 Whittier Narrows

earthquake, the 1994 Northridge earthquake, and the 2001 Nisqually earthquake) were due to rupture of thrust (compressional) faults that did not break the ground surface. Thrust faults that do not break the ground surface are termed *blind thrust* faults. Figure 2-5 illustrates a blind thrust fault in which rupture does not propagate to the ground surface.

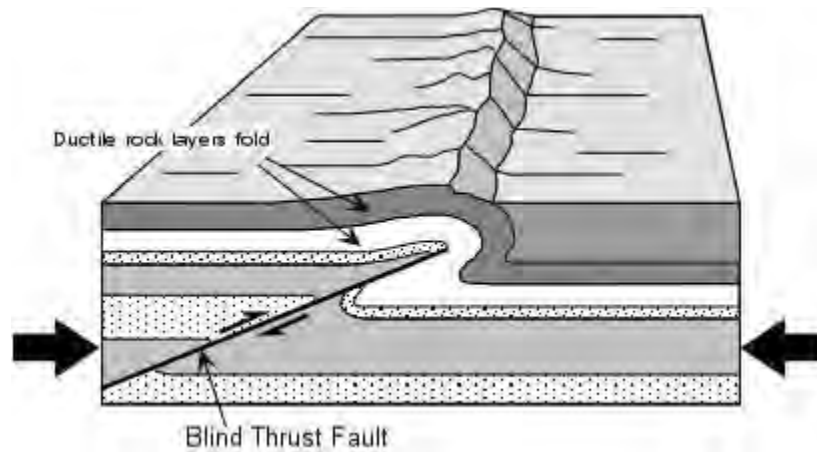


Figure 2-5 Blind Thrust Faulting (www.earthsci.org)

Strong shaking associated with fault rupture may also generate ground deformations such as ridge-top shattering, landslides, graben structures (depressions behind large landslide masses), and liquefaction-induced lateral spreads. These types of secondary ground breakage are not considered surface manifestations of the fault.

2.2.4 Fault Activity

Identifying faults capable of producing damaging ground motions at a project site and assessing the potential size (*magnitude*) and frequency of occurrence (*recurrence*) of earthquakes on those faults is part of a process referred to as a *seismic hazard assessment*. Whether or not a fault has the potential to produce earthquakes is generally categorized by the recency of previous fault movements. Considering the slow rate at which geologic processes evolve, if a fault has undergone relative displacement in relatively recent geologic time (within the time frame of the current tectonic setting), it is reasonable to assume that this fault has the potential to move again. If a fault has propagated up to the ground surface in recent geologic time, evidence of faulting is usually found in geomorphic features associated with fault rupture (e.g., relative displacement of geologically young sediments). Age dating of the last sediment

layer to be displaced by the fault and the first layer not displaced by the fault can be used to bound when the fault last moved. For faults that do not propagate all the way to the ground surface, geomorphic evidence of previous earthquakes may be more subdued and more difficult to evaluate (e.g., near surface folding in sediments or evidence of liquefaction or slumping generated by the earthquakes). Faults that have moved in Holocene time (the current geologic epoch, generally the past 11,000 years) are considered active. However, faults that have not moved in Holocene time or for which there is no evidence of Holocene movement but are located in a tectonic stress regime capable of generating earthquakes may still be considered potentially active and incorporated into a seismic hazard assessment. If a fault has moved in the distant geologic past but there is no evidence of movement in the current tectonic stress regime (i.e. under the current configuration of the earth's tectonic plates), it will generally not be included in a seismic hazard assessment unless there is concern that anthropogenic activities, e.g. reservoir impoundment, may trigger fault movement.

Geomorphic evidence of fault movement cannot always be dated. In practice, if a fault displaces the base of unconsolidated alluvium, glacial deposits, or surficial soils, then the fault is generally considered to be active. Also, if there is microseismic activity (i.e. small magnitude earthquakes identified using sensitive instruments) associated with the fault, the fault is typically judged as active. Microseismic activity is particularly useful in identifying seismic sources with little to no surface manifestation (e.g. blind thrust faults, intraplate faults and other faults at great depth, faults with long recurrence intervals). However, shallow microseismic events (i.e. earthquakes of magnitude 3 or less) may sometimes be associated with blasting for mining or other non-seismogenic mechanisms. If there is no geomorphic evidence of seismic activity and there is no microseismic activity in the area, then faults in the area are unlikely to be capable of generating damaging earthquakes.

Faults are generally of finite length and are subject to certain frictional and geometric constraints that cause them to move only after certain threshold levels of accumulated stress (or built up strain) are achieved. Thus, a fault may tend to produce earthquakes within a range of magnitudes that are characteristic for that particular fault. The maximum potential size of an earthquake on an active or potentially active fault is generally related to the size of the fault (i.e., a small fault produces small earthquakes and a large fault produces large earthquakes). Fault length is the primary (though not the sole) measure of fault size; fault plane surface area is also sometimes used. The average annual displacement along a fault, termed the *slip rate*, is also a measure of the maximum potential size earthquake a fault is capable of generating. Field evidence shows that faults that have a larger slip rate are generally associated with larger magnitude earthquakes. A long fault, like the San Andreas Fault in California or the Wasatch Fault in Utah, will generally not rupture along its entire length in any one

earthquake. Such faults typically move in portions (or segments), one segment at a time, although sometimes multiple fault segments will rupture simultaneously or sequentially. Earthquake hazard scenarios typically consider the possibility of both individual segments rupturing separately and multiple segments rupturing simultaneously or sequentially (and generating a larger magnitude event). An immobile (or "locked") fault segment, i.e. a fault segment which has remained stationary while the adjacent segments of the fault have moved, is a strong candidate for the next episode of movement (i.e. the next damaging earthquake) along a given fault. The lengths of fault segments may be interpreted from geomorphic evidence of prior movements or from fault geometry and kinematic constraints (e.g., segments may be defined by abrupt changes in the orientation of the fault).

Short, disconnected surface fault traces aligned in a generally parallel manner in sediments at the ground surface may well be continuous at depth, with their surface expression modified by the near surface geologic structure. Thus, the observed length of a group of such fault traces at the ground surface is often shorter than the true length of the causative fault. However, these fault traces may also move in distinct segments. The true length of the fault associated with a group of short surface fault traces may be identified by the continuity of the geomorphic evidence (e.g. by consistency in the age of the displaced features along the fault).

A variety of correlations between the size of an earthquake (usually expressed in terms of earthquake magnitude, using various definitions of magnitude), the length or area of a fault plane, and the amount of displacement along the fault are available (e.g. Bonilla, *et al.*, 1984; de Polo and Slemmons, 1990). However, evaluation of fault segmentation and magnitude potential is a complex task that is best left to qualified geologists and seismologists and should not be attempted by engineers who do not have expertise in this area.

Finally, even in the best of circumstances, with a thorough understanding of local geology, geomorphology, and seismicity, one cannot assume that all active faults in a region have been identified. Engineering evaluations should be made in such a way that the potential for earthquakes from unknown faults is considered. For this purpose, *floating* or *random earthquakes* of a characteristic size (magnitude) and recurrence rate determined based upon regional geology and seismology are often included in an engineering assessment of seismic hazard. These random earthquakes are assumed to occur anywhere within a defined earthquake zone. Chapter 3 will have more discussions on this subject.

2.3 SEISMIC WAVES

The elastic rebound of the rock along both sides of a fault that ruptures generates seismic waves that radiate away from the fault. These seismic waves are the source of the ground shaking that is characteristic of earthquakes. In general, these waves can be separated into two broad categories: body waves that travel (propagate) through the interior of the earth and surface waves that travel (propagate) along the earth's surface. Body waves can be further divided into compressional (pressure) waves, or P-waves, and shear waves, or S-waves. In a P-wave, particle motion is in the same direction as wave propagation while in S-waves particle motion is orthogonal (perpendicular) to the direction of wave propagation. Shear waves can be sub-divided into SV-waves, or shear waves in which the direction of particle motion is in a vertical plane, and SH-wave, or shear waves in which the direction of particle motion is in a horizontal plane. Figure 2-6 illustrates the direction of particle motion relative to the direction of wave propagation for horizontally propagating P-waves and SV-waves.

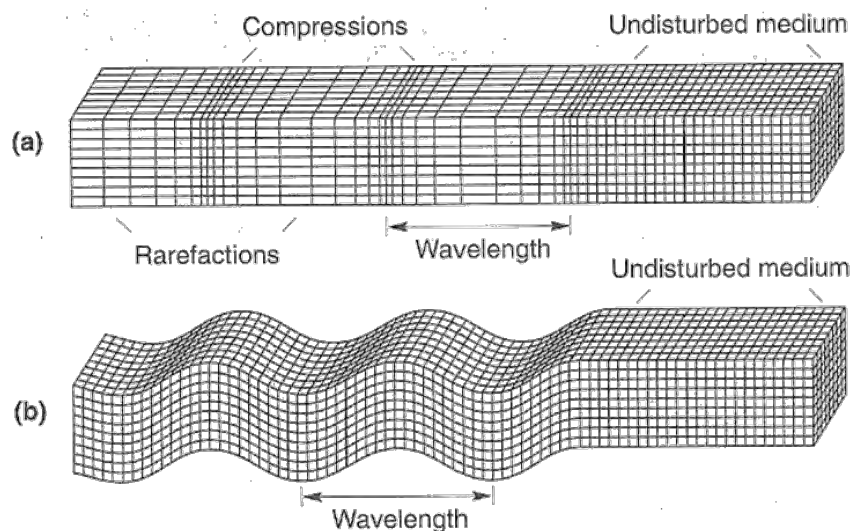


Figure 2-6 Deformations Produced by Body Waves: (a) P-waves; (b) SV-Waves (Source: Earthquakes, by Bolt, W.H. Freeman and Company, 1993)

Surface waves are generated when body waves interact with a free surface, e.g. the ground surface. Because surface waves attenuate (decay) at a slower rate than body waves, ground motions due to surface waves may predominate over body waves at longer distances from the earthquake source. Rayleigh waves are the predominant form of surface wave generated in earthquakes. Rayleigh waves are generated

by the interaction of P-waves and SV-waves with the ground surface. Particle movement during Rayleigh wave propagation tends to follow a retrograde orbital path similar to that in a water wave, as illustrated in Figure 2-7. Another type of surface wave is a Love wave. Love waves are generated when SH-waves are trapped in a soft surficial layer. Neither Love waves nor Rayleigh waves are generally considered explicitly in a seismic hazard analysis.

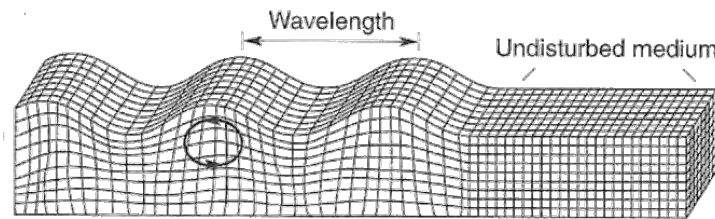


Figure 2-7 Deformations Produced by Rayleigh Waves (Source: Earthquakes, by Bolt, W.H. Freeman and Company, 1993)

The propagation velocity of seismic waves depends upon the stiffness of the medium through which they are propagating. Because the bulk (compressional) stiffness of geologic media is greater than the shear stiffness, P-waves travel faster than S-waves (and surface waves) and thus are generally the first earthquake waves to arrive at a site. The P-wave velocity of saturated sediments (particularly in loose or soft ground) tends to be governed by the compressibility of water. Thus, it is hard to distinguish among the characteristics of saturated sediments based upon P-wave velocity. However, because water has essentially no shear stiffness, S-wave velocity in sediments is governed by the shear stiffness of the soil skeleton. Thus, S-wave velocity can be used as an indicator of soil characteristics such as stiffness and density.

2.4 STRONG MOTION RECORDS (TIME HISTORIES)

Earthquake ground motions that are capable of damaging engineered structures are generally referred to as *strong ground motions*. A record of strong ground motion versus time (a strong ground motion *time history*) is called a *strong motion record*. Strong motion records are captured in an earthquake by a *strong motion instrument* (as opposed to a seismometer, which is used to capture weak motions from small or distant earthquakes). Strong motion records can also be generated analytically (numerically) by simulation. Strong motion instruments used to capture time histories of ground acceleration, the most

common type of strong motion record, are sometimes called strong motion *accelerometers*.

Acceleration time histories can be integrated to yield time histories of ground velocity and displacement. Figure 2-8 shows the recorded time history of acceleration and calculated time histories of velocity and displacement for one horizontal component of ground motion at the ground surface during the 1989 Loma Prieta earthquake. The time history of ground motions in three orthogonal directions is required to completely describe the time history of ground motion at a point.

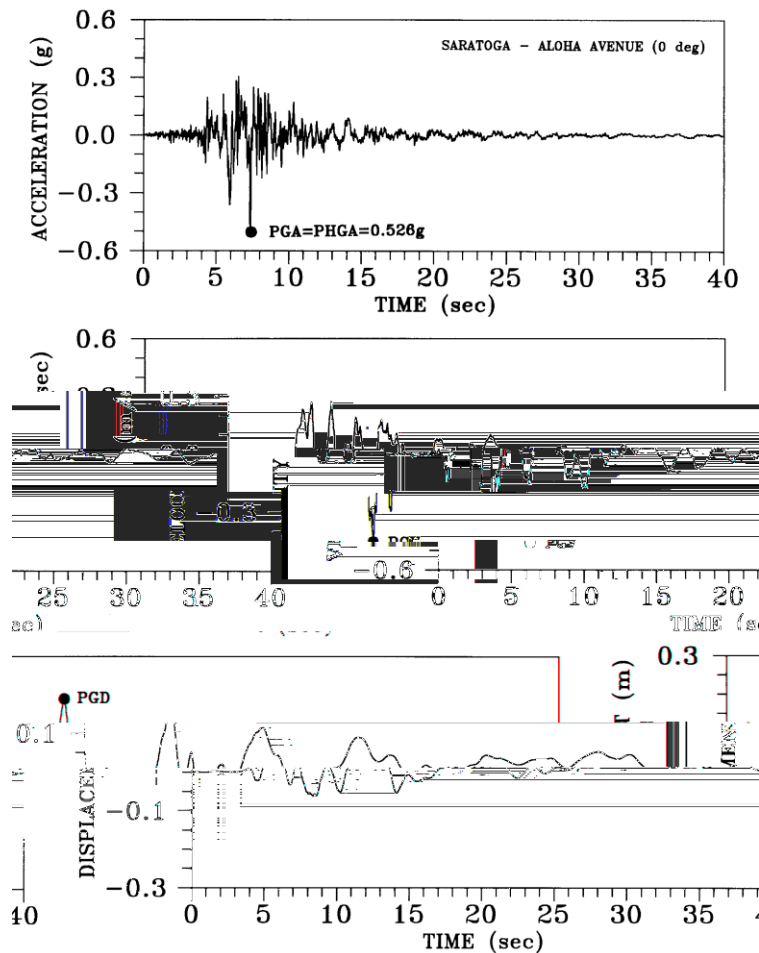


Figure 2-8 Acceleration, Velocity, and Displacement Strong Ground Motion Time Histories (FHWA, 1998)

The acceleration time history, sometimes referred to as an *accelerogram*, is the form of strong ground motion record used most often in engineering practice. However, velocity and displacement time histories also have their uses in engineering practice. The processing of recorded time histories of acceleration to correct for instrument bias and other sources of error is a complicated process. However,

catalogs of numerous (thousands) of processed (corrected) time histories are available on line from a variety of different sources. Reputable sources for corrected strong motion records include the Pacific Earthquake Engineering Research Center (PEER), the National Geophysical Data Center (NGDC), and the Multi-Disciplinary Center for Earthquake Engineering Research (MCEER).

2.5 PARAMETERS DESCRIBING EARTHQUAKE SIZE AND LOCATION

2.5.1 Earthquake Magnitude

In practice, the size of an earthquake is quantified by the *earthquake magnitude*, M , a measure of the energy released by an earthquake. A variety of different earthquake magnitude scales exist. The differences among these scales are attributable to the earthquake characteristics used to quantify the energy content. Characteristics used to quantify earthquake energy content include the local intensity of ground motions, the amplitude of the body waves generated by the earthquake, and the amplitude of the surface waves generated by the earthquake. The first earthquake magnitude scale, and the magnitude scale most commonly referred to (often incorrectly) in media reports and non-technical publications, is the Richter magnitude scale. *Richter magnitude* is sometimes also referred to as the *local magnitude* as it is based upon the local intensity of the ground motion. Richter magnitude is often designated by the symbol M_L (for local magnitude). In the eastern United States, earthquake magnitude was often measured historically as a *short period body wave magnitude*, m_b . However, the long period body wave magnitude, m_B , was also sometimes used in the central and eastern United States. In California, earthquake magnitude was historically measured as either M_L or as *surface wave magnitude*, M_s . The *Japan Meteorological Agency Magnitude* (M_{JMA}) scale was commonly used in Japan.

Due to the limited strength of near surface geologic materials, the historical magnitude scales cited above tend to reach an asymptotic upper limit (a phenomenon referred to as *saturation*). To compensate for this phenomenon and provide a consistent and logical basis for quantifying the size of earthquakes, the *moment magnitude*, M_w , was defined by Hanks and Kanamori (1979). The moment magnitude of an earthquake is a direct measure of the kinetic energy released by the earthquake. M_w is proportional to the *seismic moment*, defined as a product of the material rigidity (i.e. the elastic modulus of the fault), the fault rupture area, and the average dislocation (relative displacement, or *slip*) across the rupture surface. Moment magnitude has been adopted by most of the earthquake engineering community as a unifying, consistent magnitude measure of earthquake energy content. For this reason, moment magnitude is used in this document to describe earthquake magnitude unless it is otherwise noted. Figure 2-9 (Heaton, *et*

al., 1986) provides a comparison of the various other magnitude scales with the moment magnitude scale. Note that in the magnitude range of 3 to 6, moment magnitude M_w is approximately equal to the local (Richter) magnitude M_L , while in the magnitude range of 6 to 7.5, moment magnitude M_w is approximately equal to the surface wave magnitude M_s .

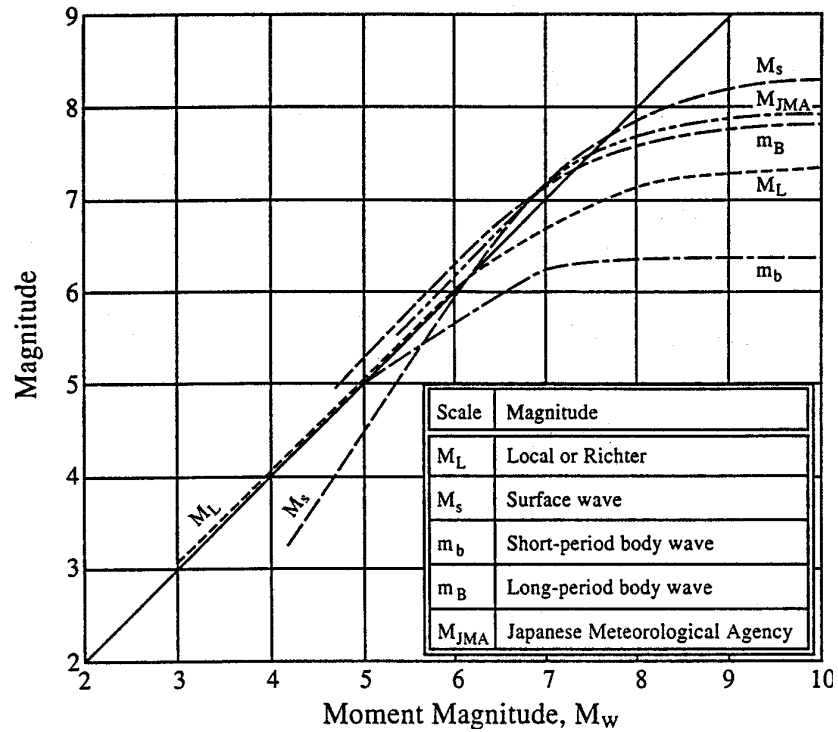


Figure 2-9 Comparison of Earthquake Magnitude Scales (Heaton, *et al.*, 1986)

2.5.2 Earthquake Location

The location (or origin) of an earthquake is generally described by either the hypocenter or epicenter. The *hypocenter* (focus) of an earthquake is the point from which the seismic waves first emanate. Conceptually, it may be considered as the point on a fault plane where the slip responsible for the earthquake was initiated. The *epicenter* is the point on the ground surface directly above the hypocenter. The *zone of energy release* may also be used to describe the location of an earthquake. The zone of energy release, sometimes referred to as the *zone of seismogenic rupture*, is the area on the fault plane from which the seismic waves that generate strong ground motions emanate. The zone of energy release is typically assumed to be the portion of the fault rupture zone that is within crystalline rock. Therefore, even if the fault plane ruptures to the ground surface, the zone of energy release may not extend to the

ground surface. Figure 2-10 shows the relationship between the hypocenter, epicenter, fault plane, and rupture zone of an earthquake. Figure 2-10 also illustrates the definitions of the strike and dip of the fault plane. The strike is the map orientation (in plan) of a horizontal line on the fault plane, e.g. N30°W. The dip is the inclination from the horizontal of a line on the fault plane that is perpendicular to the strike.

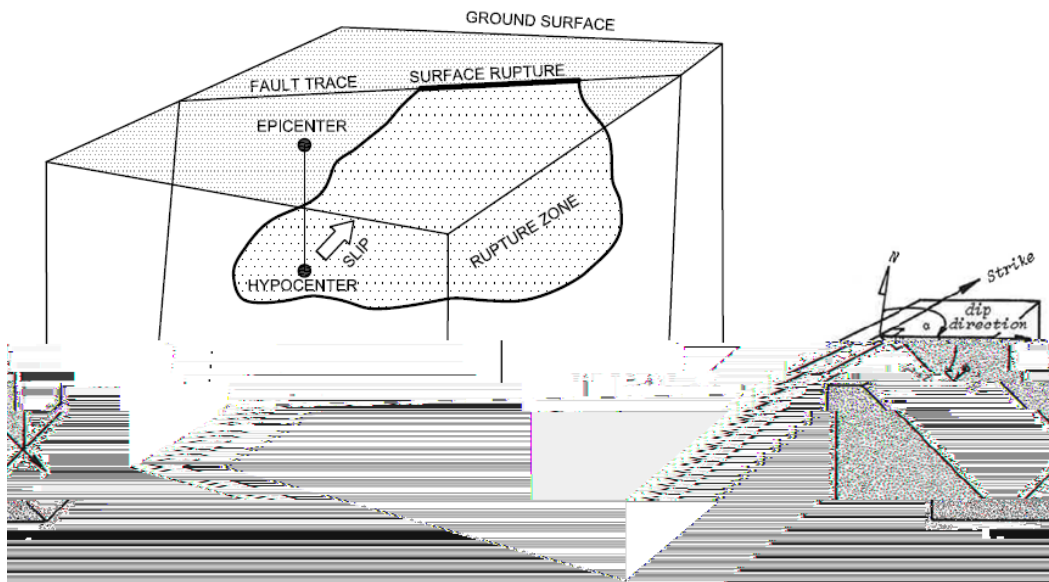


Figure 2-10 Basic Fault Geometry and Definition (after FHWA, 1998)

The distance between the site of engineering interest and the location of the earthquake, generically referred to as the *site-to-source distance*, is used in engineering analyses to estimate the intensity of earthquake ground motions at the site if interest. The site-to-source distance depends upon the measure used to describe the earthquake location. Figure 2-11 illustrates graphically the definitions of various site-to-source distances commonly used to estimate the intensity of earthquake-induced ground motions in engineering analyses. In the eastern United States, epicentral distance, R_E , is commonly used. In the western United States, the rupture distance, R_R , the seismogenic distance, R_S , the hypocentral distance, R_H , and, the so-called Joyner and Boore distance, R_{JB} , are commonly used. Different definitions can result in significant differences in site-to-source distance, particularly for sites close to the earthquake origin. For instance, if the site is located within the vertical projection of the fault plane, then R_{JB} is equal to zero. However, the hypocentral distance to the site can be 10 kilometers or more if the earthquake originated at depth. Due to the variety of site-to-source distance definitions used in practice, care must be taken to ensure that the correct site-to-source distance is used in any engineering analysis. The site-to-source distance used in an analysis must be consistent with the site-to-source distance employed in developing the analytical method or equation.

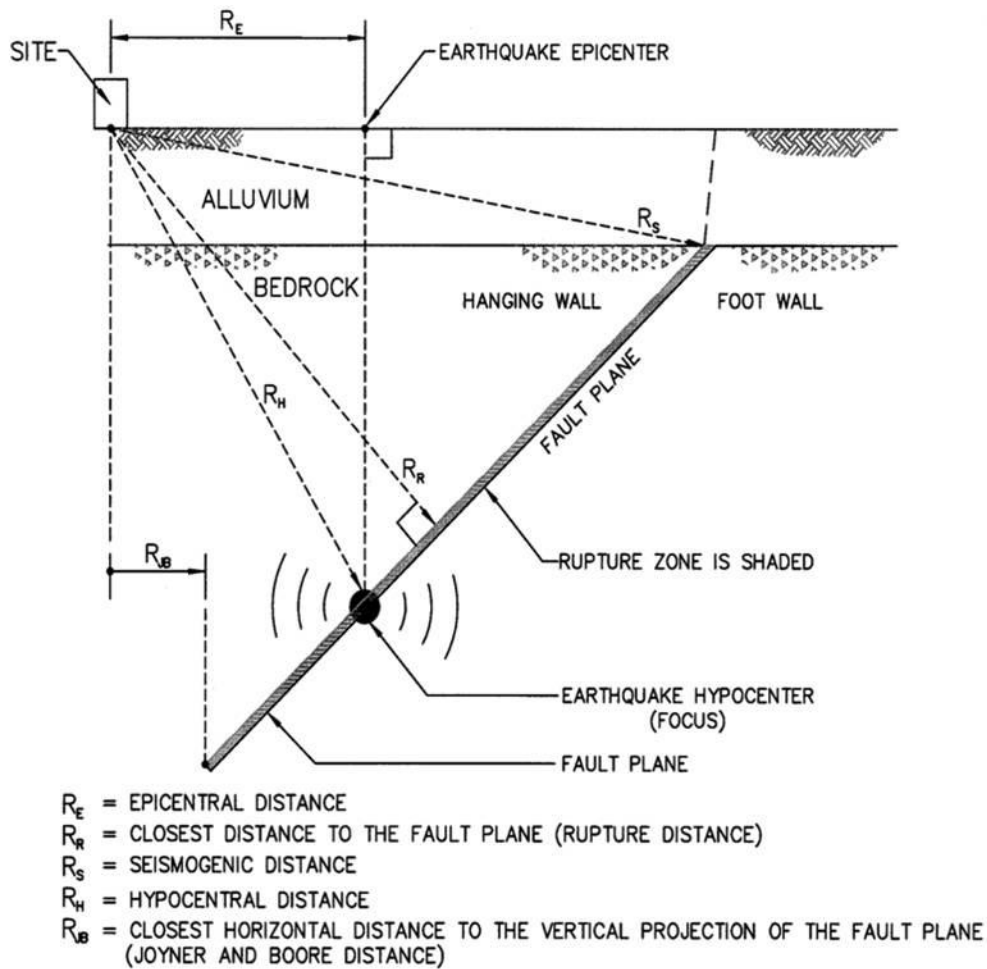


Figure 2-11 Various Site-to-Source Distance Measures Used in Earthquake Engineering

2.5.3 Earthquake Recurrence

The rate at which a specific earthquake source (e.g. a fault) generates earthquakes is referred to as the *recurrence rate*. The recurrence rate is usually described in terms of the number of events per year equal to or exceeding a specified magnitude. For magnitudes of engineering significance, the average number of earthquakes generated each year from a specific source is generally less than one and thus the recurrence rate (expressed in the number of events per year) will be less than 1.0. The reciprocal of the recurrence rate is sometimes referred to as the *recurrence interval*, and describes the average number of years between events equal to or greater than the specified magnitude. Recurrence rate and recurrence

interval are also sometimes used to describe the rate of occurrence of ground motion parameters such as the peak ground acceleration. However, the *annual probability of exceedance* and the *return period* are the terms more properly used to describe the frequency of occurrence of ground motions at a site. Recurrence rate depends upon earthquake magnitude. The relationship between recurrence rate and earthquake magnitude is referred to the *recurrence relationship*. The most common type of recurrence relationship is an exponential model in which a plot of the logarithm of the recurrence rate versus earthquake magnitude forms a straight line. This is the basis for the well-known Gutenberg-Richter recurrence model. To account for the fact that the magnitude of earthquake that can be generated by a specific fault is limited by the size of the fault, Gutenberg-Richter (or exponential) recurrence models used in practice are often truncated at the maximum magnitude for the fault (established based upon geological considerations), as illustrated in Figure 2-12.

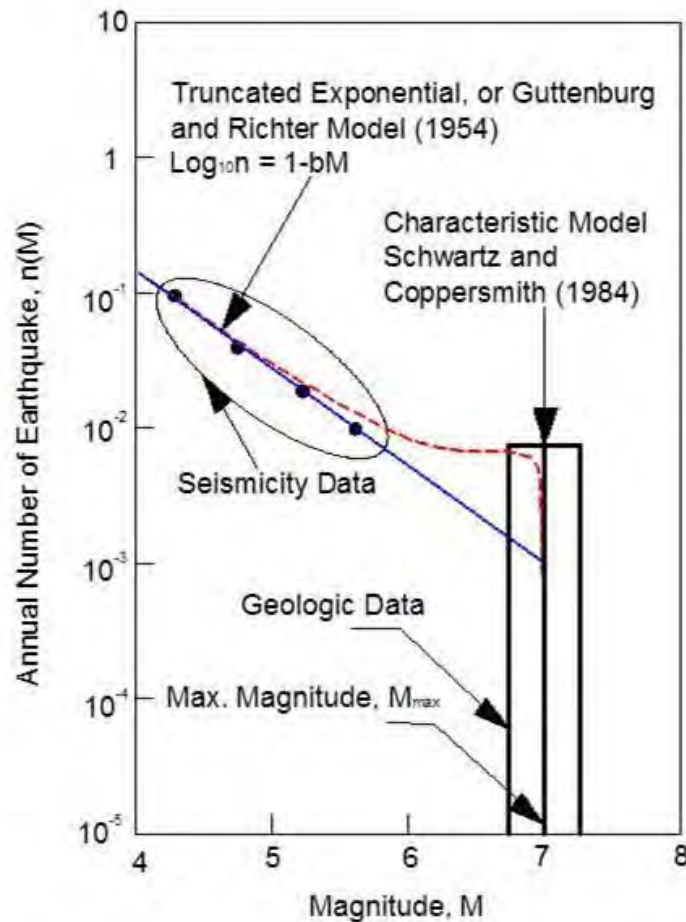


Figure 2-12 Truncated Gutenberg Richter and Characteristic Magnitude-Recurrence Models (Young and Coopersmith, 1985)

Another common earthquake recurrence relationship is a characteristic earthquake recurrence model. The characteristic model is used when geologic evidence indicates that the magnitude of earthquake generated by a fault falls within a relatively narrow range (typically within a band of 0.5 on the magnitude scale), as illustrated in Figure 2-12. In a characteristic recurrence model, the earthquake magnitude is typically uniformly distributed across this range and is assigned a recurrence rate, or recurrence rate distribution, based upon geologic evidence. The characteristic recurrence model was developed because in some areas geologic evidence suggests that the exponential model under-predicts the frequency of large magnitude earthquakes, as illustrated in Figure 2-12. Seismic hazard analyses often use a combination of exponential and characteristic recurrence models, calculating results using each model separately and then combining the results as a weighted average based upon the relative confidence in each model. In some cases, a combined recurrence model that employs an exponential relationship for small magnitude earthquakes and a characteristic relationship at larger magnitudes has been employed.

2.6 PARAMETERS DESCRIBING FAULTING

Faults may be broadly classified according to their mode, or style, of relative movement. The principal modes of relative displacement along a fault are illustrated in Figure 2-13 and are described below.

Strike Slip Faults: Faults along which relative movement is essentially horizontal (i.e., parallel to the strike of the fault) are called strike slip faults. Strike slip faults are often expressed as essentially linear (or planar) features in the landscape. Strike slip faults that are not fairly linear may produce complex surface features. The San Andreas Fault in California is a strike slip fault that is essentially a north-south linear feature over most of its length. However, the “Big Bend” in the San Andreas Fault just north of Los Angeles produces thrusting (compression) that results in mountain building. Strike slip faults may sometimes be aligned as individual sub-parallel segments along a linear trend. This type of strike slip faulting is sometimes accompanied by step over zones, i.e. zones where the ends of the individual fault segments overlap along the linear trend but are separated laterally (perpendicularly to the linear trend) by tens to hundreds of feet. Ground rupture patterns within these zones may be particularly complex.

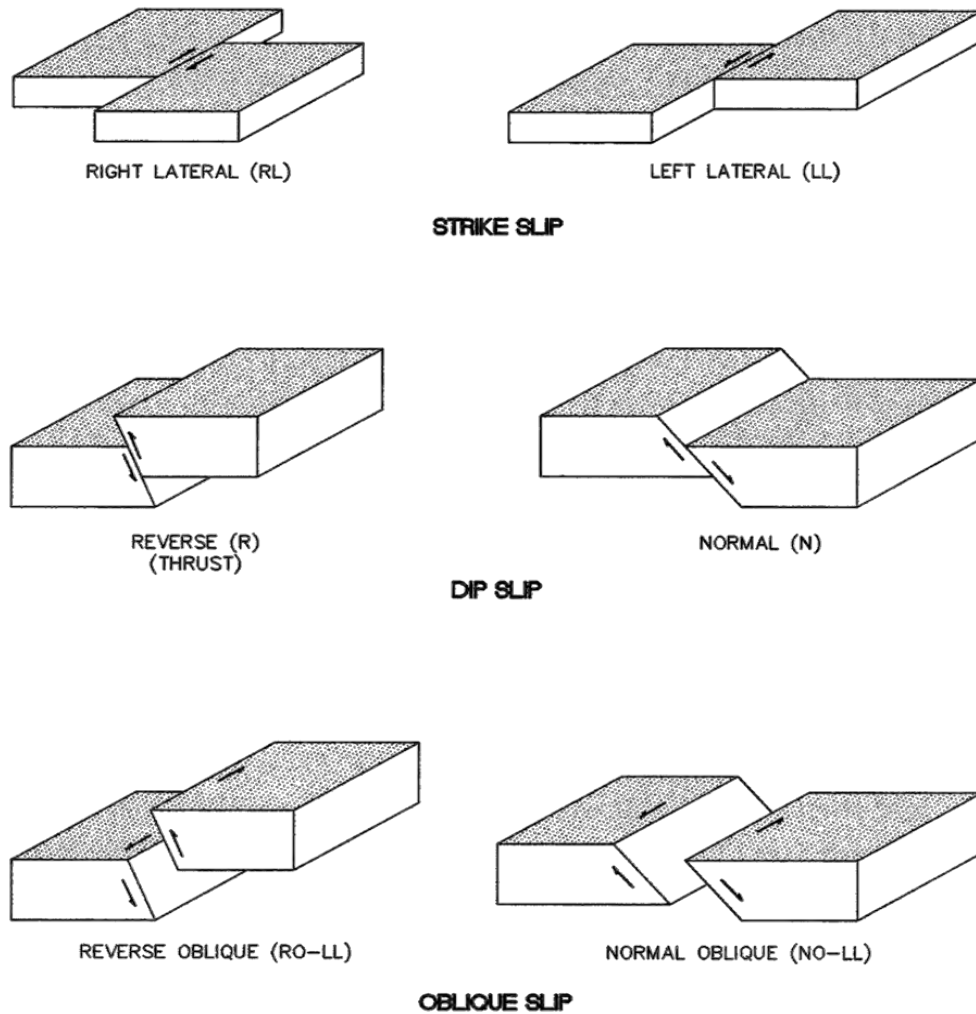


Figure 2-13 Types of Fault Movement (FHWA, 1998)

Dip Slip Faults: Faults in which the deformation is perpendicular to the strike of the fault may occur due to either *normal* (extensional) or *reverse* (compressional) motion. These faults are sometimes referred to as *dip slip* faults. Reverse (compressional) faults are also referred to as *thrust faults*. Dip slip faults may produce multiple fractures within rather wide and irregular fault zones. Some dip slip faults, e.g. blind thrust faults, may produce broad deformational features such as pressure ridges and sags rather than clearly defined fault scarps or shear zones (Hart, 1980).

Other Special Cases: Faults that show both strike slip and dip slip displacement may be referred to as *oblique slip faults*. In some cases, due to changes in fault alignment, the type of a given fault may be mixed. A good example of this is in the vicinity of the so-called "big-bend" in the alignment of the San Andreas Fault in California, where the fault, generally north-south trending, bends into a generally east-west alignment. In the vicinity of the big-bend, the generally strike slip lateral movement along the plate boundary is transferred into thrusting and compression, generating deformation perpendicular to the east-west trending fault plane.

2.7 PARAMETERS DESCRIBING GROUND SHAKING

2.7.1 Intensity

Intensity refers to the local strength and of earthquake ground motions. There are several earthquake intensity measures commonly used to describe qualitatively the strength of earthquake shaking at a site. These qualitative intensity measures are generally based upon verbal descriptions of the earthquake effects, including how humans and animals react to the shaking, observations of damage to structures and their contents, and other earthquake-related phenomenon such as ground cracking and sloshing of water in lakes and ponds. Qualitative intensity measures are particularly useful in studying historic earthquakes for which there are no instrumentally recorded ground motions, as they provide the sole basis for estimating the magnitude of such events. However, to be reliable, qualitative intensity information must be collected over a broad geographic area in order to average out local site effects, i.e. in order to discount local increases or decreases in intensity due to topography or local soil conditions.

The most commonly used qualitative intensity scale in the United States is the Modified Mercalli Intensity (MMI) scale. The MMI scale is a twelve point Roman numeral scale that varies from MMI I, representing an earthquake that is not felt except by a few people in favorable circumstances to MMI XII, representing an earthquake where damage is total, practically all engineered facilities are damaged or destroyed. Table 2-1 presents the MMI scale.

TABLE 2-1 MODIFIED MERCALI INTENSITY SCALE

(Source: <http://earthquake.usgs.gov/learning/topics/mercalli.php>)

- I.** Not felt except by a very few under especially favorable conditions.
- II.** Felt only by a few persons at rest, especially on upper floors of buildings.
- III.** Felt quite noticeably by persons indoors, especially on upper floors of buildings. Many people do not recognize it as an earthquake. Standing motor cars may rock slightly. Vibrations similar to the passing of a truck. Duration estimated.
- IV.** Felt indoors by many, outdoors by few during the day. At night, some awakened. Dishes, windows, doors disturbed; walls make cracking sound. Sensation like heavy truck striking building. Standing motor cars rocked noticeably.
- V.** Felt by nearly everyone; many awakened. Some dishes, windows broken. Unstable objects overturned. Pendulum clocks may stop.
- VI.** Felt by all, many frightened. Some heavy furniture moved; a few instances of fallen plaster. Damage slight.
- VII.** Damage negligible in buildings of good design and construction; slight to moderate in well-built ordinary structures; considerable damage in poorly built or badly designed structures; some chimneys broken.
- VIII.** Damage slight in specially designed structures; considerable damage in ordinary substantial buildings with partial collapse. Damage great in poorly built structures. Fall of chimneys, factory stacks, columns, monuments, walls. Heavy furniture overturned.
- IX.** Damage considerable in specially designed structures; well-designed frame structures thrown out of plumb. Damage great in substantial buildings, with partial collapse. Buildings shifted off foundations.
- X.** Some well-built wooden structures destroyed; most masonry and frame structures destroyed with foundations. Rails bent.
- XI.** Few, if any (masonry) structures remain standing. Bridges destroyed. Rails bent greatly.
- XII.** Damage total. Lines of sight and level are distorted. Objects thrown into the air.

2.7.2 Peak Ground Motions

The intensity of earthquake-induced ground motion, i.e. the strength of the ground motions at a given site, is often described quantitatively by the peak value of the acceleration time history, *the peak ground acceleration* (PGA). *Peak ground velocity* (PGV) and/or *peak ground displacement* (PGD) are also sometimes used as quantitative indices of earthquake damage potential. Peak ground motions are generally specified for the motions in the horizontal plane, as the horizontal ground motions generated by an earthquake tend to be the motions that cause the greatest damage. Figure 2-8 illustrates the acceleration, velocity, and displacement time histories from the horizontal component of an earthquake. The corresponding *peak horizontal ground acceleration* (PHGA), *peak horizontal ground velocity* (PHGV), and *peak horizontal ground displacement* (PHGD) values are indicated on Figure 2-8 by solid dots.

2.7.3 Energy Content

The *energy content* of the acceleration time history provides another means of characterizing quantitatively the intensity of strong ground motions. The energy content of a strong ground motion record is proportional to the square of the acceleration. In engineering practice, the energy content of the motion is typically expressed in terms of either the *root-mean-square* and *duration* of the acceleration time history or the *Arias intensity*, I_A . The *Arias intensity*, I_A , is proportional to the square of the acceleration integrated over the entire acceleration time history:

$$I_A = \frac{\pi}{2g} \int_0^{t_f} [a(t)]^2 dt \quad 2-1$$

where $a(t)$ is the time history of acceleration (the accelerogram), g is the acceleration of gravity and t_f is the duration of strong shaking. Arias (1969) showed that this integral is a measure of the total energy of the accelerogram.

The root-mean-square of the acceleration time history, or *RMSA*, is the square root of the square of the acceleration integrated over the duration of the motion and divided by the duration:

$$RMSA = \sqrt{\frac{1}{t_f} \int_0^{t_f} [a(t)]^2 dt} \quad 2-2$$

where $a(t)$ is the acceleration time history, and t_f is the duration of strong ground shaking. The RMSA represents an average value of acceleration over the duration of strong shaking. The square of the RMSA multiplied by the duration of the motion is directly proportional to the energy content of the motion, i.e. Arias intensity is related to the RMSA as follows:

$$I_A = \frac{\pi}{2g} (\text{RMSA})^2 \times t_f \quad 2-3$$

The value of the Arias Intensity is independent of the duration of strong shaking, while RMSA depends upon the definition of the strong shaking duration. However, as the energy content of the motion is fixed, the product of the RMSA and the squared duration will remain constant, as suggested by Equation 2-3. The definition of the duration of strong shaking for an acceleration time history can be somewhat arbitrary (as discussed subsequently), as relatively low intensity motions may persist for a long time towards the end of a strong motion record. If the defined duration of strong motion is increased to include these low intensity motions, the Arias intensity will remain essentially constant but the RMSA will decrease. Therefore, some investigators prefer Arias intensity to RMSA as a measure of energy content, as the Arias intensity is essentially a fixed value while the RMSA depends upon the definition of the duration of strong ground motion.

Arias intensity and/or RMSA and duration are useful parameters in selecting time histories for geotechnical analysis. This is particularly true if a *seismic deformation analysis* is to be performed, as the deformation potential of a strong motion record is related to the energy content, which can be expressed as a function of either Arias intensity or the product of the RMSA and duration of the record.

2.7.4 Duration

The duration of shaking is an important factor in determining the damage potential of strong ground motions. While duration is often neglected or treated indirectly in some common methods for evaluating the dynamic response of structures (e.g. response spectra analysis using modal superposition), duration is accounted for either explicitly (e.g. in analyses that use acceleration time histories as input) or implicitly based upon magnitude or peak ground velocity (e.g. in geotechnical problems such as liquefaction and

slope stability analyses). Duration is an important parameter in selecting representative time histories for use in advanced time and frequency domain structural and geotechnical analyses. Common definitions of strong ground motion duration include the bracketed duration and the significant duration. The *bracketed duration of strong motion*, D_b , as defined by Bolt (1973), is the elapsed time between the first and last acceleration excursion of the acceleration time history greater than a specified threshold level. Figure 2-14 illustrates calculation of bracketed duration for the Saratoga - Aloha Avenue accelerogram from the 1989 M_w 6.9 Loma Prieta earthquake (the acceleration time history used in Figure 2-8) for a threshold acceleration of 0.05 g.

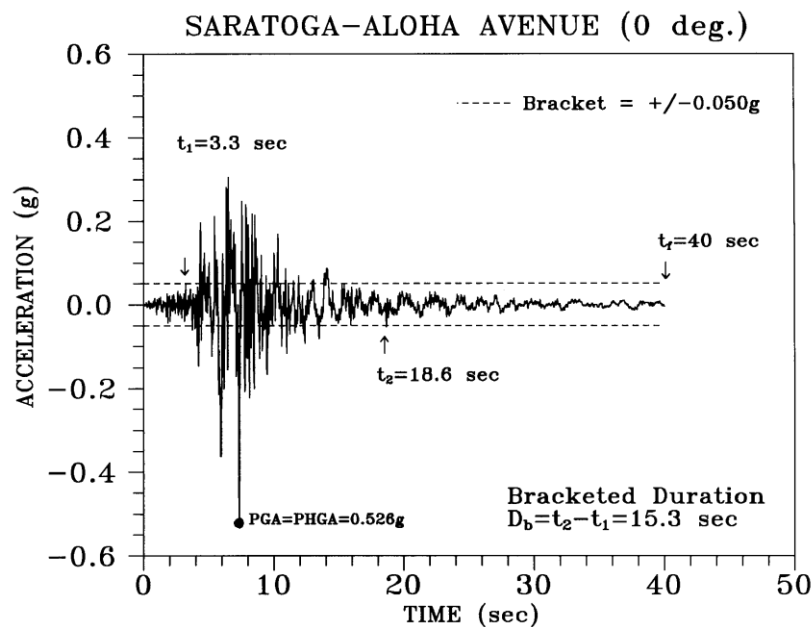


Figure 2-14 Bracketed Duration of Strong Shaking

While the bracketed duration is intuitively satisfying, it is not a unique property of an accelerogram if scaling of the accelerogram is allowed (as often done in engineering practice). If an acceleration time history is scaled to a different peak ground acceleration, the bracketed duration will change. Furthermore, use of the bracketed duration produces a decrease in the duration of strong shaking with increasing distance from the earthquake source, a somewhat counter-intuitive result as earthquake waves are known to spread out as they move away from the source, increasing the duration of shaking.

Many engineers and seismologists find the *significant duration*, D_s , proposed by Trifunac and Brady (1975) to be the most appropriate duration definition. Trifunac and Brady (1975) defined the significant duration as the time interval between 5 and 95 percent of the total Arias intensity on a plot of Arias intensity versus time for an accelerogram. This type of plot is known as a Husid plot as it was first proposed by Husid (1969) to portray the evolution of energy release for a ground motion record. The Trifunac and Brady definition of the significant duration is illustrated on the Husid plot in Figure 2-15 for the Saratoga-Aloha Avenue record from the 1989 M_w 6.9 Loma Prieta earthquake (the strong motion record for this motion is shown in Figure 2-14). This significant duration is a unique property of the time history, independent of any scaling of acceleration.

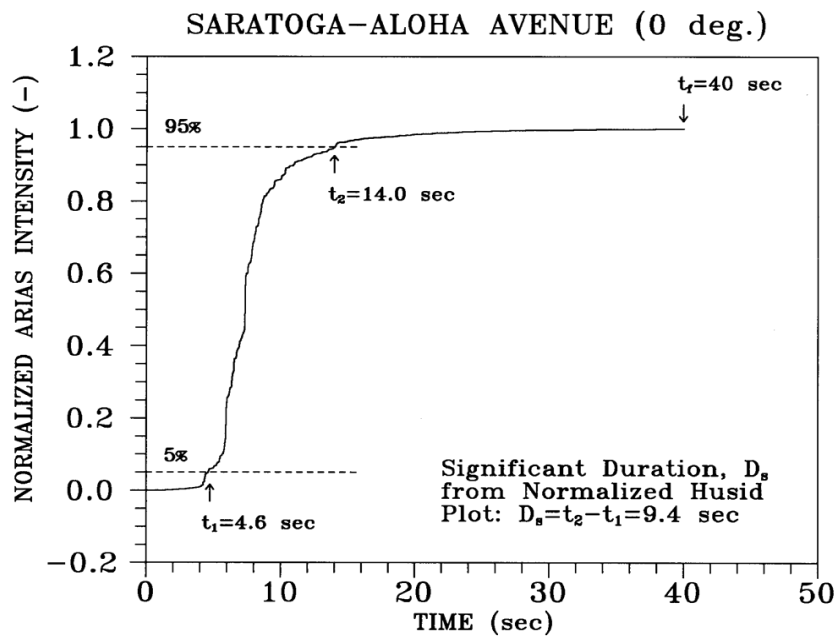


Figure 2-15 Significant Duration of Strong Shaking

For problems related to soil liquefaction, duration is sometimes expressed in terms of the *number of equivalent uniform cycles* (e.g., see Seed, *et al.*, 1975). The number of equivalent uniform cycles is typically expressed as a function of earthquake magnitude to reflect the general increase in duration with increasing magnitude. Recommendations for the number of equivalent uniform cycles as a function of earthquake magnitude for use in liquefaction and seismic settlement analyses are discussed in Chapter 6.

2.7.5 Response Spectrum

The *response spectrum* of an earthquake record is a plot of the maximum response of a linear single degree-of-freedom (SDOF) system versus the natural period of the system for a specified damping ratio. Response spectra used in practice include the acceleration (S_a), relative velocity (S_v), and relative displacement (S_d) response spectra. The acceleration response spectrum is the sole loading parameter for the most common method for seismic analysis of structures (modal superposition). It is also commonly used in the selection of representative earthquake time histories for use in analysis. Development of an acceleration response spectrum for a single earthquake time history is illustrated on Figure 2-16. A series of linear elastic SDOF systems of stiffness k , mass m , and damping c , each with a different undamped *resonant (or fundamental) period*, T , but the same *fraction of critical damping (or damping ratio)*, β , are subject to the same earthquake time history. The peak acceleration of each SDOF, a_{\max} , also referred to as the spectral acceleration, S_a , is plotted versus T to create the acceleration response spectrum for that motion. Velocity and displacement spectrum can be generated in the same manner (by plotting the peak value for each SDOF versus the fundamental period of the SDOF). It should be noted that the spectral acceleration for a SDOF with a fundamental period of zero (an infinite stiffness) is equal to the peak ground acceleration of ground motion. Also, as illustrated in Figure 2-16, the response spectrum is a function of the damping ratio, β , of the SDOF.

The undamped resonant period of the linear SDOF is the square root of its mass, m , divided by its stiffness, k , as presented in Equation 2-4:

$$T = \sqrt{\frac{m}{k}} \quad 2-4$$

The damping of the linear SDOF system is represented by the *viscous damping coefficient*, c . The critical damping coefficient for the SDOF system, c_{crit} , is the damping that results in the quickest approach (shortest time) to the at-rest condition for the system during free vibration. With less damping, the system reaches the at-rest position faster but oscillates around that position, while with more damping the system approaches the at-rest position without oscillation but at a slower rate. The critical damping coefficient, c_{crit} , is the square root of the mass times the stiffness of the SDOF:

$$C_{\text{crit}} = 2 \cdot \sqrt{(k \cdot m)} \quad 2-5$$

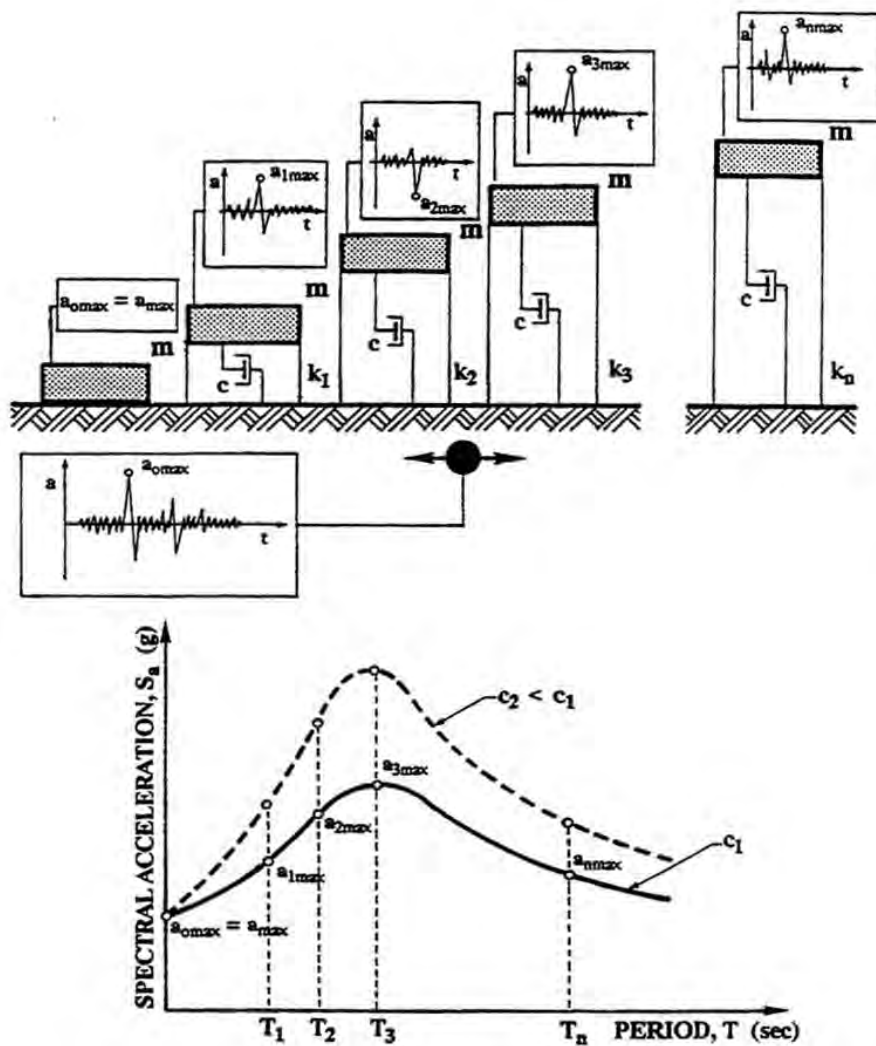


Figure 2-16 Schematic Representation of Acceleration Response Spectra (Reproduced from Matasovic, 1993)

The ratio of the viscous damping coefficient to the critical damping coefficient, c/c_{crit} , is fraction of critical damping, or damping ratio β (when expressed as a percent).

$$\beta = \frac{C}{C_{crit}} \cdot 100\% \quad 2-6$$

In the context of a response spectrum, β is sometimes referred to as the *spectral damping*. In earthquake engineering, a spectral damping of 5% is commonly selected for development of response spectra.

A tripartite spectral plot is sometimes used to graphically portray response spectra. Figure 2-17 shows an example of such a tripartite plot for a smoothed response spectra developed by averaging or enveloping a large number of spectra representative of a specified condition. A tripartite plot simultaneously displays the spectral acceleration, S_a , as well as the spectral velocity, S_v , and the spectral displacement, S_d , values (determined in the same way as S_a as the peak values for the SDOFs in Figure 2-16) for the selected spectral damping. For a given fundamental period, T , (or fundamental frequency $f = 1/T$), S_a , S_v , and S_d are read from the appropriate ordinates. For example, as indicated on Figure 2-17, for $T = 0.7$ s ($f = 1.4$ Hz), $S_a = 0.19$ g, $S_v = 10$ in/s, and $S_d = 1.2$ in.

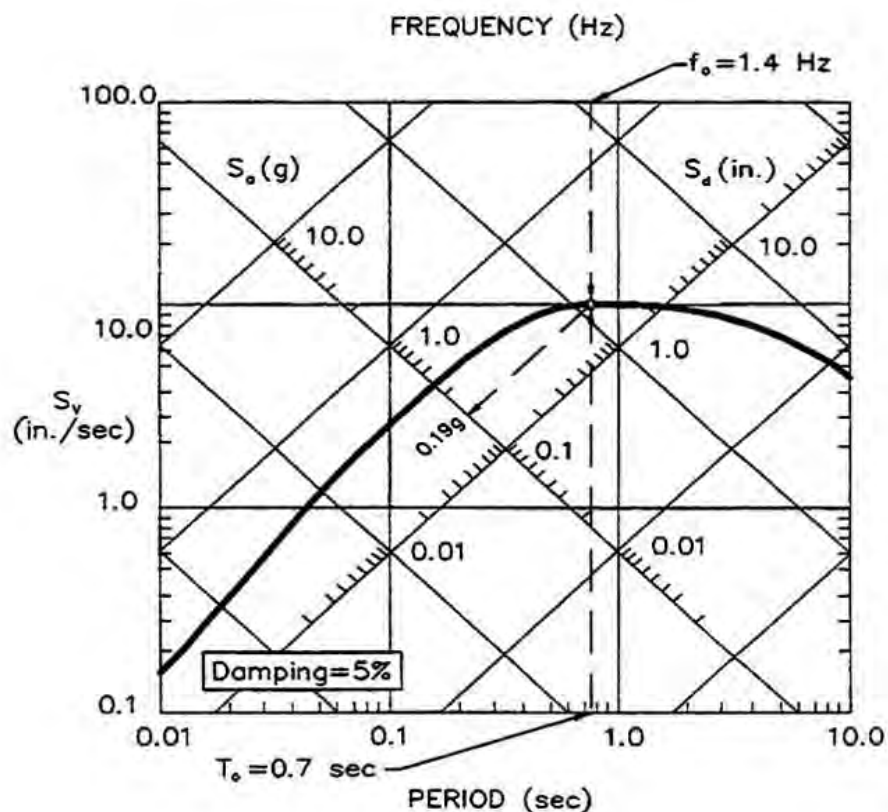


Figure 2-17 Tripartite Representation of Acceleration, Velocity, and Displacement Response Spectra.

2.7.6 Smoothed Uniform Hazard Spectra

Seismic hazard analyses often must consider the contributions to seismic risk from a variety of different earthquake sources. Furthermore, even when there is only a singular source under consideration, that source may be capable of generating earthquakes of different magnitudes at different distances and recurrence rates. One method often used to consider the relative contributions of more than one source

and/or of multiple events of different magnitude, distance, and recurrence from the same source is a probabilistic seismic hazard analysis. In a probabilistic seismic hazard analysis, the probability of exceeding a specified level of ground motion for a specified time period is calculated. The specified ground motion parameter may be a peak ground motion parameter (e.g. PGA, PGV, or PGD) or a spectral parameter (e.g. S_a , S_v , or S_d) at a specified spectral period. One particularly useful output from a probabilistic hazard analysis is a plot of a desired spectral parameter (e.g. spectral acceleration, S_a) over the entire range of spectral periods of interest for a specified probability of exceedance over a specified time period (e.g. for a 7% probability of exceedance in a 75 year period, per the AASHTO seismic design specifications). Such a plot is referred to as a uniform hazard spectrum (as each point has the same annual probability of being exceeded), or UHS. A UHS typically represents the statistically averaged contributions from multiple events on multiple seismic sources, thus the resulting spectra are generally represented by a smooth curve. Figure 2-18 presents the uniform hazard acceleration response spectrum for a site in Memphis, Tennessee, from the USGS National Seismic Hazard Mapping Program for ground motions with a 5 percent probability of being exceeded in a 50-year period (probabilistically equivalent to a 7% probability of being exceeded in a 75-year period). More discussions in seismic hazard analysis and uniform hazard spectra are presented in Chapter 3.

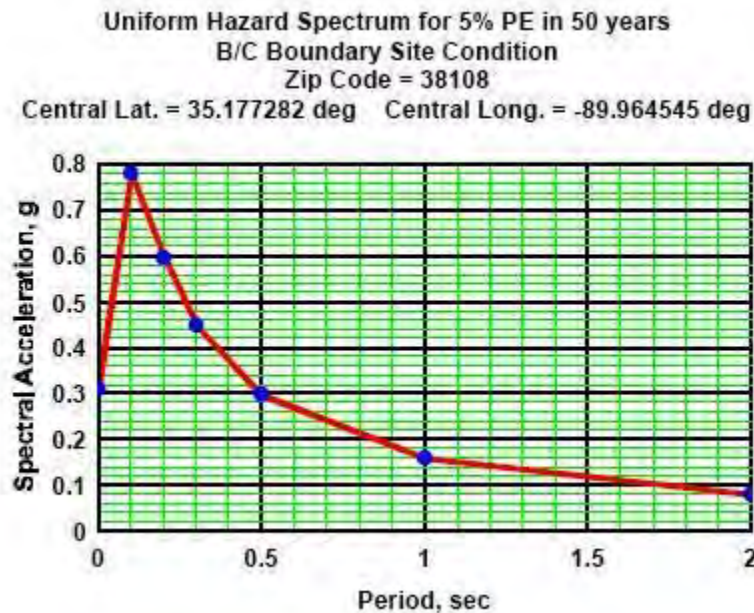


Figure 2-18 Uniform Hazard Acceleration Response Spectra for Memphis, Tennessee, with a 5% Probability of Exceedance 50-years (USGS National Seismic Hazard Mapping Program)

2.7.7 Ground Motion Attenuation Relationships

An *attenuation relationship* describes the relationship between earthquake magnitude, site-to-source distance, and the value of a peak or spectral ground motion parameter (e.g., peak ground acceleration, peak ground velocity, peak ground displacement, or spectral parameters S_a , S_v , or S_d at a specified spectral period). Attenuation relationships are essential input parameters for seismic hazard analyses. Acceleration attenuation relationships (for both peak and spectral values) are the most common form of attenuation relationship. Attenuation relationships are usually developed by statistical analysis of ground motions recorded in previous earthquakes. The variability in the ground motion parameter of interest for a given magnitude and distance is generally characterized by the standard deviation of the statistical data. This variability is usually assumed to be log-normally distributed (i.e., the logarithm of the parameter value is normally distributed).

Numerous attenuation relationships can be found in the technical literature. Typical factors included in an attenuation relationship are tectonic regime (e.g. shallow crustal earthquakes, subduction zone earthquakes, intraplate earthquakes), earthquake magnitude, site-to-source distance, and some measure of local ground conditions (e.g. stiff soil, soft soil, or rock or, more recently, shear wave velocity in the upper 30 meters of the site). Figure 2-11 identifies the distance measures associated with the most common attenuation relationships used in engineering practice. The style of faulting (e.g., slip-strike versus normal faulting) and, for normal faulting, the location of the site with respect to the orientation of the fault, are also used in some attenuation relationships.

Attenuation relationships can be particularly sensitive to tectonic setting. Field data indicate that attenuation in subduction zone events differs from attenuation in shallow crustal events, which in turn differs from attenuation in intraplate events. In particular, intraplate events appear to attenuate at a significantly slower rate (decay slower with distance) than shallow crustal events. Hence, strong ground motions from an intraplate event is likely to be experienced over a much broader area than strong motions from a shallow crustal event of the same magnitude. Attenuation relationships are addressed in more detail in Chapter 3 of this document.

2.7.8 Predominant Period of the Strong Ground Motions

Earthquake ground motions tend to have a predominant period (or frequency), i.e. a period, or range of periods, of vibration where the greatest amount of strong motion energy is concentrated. This

predominant period can be identified in an approximate manner as the period, or range of periods, corresponding to the peaks of the acceleration response spectrum. Sites with a soil layer (or layers) overlying either bedrock or another soil layer that differs significantly in stiffness and density will have a resonant period governed by the thickness, density, and stiffness (or shear wave velocity) of the overlying soil layer(s). Similarly, an engineered facility is likely to have one or more fundamental (or resonant) periods, i.e. a period at which the structural response is the greatest. The damage potential of strong ground motions with respect to a specific engineered facility is affected by the fundamental period of the base earthquake motion, the resonant period of any soil layer at the site, and the resonant period of the engineered facility. When the predominant period of the earthquake motion is close to the resonant period of the soil layer, there is a significant potential for amplification of the earthquake motion. In fact, the spectral acceleration of the earthquake motion will always be amplified around the resonant period of the soil layer. So, the damage potential of an earthquake ground motion increases when the predominant period of the earthquake motion is close to the resonant period of the site and when the resonant period of the site is close to the fundamental period of the structure. The damage potential of an earthquake ground motion will be greatest when all three of these predominant or fundamental periods coincide.

2.7.9 Magnitude-Distance Deaggregation

Each point on a uniform hazard spectrum is typically composed of contributions from a family of earthquakes of different magnitude and distance. The distribution of magnitude and distance may be different for each point on the uniform hazard spectrum. This distribution is referred to as the magnitude-distance deaggregation. The magnitude-distance deaggregation is important as it provides the basis for assigning a representative magnitude and distance to a design earthquake ground motion. Figure 2-19 shows the magnitude-distance deaggregation for one point on a uniform hazard spectrum for Oceano, California.

Figure 2-19 indicates that the primary contribution to the seismic hazard at the site is from a M 7.5 event at a distance of approximately 3 miles from the site but that there is also a M 8 source about 12.5 miles from the site that contributes to the hazard. Magnitude-distance deaggregation is described in more detail in Chapter 3.

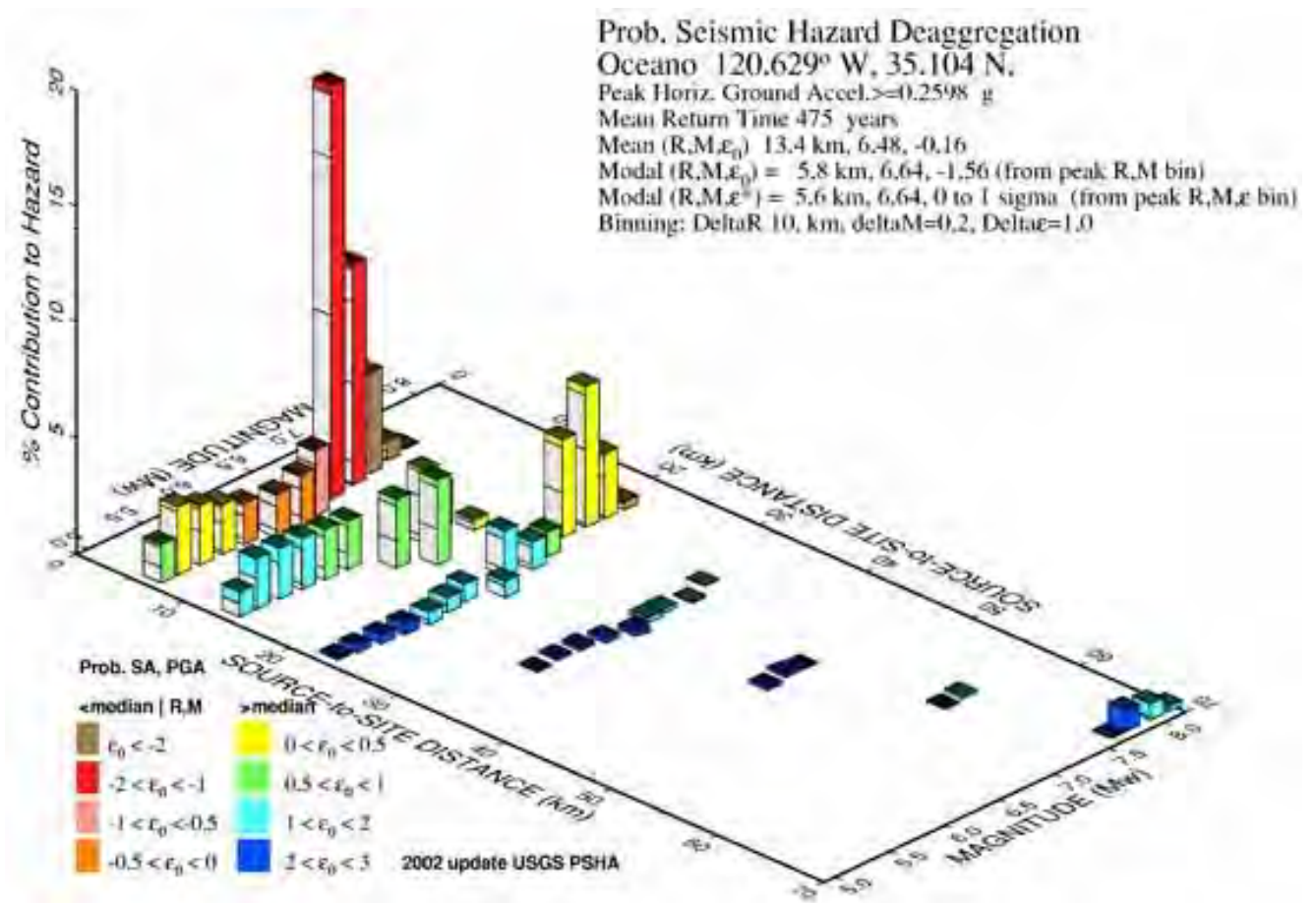


Figure 2-19 Magnitude-Distance Deaggregation for Oceano, California (Source: USGS National Seismic Hazard Mapping Program)

2.8 SUMMARY

This chapter presents an overview of the mechanisms of earthquakes and earthquake source zones. It also defines the basic parameters describing faults and the recurrence of earthquakes and strong ground motions generated by earthquakes. The mechanisms of earthquakes are described to provide the reader with a physical understanding of earthquake phenomenon. Earthquake sources are discussed within the framework of plate tectonics to give the reader an appreciation of the sources of damaging earthquakes within the United States. Earthquake source mechanisms are also important because the rate at which earthquake motions attenuate is related to source mechanism, with intraplate earthquakes in the central and eastern United States attenuating less rapidly with distance compared to earthquakes at transform boundaries and other shallow crustal events.

Earthquakes are generated by fault rupture. The energy released by an earthquake is quantified by the earthquake magnitude. Moment magnitude is presented as a uniform measure of earthquake magnitude. The geometric parameters describing the ruptured fault include parameters describing the location of the fault such as hypocenter and epicenter, parameters describing its orientation such as strike and dip, and the zone of energy release. The measures used to describe the distance of a project site from the earthquake source vary depending on the location parameter used in their definition. The rate at which earthquakes occur on a given fault is referred to as the recurrence rate. The two models commonly used to define the recurrence of earthquakes in a seismic hazard assessment, the truncated exponential Gutenberg-Richter model based upon primarily instrumentally recorded earthquakes, and the characteristic model developed based upon geologic data, are briefly described.

The engineering parameters describing strong shaking in earthquakes that are defined in this chapter include strong motion time histories, peak ground motion parameters, elastic response spectra, ground motion attenuation relationships, uniform hazard spectra and the associated magnitude deaggregation, and various energy and duration measures. These parameters are generally related to the return period, or annual probability of occurrence, of the ground motion. The evaluation of these strong ground motion parameters in accordance with both probabilistic and deterministic earthquake design criteria is discussed in Chapters 3 and 5. Chapter 3 further discusses the development of acceleration response spectra that satisfies the AASHTO seismic design criteria and modification of the AASHTO response spectra to account for local site conditions, while Chapter 5 further discusses modifications to ground motion design parameters based upon site-specific site response analysis. Subsequent chapters of this document then discuss the use of these design ground motion parameters in geotechnical analysis of the performance of transportation facilities in earthquakes including:

- The use of earthquake magnitude and peak ground acceleration, spectral acceleration, peak ground velocity, and/or a suite of representative time histories to evaluate liquefaction potential, liquefaction-induced ground displacement, seismic slope stability and deformation, and seismic settlement in Chapter 6;
- The use of representative time histories in soil-structure interaction analyses in Chapter 8;
- The use of peak ground acceleration, spectral velocity, or representative ground motions to evaluate lateral earth pressures and design earth retaining structures in Chapter 12; and
- The use of representative ground motions to design buried structures for seismic loads in Chapter 13.

CHAPTER 3

SEISMIC HAZARD ANALYSIS AND GROUND MOTION CHARACTERIZATION

3.1 GENERAL

Seismic hazard analysis is the process by which the appropriate ground motions (or ground motion parameters) are established for seismic design. This chapter describes the two basic types of seismic hazard analyses (i.e. probabilistic and deterministic analyses) commonly employed in design practice as well as characterization of the design ground motions based upon the results of these analyses. AASHTO uses a probabilistic approach and has recently adopted a **1,000-year** return period as the basis for bridge design. The 1000-year return period may also be logically assumed to be appropriate for non-bridge highway transportation facilities (e.g., embankments, tunnels, culverts, retaining walls, etc.) for consistency. However, occasionally a different return period, or a deterministic analysis, may be employed to provide a basis upon which to establish earthquake ground motions for use in design. Furthermore, the designer may wish to evaluate performance of a structure or facility for more than one return period or to assess the sensitivity of seismic performance to the return period.

This chapter describes the fundamental principles of seismic hazard analysis and discusses the relative merits of, and fundamental differences between, the probabilistic and deterministic approaches to seismic hazard analysis. The procedure for obtaining design ground motion parameters in accordance with the AASHTO criteria for LRFD seismic design, procedures for establishing a suite of representative acceleration time histories for use in design, and special considerations in determining design ground motions not addressed by the AASHTO specification, including near-field ground motions, shallow bedrock and deep soil basin sites, and spatial variability in ground motions, are also addressed in this chapter.

Figure 3-1 portrays the four fundamental steps in a probabilistic seismic hazard analysis. In Step 1 (Seismic Source Identification), the seismic sources capable of generating strong ground motions at the project site(s) are identified and the characteristics and geometries of these sources (i.e. their tectonic mechanism, style of faulting, location and spatial extent) are defined. In Step 2 (Magnitude-Recurrence), a recurrence relationship describing the rate at which various magnitude earthquakes are expected to occur, is assigned to each of the identified seismic sources. Together Steps 1 and 2 may be referred to as “seismic source characterization”. In Step 3 (Ground Motion Attenuation), an attenuation relationship

that describes the link between earthquake magnitude, site-to-source distance, and the ground motion parameter of interest is assigned to each seismic source. In Step 4 (Probability of Exceedance), the results from the first three steps are combined to produce a curve relating the value of the ground motion parameter of interest at the site(s) of interest to the probability that it will be exceeded in a specified time interval.

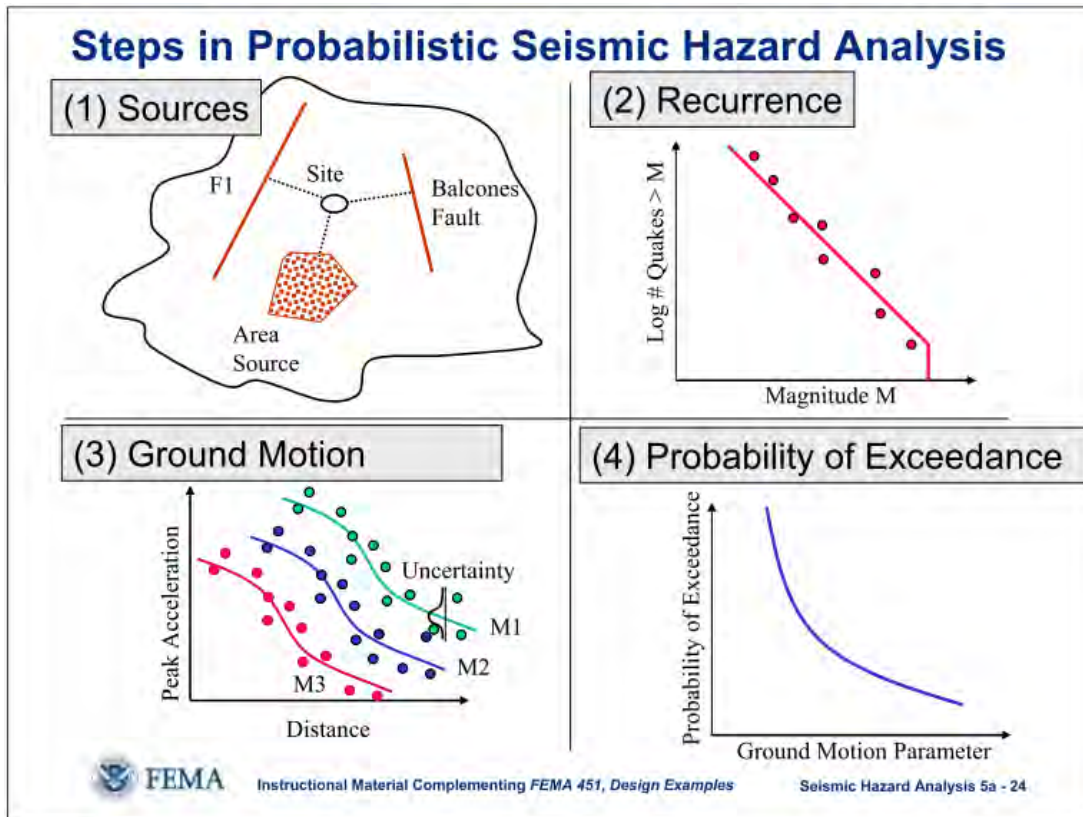


Figure 3-1 Steps in Probabilistic Seismic Hazard Analysis

A deterministic seismic hazard analysis may also be described by the four step process illustrated in Figure 3-1. However, in a deterministic analysis, Step 2 (Magnitude-Recurrence) is abbreviated by assigning a discrete, deterministic magnitude to each seismic source. The magnitude assigned to each source is generally some sort of maximum magnitude. Then, Step 4 consists solely of determining which source generates the maximum (or most damaging) value of the ground motion parameter of interest (though it may sometimes be necessary to consider more than one source due to the interrelationship between damage potential, intensity, and duration).

Each of the steps described above for the probabilistic and deterministic methods of analysis is discussed in the following sections. How the deterministic approach differs from the probabilistic approach is also addressed herein. Other important subjects that are discussed in the following sections include selection of the target ground motion level for use in design, characterization of the design ground motions from the results of a probabilistic or deterministic seismic hazard analysis, details of the procedure for obtaining design ground motions in accordance with the AASHTO probabilistic seismic hazard design criteria, and special topics such as near field (near fault) effects such as directivity and the near field pulse of ground motion, spatial variation of ground motions, and vertical ground motions.

3.2 SEISMIC HAZARD ANALYSIS

3.2.1 Seismic Source Identification

The first step in a seismic hazard analysis usually is to identify and characterize the seismic sources capable of generating strong ground motions at the project site. The characteristics of seismic sources capable of generating strong ground motions at the project site were discussed in Chapter 2. In addition to simply identifying the seismic sources impacting a site, the type of seismic source zone (e.g. shallow crustal fault zone, subduction zone, or intraplate zone), the style of faulting (e.g. strike-slip, dip-slip, oblique) must be identified and a model of the geometry of each seismic source must be developed. There are two basic geometries used to model seismic sources in a seismic hazard analysis: area source zones (sometimes discretized into a series of point sources), and discrete fault sources (typically modeled as line sources). Both types of sources are conceptually illustrated in Figure 3-2.

Well-defined faults may be modeled as line sources, while area source zones are used to model spatially distributed seismicity. In the 1970s and early 1980s, seismic source characterization was typically based on area sources that were defined using historical seismicity data. In many parts of the world, particularly those without well-defined active faults, modeling seismic sources using area sources is still the standard of practice. However, even in regions with well known faults, area sources are commonly included in the source characterization to account for background seismicity and for earthquakes that do not occur on known faults or fault zones.

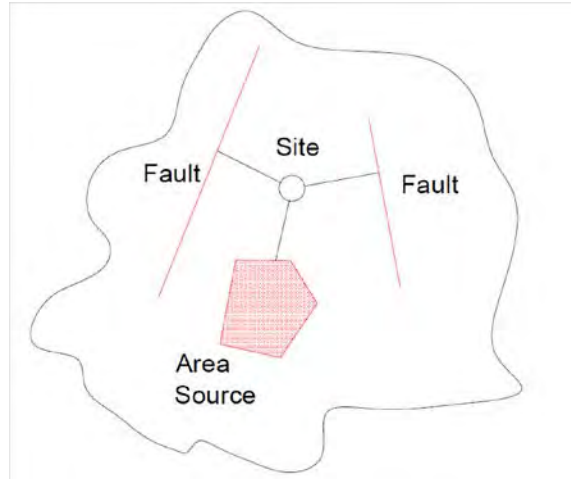


Figure 3-2 Geometry of Seismic Sources in Seismic Hazard Analysis

In the United States (especially in the western U.S.), faults that have the potential to produce strong ground shaking have generally now been well defined by geological and seismological studies and therefore discrete fault source modeling can be employed. In state-of-the practice seismic hazard analyses, fault sources are usually treated as planes to account for the variable depth of the seismic activity. Area sources may be treated as volumes to account for uncertainty in the depth of seismic activity. Accounting for the depth of seismic source is necessary to properly account for the depth-dependence of the site to source in many attenuation relationships. This subject is further discussed in Section 3.2.3 in the discussion on ground motion attenuation relationships.

3.2.2 Magnitude-Recurrence Relationships

After defining the characteristics and geometry of each seismic source that can contribute to the strong ground shaking at the project site, the next is to define the size (i.e. magnitude) and frequency of occurrence (recurrence) of the earthquake(s) associated with each seismic source. As noted in Chapter 2, Moment Magnitude, M_w , has been generally adopted by seismologists and engineers as the measure of the size of an earthquake. M_w was defined by Hanks and Kanamori (1979) using the following equation:

$$M_w = \frac{2}{3} \log_{10}(M_o) - 10.7 \quad 3-1$$

where M_o is defined as the ‘seismic moment’ (in dyne-cm), given by the following equation:

$$M_o = \mu \times A \times D \quad 3-2$$

where μ is the rupture strength (shear modulus) of the crust (dyne/cm²),
 A is the area of the fault rupture (cm²), and
 D is the average displacement (slip) over the rupture surface (cm).

M_w and M_o both have units of force times length (dyne-cm), or work done, and hence, both are direct measures of the energy released by fault rupture during an earthquake.

From Equation 3-1, it can be shown that seismic moment is related to moment magnitude as follows:

$$M_o = 10^{(3/2(M_w + 10.7))} \quad 3-3$$

From Equations 3-1 and 3-3, it can be seen that the relationship between the energy released by an earthquake (M_o) and earthquake magnitude (M_w) is logarithmic, i.e. for each unit increase in moment magnitude, M_w , the seismic moment, M_o (energy released by fault rupture), increases by a factor of 31.6. Hence, compared to the energy released by a magnitude 5 earthquake, the energy released by magnitude 6, 7 and 8 earthquakes will be 31.6, 1,000 and 31,623 times greater, respectively. A larger magnitude (greater energy release) generally results in stronger and longer shaking from the earthquake. However, the additional energy associated with a very large magnitude earthquake may not necessarily induce stronger shaking at the site in the near field (i.e. close to the zone of energy release for the earthquake) due to the limited strength of near surface soils (which limits the amplitude of the waves they can transmit). Even if the amplitude of shaking is limited, a very large magnitude event will still subject a much larger area to strong shaking and cause a longer shaking duration.

In both deterministic and probabilistic seismic hazard analyses, the maximum magnitude earthquake that can be generated for each seismic source must be defined. In a deterministic seismic hazard analysis, knowledge of the maximum magnitude, or a characteristic magnitude, for each source is generally sufficient for seismic source characterization purposes (in addition to the tectonic mechanism, style of faulting, source location, and geometry). In a probabilistic seismic hazard analysis, a magnitude-

recurrence relationship (i.e. the rate of occurrence of various magnitude earthquakes) needs to be defined in addition to the maximum earthquake magnitude. As discussed in Chapter 2, the magnitude-recurrence relationship relates earthquake magnitude to the number of earthquakes per year equal to or greater than that magnitude for a seismic source. The reciprocal of the recurrence rate is the average time period (in years) between events equal to or greater than the associated magnitude. (Note that the reciprocal of the recurrence rate, or recurrence interval, which is the average time period (in years) between occurrences of an earthquake of a given magnitude, is generally distinguished from the return period, which is the average time period (in years) between occurrences of a specified ground motion level.)

The need to define the frequency of occurrence of earthquakes in a magnitude-recurrence relationship is one of the main distinctions between deterministic and probabilistic seismic hazard analyses. The Gutenberg-Richter recurrence model (sometimes referred to as the exponential model) was widely used as the sole means of characterizing magnitude-recurrence relationships in the 1970s and early 1980s, and is given by the following equation (Gutenberg and Richter, 1944):

$$\text{Log}_{10}(n) = a + b \times M_w \quad 3-4$$

where n is the annual number of earthquakes with magnitude M_w , and the a and b parameters define the recurrence rate based on curve fitting to historical seismicity data.

One shortcoming of the Gutenberg-Richter model is that it is not limited in magnitude (i.e. there is a small but finite frequency of earthquakes of magnitude 9, 10, and greater). To compensate for this shortcoming, Gutenberg and Richter proposed truncating the exponential model at a limiting (or maximum) magnitude (Gutenberg and Richter, 1954). The truncated Gutenberg-Richter model (i.e. a truncated exponential model) works well for large regions (e.g. for the worldwide seismicity data base) but does not always fit the observed behavior of finite fault sources (Schwartz and Coppersmith, 1984) or for seismicity data measured over smaller regions during the relatively short time frame of instrumental seismicity (i.e., since 1933, the start of instrumental seismicity measurements using scientific instruments).

While the use of recorded seismicity data may intuitively seem like the preferred method for development of a recurrence relationship, the short history of the instrumental record is insufficient to reflect geologic processes in most areas. Therefore, other means, e.g. the use of geologic data, are usually necessary to

develop recurrence relationships. Even when representative instrumental data is available for small magnitude events, geologic evidence usually is used to anchor the recurrence model at the large earthquake end of the magnitude-recurrence relationship, i.e. for the maximum magnitude earthquake, M_{\max} .

The current preferred approach to account for the recurrence of large magnitude earthquakes on well known faults is to complement the instrumental seismicity data for smaller magnitude earthquakes with a characteristic magnitude-recurrence model for maximum magnitude events. In the characteristic model, the rate at which earthquakes of the characteristic (or maximum) magnitude occur is based on both geodetic data (i.e. the tectonic slip rate for the fault) and geologic data (i.e. paleoseismic studies) that can cover a much longer history of the earth's geologic processes than instrumental seismicity. The characteristic model assumes that individual faults tend to generate earthquakes of a preferred magnitude due to the geometry of the fault and the rate of accumulation of stress due to tectonic forces (i.e. the average annual rate of movement, or tectonic slip rate). As a result of this phenomenon, there is a 'characteristic' size (magnitude) of earthquake that a given fault segment tends to generate based on the dimension of the fault segment and associated slip rate.

As discussed in Chapter 2, Figure 2-12 (also shown hereafter as Figure 3-3) shows a composite of the Gutenberg-Richter and Characteristic models is often used to describe magnitude-recurrence in seismic hazard analysis. The Gutenberg-Richter model is used to describe the recurrence of small magnitude events based on instrumental seismicity and the Characteristic model is used to describe magnitude recurrence in the large magnitude range based upon geologic data such as the fault's length and/or historic slip rate. One such composite model is the Youngs and Coppersmith (1985) model, which is contrasted in Figure 3-3 to the truncated exponential model. The Youngs and Coppersmith model employs a uniform distribution for the large magnitude characteristic earthquakes. The uniform distribution illustrated in Figure 3-3 is centered on the mean characteristic magnitude and has a width of 0.5 magnitude units.

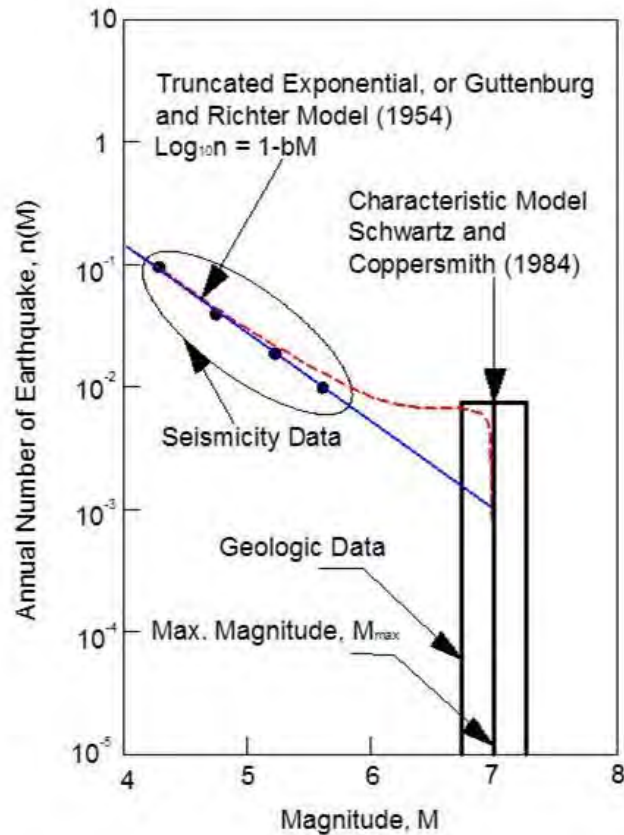


Figure 3-3 Truncated Gutenberg Richter and Characteristic Magnitude-Recurrence Models (Youngs and Coopersmith, 1985)

Since a composite model employs two different magnitude distributions, an additional constraint is needed to define the relative amplitudes of the two distributions. One commonly adopted constraint is to set the height of the uniform distribution equal to the value of the exponential distribution at 1.0 magnitude unit below the lower end of the uniform characteristic distribution (1 magnitude unit less than the smallest magnitude of the uniform characteristic magnitude distribution). This additional constraint sounds rather arbitrary, but it has a basis in empirical data on earthquake recurrence. A key feature of the Young and Coppersmith model is that this constraint results in about 94% of the total energy associated with a seismic source being released in characteristic earthquakes and about 6% of the total energy being released in the smaller earthquakes that fall within the range of the exponential model.

An additional consideration in assigning magnitude-recurrence to a seismic source is the distribution of the earthquake occurrences over the source, i.e. the locations of the ruptures. In practice, a uniform distribution of earthquake occurrence over the seismic source is commonly used.

3.2.3 Strong Motion Attenuation Relationships

The third step in a seismic hazard assessment (after characterizing seismic source geometry and magnitude-recurrence) involves defining the appropriate attenuation relationship(s) for the strong ground motions. An attenuation relationship relates the design ground motion shaking parameter(s) of interest (e.g. peak ground acceleration or spectral acceleration as a function of spectral period) to the combination of magnitude (M) and distance (D), as shown in Figure 3-4. The preferred method for developing an attenuation relationship is to conduct statistical analysis of recorded strong motion data. However, in some tectonic regimes there is not sufficient historical strong motion data from which to develop such a relationship. Furthermore, there is often a lack of data on attenuation in very large magnitude events for a given tectonic regime, particularly in the near field. In these cases, empirical and analytical seismological models are employed to supplement the available historical data.

Historical strong motion data from earthquakes show a wide range of scatter, even after reconciling discrepancies due to earthquake magnitude, source mechanism, tectonic regime, and site conditions. This variation among recorded data within a single earthquake event is referred to as intra-event variability, while the variability among records from different earthquakes is referred to as inter-event variability. It is generally recognized that attenuation relationships need to reflect both sources of variability (i.e. the total uncertainty) in the strong motion data. Hence, an attenuation relationship is typically presented in terms of a median attenuation relationship with the scatter about the median modeled by a statistical distribution function. If the functional form of the distribution is known (or assumed), the scatter of the ground motion about the median can be characterized simply in terms of the standard deviation or variance of the distribution. Most current attenuation models assume a log-normal distribution for this scatter (i.e., the logarithm of the response parameter has a normal (Gaussian) distribution). Hence, modern attenuation relationships are typically defined by an equation for the median value of the ground motion parameter as a function of magnitude and distance (and any other parameters included in the attenuation model) plus the standard deviation (sigma, or σ , value) for the stated distribution shape. The standard deviation may also be a function of magnitude and/or distance. Most current attenuation models provide for prediction of both the peak ground acceleration and the spectral acceleration at various spectral periods. Attenuation models may also provide values for other ground response parameters of interest, e.g. peak ground velocity.

Figure 3-4 presents an example of a common attenuation relationship for the peak horizontal ground acceleration (PHGA) along with the historical strong motion data used to develop it. The dots in Figure 3-4 represent the historical data points while the solid lines represent the median values. The dashed lines in Figure 3-4 represent the 95% confidence interval from the statistical analysis (i.e. the 2σ bounds assuming a log normal distribution). The bell-shaped curves in Figure 3-4 show the assumed statistical log normal distribution of the ground motion parameter (the peak ground acceleration) at a distance of 0.6 miles.

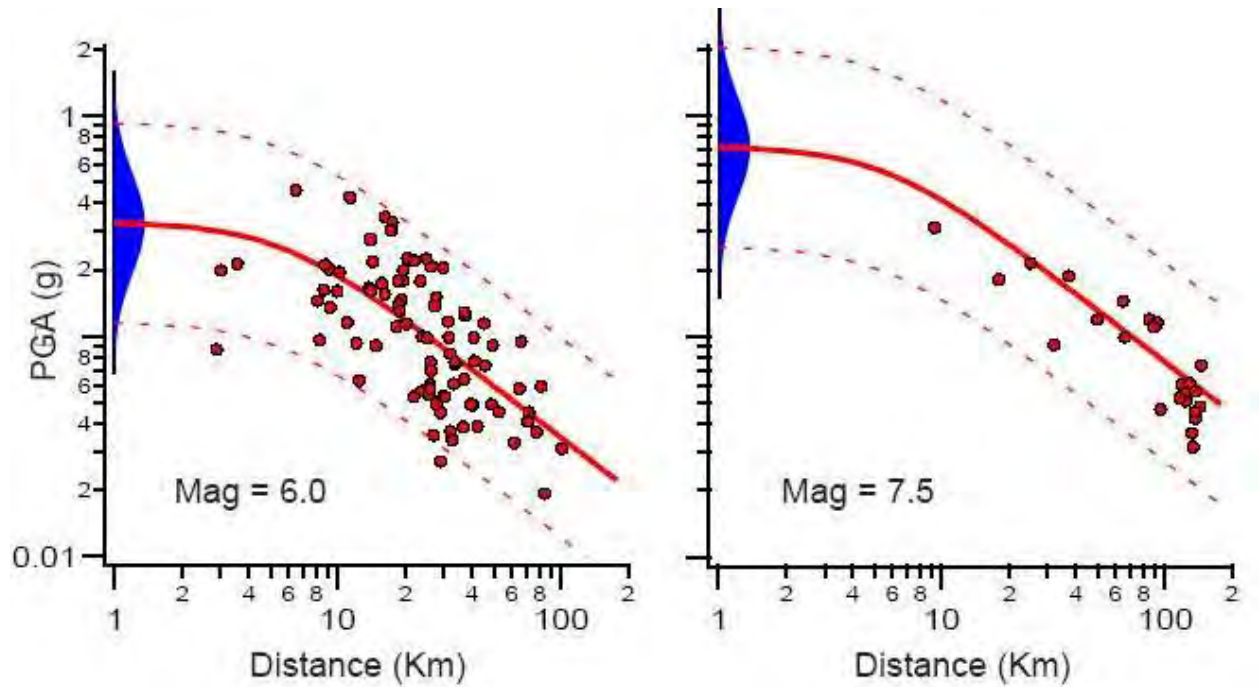


Figure 3-4 Example of Peak Horizontal Ground Acceleration Attenuation Relationship for Strike-Slip Earthquakes and Soil Sites (Boore, Joyner, and Fumal (1997))

Individual attenuation modelers often have different viewpoints about earthquake mechanisms and hence often employ different variables in their attenuation relationship. In particular, the measure of the site-to-source distance, D , which is employed in the attenuation equations varies among common attenuation relationships. There are several variations of site-to-source distance used by different attenuation modelers, as discussed in Chapter 2 and depicted in Figure 3-5.

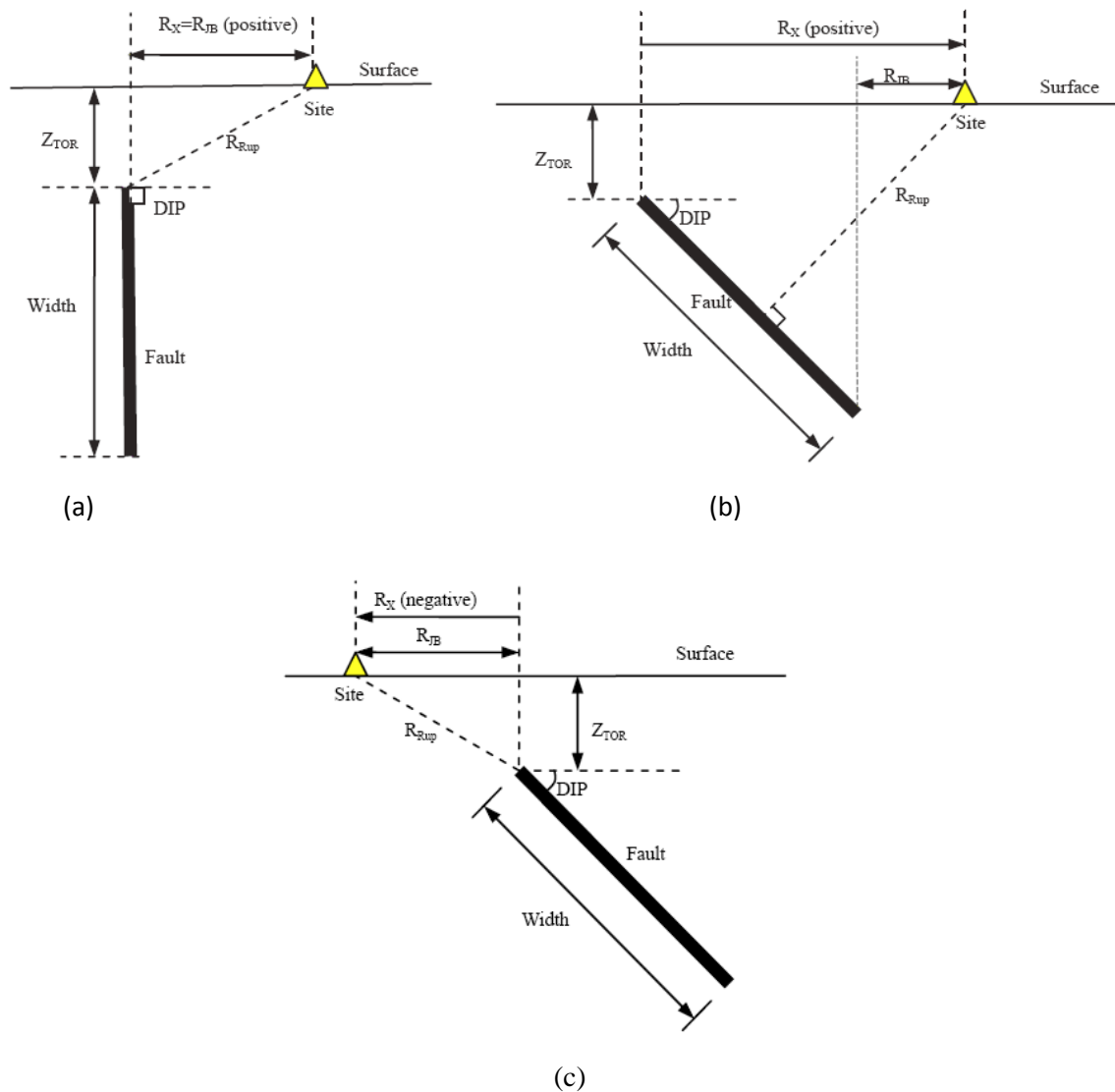


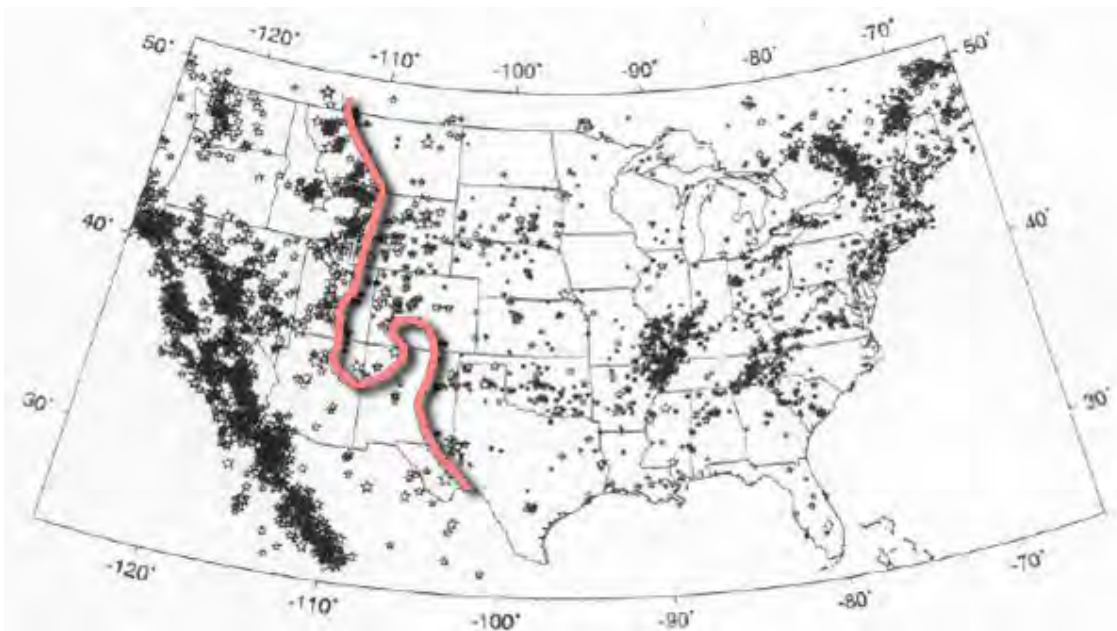
Figure 3-5 Variation in Definitions on Distance (site to seismic source) in Commonly Used Attenuation Relationships; (a) Strike Slip Faulting; (b) Reverse or Normal Faulting, Hanging-wall Site; (c) Reverse or Normal Faulting, Foot-wall Site

The role the attenuation relationship(s) play in the outcome of both probabilistic and deterministic seismic hazard analysis cannot be over-emphasized. Furthermore, the state-of-the-art on this subject is constantly evolving: almost every major earthquake has led to a change in attenuation relationships. As the state-of-the-art progresses, these relationships become more complex and greater expertise may become necessary in selecting and implementing the appropriate relationships. For example, attenuation relationships are particularly sensitive to tectonic regime. In the United States, the tectonic regimes that may be encountered include:

- 1) Shallow crustal earthquakes along active tectonic boundaries, e.g. for the western U.S.
- 2) Subduction zone earthquakes in Alaska and the northwestern U.S.
- 3) Stable continental regions in the central and eastern U.S.
- 4) Extensional tectonic regions such as those in Nevada and Arizona

As noted above and in Chapter 2, the current viewpoint among seismologists is that there are fundamental differences in strong motion attenuation between different tectonic regimes such as between the western U.S. (WUS) and the central and eastern U.S. (CEUS), leading to the adoption of different attenuation models in different regimes. The boundary between WUS and CEUS tectonic regimes is shown in Figure 3-6, lying approximately along the Rocky Mountains. West of this boundary is referred to as the more seismically active WUS region and east of the boundary is the less active CEUS region. In general, probabilistic ground shaking levels are higher in the WUS compared to the CEUS due to higher activity rates, especially at longer spectral periods (for example, 0.5 seconds or more). However, ground motions appear to attenuate with distance less rapidly in the CEUS compared to the WUS.

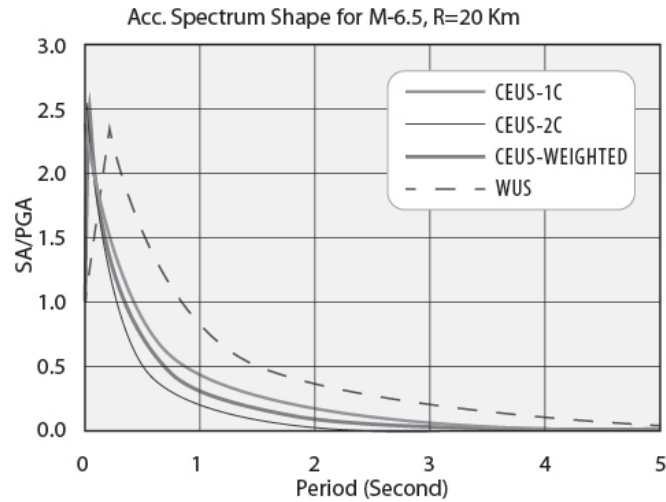
USGS Seismic Hazard Regions



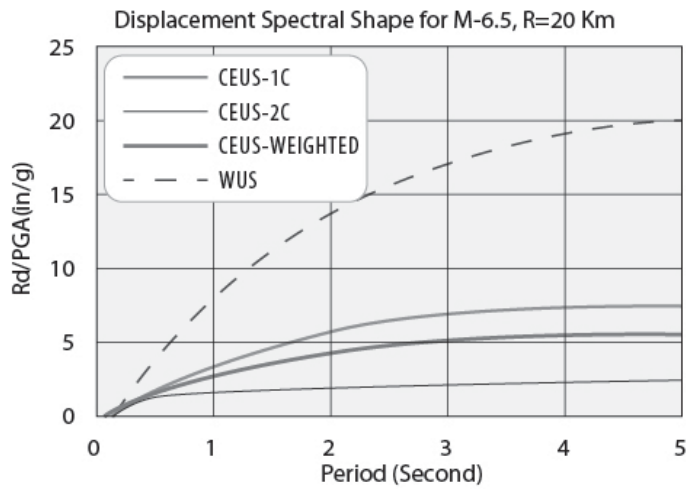
Note: Different attenuation relationships used for different regions

Figure 3-6 Boundary Defining WUS and CEUS Seismic Hazard Regions Based on Change in Attenuation Relationship (USGS, 2002)

Figure 3-7 compares spectral shapes from WUS and CEUS attenuation models for a typical Magnitude 6.5 event at a site-to-source distance of 12 miles (20 km). The CEUS curves in Figure 3-7 includes two attenuation models to compensate for the lack of sufficient strong motion data plus and a third curve that is a weighted average of the first two models. Figure 3-7a presents a comparison of the acceleration response spectra shapes (i.e. the acceleration response spectra normalized by their respective PGA) and Figure 3-7b presents a comparison of displacement response spectra shapes.



(a)



(b)

Figure 3-7 Comparison between Spectral Curve Shapes for the WUS and CEUS Hazard Regions (after NUREG, 2001); (a) Acceleration Spectra for M=6.5, and R=20 km; (b) Displacement Spectra for M=6.5, and R=20 km

The CEUS acceleration response spectra shape in Figure 3-7a has a higher amplitude than the WUS spectral curve shape at shorter spectral periods ($T < 0.1$ sec). The WUS spectral curve shape is higher than the CEUS curve shape for spectral periods greater than 0.1 second, the range of periods of importance in most structural designs. At a period of one second, the normalized WUS spectral acceleration is about twice the normalized CEUS acceleration. The normalized WUS acceleration spectral amplitude is over 3 times the normalized amplitude of CEUS spectrum at a period of 3 seconds. Furthermore, there may be even more intense, long-period motions associated with forward directivity of near-fault ground motions that can be encountered in the WUS (as discussed subsequently).

Table 3-1 summarizes several of the attenuation relationships used to develop the 2002 USGS National Seismic Hazard Maps. The 2002 USGS National Seismic Hazard Maps provide the basis for current AASHTO seismic design criteria. There is a more recent 2008 update to these 2002 maps and some building codes (but not AASHTO) require the use of ‘the most current version of the USGS National Seismic Hazard Maps’. During deliberations on the current seismic design criteria, AASHTO decided that, whereas there are good rationales to continuously implement the updated USGS National Seismic Hazard Maps, changes to the AASHTO design criteria need to be managed by the AASHTO balloting process for technical stability and to control cost impacts. Therefore, it was decided that AASHTO would not automatically adopt new USGS maps upon their dissemination and that the 2002 USGS maps would remain the basis for seismic design of transportation facilities at the current time.

There are three general categories of attenuation relationships presented in Table 3-1: one for each of the three predominant tectonic regimes associated with the United States. These tectonic regimes are categorized as follows: (1) shallow crustal earthquakes in the western U.S. (including extensional and volcanic faulting regimes), (2) intra-plate earthquakes in the central and eastern U.S. and (3) subduction zone earthquakes in the Pacific Northwest, Alaska, and the Caribbean. Category 1 includes both the active tectonic regime along the west coast of the US, the extensional tectonic regime in Arizona and Nevada, and earthquakes associated with volcanism in Hawaii and the Pacific northwest. The attenuation equations for shallow crustal earthquakes and, to a lesser extent, subduction zone earthquakes are based on empirical strong motion recordings. However, there are little strong motion data from significant intraplate earthquakes in the central and eastern U.S. (CEUS), or from other analogous tectonic regimes around the world, that is suitable for developing intraplate earthquake attenuation equations.

TABLE 3-1 SELECTED ATTENUATION RELATIONSHIPS USED TO DEVELOP USGS SEISMIC HAZARD MAPS

Attenuation Relationship for Western US (Shallow Crustal Earthquakes)

No.	Reference	Attenuation Equation	Standard Deviation	Explanation
1	Abrahamson and Silva (1997)	$\ln Sa(g) = a_1 + a_2(M-c_1) + a_{12}(8.5-M)^0 + [a_3 + a_{13}(M-c_1)] \ln R$ for $M \leq 6.4$ $\ln Sa(g) = a_1 + a_4(M-c_1) + a_{12}(8.5-M)^0 + [a_3 + a_{13}(M-c_1)] \ln R$ for $M > 6.4$	$\sigma_{\text{site}}(M) = \begin{cases} b_4 \text{ for } M \leq 5.0 \\ b_5 - b_6(M-5) \text{ for } 5.0 < M < 7.0 \\ b_5 - 2b_6 \text{ for } M \geq 7.0 \end{cases}$	$R = \sqrt{(r_{rup}^2 + c_4^2)}$ where r_{rup} is the closest distance to the rupture surface and $a_1, a_2, a_3, a_4, a_{12}, a_{13}, b_1, b_2, c_1$ and c_4 are regression coefficients.
2	Boore et al. (1997)	$\ln Sa(g) = b_1 + b_2(M-6) + b_{11}(M-6)^2 + b_5 \ln r$	Period dependent standard of deviations in tables.	$r = \sqrt{r_{3b}^2 + h^2}$ where b_1, b_2, b_3, b_5 and h are regression coefficients.
3	Campbell (1997)	$\ln PGA(g) = -3.512 + 0.904M - 1.328 \ln \sqrt{R_{seis}^2 + [0.149 \exp(0.64M)]^2}$	For PGA $\sigma = 0.55$ for $PGA < 0.068g$ $\sigma = 0.173 - 0.14 \ln(PGA)$ for $0.068 \leq PGA \leq 0.2g$ $\sigma = 0.39$ for $PGA > 0.2g$	R_{seis} is Distance to Seismogenic Zone. c_1, c_2, c_3, c_4 , and c_5 are regression coefficients.
		$\ln Sa(g) = \ln(PGA) + c_1 + c_2 \tanh [c_3(M-4.7)] + (c_4 + c_5 M)R_{seis}$	For S_s $\sigma = 0.889 - 0.069 \ln M$ when $M < 7.4$ $\sigma = 0.38$ for $M \geq 7.4$	
4	Sadigh et al (1997)	$\ln Sa(g) = c_1 + c_2 M + c_3(8.5M)^2 + c_4 \ln [r_{rup} + \exp(c_5 + c_6 M)] + c_7 \ln (r_{rup} + 2)$	Period and magnitude dependent standard of deviations in tables.	r_{rup} is the closest distance to the rupture surface and $c_1, c_2, c_3, c_4, c_5, c_6$, and c_7 are regression coefficients.

Notes:

Only the most basic form of attenuation equations are presented above. Most of the authors above included additional modification factors applied to the above equations for style of faulting, site factors, and other (e.g. Hanging wall) effects.

M is Moment Magnitude, M_w in above cited attenuation equations.

Attenuation Relationship for Subduction Zone Earthquakes

No.	Reference	Attenuation Equation	Standard Deviation	Explanation
1	Atkinson, G.M. and Boore, D.M. (2002)	$\ln Sa(g) = c_1 + c_2(M) + c_3 h + c_4 R - g \log R$	Period dependent standard deviations in tables.	$R = \sqrt{(D_{sub}^2 + \Delta^2)}$ where D_{sub} is the closest distance to fault surface in kilometers, and Δ is given by $\Delta = 0.00724 \times 10^{0.697M}$, h is focal depth in kilometers no larger than 100, and c_1, c_2, c_3, c_4 are regression coefficients that varies depending on (i) interface or (ii) inter slab event.
2	Gregor et al., (2002)	$\ln Sa(g) = c_1 + c_2(M) + (c_3 + c_4 M) \ln [R + \exp(c_5)] + c_6 (M-10)^3$	Period dependent standard deviations in tables.	R is the closest distance to fault surface in kilometers, and c_1, c_2, c_3, c_4 and c_5 are regression coefficients that varies depending on soil or rock sites.

Attenuation Relationship for Central Eastern US (CEUS) Earthquakes

No.	Reference	Attenuation Equation	Standard Deviation	Explanation
1	Atkinson, G.M. and Boore, D.M. (1995)	$\log Sa(\text{cm/s}^2) = c_1 + c_2(M-6) + c_3(M-6)^2 - \log R - c_4 R$	Frequency dependent varying from 0.24 to 0.27	R is the closest distance to the seismic source zone in kilometers, and c_1, c_2, c_3, c_4 are regression coefficients. Note that S_a in the regression equation is in cm/s^2 as opposed to in g 's and instead of natural logarithm, the logarithm is in based 10 for this equation as opposed to natural log for other cited equations.

Therefore, the CEUS attenuation equations are based largely on analytical and numerical modeling of strong motion attenuation in these regions. Toro et al. (1997) discuss the uncertainties associated with CEUS attenuation relationships and present another CEUS attenuation relationship commonly used in practice.

The attenuation relationships listed in Table 3-1 provide for prediction not only of the PGA but also of the spectral acceleration at various periods. While all of these equations depend upon site-to-source distance, each attenuation model uses a different definition for distance. Figure 3-5 illustrates the differences among the various distance definitions used in these models. The equations for shallow crustal earthquakes presented in Table 3-1 are simplified versions of the complete attenuation equations for these models in that they apply solely to strike-slip earthquakes at rock sites. The complete equations include additional terms and coefficients to account for style of faulting, site soil conditions, and which side of the fault the site is on (for thrust faulting). The treatment of uncertainty (i.e. values of equations for the standard deviation) also varies widely among different attenuation equations. However, all of the attenuation relationships in Table 3-1 assume a log normal distribution for the ground motion. Therefore, only the standard deviation is required to characterize the uncertainty in the predicted median response spectral acceleration values. However, the standard deviation typically depends upon magnitude and distance.

The widely used Abrahamson and Silva (1997) attenuation relationship (one of the relationships used to represent attenuation in shallow crustal earthquakes when developing the 2002 USGS maps) can be used to illustrate some of the important features of an attenuation relationship. Table 3-2 presents the regression coefficients used to predict the median spectral acceleration for the 1997 Abrahamson and Silva attenuation equation. These coefficients can be used in the basic equation shown in Table 3-1 to compute the spectral acceleration for any combination of magnitude and distance for a scenario earthquake. Abrahamson and Silva (1997) tabulated the regression coefficients for 28 spectral periods ranging from 0.01 second to 5 second. Note that, because the equations predict the log of the spectral acceleration, there is no coefficient for a spectral period of zero, the spectral period corresponding to the PGA. Instead, the spectral acceleration at a spectral period of 0.01 is used to represent the PGA.

To illustrate the use of the Abrahamson and Silva (1997) attenuation equation, consider a site located 10 kilometers from the fault rupture plane of a moment magnitude 7 strike-slip earthquake (i.e. $M_w = 7$ and $R_{rup} = 10$ km). From Table 3-2, at period of 0.01 second (the period used to find the PGA), the regression coefficients are: $a_1 = 1.64$, $a_4 = -0.144$, $c_1 = 6.4$, $a_{12} = 0$, $n = 2$, $a_3 = -1.145$, $a_{13} = 0.17$ and $c_4 = 5.6$.

TABLE 3-2 COEFFICIENTS FOR THE ABRAHAMSON AND SILVA (1997) ATTENUATION MODEL

Period	c ₄	a ₁	a ₂	a ₃	a ₄	a ₅	a ₆	a ₉	a ₁₀	a ₁₁	a ₁₂	a ₁₃	c ₁	c ₅	n
5.00	3.50	-1.460	0.512	-0.7250	-0.144	0.400	-0.200	0.000	0.664	0.040	-0.2150	0.17	6.4	0.03	2
4.00	3.50	-1.130	0.512	-0.7250	-0.144	0.400	-0.200	0.039	0.640	0.040	-0.1956	0.17	6.4	0.03	2
3.00	3.50	-0.690	0.512	-0.7250	-0.144	0.400	-0.156	0.089	0.630	0.040	-0.1726	0.17	6.4	0.03	2
2.00	3.50	-0.150	0.512	-0.7250	-0.144	0.400	-0.094	0.160	0.610	0.040	-0.1400	0.17	6.4	0.03	2
1.50	3.55	0.260	0.512	-0.7721	-0.144	0.438	-0.049	0.210	0.600	0.040	-0.1200	0.17	6.4	0.03	2
1.00	3.70	0.828	0.512	-0.8383	-0.144	0.490	0.013	0.281	0.423	0.000	-0.1020	0.17	6.4	0.03	2
0.85	3.81	1.020	0.512	-0.8648	-0.144	0.512	0.038	0.309	0.370	-0.026	-0.0927	0.17	6.4	0.03	2
0.75	3.90	1.160	0.512	-0.8852	-0.144	0.528	0.057	0.331	0.320	-0.500	-0.0862	0.17	6.4	0.03	2
0.60	4.12	1.428	0.512	-0.9218	-0.144	0.557	0.091	0.370	0.194	-0.890	-0.0740	0.17	6.4	0.03	2
0.50	4.30	1.615	0.512	-0.9515	-0.144	0.581	0.119	0.370	0.085	-0.121	-0.0635	0.17	6.4	0.03	2
0.46	4.38	1.717	0.512	-0.9652	-0.144	0.592	0.132	0.370	0.200	-0.136	-0.0594	0.17	6.4	0.03	2
0.40	4.52	1.860	0.512	-0.9880	-0.144	0.610	0.154	0.370	-0.065	-0.160	-0.0518	0.17	6.4	0.03	2
0.36	4.62	1.955	0.512	-1.0052	-0.144	0.610	0.170	0.370	-0.123	-0.173	-0.0460	0.17	6.4	0.03	2
0.30	4.80	2.114	0.512	-1.0350	-0.144	0.610	0.198	0.370	-0.219	-0.195	-0.0360	0.17	6.4	0.03	2
0.24	4.97	2.293	0.512	-1.0790	-0.144	0.610	0.232	0.370	-0.350	-0.223	-0.0238	0.17	6.4	0.03	2
0.20	5.10	2.406	0.512	-1.1153	-0.144	0.610	0.260	0.370	-0.445	-0.245	-0.0138	0.17	6.4	0.03	2
0.17	5.19	2.430	0.512	-1.1350	-0.144	0.610	0.260	0.370	-0.552	-0.265	-0.0040	0.17	6.4	0.03	2
0.15	5.27	2.407	0.512	-1.1450	-0.144	0.610	0.260	0.370	-0.557	-0.280	0.0050	0.17	6.4	0.03	2
0.12	5.39	2.272	0.512	-1.1450	-0.144	0.610	0.260	0.370	-0.591	-0.280	0.0180	0.17	6.4	0.03	2
0.10	5.50	2.160	0.512	-1.1450	-0.144	0.610	0.260	0.370	-0.598	-0.280	0.0280	0.17	6.4	0.03	2
0.09	5.54	2.100	0.512	-1.1450	-0.144	0.610	0.260	0.370	-0.609	-0.280	0.0300	0.17	6.4	0.03	2
0.075	5.58	2.037	0.512	-1.1450	-0.144	0.610	0.260	0.370	-0.628	-0.280	0.0300	0.17	6.4	0.03	2
0.06	5.60	1.940	0.512	-1.1450	-0.144	0.610	0.260	0.370	-0.665	-0.280	0.0300	0.17	6.4	0.03	2
0.05	5.60	1.870	0.512	-1.1450	-0.144	0.610	0.260	0.370	-0.620	-0.267	0.0280	0.17	6.4	0.03	2
0.04	5.60	1.780	0.512	-1.1450	-0.144	0.610	0.260	0.370	-0.555	-0.251	0.0245	0.17	6.4	0.03	2
0.03	5.60	1.590	0.512	-1.1450	-0.144	0.610	0.260	0.370	-0.470	-0.230	0.0143	0.17	6.4	0.03	2
0.02	5.60	1.640	0.512	-1.1450	-0.144	0.610	0.260	0.370	-0.417	-0.230	0.0000	0.17	6.4	0.03	2
0.01	5.60	1.640	0.512	-1.1450	-0.144	0.610	0.260	0.370	-0.417	-0.230	0.0000	0.17	6.4	0.03	2

For $R_{rup} = 10$ kilometer, the distance parameter R in the attenuation equation is calculated as:

$$R = \sqrt{R_{rup}^2 + c_4^2} = \sqrt{10^2 + 5.6^2} = 11.46$$

From the basic attenuation equation for the median spectral acceleration at 0.01 second (i.e. the median PGA), we get:

$$\begin{aligned} \ln S_a(g) &= a_1 + a_4(M - c_1) + a_{12}(8.5 - M)^n + [a_3 + a_{13}(M - c_1)] \ln(R) \\ &= 1.64 - 0.144(7 - 6.4) + 0(8.5 - 7)^2 + [-1.145 + 0.17(8 - 6.4)] \ln(11.46) \\ &= -0.99025. \end{aligned}$$

Hence, the median PGA from the Abrahamson and Silva (1997) attenuation equation for $M_w=7$ and $R_{rup}=10$ would be $e^{-0.99025}$, or 0.371 g.

Abrahamson and Silva (1997) also define a magnitude-dependent standard deviation, σ , in their model. For $M_w = 7$, the standard deviation is given by the following equation.

$$\sigma = b_5 - 2b_6 = 0.7 - 2(0.135) = 0.43$$

Based upon the assumption of a log normal distribution for the ground motion, the median-minus-sigma (84th percentile) PGA would then be:

$$\exp(-0.99025-0.43) = \exp(-1.42025) = 0.242 \text{ g}$$

and the median-plus-sigma (16th percentile) PGA would be:

$$\exp(-0.99025+0.43) = \exp(-0.56035) = 0.571 \text{ g.}$$

Using the regression coefficients tabulated for the other spectral periods in Table 3-2, one can solve for the corresponding median, median-minus-sigma, and median-plus-sigma spectral ordinates at other periods. This data can then be used to plot the median, median-minus-sigma, and median-plus-sigma acceleration response spectra shown in Figure 3-8 for the M_w 7 strike-slip scenario earthquake at a rupture distance, R_{rup} , 10 kilometers from the site.

As noted above, there are many variations among specific attenuation relationships and these relationships are constantly being updated. For instance, a set of Next Generation Attenuation (NGA) relationships for shallow crustal earthquake in the western US (discussed briefly in Section 3.5 of this chapter) were recently published. Readers are encouraged to refer to the cited publications for complete details of these relationships, including the attenuation coefficients and any special conditions or constraints considered for specific attenuation models.

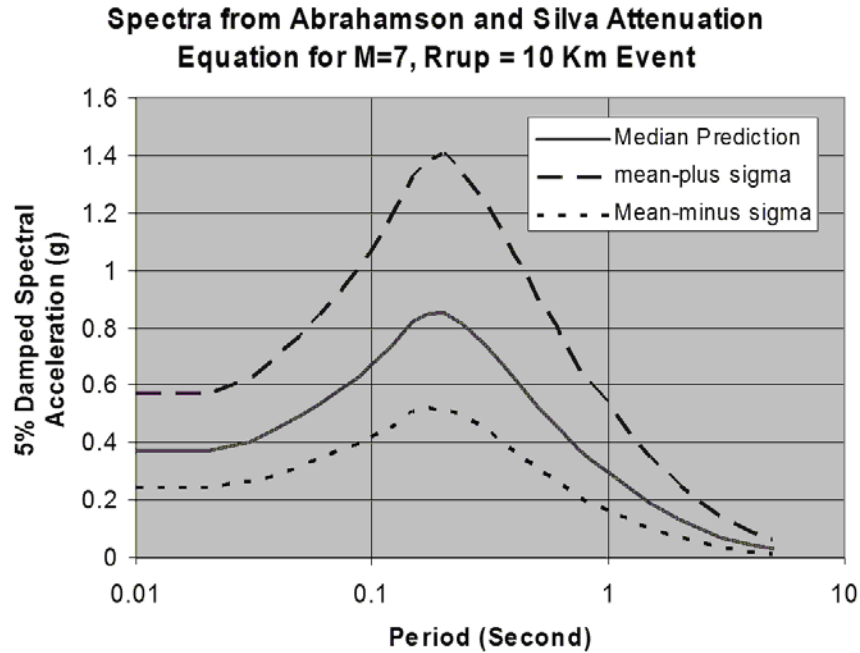


Figure 3-8 Acceleration Response Spectra from Abrahamson and Silva (1997)

3.2.4 Uniform Hazard Spectra

An essential output from a probabilistic seismic hazard analysis is a plot of the ground motion parameter of interest, say PGA, versus the annual probability of exceeding that parameter. This plot is called a seismic hazard curve. Figure 3-9 shows a plot of PGA versus the annual probability of exceedance (i.e. the seismic hazard curve) from the seismic hazard analysis for a port facility in southern California. The inverse of the annual probability of exceedance (return period in years, i.e. the average interval between earthquake ground motions equal to or greater than the associated value), is shown on the right vertical axis. Figure 3-9 shows not only the total probability of exceedance at the site but also the contributions from individual seismic sources for this example. The annual probability of exceedance from each source is summed to give the total hazard curve as shown in Figure 3-9.

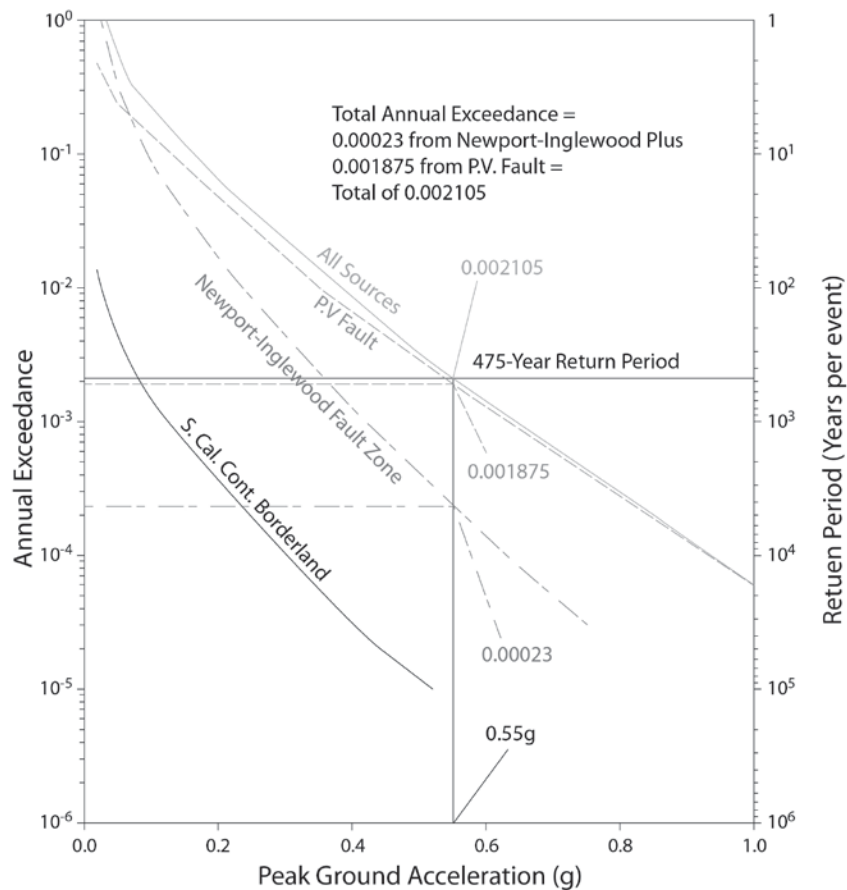


Figure 3-9 Seismic Hazard Curves for Site in Southern California: Total Hazard and Individual Contributions from Three Major Faults

A hazard curve such as the one in Figure 3-9 may be used in several ways. For example the level of ground motion with a 10% probability of exceedance in 50 years at this site, is 0.55g. (10% exceedance in 50 years is an annual exceedance of 0.0021, or a return period of 475 years.) This same curve indicates that if the return period was doubled to 1,000 years the design ground motion would be 0.65g, so it can be observed that doubling the return period does not double the design ground motion. Similarly, if a bridge at this site has an elastic strength that is exceeded when the design ground motion exceeds 0.2g, the elastic capacity of the bridge will be exceeded about once every 15 years (annual probability of exceedance for this ground motion = 0.07).

Similar hazard curves can be generated for the spectral acceleration at selected spectral periods. Then, by plotting the spectral acceleration against period for a specified annual probability of exceedance, a

uniform hazard acceleration response spectrum for the specified annual probability of exceedance (or specified return period) can be extracted from these hazard curves. The resulting spectrum is called a uniform hazard spectrum (UHS) because the ground motion parameter at all periods in this spectrum represents the same, consistent seismic hazard level, or return period.

3.2.5 Return Period and Seismic Risk

The return period is a fundamental parameter for quantifying the risk assumed in design. The inverse of the return period in years is essentially the annual risk. As noted earlier, AASHTO adopted a 1,000-year return period (corresponding to a 0.001 annual risk) in 2007 for the no-collapse design limit state for ordinary bridges. Therefore, under the AASHTO criteria for seismic design of ordinary bridges, damage may be expected to occur when the bridge is subjected to the 1,000-year ground motions but collapse of one or more spans and loss of life is not expected. The annual risk level of 0.001 associated with the 1,000 year return period ground motion may be compared to that for other natural hazards such as extreme weather (floods and high wind) when making decisions regarding the risk level for design. An annual risk of 0.001 is lower than the annual risk associated with bridge design for flooding and scour, but public acceptance of the risk associated with the widespread loss of life, damage and business disruption that may occur in a major earthquake dictates this criterion for seismic design. Furthermore, in some circumstances even lower risk levels than that associated with the AASHTO 1,000-year return period may be appropriate, such as for particularly important bridges. For example, a 1,500-year return period (0.00067 annual risk) was adopted for the design of the new East Bay Spans for the San Francisco Oakland Bay Bridge, based upon recommendations from Caltrans's Seismic Advisory Board. Elsewhere, a 2,500-year return period (0.0004 annual risk) has been employed for design of other major critical water crossings in the U.S., including the seismic retrofit of several long-span bridges in New York City, and the design of the Arthur Ravenal, Jr. (Cooper River) Bridge in Charleston and the Tacoma-Narrows Second Crossing in Seattle.

While the return period (or annual risk) is a convenient way to interpret the risk associated with design ground motions, many design engineers prefer to look at the risk over the design life of a facility, sometimes referred to as the exposure period. Risk over a specified exposure period is quantified by the probability of exceedance over that exposure period. By assuming that earthquakes occur randomly (i.e. assuming a Poisson distribution of earthquake in time, e.g. that even if an earthquake occurs today, it has the same chance of occurring tomorrow), the following equation can be used to relate the probability of

exceedance, P, for an exposure period t to the annual risk γ (i.e. to the annual probability of exceedance, which is the inverse of the return period, R):

$$P = 1 - \exp(-\gamma \times t) \quad 3-5$$

At relatively small probabilities of exceedance (e.g. 10% or less), this exponential relationship in Equation 3-5 can be replaced by a simple proportional relationship between the annual risk and the exposure period, t, or return period, R:

$$P = t \times \gamma \quad 3-6$$

$$P = \gamma / R \quad 3-7$$

So, for example, for a return period of 1,000-year, $\gamma=0.001$ and the probability of exceedance during a 50-year exposure period ($t = 50$ years) is about 5% in accordance with Equations 3-6 and 3-7. If the exposure period becomes 75 years (a common assumption for the design life of highway bridges), the probability of exceedance is approximately 7% for a 1,000-year return period. Note, however, that at higher probabilities of exceedance (e.g. for a 50% probability of exceedance in 75 years), the exponential relationship in Equation 3-5 must be used.

Care must be exercised in choosing the exposure period, or design life, for an engineered facility. If the design life is too short, the design earthquake ground motion can become so low that it has little chance of representing the ground motion in a real earthquake. Also, while a design life of 50 years is commonly assumed for economic analysis of many engineered structures, this rarely represents the true exposure period for a transportation facility, especially for more critical structures. For example, the Manhattan Bridge in New York City was opened to traffic in 1909. The bridge has now been in service for about 100 years. But, it is inconceivable that this bridge would be demolished today and chances are that with routine maintenance it will be in service for at least another 50 years. However, if the designer assumes a very long design life for a critical structure (e.g. 2500 years), the probabilistic design ground motions may become exceedingly high, in some cases significantly greater than the median value of or even median plus one standard deviation from the maximum magnitude earthquake for the site (particularly in areas of high seismicity). For this reason, some seismic codes and design specifications place a deterministic cap on the level of ground motions used in design.

3.2.6 De-aggregation of Design Earthquake, Magnitude and Distance

While the uniform hazard spectrum (UHS) is the most common means of characterizing the seismic hazard for use in design, some structural and many geotechnical analyses require additional information about the design earthquake that is associated with the UHS, e.g. the earthquake magnitude. Magnitude is used, for example, when developing acceleration time histories for structural and geotechnical time history analyses. The UHS typically consists of contributions for many different combinations of earthquake magnitude and distance. To obtain information on a representative earthquake magnitude, the UHS can be decomposed into the contributions from individual seismic sources and the corresponding magnitude and distance combinations through a process known as deaggregation. This process enables the identification of the magnitude and distance combinations that make the most significant contributions to the seismic hazard. The deaggregated magnitude information can also be used to determine the representative magnitude for magnitude-dependent analyses, including the evaluation of liquefaction potential, as well as for selection of representative time histories.

Selecting a design earthquake magnitude from the deaggregated magnitude data is complicated because each spectral period in a UHS will have a different, unique magnitude deaggregation. The dependence of magnitude deaggregation on spectral period occurs because the dependence of earthquake ground motion attenuation upon magnitude and distance is different for every spectral period. The spectral acceleration at short periods (including the zero period, or peak ground acceleration) tends to attenuate faster than at longer periods. Furthermore, large magnitude earthquakes tend to have more energy at longer periods when compared to smaller magnitude events. Therefore, magnitude deaggregation for shorter spectral periods tend to be biased towards smaller magnitude and closer earthquakes compared to the magnitude deaggregation for longer spectral periods. Table 3-3 illustrates this effect, presenting the magnitude deaggregation for the seismic hazard at a site in Bakersfield, California at periods of 0.0 second (the PGA) and 1.0 second (a frequency of 1 Hz) for a 2,500-year return period. For the PGA, almost 70% of the hazard is associated with earthquakes of Magnitude 6.5 or less, and almost 92% of the hazard is associated with an earthquake of magnitude 7 or less. At a period of 1 second, over 50% of the hazard is associated with earthquakes of magnitude 7.5 or greater. Therefore, selection of a single representative magnitude for design may still be a subjective decision made of the basis of engineering judgment. This judgment should be guided by the engineer's understanding of the sensitivity of the analysis for which magnitude is required to spectral period.

TABLE 3-3 MAGNITUDE DEAGGREGATION FOR BAKERSFIELD, CALIFORNIA, FOR A 2500 YR RETURN PERIOD

Deaggregated Seismic Hazard PE = 2% in 50 years pga										
Bakersfield CA 35.373 deg N 119.018 deg W PGA=0.42440 g										
M<=	5.0	5.5	6.0	6.5	7.0	7.5	8.0	8.5	9.0	
d<= 25.	0.000	18.239	18.339	32.288	18.484	0.000	0.000	0.000	0.000	
50.	0.000	0.019	0.024	0.086	4.200	7.059	0.000	0.000	0.000	
75.	0.000	0.000	0.001	0.006	0.033	0.019	1.154	0.000	0.000	
100.	0.000	0.000	0.000	0.000	0.015	0.008	0.000	0.000	0.000	
125.	0.000	0.000	0.000	0.000	0.009	0.002	0.000	0.000	0.000	
150.	0.000	0.000	0.000	0.000	0.001	0.003	0.000	0.000	0.000	
175.	0.000	0.000	0.000	0.000	0.001	0.000	0.000	0.000	0.000	
200.	0.000	0.000	0.000	0.000	0.007	0.002	0.000	0.000	0.000	

Deaggregated Seismic Hazard PE = 2% in 50 years lhz										
Bakersfield CA 35.373 deg N 119.018 deg W SA= 0.38360 g										
M<=	5.0	5.5	6.0	6.5	7.0	7.5	8.0	8.5	9.0	
d<= 25.	0.000	0.957	2.329	17.096	16.216	0.000	0.000	0.000	0.000	
50.	0.000	0.004	0.019	0.272	12.374	23.708	0.000	0.000	0.000	
75.	0.000	0.000	0.001	0.019	0.254	0.208	26.228	0.000	0.000	
100.	0.000	0.000	0.000	0.001	0.074	0.097	0.000	0.000	0.000	
125.	0.000	0.000	0.000	0.001	0.037	0.016	0.000	0.000	0.000	
150.	0.000	0.000	0.000	0.000	0.006	0.029	0.008	0.000	0.000	
175.	0.000	0.000	0.000	0.000	0.002	0.006	0.000	0.000	0.000	
200.	0.000	0.000	0.000	0.000	0.015	0.025	0.000	0.000	0.000	

Another complicating factor when selecting a design magnitude from deaggregation data is the distributed nature of the magnitude data. Sometimes, the magnitude deaggregation falls in a narrow band, as illustrated by the bold points in Table 3-3. In this case, selection of the dominant magnitude for a given period is relatively straight forward. However, in some cases the magnitude distribution is broadly distributed or multi-modal. Figure 3-10 graphically illustrates the bi-modal distribution of the deaggregated seismic hazard for Augusta, Georgia, at a period of 1.0 second for a 2,500-year return period. The deaggregated magnitude in this case is split between two major seismic sources: the M_w 7.3 Charleston source and the M_w 8.0 New Madrid source. While the Charleston source contributes a greater percentage to the overall hazard (and is thus identified in the figure as the dominant source), the New Madrid source is potentially more damaging to certain types of structures. Furthermore, if the site of interest is moved closer to New Madrid and away from Charleston, the magnitude distribution would become more weighted towards the larger New Madrid event. The choice of dominant magnitude is therefore not that straight forward and requires engineering judgment.

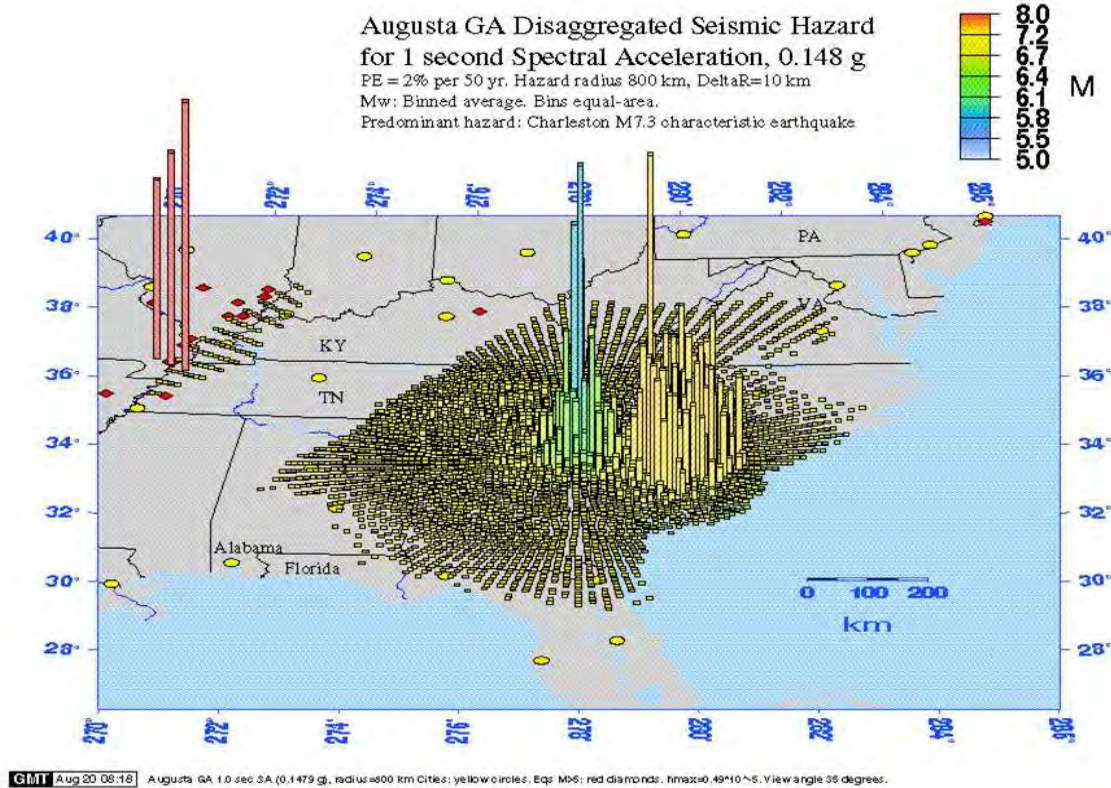


Figure 3-10 Magnitude Deaggregation for Augusta, GA, at 1.0 sec Period for a 2500-year Return Period: Predominant Hazard is Charleston M7.3 Characteristic Earthquake

3.2.7 Deterministic Maximum Magnitude and Ground Motion Evaluation

In a deterministic seismic hazard analysis, individual earthquake scenarios (i.e. earthquakes of a specified magnitude and location) are developed for each relevant seismic source. The design ground motion parameter is then calculated for each earthquake scenario. Typically, either (i) the median (i.e. the zero standard deviation), or (ii) the median-plus-one standard deviation (i.e., the 84-percentile confidence limit) ground motion attenuation relationship is employed to compute the design ground motion parameter, depending on the potential consequences of failure. The maximum value of this parameter from all of the scenario earthquakes is then employed for design. The approach is ‘deterministic’ in the sense that a single value of the design ground motion parameter corresponding to a deterministic magnitude and distance is selected for design.

In practice, the scenario earthquake for each seismic source is usually some sort of maximum magnitude event, e.g. the maximum magnitude expected in the currently known tectonic framework (sometimes

termed the maximum credible earthquake, or MCE) or the maximum magnitude earthquake expected during some specified exposure period (for instance, over a 100-year period). Furthermore, this maximum magnitude event is usually placed at the closest approach of the seismic source to the site, sometimes referred to as the “worst case scenario.” However, if the median ground motion attenuation relationship is used, as is the current practice for many transportation facilities that use the deterministic approach, the resulting ground motion will not, in fact, be a worst case scenario. When the median attenuation relationship is used, 50% of the time an earthquake of the maximum magnitude occurs at the specified location the ground shaking will exceed the median value. Furthermore, if the goal of the deterministic analysis is to determine the most damaging event, it may be necessary to consider more than one scenario event in the design analysis, as damage depends upon both the intensity of shaking and the duration of shaking. So, it may not be possible to distinguish *a priori* whether the most damaging event is a nearby relatively small magnitude event or a more distant larger magnitude event with a smaller intensity.

3.2.8 Probabilistic versus Deterministic Analysis Methods

In the probabilistic seismic hazard approach, the relative likelihood of all possible and relevant earthquake scenarios (all possible magnitude and location combinations capable of inflicting damage) are considered along with the range of possible ground motion probability levels. Therefore, the probabilistic approach incorporates uncertainties with respect to earthquake location, magnitude, and ground motion attenuation, producing a weighted average of all possibilities that is a best estimate of the hazard associated with seismic activity. For this reason, the probabilistic approach is often considered an appropriate basis for making rational design decisions about risk versus benefit. The probabilistic approach has been widely adopted by the engineering community for use in establishing design ground motions. However, even after the probabilistic approach has been embraced, a decision still must be made about the appropriate level of hazard to use in design.

For critical engineering facilities (e.g. lifeline bridges, hospitals, nuclear power plants, and high hazard dams), engineers and other decision makers are sometimes uncomfortable with use of a probabilistically-based design level. Oftentimes, the decision makers express a desire to design these critical facilities for a so called worst case scenario. In such cases, the deterministic approach of employing a Maximum Credible Earthquake (maximum magnitude earthquake) is sometimes used. However, as noted above, the deterministic approach may not necessarily lead to a worst case ground motion prediction, particularly

if the median attenuation relationship is used, due to uncertainties regarding ground motion attenuation. Use of a median plus one standard deviation (84 percentile) ground motion level, as practiced for some critical structures (e.g. high hazard dams and sometimes critical buildings such as hospitals and schools) can provide a higher level of certainty regarding the maximum anticipated ground motions. However, designing to an 84 percentile attenuation basis is not traditionally done by transportation agencies, as it often results in extremely costly seismic design requirements. In fact, the risk associated with either the median or 84 percentile ground motions from a deterministic seismic hazard analysis is unknown because the analysis only considers uncertainty with respect to ground motion attenuation and does not consider uncertainties with respect to earthquake location, magnitude, or rate of occurrence.

As noted previously, designing to an arbitrarily high probabilistic design level (i.e. a very long return period) can also produce unrealistically high ground motions due to compounding of uncertainties at low probability levels. One alternative approach that has been used for design of important facilities to compensate for the deficiencies in both probabilistic and deterministic analyses is to combine these two approaches. For example, Caltran's seismic peer review panel and the state of California Seismic Safety Advisory Board recommended the use of both probabilistic and deterministic ground motion levels (including considering both median and median-plus one standard deviation values for the deterministic scenario events) when setting the design ground motions for the Toll Bridge Retrofit Program in California.

In summary, fundamentally there is relatively little difference in the basic methodology for deterministic and probabilistic seismic hazard approaches. The probabilistic approach can be regarded as an approach providing explicitly defined hazard levels in terms of return period or the annual rate of exceedance for use in design: information that can then be the basis for design decisions balancing cost versus risk. The estimated hazard from a probabilistic assessment can also be compared to the hazard associated with other extreme environmental loading conditions to produce a balanced design. A probabilistic approach also has the merit of being able to distinguish relative contributions to the hazard from the more active versus less active faults. However, a deterministic hazard approach is simpler than a probabilistic approach and can be conducted by most engineers (probabilistic analyses should preferably be conducted by qualified professionals who specialize in this area). It is very difficult, and sometimes impossible, to verify probabilistic solutions by independent checks. Furthermore, as noted previously, the results of probabilistic hazard solutions can sometimes be unreasonable, or at least questionable, at very long return periods (low probability levels). It is generally believed prudent to, as a minimum, employ deterministic solutions as a sanity check on the results of probabilistic analyses for long return periods. To account for

the large uncertainties associated with low probability levels, a median-plus-one standard deviation deterministic hazard solution using maximum magnitudes can be regarded as an upper bound on the results of a probabilistic hazard analysis when designing transportation facilities.

3.3 HAZARD LEVELS AND RETURN PERIODS FOR FUNCTIONAL AND LIFE SAFETY DESIGN

3.3.1 Performance Levels for Seismic Design

The choice of the design ground motion level, whether based upon probabilistic or deterministic analysis, cannot be considered separately from performance standard specified for the design event. Sometimes, facilities may be designed for multiple performance standards, with a different ground motion level assigned to each performance standard. Common performance standards used in design of transportation facilities include protection of life safety and maintenance of function after the event. A life safety level design earthquake criterion is routinely employed for all types of facilities in seismic design. Keeping a facility functional after a large earthquake, a more rigorous requirement than simply maintaining life safety, is often also employed for essential and critical facilities. An even more rigorous performance standard is a no damage criterion. A no damage seismic performance standard is typically only required for critical facilities, e.g. “lifeline” bridges.

Current AASHTO specifications employ a single seismic performance standard. The AASHTO seismic performance standard for conventional (or ordinary) bridges is based upon preventing collapse and protecting life safety: an ordinary bridge should not collapse and threaten life safety in the design event, though it may suffer significant damage that requires complete replacement of the structure. AASHTO seismic design provisions also note that more stringent performance standards may be appropriate for critical and essential structures (AASHTO calls for bridges are to be classified by the owner as critical, essential, and other (ordinary) bridges, in descending order of importance, depending on their function). A critical bridge is a bridge that is expected to remain open to all traffic, including for emergency vehicles and defense and security purposes, after the design earthquake. Essential bridges are bridges that are expected to be useable by emergency vehicles and for security and defense purposes after the design earthquake. Bridges that don't fall into the categories are designated as ordinary bridges. Table 3-4 presents a two-level, performance-based, set of seismic design criteria for transportation facilities that were developed for a proposed revision to the AASHTO LRFD seismic design specifications under the

sponsorship of the National Cooperative Highway Research Program (NCHRP, 2001). Two levels of design ground motions, (a 'rare' earthquake and an 'expected' earthquake), are specified for two different performance standards: 'life safety' for ordinary facilities and 'operational' for critical facilities. Performance criteria are specified for each ground motion level and performance standard. For instance, in a 'rare' earthquake, an ordinary facility is expected to suffer significant disruption in service and significant damage (but not loss of life), while a critical facility is expected to remain in service (for emergency vehicles, at a minimum) with minimal damage. In the 'expected' earthquake, both ordinary and critical facilities are expected to be serviceable after the earthquake, with an ordinary facility suffering minimal damage while a critical facility should suffer only minimal to no damage.

TABLE 3-4 PERFORMANCE BASED SEISMIC DESIGN CRITERIA FOR TRANSPORTATION FACILITIES (NCHRP, 2001)

Probability of Exceedance For Design Earthquake Ground Motions ⁽⁴⁾		Performance Level ⁽¹⁾	
		Life Safety	Operational
Rare Earthquake (MCE) 3% PE in 75 years/1.5 Mean Deterministic	Service ⁽²⁾	Significant Disruption	Immediate
	Damage ⁽³⁾	Significant	Minimal
Expected Earthquake 50% PE in 75 years	Service	Immediate	Immediate
	Damage	Minimal	Minimal to None

Notes:

(1) Performance Levels

These are defined in terms of their anticipated performance objectives in the upper level earthquake. Life safety in the MCE event means that the bridge should not collapse but partial or complete replacement may be required. Since a dual level design is required the Life Safety performance level will have immediate service and minimal damage for the expected design earthquake. For the operational performance level the intent is that there will be immediate service and minimal damage for both the rare and expected earthquakes.

(2) Service Levels*

- *Immediate* – Full access to normal traffic shall be available following an inspection of the bridge.
- *Significant Disruption* – Limited access (Reduced lanes, light emergency traffic) may be possible after shoring, however the bridge may need to be replaced.

In the two-level criteria presented in Table 3-4, the 'rare' earthquake was defined as one with a 3% probability of exceedance in 75 years (corresponding approximately to a 2,500-year return period), while the 'expected' earthquake was one with a 50% probability of exceedance in 75 years, corresponding approximately to a 100-year return period. The 2006 Edition of the *Retrofitting Manual for Highway Structures* published by the Federal Highway Administration (FHWA 2006) also recommends a dual-

level performance criterion for use when retrofitting bridges. This Manual uses the terms ‘upper’ and ‘lower’ level to describe the dual-level ground motions. The upper level motions have a return period of 1,000 years and the lower level motions have a return period of 100 years.

AASHTO first adopted a probabilistic approach to seismic design in 1981 with the publication of Guide Specifications for Seismic Design of Bridges (AASHTO 1981). These specifications were an approved alternative to the seismic provisions in the Standard Specifications for Highway Bridges in use at that time and were based on a 500-year return period seismic hazard map prepared by USGS. In developing the current AASHTO design criteria (AASHTO 2007, 2009), the two-level design approach proposed in the 2001 NCHRP study (NCHRP 2001) was considered to be unjustified for most transportation facilities in the US and thus was not adopted. Furthermore, when considering the return period for the ‘design’ earthquake (the term used in single-level design), 2,500 years was considered to be too long (too inconsistent with the return periods for other natural hazards) and potentially too costly, especially in the design of foundations. There was also concern that the cost of retrofitting existing bridges, many of which were designed for a 500-year return period, to this new hazard level would be cost prohibitive.

Nevertheless the arguments for raising the hazard level were persuasive and in 2007 AASHTO elected to adopt a 1,000-year hazard level for the design of ordinary bridges. This hazard level is used in both the 2008 interim of 4th Edition LRFD Specifications (AASHTO 2007) and the LRFD Guide Specifications for Seismic Bridge Design (AASHTO 2009). The Guide Specifications were developed under NCHRP Project 20-07/193 which showed that the hazard level for the 2,500-year return period corresponds to a shaking level at about the median-plus-one standard deviation level in many parts of country. Considering Caltrans’ practice, which uses median attenuation models for setting the safety level limit state ground motion criteria for ordinary bridges, it can be argued that a 2,500-year hazard level (corresponding to the median-plus-one standard deviation ground motion in many areas) is too conservative for ordinary (conventional) bridges. Hence, one can infer that the AASHTO’s decision for not accepting the 2,500-year return period and adopting a 1,000-year return period is appropriate. The NCHRP 20-07/193 study also showed that the return period that best correlated with historical earthquakes in various parts of the country varied widely, ranging from less than 500 years for the seismically active western U.S. to close to 2,000-years in some parts of central and eastern U.S. Thus AASHTO’s selection of a 1,000-year return period is a compromise which can be reconciled against many of the historical earthquakes that have occurred in the central and eastern parts of U.S. (on a median attenuation basis).

AASHTO has no explicit requirements for checking bridge performance for more frequently occurring ground motions than those that occur every thousand years, on average. But some owners may wish to check that certain important bridges will remain functional in frequently occurring earthquakes such as those with return periods of the order of a hundred years or so. In practice, where owners have chosen to check functionality, the selected return period has varied from project to project, even within the same geographic region. A 72-year return period has been used in California for toll road projects in Orange County, CA, and for designing wharf structures in the ports of Los Angeles and Long Beach. A 92-year return period has been used for the functional earthquake for the East Bay Spans of the San Francisco Oakland Bay Bridge. However, for major bridge structures in less active seismic states, longer return periods have been used for the functional earthquake. For example, 500 years has been used as the return period for the functional level ground motion for the retrofit of the major water crossing bridges in New York City and for design of the new Arthur Ravenel, Jr. (Cooper River) cable-stayed bridge in Charleston, South Carolina. The decision on whether or not to design for functionality involves balancing the risk of service disruption and the cost of disruption versus the cost associated with additional design and construction or retrofit measures. While this decision is the owners' responsibility, it is the engineer's responsibility to provide the owner with sufficient information with which to make this economic decision and, having made the decision to use a functional level earthquake, to set the functional level earthquake criteria on a project specific basis.

3.3.2 Return Period for Use in Design

As discussed above, a 1,000-year return period has been adopted by AASHTO for safety level design of ordinary bridges. However, owners may choose to deviate from the 1,000-year return period ground motion criteria for transportation facilities as the situation warrants it. The following are some of the reasons that have been cited for deviation from the AASHTO criteria:

- 1) A longer return period may be justified for critical structures, when (a) the structure is part of a lifeline route for emergency operations, or (b) an extended duration in loss of operation of the structure would have an undue cost impact to the community. For these critical structures, especially when they are complex structural systems such as long span water crossing structures, project-specific ground motions and performance criteria should be developed with the assistance of a peer review panel.

- 2) A shorter return period may be justified, if (a) the capital cost for design of the structure to the 1,000-year return period is deemed too costly, (b) it is required by the owner and regulatory agencies, or (c) in retrofit situations the existing facility has limited remaining operating life and the facility is expected to be replaced. It is noted that the FHWA retrofit manual (FHWA 2006) does not favor a reduction in the return period for older structures. Instead, the minimum level of retrofit is adjusted to account for the remaining service life, with little or no retrofit recommended for a bridge about to be closed or replaced.
- 3) The return period may also be reduced when the 1,000-year return period ground motion is excessive, e.g. when it is higher than a median-plus-one standard deviation ground motion from the maximum credible earthquake. This situation may occur in seismically active areas such as some parts of California where the faults have relative short rupture recurrence intervals (i.e. rupture recurrence intervals on the order of a few hundred years). For such situations, it is common to place a deterministic cap on the probabilistic ground motions, e.g. the median-plus-one standard deviation MCE ground motions.

3.3.3 Site Specific Analysis versus USGS National Seismic Hazard Maps

The AASHTO seismic design criterion is based upon the 2002 USGS National Seismic Hazard Maps. However, owners can, at their discretion, use more recent versions of the USGS National Seismic Hazard maps or commission site-specific seismic hazard analyses to determine design ground motion parameters. The USGS hazard mapping efforts are comprehensive, employing state-of-the-art attenuation relationships and regional workshops to gather local geological data and to develop consensus within the geoscience community on the resultant seismic source models. This level of effort cannot be easily duplicated and thus site-specific seismic hazard analyses are generally not justified for small scale projects. Furthermore, site specific studies often result in discrepancies with the USGS maps and other models for the predicted ground shaking that require investigation and explanation, often leading to controversies and delay for the project. Therefore, site-specific seismic hazard studies should only be exercised with good justification, conducted by qualified experts, and subject to peer review by experts in regional seismicity and seismic hazard evaluation. In general, site specific seismic hazard studies for transportation facilities are usually confined to major bridge projects (e.g. major water crossing bridges) or regional transportation projects that cover a wide geographic area. Some of the justifications for conducting a site specific seismic hazard analysis include:

- 1) Failure of a major transportation facility or disruption of a transportation network may have tremendous impact on the local economy. Many transportation facilities may be classified as important or critical structures, and some may be classified as lifeline structures. Hence, the appropriate ground motion and especially the performance criteria may be considered to be different from ordinary bridges. Projects that deviate from the 1,000-year return period would therefore often be good candidates for site specific studies. For example, many of the water crossing bridges in the east coast, including at New York City and the Arthur Ravenal, Jr. bridge in Charleston, and the Tacoma Narrows Second Crossing Bridge in Seattle have adopted a 2,500-year return period for seismic design. The California State Seismic Advisory Board and the Seismic Peer Review Panel recommended a 1,500-year return period for seismic design of the San Francisco-Oakland Bay Bridge East Span Replacement project. Due to the potential economical impacts of service disruption for such structures, it is common for these projects to employ a site specific seismic hazard analysis.
- 2) Major bridges and viaducts are complicated structures and therefore often require time history analyses. There is a high level of expertise required for generating the appropriate input time histories to support design of such bridges. Therefore, such structures would logically be candidates for site specific studies due to the requirement for developing input time histories.

A peer review process is recommended for any project that employs a site-specific seismic hazard analysis. As major transportation projects of the type that require a site specific seismic hazard analysis often involve oversight by a peer review panel, this peer review panel can often also be employed to provide the proper review of results from a site specific ground motion hazard study.

3.3.4 Ground Motion Characterization

While a response spectrum developed in a probabilistic or deterministic seismic hazard analysis can be input directly to a structural response analysis, more often than not a modified version of the spectra from the seismic hazard analysis is used for structural design. In general, the acceleration response spectrum from a seismic hazard analysis may be modified for use in design in two ways: 1) the shape may be modified from the relatively peaked shape typically produced by a seismic hazard analysis to the more truncated standard shape typically used in structural analysis; and 2) the amplitude of the spectral ordinates may be modified to account for local soil conditions. As noted previously, a deterministic cap may also be placed on a probabilistically-derived acceleration spectrum developed from a seismic hazard

analysis in areas of high seismicity. This cap limits the amplitude of the spectrum in the short period range. Furthermore, the USGS National Seismic Hazard Maps are produced for a site where the average shear wave velocity within the upper 100 feet of the site profile ranges from 2,500 to 5,000 feet per second (ft/sec). If the shear wave velocity in the upper 100 ft differs from this range of values, the design response spectra must be modified to account for the local site conditions.

Modifications to the response acceleration spectrum developed from the USGS National Seismic Hazard maps to develop the acceleration response spectrum for structural design purposes is generally based upon the standard spectral shape shown in Figure 3-11.

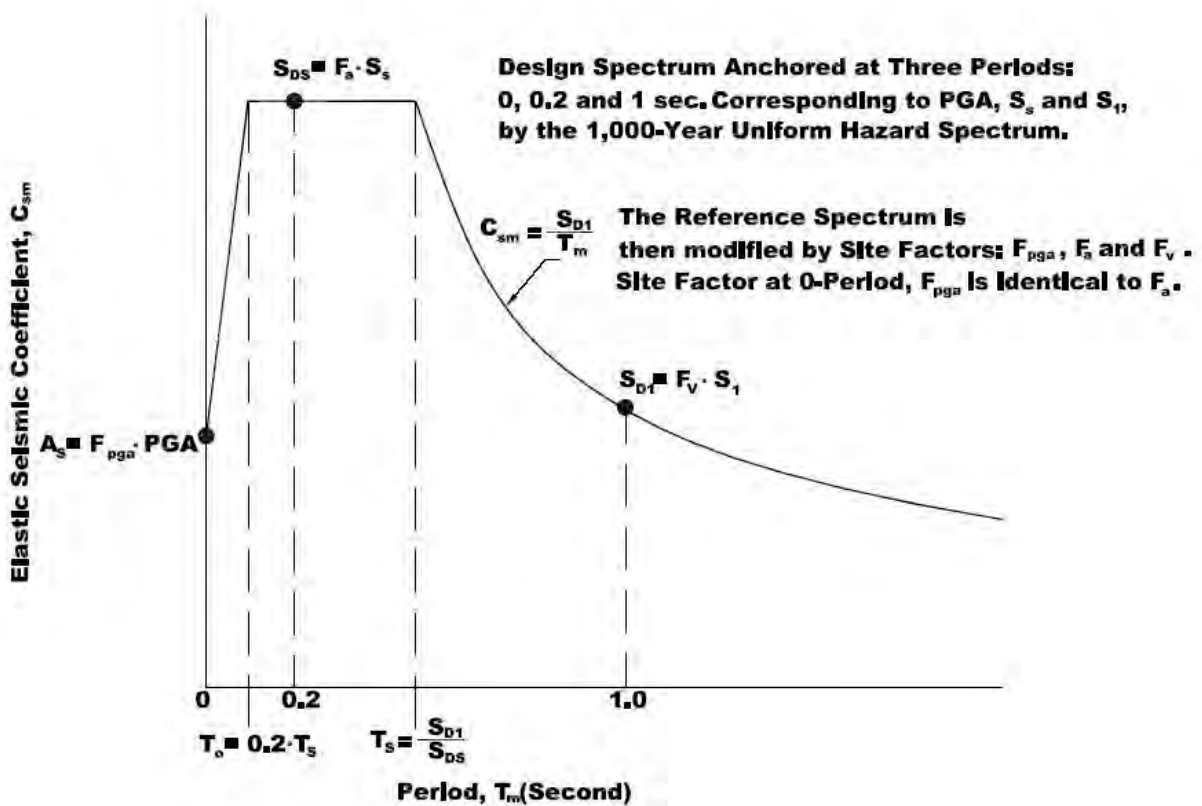


Figure 3-11 Design Response Spectrum Constructed with the Three-Point Method

Three spectral ordinates, the spectral acceleration at 0.0, 0.2 and 1.0 seconds, are used to develop the modified spectral curve shape from the seismic hazard analysis results. The values for these parameters obtained from a seismic hazard analysis for soft rock site conditions, e.g. from the 2002 USGS National Seismic Hazard Maps, are modified by site factors F_{PGA} (i.e., F_{PGA}), F_a and F_v that depend upon V_{S30} , the average shear wave velocity in the top 100 ft (30 m) of the site, to account for local site conditions when

developing the acceleration response spectrum for structural design (these site factors are discussed in detail in Section 3.4.7). This method of modifying the acceleration response spectrum, sometimes referred to as the three-point method, was developed as part of the recommended seismic design provisions from the National Earthquake Hazard Reduction Program (NEHRP). This three-point method is employed not only in the AASHTO LRFD and NEHRP seismic design provisions but also in the International Building Code (IBC). The primary difference among the NEHRP, AASHTO, and IBC seismic design provisions is the return period used to determine the three anchoring spectral accelerations. For example, while AASHTO uses the 1,000-year return period, the IBC multiplies the spectral ordinates for a 2,500-yr return period by a reduction factor of 2/3. One important difference between the current AASHTO procedure (described in Section 3.7) and the other versions of this procedure is that the current AASHTO procedure uses the PGA to anchor the design spectrum at zero period. Other versions of this procedure simply assumed the PGA to be equal to 0.4 times the spectral acceleration at 0.2 second.

Figure 3-12 compares the UHS acceleration response spectrum developed from the USGS National Seismic Hazard mapping program data with the AASHTO truncated structural design spectrum developed using the three-point fitting method for a site in Memphis, Tennessee for a 1,000-year return period.

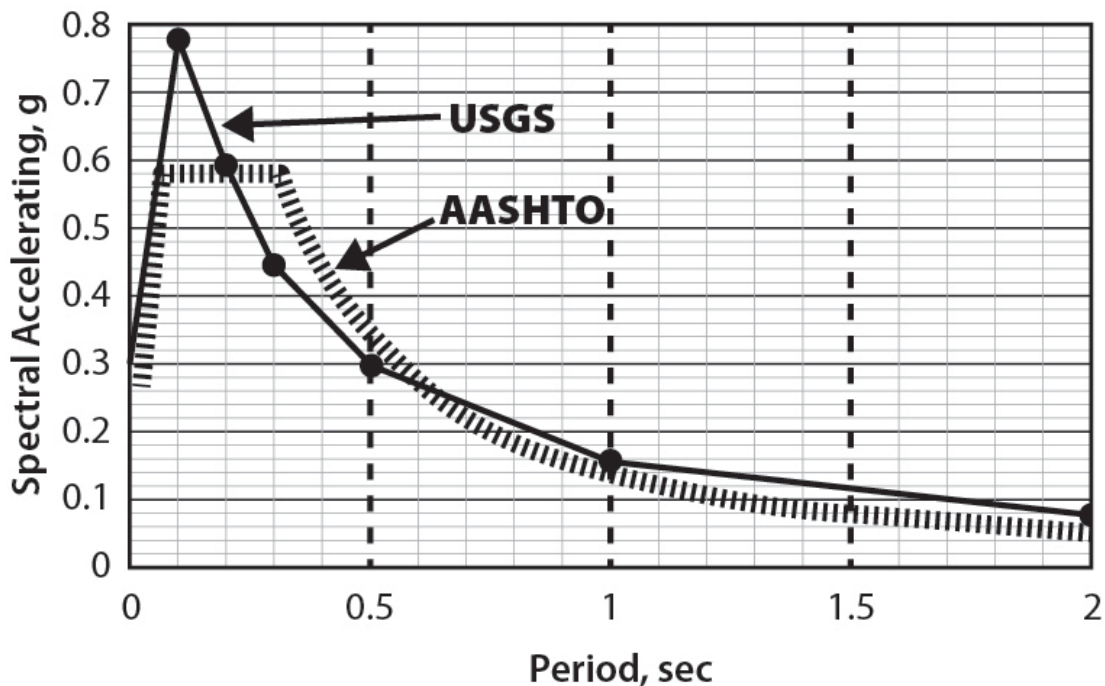


Figure 3-12 Comparison of USGS Spectra to AASHTO Spectra for a Rock Site in Memphis, Tennessee (1,000-yr Return Period)

Figure 3-12 clearly illustrates the truncation of the peaked USGS 1000-year return period UHS spectrum to develop the spectrum for use in structural design, e.g. in a structural analysis that employs an elastic response spectra and the principle of modal superposition to calculate structural response.

3.3.5 Correlation for Peak Ground Velocity

The Peak Ground Velocity (PGV) is an important parameter in both structural and geotechnical design analyses. In structural design, it is generally acknowledged that damage potential is more closely correlated to PGV than to any other single earthquake loading parameter. In geotechnical analysis, PGV can be used in Newmark displacement analysis for predicting permanent seismically induced displacement of slopes and earth retaining structures. USGS (in their national hazard mapping program) does not provide maps for PGV. Therefore, it is often necessary to derive PGV for a representative deterministic scenario event from an attenuation relationship or by correlation with other earthquake parameters.

Several correlations between PGV and ground motion parameters were developed during the NCHRP 12-70 project. After reviewing the available information, a revised form of a Peak Ground Velocity (PGV) correlation suggested by Abrahamson (2005) for the estimation of PGV from the spectral acceleration at one second (S_1) was recommended in NCHRP 12-70 (NCHRP 2008). This correlation is given as:

$$PGV = 0.3937 \times 10^{0.434C_1} \quad 3-8$$

where PGV is in inches/sec,

$$C_1 = 4.82 + 2.16 \log_{10} F_V S_1 + 0.013 [2.30 \log_{10} (S_1 F_V) + 2.93]^2 \quad 3-9$$

and S_1 is the spectral acceleration (in g) at a spectral period of 1 second and F_V is the site factor for the spectral acceleration at a period of 1 second. For design purposes, Equation 3-6 was simplified to the following equation:

$$PGV \left(\frac{\text{in}}{\text{sec}} \right) = 38 \cdot F_V S_1 \quad 3-10$$

It is expected that in the future the USGS will include PGV in their national seismic hazard mapping program and will provide map values for a 1,000-year return period. In that case, the S_1 -PGV correlation will be replaced in favor of design PGV values from the USGS maps (unless PGV is available from the results of a project-specific seismic hazard analysis).

3.3.6 Acceleration Response Spectra versus Displacement Spectra

The most common method of seismic design for bridges focuses on providing sufficient strength to resist the earthquake force demands. This approach is called a ‘force-based’ approach and it employs acceleration response spectra to calculate the earthquake demands. However, there is a growing trend in bridge design to move away from ‘force-based’ methods to ‘displacement-based’ methods where the focus is on providing sufficient displacement capacity. This approach employs displacement response spectra to calculate the earthquake displacement demands. A displacement response spectrum may be derived from an acceleration response spectrum using the following equation:

$$S_d = \frac{T^2}{(2\pi)^2} S_a \quad 3-11$$

where S_d is spectral displacement, S_a is spectral acceleration, and T is period.

The spectral displacement demand from the above equation is the relative displacement between the center of mass of the structure and the point where ground motion is input to the structure.

3.3.7 Near-Fault (Near-Field) Directivity Effects

Research over the last 15 years (e.g. Sommerville et al., 1997) has shown that certain combinations of site location, the configuration of the seismic source, and the direction of fault rupture can result in a significant enhancement to the long period motions at a site that can result in directivity effects that can be very damaging to certain structures, particularly in the near field, i.e. when the site is close (within 15 km) to the fault. Figure 3-13 illustrates the effect of directivity in near-fault ground motions by comparing the velocity time histories from two sites subject to the 1992 M_w 7.2 Landers earthquake in Southern California at the same distance from the earthquake epicenter but located in different directions from the epicenter with respect to the direction of rupture propagation along the fault. It is seen in this figure that the ground motion recorded during the earthquake at the station oriented in the direction of

fault rupture propagation relative to the earthquake origin, the Lucerne recording station, is significantly different from that recorded which is in opposite direction of fault rupture, the Joshua Tree station. The Lucerne record shows a very large velocity pulse, with a peak ground velocity of 53.5 in/s, compared to the Joshua Tree record, which has a much lower amplitude of peak ground velocity of 16.9 in/s, even though the duration of shaking is longer in the Joshua Tree record.

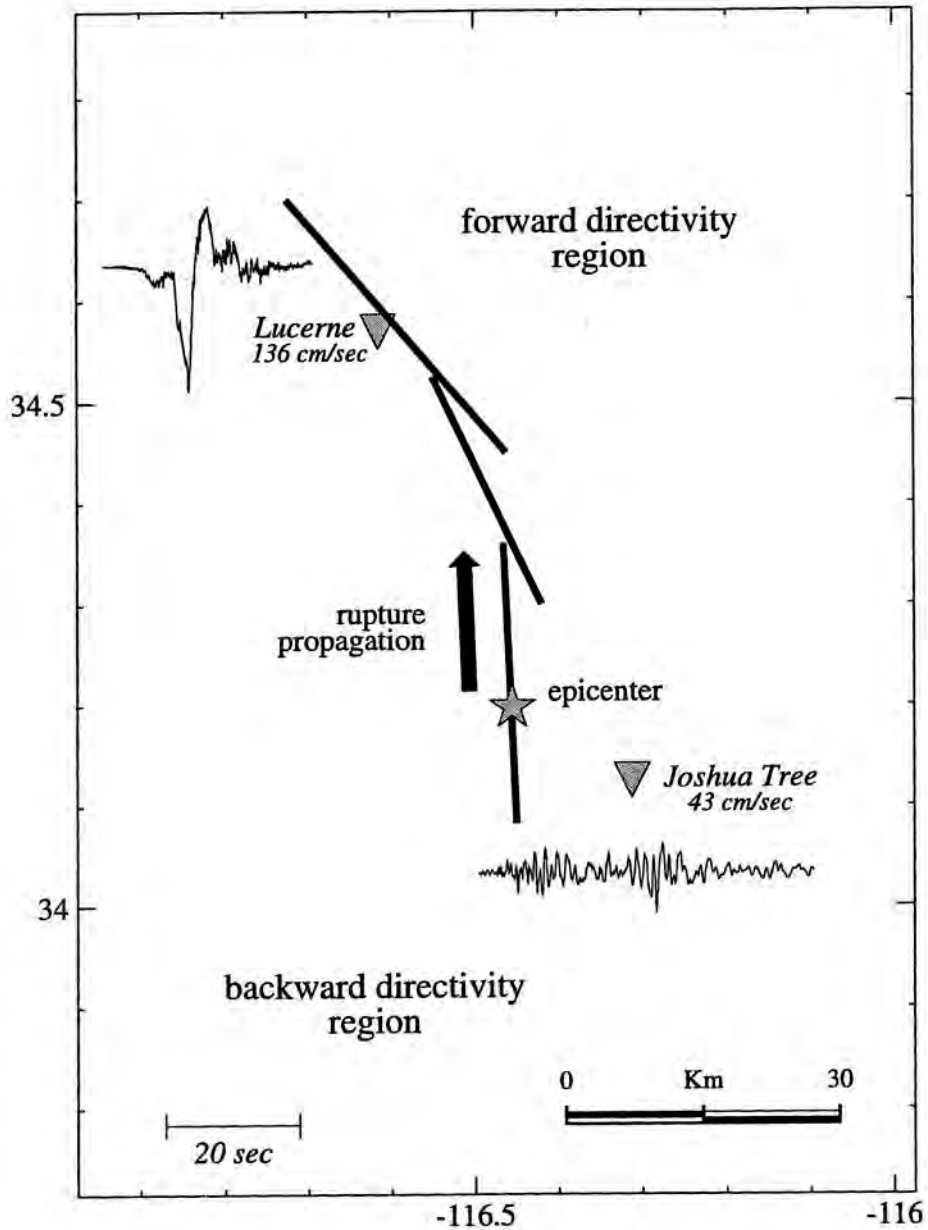


Figure 3-13 Influence of Rupture Directivity on Velocity Time Histories Recorded at the Lucerne and Joshua Tree Sites During the 1992 Landers Earthquake (Somerville et al., 1997)

Figure 3-13 shows that if a site is located sufficiently near to a fault and the earthquake fault ruptures toward the site, a ground motion with a very large velocity pulse can occur. Because these kinds of pulses can be very damaging to long-period bridges, it is necessary to take special design measures in these situations. However, the methods used to account for these near-fault directivity effects vary from project to project, in part because the subject matter is still under research. In particular, the means for quantifying the velocity pulse and relating it to structural response is still a subject of research, although a time history analysis using appropriate time histories is one way this can be accomplished. The need to consider near fault directivity is, in general, limited to those states with well-defined shallow active faults (e.g. California, Washington, and Utah). Furthermore, only project sites within about 10 miles (15 kilometers) of the rupturing fault subject to relatively large magnitude earthquakes ($M > 6.5$) need be considered for fault directivity effects.

3.3.8 Local Site Effects

As noted previously, local site conditions have a significant effect on the characteristics of earthquake ground motions. The local site conditions effect needs to be properly taken into account when establishing design ground motions. There are, in general, three methods that can be used to account for the influence of local site conditions on earthquake ground motions: 1) the use of site factors to modify the results of the seismic hazard analysis to account for local soil conditions; 2) the use of soil site attenuation relationships to directly account for the local soil conditions in the seismic hazard analysis; and 3) the use of site-specific site response analysis. Until recently, soil site attenuation relationships were generally considered too crude to properly account for local soil conditions, as they tended to group all soil sites into one or two site classes. However, a new generation of attenuation relationships that discriminates among soil sites on the basis of the shear wave velocity in the upper 100 ft has recently been developed for shallow crustal faults in the western United States. This new generation of attenuation relationships, termed the Next Generation Attenuation (NGA) relationships, is discussed in more detail in Section 3.8. The use of site response analysis to account for local soil conditions is discussed in Chapter 5 of this document.

The use of site factors to account for the influence of local soil conditions on ground motion characteristics is illustrated in Figure 3-11. Using the site factor approach, the three anchoring spectral accelerations for the design response spectrum are modified by site response factors F_{pga} (for the PGA, or spectral acceleration at a spectral period of 0.0 seconds), F_a (for the spectral acceleration at 0.2 second spectral period) and F_v (for the spectral acceleration at 1 second spectral period). Note that on Figure

3-11 the site response factor F_{pga} (for the 0.0 second spectral period) is shown as equal to F_a (for the 0.2 second period). While this is the case for the NEHRP spectrum, which assumes the PGA is 0.4 times the spectral acceleration at 0.2 second spectral period, it may not always be the case for the AASHTO spectrum (for which the PGA is evaluated independently). The values of F_{pga} , F_a and F_v depend upon both the local site conditions and the amplitude of the associated spectral accelerations. Local site conditions are defined on the basis of the average shear wave velocity for the top 100 ft of the site, sometimes referred to as V_{S30} (the subscript “30” refers to 30 meters, the metric equivalent of 100 ft). Six site classes, designated Site Class A through F, have been established on the basis of V_{S30} . These site classes, referred to as the NEHRP site classes because they were initially established under the NEHRP program, are shown in Table 3-5. Note that for Site Class F site factors cannot be used and a site-specific response analysis must be conducted to evaluate the influence of local site conditions on seismic site response. Also note that Site Classes C, D, and E can also be defined on the basis of the average Standard Penetration Test blow count, \bar{N} , or the average undrained shear strength, \bar{s}_u . The average blow count, \bar{N} , is generally defined on the basis of the normalized, standardized blow count $(N_1)_{60}$ discussed in Chapter 4.

TABLE 3-5 NEHRP SITE CLASSIFICATION SYSTEM

SITE CLASS DEFINITIONS				
SITE CLASS	SOIL PROFILE NAME	AVERAGE PROPERTIES IN TOP 100 feet, SEE SECTION 1613.5.5		
		Soil shear wave velocity, \bar{v}_s , (ft/s)	Standard penetration resistance, \bar{N}	Soil undrained shear strength, \bar{s}_u , (psf)
A	Hard rock	$\bar{v}_s > 5,000$	N/A	N/A
B	Rock	$2,500 < \bar{v}_s \leq 5,000$	N/A	N/A
C	Very dense soil and soft rock	$1,200 < \bar{v}_s \leq 2,500$	$\bar{N} > 50$	$\bar{s}_u \geq 2,000$
D	Stiff soil profile	$600 \leq \bar{v}_s \leq 1,200$	$15 \leq \bar{N} \leq 50$	$1,000 \leq \bar{s}_u \leq 2,000$
E	Soft soil profile	$\bar{v}_s < 600$	$\bar{N} < 15$	$\bar{s}_u < 1,000$
E	—	Any profile with more than 10 feet of soil having the following characteristics: 1. Plasticity index $PI > 20$, 2. Moisture content $w \geq 40\%$, and 3. Undrained shear strength $\bar{s}_u < 500$ psf		
F	—	Any profile containing soils having one or more of the following characteristics: 1. Soils vulnerable to potential failure or collapse under seismic loading such as liquefiable soils, quick and highly sensitive clays, collapsible weakly cemented soils. 2. Peats and/or highly organic clays ($H > 10$ feet of peat and/or highly organic clay where H = thickness of soil) 3. Very high plasticity clays ($H > 25$ feet with plasticity index $PI > 75$) 4. Very thick soft/medium stiff clays ($H > 120$ feet)		

Table 3-6 provides values for the PGA site factor F_{pga} , Table 3-7 provides values of the short period (0.2-second period) site factor, F_a , and Table 3-8 provides values for the long period (1-second) site factor, F_v .

These site factors are applied to the PGA, 0.2 second, and 1 second spectral accelerations, respectively. The site factor F_{pga} , which is used to adjust the PGA (i.e. the zero period spectral acceleration), is based upon F_a . However, the intensity-dependent categories in the top row of Table 3-7 are divided by 2.5 to create the values for F_{pga} in Table 3-6. For intensity values intermediate to the values at the top of the columns in Tables 3-6, 3-7, and 3-8 linear interpolation is used. For intensity values less than the values in the first column of these tables, the site factor values in the first column is used and for intensity values greater than the values in the last column the values in the last column are used.

The site factors in Tables 3-6, 3-7, and 3-8 are used to create the three-point truncated design spectrum that accounts for local site conditions. In most cases, these site factors are greater than 1.0 (and as great as 3.5 in one case), resulting in amplification of the spectral accelerations by local site conditions. But for hard, crystalline rock sites (i.e., Site Class A, sites where V_{s30} is in excess of 5,000 ft/s) the site factors are equal to 0.8, resulting in reduction of the spectral accelerations from the seismic hazard analysis. The site factors are also less than 1.0 for short period (0.2 second) spectral accelerations in excess of 1 g (and therefore for PGA values in excess of 0.4 g) for Site Class E (V_{s30} less than 600 ft/s), where the low shear strength of the soil limits the intensity of the ground motions. Note that site factors are not given in Table 3-6, 3-7, and 3-8 for Site Class F. A site-specific geotechnical investigation and dynamic site response analysis is recommended to evaluate the influence of local soil conditions on the site response for Site Class F.

TABLE 3-6 VALUES OF F_{pga} AS A FUNCTION OF SITE CLASS AND THE SITE CLASS B PEAK GROUND ACCELERATION

Site Class	Mapped Spectral Response Acceleration at Short Periods				
	PGA ≤ 0.1 g	PGA = 0.2 g	PGA = 0.3 g	PGA = 0.4 g	PGA ≥ 0.5 g
A	0.8	0.8	0.8	0.8	0.8
B	1.0	1.0	1.0	1.0	1.0
C	1.2	1.2	1.1	1.0	1.0
D	1.6	1.4	1.2	1.1	1.0
E	2.5	1.7	1.2	0.9	0.9
F	a	a	a	a	a

Table notes: Use straight interpolation for intermediate values of S_s , where S_s is the spectral acceleration and 0.2 second obtained from the ground motion maps.

a Site-specific geotechnical investigation and dynamic site response analyses shall be performed (Article 3.4.3)

TABLE 3-7 VALUES OF F_a AS FUNCTION OF SITE CLASS AND THE SITE CLASS B SHORT PERIODS (0.2 SECONDS) SPECTRAL ACCELERATION

Site Class	Mapped Spectral Response Acceleration at Short Periods				
	$S_s \leq 0.25 \text{ g}$	$S_s = 0.50 \text{ g}$	$S_s = 0.75 \text{ g}$	$S_s = 1.00 \text{ g}$	$S_s \geq 1.25 \text{ g}$
A	0.8	0.8	0.8	0.8	0.8
B	1.0	1.0	1.0	1.0	1.0
C	1.2	1.2	1.1	1.0	1.0
D	1.6	1.4	1.2	1.1	1.0
E	2.5	1.7	1.2	0.9	0.9
F	a	a	a	a	a

Table notes: Use straight interpolation for intermediate values of S_s , where S_s is the spectral acceleration and 0.2 second obtained from the ground motion maps.

a Site-specific geotechnical investigation and dynamic site response analyses shall be performed (Article 3.4.3)

TABLE 3-8 VALUES OF F_v AS A FUNCTION OF SITE CLASS AND THE SITE CLASS B LONG PERIOD (1 SECOND) SPECTRAL ACCELERATION

Site Class	Mapped Spectral Response Acceleration at 1 Second Periods				
	$S_1 \leq 0.1 \text{ g}$	$S_1 = 0.2 \text{ g}$	$S_1 = 0.3 \text{ g}$	$S_1 = 0.4 \text{ g}$	$S_1 \geq 0.5 \text{ g}$
A	0.8	0.8	0.8	0.8	0.8
B	1.0	1.0	1.0	1.0	1.0
C	1.7	1.8	1.5	1.4	1.3
D	2.4	2.0	1.8	1.6	1.5
E	3.5	3.2	2.8	2.4	2.4
F	a	a	a	a	a

Table notes: Use straight interpolation for intermediate values of S_s , where S_s is the spectral acceleration and 0.2 second obtained from the ground motion maps.

a Site-specific geotechnical investigation and dynamic site response analyses shall be performed (Article 3.4.3)

3.3.9 Representative Ground Motion Time Histories

While the response spectrum method is the most common method of seismic analysis for conventional structural seismic design, many geotechnical analyses and some of the more complex structural analyses require the input of representative acceleration time histories for the design earthquake. The process of developing appropriate time histories for these analyses generally starts with establishing the target response spectra (median and plus and minus one standard deviation spectra). Then, time histories for use in the design analyses are developed by first selecting a candidate set of appropriate naturally recorded strong motion records (sometimes referred as the startup time histories or seed time histories). These candidate time histories are usually based on the peak ground acceleration, earthquake magnitude, and other relevant seismic source characteristics (e.g. source mechanism, strong motion duration, arias intensity or energy content). The candidate strong motion records are then scaled so that the resultant response spectra for the strong motion records best match the target design response spectra. Ideally, the suite of candidate time histories should average out to the median spectrum and “fill the envelope” between the plus and minus one standard deviation spectra. The accelerations of a candidate records may be scaled by a constant factor to meet this criterion. Candidate records may also be modified in the time or frequency domain to match the target spectrum, if necessary. Modification of candidate time histories to match the intended design response spectrum will be further discussed in the next section.

There are various approaches to the selection of candidate ground motions for time history design analyses. These approaches typically involve selecting the candidate time histories from one of the many available catalogs of time histories on the basis of peak ground acceleration, seismic source mechanism, earthquake magnitude, and other earthquake parameters. One of the more comprehensive catalogs of earthquake ground motions is the one developed by the Nuclear Regulatory Commission for use in design of Nuclear Power Plants (NUREG/CR-6728: Technical Basis for Revision of Regulatory Guidance on Design Ground Motions: Hazard- and Risk Consistent Ground Motion Spectra Guidelines). NUREG/CR-6728 provides a catalog of over 500 sets of three component time history records classified into (1) two tectonic regions: the western US (WUS) and the central and eastern U.S. (CEUS), (2) two site classes: rock or soil sites, and (3) magnitude (M- 5 to 6, M- 6 to 7, and 7+) and distance (R from 0-6 miles, 6 to 30 miles, 30 to 60 miles and >60 miles) . The Nureg/CR-6728 report also includes a set of CD-ROMs containing the time histories. The NUREG time history records for the WUS are actual recordings while, due to lack of actual data, the CEUS NUREG records were developed by modifying WUS records to account for differences in seismic source and crustal properties between the two regions based on seismological modeling. The Pacific Earthquake Engineering Research Center (PEER) and the State

California Department of Conservation (Strong Motion Instrumentation Program-CSMIP) in California are other sources of databases for earthquake time histories. However, these two data sets are biased toward strong motion records for the WUS. The Multidisciplinary Center for Earthquake Engineering Research (MCEER) also maintains a catalog of earthquake time histories, providing some strong motion records relevant to the CEUS. See http://peer.berkeley.edu/products/strong_ground_motion_db.html for the PEER database and http://mceer.buffalo.edu/infoservice/Reference_Services/strongMotionGuide.asp for the MCEER database.

After establishing a data set of appropriate strong motion records, subsequent steps in developing a set of time histories for use in design involves establishing:

- 1) The target ground shaking spectra
- 2) The number of input time histories
- 3) The specific time history records to be employed

The following discussion provides some general guidance on this subject matter.

The uniform hazard spectra from a probabilistic analysis and/or a deterministic scenario earthquake are common bases for setting the target response spectra for selection of candidate time histories. The 1,000-year UHS adopted by AASHTO generally serves as the appropriate target spectrum for most ordinary bridges and other transportation facilities within the transportation network for the life safety performance goal. Then, a representative magnitude and distance can be selected based upon the magnitude deaggregation of the UHS and deterministic median and plus and minus one standard deviation spectra for the representative event can be generated using one of the available attenuation relationships. Note that if the mean spectrum does not conform to the UHS over the period range of engineering the selection of the representative magnitude and distance should be reconsidered. Critical facilities (e.g. major water crossing long-span bridges) might involve the use of other project specific ground motion criteria for design, as discussed earlier.

With respect to the number of time histories adopted for design, theoretically the number of time histories should be sufficiently large so that the median and variability (standard deviation) of the demand predicted by the time history analyses is statistically stable. The number of time histories to achieve this objective may depend on the application as well as specifics of the adopted procedures for modifying the

startup time history records. The most basic objective in a design analyses, predicting the peak response, generally requires a fewer number of input time histories to achieve statistical stability than design objectives such as predicting permanent deformation.

Generally accepted practice is to use a minimum of 3 sets of input time histories for a time-history analysis. However, three sets of input motions are generally insufficient to achieve the desired statistical stability for the demand. Therefore, it is common practice to employ the maximum response from a set of three input motions (rather than the median response) for design purposes. The IBC calls for the use of at least seven sets of input motions if the median response from a time-history analysis is to be employed. This same criterion for the number of time histories has been used on some recent bridge projects. However, for very complex or unusual structures (e.g. for bridges involving isolation devices), the designer may chose to design the structure for the maximum response even if a minimum of seven sets of input motions are employed.

The use of naturally recorded time histories is generally preferred to the use of modified or synthetic (i.e. numerically generated) time histories. To select an appropriate data set of candidate strong motion records, the designer usually identifies a set of records from available databases based upon the appropriate tectonic conditions, magnitude, site-to-source distance, peak ground acceleration, and site class (e.g., rock or soil site). To narrow this data set down further, other strong motion parameters, including the duration of strong shaking and Arias intensity, may also be used as a basis for discriminating among records for analysis. The response spectra for the reduced set of candidate records can then be compared to the target response spectra for the design earthquake. The final suite of time histories is selected based upon the goal of conforming, on the average, to the median spectrum for the representative event or to the UHS from a probabilistic analysis and filling the envelope between the plus and minus one standard deviation spectra from the representative event. If necessary, records can be manipulated to meet this goal. However, it is preferable to minimize changes to the selected time history records, thus the response spectrum from the selected candidate time histories should be as good a match as available to the target spectra over the range of period of design interest.

If the candidate time histories selected for design must be manipulated, simple constant scaling of the acceleration is preferable to other methods of time history manipulation. However, some transportation projects may employ spectrum-compatible motions (motions that closely conform to the UHS or median spectrum for the scenario earthquake). Development of spectrum compatible motions usually involves complex manipulation of a natural time history to fit the smooth UHS target spectrum (or median

spectrum from the representative event). A spectrum compatible time history is illustrated in Figure 3-14. Some engineers do not approve of the use of spectrum compatible time histories, as they do not, in general, simulate real earthquake ground motions. Even if a spectrum compatible time history approach is employed, it is desirable to minimize the degree of modification to the original time history record by selecting records that have a reasonable initial match to the target spectrum in terms of the amplitude and overall spectral shape.

An important step in the process of selecting appropriate time histories for use in design involves comparing the response spectrums of the selected records to the target spectrum. There are a variety of free computer software tools available for this purpose. SEISMOSIGNAL is a free program for processing strong motion records, including plotting response spectra and calculating duration and Arias Intensity. SEISMOSIGNAL can be downloaded at www.seismosoft.com. PEER and the California Geological Survey have developed an automated program with an associated library of strong motion records for selection of design time histories called the Design Ground Motion library, or DGML (Powers, 2004; Powers et al., 2004). The trial version of the DGML allows the user to generate target spectra from three common WUS attenuation relationships or to input their own project-specific target spectrum (e.g. the 1,000-year uniform hazard spectrum for an AASHTO project). The user then specifies the range of strong motion parameters that will be employed to screen the DGML database for the appropriate time history records. Screening parameters include fault type(s), and ranges for acceptable magnitudes, Joyner and Boore distance, the shortest distance to the fault rupture plane, and average shear wave velocity in the upper 100-ft at the recording station. Other parameters specified by the user include the scaling procedure and the period range of interest. The DGML then generates a list of candidate earthquake records which satisfy the defined screening parameters and automatically ranks the seven best candidate records based on minimizing the mean square error between the spectral acceleration of a record and the target spectrum and a user-defined period weighting scheme. The DGML is still in a development stage and its status for public distribution is not clear. Nevertheless, this discussion should provide some appreciation of the steps involved in selecting the appropriate time histories for design.

Other methods for selecting representative time histories do exist. Kottke and Rathje (2008) present a semi-automated procedure for selecting scaling factors and ranking input motions for fitting a target acceleration response spectrum. The Kottke and Rathje (2008) method represents one of the few studies describing a systematic automated algorithm for selecting ground motion time histories and their corresponding scaling factors. This method is specific for natural time history records to which a constant scaling factor is applied.

3.3.10 Adjusting Time Histories to a Target Spectrum

Best practice for selection of startup time histories for use in seismic design is to employ actual recorded acceleration time histories whenever possible, as opposed to manipulated records or artificially generated synthetic records. However, even when actual recorded time histories are used, some modification of these time histories is generally required to match the target spectrum. The simplest form of time history modification is simple scaling of the accelerations in a record by a constant factor. Scaling of a recorded time history by a factor between 0.5 and 2.0 is a non-controversial process that is widely accepted. However, scaling by factors outside of this range must be done with caution and is subject to argument. Even after it is scaled, a naturally recorded time history will usually fit the target spectrum over only a very narrow range of spectral periods. Therefore, a suite of scaled time histories is generally required to encompass the entire design spectrum. As noted above, a minimum of three and preferably seven scaled time histories are usually employed in a time history analysis. If three time histories are used the maximum response is generally used in design, while if seven time histories are used a median response can be employed in design.

Many engineers prefer using only constant scaling to modify time histories for use in design, as opposed to modification of records in the time or frequency domain. The preference for constant scaling only is based upon the belief that this is the best way to preserve the phasing characteristics of the time history record and the correlation among the three orthogonal components of a ground motion. However, the computational effort required for a design analysis that employs multiple time histories can be significant, particularly if seven sets of three-component time histories are used. This large computational effort may present significant practical problems for design applications. To limit the number of time histories employed in design for practical reasons, some bridge design analyses employ spectrum-compatible time histories. As illustrated in Figure 3-14, a spectrum-compatible time history record is developed by modifying the candidate time history in the time and frequency domain so that it closely conforms to the design spectrum. Even in a spectrum compatible motion analysis, it is recommended to use 3 (or more in some cases) sets of spectrum compatible motions to achieve a statistically stable response result. The argument against this type of analysis is that a spectrum compatible time history may not represent a realistic earthquake ground motion. The argument in favor of this type of analysis is that it can significantly reduce computation effort.

There are two basic ways to modify naturally recorded startup motions to develop a spectrum-compatible motion: (1) time domain adjustment (Lilhanand and Tseng, 1988) and (2) frequency domain adjustment

(Silva and Lee, 1987). There are relative merits for both approaches and, ultimately, the best way to achieve spectrum-compatibility of the resultant motion would be the one that makes the least changes to the original startup motion. Development of spectrum compatible design motions should only be done by engineers experienced with these procedures. Further discussion on this topic is provided in Lam and Law (2000).

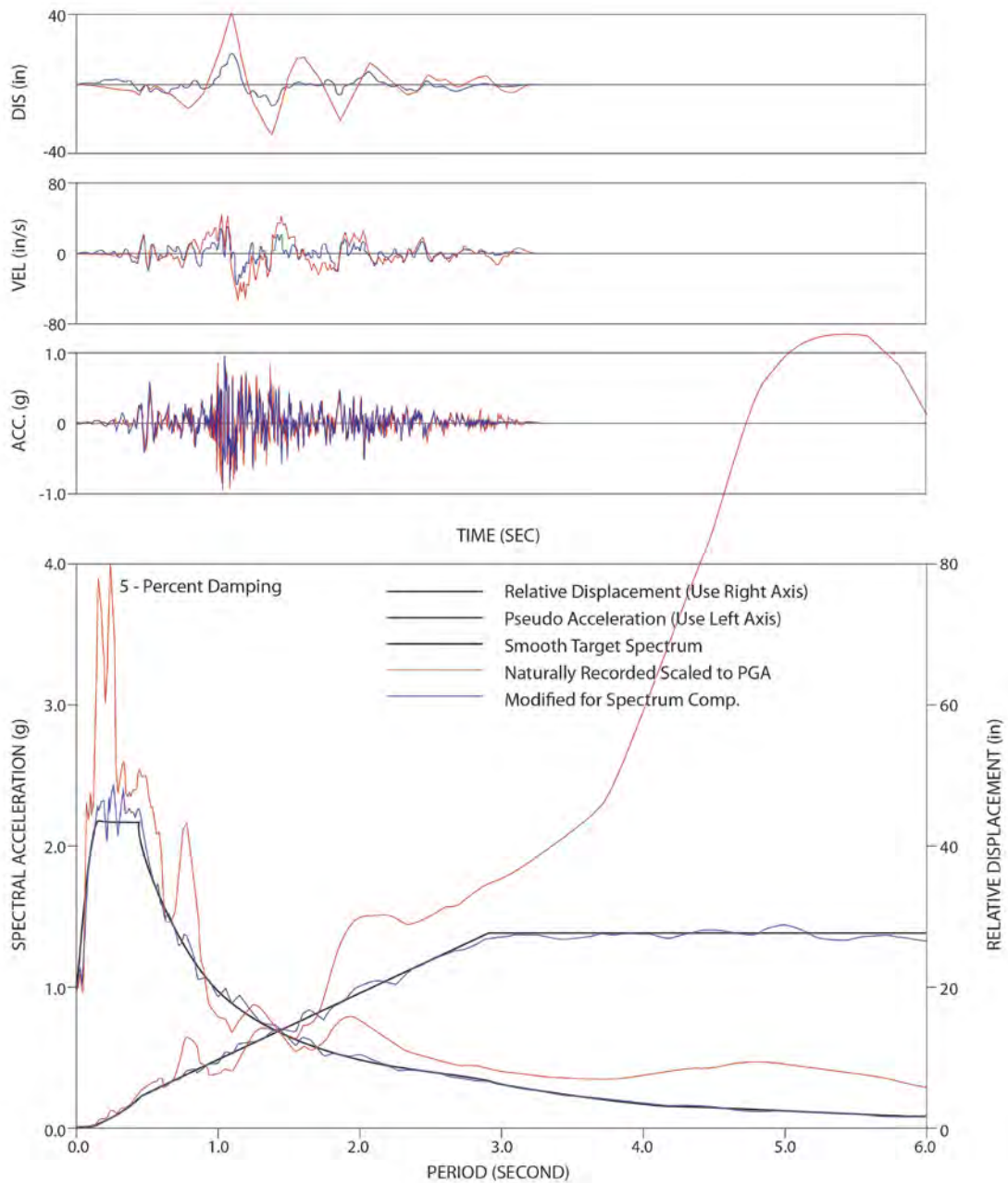


Figure 3-14 Representative Scaled versus Spectrum-Compatible Adjusted Motion

3.3.11 Spatially Varying Ground Motions

Because transportation systems are lineal systems that extend over large distances, it is sometimes necessary to consider the effect of the spatial variation of earthquake ground motions across the project site. This usually involves analyzing the system (e.g. a long-span bridge, multi-span viaduct, or a tunnel) with input motions that differ from support to support. In such circumstances, time histories of both acceleration and displacement are required at each support.

Several factors contribute to spatial variability and these include:

- 1) **Wave Passage Effect.** The wave passage effect is due to non-vertical wave propagation and produces systematic time shifts in the arrival of the seismic waves at each support. This effect can be modeled by applying a time shift to each support time history. Based on field measurements, an apparent wave speed of 8,250 ft/s may be used to calculate this time shift. This velocity is toward the lower end of the range of measured apparent wave speed, leading to somewhat conservative (upper bound) estimates of the time shifts.
- 2) **Attenuation over Distance.** When the seismic source is close to a long structure, the different distances to the various support locations can result in different ground motions at each support due to the attenuation of the ground motion with distance. Conventional attenuation relationships may be used to estimate this difference in the ground motions.
- 3) **Complex Wave Scattering.** Wave propagation can result in spatial incoherency (spatial differences) in both the amplitude and phase of the ground motions. These effects are sometimes referred to as wave scattering effects and are observed empirically in the recorded data from closely spaced strong motion instruments. Empirical models for the coherency function for the horizontal and vertical components of ground motion have been developed by Abrahamson (1992) and are shown in Figure 3-15 and Figure 3-16. These plots show that the degree of coherency decreases, and incoherency increases, at higher frequencies and larger spatial distances.
- 4) **Variation due to Local Soil Condition.** The change in soil profile and soil properties across a site can lead to significant variations in ground motions at or near the ground surface. This is perhaps the most significant source of spatially-varying input for most cases. Variations in local soil conditions are generally accounted for by conducting site response analyses for representative soil

columns at each support. Each soil column is subjected to the free-field design ground motion at its base and the difference in response of the soil columns is assumed to represent the variation in motions due to local soil conditions.

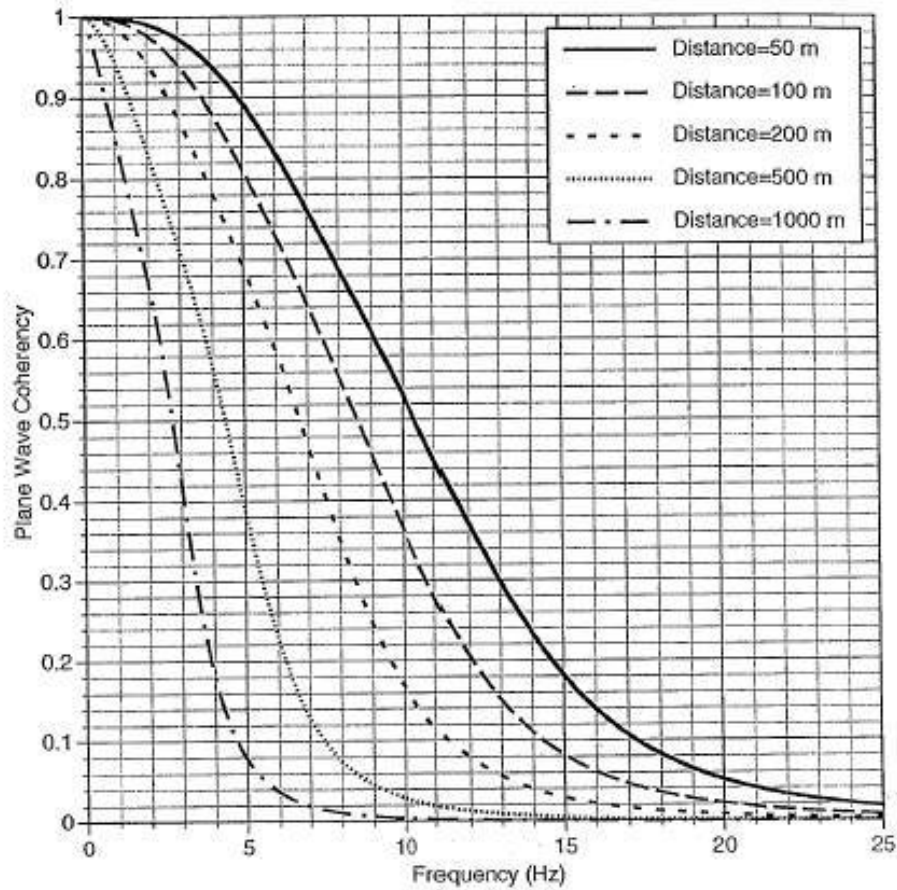


Figure 3-15 Coherency Function for Horizontal Component Motion (Abrahamson, 1992)

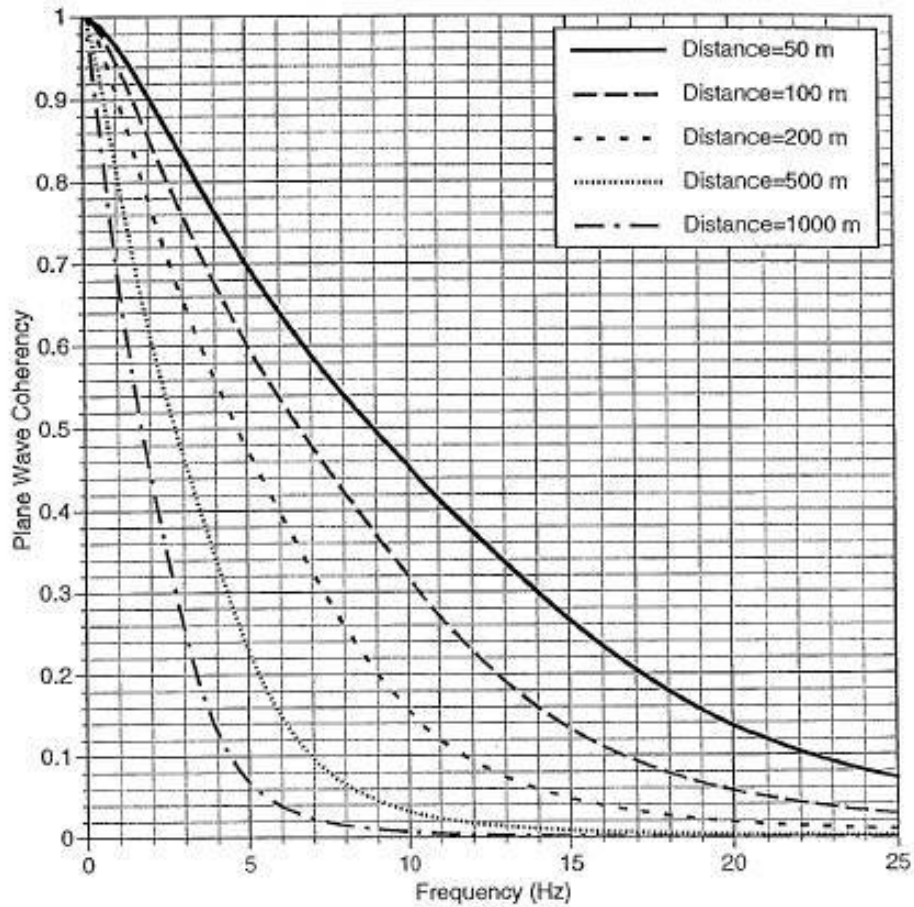


Figure 3-16 Coherency Function for Vertical Component Motion (Abrahamson, 1992)

Each of the above phenomena can contribute to differences in the ground motions at the supports of a long bridge or tunnel. However, experience has shown that the effect of the first three phenomena is usually very small and may be ignored, with the exception of the wave passage effect on long span structures. The most important factor contributing to differential ground motion is likely to be variability in the soil conditions from support to support. It is most important to include this factor when developing spatially varying, multiple support motions for use in time history analyses. Both displacement and acceleration time histories may be required to correctly model the response of a bridge, although some computer programs will compute one from the other if both are not available. Approximate methods that use a modified response spectrum to account for the spatial variability of ground motions, thereby avoiding time history analysis, have been proposed but not yet been shown to be reliable.

3.3.12 Vertical Ground Motions

The subject of vertical ground motions sometimes leads to heated debates among academics and practicing engineers. An in-depth discussion on this subject is outside the scope of this document. A brief discussion of the issues surrounding vertical ground motion is given below.

- 1) Few structural design codes and specifications and essentially no geotechnical design provisions require consideration of vertical ground motions.
- 2) Vertical design spectra are not available from the USGS National Seismic Hazard mapping program. If vertical motions are to be considered in design, project-specific generation of vertical ground motions and/or spectra will be necessary.
- 3) The method of most technical merit for the development of a vertical ground motion spectrum makes use of the magnitude and distance data from the deaggregation of the hazard curve and an appropriate attenuation relationship to develop a period dependent V/H (vertical to horizontal) ground motion spectrum ratio. This V/H function can then be applied to the horizontal design spectrum to generate a target vertical spectrum for design.
- 4) In many situations (particularly for the CEUS) an appropriate attenuation relationship for vertical ground motions may not exist. In these circumstances, the rule of thumb of scaling the horizontal design response spectrum by $2/3$ can be used to develop a target vertical spectrum for design. However, this rule-of-thumb can break down at high frequencies (i.e. at spectral periods less than 0.15 second), especially where the site to seismic source distance is less than 50 km. Use of the $2/3^{\text{rds}}$ rule-of-thumb procedure for bridges with short fundamental periods and close to active faults is therefore not advised.

Some investigators have suggested the use of one-dimensional wave propagation theory to account for the influence of local soil conditions on vertical ground motions. However, it is not clear that one-dimensional wave propagation theory (the most common approach in a site-specific response analysis – see Chapter 5 of this report) is the proper approach to account for the impact of local soil conditions on vertical ground motions. Experience indicates that modeling the propagation of compressional waves using a one-dimensional soil column model usually leads to unrealistic vertical motions, especially at high excitation levels. Until further studies are available, it is recommended to rely on empirical adjustments for local soil effects (e.g. establishing the spectral period-dependent V/H ratio based on attenuation relationships) when developing acceleration spectra for vertical ground motions if they are required for analysis.

3.4 DEVELOPMENT OF AASHTO ACCELERATION RESPONSE SPECTRUM

In most situations, the seismic design of a conventional bridge is based on the 1,000-yr return period national seismic hazard maps developed by the USGS for AASHTO in 2007. These maps provide the spectral acceleration at periods of 0.0, 0.2, and 1.0 seconds for use in constructing the acceleration design response spectra shown in Figure 3-11 in accordance with the AASHTO LRFD Specifications (2007, 2009). The FHWA Retrofitting Manual (2006) uses the same maps and procedure.

1,000-yr return period maps were not part of the original 2002 National Seismic Hazard mapping project but were developed by USGS specifically for AASHTO. Originally only available on a special CD provided by AASHTO, the computer program and database developed by USGS for AASHTO to evaluate the 1000-yr return period ground motions is now available for download from the USGS seismic hazard website at <http://earthquake.usgs.gov/hazards/designmaps/aashtocd.php>. The program provides spectral accelerations for the reference AASHTO weak rock site class, Site Class B, along with routines for adjusting these reference site values for local site conditions based upon V_{S30} using the procedure described in Section 3.5.5. Values of spectral accelerations for a 1,000 year return period from the most recent National Seismic Hazard map can also be obtained from the USGS website if the owner decides to use this data in design. The balance of this section steps through the use of both the USGS website and the USGS/AASHTO CD ROM to evaluate the 1,000-yr return period design response spectra and use of the USGS website for estimation of the associated magnitude deaggregation.

In some special cases, e.g. for major bridge projects or in regions where there have been significant advances in the understanding of the local seismic environment since development of the USGS National Seismic Hazard maps, a site-specific seismic hazard analysis may be justified. In such cases, the qualified professionals conducting the site-specific analysis can provide the designer with the uniform hazard response spectra for any desired return period and the associated magnitude deaggregation for any specified spectral period. However, unless an attenuation relationship that accounts for local site conditions (e.g. one or more of the Next Generation Attenuation relationships described in Section 3.5) is employed in the seismic hazard assessment, the results must still be corrected for local site conditions. This correction can be accomplished using either the procedure described in the next section to correct the spectral acceleration values for V_{S30} or a site-specific seismic response analysis as described in Chapter 5. Furthermore, if a modal superposition structural analysis is going to be conducted, the AASHTO design spectra must still be generated from the site-corrected spectral acceleration values as described in the Section 3.3.8 of this chapter.

3.4.1 Use of the USGS Website

To obtain the anchoring points for the AASHTO 1,000-yr response spectrum (or for any other desired return period) from the USGS website, the *Seismic Design Values for Buildings* option at <http://earthquake.usgs.gov/research/hazmaps/design/> must be used. Figure 3-17 shows the initial screen for this page of the website.

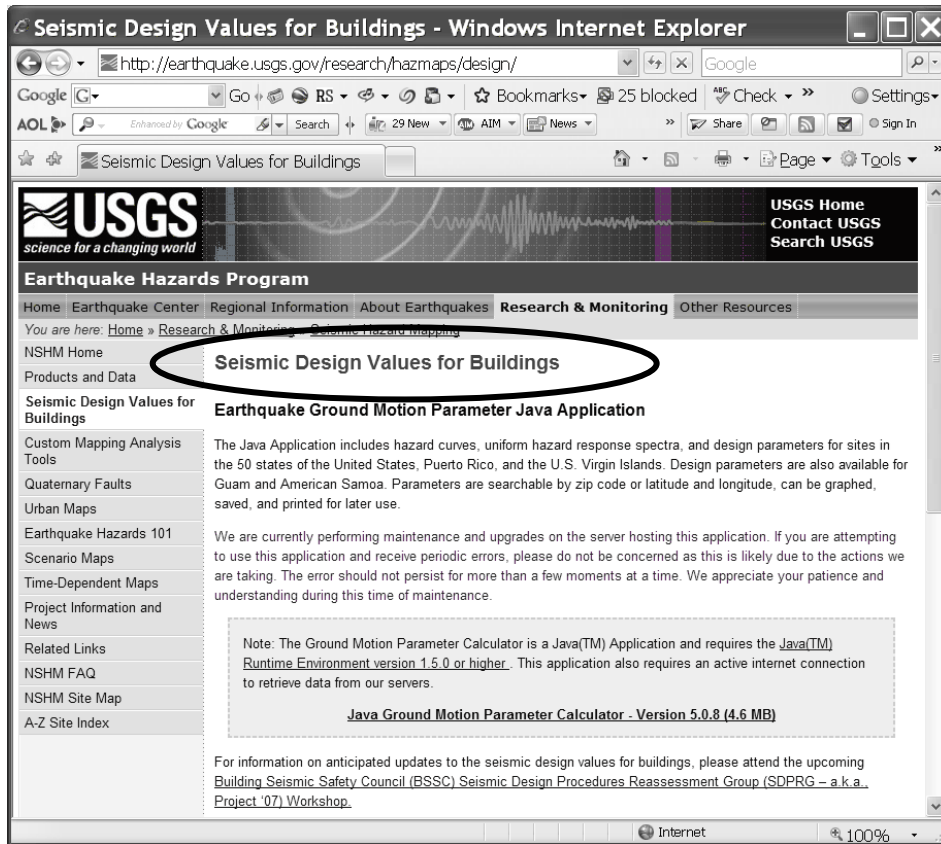


Figure 3-17 Initiation Screen for the *Seismic Design Values for Buildings* option

Clicking on the link for the Java Ground Motion Parameter Calculator – Version 5.0.8 (4.6 MB), circled in bold at the bottom of the screen shown in Figure 3-17, will bring up a dialog box for this application. Clicking on the OPEN button in the dialog box brings up the screen shown in Figure 3-18 for Seismic Hazard Curves, Response Parameters, and Design Parameters.

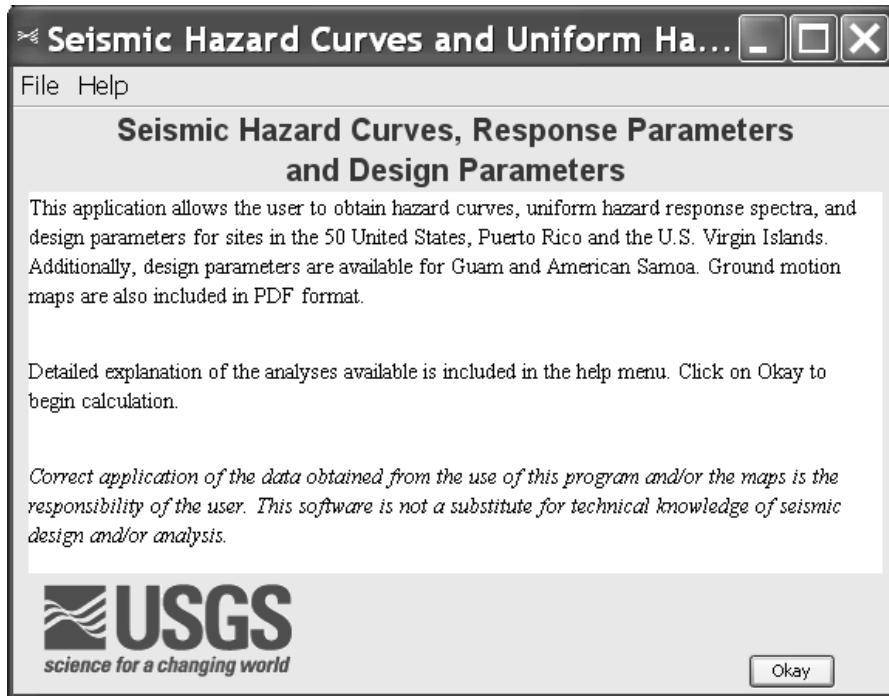


Figure 3-18 Initial Screen for Seismic Hazard Curves and Uniform Hazard Response Spectra

Clicking the OKAY button on the lower right of Figure 3-18 brings up the basic input screen shown in Figure 3-19. The essential information for obtaining the reference site class (Site Class B) peak ground acceleration and spectral accelerations for 0.2 second and 1 second periods for the 1,000-yr return period (or any other return period desired) is input on this screen. To obtain values for the 1,000-yr return period, the “Probabilistic Seismic Hazard Curve” option in the pull-down menu at the top of the screen in Figure 3-19 must be selected. This will bring up the screen shown in Figure 3-20.

The latitude and longitude for the site is entered into the appropriate boxes in the center of the screen in Figure 3-20 and a 1,000-year return period is selected in the drop down menu at the bottom of the screen. (Note: the search by zip codes option is not recommended, as some zip code areas are excessively large.) Then, by clicking on the CALCULATE button at the very bottom of the screen, the screen shown in Figure 3-21 will appear. The data points for the PGA seismic hazard curve and the singular value for PGA corresponding to a 1,000-yr return period are provided in this screen. For illustration purposes, the San Francisco-Oakland Bay Bridge East Span location was arbitrarily chosen as the input location for the screen shown in Figure 3-20. The coordinates employed in the demonstration (latitude 37.814° north and longitude -122.359° west) corresponds to the far eastern point of the East Span at Yerba Buena Island. As

shown in Figure 3-21, the PGA corresponding to a 1,000-yr return period for the Site Class B reference condition at this location is 0.571 g. The reference site condition spectral accelerations for periods of 0.2 and 1 second are then generated by selecting “Hazard Curve for 0.2sec” and “Hazard Curve for 1.0sec” from the Seismic Hazard Curve drop down box near the bottom of the screen of the left hand side and clicking the calculate button for each of the seismic hazard curves. The resulting screens, shown in Figure 3-22 and Figure 3-23, show that for the Site Class B reference condition at this location and a 1,000-yr return period the spectral acceleration for 0.2 second period is 1.386 g and the spectral acceleration for 1.0 second period is 0.608 g.

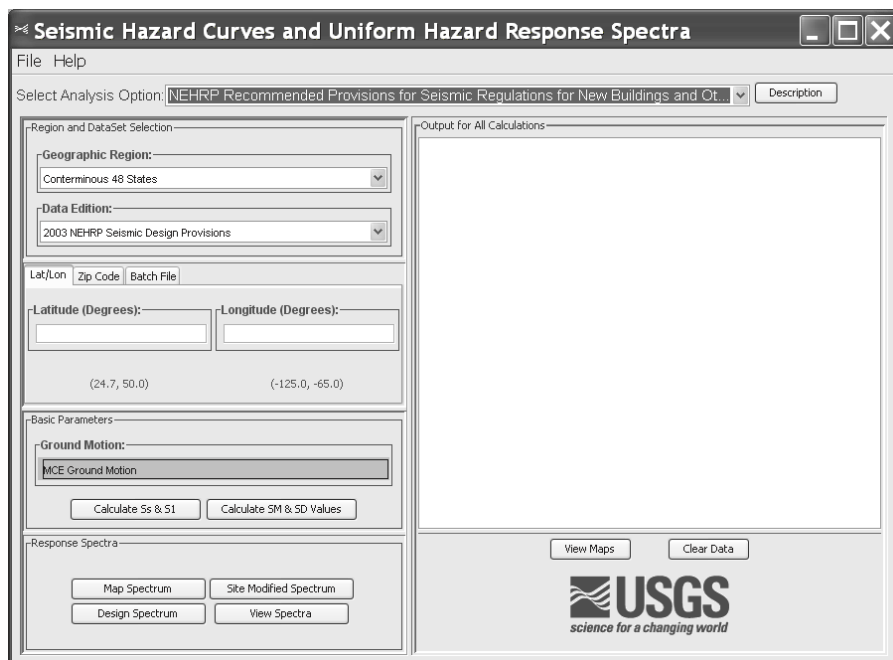


Figure 3-19 Input Screen for Seismic Hazard Curves, Response Parameters, and Design Parameters

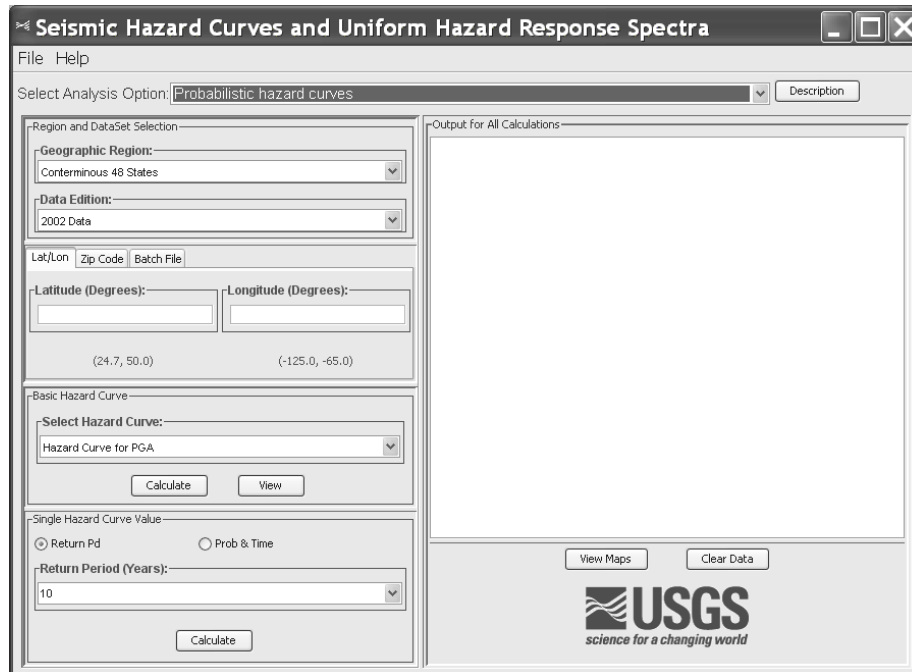


Figure 3-20 Input Screen for Probabilistic Hazard Curves

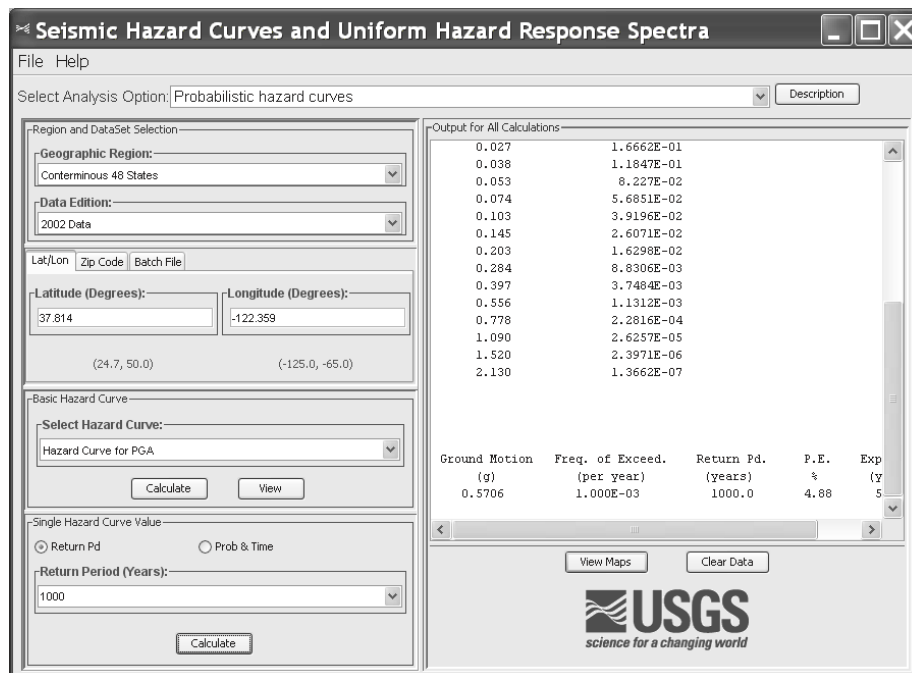


Figure 3-21 Screen for PGA for 1000-yr Return Period

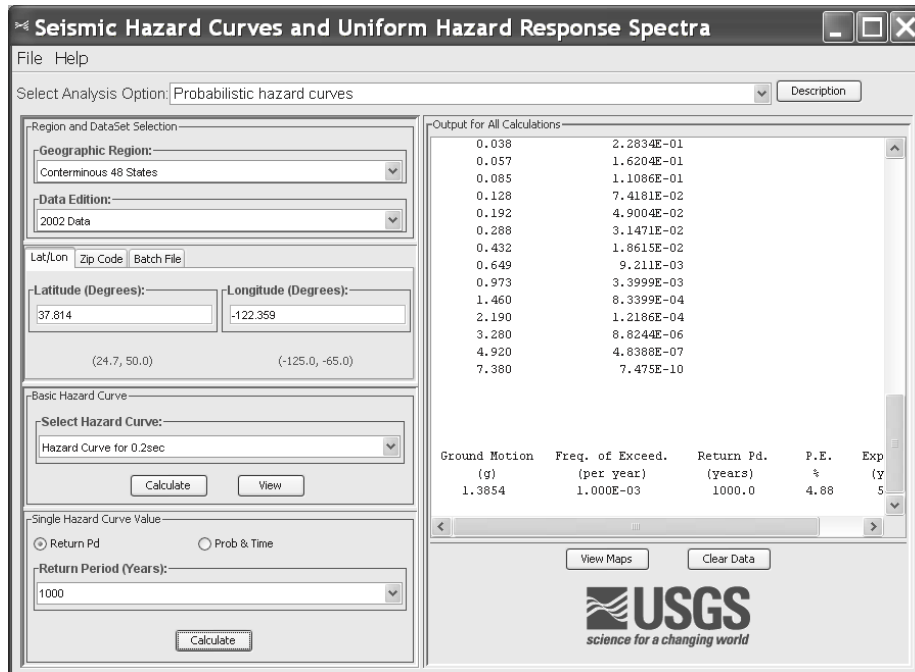


Figure 3-22 Screen for 0.2 sec Spectral Acceleration for 1000-yr Return Period

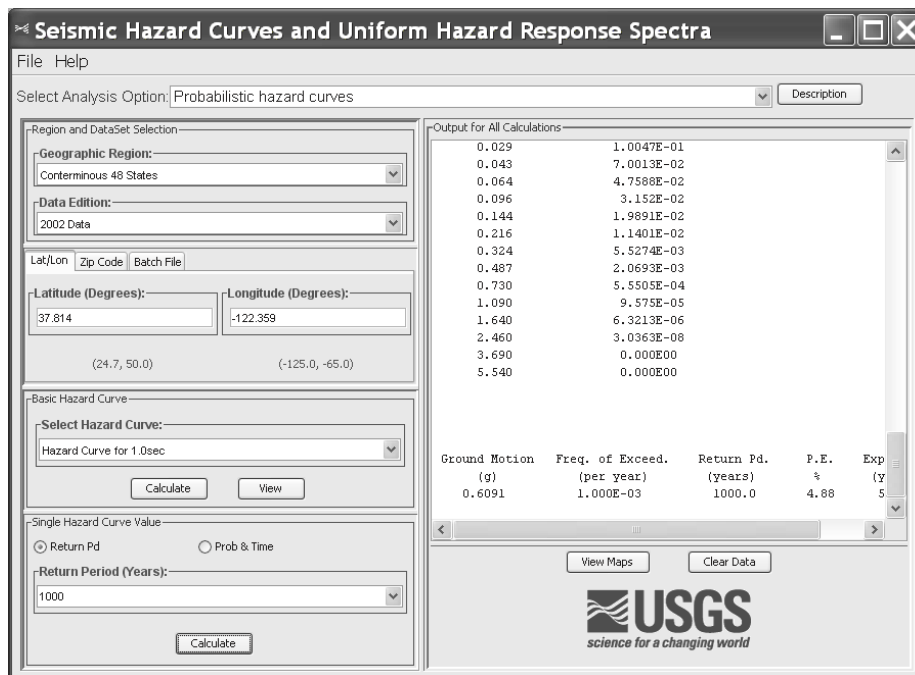


Figure 3-23 Screen for 1.0 sec Spectral Acceleration for 1000-yr Return Period

The PGA and spectral accelerations for the Site Class B reference site condition must still be adjusted for site-specific ground conditions using the Site Class factors presented in Tables 3-6, 3-7 and 3-8. Assuming Site Class C for illustration purposes, Table 3-6 yields a value for F_{pga} , the PGA site factor, of 1.0 for PGA values in excess of 0.5 g. Table 3-7 yields a value for the F_a , the short period site factor, of 1.0 for short period (0.2 second period) spectral accelerations in excess of 1.25 g. Table 3-8 yields a value of F_v , the long period site factor, of 1.3 for spectral accelerations at 1.0 second in excess of 0.5 g. To calculate the appropriate spectral values for Site Class C, the PGA is multiplied by F_{pga} (i.e. multiplied by 1.0 for this example) the 0.2 second spectral acceleration is multiplied by F_a (i.e. multiplied by 1.0 for this example), and the 1.0 spectral acceleration is multiplied by F_v (1.3 for this example). Applying these site factors to the reference site class (Site Class B) values yields a site class-corrected value of 0.571 g for the PGA, 1.39 g for the spectral acceleration at 0.2 second, and 0.792 g for the spectral acceleration at 1.0 second for Site Class C at the example site for a 1,000-yr return period.

The Site Class C PGA and spectral accelerations can then be used to construct the AASHTO design spectrum in accordance with Figure 3-11. As shown in this figure, the anchoring periods for the plateau of the AASHTO spectrum, T_s and T_0 , are calculated as follows: T_s is calculated as the spectral acceleration at 1.0 second divided by the spectral acceleration at 0.2 second and T_0 is calculated as $0.2 T_s$. For the example above, this procedure yields $T_s = 0.792/1.39 = 0.57$ second and $T_0 = 0.2 T_s = 0.11$ second. The resulting AASHTO design spectrum for the example site for a 1,000-yr return period for Site Class C is shown in Figure 3-24. Spectral acceleration values at spectral periods greater than 0.57 second can be calculated by assuming that the spectral acceleration decays as $1/T$ in this range. Based upon this assumption and a spectral acceleration of 0.792 at 1 second, the following values can be calculated for the spectral acceleration, S_a , at periods greater than 0.57 g: $S_a = 1.056$ at $T = 0.75$ sec; $S_a = 0.528$ at $T = 1.5$ sec; $S_a = 0.396$ at $T = 2$ sec; $S_a = 0.317$ at $T = 2.5$ sec; $S_a = 0.264$ at $T = 3.0$ sec; $S_a = 0.198$ at $T = 4.0$ sec.

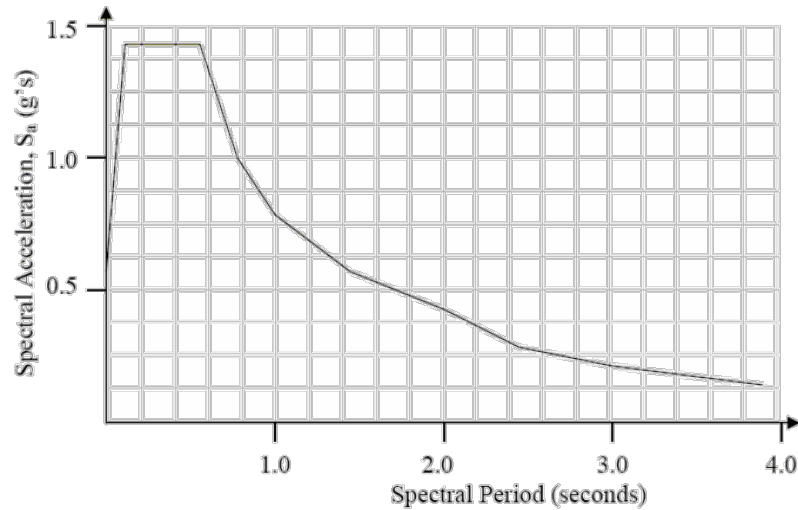


Figure 3-24 Bay Bridge Site AASHTO Design Spectrum for Site Class C Conditions

3.4.2 Use of the USGS/AASHTO CD

The initial screen for the 1,000-Year Ground Motion CD produced by the USGS for AASHTO is shown in Figure 3-25. After clicking the “Okay” button on this initial screen, the screen shown in Figure 3-26 appears. As shown in Figure 3-26, the next step after initiation of the ground motion CD program involves inputting the site location, either in terms of the geographic coordinates (latitude and longitude) or the zip code. As noted before, use of geographic coordinates is more accurate and the use of the zip code option is not recommended. In the following example, we use the same location employed to illustrate the AASHTO design spectrum in Figure 3-11: a site in Memphis, Tennessee with latitude 35.18° north and longitude -89.97° west. After inputting the site location, the desired hazard level is selected (in this example, a 7% probability of exceedance in 75 yr, corresponding to the 1,000-yr return period). Next, upon clicking the “Calculate PGA, S_s , and S_1 ” button, the program provides the three design spectrum anchoring points, i.e. the spectral accelerations at 0.0, 0.2, and 1.0 seconds, for the reference Site Class B site condition of an average shear wave velocity over the top 100 ft of between 2500 and 5000 ft/s. For the example site location, the three anchoring points provided by the program are 0.388 g for the spectral acceleration at 0 seconds (the PGA), 0.725 g for the short period spectral acceleration, S_s (i.e. the spectral acceleration at 0.2 second), and 0.185 g for the long period spectral acceleration, S_1 (i.e. the spectral acceleration at 1 second).

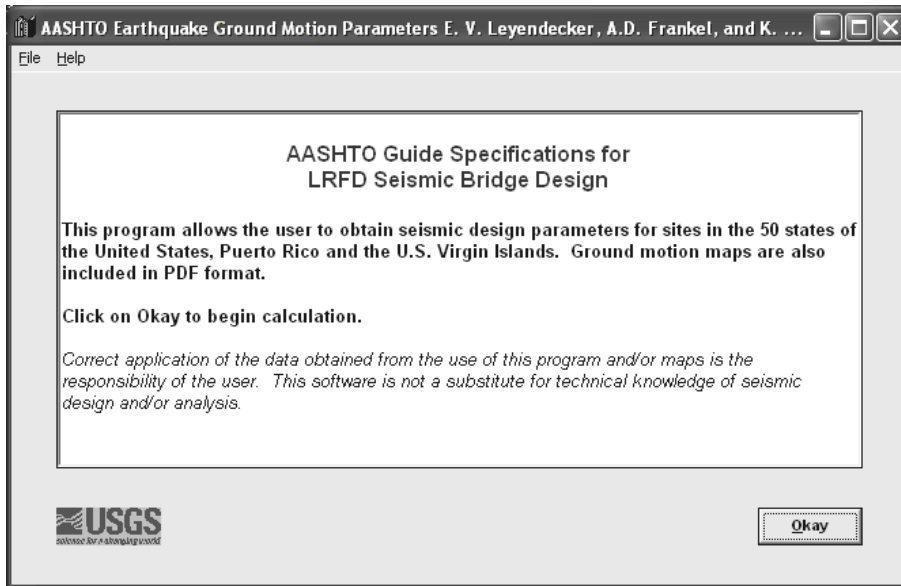


Figure 3-25 Initiation Screen in the USGS/AASHTO Ground Motion CD

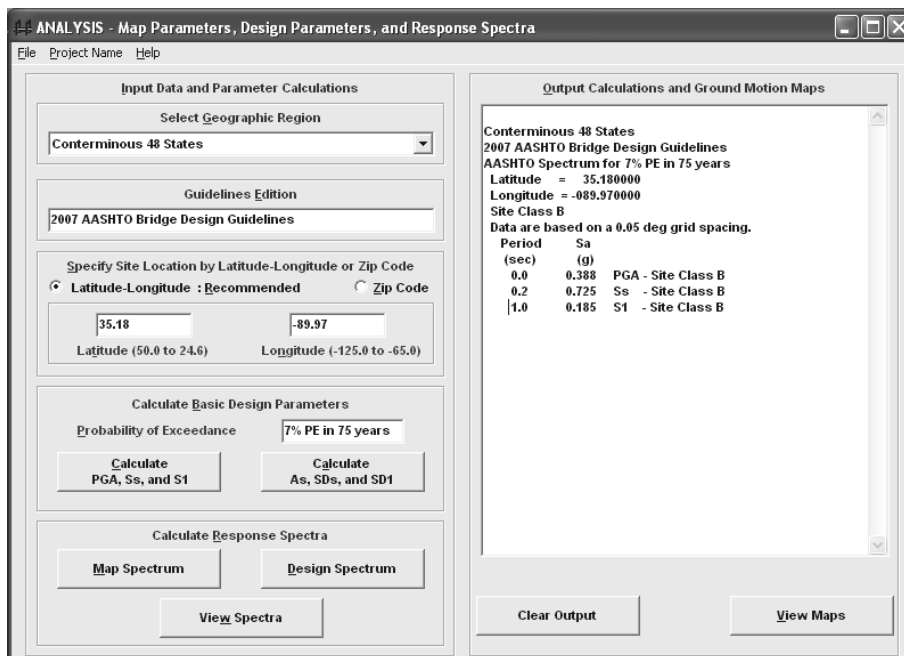


Figure 3-26 Screen No. 2: Site Location and Design Hazard Level

Following the evaluation of the spectral accelerations associated with the reference Site Class B site condition, the site soil factors are calculated by clicking the “Calculate As, SDs, and SD1” box in Screen

2 (Figure 3-26). Upon clicking the “Calculate A_s , S_D s and S_{D1} ” box, the screen shown in Figure 3-27 appears showing the NEHRP site factors for site classes A, B, C, D, and E. At this point, the user selects the appropriate site class from the box on the left hand side of the screen in Figure 3-27. In this example, we elected to conduct the analysis for Site Class D. Upon clicking the “Site Class D” box on the left hand side of the screen, interpolated site coefficient factors of $F_{pga} = 1.11$, $F_a = 1.22$, and $F_v = 2.06$ will be used to scale the reference site class (Site Class B) values for the PGA (0.388 g), S_s (0.725g) and S_1 (0.185g), to the appropriate site specific values for Site Class D.

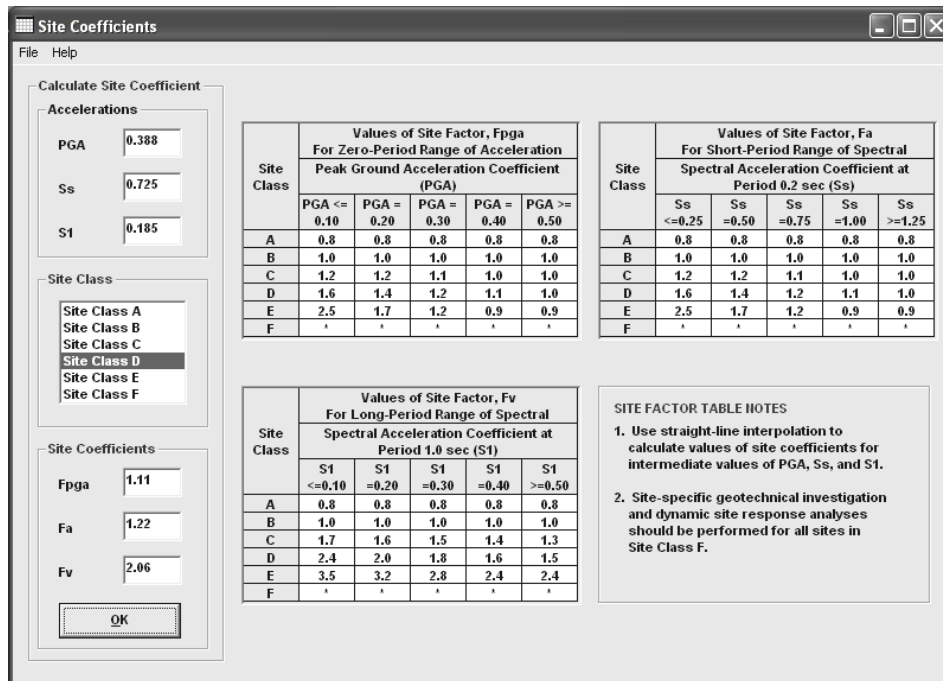


Figure 3-27 Screen No. 3: Site Factor Table.

After clicking the “OK” tab at the lower left corner of Screen 3 in Figure 3-27, the program produces the screen shown in Figure 3-28 with a tabulation of the spectral accelerations for the three anchoring periods for the Class D design spectrum ($A_s = F_{pga} \times \text{PGA} = 0.473$; $S_{DS} = F_a \times S_s = 0.884$; $S_{D1} = F_v \times S_1 = 0.381$) along with the values for the initial reference Class B site condition.

From the screen in Figure 3-28, the user has the option of plotting the spectrum for the reference Class B site by clicking the “Map Spectrum” button or the Site Soil Adjusted spectrum (the Class-D Spectrum in

this demonstration) by clicking the “Design Spectrum” button. The user can also click both buttons to generate both spectra.

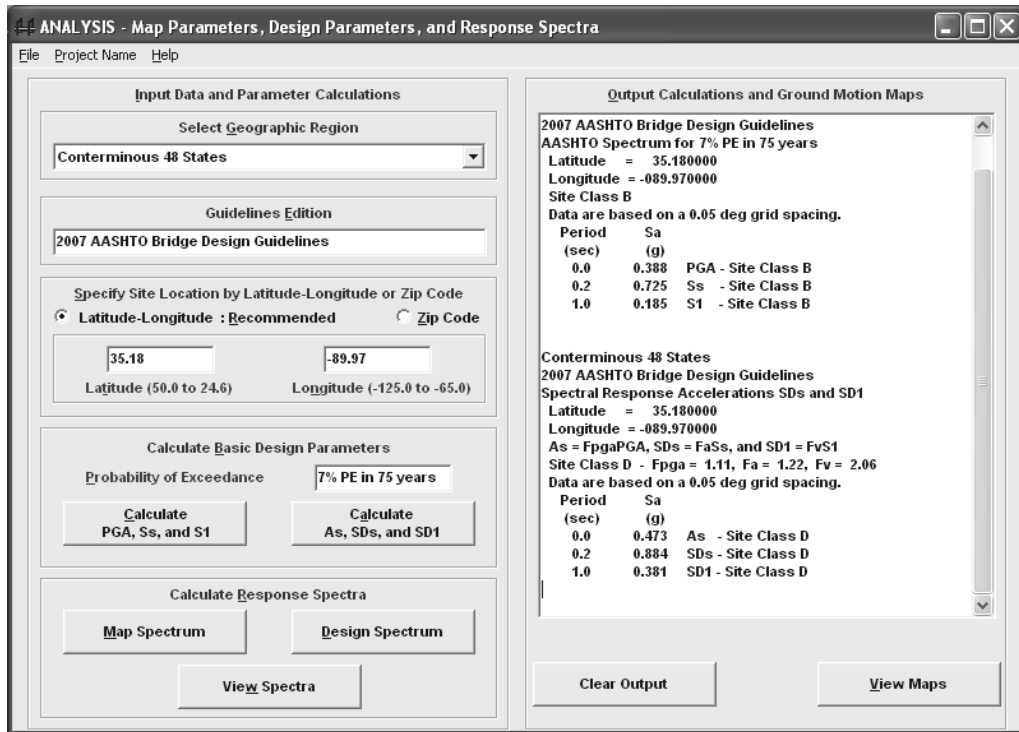


Figure 3-28 Screen No. 4: Site Class Adjusted Anchoring Points for Design Spectrum

By clicking the “Map Spectrum” tab, the screen shown in Figure 3-29 (Screen 5) is created with a tabulation of the AASHTO reference site (Site Class B) acceleration response spectrum. By clicking the “Design Spectrum” tab, the screen shown in Figure 3-30 (Screen 6) is created with a tabulation of the AASHTO design spectrum for Site Class D.

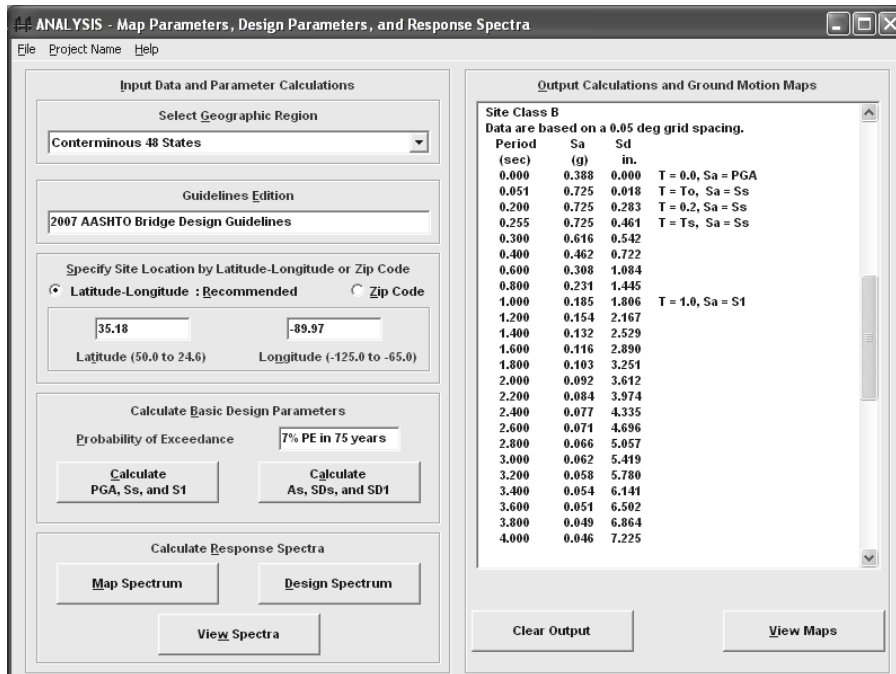


Figure 3-29 Screen No. 5: Reference Site Spectrum Values

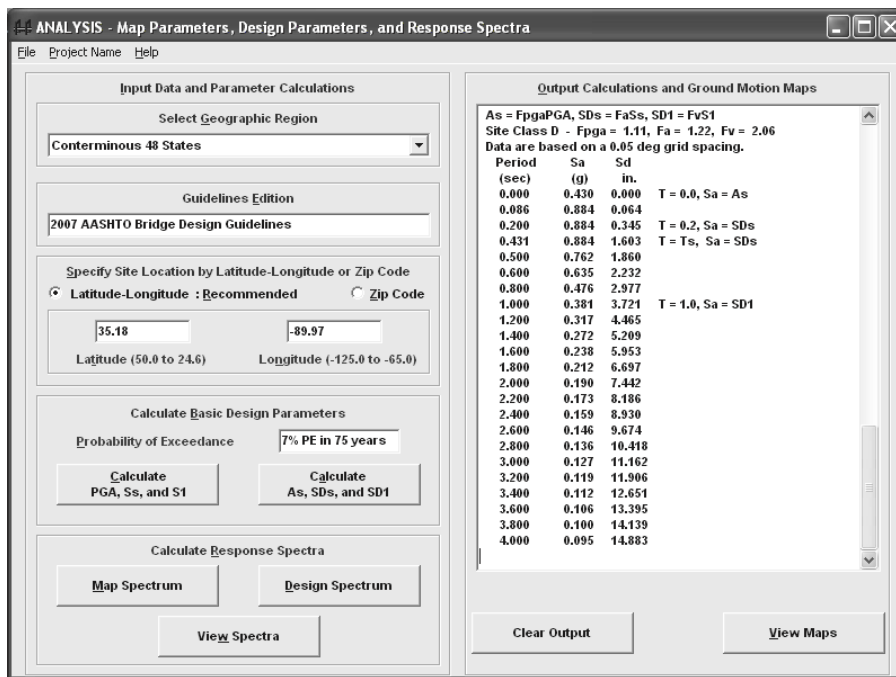


Figure 3-30 Screen No. 6: Site Class D Spectrum Values

At this point, the calculations for both the initial reference site condition (the “Map Spectrum”) and the site class adjusted spectrum (the “Design Spectrum”) are complete. In the next step, the AASHTO/USGS ground motion CD allows graphical display of the various developed spectra. One can initiate the display options by clicking the “View Spectra” button at the bottom the prior screen. Then one can click on the Select Graph button from the pull down menu in the subsequent screen (Screen 7) which will display the various options listed below:

- 1) Map Spectrum for S_a vs. T.
- 2) Map Spectrum for S_a vs. S_d , (plot spectral acceleration versus spectral displacement).
- 3) Design Spectrum for S_a vs. T.
- 4) Design Spectrum for S_a vs. S_d .
- 5) All S_a vs. T Spectra (for viewing comparison between the mapped spectrum and the Design Spectrum), and
- 6) All S_a vs. S_d Spectra.

Figure 3-31 (Screen No. 7) presents the screen obtained when selecting Option 1 above for the Map Spectrum for S_a vs. T (for Site Class B). Figure 3-32 (Screen No. 8) presents the screen obtained when selecting Option 5, the All S_a versus T Spectra option, and shows both the Map Spectrum (for Site Class B) and the adjusted Design Spectrum for Site Class D. Figure 3-33 (Screen No. 9) presents the screen obtained when selecting Option 6, the All S_a vs. S_d Spectra option, showing spectral acceleration versus displacement for both Site Class B and Site Class D.

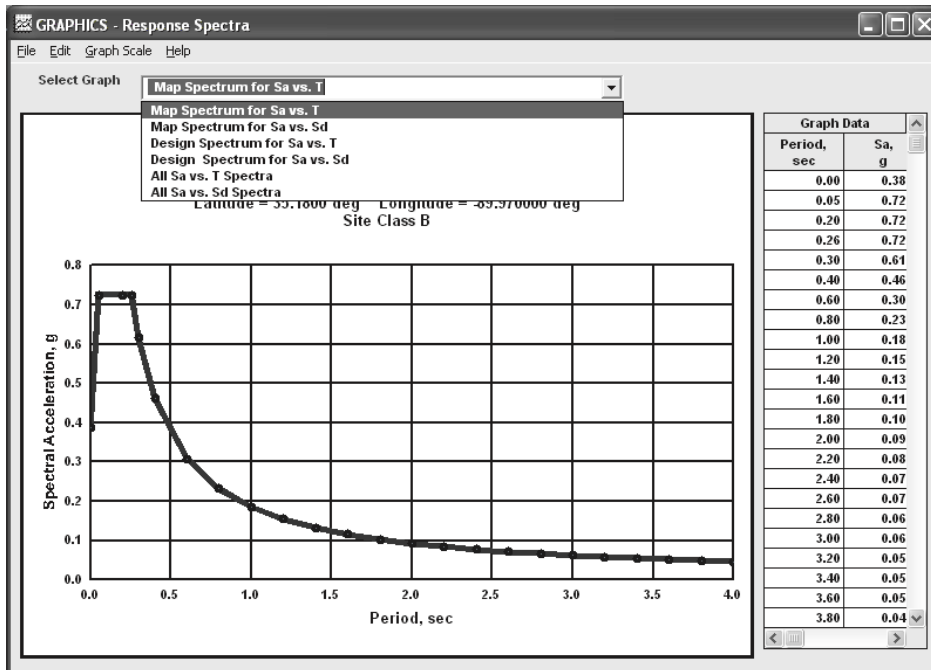


Figure 3-31 Screen No. 7: Options for Viewing Various Spectra

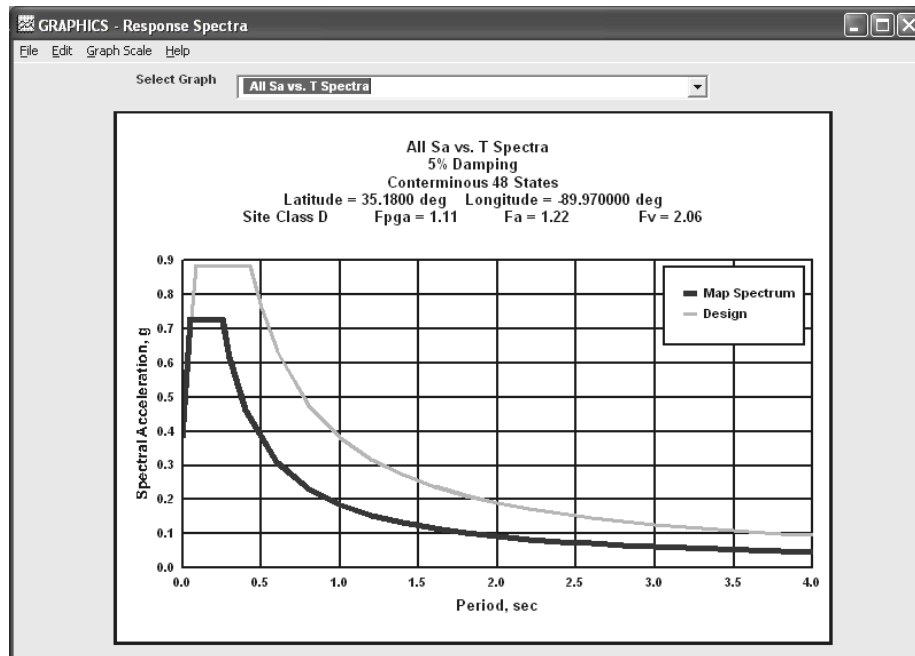


Figure 3-32 Screen No. 8: Example of “All S_a vs. T Spectra” Option

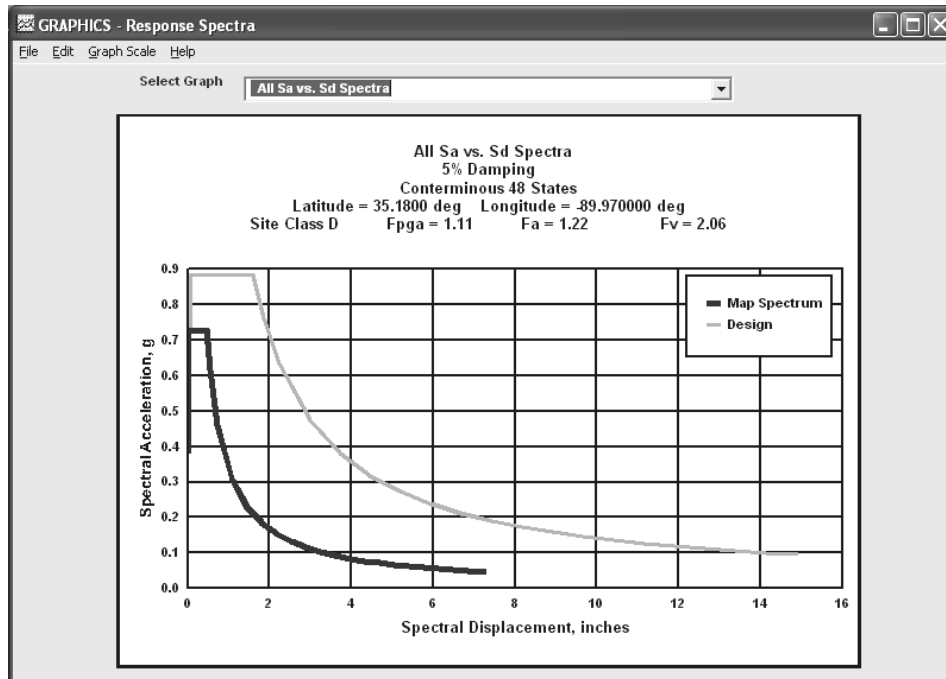


Figure 3-33 Screen No. 9: Example of “All S_a vs. S_d Spectra” Option

3.4.3 Magnitude Deaggregation

The 1,000-year Ground Motion CD distributed by AASHTO/USGS has been designed solely for construction of the 1,000-year return period uniform hazard spectra. There is no provision on the Ground Motion CD for extracting the deaggregated magnitude and distance information for design. Currently, deaggregation of the design earthquake, including for the 1,000-year return period event derived from the AASHTO/USGS Ground Motion CD, needs to be conducted through the USGS web site. The following link will take the user to the USGS deaggregation web page: <http://eqint.cr.usgs.gov/deaggint/>. The screen associated with this link is shown below in Figure 3-34.

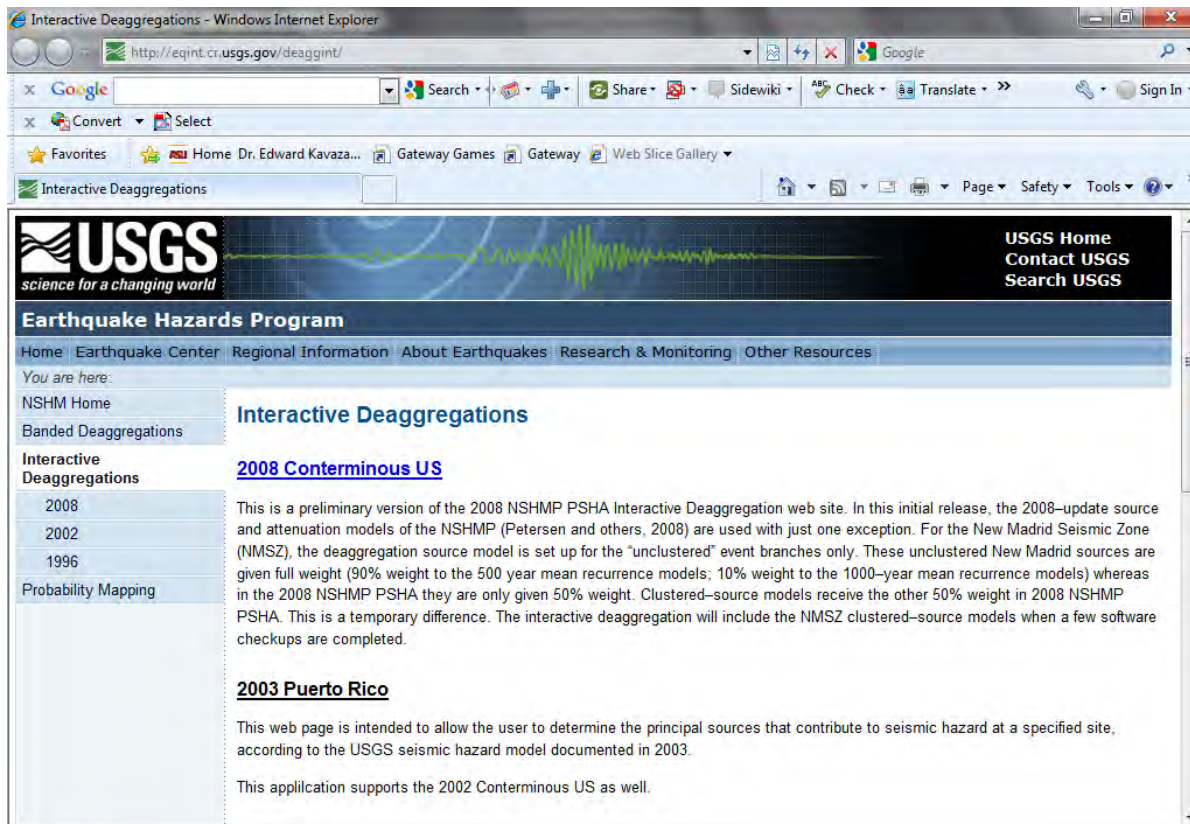


Figure 3-34 Initial Screen from the USGS Web Site for Interactive Deaggregation

The deaggregation data for the AASHTO design seismic hazard design event (i.e. for a 100-yr return period and the 2002 USGS seismic hazard data) can be obtained by clicking on the “Interactive Deaggregation 2002” button on the left hand side of the screen shown in Figure 3-34. Clicking on the 2002 deaggregation button leads to screen shown in Figure 3-35. On this screen, the user inputs the site location and selects the desired hazard level (similar to screen 2 from the USGS/AASHTO CD ROM) as well as the spectral frequency (the inverse of the spectral period) for which the deaggregation is desired.

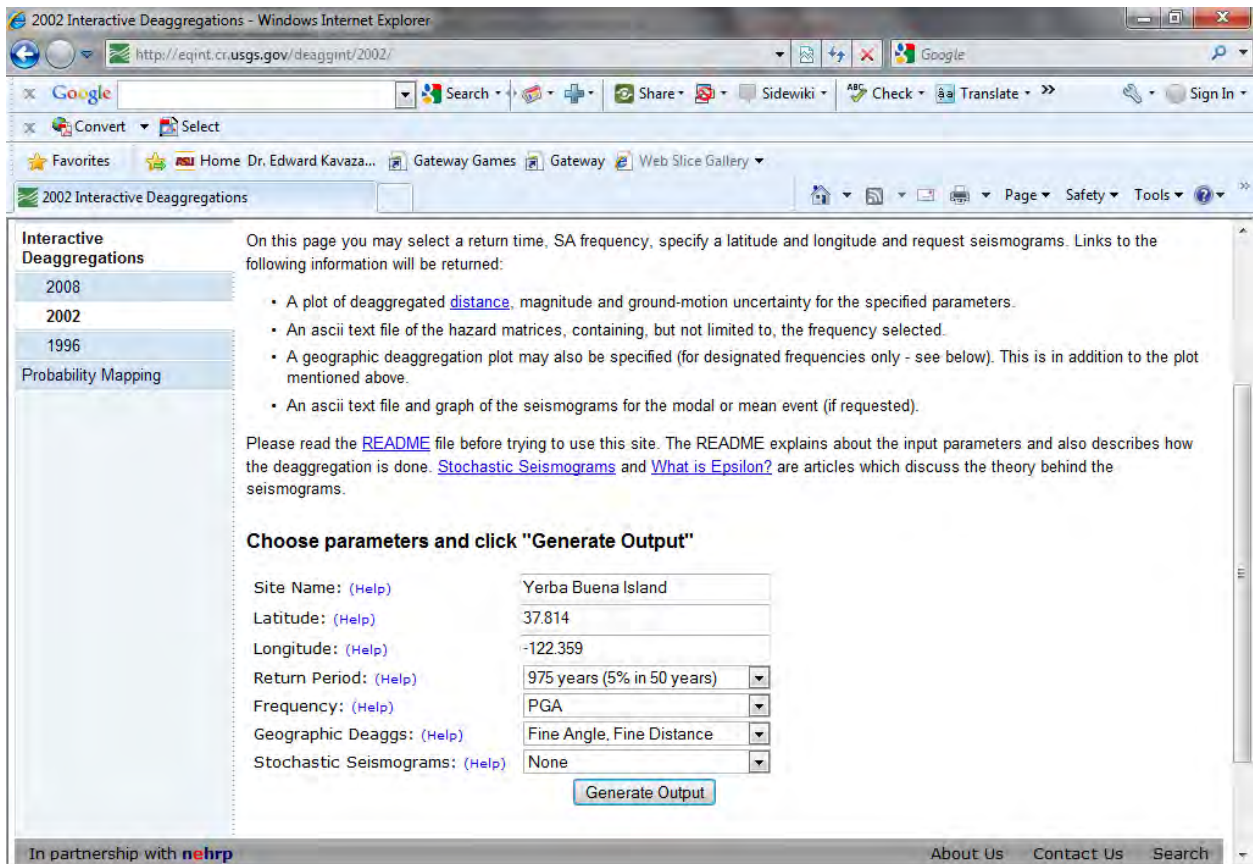


Figure 3-35 Screen for Specifying Location and PSHA Return Period

After specifying the ground motion parameters for deaggregation and clicking the Generate Output tab on the screen in Figure 3-35, the screen shown in Figure 3-36 appears. The screen shown in Figure 3-36 allows the user to select one of the three types of output files:

- 1) Report
- 2) Deaggregation
- 3) Geographic deaggregation



Figure 3-36 Available Interactive Deaggregation Results

Figure 3-37 and Figure 3-38 show the screens that will appear following clicking the Deaggregation tab and the Geographic Deaggregation tab, respectively. Figure 3-37 is a bar chart of the magnitude/distance deaggregation from which the designer can extract magnitude and distance combinations appropriate for design. The report tab provides tabular output for this data. Figure 3-38 plots the magnitude distribution on a map and can be used to clarify the specific seismic sources contributing to the seismic hazard. Note that the plots in Figure 3-37 and Figure 3-38 show a bi-modal hazard, with half the hazard coming from an earthquake on the Hayward fault with a characteristic magnitude of 7 and half the seismic hazard coming from an event on the San Andreas fault with a characteristic magnitude of 7.9.

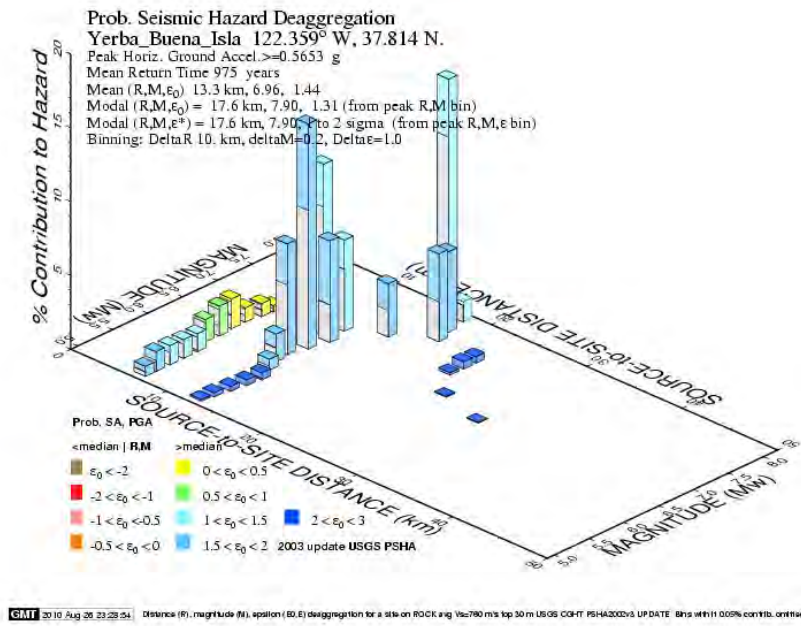


Figure 3-37 Hazard Deaggregation for Combinations of Magnitude and Distance

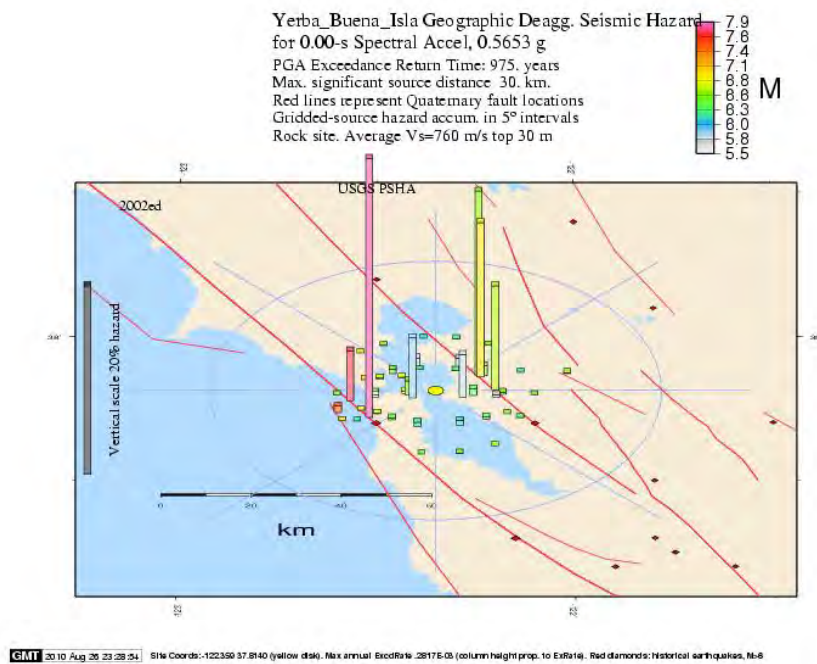


Figure 3-38 Geographic Hazard Deaggregation

3.5 RECENT ADVANCES IN ENGINEERING SEISMOLOGY AND GROUND MOTION CHARACTERIZATION

One of the most significant recent developments in engineering seismology and ground motion characterization is the Next Generation Attenuation (NGA) project sponsored by the National Science Foundation, Caltrans, and Pacific Gas and Electric Company. This project has recently completed an update of the commonly used attenuation models for shallow crustal earthquakes in active tectonic regions (e.g. the WUS). The 2009 USGS National Seismic Hazard Maps have implemented this new generation of attenuation relationships. The same consortium has embarked upon a similar update for CEUS attenuation relationships. Subsequent phases of the NGA project, hopefully including attenuation relationships for subduction zones, will most likely lead to further updates in the USGS ground motion hazard maps for U.S.

The NGA project is being coordinated by the Lifelines Program of the Pacific Earthquake Engineering Research Center (PEER), in partnership with the U.S. Geological Survey and the Southern California Earthquake Center. In the developing attenuation relationships for the WUS, five sets of ground-motion models were developed by teams working independently but interacting with one another throughout the development process. The development of these WUS NGA ground motion models was supported by other project components, including (1) development of an updated and expanded PEER database of recorded ground motions, earthquake sources, travel path, and recording station site conditions (see http://peer.berkeley.edu/products/strong_ground_motion_db.html); (2) supporting research projects to provide guidance on the selected functional forms of the ground motion models; and (3) a program of interactions throughout the development process to provide input and reviews from both the scientific research and engineering user communities. A special February, 2008 issue publication of the EERI Earthquake Spectra provides documentation of this initial phase of the NGA project (e.g. Abrahamson et al., 2008).

The NGA models have increased the level of sophistication required to apply attenuation equations. Four of the five NGA attenuation models (all but the Idriss model) require many more input parameters than the traditional parameters of magnitude, distance, and style of faulting in their attenuation equations. The average engineer may not have sufficient understanding on what some of these parameters mean and there is no easy way to measure some of the required input parameters. With the exception of the Idriss NGA model, there are as many as 15 parameters involved in the NGA models. An important facet of the NGA models is that they account for the influence of local site conditions directly by using V_{s30} as one of

the input parameters in the attenuation model (as opposed to the use of site factors to modify the reference site spectrum). Two of the NGA models also use the depth to a shear wave velocity of 3300 ft/s (1000 m/s) and another model uses the depth to a shear wave velocity of 8250 ft/s (2500 m/s) as discriminating factors that reflect local site conditions.

Two and three dimensional site response effects and deep soil basin effects are also a subject of much current research, as is the response of other types of stratigraphic profiles that do not conform to stratigraphy assumed in the development of the NEHRP site factors. Observed multi-dimensional site response effects include Basin Edge effects, wherein the ground motions around the edge of a soil basin are influenced by the direction of the propagating seismic wave (i.e. from within the basin or from outside of the basin). However, there are no simple methods to account for the effects of wave propagating to the site from outside the basin edge at the present time. Site response analyses have also shown that response of deep soil basins (i.e. basins with over 500 ft of sediments) and of soil sites with a bedrock interface or other layer interface across which there is a significant contrast in soil stiffness and density within 150 to 200 ft of the ground surface is not properly described by the NEHRP soil site factors. These deep soil basin and shallow bedrock conditions can be accounted for using appropriate one-dimensional site response analysis, as discussed in Chapter 5 of this document.

The near-fault directivity effect (e.g. Sommerville et al., 1997) discussed previously is another area of current research and development. This effect has been included in development of input ground motions for seismic retrofit of the long-span bridges in California for over 10 years (starting from about 1995). Inclusion of the near field effect using a 1995 Somerville procedure drastically impacted the response of several of these bridge structures, leading to a very significant increase in retrofit cost. However, subsequent developments, e.g. the Sommerville 1997 near-fault forward directivity adjustment procedure, suggest that the 1995 Sommerville near-fault directivity adjustment procedure was overly conservative (Abrahamson, 2000). This lesson suggests that one needs to be careful in implementing new state-of-the-art procedures in design until these procedures have been properly vetted.

3.6 SUMMARY

This chapter describes the methods used to assess and characterize strong ground motions for use in seismic design. The fundamental steps in a seismic hazard analysis are described, including seismic source characterization, strong motion attenuation, and prediction of design ground motion parameters. Both probabilistic and deterministic seismic hazard analyses are described and the advantages and disadvantages of these two types of analysis are discussed. A detailed discussion of strong ground motion attenuation relationships is provided along with examples of common attenuation relationships for the tectonic regimes encountered in the United States. Application of a typical attenuation relationship, the Abrahamson and Silva (1997) relationship, is illustrated through an example. The essential products of a probabilistic seismic hazard analysis, including the development of uniform hazard spectra and the associated magnitude-distance deaggregation, are described in detail. Uniform hazard spectra describe the intensity of seismic loading. The magnitude-distance deaggregation is used to establish a representative magnitude and distance for use in design. Development of acceleration response spectra for deterministic scenario earthquakes is also described. The selection of the design earthquake for both safety and functionality is discussed.

The procedure for developing the acceleration response spectra for structural design in accordance with AASHTO seismic design provisions, including adjustments for local soil conditions, is presented. A correlation between spectral acceleration and peak ground velocity and an equation for deriving the displacement spectra from the acceleration response spectra are included in the discussion of seismic design input parameters. The importance in design of a variety of special considerations, including near-field fault directivity effects, vertical motions, and the spatial variability of ground motions, is discussed. The procedures used to select a suite of representative time histories for use in time-domain analysis is presented. Step-by-step procedures are presented for developing the AASHTO 1,000-year return period acceleration response spectra for safety-level design of transportation facilities from the USGS web site and the special CD prepared by the USGS for AASHTO. Finally, current topics in seismic hazard assessment, including the development of the next generation attenuation (NGA) equations under the auspices of the Pacific Earthquake Engineering Research (PEER) Center are discussed.

Design ground motion parameters developed in accordance with the methods described in this chapter, are essential input to structural and geotechnical seismic design analyses. These parameters include the value of peak parameters (e.g. peak ground acceleration, peak ground velocity), acceleration and displacement response spectra, and representative time histories. The most common type of structural

analyses for seismic design, described in a companion document on seismic design of bridge structures, employs the acceleration response spectra described in this chapter as input. More sophisticated structural analyses may require the design earthquake displacement spectra or a suite of representative acceleration time histories, developed as described in this chapter, for input. The representative acceleration time histories described in this chapter are also essential input for the one-dimensional site response analyses described in Chapter 5 and the soil-structure interaction analyses described in Chapter 8 of this document. Peak ground acceleration, peak ground velocity, and deaggregated magnitude data for the design earthquake, developed as described in this chapter, are essential input to the geotechnical hazard analyses described in Chapter 6, the earthwork and foundations seismic performance analyses described in Chapters 7 through 12, and the buried structure performance analyses described in Chapter 13.

CHAPTER 4

SITE CHARACTERIZATION

4.1 INTRODUCTION

This chapter describes site characterization for the seismic design of geotechnical transportation features, including structural foundations, earth retaining structures, earthworks, and underground structures. The relevant soil parameters for seismic site characterization, their importance for seismic analyses, and the available evaluation techniques are described in detail. It is assumed that the basic geological, geotechnical, and hydrological investigations required for the general design of the structural foundation or feature under consideration have been (or will be) conducted according to the state of practice. Therefore, the emphasis of this chapter is on the supplemental information required for seismic design. Soil parameters required for seismic analyses include the initial (small strain) dynamic shear modulus, the small strain viscous damping ratio, shear modulus reduction and strain-dependent hysteretic damping characteristics, dynamic shear strength and liquefaction resistance parameters, and post-liquefaction residual shear strength.

Three broad categories of site investigation activities can be included in a subsurface exploration program. The first category is a conventional geotechnical boring program, including laboratory testing on undisturbed or remolded samples. The second category is in situ testing, wherein the parameters that describe soil properties are estimated in situ using penetrometers and other types of probes and invasive in situ testing devices. The third category is geophysical exploration. Conventional geotechnical site characterization techniques using all the three categories of site investigations are discussed in detail in other FHWA and Transportation Research Board publications (e.g. FHWA 2002, 2002a, 2006; Mayne, 2007). Only brief discussions of these conventional techniques as they relate to characterization of a site for seismic studies are presented herein. However, special attention is paid to the use of the cone penetrometer for site investigation due to its utility and reliability and the availability of recently-developed correlations with engineering properties that many geotechnical engineers are still unfamiliar with.

4.2 SUBSURFACE PROFILE DEVELOPMENT

4.2.1 General

As for all geotechnical engineering analyses, seismic analysis requires knowledge of the subsurface profile, or stratigraphy, at the site under study. The required stratigraphic information includes data on the water level, soil layering, and the depth to the underlying bedrock. Stratigraphy can be obtained using classical investigation techniques (field reconnaissance, geologic mapping, test pits, drilling and sampling), in situ tests, or by geophysical means.

As in many other geotechnical problems, identification and quantification of relatively thin, weak layers in the soil or rock can be an important part of seismic site characterization. However, the "weak" layer in a seismic analysis may differ from the "weak" layer in a static analysis. For instance, a saturated sand layer considered a suitable foundation material with respect to static loads may be susceptible to liquefaction under earthquake loads and thus becomes a weak layer in a seismic analysis. In other cases, such as soft material between beds of rock or stiff soil on a hillside, the same material that is a weak material for static analyses may also represent a potential problem under earthquake loads. Therefore, attention must be paid to characterize these thin layers in the site exploration program, e.g. through the use of continuous sampling or CPT soundings that yield a continuous stratigraphic profile.

4.2.2 Water Level

Groundwater may play an important role in seismic analysis, particularly if the soil deposits are liquefiable. Therefore, accurate characterization of the groundwater level (or levels) is an essential part of seismic site characterization. Furthermore, seasonal variability in the water level should be considered in developing the stratigraphic profile and performing liquefaction potential analyses.

Groundwater level information is often obtained by observation of the depth to which water accumulates in an open borehole. However, water level observations in boreholes may be unreliable due to a variety of factors, including:

- Insufficient time for equilibrium in borings in fine-grained soils;
- Artesian pressures in confined aquifers; and
- Perched water tables in coarser soils overlying fine-grained deposits.

Furthermore, borehole observations do not, in general, permit observations of seasonal fluctuations in water levels. Piezometers or observation wells installed in a borehole provide a much more reliable means of monitoring water levels in the subsurface. In deposits where layers of fine-grained soils are present and multiple water levels are suspected, multiple-point piezometers can be installed in a single borehole or multiple boreholes of different depths can be fit with single point piezometers.

A cone penetrometer with pore pressure measuring capabilities, referred to as a piezocone, can also be used to estimate water level elevations. By holding the cone at a constant elevation and waiting until the pore pressure drops to a constant value, the piezocone can be used to determine the steady state pore pressure at a specified elevation at the time of exploration. The potential for perched water tables or confined aquifers can be assessed with the piezocone by combining steady-state pore pressure readings at several elevations with stratigraphic information developed from the tip and sleeve resistance of the cone.

Geophysical stratigraphic profiling methods used in seismic site investigation are generally not used to evaluate the depth to groundwater. Geophysical methods used to evaluate soil stratigraphy and soil properties for seismic design are often targeted towards shear wave or Rayleigh wave velocity and thus are generally insensitive to the water level. Some resistivity methods (e.g., down hole resistivity surveys) can detect the presence of water in the soil pores but cannot measure the pressure in the water. Therefore, such methods can neither distinguish between soil above the water table saturated by capillarity and soil below the water table in a fine-grained soil nor measure an artesian pressure in a confined aquifer.

4.2.3 Soil Stratigraphy

The subsurface investigation should provide a detailed description of the soil stratigraphy at the site, including the thickness and elevation of the different layers. Potentially liquefiable soils should be clearly identified and quantified by one of the methods described later in this chapter. Both conventional boring with continuous sampling and in situ testing using the CPT offer the possibility of development of a continuous soil profile in which layers as small as 75 mm can be identified. Thin continuous layers of weak or potentially liquefiable soil encountered between beds of more competent soil may prove to be the critical plane in seismic slope stability analyses.

Borings offer the advantage of recovery of a physical sample for visual classification and, if desired, laboratory testing. In a boring in which continuous Standard Penetration Test (SPT) sampling is performed, layers of soil can be visually identified from the sample recovered from the split spoon to

develop a stratigraphic profile. However, the SPT blow count, the primary measurement of cohesionless soil strength and consistency obtained using the SPT, generally applies only to the gross behavior of a relatively large 300 mm interval of the boring and thus cannot be used to characterize the liquefaction susceptibility of thin lenses of soil visually identified in the split-spoon sample.

In the Cone Penetrometer test (CPT) the resistance of the tip and sleeve of the cone to penetration can be used to develop continuous profiles of the soil layers and the shear strength of the soil that are applicable to layers as thin as 3 in (75 mm). When the CPT is used, soil classification, consistency, shear strength, and liquefaction potential are based upon correlation with the tip and sleeve resistance of the cone, as discussed subsequently. As discussed previously, a CPT with a pore pressure transducer (a piezocone) can also be used to evaluate groundwater conditions.

Geophysical methods will provide information on the stratigraphy of the soil with respect to the measured geophysical property. The measured geophysical property may be a physical property of direct interest in a seismic analysis (e.g., shear wave velocity) or may be correlated to a physical property of interest (e.g., electrical resistivity and water level). The ability of geophysical methods to resolve layering in the ground varies among the available methods. In general, geophysical methods identify contrasts in the measured geophysical property. Therefore, if contiguous layers of a stratigraphic profile have the same or similar values of the measured geophysical property (e.g. electrical resistivity) they will be characterized as a single layer in the geophysical profile. The ability of geophysical methods to delineate stratigraphy, in general, decreases with depth unless a down-hole method is used (in which case a boring or in situ probe is required).

4.2.4 Depth to Bedrock

Ideally, the soil profile developed for a seismic analysis should extend to *competent bedrock*, where competent bedrock is defined as material with a shear wave velocity of at least 2,500 ft/s (760 m/s) (AASHTO Site Class B) and the physical properties of the soil over the entire interval between the ground surface and competent bedrock should be defined. However, if competent bedrock is not reachable at a reasonable depth, the depth over which the physical properties of the soil for seismic analyses are defined should be at least 200 ft (60 m). Furthermore, the depth to which the soil profile is developed should be at least as deep as required for conventional geotechnical analyses. However, the results of a seismic analysis are generally not sensitive to the properties of the bedrock assuming its shear wave velocity exceeds the shear wave velocity of the overlying soil.

4.2.5 Rock Mass Characterization

Characterization of the rock mass may be required for seismic stability evaluation of rock slopes and seismic design of underground openings. Rock mass characterization may include field mapping, rock borings, and geophysical exploration. The most important element in rock mass characterization is characterization of the orientation and nature of its discontinuities, including fractures, joints, shear zones, and faults. The orientation of discontinuities can be established by field mapping of exposures, logging of oriented core, down hole logging of large -diameter boreholes, and borehole geophysical methods such as the acoustic televiewer (NCHRP, 2006). The characteristics of the rock mass discontinuities, including surface roughness, cementation, and joint filling, are generally evaluated based upon visual examination of outcrops and rock core. If fresh rock surfaces are to be exposed by the project, rock durability (e.g. slake durability) may also be a concern. Indices of rock quality, including Rock Quality Designation (RQD) and the Q-value (Barton, 2002), can be used to quantify rock mass characteristics for engineering purposes.

4.3 REQUIRED SOIL AND ROCK PARAMETERS

4.3.1 General

At a minimum, a seismic analysis requires the same parameters used to describe soil properties for the static analyses of the foundations, earth structures, and underground openings under consideration. During the course of a typical geotechnical investigation, the following information is obtained for the soil units of interest:

- Soil classification and index parameters;
- Unit weight of the soil; and
- Compressibility and shear strength parameters of the soil

For rock units of interest, typical information includes:

- Unconfined compressive strength
- The orientation and characteristics of the discontinuities
- Durability characteristics (e.g. slake durability)

For seismic design purposes, a series of other soil and rock parameters and properties may need to be evaluated. For a seismic analysis, these may include:

- A measure of the consistency of the soil (e.g. relative density or overconsolidation ratio)
- Shear wave velocity or initial (small strain) shear modulus
- Cyclic stress-strain behavior
- Residual shear strength

4.3.2 Unit Weight and Relative Density

Measures of both the unit weight and relative density of the soil may be required for seismic analysis. The unit weight of the soil is used to calculate the total and effective vertical stresses for liquefaction and slope stability analyses. Unit weight is also an important parameter in dynamic site response analysis and stability analysis, as the inertia force of a soil element is equal to the acceleration times its total weight. Total unit weight may be assessed on the basis of measured values from undisturbed samples or from the water content and specific gravity of saturated soil.

Relative density is an important parameter with respect to the potential for soil liquefaction and seismically-induced settlement of cohesionless soils. The relative density is a measure of the relative consistency of the soil. Mathematically, relative density, D_r , is related to the maximum dry density ($\gamma_{d\max}$) or minimum void ratio (e_{\min} , the densest state to which the material can be compacted) and the minimum density ($\gamma_{d\min}$) or maximum void ratio (e_{\max} , the loosest state the material can attain) by Equation 4-1:

$$D_r = \frac{e_{\max} - e_0}{e_{\max} - e_{\min}} = \left(\frac{1 - \frac{\gamma_{d\min}}{\gamma_{do}}}{1 - \frac{\gamma_{d\max}}{\gamma_{do}}} \right) 100\% \quad 4-1$$

where e_0 is the in situ void ratio of the material and γ_{do} is the in situ dry unit weight. The relative density is an important parameter with respect to liquefaction and seismic settlement potential because it is related to the potential for a granular material to decrease in volume when subjected to disturbance.

Relative density is rarely measured directly. Generally, an index of the relative density is measured in situ. Commonly used indices of the relative density, or relative consistency, of soil in situ are the SPT blow count, N , and the tip and sleeve resistance of the CPT probe, q_t , and f_s , respectively.

4.3.3 Shear Wave Velocity

The shear wave velocity of a soil is used to establish the stiffness of the soil at small strains. The small strain (initial) shear modulus of a soil, G_{\max} , is related to the shear wave velocity, V_s , and the mass density, ρ , of the soil by Equation 4-2:

$$G_{\max} = \rho \cdot V_s^2 \quad 4-2$$

Mass density of the soil is related to the total unit weight of the soil, γ_t , by the acceleration of gravity, g , as described in Equation 4-3:

$$\rho = \frac{\gamma_t}{g} \quad 4-3$$

As noted previously, the unit weight of soil or rock can be evaluated from undisturbed samples or, for saturated soil, from knowledge of the water content and the specific gravity of the soil solids. The unit weight of most soils can also usually be estimated reasonably (+/- 10%) from correlation with CPT resistance (as discussed subsequently) or from SPT blow count, soil classification, and location relative to the water table. Therefore, measurement of shear wave velocity provides a reliable means for evaluating the small strain shear modulus of the soil if the stratigraphic profile is known.

Small strain (initial) shear modulus is related to small strain Young's modulus, E_{\max} , as a function of Poisson's ratio, ν , by the theory of elasticity in accordance with Equation 4-4:

$$E_{\max} = 2(1 + \nu)G_{\max} \quad 4-4$$

For practical purposes, Poisson's ratio of soil can be assumed equal to 0.35 for sands and 0.48 for saturated clays. Alternatively, if results of geophysical measurements are available, Equation 4-5 may be used to estimate ν :

$$\nu = 1 - \frac{1}{2 \left(1 - (V_s/V_p)^2 \right)} \quad 4-5$$

where V_s and V_p are shear and compressional wave velocities, respectively. Young's modulus can also be evaluated from the compressional wave velocity and mass density of the soil using the analog to Equation 4-2. Consequently an efficient and reliable means of obtaining the small-strain elastic properties of the soil is through the measurement of shear and compressional wave velocities.

4.3.4 Cyclic Stress-Strain Behavior

During an earthquake, a soil deposit is subjected to a complex system of stresses and strains resulting from the ground motions induced by the earthquake. In general, these stresses and strains will be cyclical due to the vibrational nature of the earthquake loading. To evaluate the seismic response of the soil deposit, it is necessary to estimate how the soil responds to this cyclic loading.

The earthquake-induced stresses and strains that produce the most damage in soils are generally considered to be due to cyclic shearing of the soil. Shear waves propagate primarily upward near the ground surface. Therefore, most geotechnical earthquake engineering analyses assume that earthquake ground motions are generated by vertically-propagating shear waves.

The cyclic stresses induced on a soil element by a vertically-propagating shear wave, the type of earthquake wave most commonly considered in a seismic analysis, are schematically presented in Figure 4-1. The stress-strain response of soil to this type of cyclic loading is commonly characterized by *hysteresis*. A typical hysteresis loop from uniform cyclic loading of soil is shown on Figure 4-2. Various constitutive models have been developed to characterize soil hysteresis loops. The most common model used to represent the hysteretic behavior of soil in seismic analysis is the *equivalent-linear* model (Seed and Idriss, 1970). Various non-linear constitutive models (Kondner and Zelasko, 1963; Martin, 1975; Matasovic and Vucetic, 1993; Hashash and Park, 2001) have also been developed to represent hysteretic soil behavior. Non-linear constitutive models for the hysteretic behavior of soil are discussed in more detail in Chapter 5 of this document.

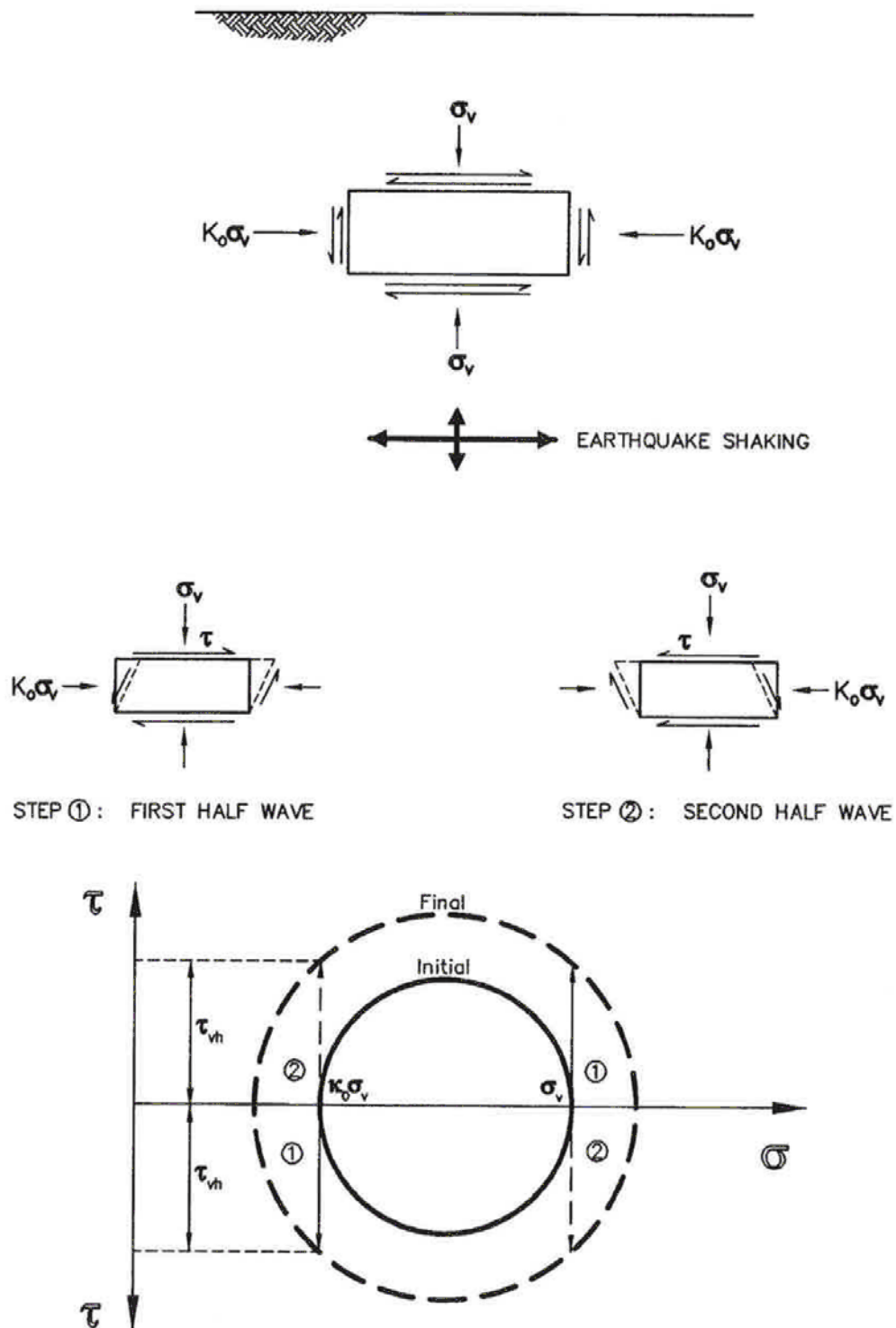


Figure 4-1 Stresses Induced in a Soil Element by Vertically Propagating Shear Wave

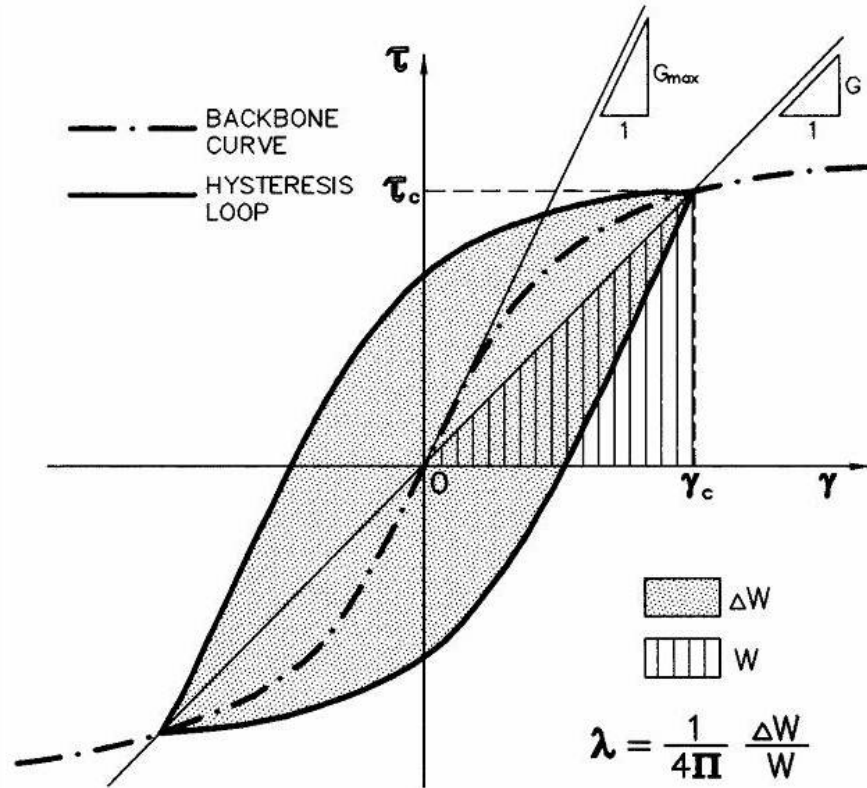


Figure 4-2 Hysteretic Stress-Strain Response of Soil Subjected to Cyclic Loading

The equivalent-linear model represents non-linear hysteretic soil behavior using an equivalent shear modulus, G , equal to the slope of the line connecting the tips of the hysteresis loop and an equivalent viscous damping ratio, λ , proportional to the enclosed area of the loop. The equivalent modulus and viscous damping ratio depend upon the cyclic shear strain, γ_c . The shear strain dependence of the equivalent modulus and damping ratio are described by the *modulus reduction* and *damping curves* shown on Figure 4-3. The equivalent viscous damping ratio is evaluated from the area of the hysteresis loop as shown on Figure 4-2 and is typically expressed as β , the percentage of the critical damping ratio. Modulus reduction and damping curves strictly apply only to uniform cyclic loading. However, these curves are typically also used to model the soil behavior under irregular (non-uniform) cyclic loading generated by earthquakes based upon a representative shear strain.

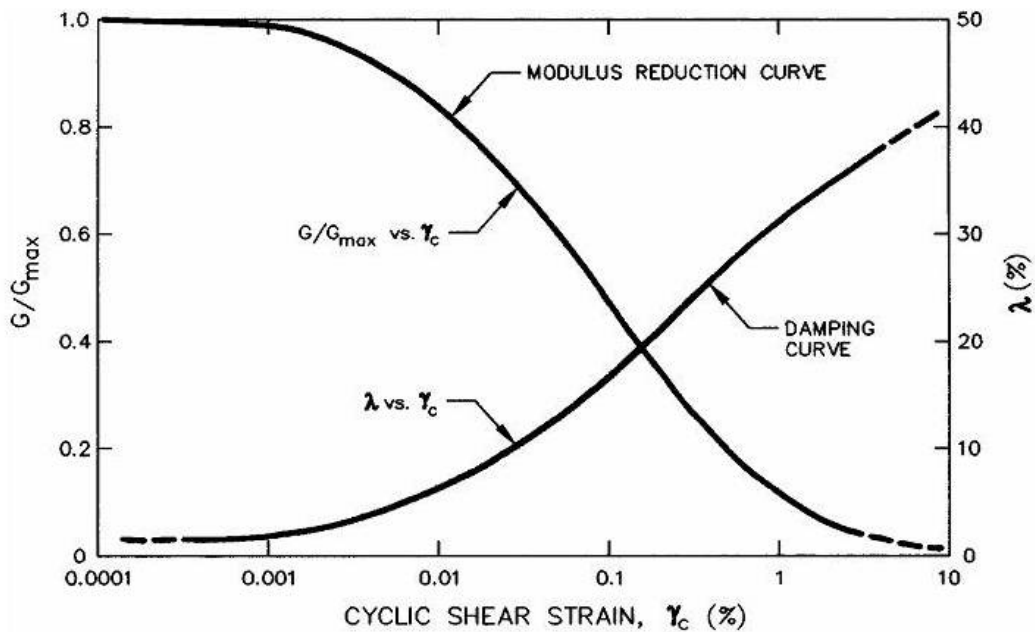


Figure 4-3 Shear Modulus Reduction and Equivalent Viscous Damping Ratio Curves

Cyclic loading can break bonds between soil particles and rearrange the particles into a denser state. In a dry soil, this rearrangement will be manifested as compression of the soil and will result in seismic settlement. If the soil is saturated, volume change cannot occur instantaneously and the load carried by the soil skeleton is transferred to the pore water as the particles are rearranged. If the rearrangement is sufficient in magnitude, the soil skeleton can shed its entire load to the pore water, resulting in a pore pressure equal to the overburden pressure, complete loss of shear strength, and, consequently, liquefaction of the soil.

4.3.5 Peak and Residual Shear Strength

Peak and residual shear strengths are important elements in the evaluation of seismic stability. The peak shear strength refers to the maximum shearing resistance an element of soil can sustain during and after cyclic loading. The peak shear strength may be used to calculate the *yield acceleration* of a soil (the horizontal acceleration above which permanent seismic deformations begin to accumulate) if buildup of seismically-induced pore pressure is not anticipated. Residual shear strength refers to the shear strength of the soil after significant static and/or cyclic shearing has occurred. In the context of this document, it is also used to represent the shear strength of a soil element after it has liquefied. Residual shear strength may be used to evaluate post-liquefaction bearing capacity and stability and to calculate the accumulation

of permanent seismic deformation in a post-liquefaction stability and deformation analysis for a foundation or earth structure.

While there is some limited information to indicate that the shear strength of soil increases with increasing strain rate, the peak shear strength of soil subjected to cyclic loading is generally assumed to be equal to or less than the peak static strength. If the soil is dry, the static drained shear strength may be used. If the soil is saturated, even if the soil is relatively free draining, the undrained shear strength should be used for seismic analyses because of the rapid nature of earthquake loading. For cohesive soils of low to intermediate sensitivity, the static shear strength of the soil may be reduced by 10-15% when subjected to large magnitude earthquakes ($M \geq 7$) to account for a potential reduction in shear strength due to cyclic loading. This potential strength reduction is discussed in more detail in Chapter 6.

The residual shear strength is perhaps the most important parameter with respect to evaluation of the impacts of liquefaction. If the static factor of safety against bearing capacity or slope failure is greater than 1.0 when evaluated using the residual shear strength, liquefaction-induced deformations may be small enough to be acceptable without extensive remediation. If the static factor of safety evaluated using the residual shear strength is less than one, large deformations or a flow slide should be anticipated unless remedial action is taken. Recent advances in geotechnical earthquake engineering have facilitated much more accurate assessment of residual shear strength than possible previously. These recent advances allow the residual shear strength to be evaluated as an undrained shear strength that is a fraction of the effective overburden pressure.

4.4 EVALUATION OF SOIL AND ROCK PROPERTIES FOR SEISMIC ANALYSIS

4.4.1 General

The key soil and rock parameters required to perform a seismic analysis are the shear wave velocity, modulus reduction and damping curves, peak and residual shear strength, and the soil resistance parameters needed to evaluate soil liquefaction potential and seismic settlement. A value for Poisson's ratio may also be required. These parameters can either be directly evaluated from laboratory or in situ test results or indirectly evaluated by correlation with index properties of soils. Laboratory tests generally provide a direct means of evaluating soil parameters for seismic analyses. However, laboratory tests are subject to limitations on the recovery and testing of representative samples as well as on the limitations of the testing itself. In most cases, in situ testing provides the most reliable and cost effective means of soil

and rock property evaluation for seismic analysis. However, in many cases, empirical correlation with index parameters is the most practical means of evaluating soil parameters for seismic analyses. Sometimes, for particular geographical areas and soils (e.g., Piedmont region residual soils, see Borden, et al., 1996) typical dynamic soil parameters have been established.

4.4.2 In Situ Testing

Standard Penetration Testing (SPT)

Probably the most common in situ test used in geotechnical practice is the SPT. The SPT measures the resistance to penetration of a standard split-spoon sampler in a boring. The test method is rapid and yields useful data, although there are many factors that affect the results. The procedure used to perform the SPT is codified under ASTM Standard D 1586. The SPT consists of driving a standard split barrel sampler with a 140 lb hammer dropping 30-in. in a free fall. The sampler is driven 18 inches into the bottom of the borehole. The number of hammer blows required to drive the sampler the final 12 inches is the uncorrected SPT blow count, N .

Measurements show that in a typical Standard Penetration Test using a safety hammer and a rope and cathead to raise the hammer approximately 60 percent of the theoretical kinetic energy of the free-falling hammer is delivered to the drill rods. However, other types of equipment that are allowed within the ASTM standard for the SPT typically show a different level of energy efficiency and even for a consistent equipment set-up the delivered energy can vary widely not only from site to site but also from blow to blow. To compensate for the variability in the average amount of energy delivered by the hammer to the drill rod due to the equipment set-up, the uncorrected SPT blow count, N , is generally transformed to N_{60} , the SPT blow count standardized to an energy efficiency of 60 percent. Standardization is based either on the typical efficiency for the equipment used in a particular test or on the measured delivered energy when this information is available.

SPT blow count also depends on overburden pressure. To provide a basis for comparison of blow counts at different depths or overburden pressures, the standardized blow count is sometimes normalized to an overburden pressure of 1 ton per square foot, $(N_1)_{60}$

Although widely recognized as an unsophisticated test, the SPT is performed routinely worldwide and, when performed properly, yields useful results. Extensive work has been conducted to understand the

limitations of the test and develop reliable correction factors accounting for the influence of vertical stress, soil gradation, hammer efficiency, and other factors on test results. Standardized and normalized SPT blow count values can be used to estimate:

- The relative density of sand
- Shear strength parameters of cohesionless soils
- Bearing capacity
- Seismic settlement potential of sands
- Liquefaction potential of saturated sands
- Shear wave velocity

Most soil mechanics text books contain correlations relating SPT blow counts to soil shear strength and foundation bearing capacity (e.g., Bowles, 1988; Coduto, 2001). SPT blow counts may also be used to estimate the relative density of sand and dynamic soil properties (e.g., cyclic resistance against liquefaction and residual undrained shear strength) are often correlated to the relative density of the soil.

The procedure used to account for the effects of energy variations and overburden pressure on the field SPT blow counts is presented below.

Step 1: Evaluate the *standardized* SPT blow count, N_{60} , i.e. the blow count for a hammer with an energy efficiency of 60 percent (60 percent of the theoretical SPT energy is delivered to the drill rod). The "standardized" equipment corresponding to an efficiency of 60 percent is specified in Table 4-1. If nonstandard equipment is used, N_{60} is obtained from the equation:

$$N_{60} = N \cdot C_{60} \tag{4-6}$$

where C_{60} is the product of various correction factors. The equation for the global correction factor, C_{60} , in Equation 4-6 can be written as:

$$C_{60} = H_E \cdot C_{SS} \cdot C_{RL} \cdot C_{BD} \tag{4-7}$$

where H_E is the hammer energy correction factor and C_{SS} , C_{RL} , and C_{BD} are the Sampler Setup, Rod Length, and Borehole Diameter factors, respectively.

The values for the C_{SS} , C_{RL} , and C_{BD} correction factors recommended by various investigators for some common non-standard SPT configurations are provided in Table 4-2 (Richardson, *et al.*, 1995).

The hammer energy correction factor, H_E , is a combination of a Non-Standard Hammer Type factor, C_{HT} , and a Non-Standard Hammer Weight or Height of Fall factor, C_{HW} :

$$H_E = C_{HT} \cdot C_{HW} \quad 4-8$$

Evaluation of C_{HT} and C_{HW} is described in Table 4-2. However, for important projects, H_E may be calculated directly, by measuring the hammer energy. There are two commercially available methods for measuring hammer energy: the Force Squared (F2) method and the Force Velocity (FV) method. However, in general the F2 method is not considered as reliable as the FV method and is not recommended for correcting SPT blow counts.

In the FV method, the product of the force times the velocity is integrated over time. The FV method requires both load cells to measure the transmitted force to the drill rods and an accelerometer to measure the velocity time history of the rods. The equipment for making FV measurements is similar to pile driving analyzer equipment for dynamic load testing of driven piles.

Using the energy measured by the FV method, F_{VE} , the energy correction factor H_E may be evaluated as:

$$H_E = \frac{F_{VE}}{0.6 F_{max}} \quad 4-9$$

where F_{max} is the theoretical maximum kinetic energy of the SPT hammer (350 ft-lb).

TABLE 4-1 RECOMMENDED “STANDARDIZED” SPT EQUIPMENT
 (After Seed, *et al.*, 1985 and Riggs, 1986, Reprinted by Permission of ASCE)

Element	Standard Specification
Sampler	Standard split-spoon sampler with: (a) Outside Diameter, O.D. = 2 in (51 mm), and (b) Inside Diameter, I.D. = 1.38 in (35 mm) (no room for liners in the barrel)
Drill Rods	A or AW-type for depths less than 50 ft (15.2 m); N- or NW-type for greater depths
Hammer	Standard (safety) hammer with: (a) weight = 140 lbs (63.5 kg); (b) drop = 30 in (762 mm) (delivers 60% of theoretical free fall energy)
Rope	Two wraps of rope around the pulley
Borehole	4 to 5 in (100 to 130 mm) diameter rotary borehole with bentonite mud for borehole stability (hollow stem augers where SPT is taken through the stem)
Drill Bit	Upward deflection of drilling mud (tricone or baffled drag bit)
Blow Count Rate	30 to 40 blows per minute
Penetration Resistance Count	Measured over range of 6 to 18 in (150 to 460 mm) of penetration into the ground
Notes: (1) If the equipment meets the above specifications, $N = N_{60}$ and only a correction for overburden is needed. (2) This specification is essentially the same as the ASTM D 1586 standard.	

**TABLE 4-2 CORRECTION FACTORS FOR NON-STANDARD SPT PROCEDURE AND EQUIPMENT
(Richardson, *et al.*, 1995; Youd and Idriss, 1997)**

Correction for	Correction Factor	Reference
Nonstandard Hammer Type and Hammer Release (DH = doughnut hammer; SH = Safety Hammer; ER = energy ratio)	$C_{HT}=0.75$ for DH with rope and pulley $C_{HT}=1.33$ for SH with trip/auto & ER=80	Seed, <i>et al.</i> (1985)
Nonstandard Hammer Weight or Height of Fall (H = height of fall in mm; W = hammer weight in kg)	$C_{HW} = \frac{H \cdot W}{63.5 \cdot 762}$	calculated per Seed, <i>et al.</i> (1985)
Nonstandard Sampler Setup (standard samples with room for liners, but used without liners)	$C_{SS} = 1.10$ for loose sand $C_{SS} = 1.20$ for dense sand	Seed, <i>et al.</i> (1985)
5 - 13 (Part I) Nonstandard Sampler Setup (standard samples with room for liners, and liners are used)	$C_{SS} = 0.90$ for loose sand $C_{SS} = 0.80$ for dense sand	Skempton (1986)
Short Rod Length	$C_{RL} = 0.75$ for rod length 0 – 13 ft (0-4 m) $C_{RL} = 0.85$ for rod length 13 – 20 ft (4-6 m) $C_{RL} = 0.95$ for rod length 20 – 33 ft (6-10 m) $C_{RL} = 1.0$ for rod length 33 – 100 ft (10-30 m) $C_{RL} < 1.0$ for rod length > 100 ft (30 m)	Seed, <i>et al.</i> (1983); Youd and Idriss (1997)
Nonstandard Borehole Diameter	$C_{BD} = 1.05$ for 6 in (150 mm) borehole diameter $C_{BD} = 1.15$ for 8 in (200 mm) borehole diameter	Skempton (1986)
Notes: N = Uncorrected SPT blow count.		
$C_{60} = C_{HT} \cdot C_{HW} \cdot C_{SS} \cdot C_{RL} \cdot C_{BD}$	$N_{60} = N \cdot C_{60}$	
$C_N =$ Correction factor for overburden pressure.	$(N_1)_{60} = C_N \cdot N_{60} = C_N \cdot C_{60} \cdot N$	

Step 2: Calculate the normalized and standardized SPT blow count, $(N_1)_{60}$. $(N_1)_{60}$ is the standardized blow count normalized to an effective overburden pressure of 1 tsf (96 kPa) in order to eliminate the influence of confining pressure. The most commonly used technique for normalizing blow counts is via the correction factor, C_N , shown in Figure 4-4 (Seed, *et al.*, 1983). However, the closed-form expression proposed by Liao and Whitman (1986) may also be used:

$$C_N = 9.79 \left(\frac{1}{\sigma'_v} \right)^{1/2} \quad 4-10$$

where σ'_v equals the vertical effective stress at the sampling point in psf.

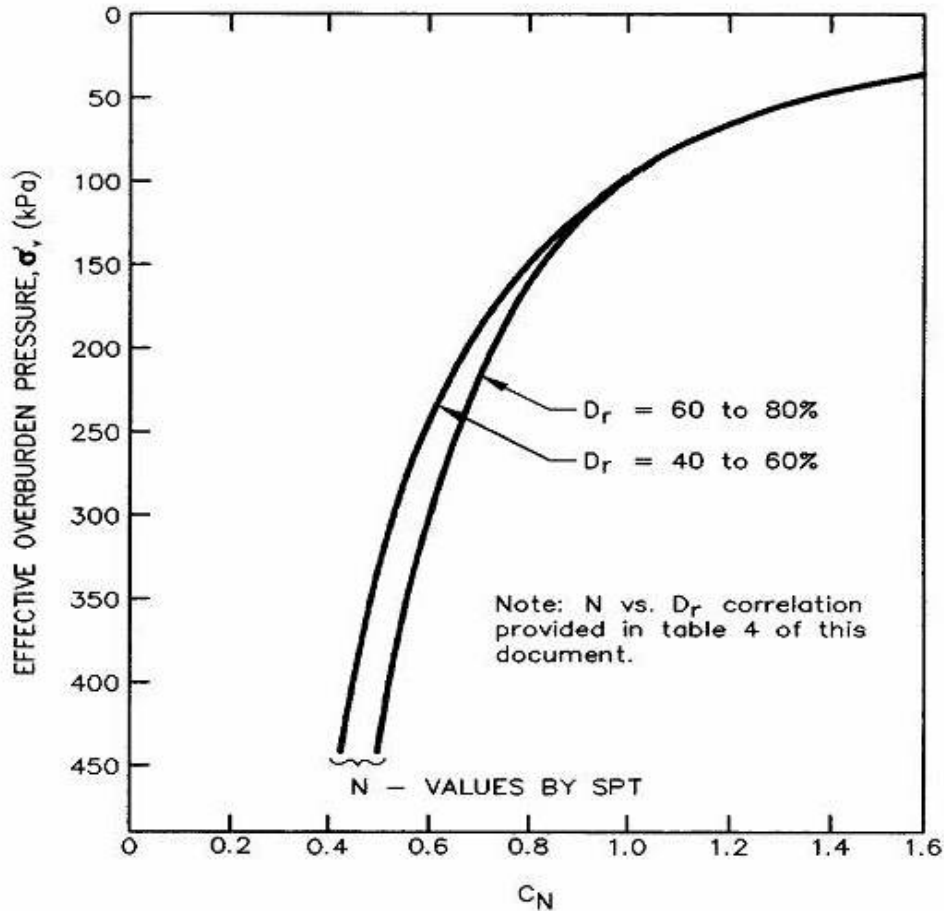


Figure 4-4 Correction Factor for the Effective Overburden Pressure, C_N (Seed, *et al.*, 1983, reprinted by permission of ASCE)

As shown in Figure 4-4, the Seed, et al. (1983) effective overburden correction factor curves are valid only for depths greater than approximately 10 ft (3 m), or for effective overburden pressures greater than approximately 1000 psf (48 kPa). A similar plot presented by Liao and Whitman (1986) suggests that C_N in Equation 5-10 should be limited to 2.0 at depths greater than 3 m. Once the value of C_N is estimated, the normalized and standardized blow count is then calculated as:

$$(N_1)_{60} = C_N \cdot N_{60} \quad 4-11$$

Other factors, such as grain size distribution, may influence C_N (Marcuson and Bieganousky, 1977). However, considering the uncertainties involved in the SPT itself, the application of equipment and overburden pressure correction factors should be sufficient for engineering purposes.

Cone Penetration Testing (CPT)

The CPT test involves pushing a standard dimension conical probe into the ground at a standard rate and measuring the resistance of the tip of the cone and along the side of the cone to penetration. The cone tip resistance, q_t , combined with the friction ratio, FR (the ratio between the side resistance, f_s , of the cone and q_t), has been shown to be strongly correlated to soil type and soil strength. In recent years, cone penetration testing probes have been fitted with pore pressure cells (piezocones) to measure pore pressure during penetrations and pore pressure dissipation after penetration, facilitating in situ measurement of consolidation properties and water table depth. The CPT can also be fitted with a geophone for use in “down hole” seismic profiling to determine shear wave velocity.

CPT testing is codified as ASTM Standard D 3441. A comprehensive review of CPT equipment, procedures, and testing is provided by Mayne (2007). The CPT is relatively easy to perform and provides a continuous profile of soil stratigraphy that can be invaluable in identifying the extent of liquefiable soils at a site. Figure 4-5 shows the soil classification chart developed by Robertson et al. (1986) based on cone penetration resistance readings. Data from the CPT can also be used to establish soil shear strength, unit weight, relative density, overconsolidation ratio, shear wave velocity, allowable bearing capacity, and for pile design (Mayne, 2007).

Figure 4-5 Soil Classification Chart Based on the CPT (Robertson et al., 1986)

Until recently, correlations between SPT N values and CPT cone resistance were employed to allow for the use of CPT data with relationships between SPT values and soil properties (e.g., liquefaction potential). Figure 4-6 presents the relationship developed by Robertson et al. (1983) among cone resistance, SPT N value, and mean grain size, D_{50} . However, most soil properties, including liquefaction potential and shear wave velocity, are now correlated directly with CPT data, eliminating the need for this correlation in most situations.

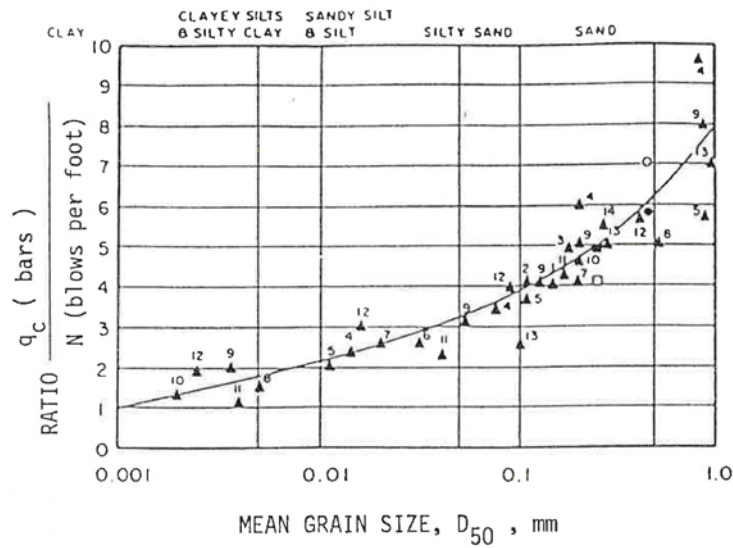


Figure 4-6 CPT-SPT Correlation Chart (Robertson et al., 1983, reprinted from FHWA-SA-91-043)

4.4.3 Unit Weight and Relative Density

The total density of soil is usually expressed in terms of total unit weight (total density times the acceleration of gravity). Typical values of the total unit weight are often adequate for use in engineering analysis. However, a higher degree of accuracy can be obtained by evaluating the unit weight from measurements made on undisturbed samples, from the water content and the specific gravity in saturated cohesive soils, or from correlations with CPT parameters. Mayne (2007) developed the correlation presented in Figure 4-7 between dry unit weight and normalized cone tip resistance, q_{T1} , for uncemented, un-aged quartz sands (q_{T1} is defined in the figure). However, this correlation, developed from the results of large-scale calibration chamber tests, has a correlation coefficient, r^2 , of only 0.488. The scatter of the data in the figure also gives an idea of the accuracy of the correlation.

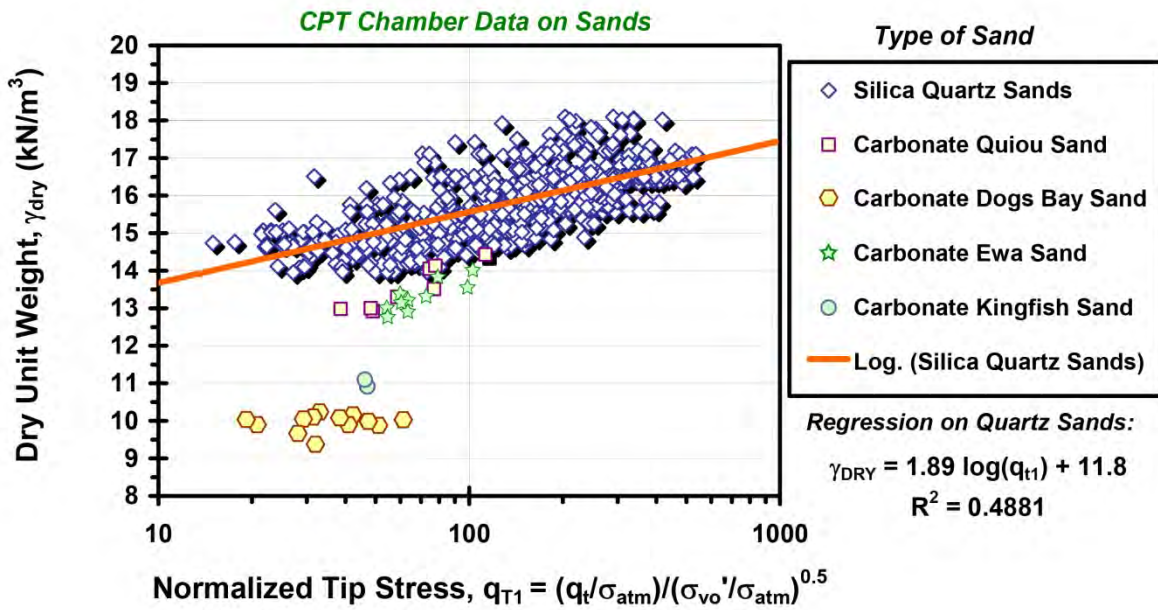


Figure 4-7 Correlation between Dry Unit Weight and Normalized Cone Tip Resistance (Mayne, 2007)

Mayne (2007) developed a more robust correlation for the unit weight of saturated soils as a function of shear wave velocity and depth. This correlation, presented in Figure 4-8, includes data from soft to stiff clays and silts, loose to dense sands and gravels, and mixed geomaterials. The correlation coefficient for the 727 data points in Figure 4-8 is 0.808. By using a correlation between cone penetrometer resistance and shear wave velocity (presented subsequently) and assuming a characteristic specific gravity for

different types of soil, the correlation between cone penetration resistance, saturated unit weight, and specific gravity presented in Figure 4-9 was developed.

Figure 4-8 Correlation among Saturated Weight, Shear Wave Velocity, and Depth (Mayne, 2007)

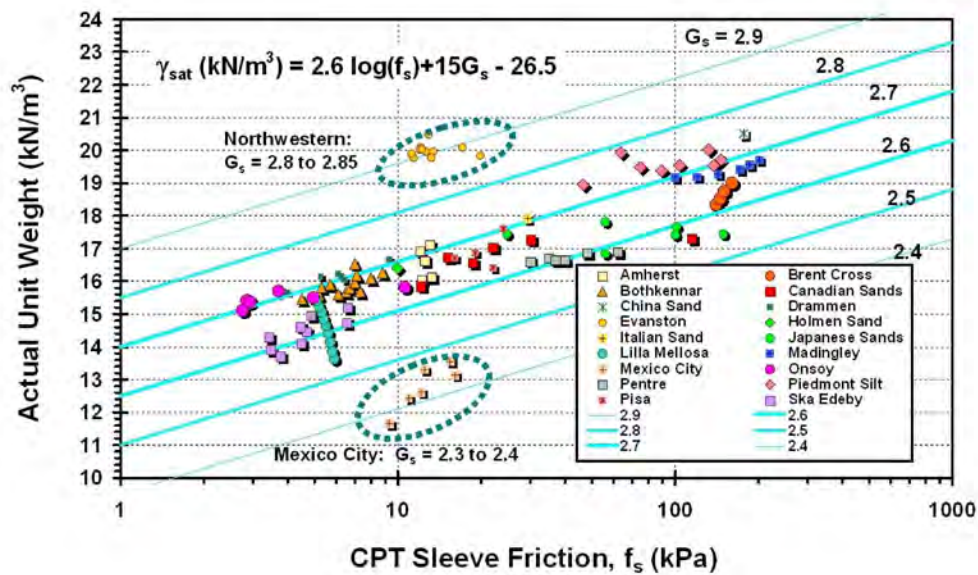


Figure 4-9 Correlation among Saturated Weight, CPT Sleeve Friction, and Specific Gravity (Mayne, 2007)

Relative density, D_r , is rarely measured directly for geotechnical engineering purposes. Instead, relative density is generally derived from correlation with SPT blow count or the CPT resistance. Table 4-4, after

Terzaghi and Peck (1948), presents a rough correlation between SPT blow count and the relative density of sandy soils.

Kulhawy and Mayne (1990) give the following equation for the relative density, D_r , of cohesionless soil as a function of the standardized normalized SPT blow count:

$$D_r = \left[\frac{(N_1)_{60}}{C_p \cdot C_A \cdot C_{OCR}} \right]^{0.5} \cdot 100\% \quad 4-12$$

where C_p is a grain-size correction factor, C_A is an aging factor, and C_{OCR} is an overconsolidation correction factor. These factors may be evaluated as follows:

$$C_p = 60 + 25 \cdot D_{50} \quad 4-13$$

$$C_A = 1.2 + 0.05 \cdot \log\left(\frac{t}{100}\right) \quad 4-14$$

$$C_{OCR} = OCR^{0.18} \quad 4-15$$

where D_{50} is the grain size, in mm, at which 50 percent of the soil is finer, by weight and t is the time since deposition of the soil in years. Coduto (2001) suggest that, in the absence of geologic data, t equal to 1000 years and an OCR varying from 1 for loose soils ($(N_1)_{60} < 10$) to 4 for dense soils ($(N_1)_{60} > 50$) should be sufficient for use with these equations. Alternatively, Mayne (2005) presents the following equation, developed using 636 data points from large chamber tests, for the OCR of clean quartz sands as a function of CPT tip resistance, vertical effective stress (σ'_{vo}), and effective friction angle (ϕ'):

$$OCR = \left[\frac{\left(0.192 \left(\frac{q_t}{\sigma_{atm}} \right)^{0.22} \right)}{\left((1 - \sin \phi') \left(\frac{\sigma'_{vo}}{\sigma_{atm}} \right)^{0.31} \right)} \right] \cdot e^{\left[\frac{1}{\sin \phi' - 0.27} \right]} \quad 4-16$$

where σ_{atm} is atmospheric pressure.

TABLE 4-3 RELATIVE DENSITY OF SANDY SOILS (After Terzaghi and Peck, 1948)

Relative Density, D_r (%)	Penetration Resistance, N (blows/ft)	Descriptive Term
0-15	0-4	Very Loose
15-35	5-10	Loose
35-65	11-30	Medium
65-85	31-50	Dense
85-100	> 50	Very Dense

Figure 4-10 presents the correlation developed by Jamiolkowski et al. (2001) among normalized cone tip resistance, relative density, and compressibility for clean sands (less than 15% fines). Carbonate and calcareous sands are expected to fall on the high compressibility side of this correlation while silica sands should fall on the low compressibility side.

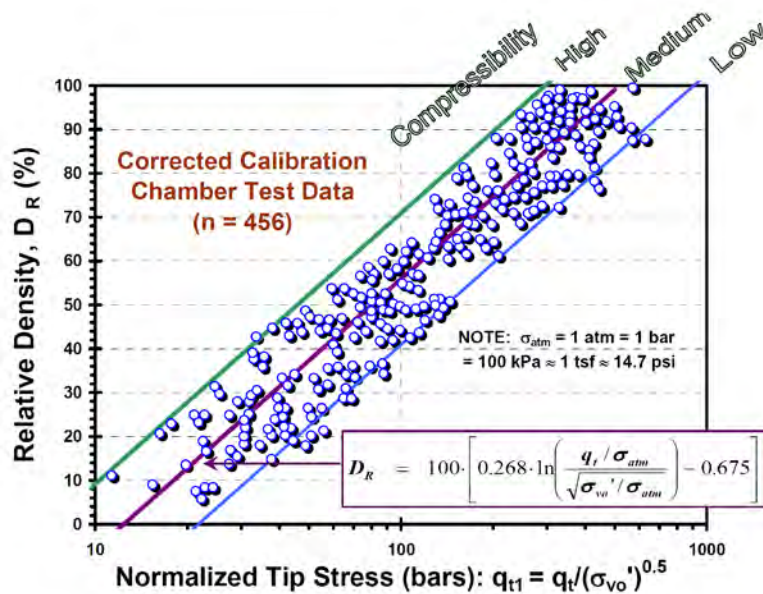


Figure 4-10 Correlation among CPT Tip Resistance, Relative Density, and Compressibility for Clean Sands (Jamiolkowski et al., 2001)

4.4.4 Shear Wave Velocity

General

The initial (small strain) shear modulus, G_{\max} , required for input to a site response analysis can be calculated from the total unit weight and the shear wave velocity of the soil. Shear wave velocity is relatively easily and inexpensively measured in the field using geophysical techniques. Therefore, it is recommended that shear wave velocity be directly measured in the field. However, for preliminary analyses and for projects where the results of the site response analysis are not considered critical, shear wave velocity can be estimated based upon soil type and consistency, by using the empirical correlations, or from CPT data. Shear wave velocity can also be evaluated in the laboratory using resonant column tests. However, field geophysical measurements are generally more reliable and cheaper for estimating the in situ shear wave velocity. Thus laboratory testing is rarely used in practice to evaluate shear wave velocity on transportation projects.

Figure 4-11 illustrates the variety of methods commonly used in the field and laboratory to measure shear wave velocity. Field measurements of shear wave velocities are typically based on measuring the wave travel time along a known propagation path. From knowledge of travel path distance and travel time, the velocity is obtained. Wave velocity may be measured using intrusive methods such as boreholes and CPT soundings (seismic cone) or non-intrusively using seismic reflection, refraction, and surface wave profiling.

Compressional wave velocity may sometimes be required for seismic analyses. Compressional wave velocity can be directly measured in a geophysical test or laboratory test. Alternatively, the compressional wave velocity can be calculated from the shear wave velocity and Poisson's ratio using Equation 4-5.

Geophysical Surveys

Geophysical techniques for subsurface exploration are described by Woods (1994) and in FHWA (2002a) and FHWA (2006). Geophysical techniques commonly used in geotechnical practice to measure shear wave velocity are briefly summarized in the following paragraphs. Two general types of geophysical techniques are available to measure shear wave velocities in the field:

- Intrusive techniques whereby measurements are made using probes and sensors that are lowered in boreholes or pushed into the ground; and
- Non-intrusive techniques whereby the measurements are made from the ground surface.

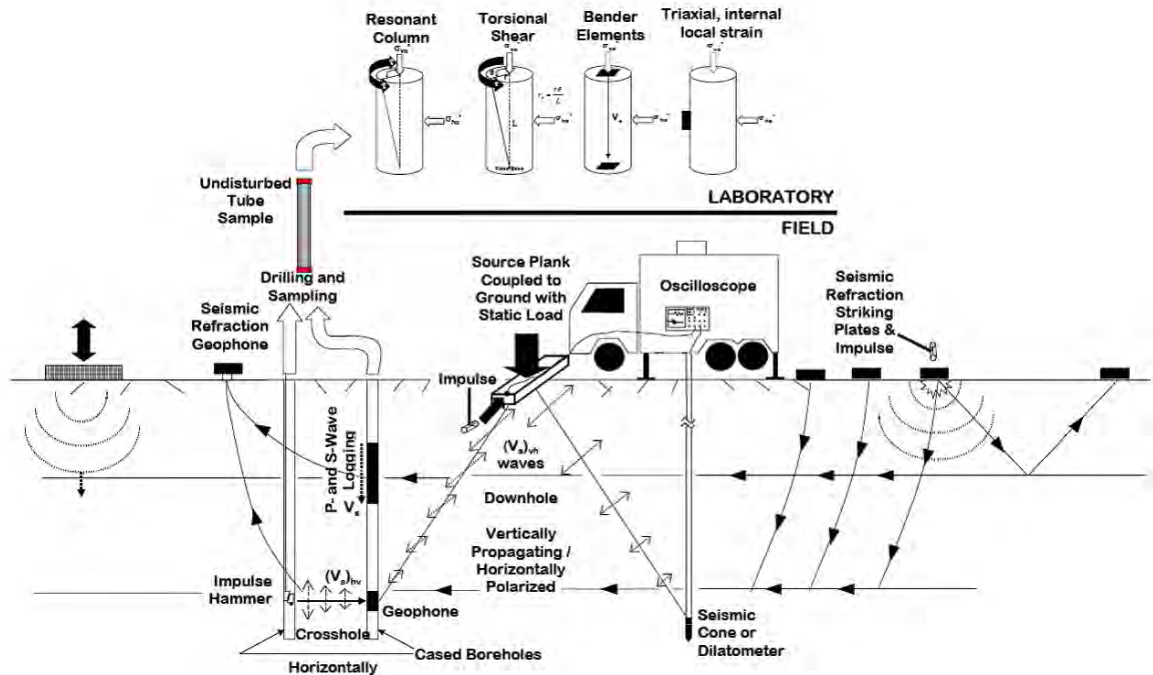


Figure 4-11 Field and Laboratory Methods for Evaluating Shear Wave Velocity (FHWA, 2002)

Borehole Surveys

In a borehole seismic survey, one or more boreholes are drilled into the soil to the desired depth of exploration. Wave sources and/or receivers are then lowered into the boreholes to perform the desired tests. There are three approaches to borehole seismic surveys:

- *Cross Hole Survey*: In a cross hole survey, the energy source is located in one boring and the detector (or detectors) is placed at the same depth as the energy source in one or more surrounding boreholes at a known spacing. Travel time between source and receiver is measured to determine the wave velocity. The cross hole survey method is illustrated at the bottom left of Figure 4-11.

- *Down Hole Survey:* In a down hole survey, the energy source is located on the surface and the detector, or geophone, is placed in the borehole. The travel time is measured with the geophone placed at progressively increasing depth to evaluate the wave velocity profile. The down hole survey method is illustrated in the left-center of Figure 4-11. Seismic cone penetration testing (SCPT) is another form of down hole survey. SCPT surveys can be combined with conventional cone penetration testing. SCPT testing is illustrated in the center of Figure 4-11.
- *Up Hole Surveys:* Up hole surveys are similar to down hole surveys except that geophones are placed on the surface adjacent to the borehole and the source in the borehole. The energy source usually is set off within the borehole at successively decreasing depths starting at the bottom of the hole. The energy source may be either explosives or a mechanical pulse instrument composed of a stationary part and a hammer held against the side of the borehole by a pneumatic or hydraulic bladder.

The cross hole technique generally offers the highest resolution and greatest accuracy among the three types of borehole geophysical surveys. However, cross hole measurements require a very precise evaluation of the distance between the energy source and the detector. An inclinometer reading is generally performed in the boreholes used in a cross hole survey to correct the results for deviation of the boreholes from verticality. Cross hole geophysical testing is codified in ASTM Standard D 4428.

Seismic Refraction and Seismic Reflection Methods

Seismic refraction and reflection exploration surveys are conducted from the surface and do not require boreholes. Seismic refraction surveying is illustrated on the right hand side of Figure 4-11. The resolution of these methods is relatively poor and decreases with depth. These methods are most suitable as a means of identifying the depth to competent rock and the location of prominent soil horizons that have a large contrast in density and stiffness compared to the overlying soil as opposed to making precise measurements of in situ wave velocities.

Spectral Analysis of Surface Waves (SASW)

Spectral Analysis of Surface Waves (SASW) is a non-intrusive geophysical technique used primarily for evaluating subsurface shear wave velocity profiles. SASW testing evaluates shear wave velocity indirectly by direct measurement of Rayleigh, or surface wave, velocity. Rayleigh wave velocity is

related to shear wave velocity by Poisson's ratio. The two velocities are usually within 5 percent of each other for most soils. SASW can be a very cost-effective method of investigation. Excitation at the ground surface is used to generate the Rayleigh, or surface, waves at various frequencies. By spectral analysis of the ground surface response (velocity or acceleration) at two points a known distance apart, the Rayleigh wave velocity can be obtained at discrete frequencies. Usually, an inversion process (trial and error) is used to determine the velocity profile. The ease and rapidity of field measurements and automated algorithms for data processing and inversion allow for evaluation of subsurface conditions at a relatively large number of points at a fraction of the cost of conventional intrusive exploration techniques. Measurements are not affected by the depth to the water table.

The concept of measuring the velocity of Rayleigh waves of different frequencies to determine the profile of shear wave velocity with depth was first proposed by Jones (1962), in Great Britain, for pavement surveys and by Ballard (1964), at the Waterways Experiment Station in Vicksburg, Mississippi, for geotechnical analyses. These investigators used impact loading as the source excitation and developed an analysis based upon the assumption of a uniform, homogeneous layer. Stokoe and Nazarian (1985) at the University of Texas, Austin, extended the analysis to consider multi-layered media. SASW surveys can resolve the shear wave velocity profile to depths in excess of 200 ft when heavy equipment or large electro-hydraulic vibrators are used to generate the surface excitation.

4.4.5 Cyclic Stress-Strain Parameters

Laboratory Testing

Laboratory testing for evaluation of cyclic stress-strain parameters of soil is appealing to many engineers because direct measurements are made of the hysteretic stress-strain behavior of soils. However, cyclic laboratory testing is subject to a variety of constraints, including:

- Difficulty in reproducing field stresses (and strains);
- Difficulty in recovering and testing undisturbed cohesionless soil samples; and
- The time and expense associated with cyclic laboratory testing.

A brief summary of the different types of cyclic laboratory tests used in geotechnical practice and their advantages and limitations follows. More details on cyclic laboratory testing can be found in Kramer (1996).

Cyclic Direct Simple Shear Test

The cyclic direct simple shear (CyDSS) test may provide the most accurate representation of the stress state resulting from a vertically propagating shear wave in a horizontally layered soil deposit of any laboratory test (see Figure 4-1). The simple shear device consists either of a rectangle box made of hinged plates, a cylindrical specimen confined by a wire-reinforced membrane, or stacked rings which surround the sample and restrain it from deforming laterally during the test. The apparatus includes either an arrangement for applying a constant vertical load or for maintaining a constant sample height while measuring the vertical load and a mechanism for applying a horizontal cyclic shear load. Reconstituted samples are usually formed directly in the simple shear device. However, undisturbed samples of cohesive soil or frozen sand can be tested in devices that use wire-reinforced membranes.

Cyclic Triaxial Test

The cyclic triaxial test was developed for geotechnical purposes by Seed and his co-workers at the University of California at Berkeley in the 1960s and has been used extensively to evaluate cyclic behavior of soils. The device consists of a regular triaxial cell and a cyclic, often sinusoidal loading machine attached to the loading piston. The sample is isotropically consolidated in the triaxial cell and then subjected to a cyclic axial load in extension and compression. The primary drawback of the cyclic triaxial tests is that it does not provide a good representation of the stress state induced in the ground by an earthquake (see Figure 5-1 in Chapter 5). The main difference in cyclic triaxial test stress conditions compared to the field conditions are: (1) the laboratory soil sample is isotropically consolidated, whereas the soil is under a K_0 condition in the field; (2) in the field there is a continuous reorientation of the principal stresses whereas in the triaxial test, the reorientation angle is either 0 or 90 degrees; (3) the cyclic shear stress is applied on a horizontal plane in the field but on a 45 degree plane in the triaxial test; and (4) the mean normal stress in the field is constant while the mean normal stress in the laboratory varies cyclically.

Torsional Simple Shear Test

In order to overcome some of the limitations of the CyDSS and triaxial tests, Ishibashi and Sherif (1974) developed a torsional simple shear test. The sample is a hollow cylinder with outer to inner radius and outer to inner height ratios of about two. This shape ensures a relatively uniform shear strain on the

horizontal plane throughout the sample. The torsional simple shear test offers several advantages over CyDSS and cyclic triaxial tests, including:

- Close simulation of the field stress (and strain) conditions (like the CyDSS);
- The ability to apply vertical and horizontal stresses independently; and
- The ability to keep the octahedral normal stress constant during the test.

There are also some disadvantages associated with this test, including:

- Interpretation of the results is rather complicated and the definition of liquefaction (Ishibashi and Sherif, 1974) does not permit correlation of torsional simple shear results with those of other tests;
- Mobilization of enough interface shear between the sample and the top and bottom plates to prevent slippage may be difficult, however steel pins cast into porous stones will provide good contact between the sample and the plates; and
- The shape of the sample makes the device impractical for use in conventional practice, particularly for undisturbed samples.

Resonant Column Test

The resonant column test for determining the dynamic properties of soils is based on the theory of wave propagation in rods. Either compression or shear waves can be propagated through the soil specimen in resonant column testing. Solid or hollow specimens can be used in the apparatus. Either a sinusoidal torque or a vertical compressional load is applied to the top of the sample through the top cap. The deformation of the top of the specimen is measured. The excitation frequency is adjusted until the specimen resonates. The wave velocity or modulus is computed from the resonant frequency and the geometric properties of the sample and driving apparatus. Damping is determined by switching off the current to the driving coil at resonance and recording the amplitude of decay of the vibrations. The decay of the amplitude with time is used to determine the *logarithmic decrement* (the percentage decay over one log cycle of time), which is directly related to the viscous damping ratio.

The primary limitation associated with using resonant column tests to measure dynamic soil properties is that the test is generally limited to small to intermediate shear strains by the applied force requirements and resonant frequencies. Furthermore, at larger strains, hollow samples must be used to maintain a relatively constant shear strain across the sample. For these reasons, resonant column testing is primarily

used to estimate small strain shear modulus and damping. However, resonant column testing can be conducted in the same device as torsional shear test in a device known as a Resonant Column Torsional Shear (RCTS) device. An RCTS device can be used to determine both the small strain modulus and damping of the soil and modulus reduction and hysteretic damping in intermediate strain range.

Use of Empirical Correlations

Parameters describing the cyclic soil properties required for a dynamic analyses include the initial (small strain) damping, λ , the initial (small strain) shear modulus at small shear strain, G_{max} , and the modulus reduction and damping curves for the soil. Small strain damping is difficult to evaluate. A viscous damping ratio of 2 to 5 percent is commonly assumed as the small-strain damping. The small strain shear modulus, commonly referred to as the *initial shear modulus*, G_{max} , can be obtained from site-specific investigations or by using empirical correlations with index soil properties. Geophysical methods for establishing shear wave velocity (V_s), from which G_{max} may be determined, were previously described. Table 4-4 presents the typical range of V_s and of G_{max} for several generic soil types.

TABLE 4-4 TYPICAL VALUES OF INITIAL SHEAR MODULUS

Type of Soil	Small-Strain Shear Wave Velocity, V_s (ft/s)	Initial Shear Modulus, G_{max} (tsf)
Soft Clays	130 - 300	30 - 140
Firm Clays	220 - 460	70 - 360
Loose Sands	420 - 900	290 - 1,440
Dense Sands and Gravel	660 - 1,350	720 - 3,600

The parameter G_{\max} has been empirically related to both the SPT blow count value and CPT resistance. Seed, et al. (1984) suggested that G_{\max} can be related to standardized and normalized SPT blow count, $(N_1)_{60}$, by the following equations:

$$G_{\max} = 1000 (K_2)_{\max} \cdot (\sigma'_m)^{0.5} \quad 4-17$$

$$(K_2)_{\max} = 20[(N_1)_{60}]^{0.33} \quad 4-18$$

where G_{\max} is in psf and σ'_m is the mean effective normal stress (in psf), evaluated as:

$$\sigma'_m = \left[\frac{1 + 2K_o}{3} \right] \cdot \sigma'_v \quad 4-19$$

Seed et al. (1984) also note that $(K_2)_{\max}$ can vary from 80 to 180 for loose to dense well graded gravels. Imai and Tonouchi (1982) present the following equation for G_{\max} as a function of the standardized blow count, N_{60} :

$$G_{\max} = 325 (N_{60})^{0.68} \quad 4-20$$

Table 4-5 presents the correlations presented in Equations 4-17 and 4-20 in SI units along with several additional index correlations for G_{\max} . Small strain modulus can also be derived from shear wave velocity and unit weight using Equations 4-2 and 4-3.

Figure 4-12 presents a correlation between CPT tip resistance and shear wave velocity developed by Baldi et al. (1989) for clean quartz sands. Figure 4-13 presents a correlation between shear wave velocity and CPT tip resistance developed by Mayne and Rix (1995) for clay soils.

TABLE 4-5 INDEX PROPERTY CORRELATIONS FOR ESTIMATING THE INITIAL (SMALL STRAIN) SHEAR MODULUS, G_{max}

CORRELATIONS FOR ESTIMATING INITIAL SHEAR MODULUS

Reference	Correlation	Units	Limitation
Seed, <i>et al.</i> (1984)	$G_{max} = 220 (K_2)_{max} (\sigma'_m)^{1/2}$ $(K_2)_{max} \approx 20(N_{1,60})^{1/3}$	kPa	$(K_2)_{max} \approx 30$ for very loose sands and 75 for very dense sands; ≈ 80 -180 for dense well graded gravels; Limited to cohesionless soils
Imai and Tonouchi (1982)	$G_{max} = 15,560 N_{60}^{0.68}$	kPa	Limited to cohesionless soils
Hardin (1978)	$G_{max} = \frac{625}{(0.3 + 0.7 e_o^2)} (P_a \cdot \sigma'_m)^{0.5} OCR^k$	kPa ^{(1) (3)}	Limited to cohesive soils P_a = atmospheric pressure
Jamiolkowski, <i>et al.</i> (1991)	$G_{max} = \frac{625}{e_o^{1.3}} (P_a \cdot \sigma'_m)^{0.5} OCR^k$	kPa ^{(1) (3)}	Limited to cohesive soils P_a = atmospheric pressure
Mayne and Rix (1993)	$G_{max} = 99.5 (P_a)^{0.305} (q_c)^{0.695} / (e_o)^{1.13}$	kPa ⁽²⁾	Limited to cohesive soils P_a = atmospheric pressure

Notes: ⁽¹⁾ P_a and σ'_m in kPa

⁽²⁾ P_a and q_c in kPa

⁽³⁾ The parameter k is related to the plasticity index, PI, as follows:

PI	k
0	0
20	0.18
40	0.30
60	0.41
80	0.48
> 100	0.50

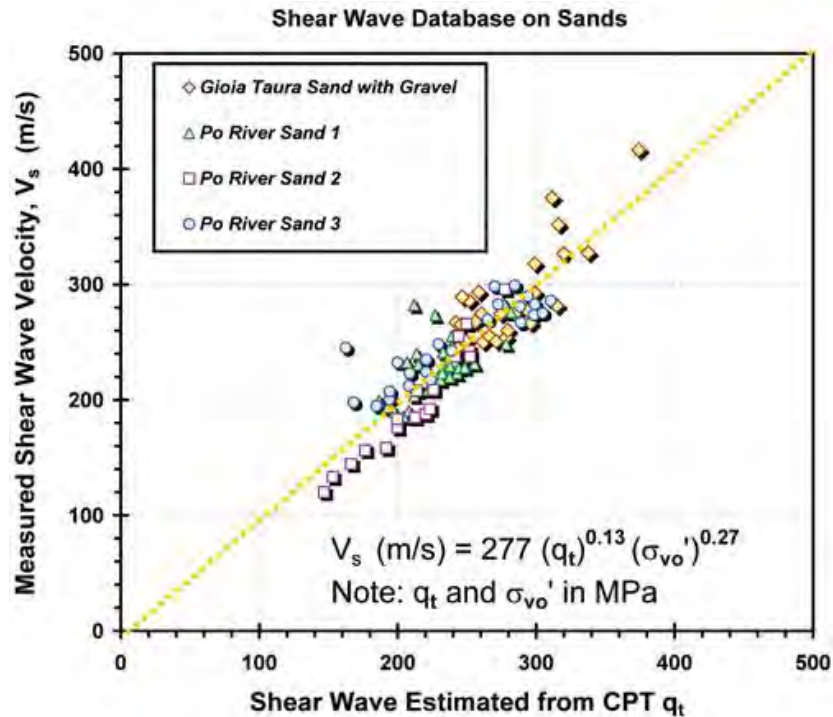


Figure 4-12 CPT – Shear Wave Velocity Correlation for Clean Quartz Sands (Baldi et al., 1989)

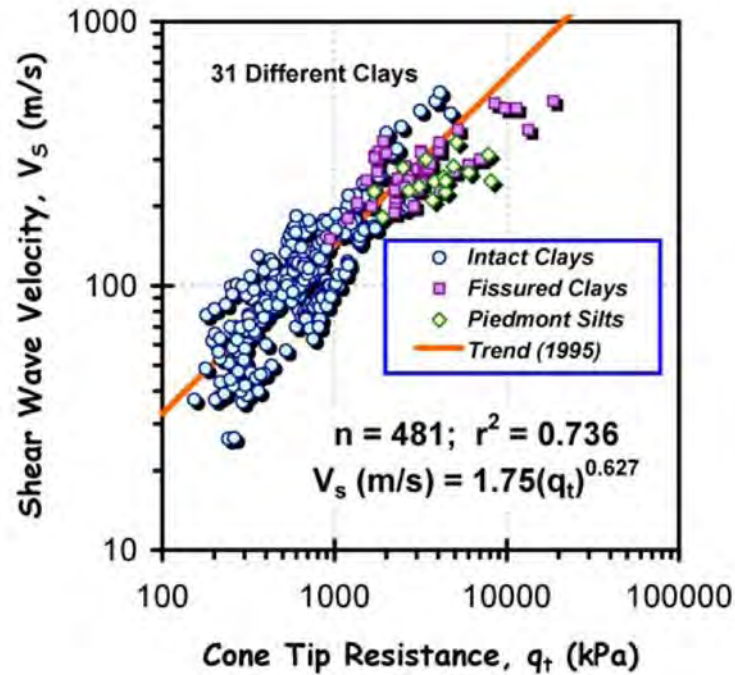


Figure 4-13 CPT – Shear Wave Velocity Correlation for Clay Soils (Mayne and Rix, 1989)

Damping and normalized modulus reduction curves are generally presented as a function of soil type or plasticity index, with a PI = 0 representing cohesionless soil. However, since the modulus reduction curve is normalized with respect to the small strain, the absolute value of the shear modulus depends not only on shear strain but on the factors influencing the small strain modulus. Traditional modulus reduction and damping curves are independent of overburden pressure. Traditional curves still widely used in practice include the Seed and Idriss (1970) and Seed et al. (1986) sand curves (presented as a band of data, with the mean value typically used in practice), the Seed et al. (1984) gravel curves, and families of PI-dependent curves for cohesive soils developed by Sun et al. (1988) and Vucetic and Dobry (1991). Subsequent work has shown that both modulus reduction and damping depend upon overburden pressure. However, these traditional curves can still be used with good confidence for soil layers in the top 50 ft of the profile.

Iwasaki, et al. (1978) found that the mean normal effective stress is a significant factor influencing modulus reduction and damping in cohesionless soils. The stress dependent modulus reduction curves developed by these investigators are shown in Figure 4-14.

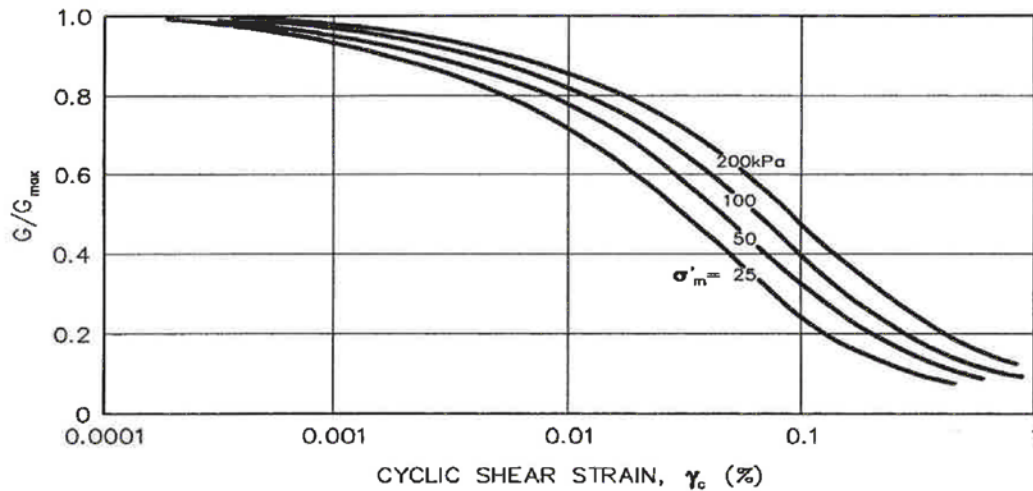


Figure 4-14 Shear Modulus Reduction Curves for Sands. (Iwasaki, *et al.*, 1978, reprinted by permission of Japanese Society of Soil Mechanics and Foundation Engineering)

It is now recognized that it is essential to capture the confining pressure dependence of modulus reduction in order to properly model the seismic response of deep soil deposits. In particular, the traditional confining pressure independent curves have been shown to significantly over-damp site response in soil profiles greater than 300 ft thick, filtering out high frequency motions and attenuating peak accelerations. Confining pressure dependent curves frequently used in practice today include families of curves developed by EPRI (1993), Hashash and Park (2001), and Darendeli (2001). Figure 4-15 compares upper bound, average, and lower bound Seed *et al.* (1986) confining pressure independent modulus reduction and damping curves to the confining pressure dependent curves of Darendeli (2001) for $PI = 0$.

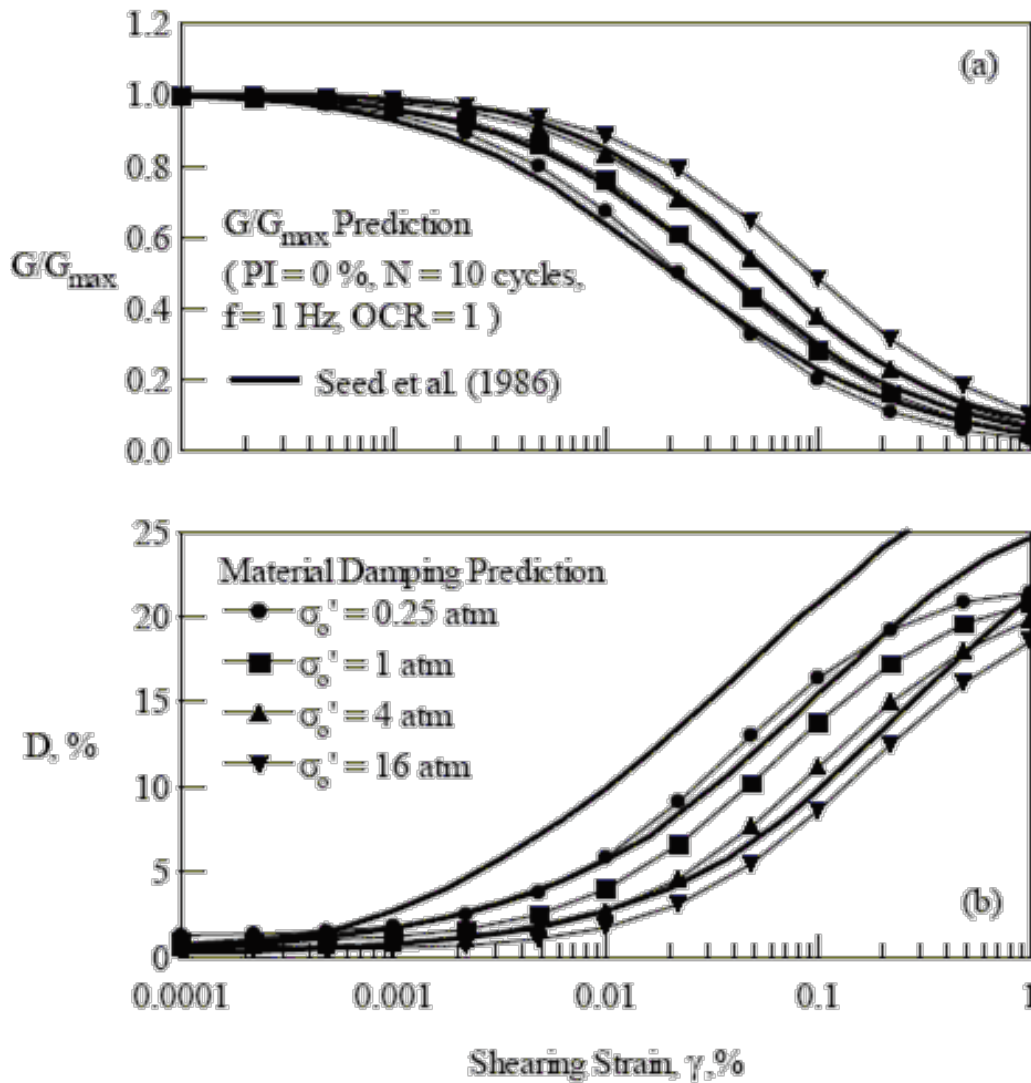


Figure 4-15 Comparison of Seed et al. (1985) Modulus Reduction and Damping Curves for Sand with Darendeli (2001) Curves for PI = 0. (Darendeli, 2001)

Figure 4-16 presents the Darendeli (2001) confining pressure dependent modulus reduction and damping curves for a PI equal to 30. Figure 4-17 compares modulus reduction and damping curves from Hashash and Park (2001), used to model seismic response of soil and weak rock columns in the Mississippi embayment over 3000 ft thick, with the EPRI (1993) confining pressure dependent modulus reduction and damping curves. EPRI (1993) also provides modulus reduction and damping curves for weak rock. Most computer programs for seismic site response analysis will have one or more of these confining pressure dependent models built into them.

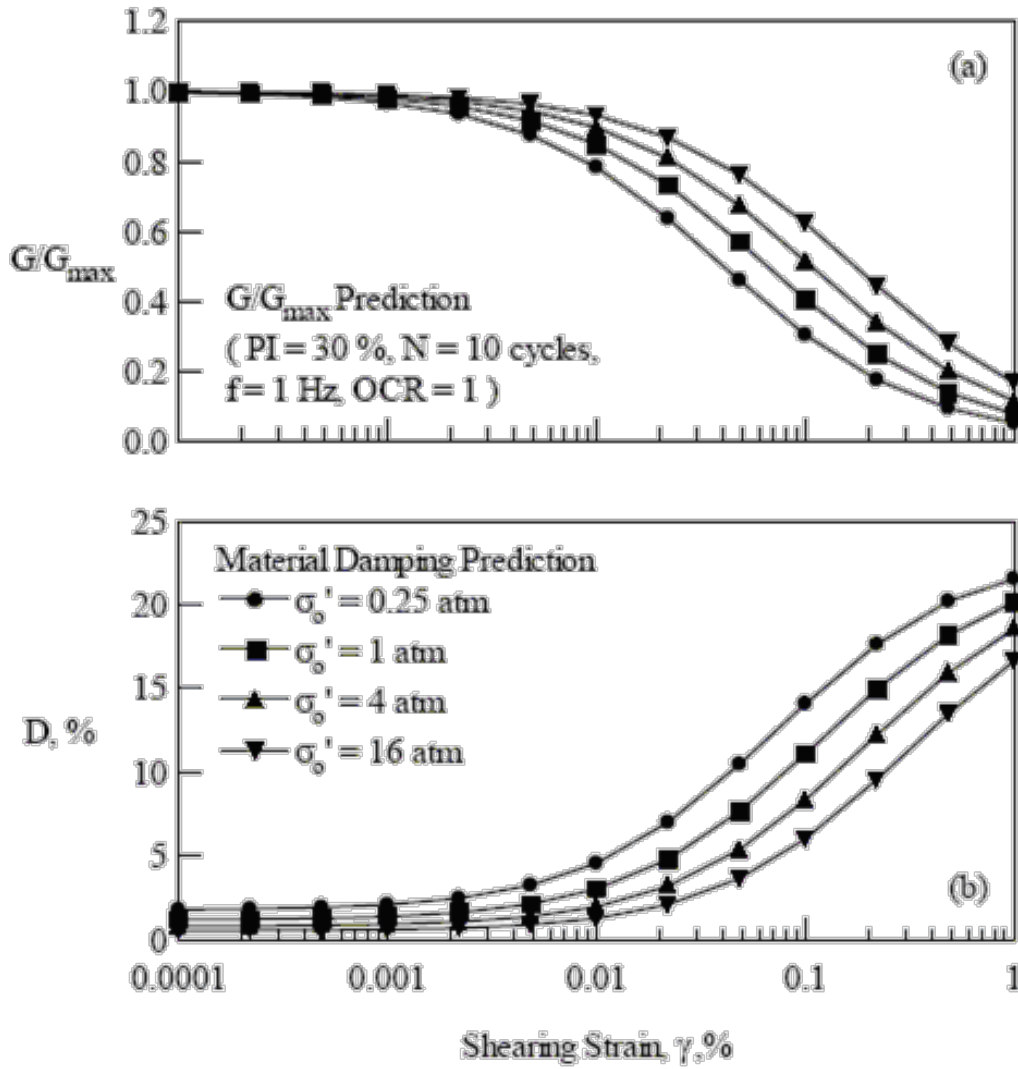


Figure 4-16 Darendeli (2001) Confining Pressure Dependent Curves for PI = 30. (Darendeli, 2001)

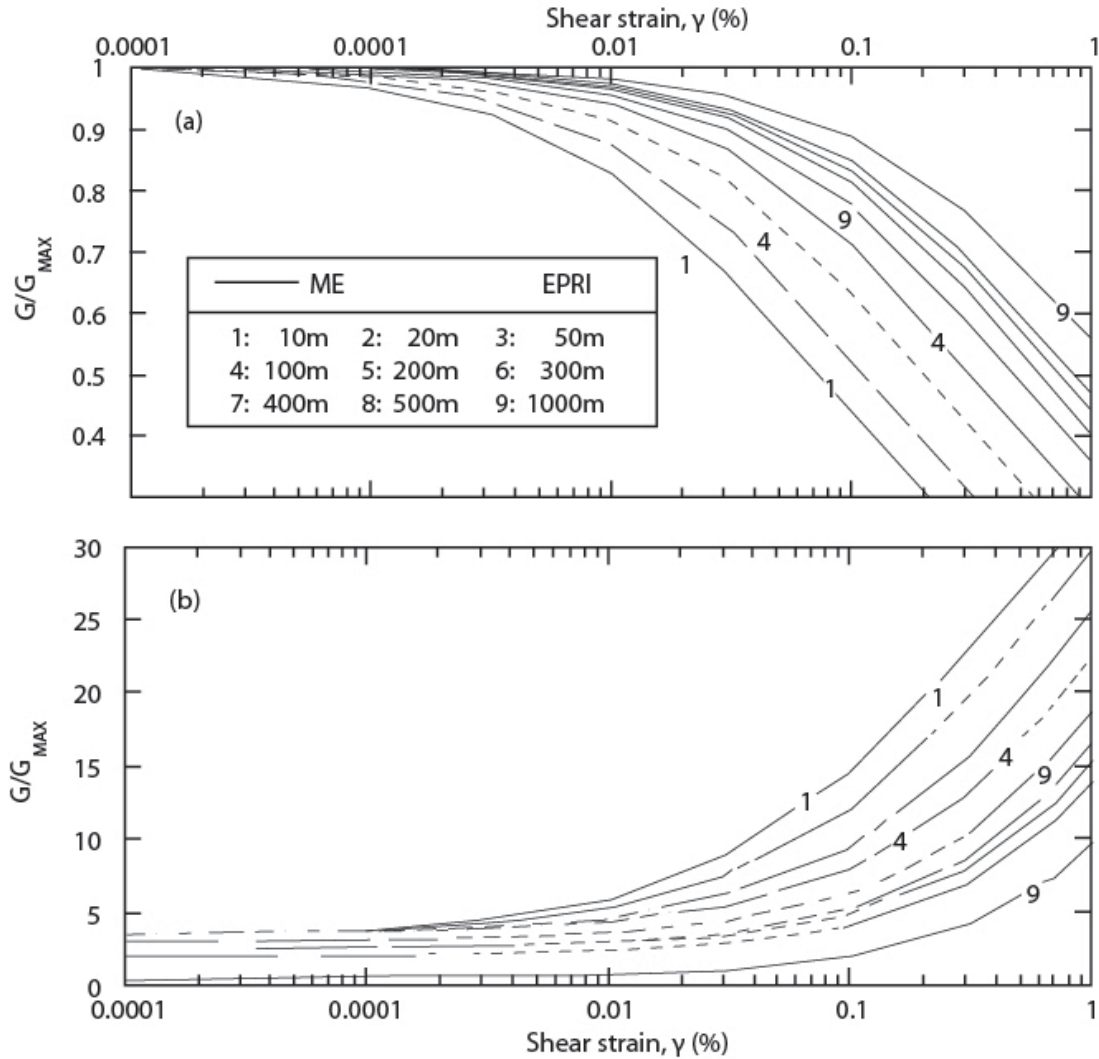


Figure 4-17 Comparison of Hashash and Park (2001) Modulus Reduction and Damping Curves for the Mississippi Embayment with EPRI (1993) curves (after Darendeli, 2001)

4.4.6 Peak and Residual Shear Strength

The peak shear strength of soil not subject to strength degradation under cyclic loading may be evaluated using conventional methods, including laboratory and in situ testing and correlations with soil index properties. A key difference in seismic problems compared to static problems is that undrained strength parameters are typically used for the strength of saturated soils subjected to cyclic loading, even for cohesionless soils (e.g., sands, gravels) because of the relatively rapid rate of earthquake loading.

The undrained shear strength of a soil subject to cyclic loading may be influenced by the amplitude of the cyclic deviator stress, the number of applied loading cycles, and the plasticity of the soil. Makdisi and Seed (1978) point out that substantial permanent strains may be produced by cyclic loading of clay soils to stresses near the yield stress, while essentially elastic behavior is observed for large numbers of (>100) cycles of loading at cyclic shear stresses of up to 80 percent of the undrained strength. Therefore, these investigators recommend the use of 80 percent of the undrained strength as the “dynamic yield strength” for soils that exhibit small increases in pore pressure during cyclic loading, such as clayey materials, and partially saturated cohesionless soils. However, the investigators in the NCHRP 12-70 project found little evidence of cyclic strength loss in cohesive soils during earthquakes and noted that cohesive soils also tend to show an increase in undrained shear strength when subject to rapid loading. These investigators concluded that, except for earthquakes of greater than magnitude 7 wherein it may be prudent to assume a 10-15% strength loss, there was no reason to reduce the undrained shear strength of low to intermediate sensitivity cohesive soils to account for cyclic strength loss.

For saturated cohesionless soils, even relatively modest cyclic shear stresses can lead to pore pressure rise and a significant loss of undrained strength. Direct evaluation of the potential for shear strength reduction in a saturated or almost saturated cohesionless soil (low plasticity silt, sand, or gravel) subjected to cyclic loading would require sophisticated cyclic laboratory testing. Alternatively, a residual strength may be assigned to the soil based upon in situ test results.

The undrained residual shear strength after cyclic loading, S_r , is of critical importance in assessing the post-liquefaction stability of a foundation or earth structure. Saturated soils which liquefy typically possess some "residual" shear strength even when in the liquefied state. In initially loose soils, this residual strength may be very small and of little consequence. In denser soils (particularly in dense granular soils which tend to dilate or expand in volume), this residual strength can be high enough to render the impact of liquefaction relatively insignificant. For medium dense soils, the residual shear strength can be the most important factor in determining whether or not remediation is necessary

Poulos, et al. (1985) proposed a methodology for evaluating S_r based on obtaining high-quality soil samples with minimal disturbance. The high-quality samples were tested in the laboratory and the laboratory strengths were then adjusted for field conditions using specially developed techniques to correct the resulting laboratory S_r values for effects of void ratio changes due to sampling, handling, and test set-up. Due to the sensitivity of S_r to even small changes in void ratio, the laboratory techniques proposed by Poulos, et al. do not appear to represent a reliable basis for engineering analyses unless very

conservative assumptions and high factors of safety are employed to account for the considerable uncertainties involved.

Because of the difficulties in measuring steady-state strength in the laboratory, Seed (1987) proposed an alternate technique for evaluation of in situ undrained residual shear strength based on the results of SPT testing. He back analyzed a number of liquefaction-induced failures from which residual strength could be calculated for soil zones in which SPT data was available, and proposed a correlation between *residual strength*, S_r , and $(N_1)_{60-cs}$. $(N_1)_{60-cs}$ is a "corrected" normalized standardized SPT blow count, in which the normalized standardized $(N_1)_{60}$ value is further adjusted with a correction factor for fines content, N_{corr} , is applied to generate an equivalent "clean sand" blow count. The original Seed (1987) relationship was subsequently updated by Seed and Harder (1990). However, uncertainty due to the large spread of the data and the limited number of case studies back analyzed by Seed and Harder (1990) limited the usefulness of their work in practice.

The work of Seed and Harder in back-analyzing case histories of liquefaction flow slides to evaluate S_r has subsequently been extended by Olsen and his co-workers (Olsen and Stark, 2002; Olsen and Johnson, 2008) and Idriss and Boulanger (2007) to develop correlations between the residual undrained strength ratio, S_r/σ'_{vo} , and SPT blow count. Olson and Johnson (2008) back analyzed case histories of both lateral spreading and liquefaction flow failures to develop relationships between the undrained residual shear strength ratio and both the standardized normalized blow count, $(N_1)_{60}$ and the normalized CPT tip resistance, q_{c1} . These authors state that they used the average of CPT tip resistance normalization procedures suggested by Jamiolkowski et al. (2001) and Tatsuoka et al. (1995) in developing their correlation with CPT tip resistance. However, for practical purposes the following normalization equation presented in Mayne (2007) can be used:

$$q_{c1} = \frac{q_t}{(\sigma'_{vo} - \sigma_{atm})^{0.5}} \quad 4-21$$

The undrained residual shear strength ratio correlations developed by Olson and Johnson (2008) are presented in Figure 4-18.

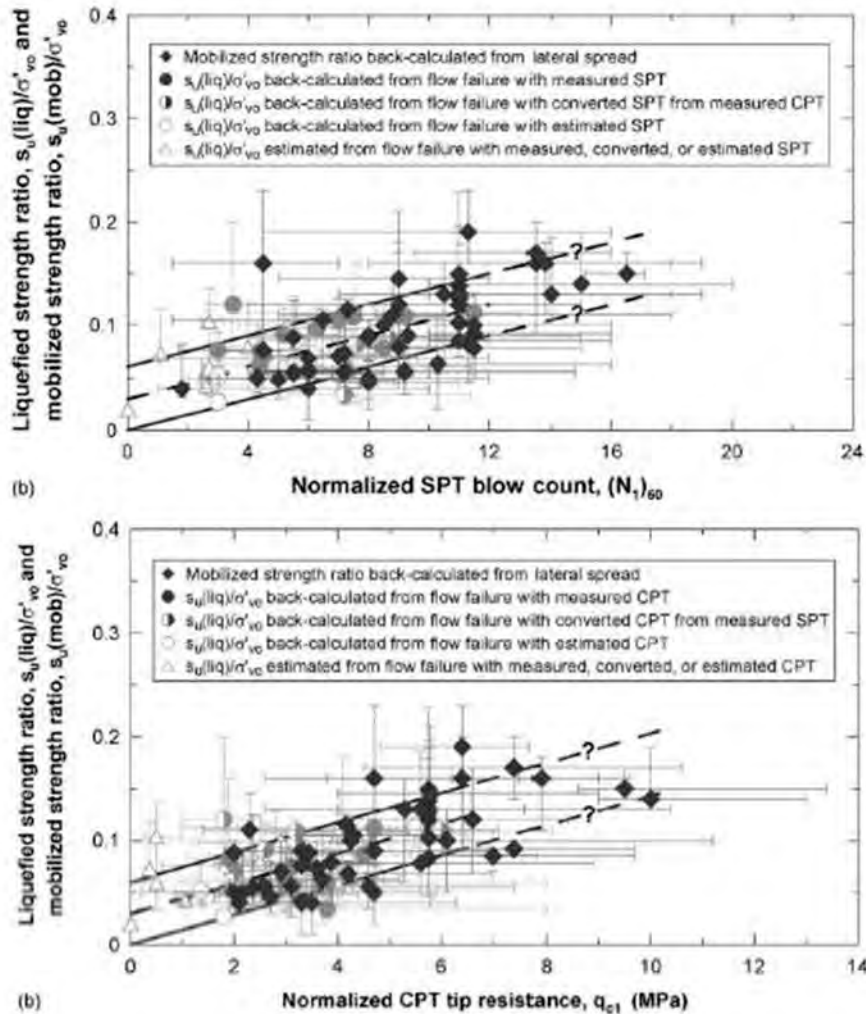


Figure 4-18 Correlation between the Undrained Residual Strength Ratio, S_r/σ'_{vo} and a) standardized normalized SPT blow count, $(N_1)_{60}$ and b) normalized CPT tip resistance, q_{c1} (Olson and Johnson, 2008)

Idriss and Boulanger (2007) also developed correlations between the undrained residual shear strength ratio and both SPT and CPT penetration resistance. The SPT correlation developed by Idriss and Boulanger (2007) is presented in Figure 4-19. These investigators used the equivalent clean sand blow count of Seed and Harder (1990), $(N_1)_{60-cs}$, presented in Equation 4-22, as their SPT resistance parameter:

$$(N_1)_{60-cs} = (N_1)_{60} + N_{corr} \quad 4-22$$

where N_{corr} depends upon the percent, by weight, passing the number 200 sieve as presented in Table 4-6.

TABLE 4-6 BLOW COUNT CORRECTION, N_{corr} , FOR THE EQUIVALENT CLEAN SAND BLOW COUNT, $(N_1)_{60cs}$

% passing #200 sieve	N_{corr}
0-9	0
10-24	1
25-49	2
50-74	4
>75	5

Idriss and Boulanger (2007) limit the application of their correlations to an effective overburden pressure of 8000 psf. In developing their correlations, Idriss and Boulanger (2007) differentiated between cases where void ratio redistribution may be anticipated due to the presence of an overlying confining pressure, as illustrated in Figure 4-20, and cases where no void ratio redistribution was anticipated. Figure 4-19 shows their suggested correlation for cases where void ratio redistribution is expected. However, this portion of their correlation is supported by few data points and therefore should be used with caution.

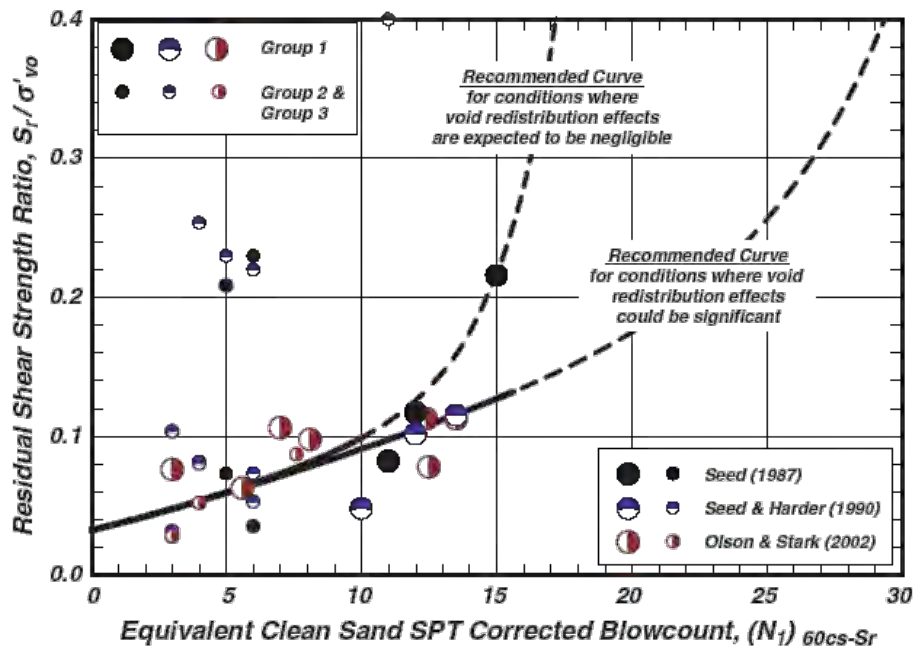


Figure 4-19 Correlation between the Residual Undrained Strength Ratio, S_r/σ'_{vo} and equivalent clean sand SPT blow count, $(N_1)_{60cs}$ (Idriss and Boulanger, 2007)

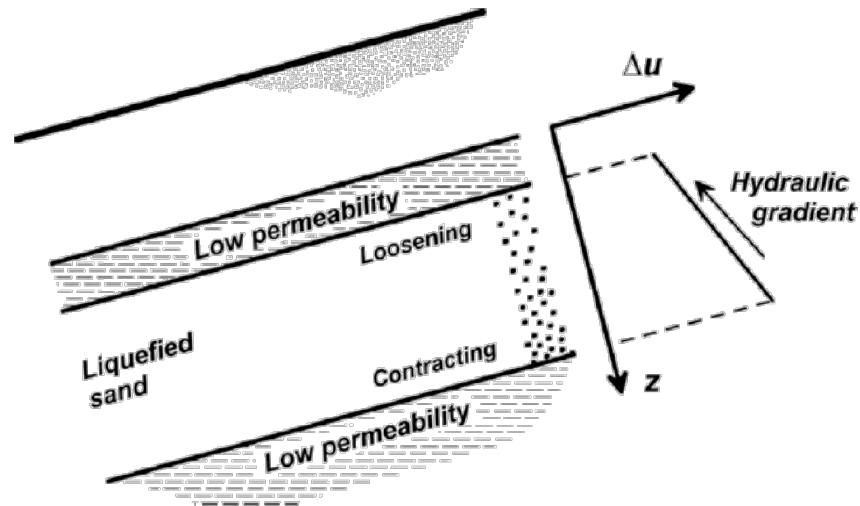


Figure 4-20 Void Ratio Redistribution Due to an Overlying Confining Layer (Idriss and Boulanger, 2007)

4.5 ROCK MASS PROPERTIES

4.5.1 Rock Mass Categories

In a seismic analysis, rock may be treated as either a linear elastic material with a constant shear modulus and no damping or as an equivalent linear material with an initial small strain modulus, a slight potential for modulus degradation, and a small amount of damping. The elastic modulus for the rock mass is generally based upon either shear wave velocity measurements or, in cases where the value of the modulus is not critical (i.e. when the modulus is merely used to characterize the impedance contrast at the bottom of a soil column), using typical properties. Modulus reduction and damping are typically based upon generic equivalent linear modulus reduction and damping curves (e.g. the generic curves for soft rock from Silva et al. 1997).

The shear strength of the rock mass is required for seismic stability analyses. The shear strength of a rock mass is, in general, less than the shear strength of the intact pieces of rock. However, the shear strength of the intact rock may still influence the rock mass shear strength. For the purpose of characterizing rock mass shear strength, rock masses may be divided into two broad categories: highly fractured rock masses and rock masses with discrete discontinuities. The shear strength characteristics of both categories of rock mass are described below.

4.5.2 Highly Fractured Rock Masses

The shear strength parameters for highly fractured rock masses may be determined from either of two empirical methods (FHWA 1998a, 2002): (i) An empirical method (i.e. Hoek-Brown failure criterion with Geological Strength Index) developed by Hoek (1983) and Hoek and Brown (1988, 1997), and updated by Hoek et al. (2002); and (ii) back analysis of a failed or failing slope. The applicability of the Hoek-Brown method is more suitable for intact rock or heavily jointed rock masses such as the Group I and Group III rock mass systems shown in Figure 4-21. Representative values of cohesion and friction angle c and ϕ from back analysis of rock mass failures are shown in Figure 4-22.

The generalized Hoek-Brown failure criterion defining the rock mass strength for jointed rock masses is expressed as:

$$\sigma'_1 = \sigma'_3 + \sigma'_{ci} \left(m_b \frac{\sigma'_3}{\sigma'_{ci}} + s \right)^a \quad 4-23$$

where

- σ'_1 and σ'_3 are the maximum and minimum effective stresses at failure,
- m_b is the value of the Hoek-Brown constant for the rock mass,
- s and a are constants which depend upon the rock mass characteristics, and
- σ_{ci} is the uniaxial compressive strength of the intact rock pieces.

As shown by Equation 4-23, the strength of a jointed rock mass depends on the uniaxial compressive strength (σ_{ci}) and other properties of the intact rock pieces as well as upon the freedom of these pieces to slide and rotate under different stress conditions. This freedom is controlled by the geometrical shape of the intact rock pieces as well as the condition of the surfaces separating the pieces. Angular rock pieces with clean, rough discontinuity surfaces will result in a much stronger rock mass than one which contains rounded particles surrounded by weathered and altered material. Table 4-7 presents typical field estimates of uniaxial compressive strength of intact rock.

The values of m_b , s , and a for use in Equation 4-23 have been correlated to the Geological Strength Index (GSI) introduced by Hoek (1994) and Hoek, Kaiser and Bawden (1995). The GSI provides a system for estimating the reduction in rock mass strength for different geological conditions. This system is presented in Table 4-8.

TABLE 4-7 FIELD ESTIMATES OF UNIAXIAL COMPRESSIVE STRENGTH OF INTACT ROCK (MARINOS AND HOEK, 2000)

Grade*	Term	Uniaxial Comp. Strength (MPa)	Point Load Index (MPa)	Field estimate of strength	Examples
R6	Extremely Strong	> 250	>10	Specimen can only be chipped with a geological hammer	Fresh basalt, chert, diabase, gneiss, granite, quartzite
R5	Very strong	100 - 250	4 - 10	Specimen requires many blows of a geological hammer to fracture it	Amphibolite, sandstone, basalt, gabbro, gneiss, granodiorite, peridotite, rhyolite, tuff
R4	Strong	50 - 100	2 - 4	Specimen requires more than one blow of a geological hammer to fracture it	Limestone, marble, sandstone, schist
R3	Medium strong	25 - 50	1 - 2	Cannot be scraped or peeled with a pocket knife, specimen can be fractured with a single blow from a geological hammer	Concrete, phyllite, schist, siltstone
R2	Weak	5 - 25	**	Can be peeled with a pocket knife with difficulty, shallow indentation made by firm blow with point of a geological hammer	Chalk, claystone, potash, marl, siltstone, shale, rocksalt,
R1	Very weak	1 - 5	**	Crumbles under firm blows with point of a geological hammer, can be peeled by a pocket knife	Highly weathered or altered rock, shale
R0	Extremely Weak	0.25 - 1	**	Indented by thumbnail	Stiff fault gouge

* Grade according to Brown (1981).

** Point load tests on rocks with a uniaxial compressive strength below 25 MPa are likely to yield highly ambiguous results.

Once the Geological Strength Index has been estimated, the parameters that describe the rock mass strength characteristics for use in Equation 4-23 are calculated as follows:

$$m_b = m_i \exp\left(\frac{GSI - 100}{28 - 14D}\right) \quad 4-24$$

where m_i is the value of the Hoek-Brown constant for the intact rock shear strength which can be obtained based upon the typical values shown in Table 4-9.

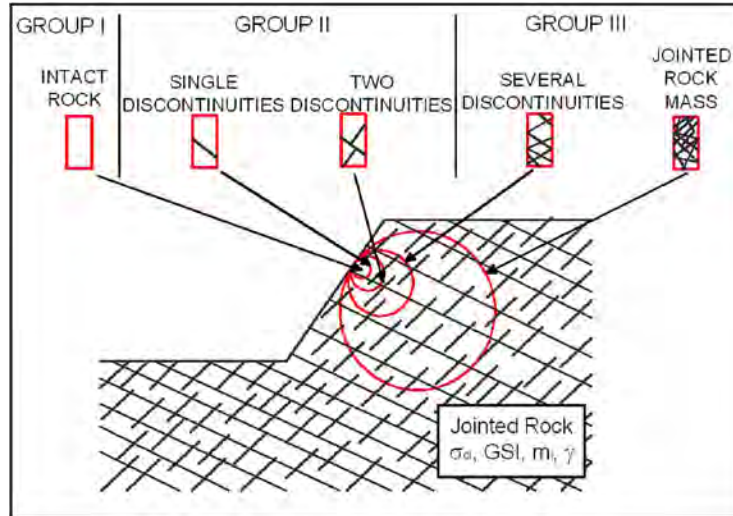


Figure 4-21 Classes of Rock Mass Discontinuities (FHWA 1998)

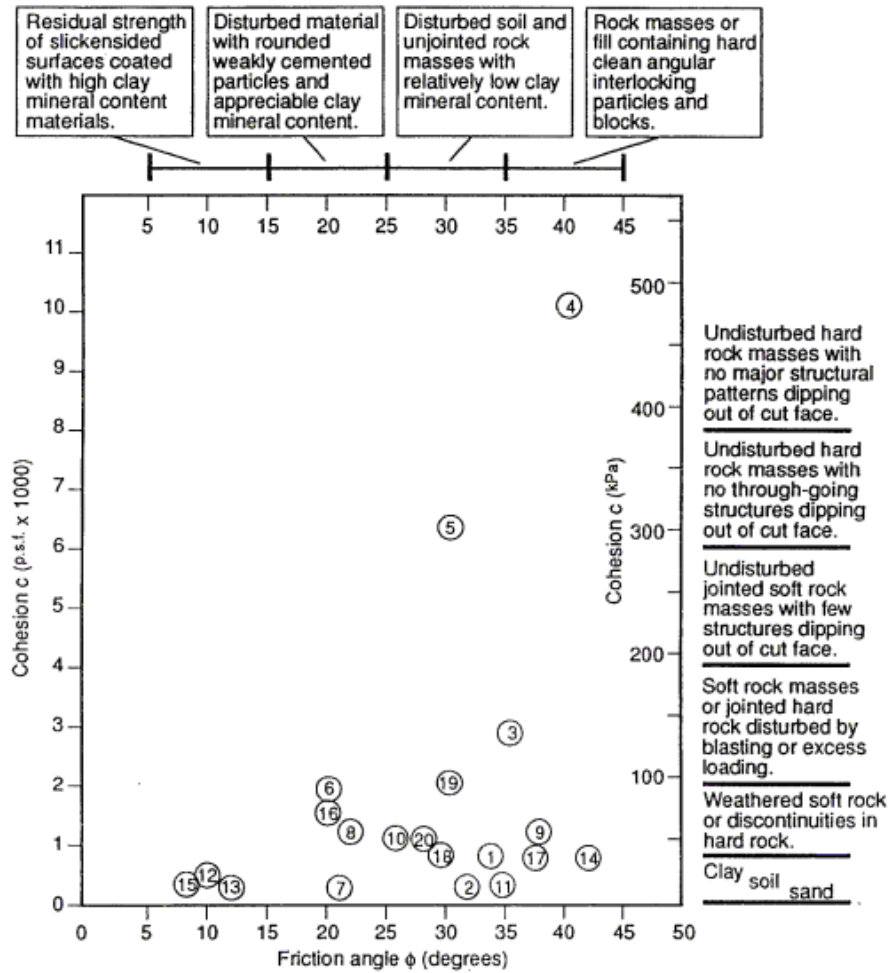








Figure 4-22 Relationship between Friction Angles and Cohesive Strength Mobilized at Failure for Slopes (Hoek and Bray, 1977)

**TABLE 4-8 GEOLOGICAL STRENGTH INDEX (GSI)
FOR JOINTED ROCK MASSES (Hoek and Marinos, 2000)**

<p>GEOLOGICAL STRENGTH INDEX FOR JOINTED ROCKS (Hoek and Marinos, 2000)</p> <p>From the lithology, structure and surface conditions of the discontinuities, estimate the average value of GSI. Do not try to be too precise. Quoting a range from 33 to 37 is more realistic than stating that GSI = 35. Note that the table does not apply to structurally controlled failures. Where weak planar structural planes are present in an unfavourable orientation with respect to the excavation face, these will dominate the rock mass behaviour. The shear strength of surfaces in rocks that are prone to deterioration as a result of changes in moisture content will be reduced if water is present. When working with rocks in the fair to very poor categories, a shift to the right may be made for wet conditions. Water pressure is dealt with by effective stress analysis.</p>		<p>SURFACE CONDITIONS</p> <p>VERY GOOD Very rough, fresh unweathered surfaces</p> <p>GOOD Rough, slightly weathered, iron stained surfaces</p> <p>FAIR Smooth, moderately weathered and altered surfaces</p> <p>POOR Slickensided, highly weathered surfaces with compact coatings or fillings or angular fragments</p> <p>VERY POOR Slickensided, highly weathered surfaces with soft clay coatings or fillings</p> <p align="center">DECREASING SURFACE QUALITY →</p>				
<p>STRUCTURE</p>						
 <p>INTACT OR MASSIVE - intact rock specimens or massive in situ rock with few widely spaced discontinuities</p>	90			N/A	N/A	
 <p>BLOCKY - well interlocked undisturbed rock mass consisting of cubical blocks formed by three intersecting discontinuity sets</p>	80	70	60			
 <p>VERY BLOCKY- interlocked, partially disturbed mass with multi-faceted angular blocks formed by 4 or more joint sets</p>		50	40			
 <p>BLOCKY/DISTURBED/SEAMY - folded with angular blocks formed by many intersecting discontinuity sets. Persistence of bedding planes or schistosity</p>			30			
 <p>DISINTEGRATED - poorly interlocked, heavily broken rock mass with mixture of angular and rounded rock pieces</p>			20			
 <p>LAMINATED/SHEARED - Lack of blockiness due to close spacing of weak schistosity or shear planes</p>	N/A	N/A			10	

**TABLE 4-9 VALUES OF m_i FOR INTACT ROCK
BY ROCK GROUP (Marinos and Hoek, 2000)**

Rock type	Class	Group	Texture			
			Coarse	Medium	Fine	Very fine
SEDIMENTARY	Clastic		Conglomerates *	Sandstones 17 ± 4	Siltstones 7 ± 2	Claystones 4 ± 2
			Breccias *		Greywackes (18 ± 3)	Shales (6 ± 2) Marls (7 ± 2)
	Non-Clastic	Carbonates	Crystalline Limestone (12 ± 3)	Sparitic Limestones (10 ± 2)	Micritic Limestones (9 ± 2)	Dolomites (9 ± 3)
		Evaporites		Gypsum 8 ± 2	Anhydrite 12 ± 2	
METAMORPHIC	Non Foliated		Marble 9 ± 3	Hornfels (19 ± 4) Metasandstone (19 ± 3)	Quartzites 20 ± 3	
	Slightly foliated		Migmatite (29 ± 3)	Amphibolites 26 ± 6	Gneiss 28 ± 5	
	Foliated**			Schists 12 ± 3	Phyllites (7 ± 3)	Slates 7 ± 4
IGNEOUS	Plutonic	Light	Granite 32 ± 3	Diorite 25 ± 5	Granodiorite (29 ± 3)	
		Dark	Gabbro 27 ± 3 Norite 20 ± 5	Dolerite (16 ± 5)		
	Hypabyssal		Porphyries (20 ± 5)		Diabase (15 ± 5)	Peridotite (25 ± 5)
	Volcanic	Lava		Rhyolite (25 ± 5) Andesite 25 ± 5	Dacite (25 ± 3) Basalt (25 ± 5)	
		Pyroclastic	Agglomerate (19 ± 3)	Breccia (19 ± 5)	Tuff (13 ± 5)	

* Conglomerates and breccias may present a wide range of m_i values depending on the nature of the cementing material and the degree of cementation, so they may range from values similar to sandstone, to values used for fine grained sediments (even under 10).

** These values are for intact rock specimens tested normal to bedding or foliation. The value of m_i will be significantly different if failure occurs along a weakness plane.

The values of s and a are constants for the rock mass and can be evaluated as:






$$s = \exp\left(\frac{GSI - 100}{9 - 3D}\right) \quad 4-25$$

and

$$a = \frac{1}{2} + \frac{1}{6} \left(e^{\frac{-GSI}{15}} - e^{\frac{-20}{3}} \right) \quad 4-26$$

D is a factor which depends upon the degree of disturbance to which the rock mass has been subjected by blast damage and stress relaxation as shown in Table 4-10 (Hoek et. al, 2002).

Table 4-10 ESTIMATION OF DISTURBANCE FACTOR, D (Hoek et. al, 2002)

Appearance	Description of Rock Mass	Suggested Value
	Excellent quality controlled blasting or excavation by Tunnel Boring Machine results in minimal disturbance to the confined rock mass surrounding a tunnel.	$D = 0$
	Mechanical or hand excavation in poor quality rock masses (no blasting results in minimal disturbance to the surrounding rock mass. Where squeezing problems result in significant floor heave, disturbance can be severe unless a temporary invert, as shown in the paragraph, is placed.	$D = 0$ $D = 0.5$ No invert
	Very poor quality blasting in a hard rock tunnel results in severe local damage, extending 2 or 3m, in the surrounding rock mass.	$D = 0.8$
	Small scale blasting in civil engineering slopes results in modest rock mass damage, particularly if controlled blasting is used as shown on the left hand side of the paragraph. However, stress relief results in some disturbance.	$D = 0.7$ Good blasting $D = 1.0$ Poor blasting
	Very large open pit mine slopes suffer significant disturbance due to heavy production blasting and also due to stress relief from overburden removal. In some softer rocks excavation can be carried out by ripping and dozing and the degree of damage to the slope is less	$D = 1.0$ Production blasting $D = 0.7$ Mechanical excavation

For practical purposes, the Hoek-Brown failure criterion (based on major and minor principal stresses) was best-fit to the Mohr-Coulomb criterion with strength parameters c and ϕ for use in conventional limit equilibrium slope stability analyses as shown in Figure 4-23.

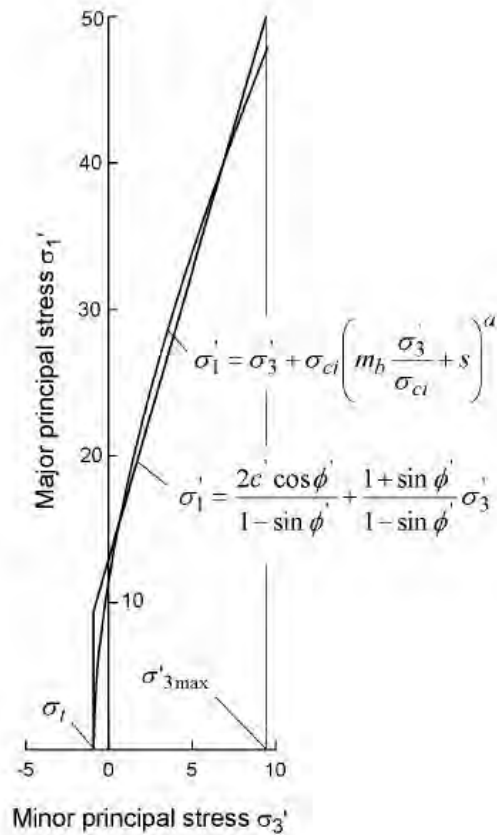


Figure 4-23 Relationships between Major and Minor Principal Stresses for Hoek-Brown and equivalent Mohr-Coulomb Criteria (Hoek, 2002)

The Mohr-Coulomb shear strength (τ) can be calculated by:

$$\tau = c' + \sigma' \tan \phi' \tag{4-27}$$

where

$$\phi' = \sin^{-1} \left[\frac{6am_b (s + m_b \sigma'_{3n})^{a-1}}{2(1+a)(2+a) + 6am_b (s + m_b \sigma'_{3n})^{a-1}} \right] \tag{4-28}$$

and

$$c' = \frac{\sigma_{ci} \left[(1+2a)s + (1-a)m_b \sigma'_{3n} \right] (s + m_b \sigma'_{3n})^{a-1}}{(1+a)(2+a) \sqrt{1 + \left(6am_b (s + m_b \sigma'_{3n})^{a-1} \right) / ((1+a)(2+a))}} \quad 4-29$$

Where

$$\sigma_{3n} = \sigma'_{3 \max} / \sigma_{ci} \quad 4-30$$

Both the Hoek-Brown failure criterion and the GSI classification system have been updated frequently by Hoek and various researchers since they were first developed. Readers are referred to Hoek and Marinos (2007) for more discussions.

4.5.3 Rock Masses with Discrete Discontinuities

The stability of rock masses with discrete discontinuities under both static and seismic loading depends on the shear strength of the discontinuity surfaces and the slope and wedge geometry. The shear strength of the discontinuity surfaces depends on the joint roughness, the strength of the intact rock material and any infill materials, and the confining pressure. The roughness of a fracture surface can be defined by a joint roughness coefficient, JRC (Barton, 1973). Barton (1976) has shown the strength of a rough rock surface may be defined by the equation:

$$\tau = \sigma' \tan \left[\phi + JRC \cdot \log_{10} \left(\frac{JCS}{\sigma'} \right) \right] \quad 4-31$$

where

JRC = joint roughness coefficient

JCS = compressive strength of the rock at the fracture surface

σ' = effective normal stress

Values of the parameter JRC may be determined by comparing a fracture surface with standard profiles as illustrated in Figure 4-24. Values of JCS may be determined from Schmidt hammer tests in the field. (Deere and Miller, 1966).

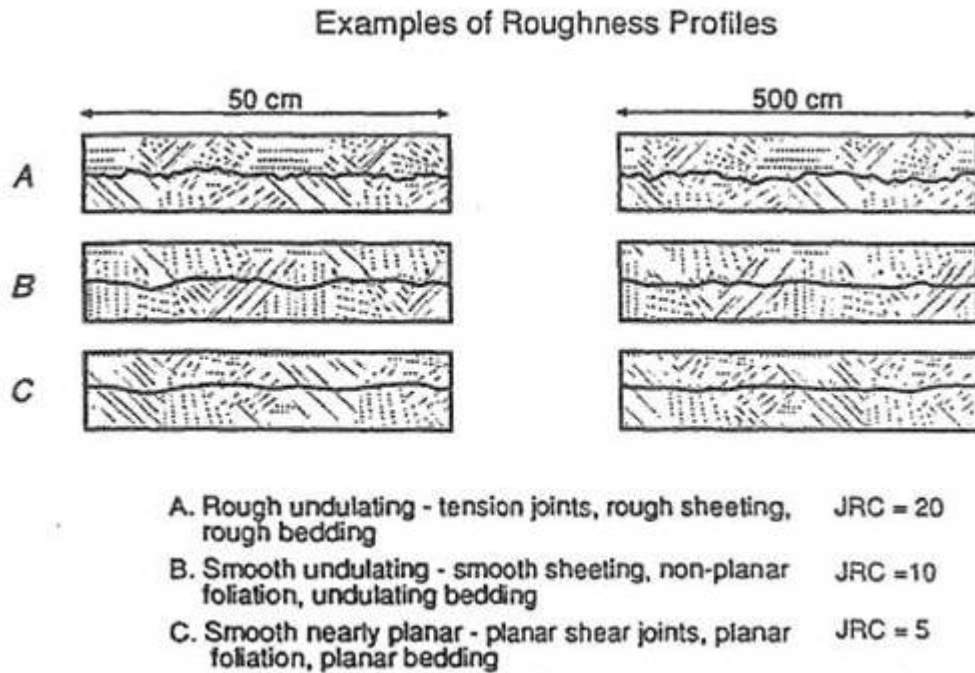


Figure 4-24 Definition of Joint Roughness Coefficient, JRC (Barton, 1973)

Equation 4-32 defines a nonlinear failure surface like that shown in Figure 4-25 from which overburden pressure-dependent instantaneous cohesion and friction angle values may be determined for stability analyses using the Mohr-Coulomb failure criterion. Computer programs for static and seismic stability based on wedge analysis are commercially available.

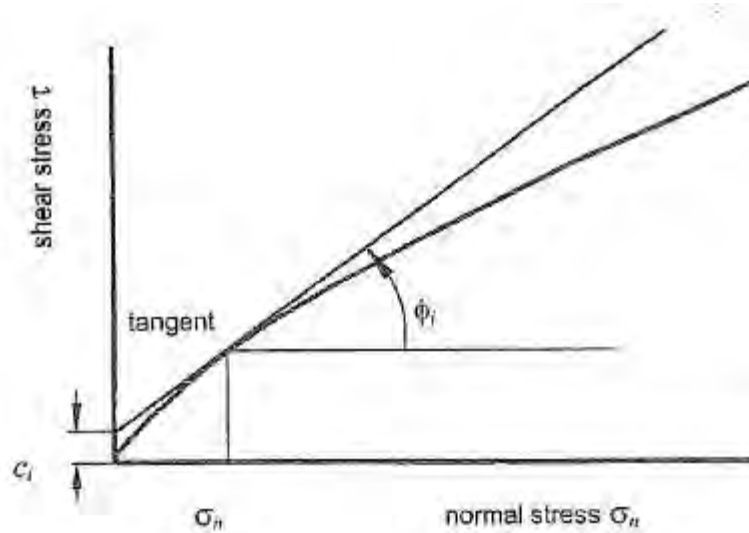


Figure 4-25 Definition of Instantaneous Cohesion c_i and Instantaneous Friction Angle ϕ_i for a Non-Linear Failure Criterion (FHWA 1998)

4.6 SUMMARY

This chapter discusses development of the subsurface profile and evaluation of representative geotechnical properties for seismic analysis of transportation facilities, including structural foundations. The discussion focuses on the information unique to seismic analysis under the assumption that basic geotechnical information for facility design (e.g. soil classification, relative density or unit weight, moisture content, and shear strength) has already been established. Essential information from which the key geotechnical properties required for seismic analysis and design may be determined includes site stratigraphy, groundwater conditions, and measures of soil consistency (e.g. SPT blow count or CPT resistance). Stratigraphic information should include soil classification, grain size information for cohesionless soils, Atterberg limits and in situ water content for cohesive soils, and depth to bedrock.

Key geotechnical properties for seismic analysis and design include the small strain shear stiffness (modulus), shear strain-dependent modulus reduction and damping curves, cyclic shear strength, and liquefaction resistance and post-liquefaction residual strength of potentially liquefiable soils. Shear modulus is generally determined from the shear wave velocity, V_s , and total unit weight of the material (soil or rock). Shear wave velocity may be measured directly by a variety of geophysical methods, including both intrusive and non-intrusive techniques. Alternatively, shear wave velocity may be determined by correlation with soil index properties or penetration resistance, including both SPT blow

count and CPT resistance. Shear strain-dependent modulus reduction and damping curves are generally assigned based on index properties and overburden pressure. Use of overburden dependent shear modulus reduction and damping curves is essential for soil layers greater than 100 ft thick.

For cohesionless soils, the shear strength for use in a dynamic stability assessment should be the lesser of the drained and undrained strengths. For saturated cohesive soils, an undrained shear strength equal to 85% of the static undrained strength is recommended for seismic stability assessment. Liquefaction resistance of liquefiable soil is described by either the normalized standardized SPT blow count, $(N_1)_{60}$, or the normalized CPT tip resistance, q_{c1} . Post-liquefaction residual shear strength is expressed as a function of the effective overburden pressure using the residual shear strength ratio, S_r/σ'_{v0} . The residual shear strength ratio may be determined as a function of either the normalized CPT resistance or the normalized standardized SPT blow count and fines content.

For characterization of shear strength, rock masses may be split into two categories: highly fractured rock masses and rock masses with discrete discontinuities. The shear strength of highly fractured rock masses may be characterized using the Hoek-Brown non-linear shear strength envelope or values of overburden-dependent equivalent cohesion and friction angle derived from the Hoek-Brown equation. The shear strength of discrete discontinuities can be characterized using Barton's (1976) equation or values of overburden-dependent equivalent cohesion and friction angle derived from the Barton equation.

The soil profile and soil property information developed in this chapter provides the basis for almost all of the geotechnical analyses presented subsequently in this report. The site stratigraphy, small-strain shear modulus, and shear strain-dependent modulus reduction and damping curves are the essential input for the site specific seismic response analysis presented in Chapter 5. The site stratigraphy, liquefaction resistance, and shear strength parameters discussed in this chapter are the fundamental parameters required for the geotechnical hazard analysis presented in Chapter 6. The dynamic shear strength parameters described in this chapter, including the residual shear strength, are used in slope stability analyses presented in Chapter 9, foundation performance analysis (e.g. bearing capacity and lateral resistance) presented in Chapters 10 and 11, and retaining wall analysis presented in Chapter 12. Seismic analysis of buried structures, presented in Chapter 13, also requires knowledge of the shear stiffness and shear strength of the surrounding soils.

CHAPTER 5

SEISMIC SITE RESPONSE ANALYSIS

5.1 GENERAL

The local soil profile at a project site can have a profound effect on earthquake ground motions. Local soil conditions can affect the intensity, frequency content, and duration of strong shaking. Amplification of peak bedrock accelerations on the order of 0.05 g to 0.10 g by a factor of three or more due to the influence of the local soil profile has been documented. Even when the peak ground acceleration is not amplified, the local soil profile is likely to alter the frequency content (i.e. the spectral accelerations) of the bedrock ground motions. Amplification of the spectral acceleration by a factor of ten or more has been observed in the vicinity of the fundamental site period, T_0 . Embankment and retained earth fills can have a similar effect on ground surface motions.

Conventional seismic hazard analyses typically provide ground motions for a weak rock site, i.e. a site with a value of V_{S30} , the average shear wave velocity over the top 100 ft, equal to 2,500 ft/sec. This corresponds to Site Class B in the AASHTO site classification system described in Chapter 3 (see Table 3-5). The probabilistic ground motions employed by AASHTO as the basis for structural design of ordinary bridges correspond to this site classification. The influence of local ground conditions on the strong ground motions at a site that differs from a site that is representative of Site Class B can be accounted for in several different ways. The peak ground acceleration (PGA) can be modified by empirical amplification factors that depend upon soil type or site class. Alternatively, the PGA and spectral accelerations at 0.2 second and 1 second can be modified using the site-class dependent PGA, short period, and long period site factors, F_{PGA} , F_a and F_v . With the modified values of peak ground acceleration and the spectral accelerations at 0.2 second and 1 second, a new response spectrum can be constructed, as discussed in Section 3.4.7. Another alternative is to conduct a site-specific seismic hazard analysis using one or more of the Next Generation Attenuation (NGA) relationships that explicitly accounts for local site conditions. Four of the five NGA relationships discussed in Section 3.6 of Chapter 3 employ V_{S30} as a dependent variable in their formulation and three of these four relationships use an additional parameter to capture the influence of local site conditions on ground motions, e.g. the depth to a shear wave velocity of 3,300 ft/s. A formal site seismic response analysis can also be used to account for the effect of local site conditions on the ground motions.

For many engineering analyses, one of the first three methods described above is sufficient to account for the effect of local soil conditions on design ground motions. However, if a detailed evaluation of the influence of local soil conditions is desired, or when it is not appropriate to use empirical PGA amplification relationships or the AASHTO site factors, a formal seismic site response analysis must be conducted. Furthermore, for Site Class F, deemed special study sites in the AASHTO seismic design provisions, a formal seismic site response analysis is required to evaluate the influence of local site conditions on the design ground motions. Sites with significant contrasts in the shear wave velocity among layers within 200 ft of the ground surface and sites with deep soil columns, e.g. soil columns in excess of 500 ft, are also good candidates for a site-specific seismic response analysis, as the differences in the soil profile at these types of sites compared to the profiles used to develop the AASHTO site factors may create significant differences in site response compared to that predicted using the AASHTO site factors.

There are a variety of design analyses for non-structural features of transportation systems for which site response analyses may also be warranted. Site response analyses can be used to determine the seismic coefficient for slope stability analyses and retaining wall design. Site response analysis can also be used to develop appropriate time histories for use in Newmark-type seismic deformation analyses for slopes, embankments, and lateral spreading of liquefied ground. The most accurate means of determining the earthquake –induced shear stress, τ_{eq} , for liquefaction analysis is through a site response analysis. Site response analyses may also be warranted to determine the free field shear strain for evaluation of the dynamic stiffness of shallow foundations and the differential shear displacement for seismic design of box-shaped underground structures, e.g. culverts and cut and cover tunnels. Furthermore, Chapter 3 described the use of site response analyses to evaluate the spatial variability of ground motions along a linear structure such as a long span bridge or viaduct. Table 5-1 summarizes the different types of design analyses where a seismic response analysis may be warranted, along with the chapter in this document where these analyses are discussed.

TABLE 5-1 USES OF SITE RESPONSE ANALYSIS IN SEISMIC DESIGN OF TRANSPORTATION FACILITIES

Analysis	Response Analysis Parameter	Chapter
<ul style="list-style-type: none"> • Structural design, including spatial incoherence 	<ul style="list-style-type: none"> • Response spectra • Acceleration time histories 	3
<ul style="list-style-type: none"> • Liquefaction 	<ul style="list-style-type: none"> • Peak ground acceleration • Earthquake-induced shear stress 	6
<ul style="list-style-type: none"> • Slope stability • Retaining wall design 	<ul style="list-style-type: none"> • Seismic coefficient 	6, 7, 11 & 12
<ul style="list-style-type: none"> • Seismic deformation of slopes and embankments 	<ul style="list-style-type: none"> • Acceleration time history 	6 & 7
<ul style="list-style-type: none"> • Soil-structure interaction 	<ul style="list-style-type: none"> • Acceleration time histories vs. depth 	8, 9, 10 & 11
<ul style="list-style-type: none"> • Shallow foundation stiffness 	<ul style="list-style-type: none"> • Strain-compatible shear modulus 	9
<ul style="list-style-type: none"> • Racking/Ovaling of underground structures 	<ul style="list-style-type: none"> • Differential subsurface shear displacement 	13

5.2 SITE-SPECIFIC SEISMIC RESPONSE ANALYSES

5.2.1 Types of Site-Specific Analysis

The most common types of site-specific seismic site response analyses are one-dimensional analyses based upon the assumption of a vertically propagating shear wave through uniform horizontal soil layers of infinite lateral extent. The assumption that shear waves propagate vertically to the ground surface is, in general, a valid engineering assumption. Even if the shear wave is not propagating vertically at depth it will refract into a near vertical position as it approaches the ground surface. This refraction is due to the general increase in shear wave velocity with increasing distance from the ground surface (i.e. increasing depth below ground), as illustrated in Figure 5-1. This phenomenon is similar to the refraction of water waves at the beach such that they usually approach the shore with their crest aligned parallel to the shore. The influence of vertical motions, compressional waves, and laterally non-uniform soil conditions are typically not accounted for in conventional seismic site response analyses. There are, however, situations where the designer may wish to consider the influence of non-uniform ground conditions on site response. In such situations, a two-dimensional site response analysis may be required.

Evaluation solely of the impact of vertically propagating shear waves in a site response analysis is consistent with current design and code practices. It is also consistent with geotechnical engineering analyses for liquefaction potential and seismic slope stability, which usually consider only the horizontal component of the seismic motions. Three different levels of one-dimensional site-specific seismic site response analysis are available to geotechnical specialists:

- Simplified analysis
- Equivalent-linear one-dimensional site response analyses
- Advanced one-dimensional site response analyses

These three levels of one-dimensional site response analysis are discussed in the remainder of this chapter.

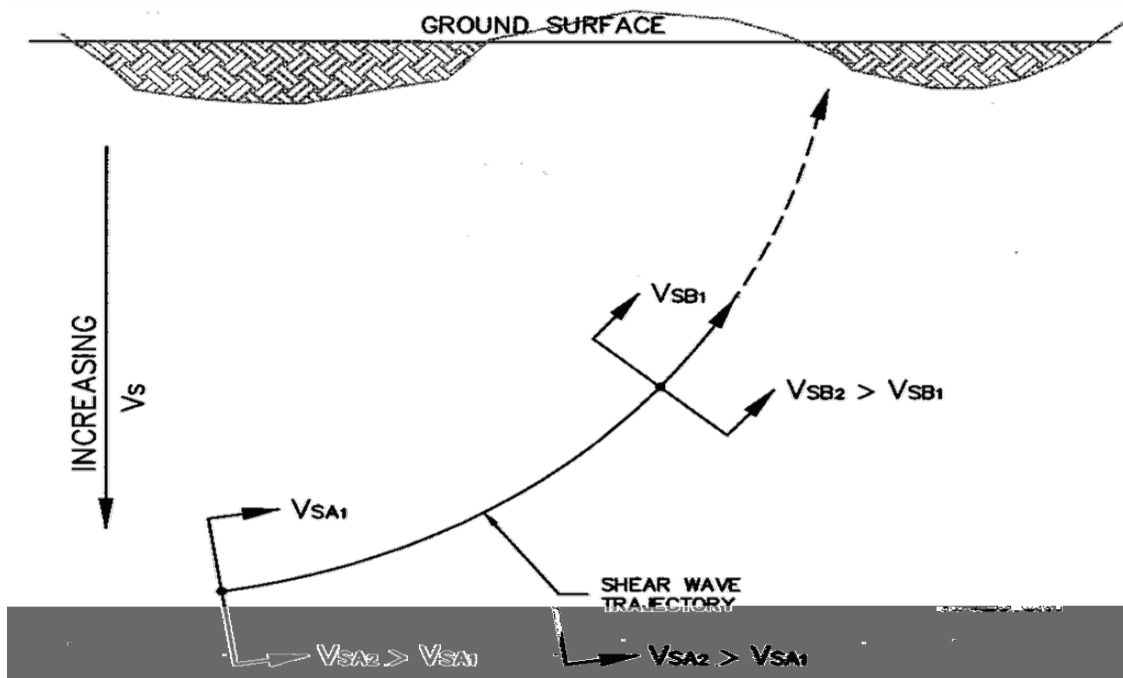


Figure 5-1 Refraction of Shear Waves Approaching the Ground Surface

5.2.2 Simple Empirical Relationships

For screening purposes and preliminary analyses, the influence of local soil conditions on seismic site response can be assessed in an approximate manner using simple empirical relationships which correlate ground motions at rock sites to those at soil sites. These relationships, developed on the basis of both observations of ground motions in earthquakes and equivalent-linear one-dimensional site response analyses, provide site response factors that can be used to estimate the *free field* (i.e., not affected by structure and/or topography) ground motion at soil sites from the free field rock site (Site Class B) ground motion determined in a seismic hazard analysis. An empirical relationship for the amplification of the transverse peak ground acceleration by earthen embankments is also available.

The most common type of simplified site response analysis used in earthquake engineering practice is the NEHRP procedure, adopted by AASHTO, for modifying the acceleration response spectra based upon V_{S30} . The NEHRP procedure for modifying the peak ground acceleration (PGA) and the short period spectral accelerations (S_S) and the spectral acceleration at 1 second (S_1) using the site response factors F_{pga} , F_a , and F_v is presented in Sections 3.3.8 and 3.5 in Chapter 3. The values of F_{pga} , F_a , and F_v , presented in Tables 3-6, 3-7, and 3-8, are related to the site class presented in Table 3-5, which depends upon V_{S30} . (Table 3-5 also provides for establishing site class based upon SPT blow count or undrained shear strength if V_{S30} is not available.) Modified values of the PGA (i.e. A_s), S_S (i.e. S_{DS}), and S_1 (i.e. S_{D1}) are then used to construct the truncated (three-point) acceleration response spectra for use in structural design. However, there are special study sites (Site Class F) where AASHTO specifies that this procedure should not be applied. Furthermore, the NEHRP procedure should not be used at sites with strong impedance contrasts among layers in the top 200 ft of the soil profile (the impedance is the product of the shear wave velocity and mass density of the soil), as these sites do not conform to the model used to develop the NEHRP/AASHTO site response factors. The NEHRP/AASHTO site factors should also be used with caution for sites with very deep soil columns (e.g. soil columns in excess of 500 ft), as these sites are also suspect with respect to conformance to the NEHRP model, as discussed subsequently.

Whereas structural analyses may require information on the spectral acceleration over a range of spectral periods to characterize the design ground motion, geotechnical analyses frequently only require knowledge of the peak ground acceleration (in combination with earthquake magnitude). Several investigators have developed empirical relationships between the peak ground acceleration at a hypothetical bedrock outcrop at the project site and the peak ground acceleration at the site as a function of the local soil conditions. Among the first of these relationships, developed by Seed and Idriss (1982),

is presented in Figure 5-2. Figure 5-2 (presented solely for historical context) relates the rock site PGA to the soil site PGA for stiff soil, deep cohesionless soil, and soft to medium-stiff clay and sand site conditions. However, no formal definition of these site conditions was provided.

While the plot in Figure 5-2 is outdated and should not be used for engineering analysis, the basic pattern of behavior illustrated by the plot remains unchanged. At low PGA values, rock site PGAs can be amplified at soft soil sites. However, at higher PGAs values the rock site PGA may be attenuated (reduced) at these same sites. The reduction in soil site PGA at higher rock site PGA values is due to the limited shear strength of the soil, resulting in yielding (shear failure) of the soil near the ground surface. Yielding of the soil limits its ability to transmit ground acceleration to overlying soil layers.

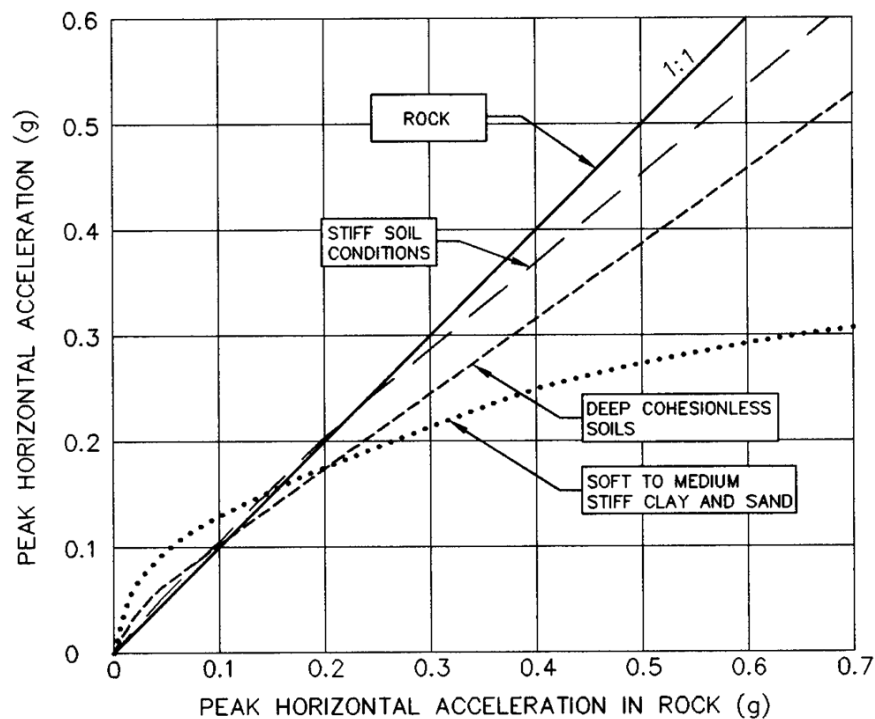


Figure 5-2 Relationship between PGA on Rock and on Other Local Site Conditions (After Seed and Idriss, 1982, reprinted by permission of EERI)

A similar plot to Figure 5-2 can be developed using the PGA site factor, F_{pga} . Figure 5-3 presents a plot of the PGA at a weak rock site (Site Class B) versus the corresponding PGA at a soil site based upon AASHTO site class (i.e. based upon V_{s30}). This plot was developed using the PGA amplification factors, F_{pga} , in Table 3-6 with slight modifications for Site Classes C and D for PGA values from 0.4 g to 0.5 g to

smooth out the curves and produce a pattern of behavior similar to Figure 5-2. Figure 5-3 can be used to modify the PGA as a function of site class (i.e. as a function of V_{s30}) without going through the entire NEHRP procedure. However, as noted previously with respect to the NEHRP procedure, the amplification factors in this figure should not be used for Site Class F (special study sites) or for sites with a strong impedance contrast in the upper 200 ft of the soil profile. Additionally, Figure 5-3 should be used with caution for deep soil sites.

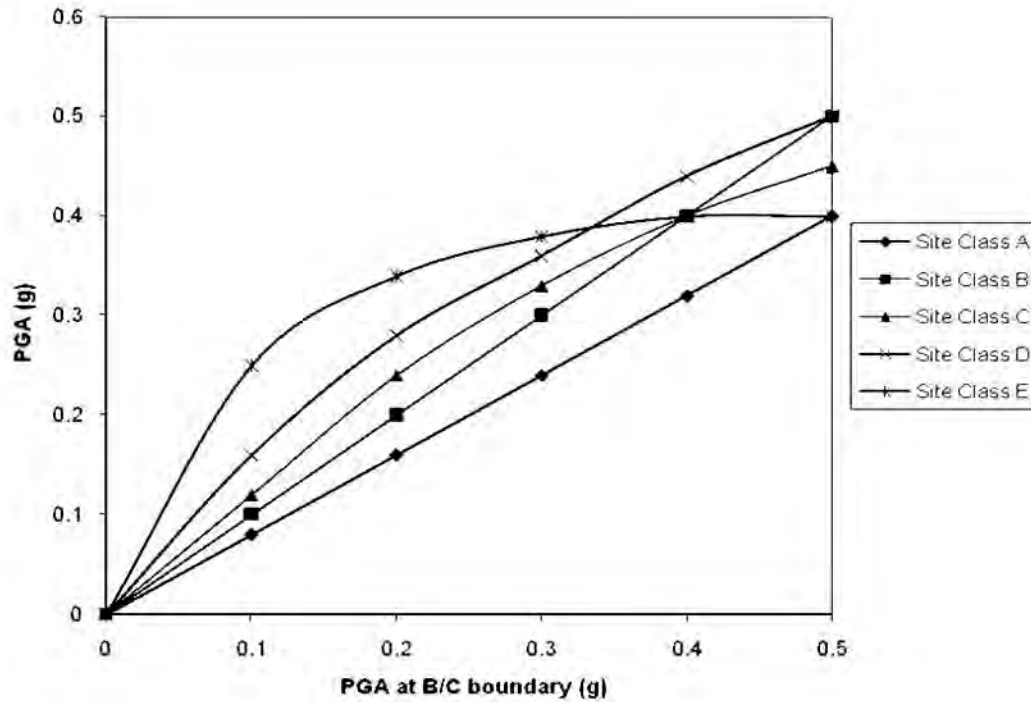


Figure 5-3 PGA Amplification Based Upon NEHRP Site Class

Figure 5-4 shows a site amplification plot developed by Idriss (1990) for soft soil sites. Figure 5-4 includes both field observations of the amplification of the PGA and the results or numerical response analysis using equivalent-linear one-dimensional site response analysis (described subsequently in this chapter). The curve in Figure 5-4 may be considered representative of the PGA response at soft soil sites, including sites classified as special study sites (Site Class F) by AASHTO because of the plasticity index (PI) or thickness of the soft soil layer.

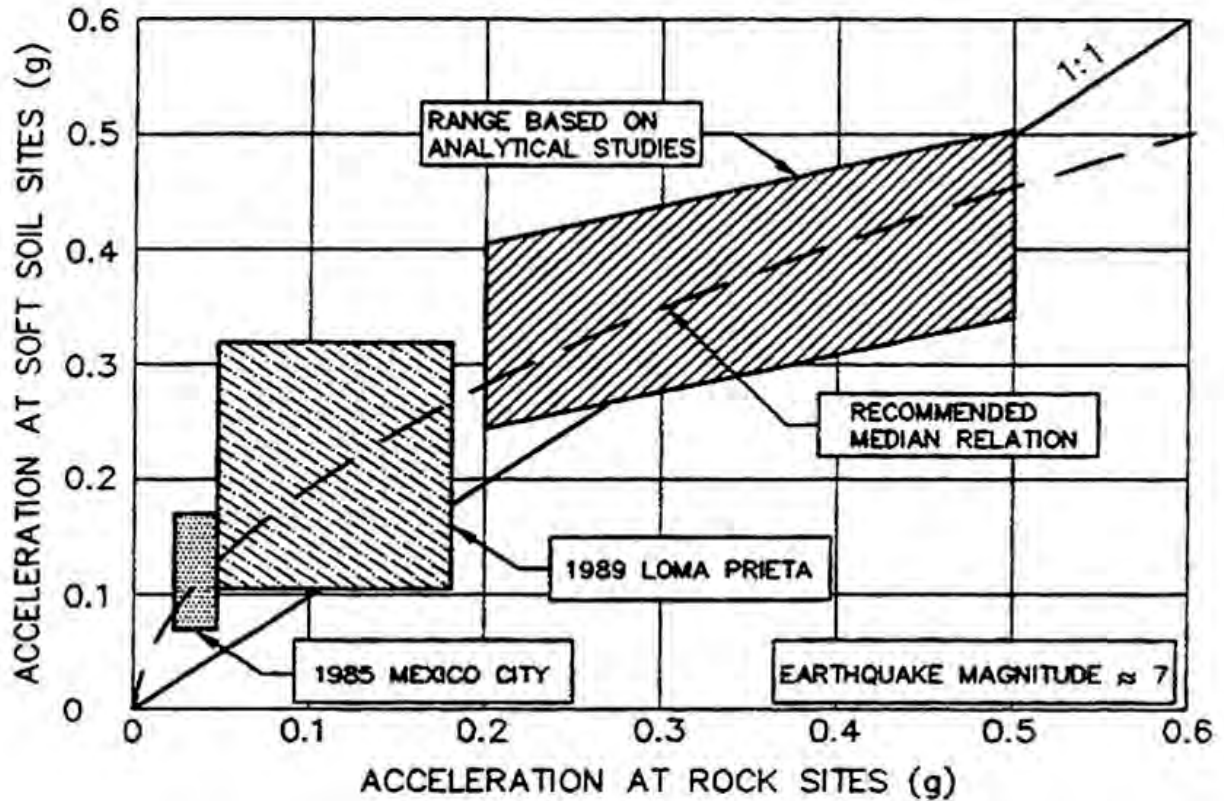


Figure 5-4 Relationship between PHGA on Rock and on Soft Soil Sites (Idriss, 1990)

Figure 5-5 presents a comparison of peak acceleration values recorded at the base (usually bedrock) of several earthen dams and the corresponding transverse peak acceleration recorded at the crest (Harder, 1991). The figure suggests that larger amplification effects may be expected in earthen structures than at free field soft soil sites. Note, however, that Figure 5-5 presents an upper bound curve (as opposed to Figure 5-4, where a mean curve is presented) and only applies to the transverse acceleration of the embankment. For the longitudinal acceleration of embankments (e.g., for end slopes) and for the acceleration of cut slopes, amplification effects may be expected to be significantly smaller than indicated by Figure 5-5.

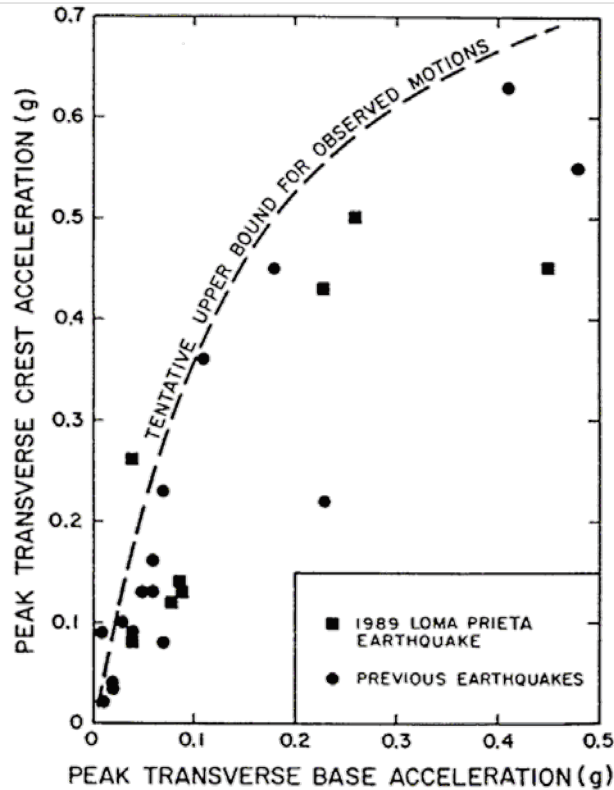


Figure 5-5 Base and Crest Peak Accelerations Recorded at the Earth Dams (Harder, 1991)

The free field amplification curves presented in Figure 5-3 and Figure 5-4 may be used in a simplified three-step site response analysis procedure to account for the influence of local soil conditions on the peak ground acceleration from a conventional seismic hazard analysis (i.e. a seismic hazard analysis for Site Class B ground conditions) for PGA values less than or equal to 0.5. The observational data presented in Figure 5-5 may be used in a fourth step to account for the influence of an embankment on the transverse peak acceleration at the crest of the embankment. The procedure is as follows:

Step 1: *Evaluate the free field bedrock acceleration at the site for NEHRP/AASHTO Site Class B.* Determine the PGA from a conventional seismic hazard analysis for NEHRP/ASHTO Site Class B.

Step 2: *Classify the site according to the NEHRP/AASHTO site classification system.* Using Table 3-5, classify the site on the basis of the average shear wave velocity for the top 100 ft (30 meters) of soil, V_{S30} .

Step 3: *Estimate the free field PGA at the site.* Estimate the potential amplification of the PGA from Step 2 from Figure 5-3 for NEHRP/AASHTO Site Classes C through E or from Figure 5-4 for NEHRP/AASHTO Site Class F (as appropriate).

Step 4: *Estimate the transverse PGA at the top of the embankment.* Estimate the potential amplification of the PGA at the top of the embankment, if an embankment is present, using the free field PGA derived in Step 3 and the earth dam amplification curve in Figure 5-5.

Step 4 in the procedure presented above is based upon the simplified “decoupled” assumption that the peak acceleration at the base of the embankment is the same as the free field peak acceleration, thereby ignoring interaction between the embankment mass and the ground. Analyses of the coupled response of embankments and foundation soils indicates that this simplified, decoupled assumption usually provides a conservative upper bound estimate of the acceleration at the base of the embankment (Bray, et al., 1995). As the amplification curve in Figure 5-5 is already an upper bound curve, the net result of using this four step procedure to estimate embankment response may be an extremely conservative assessment of the PGA at the top of the embankment. However, in general, this simplified approach is intended only to give a rough estimate of amplification effects at a site for screening analyses and preliminary design purposes. The simplified approach is not intended for use in final design of transportation facilities. Even for screening and preliminary analyses, the design engineer should decide if this approach is appropriate for the intended purpose or if it is necessary to perform a more sophisticated analysis.

The peak acceleration at the top of an embankment estimated in Step 4 may also be used in preliminary analyses for various highway ancillary structures, including retaining walls, and for structures constructed on top of embankment fills. This acceleration is not, however, the appropriate peak acceleration for use in seismic stability and deformation analyses for an embankment or bridge abutment or free-standing retaining wall. For these calculations, the *average acceleration* of the assumed failure mass, and not the acceleration at the top of the embankment, should be used. The average acceleration is directly proportional to the seismically-induced inertia forces and thus is the relevant response quantity. The average acceleration is always less than the peak ground acceleration due to spatial averaging. Appropriate reduction factors to apply to the PGA to determine the average acceleration for stability and deformation analyses of slopes and retaining walls are discussed in Chapter 6.

5.3 ONE-DIMENSIONAL SITE RESPONSE ANALYSES

5.3.1 Equivalent Linear One-Dimensional Response Analyses

When an analysis more accurate than the simplified analysis presented above is warranted, a formal seismic site response analysis can be performed. In particular, formal seismic response analyses are required for Site Class F (Special Study soils). Furthermore, as noted previously, sites with significant impedance contrasts within the top 200 ft of the soil profile and sites with thick soil columns (e.g. soil columns in excess of 500 ft) do not conform to the site model used to develop the NEHRP site response factors and thus are suspect in this respect. Therefore, a formal response analysis may be warranted at sites with shallow impedance contrasts and deep soil columns. Formal response analyses may also be warranted on important projects, projects with highly variable ground conditions over the span of a structure or other transportation facility, and for the other design purposes cited in Table 5-1.

Equivalent-linear one-dimensional analysis is by far the most common method used in engineering practice to analyze site-specific seismic response. In an equivalent-linear one-dimensional site response analysis, the soil profile is modeled as a horizontally layered, linear visco-elastic material characterized by the shear modulus and damping ratio. To account for the non-linear, strain-dependent behavior of soil, the equivalent-linear modulus is evaluated from the initial small strain modulus, G_{\max} , and the shear strain dependent modulus reduction curve. The damping ratio is evaluated from the shear strain dependent damping curve. Evaluation of G_{\max} and the shear strain dependent modulus reduction and damping curves were discussed in Chapter 4.

In an equivalent-linear analysis, strain compatible modulus and damping values are evaluated iteratively for each soil layer or sub-layer. An effective shear strain is used to calculate the strain-compatible modulus and damping and the analysis iterates until two successive iterations produce the same effective shear strain in each layer. The effective shear strain level is usually specified as:

$$\gamma_{\text{eff}} = n \gamma_{\text{max}} \quad 5-1$$

where γ_{eff} is the *effective strain*, γ_{max} is maximum value of earthquake-induced shear strain, and n is the *effective strain factor*. Because γ_{eff} is not known prior to the start of the analysis, equivalent-linear response analyses are performed in an iterative manner, using the effective strain from one iteration of the analysis to evaluate the modulus and damping ratio for the next iteration. Initial values are usually

assumed based upon experience (although the small strain modulus and damping can also be used as the initial values). Usually 5 to 10 iterations are sufficient to achieve convergence of modulus, damping, stress and strain values to within a difference of less than one percent between two successive iterations. Originally, the value of the effective strain factor, n , used in equivalent linear analysis to determine the strain compatible equivalent linear modulus and damping was 0.65. However, based upon back analysis of strong motion records obtained at soil sites in earthquakes, the consensus among geotechnical earthquake engineers is that the effective strain factor n should be related to the earthquake magnitude. Equation 5-2 presents the relationship between earthquake moment magnitude, M_w , and n proposed by Idriss and Sun (1992) and commonly used in practice today:

$$n = \frac{(M_w - 1)}{10} \quad 5-2$$

The computer program SHAKE, originally developed by Schnabel, et al. (1972) and updated by Idriss and Sun (1992) as SHAKE91, is perhaps the most commonly used computer program for one-dimensional equivalent-linear seismic site response analysis. This program idealizes the site profile as a horizontally layered soil deposit overlying a uniform visco-elastic half-space, as illustrated in Figure 5-6. SHAKE91 and its derivatives are still reliable platforms for conducting equivalent linear one-dimensional site response analyses. A DOS version of SHAKE91 is available from the National Information Service for Earthquake Engineering (NISEE) at the University of California at Berkeley for a nominal cost. However, the DOS version of SHAKE91 is somewhat cumbersome, requiring a formatted input file and direct input of time histories and newer modulus reduction and damping curves by the user. A variety of different user-friendly WINDOWS versions of SHAKE91 are now available from commercial software vendors. These commercial programs typically have built-in libraries of earthquake time histories and modulus reduction and damping curves and menu-driven input and output capabilities. Furthermore, there are several other computer programs for equivalent-linear one-dimensional seismic site response analysis that are commercially available. Most of these programs are reliable for use in engineering design, as visco-elastic response analysis is a fairly simple type of analysis to implement numerically. However, the user should carefully check the documentation provided with a program to ensure the program's reliability, as even some commercial versions of SHAKE91 are reported to have been modified from the original, validated program.

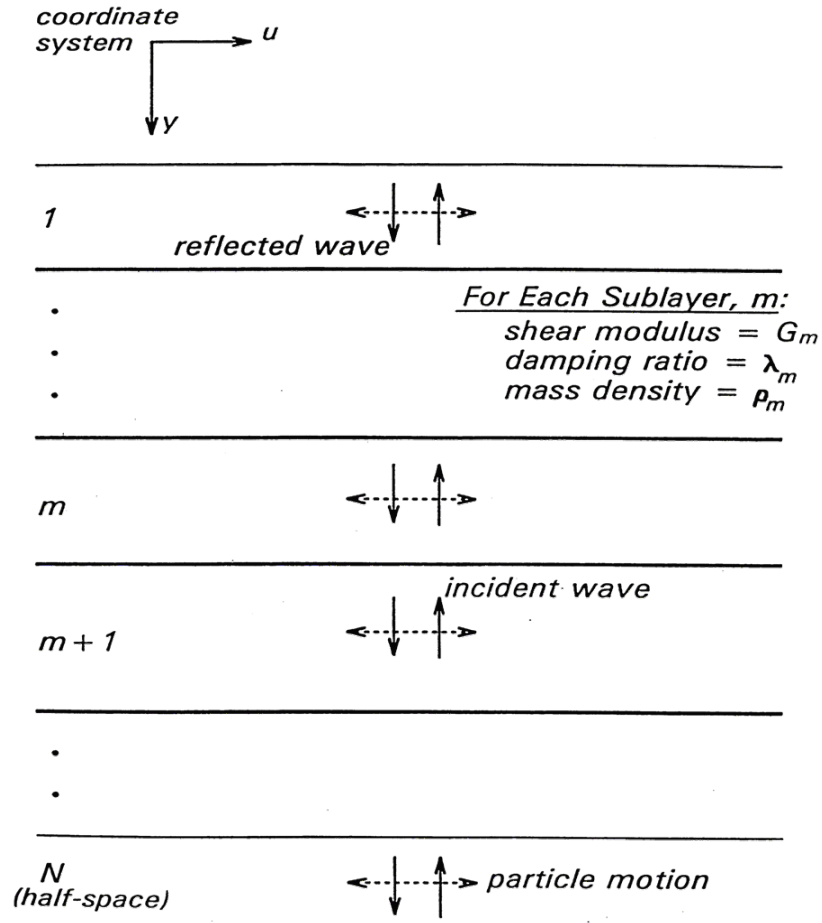


Figure 5-6 1-Dimensional Column for SHAKE Equivalent Linear Seismic Site Response Analysis (Schnabel, et al., 1972)

Basic input to an equivalent-linear seismic site response analysis includes the soil profile, soil parameters for each layer, and the input acceleration time history. Soil parameters used in the analysis include the initial (small strain) shear modulus or shear wave velocity and the total unit weight (or mass density) for each soil layer. Also, the shear strain (and sometimes overburden) dependent shear modulus reduction and damping ratio curves are required for each soil type. Evaluation of representative values for these soil properties is discussed in Chapter 4. As noted in Chapter 4, it is essential to consider the overburden dependence of the modulus reduction and damping curves when the soil profile is greater than 50 to 100 ft thick. Figure 5-7, from Hashash and Park (2001), compares the ground surface acceleration response spectrum obtained using a pressure dependent soil model to the ground surface spectrum obtained using a pressure-independent model for a 3,300 ft (1,000 m) thick soil column (representative of deep soil deposits in the Mississippi embayment). The pressure-independent model (labeled NLPI in the figure)

under-predicts spectral accelerations by a factor of 3 to 8 compared to the pressure dependent model (labeled NLPD in the figure) in the modal period range of 0.1 second to 1 second. The modulus reduction and damping curves provided with early versions of SHAKE and SHAKE 91 may not consider this dependence.

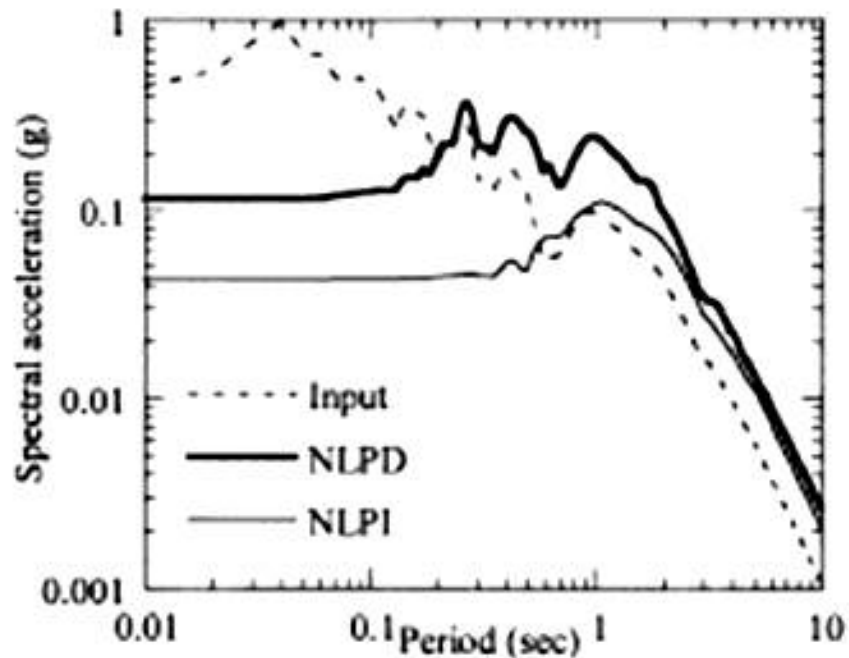


Figure 5-7 Influence of Pressure Dependent Soil Behavior on the Seismic Response of a 3,300 ft (1,000-m) Thick Soil Column in the Mississippi Embayment (Hashash and Park, 2001)

Once the soil profile and material properties have been specified, the principle remaining input to an equivalent-linear response analysis is the input earthquake acceleration time history. Selection of representative acceleration time histories for the input ground motion is discussed in Chapter 3. The acceleration-time history may be input as either the motion at a hypothetical *bedrock outcrop* at the site (the most commonly used option because it is congruent with assumptions embedded in attenuation relationships) or as a *within profile* motion (i.e. a ground motion within the soil profile) at the bedrock-soil interface at the base of the soil column (in general, not recommended and only used if a rigid, non-compliant base is used in the analysis). Results of the analysis provide shear stress-, shear strain-, and acceleration-time histories for the ground surface and for each layer within the soil profile. Most

programs will also provide response spectra and peak motions at the surface and at designated depths along with values for the strain compatible modulus in each soil layer.

While it is relatively easy to set up and perform an equivalent-linear site response analysis, the results of the analysis may be extremely sensitive to the details of the input. Factors such as the thickness and number of sub-layers, selection of appropriate input motions, the digitization interval of the input time history, the "cut-off" frequency (the highest frequency used in the Fourier transformation of the input motion), the shear wave velocity and unit weight of the underlying bedrock "half-space", and whether the input motion is specified as a within profile motion or a bedrock outcrop motion can significantly affect program output. Program documentation usually provides recommendations for these parameters. However, if the design engineer is not familiar with the program or method of analysis, or if the guidance on these parameters is vague or uncertain, a sensitivity analysis and/or a benchmark study may be warranted. Furthermore, it is recommended that all formal seismic response analyses should be reviewed by a qualified geotechnical specialist familiar with the program being used and the problem being analyzed and experienced in seismic site response analysis.

Figure 5-8 illustrates the application of equivalent-linear one-dimensional analysis to predict the seismic response of a site in Columbia, South Carolina, with a shallow impedance contrast (Martin, et al., 2008). The shear wave velocity profile used in the site response analysis, shown on the left-hand side of the figure, has a relatively abrupt change in shear wave velocity at a depth of about 120 ft (36 m). Assuming the increase in unit weight from above to below the abrupt change in shear wave velocity is on the order of 10 percent, the impedance is more than double below the shear wave velocity contrast compared to above the contrast. The site class adjusted PGA from a conventional seismic hazard analysis for NEHRP Site Class C was 0.31 g. The right hand side of Figure 5-8 compares the results of equivalent linear site response analysis using a suite of 5 representative time histories to the design spectrum from for Site Class C developed in accordance with the AASHTO provisions. The formal site response analysis shows significantly higher amplifications in the period range from 0.1 to 0.5 seconds compared to the NEHRP spectrum. Use of the AASHTO truncated (three-point) spectra at this site to design a structure with a resonant period in the short period range (i.e. 0.1 to 0.5 second) could lead to significant underestimation of the seismic loads.

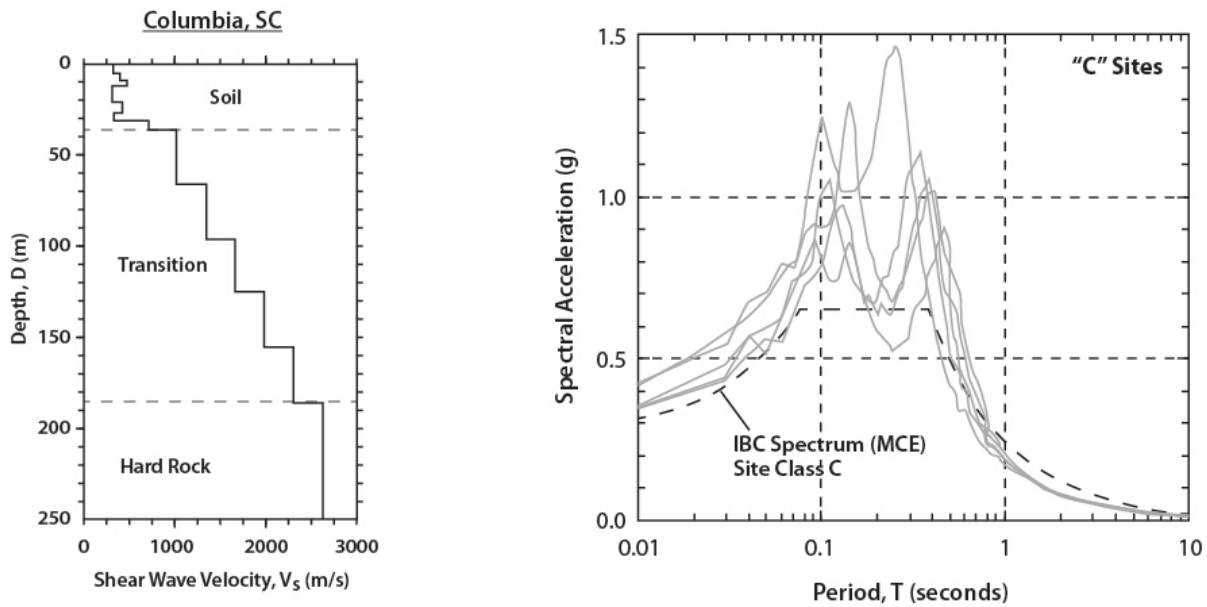


Figure 5-8 Equivalent Linear Response Analysis for a Shallow Impedance Contrast Site in Columbia, South Carolina (Martin, et al., 2008)

5.3.2 Advanced One-Dimensional Site Response Analysis

Advanced one-dimensional seismic site response analyses refer to truly non-linear response analyses that follow the actual hysteretic stress-strain behavior of the soil (rather than simply using a strain-dependent equivalent linear modulus and damping). Some of the advanced one-dimensional models site response are effective stress analyses that also have the capability of calculating pore pressure generation in the saturated soil layers due to cyclic loading and of accounting for the effect of the pore pressure generation (and dissipation) on site response. Advanced one-dimensional models must be time-domain models, i.e. they must divide the earthquake time history up into small time steps and sequentially calculate the response of the soil deposit to each time step, in order to capture non-linear soil behavior. These advanced site response models are generally much more computationally intensive than equivalent-linear models. (Equivalent-linear models can calculate soil response using a computationally efficient frequency domain analysis because, since the soil behavior is linear, the principle of superposition can be used). If pore pressure generation is modeled, the analysis may be particularly computationally intensive.

The primary difference between non-linear and equivalent-linear site response analyses is that non-linear analyses use a more realistic model to represent the behavior of soil subjected to cyclic loads. Essentially, a non-linear model traces the evolution of the hysteresis loops generated in a soil by cyclic loading in a sequential manner, whereas the equivalent-linear model only approximates soil response using representative soil stiffness and damping over the entire sequence of cyclic loads. The more realistic representation of the non-linear behavior of cyclically-loaded soils gives non-linear analyses a significant advantage over equivalent-linear seismic response analyses at higher levels of seismic shaking where non-linear effects tend to dominate.

Non-linear soil models generally describe soil behavior in terms of a backbone curve that describes stress-strain response during initial loading and a set of rules for how the soil behaves during unloading and reloading subsequent to initial loading. The backbone curve is the curve that describes the tips of the hysteresis loops developed in uniform cyclic loading. The backbone curve is usually described by some type of hyperbolic function and is easily related to the small strain modulus, G_{max} , and modulus reduction curve from the equivalent-linear model. Figure 5-9 illustrates how a typical non-linear soil model captures stress-strain behavior during non-uniform cyclic loading.

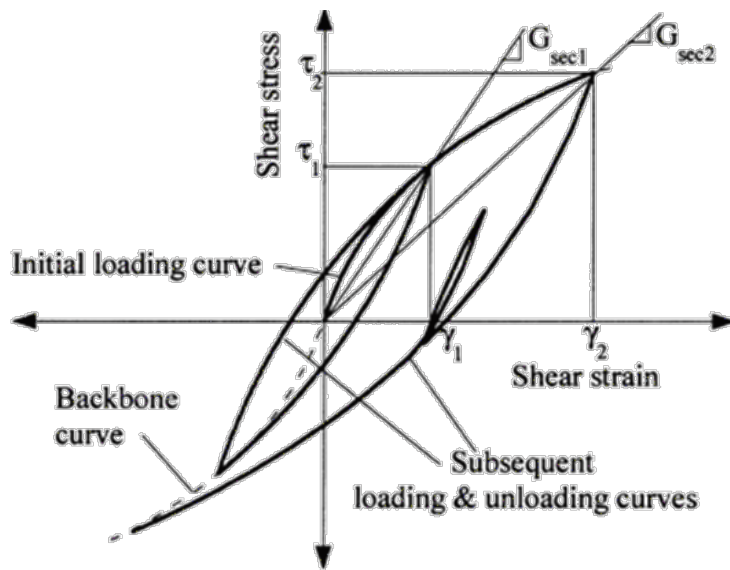


Figure 5-9 Non-Linear Soil Model for Time-Domain Site Response Analysis (Hashash and Park, 2001)

Perhaps the most common assumption with respect to unload-reload behavior is the Masing criterion. The Masing criterion says the soil stiffness during unloading and reloading is twice the stiffness of the soil during initial loading. However, the Masing criterion produces a damping curve that does not correspond in shape to a damping curve developed from uniform cyclic loading, i.e. to the equivalent linear damping curve. Therefore, many non-linear models use some sort of modified unload-reload rules that allow the damping from the non-linear model to correspond closer to the damping observed in uniform cyclic laboratory testing, i.e. to equivalent linear damping. Modified damping rules used in practice include the extended Masing criterion (Vucetic, 1990) and the Cundall-Pyke hypothesis (Pyke, 1979, 2000).

Even with modified damping rules, many non-linear soil models consistently under-predict the damping at small strains. In fact, models that use the Masing or extended Masing criterion predict essentially zero damping at small strains. Therefore, these models often add a viscous damping to the hysteretic damping predicted by the soil model. The viscous damping may be either a constant, frequency independent value or a frequency (or rate) dependent damping known as Rayleigh damping. There are simplified, full, and extended Rayleigh damping schemes used in practice. Guidelines for evaluating Rayleigh damping basically suggest matching it at the fundamental frequency of the soil layer (for simplified Rayleigh damping) or at several frequencies that are integer multiples of the fundamental frequency (for extended Rayleigh damping). A constant viscous damping value equal to the small strain damping either measured in laboratory tests or predicted by correlation for the equivalent linear damping (Kwok et al., 2006) has also been used in non-linear analysis. In this manner, close agreement with the damping measured in laboratory tests is maintained.

Equivalent-linear site response analyses are often sufficient for most geotechnical earthquake engineering problems that require a site-specific response analysis. However, when the peak ground accelerations are high enough to induce yielding (shear failure) in the soil profile, a non-linear site response analysis may be warranted. The PGA amplification curve in Figure 5-3, based upon the AASHTO site factors, suggests that non-linear site response effects will begin to accumulate at sites classified for Site Class E when the PGA for the Site Class B reference condition exceeds about 0.3 g. This is consistent with suggestions that equivalent linear analyses may be reliable up to PGA values of 0.4 to 0.5 g (see Ishihara, 1986) or earthquake-induced shear strains of up to 2 percent. A non-linear one-dimensional seismic site response analysis may also be warranted if the project is considered important or critical (e.g., a "lifeline" structure) or an analysis more accurate than a one-dimensional equivalent-linear site response analysis is

desired. Furthermore, non-linear analyses are generally required if the influence of pore pressure generation on site response is to be taken into account.

Non-linear soil models described in the literature and used in practice include DESRA-2 (Lee and Finn, 1978), MARDES (Martin, 1975), SUMDES (Li, et al., 1992), D-MOD (Matasovic and Vucetic, 1993), TESS (Pyke, 2000), DEEPSOIL (Park and Hashash, 2004), D-MOD_2 (Matasovic, 2006), and a ground response module in the OpenSees simulation platform (www.opensees.berkeley.edu). Several of these programs have user-friendly input routines that will determine the non-linear parameters that give the best fit to specified equivalent-linear modulus reduction and damping curves. Despite this apparent simplicity, in general non-linear site response models are significantly more complicated to use than equivalent linear models. Issues associated with the use of non-linear site response models are discussed in detail by Kwok, et al. (2006). In general, analyses conducted using non-linear soil models should always be validated by comparison to the results of equivalent linear models for both low intensity and high intensity input motions. For low intensity motions the two types of models should give similar results. For high intensity motions, the difference in the response predicted by the two models should be viewed with respect to anticipated differences between equivalent-linear and non-linear models, e.g. a progressive softening of the soil stiffness and lengthening of the predominant period of the site as the shaking intensifies. Furthermore, non-linear site response analyses should always be subject to independent peer review by someone experienced with the use of the model.

5.3.3 Analyses Including Pore Pressure Generation

The AASHTO bridge design guide specifications explicitly allow for a reduction in spectral accelerations of up to 33% based upon a site specific analysis. Models for computing the reduction in the intensity of ground shaking due to pore pressure generation and the consequent softening of soil stiffness have been available to researchers for over 15 years. Engineers have been slow to employ these models in practice due to the complexity of the computer programs that implement the models and the reluctance of regulatory officials to accept these analyses. However, several of the commercially available user friendly programs for non-linear site response now have the ability to account for pore pressure generation, putting this type of analysis within the reach of practicing engineers. Furthermore, as noted above, the AASHTO seismic provisions now allow for up to a 33% reduction in spectral accelerations based upon this type of analysis (putting prudent limits on the allowable reduction in shaking intensity

due to numerical modeling of pore pressure generation), making the idea of this type of analysis an attractive option in some cases

Figure 5-10, from Matasovic (1993), compares the response spectrum from a total stress analysis to two different effective stress site analyses with pore pressure generation; one with pore pressure redistribution and dissipation and another without pore pressure redistribution and dissipation. Both effective stress analyses show a significant reduction in peak acceleration and in spectral accelerations at periods of less than 1 second. However, the pore pressure generation analysis that includes pore pressure redistribution and dissipation shows significantly greater spectral accelerations at spectral periods greater than 0.2 second compared to the analysis without pore pressure redistribution and dissipation. Figure 5-10 highlights both the potential benefits of accounting for pore pressure generation as well as one of the complexities of this type of analysis, suggesting that it is essential to consider pore pressure redistribution and dissipation as well as generation in this type of analysis.

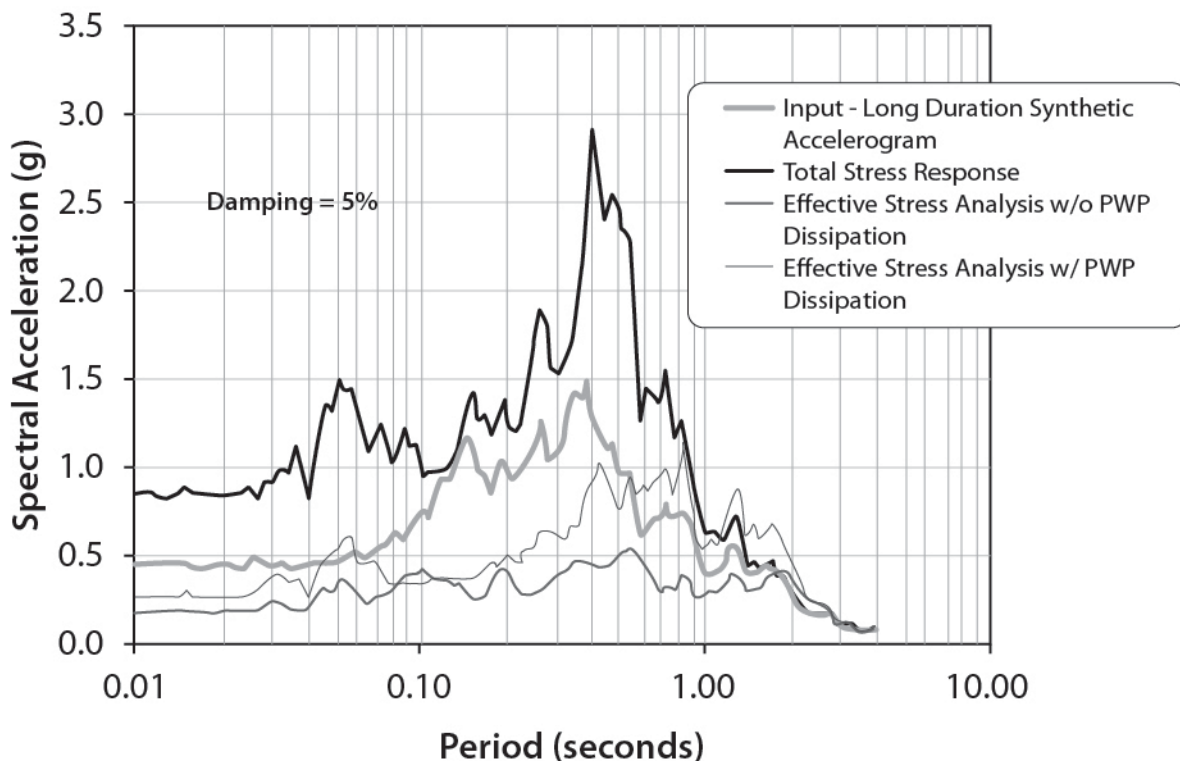


Figure 5-10 Comparison of Total Stress Site Response Analysis to Effective Stress Site Response Analyses with Pore Pressure Softening (after Matasovic, 1993)

As noted for non-linear site response analyses in general, analyses that include pore pressure generation should always be subject to independent peer review by someone experienced with the use of the model.

5.4 TWO- AND THREE-DIMENSIONAL SEISMIC SITE RESPONSE ANALYSIS

Occasionally, when the engineer wishes to analyze the influence of irregular geometry in the stratigraphic profile or irregular project geometry and for major projects of great importance, a two-dimensional site response analysis may be warranted. Three-dimensional site response analyses are rarely employed in transportation engineering practice, except as axi-symmetric analyses (even though some commercial programs boast of a three-dimensional dynamic capability). The most common type of two-dimensional seismic site response analysis conducted in practice is a quasi-two-dimensional analysis that employs multiple one-dimensional columns in a two-dimensional cross section. The quasi-two-dimensional site response is modeled by analyzing each column using one-dimensional analysis, most commonly with an equivalent-linear model. Figure 5-11 compares the results of equivalent-linear one-dimensional site response analyses of vertical columns through a two-dimensional cross section, expressed in terms of the maximum earthquake-induced shear stress versus depth, to the results of a two-dimensional equivalent-linear analysis. The results from the one-dimensional analysis are generally within 5 to 10 percent of results of the two-dimensional analysis, which provides sufficient accuracy for almost all engineering applications considering other uncertainties associated with the analysis.

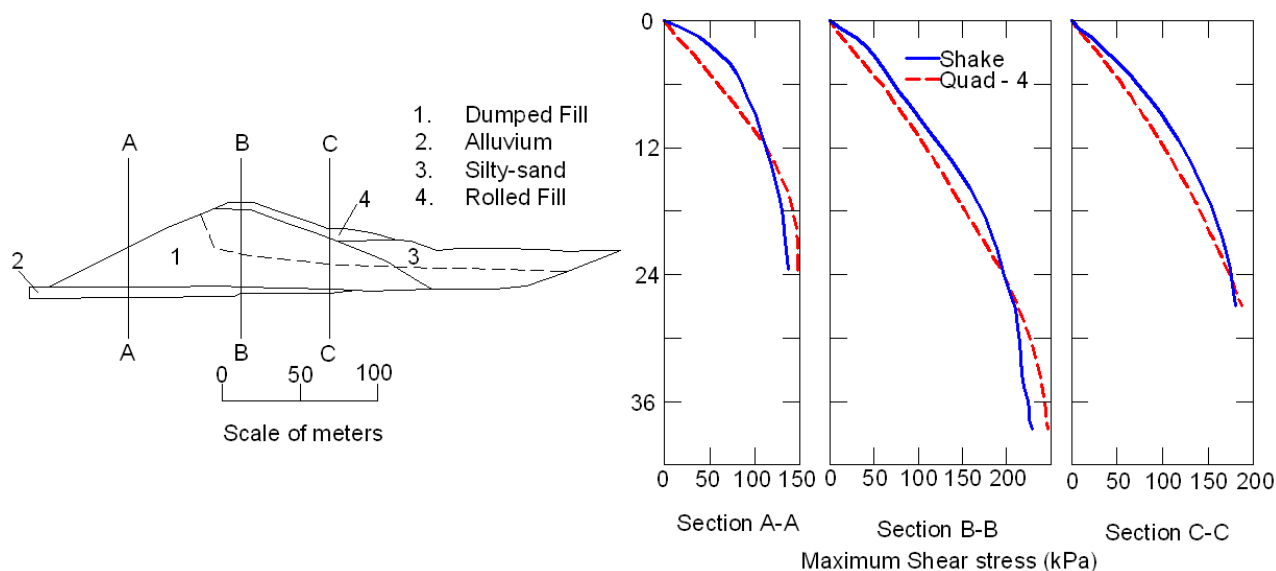


Figure 5-11 Quasi Two-Dimensional Site Response Analysis Using One-Dimensional Columns (Vrymoed and Calzascia 1978)

If a more sophisticated two-dimensional site response analysis is desired or warranted, or a soil-structure interaction analysis is to be conducted, a variety of finite element and finite difference computer programs for two-dimensional seismic site response and soil-structure interaction analysis are available. The computer program QUAD4, originally developed by Idriss and his co-workers (Idriss, et. al., 1973), updated as QUAD4M by Hudson, et. al. (1994) is among the most commonly used computer programs for two-dimensional site response analysis. One reason for the popularity of QUAD4M is that it uses the equivalent-linear soil model employed in the equivalent-linear one-dimensional site response analyses described in previous sections of this chapter. Therefore, it is relatively easy to establish appropriate input parameters for soil layers and to validate the soil model by comparison of results from QUAD4M to equivalent-linear one-dimensional analyses. Basic input to QUAD4M includes the two-dimensional soil profile, equivalent-linear soil properties, and the acceleration time history of horizontal ground motion. QUAD4M solves the equations of motion in the time domain and therefore employs a modified form of Rayleigh damping. The QUAD4M damping model requires that the equivalent-linear damping be matched to the Rayleigh damping at two frequencies specified by the user. These frequencies are generally the fundamental period of the soil layer or earth structure and four times the fundamental period. A time history of vertical ground motion may also be applied at the base of the soil profile. The base can be modeled as a rigid boundary, with design motions input directly at the base as a *within profile* motion, or as a *transmitting boundary* which enables application of ground motions as hypothetical *rock outcrop* motions. However, QUAD4M does not have structural elements and thus is not suitable for soil-structure interaction analysis.

Multi-purpose computer programs like PLAXIS (www.plaxis.com) and FLAC (www.itascacg.com) are becoming increasingly popular with practicing geotechnical engineers for all types of analysis, including seismic response and soil-structure interaction analyses. These are powerful programs with multiple features, including structural elements, energy absorbing boundaries, and sophisticated soil models that may include pore pressure generation. These programs should only be used in design by experienced professional. Furthermore, problem-specific benchmark studies (comparing program results to established solutions for problems that employ the same program features that will be used in the actual analysis) and peer review are essential when using these programs.

5.5 SUMMARY

This chapter describes the use of seismic response analysis to evaluate the effect of local site conditions on earthquake ground motions. Five different levels of site response analysis are described:

- Simplified site response analysis
- One-dimensional equivalent linear site response analysis
- One-dimensional non-linear site response analysis
- One-dimensional non-linear site response analysis with pore pressure generation and dissipation
- Two-dimensional site response analysis

Simplified site response analysis use charts based upon empirical observations of earthquake ground motions and the results of one-dimensional site response analysis to relate the ground motion at weak rock sites (i.e. AASHTO Site Class B) to the ground motion at the ground surface of the site as a function of the AASHTO site class. These analyses include the AASHTO procedure for adjusting the PGA and spectral accelerations at 0.2 and 1 second and simple charts for the adjusting just the PGA. The simple charts should only be used for screening analyses and preliminary design. Charts are also available for evaluating the amplification of the free field PGA by an embankment.

Equivalent-linear one-dimensional analyses are the most common type of site-specific seismic response analysis used in engineering practice. These analyses are required to develop design ground motions for AASHTO Site Class F (special study sites) and are recommended for sites with significant impedance contrasts within 200 feet of the ground surface and for deep soil sites (basins with soil deposits greater than 500 ft in depth). They may also be warranted for major projects and important structures and for the design purposes presented in Table 5-1. It is imperative to consider the pressure-dependence of the modulus reduction and damping curves for analyses of soil columns greater than 100 ft in thickness. One-dimensional non-linear site response analysis are only necessary for sites where the reference site PGA exceeds 0.3 g or the cyclic shear strain in the soil exceeds 2 percent or if the engineer wants to take into account the influence of pore pressure generation on site response. Non-linear analyses that account for pore pressure generation and dissipation can be used to justify reductions in spectral accelerations of up to 33%. The most common type of two-dimensional site response analysis used in practice employs one-dimensional analysis of multiple columns to represent the two-dimensional response. Formal two-dimensional site response analysis is generally only required for soil-structure interaction analysis.

In addition to evaluating the influence of local soil conditions on the design ground motions discussed in Chapter 3 of this report (e.g. on the acceleration response spectra and representative time histories), site response analyses are employed in a variety of the other analyses described in this report. Site response analyses may also be used to evaluate the seismic coefficient for stability and deformation analysis of slopes and embankments (Chapters 6 and 9) and retaining wall structures (Chapter 12), and the earthquake induced shear stress for liquefaction analysis (Chapter 6). Time histories from seismic response analyses may also be used in the formal Newmark seismic deformation analyses (Chapter 6) and to evaluate kinematic interaction in soil structure interaction analyses (Chapters 8 and 11). Other uses of seismic response analyses include evaluation of the representative free field soil modulus for evaluation of the dynamic stiffness coefficients for shallow foundations (Chapter 10) and the free field differential soil displacement for analysis of the racking/ovaling displacement induced by seismic loading on underground structures (Chapter 13).

CHAPTER 6

GEOTECHNICAL HAZARDS

6.1 GENERAL

This chapter describes geotechnical seismic hazards related to slope stability, liquefaction, ground settlement and fault rupture. There are numerous documented case histories of slope instability, liquefaction, settlement, and fault rupture generated by earthquake ground motions. Earthquake induced slope stability and bearing failures may damage bridge foundations or superstructures, block highways, or rupture pipelines or culverts. Earthquake induced liquefaction has been a major source of damage to bridge structures and non-bridge transportation facilities in past earthquakes. Fault rupture has also been a source of significant damage to transportation facilities in earthquakes.

Section 6.2 of this chapter describes methods that can be used to assess seismically-induced slope stability. Section 6.3 discusses procedures to determine the potential for triggering liquefaction, including screening procedures to assess the need for such evaluations in regions of low seismicity. Section 6.4 discusses methods to evaluate flow failure potential and lateral spreading displacements due to liquefaction. Analysis methods for post liquefaction settlement of cohesionless soils and for settlement of unsaturated cohesionless soils are discussed in Section 6.5. Section 6.6 reviews fault types and their associated rupture characteristics.

The methods of analysis presented in this chapter can be used to evaluate potential geotechnical hazards that may impact seismic performance of transportation facilities. The methods of analysis presented in this chapter are also subsequently employed in Chapter 7 for geotechnical design of earthwork features associated with transportation systems.

6.2 SEISMIC SLOPE INSTABILITY HAZARD

6.2.1 Modes of Slope Instability

Common modes of instability for soil slopes include rotational (circular) failure surfaces and sliding block (planar) failure surfaces. In a seismic analysis, all possible circular and sliding block failure mechanisms must be evaluated to find the critical failure surface, i.e. the failure surface with the lowest seismic capacity to demand (C/D) ratio or cumulative seismic displacement. However, an experienced geotechnical specialist can usually identify a limited number of failure mechanisms that need to be evaluated in the stability analysis. In general, circular failure surfaces will govern stability in a homogeneous material while sliding block failure modes also need to be evaluated in soil profiles with thin, weak layers or for relatively thin soil layers underlain by rock or much stronger soil layers.

Two important complicating factors when evaluating seismic stability are:

- The critical failure surface with respect to static stability (i.e. the potential failure surface with the lowest C/D ratio, or factor of safety, for static loading) is not necessarily the potential failure surface with the lowest yield acceleration (i.e. with the lowest seismic coefficient that yields a C/D ratio of 1.0) for seismic stability: this is particularly true for sliding block failure mechanisms.
- Due to the dependence of the seismic load on the height of the slope, the potential failure surface with the lowest yield acceleration is not necessarily the critical surface for seismic slope stability. The critical surface for seismic slope stability, i.e. the potential failure surface with the lowest C/D ratio or the largest cumulative seismic deformation, may have to be evaluated by analyzing a variety of different failure mechanisms to account for this factor.

Earthquake-induced ground accelerations can result in significant inertial forces in slopes or embankments and these forces may lead to instability or permanent deformation. Current practice for the analysis of the performance of slopes and embankments during earthquake loading is to use one of two related methods:

- 1) Limit Equilibrium using a pseudo-static representation of the seismic forces. In this approach induced seismic loads are modeled as a static horizontal force in conventional limit equilibrium analysis to either determine that the capacity is greater than the demand or to evaluate the

capacity/demand (C/D) ratio (or factor of safety) for comparison to an acceptable value. The seismic load is defined by a seismic coefficient, k , that is determined on the basis of the peak ground acceleration, the geometry of the mass of soil being loaded, and a performance criterion (i.e. the allowable displacement)

- 2) Displacement-Based Analysis using either the Newmark sliding block concept shown schematically in Figure 6-1 or more rigorous numerical modeling methods. As shown in Figure 6-1, when the average acceleration of a potential failure mass exceeds its yield acceleration (that is, when the acceleration exceeds the acceleration at which the C/D ratio in a limit equilibrium analysis is equal to 1.0), deformations accumulate leading to permanent ground displacement.

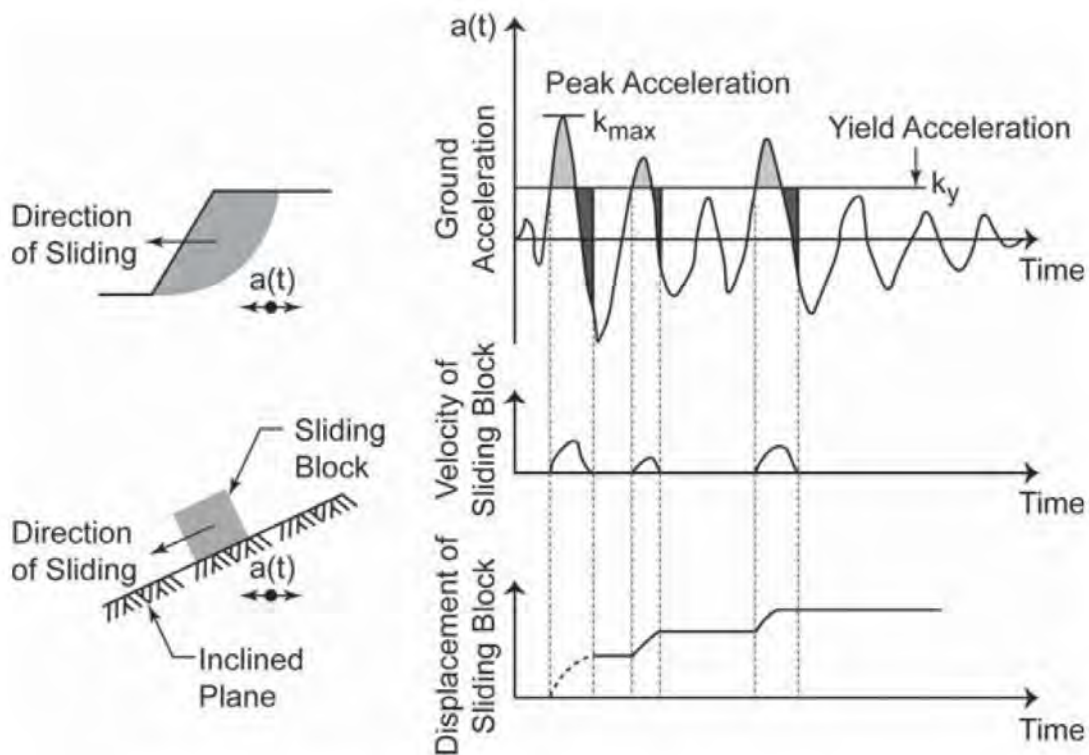


Figure 6-1 Newmark Sliding Block Concept for Slopes

The use of these methods for seismic slope design has been widely adopted both in the United States and in international practice. For example, these methods have been described in detail in the 1998 FHWA Geotechnical Earthquake Engineering Reference Manual (FHWA, 1998) and in a Southern California

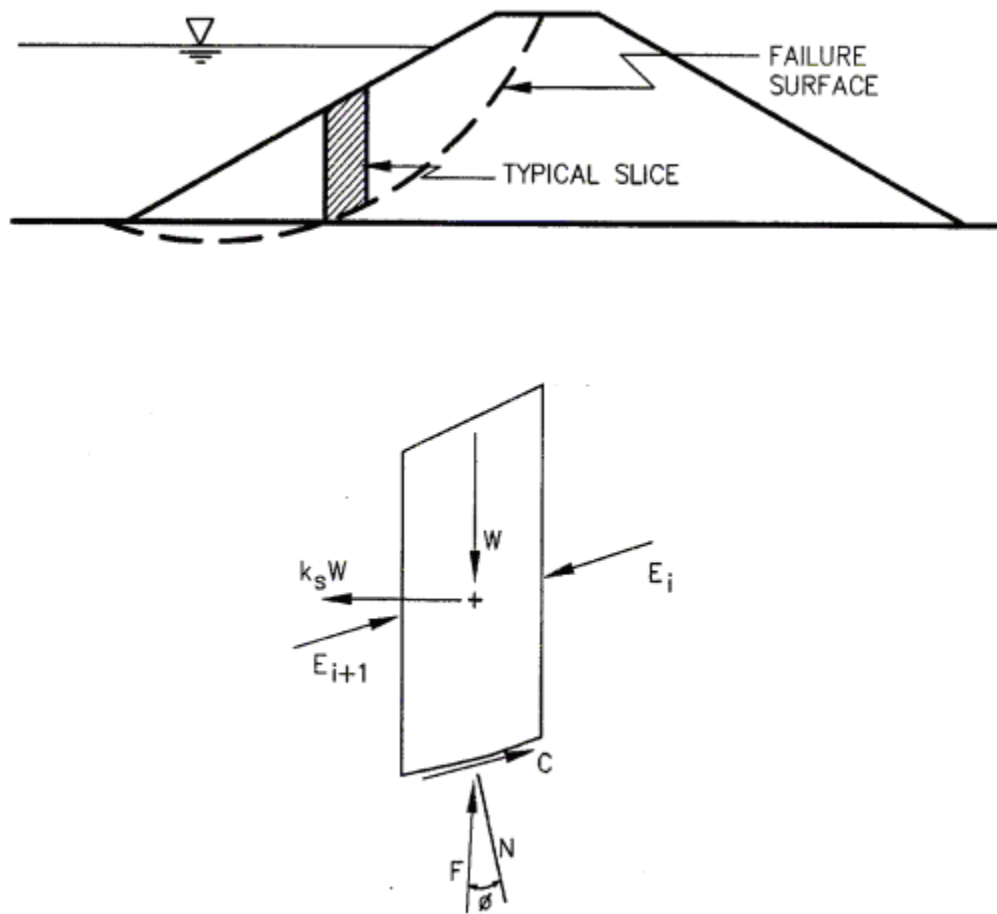


Figure 6-2 Pseudo-Static Limit Equilibrium Analysis

The reason the seismic coefficient can be less than the peak average acceleration within the potential failure mass is as follows: Earthquakes produce ground motions that in turn induce inertia forces of an alternating nature in slopes or embankments. The alternating inertia forces are of short duration and change direction many times. Therefore, even though the C/D ratio during a cycle of earthquake loading may fall below one, it will usually remain below one for only a very brief period of time, until the load reverses, as shown in Figure 6-1. During the interval when the C/D ratio is below one, permanent displacement will accumulate. However, only limited displacements will occur during any one interval because of its short duration. Therefore, even though the seismic coefficient is less than the peak average acceleration of the failure mass, the cumulative deformation that occurs over the entire earthquake will be small provided yield acceleration of the failure mass is not exceeded too many times, i.e. provided that the seismic coefficient and C/D ratio are selected appropriately. This concept not only provides a basis for

selection of an appropriate seismic coefficient but also forms the basis of the displacement based analysis approach discussed in Section 6.2.3.

A wide variety of commercially available computer programs are available that can perform the pseudo-static limit equilibrium analyses employed in the seismic coefficient method. Most of these programs provide general solutions to slope stability problems with provisions for using the modified Bishop, simplified Janbu, and/or Spencer's method of slices. Potential sliding surfaces, both circular and polygonal, can usually be pre-specified or randomly generated. Commonly used limit equilibrium slope stability programs include PCSTABL (developed at Purdue University), UTEXAS4 (developed at the University of Texas at Austin), SLOPE/W (distributed by Geo-Slope International), and SLIDE (RocScience).

An important consideration in employing the limit equilibrium approach to seismic slope stability analysis is that the rate of loading during the earthquake is relatively fast. For this reason, in most cases undrained total stress strength parameters should be used in the seismic stability model if the soil is saturated, rather than drained or effective stress parameters. The undrained total stress parameters may be obtained from static strength tests conducted in the laboratory, from in situ strength testing, or from empirical relationships.

Although the rate effects associated with earthquake loading may result in an undrained strength higher than the static undrained strength during the first cycle of loading, various studies have shown that in a saturated cohesive soil after 10 to 15 cycles of significant loading, as might occur during a seismic event, degradation of the undrained strength may occur. In consideration of the potential for strength degradation during seismic loading, the static undrained strength is generally considered to be an upper bound on the undrained strength that should be used in a seismic stability analysis. For saturated cohesive soils of low to intermediate sensitivity, the static strength may be reduced by 10-15% to account for cyclic degradation in large magnitude earthquakes ($M > 7$) to account for the potential for strength degradation. Where questionable greater potential for strength degradation is suspected (e.g. in soils of high sensitivity), cyclic loading tests can be conducted in the laboratory to obtain a more precise definition of the potential for strength degradation during cyclic loading.

As previously discussed, in the limit equilibrium approach a seismic coefficient is used to determine the horizontal inertial forces used to represent the forces imposed by the earthquake upon the potential failure mass. The vertical acceleration is normally set equal to zero based on studies which have shown that

vertical accelerations have a minor effect on a limit equilibrium seismic stability evaluation. The seismic coefficient used in the analysis is based on the peak average acceleration of the failure mass which, in turn, is based upon the site-adjusted PGA adjusted for spatial incoherence (wave scattering) effects, as discussed below.

The peak average acceleration of a potential failure mass is the theoretical peak value of the seismic coefficient for use in a limit equilibrium stability assessment. A slope with a C/D ratio greater than 1.0 when subject to this peak seismic coefficient is unconditionally stable (assuming the peak seismic coefficient and soil shear strength have been determined appropriately). However, as discussed subsequently, unconditional seismic stability is not required for most soil slopes. Most soil slopes can accommodate at least a small amount of permanent seismic deformation without threatening life safety or adjacent facilities. Under these circumstances, a seismic coefficient less than the peak seismic coefficient may be used to evaluate seismic performance of a slope.

The peak seismic coefficient for use in pseudo-static slope stability analyses can be determined by addressing two different factors. The first factor is the maximum acceleration at the ground surface beneath a fill slope or at the base of a natural slope, i.e. the site-adjusted PGA. As described in the NCHRP 12-70 Report (NCHRP 2008) and discussed in Chapter 3, the site-adjusted PGA may be estimated as the PGA for reference site conditions from the seismic hazard analysis times the appropriate site factor, F_{pga} (Table 3-6). As the peak average acceleration of the failure mass is at most equal to the site-adjusted PGA, the site-adjusted PGA is the maximum possible value of the seismic coefficient, k_{max} . Therefore, k_{max} is given by the expression:

$$k_{max} = F_{pga} \cdot PGA \quad 6-1$$

where the PGA is the USGS mapped acceleration coefficient for site class B conditions, and F_{pga} is the AASHTO peak ground acceleration site factor. However, as discussed in NCHRP Report 611 (NCHRP, 2008), the peak average acceleration of a sliding mass encompassing the full height of the slope will be less than the site-adjusted PGA (i.e less than k_{max}) due to ground motion incoherence (or wave scattering) arising from wave propagation effects. Studies conducted in preparation of NCHRP Report 611 (i.e. during the NCHRP 12-70 project) led to development of a height dependent reduction in k_{max} to get the peak average acceleration, k_{av} . This adjustment is given by the expression:

$$k_{av} = \alpha \cdot k_{max} \quad 6-2$$

where α = a slope height reduction factor and k_{av} is the average peak acceleration in the potential failure mass, taking into account spatial incoherence (or wave scattering).

The following relationship is presented in NCHRP Report 611 for the value of α for slopes and embankments of up to 100 ft in height founded upon Site Class C, D, and E soil conditions:

$$\alpha = 1 + 0.01 \cdot H \cdot (0.5 \cdot \beta - 1) \quad 6-3$$

where H = slope height (feet) and β is a function of the shape of the acceleration response spectrum and is given by:

$$\beta = F_v \cdot S_1 / k_{max} \quad 6-4$$

where F_v = AASHTO site factor for the spectral acceleration at 1 second and S_1 = the spectral acceleration at 1 second for Site Class B.

For Site Classes A and B (hard and soft rock foundation soils) the value of α from Equation 6-3 is increased by a factor of 1.2.

Figure 6-3 shows Equation 6-3 in graphical form. The curved lines in Figure 6-3 are fit to the data points developed using numerical analysis while the straight lines in the figure are engineering approximations represented by Equation 6-3. Note that the engineering approximations for α remain constant after a height of 100 ft. While a smaller value of α may be appropriate for slope heights greater than 100 ft, special studies are recommended to justify the use of smaller values of α than the value for $H = 100$ ft.. Similar height adjustment factors are recommended for evaluating the seismic coefficient for design of retaining walls, as discussed in Chapter 11.

Values of β less than 1.0 in Equation 6-3 and in Figure 6-3 would be typically associated with seismic conditions in the eastern United States, firm ground conditions, and lower acceleration levels, while values of β greater than 1.0 would be associated with the Western U.S., higher accelerations, and Site Class C or D site conditions.

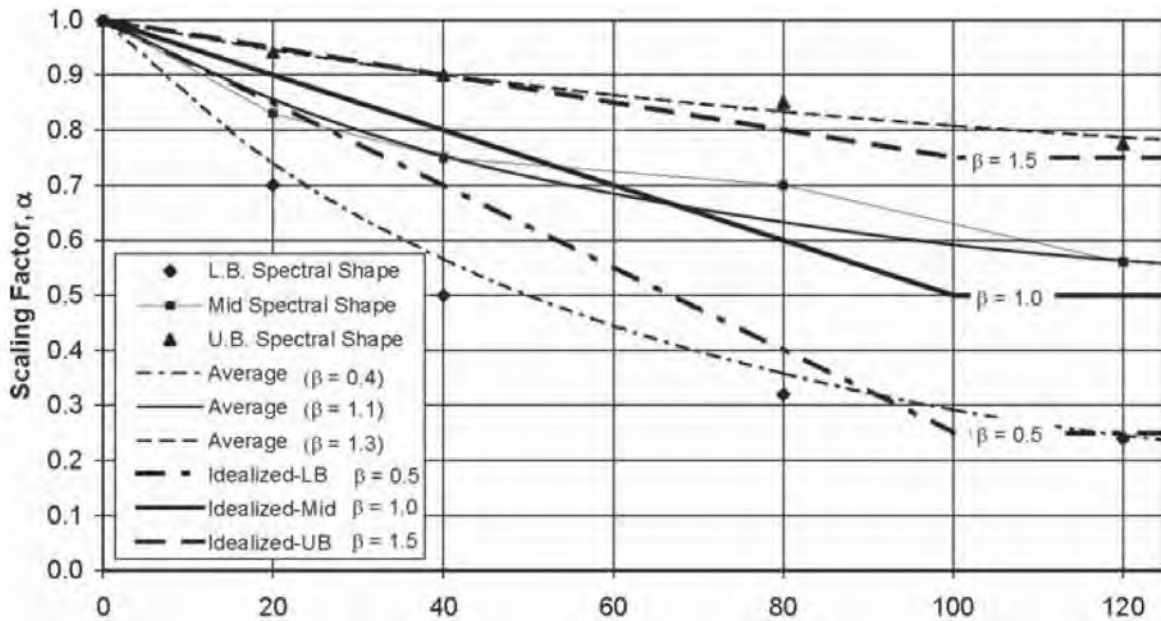


Figure 6-3 Simplified Height-Dependent Incoherence Reduction Scaling Factor, α , Recommended for Slope Stability Analysis (NCHRP 2008)

Based upon seismic displacement analyses, NCHRP Report 611 recommends that the average seismic coefficient given by Equation 6-2 be reduced by 50% to find the seismic coefficient for a required C/D ratio of 1.1, assuming the slope can accommodate 1 to 2 inches of permanent seismic displacement:

$$k_s = 0.5 \cdot \alpha \cdot F_{pga} \cdot PGA \quad 6-5$$

where k_s is the seismic coefficient for a required C/D ratio of 1.1 assuming 1 to 2 inches of permanent seismic displacement is allowable.

In summary, based upon the recommendations in NCHRP Report 611, the limit equilibrium seismic coefficient design approach entails the following steps:

- 1) Conduct static slope stability analyses using appropriate resistance factors to confirm that slope performance meets static loading requirements.
- 2) Establish the upper bound value of the seismic coefficient k_{\max} ($= F_{\text{pga}}$ PGA) and the site-adjusted spectral acceleration at one second, $F_v S_1$, from the AASHTO ground motions maps for a 1,000-year return period and the Site Class-dependent AASHTO site factors.
- 3) Modify k_{\max} to find the average peak acceleration accounting for slope height effects, k_{av} ($= \alpha k_{\max}$), in accordance with Equations 6-2 through 6-4.
- 4) Reduce k_{av} by a factor of 0.5 to find k_s (assuming 1 to 2 inches of permanent displacement are permissible). If larger permanent displacements are acceptable, further reductions in k_{av} are possible, but these would have to be determined by conducting separate calibrations studies between the resulting displacement and the ratio of k_s to k_{av} , as discussed in Section 6.2.3.
- 5) Conduct a conventional slope stability analysis using $k_s = 0.5 k_{\text{av}}$. If the resulting C/D ratio (i.e. the resulting FS) is at least 1.1, the slope meets seismic stability requirements.

6.2.3 Displacement-Based Seismic Stability Analysis

In contrast to the limit equilibrium approach, the displacement-based approach involves the explicit calculation of cumulative seismic deformation. The potential failure mass is treated as either a rigid body or deformable body, depending on whether a simplified Newmark sliding block approach or more advanced numerical modeling is used.

The Newmark sliding block approach treats the potential failure mass as a rigid body on a yielding base, as shown on Figure 6-1. The acceleration time history of the rigid body is assumed to correspond to the average acceleration time history of the failure mass. Deformation accumulates when the rigid body acceleration exceeds the yield acceleration of the failure mass, k_y , where k_y is defined as the seismic coefficient (horizontal acceleration) that results in a C/D ratio of 1.0 in a limit equilibrium analysis.

Acceleration pulses in the time history, including accelerations that exceed the yield acceleration and, once the block is moving, accelerations below the yield acceleration until the block stops moving are double integrated to calculate cumulative seismic displacement. In a Newmark analysis, relative displacement is generally assumed to accumulate in only one direction (i.e. the down slope direction). With this assumption, the yield acceleration in the other (upslope) direction is implicitly assumed to be

larger than the peak acceleration in that direction for the failure mass being analyzed. Analyses conducted by Yan et al. (1996) demonstrate that the influence of the vertical ground motion component in a Newmark analysis is generally relatively small for most situations encountered in practice and can be ignored.

The Newmark Analysis approach may be used to calibrate an appropriate pseudo-static seismic coefficient reflecting acceptable displacement performance, as discussed in Section 6.2.1. Similar discussions on the Newmark approach for slopes are presented in the FHWA publication *Geotechnical Earthquake Engineering* (FHWA, 1998). For example, Figure 6-4 shows results of Newmark seismic deformation analyses performed by Hynes and Franklin (1984) using 348 strong motion records (all soil/rock conditions; $4.5 < M_w < 7.4$) and six synthetic records. The Hynes and Franklin “upper bound” curve presented in Figure 6-4 suggests that deformations will be less than 12 inches for yield accelerations greater than or equal to one-half the peak average acceleration (i.e. for a seismic coefficient greater than or equal to $0.5 k_{av}$) in all situations.

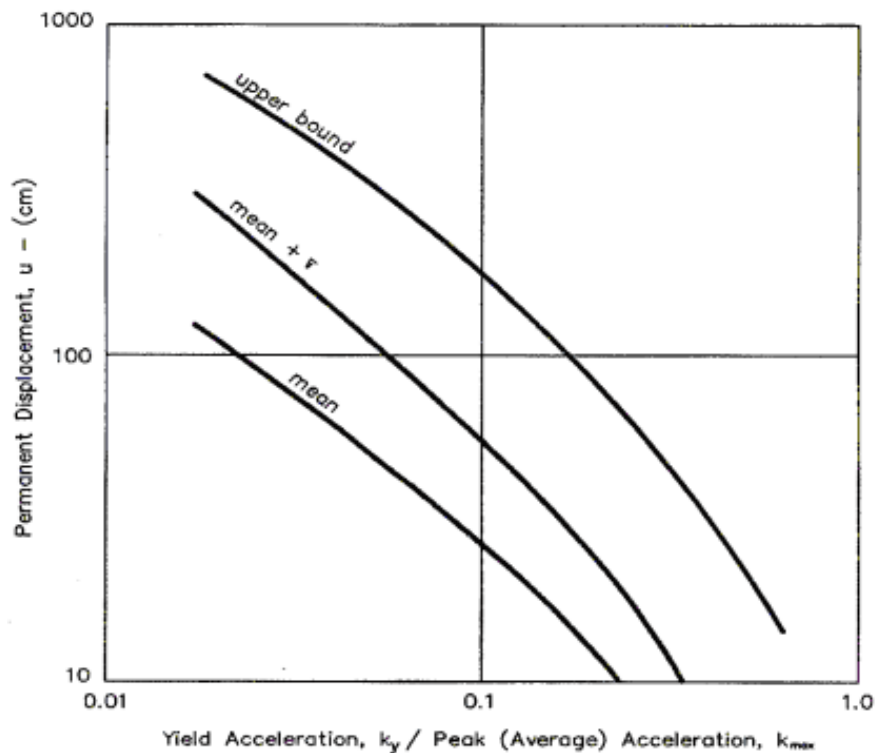


Figure 6-4 Permanent Seismic Deformation Chart (Hynes and Franklin, 1984)

As previously discussed, it must be recognized that slope-height effects should be taken into account to determine an appropriate seismic coefficient or to estimate permanent seismic displacement. This was recognized by Makdisi and Seed (1978), who developed slope displacement design charts for the seismic design of earth dams.

Newmark sliding block analyses are also used to evaluate horizontal sliding displacements of gravity retaining walls, as described in current AASHTO (2007). The current AASHTO provisions for retaining wall design employ the displacement equation of Richard and Elms (1979) in which the permanent seismic displacement of a free standing retaining wall (in inches) is given as:

$$d = 0.087 \left[\frac{(PGV)^2}{k_{max} g} \right] \cdot \left(\frac{k_y}{k_{max}} \right)^{-4} \quad 6-6$$

Newmark sliding block displacement analyses were conducted as part of the NCHRP 12-70 project using an extensive database of earthquake records. The end result of these analyses was establishment of updated relationships between permanent seismic displacement (d) and the following three terms: the ratio k_y/k_{av} , k_{av} , and the peak ground velocity (PGV). Noted that NCHRP Report 611 uses the term k_{max} in place of k_{av} in these equations but defines k_{max} in the same manner as k_{av} is defined herein (e.g. as $\alpha \times F_{pga}$ PGA). Based on regression analyses, the following simplified relationships for permanent seismic displacement were established in the NCHRP 12-70 study and are recommended herein for displacement-based slope stability assessment purposes:

- For all sites except CEUS rock (Site Class A and B) sites, the displacement (in inches) can be estimated by the following equation:

$$\log(d) = \begin{aligned} & -1.51 - 0.74 \cdot \log(k_y / k_{max}) + \\ & 3.27 \cdot \log(1 - k_y / k_{max}) - 0.80 \\ & \log(k_{max}) + 1.59 \cdot \log(PGV) \end{aligned} \quad 6-7$$

- For CEUS rock (Site Class A and B) sites, displacement (in inches) can be estimated by:

$$\log(d) = \begin{aligned} & -1.31 - 0.93 \cdot \log(k_y / k_{max}) + \\ & 4.52 \cdot \log(1 - k_y / k_{max}) - 0.46 \\ & \log(k_{max}) + 1.12 \cdot \log(PGV) \end{aligned} \quad 6-8$$

The mean value of PGV is given in NCHRP Report 611 by the approximation:

$$PGV = 38 \cdot F_v \cdot S_1 \quad 6-9$$

NCHRP Report 611 actually recommends using the mean plus one standard deviation value for PGV (equal to $55F_v S_1$) in Equations 6-7 and 6-8 to provide a margin of conservatism. However, for consistency with LRFD principles, the use of the mean value of the PGV is recommended herein.

The development of the PGV- S_1 correlation in Equation 6-9 was based on a simplification of a more precise but more complicated equation developed using regression analysis on an extensive database of recorded and synthetic accelerograms representative of both rock and soil conditions for the WUS and the CEUS. It was found that earthquake magnitude need not be explicitly included in the correlation, as its influence on PGV is captured by its influence on the value of S_1 . Figure 6-5 shows a comparison between the displacements estimated using the existing AASHTO displacement equation and Equation 6-6.

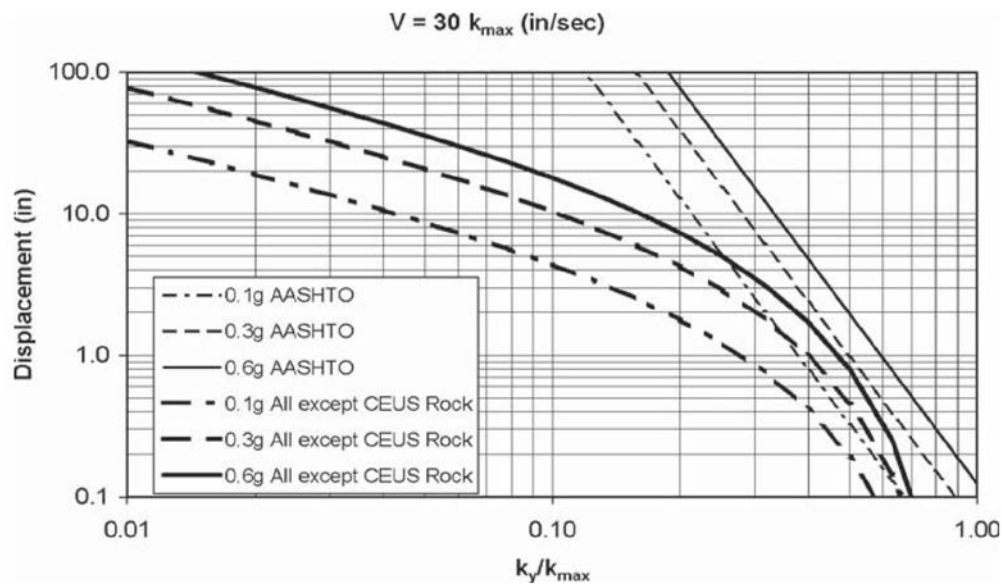


Figure 6-5 Comparison between AASHTO (2002) and Recommended Displacement Equation 6-6 for $PGV = 30k_{max}$ (in/sec)

Note that Equations 6-7 and 6-8 represent mean values and, based upon standard deviation from the statistical analysis, the resulting displacements can be multiplied by 2 to obtain displacements at the 84 percent confidence level.

Similar displacement equations to those recommended in Equations 6-7 and 6-8 were developed by Martin and Qiu (1994) from a more limited database of earthquake records, and were described in the NCHRP 12-49 Project report (NCHRP, 2003). The recommended equations shown above give displacements slightly greater than the Martin and Qiu (1994) correlations. In 2000, an approach for estimating the displacement of slopes during a seismic event was developed through the Southern California Earthquake Center (SCEC, 2002). Displacement comparisons (described in NCHRP Report 611) between the SCEC approach and the approach recommended above show similar results.

In summary, the following methodology is recommended for displacement-based seismic stability assessment of slopes and embankments:

- 1) Conduct static slope stability analyses using appropriate resistance factors to confirm that performance meets static loading requirements.
- 2) Establish the upper bound value of the seismic coefficient k_{max} ($= F_{pga}$ PGA) and the site-adjusted spectral acceleration at one second, $F_v S_1$, from the AASHTO ground motions maps for a 1,000-year return period and the Site Class-dependent AASHTO site factors.
- 3) Determine the corresponding peak ground velocity (PGV) from the correlation equation between $F_v S_1$ and PGV (i.e. $PGV = 38 F_v S_1$).
- 4) When the slope height is greater than 20 ft, modify k_{max} by multiplying it by the slope height factor, α , to get k_{av} , to account for slope height effects.
- 5) Determine the yield acceleration, k_y , using a pseudo-static stability analysis for the slope. Note that these stability analyses should normally be conducted using the undrained strength of the soil because of the short-term rapid loading from the earthquake.
- 6) Establish the earthquake slope displacement potential as a function of k_y , k_{av} , and PGV using the appropriate Newmark displacement equations.
- 7) Evaluate the acceptability of the displacement based on performance criteria established by the owner for the specific project site.

A detailed example demonstrating the application of the NCHRP 12-70 (2008) procedure outlined above for the seismic design of embankment slopes is given in Section 7.3 of this document.

6.2.4 Rock Slope Stability Analyses

Analysis approaches to evaluate rock slope seismic stability follow the same basic principles as the approaches used for soil slopes and embankments described above. However, there are unique challenges related to the rock mass characterization and the determination of rock mass strength parameters. These issues, issues which apply also to static stability evaluations, are briefly reviewed and summarized in Chapter 4. A more detailed discussion of these problems is provided in the FHWA NHI course reference manual on Rock Slopes (FHWA 1998a) and in FHWA Geotechnical Engineering Circular No. 5 on Evaluation of Soil and Rock Properties (FHWA 2002). A summary discussion on rock slope stability from these publications is given below.

With respect to rock slope stability, two distinct cases arise in practice. The first case arises with highly fractured rock masses, where the rock may be treated as an isotropic material with equivalent Mohr-Coulomb strength parameters c and ϕ . For this case, conventional two dimensional limit equilibrium stability analyses are applicable. The second case relates to where distinct bedding planes, discontinuities, or joints in the rock mass define potential planes of failure. In these cases, three dimensional stability analyses may be required.

One challenge in rock slope stability analyses is that the shear strength envelope for both a fractured rock mass and for a discontinuity is often curved. The procedure for using a curved strength envelope in a stability analysis is first, to determine the range of effective normal stresses acting along a potential rupture surface in the slope, and second to calculate the instantaneous cohesion values and friction angles (c'_i, ϕ'_i) in this stress range. Chapter 4 describes the procedure for evaluating instantaneous values of cohesion and friction angle from a curved strength envelope.

The stability analysis in a highly fractured rock mass is carried out in the same manner as for a soil slope except that a number of values of c'_i and ϕ'_i values are used corresponding to the variation in normal stress in the ground. Li et al. (2009), have developed seismic rock slope stability charts based on conventional limit analysis methods. Figure 6-6 shows that the slope parameter definitions used for the charts. Figure 6-7 shows representative results where N is a dimensionless stability number.

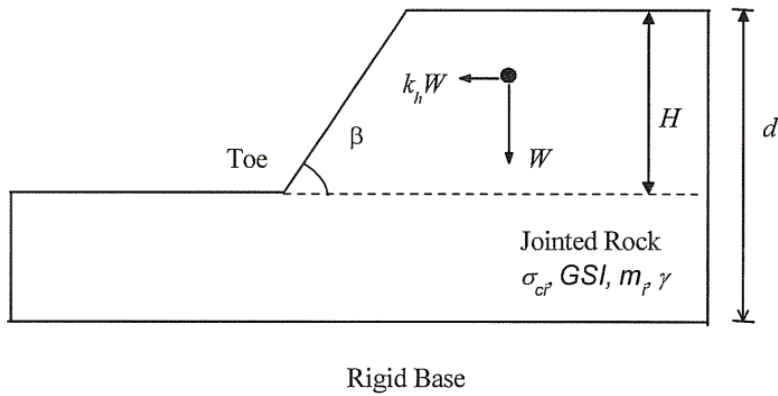


Figure 6-6 Problem Definition (Li et al., 2009)

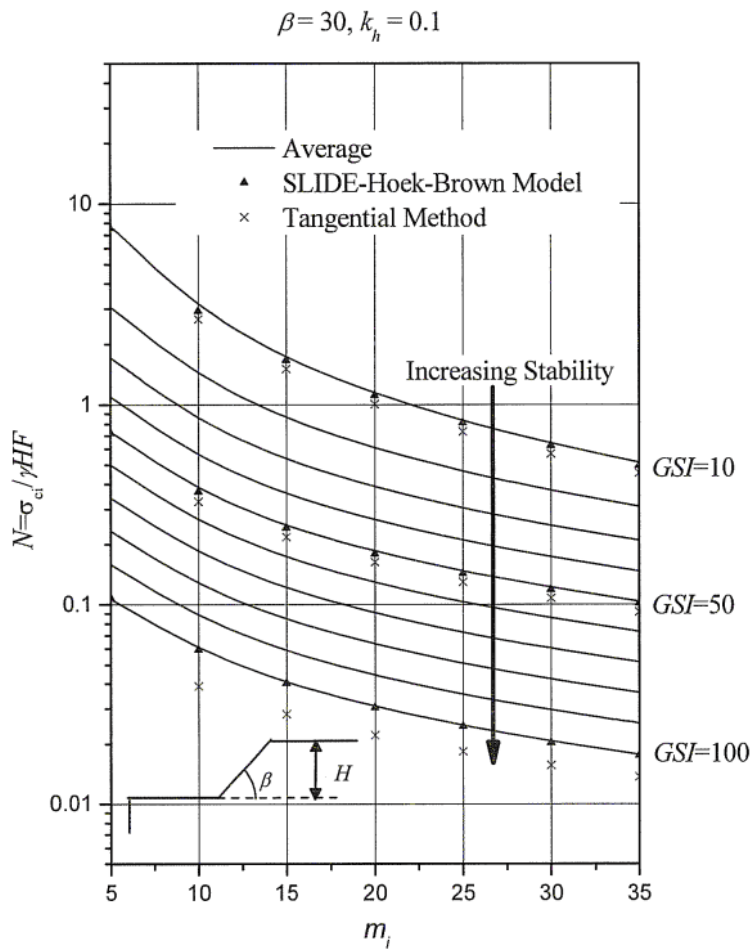


Figure 6-7 Representative Analysis Results (Li et al., 2009)

For rock masses with discrete discontinuities, stereo plots of joint systems in a rock mass will often define distinct potential failure planes as illustrated in Figure 6-8b and 6-8c and discussed in detail in the Rock Slope NHI course manual (FHWA, 1998a).

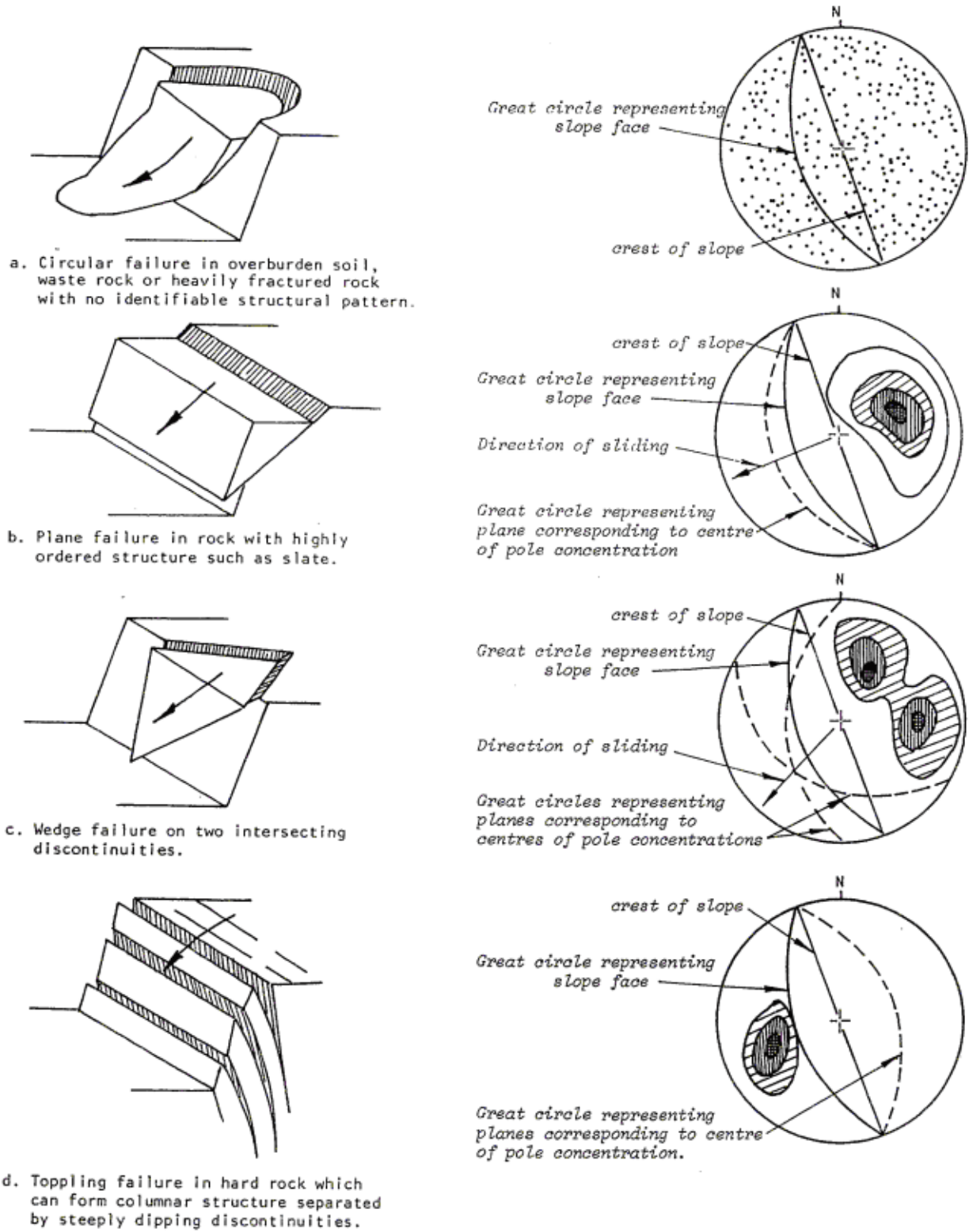


Figure 6-8 Main Types of Slope Failure and Stereoplots of Structural Conditions Likely to Give Rise to these Failures (Hoek and Bray, 1977)

6.3 SOIL LIQUEFACTION HAZARD

6.3.1 Hazard Description and Initial Screening

Soil liquefaction is a phenomenon in which a cohesionless soil deposit below the groundwater table loses a substantial amount of strength due to pore pressure generation resulting from earthquake strong ground shaking. The reason for the generation of pore pressure is that cohesionless soils tend to compact during earthquake shaking and this tendency causes the pore water pressures in the soil to increase until the pore water has time to drain (dissipate) from the soil skeleton. This pore pressure increase, in turn, causes a reduction in effective stress and associated reductions in soil strength and stiffness. Recently deposited (i.e., geologically young) and relatively loose natural soils and uncompacted or poorly compacted fill soils are susceptible to liquefaction. Loose sands and silty sands are particularly susceptible to liquefaction. Loose silts and gravels also have a significant potential for liquefaction. Dense natural soils, well-compacted fills, and cohesive soils have a relatively low susceptibility to liquefaction.

Liquefaction has been perhaps the single most significant cause of damage to bridges during past earthquakes. Most of the damage has been related to liquefaction-induced lateral movement of soil at bridge abutments. However, cases involving the loss of lateral and vertical bearing support of foundations for bridge piers due to liquefaction have also occurred.

The potential consequences of liquefaction can be grouped into the following categories:

- 1) Flow slides. Flow failures are the most catastrophic form of ground failure that can occur due to liquefaction. These large slides occur when the down slope static (gravity) loads exceed the resistance provided by low shear strengths of liquefied soils, (i.e., the static factor of safety drops below 1.0 due to liquefaction). These slides can occur even after the ground stops shaking, and commonly results in tens of feet of displacement. Further discussion of flow slides is provided in Section 6.4.2.
- 2) Lateral spreading. Lateral spreading is the most common form of lateral soil movement accompanying liquefaction. It can occur on very gently sloping ground or under embankments underlain by liquefied soil due to combined static gravity and seismically induced inertia forces in the soil mass. In lateral spreading, the static factor of safety of the soil mass is greater than one but lateral movements accumulate during the earthquake when the static plus seismically induced shear

stresses exceed the strength of liquefied soil. The resulting lateral movements can range in magnitude from inches to several feet and are typically accompanied by ground cracking with horizontal and vertical offsets. The potential for lateral movements due to lateral spreading is increased if there is a 'free face' such as a river bank in the laterally spreading mass. Lateral spreading can occur beneath a bridge approach fill or highway embankment if the underlying soil liquefies. Further discussion of lateral spreading is provided in Section 6.4.3.

- 3) Reduction in foundation bearing capacity. The occurrence of liquefaction beneath, and/or laterally adjacent to, bridge foundations can greatly reduce foundation vertical and/or lateral capacity, resulting in unacceptable foundation settlements and or lateral movements. The bearing capacity of a shallow foundation in liquefied soil can be evaluated using conventional bearing capacity theory and the residual undrained shear strength of the liquefied soil discussed in Section 4.4.6. The lateral resistance of deep foundations in liquefied soil is discussed in Section 10.6.6.
- 4) Ground settlement. Even in the absence of flow sliding, lateral spreading, or reduction in foundation bearing capacity due to liquefaction, ground settlements due to soil consolidation can occur as liquefaction-induced, excess pore water pressures in the soil dissipate. In some cases, this consolidation may take a substantial period of time to occur, perhaps hours or, in extreme cases, days after the earthquake, and may result in unacceptable total and/or differential settlement of foundations located above the liquefied layer. Furthermore, deep foundations extending through liquefied strata may be subject to downdrag as soils overlying the liquefied layers settle relative to the piles. However, the magnitude of total and differential ground settlement is typically less than that associated with flow slides, lateral spreading, or reduction in foundation bearing capacity. Further discussion of the settlement of liquefied soil is provided in Section 6.5.2.
- 5) Increased pressure on retaining walls. Liquefaction in the backfill behind a retaining wall, such as an abutment backwall or wingwall, will increase lateral earth pressures on the wall, potentially leading to wall failure or excessive deformations.

Table 6-1 presents recommendations concerning the seismic hazard level at which a liquefaction analysis is necessary from the FHWA Seismic Retrofitting Manual for Highway Structures (FHWA, 2006). In these recommendations, the need to conduct an evaluation of liquefaction is described as a function of the Seismic Hazard Level for the bridge, which depend upon the value of the Site Class-adjusted spectral acceleration at both 1 second (S_{D1}) and 0.2 second (S_{DS}). For Seismic Hazard Levels I and II, the potential for liquefaction is generally low as peak ground accelerations are likely to be less than 0.14g and

earthquake magnitudes are generally less than 6.0. In addition, little potential exists for permanent movement of the ground because of the small size and limited duration of seismic events at these levels.

TABLE 6-1 SEISMIC HAZARD LEVEL

Hazard Level	Using $S_{D1} = F_v S_1$	Using $S_{Ds} = F_a S_s$
I	$S_{D1} \leq 0.15$	$S_{Ds} \leq 0.15$
II	$0.15 < S_{D1} \leq 0.25$	$0.15 < S_{Ds} \leq 0.35$
III	$0.25 < S_{D1} \leq 0.40$	$0.35 < S_{Ds} \leq 0.60$
IV	$0.40 < S_{D1}$	$0.60 < S_{Ds}$

Notes:

1. For the purposes of determining the Seismic Hazard Level for Site Class E soils, the value of F_v and F_a need not be taken larger than 2.4 and 1.6 respectively, when S_1 is less than or equal to 0.10 and S_s is less than 0.25.
2. For the purposes of determining the Seismic Hazard Level for Site Class F soils F_v and F_a values for Site Class E soils may be used with the adjustment described in Note 1 above.

The potential for liquefaction at the higher accelerations corresponding to Seismic Hazard Levels III and IV is greater than for Seismic Hazard Levels I and II and therefore careful attention is needed to determine the potential for, and consequences of, liquefaction at sites with this hazard level. However, for Seismic Hazard Level III the following magnitude criterion may also be applied: if the mean magnitude contributing to the peak ground acceleration is less than 6.0, or if it is between 6.0 and 6.4 and either the normalized Standard Penetration Test (SPT) blow count $(N_1)_{60}$ is greater than 20, or $(N_1)_{60}$ is greater than 15 and $F_a S_s$ is less than 0.35g, a liquefaction analysis is not required.

In summary, an evaluation of the potential for, and consequences of, liquefaction in soils near the surface should be made in accordance with the following requirements:

- Seismic Hazards Levels I and II: Not required.
- Seismic Hazards Levels III: Required, unless one of the following two conditions is met:
- Mean magnitude for the design event is less than 6.0.

- Mean magnitude for the design event is less than 6.4 and equal to or greater than 6.0, and either the normalized Standard Penetration Test (SPT) blow count $(N_1)_{60}$ is greater than 20, or $(N_1)_{60}$ is greater than 15 and $F_a S_s$ is less than 0.35g.
- Seismic Hazard Level IV: Required

In addition to the above criteria, it can be assumed that a significant liquefaction hazard does not exist for Seismic Hazards Levels III and IV if any of the following screening criteria are satisfied:

- The geologic materials underlying the site are either bedrock or have very low liquefaction susceptibility according to the relative susceptibility ratings shown in Table 6-2, which are based on geologic age and general depositional environments (Youd and Perkins, 1978). Table 6-2 should be applied conservatively if there are uncertainties regarding geologic age or depositional environment.
- The soils below the groundwater table at the site are one of the following:
 1. Clayey soils which have a clay content (grain size < 0.005 mm) greater than 15 percent, liquid limit greater than 35 percent, or natural water content less than 90 percent of the liquid limit (Seed and Idriss, 1982). However, clayey soils that are highly sensitive, based on measured soil properties or local experience, should not be screened out. A highly sensitive¹ soil possesses all of the following properties:
 - a. Liquid limit less than 40 percent.
 - b. Water content greater than 0.9 times the liquid limit.
 - c. Liquidity index greater than 0.6
 - d. $(N_1)_{60}$ less than five or normalized cone penetration resistance q_{c1} , less than 20 ksf.
 2. Sand with a minimum corrected Standard Penetration Test resistance, $(N_1)_{60}$ value of 30 blows/foot or minimum corrected cone penetration test tip resistance, q_{C1N} , of 160 with a sufficient number of tests.

¹ Areas of the United States known to have highly sensitive soils include some coastal areas of Alaska, along the St. Lawrence River, some eastern and western coastal areas with estuarine soils deposits, near or within saline lakes in the Great basin and other arid areas, and soils resulting from weathering of volcanic ash (Youd, 1998).

- The water table is deeper than 50 feet below the existing ground surface or proposed finished grade at the site, whichever is lower, including considerations for seasonal, historic and possible future rises in groundwater level.

TABLE 6-2 ESTIMATED SUSCEPTIBILITY OF SEDIMENTARY DEPOSITS TO LIQUEFACTION DURING STRONG GROUND MOTION (Youd and Perkins, 1978)

Type of Deposit	General Distribution of Cohesionless Sediments in Deposits	Likelihood that Cohesionless Sediments, When Saturated, Will be Susceptible to Liquefaction (by Age of Deposit)			
		<500 yr Modern	Holocene >11 ka	Pleistocene 11 ka - 2 Ma	Pre-Pleistocene >2 Ma
(a) Continental Deposits					
River channel	Locally variable	Very high	High	Low	Very low
Floodplain	Locally variable	High	Moderate	Low	Very low
Alluvial fan and plain	Widespread	Moderate	Low	Low	Very low
Marine terraces and plains	Widespread	—	Low	Very low	Very low
Delta and fan-delta	Widespread	High	Moderate	Low	Very low
Lacustrine and playa	Variable	High	Moderate	Low	Very low
Colluvium	Variable	High	Moderate	Low	Very low
Talus	Widespread	Low	Low	Very low	Very low
Dunes	Widespread	High	Moderate	Low	Very low
Loess	Variable	High	High	High	Unknown
Glacial till	Variable	Low	Low	Very low	Very low
Tuff	Rare	Low	Low	Very low	Very low
Tephra	Widespread	High	High	?	?
Residual soils	Rare	Low	Low	Very low	Very low
Sebka	Locally variable	High	Moderate	Low	Very low
(b) Coastal Zone					
Delta	Widespread	Very high	High	Low	Very low
Estuarine	Locally variable	High	Moderate	Low	Very low
Beach					
High wave-energy	Widespread	Moderate	Low	Very low	Very low
Low wave-energy	Widespread	High	Moderate	Low	Very low
Lagoonal	Locally variable	High	Moderate	Low	Very low
Fore shore	Locally variable	High	Moderate	Low	Very low
(c) Artificial					
Uncompacted fill	Variable	Very high	—	—	—
Compacted fill	Variable	Low	—	—	—

If the above screening criteria are not satisfied, then more detailed evaluations should be used to evaluate a liquefaction hazard and its potential consequences. However, prior to initiating screening procedures for soils that are susceptible to liquefaction, a check should be made as to whether liquefaction has previously

occurred at the site (or in the near vicinity of the site in similar geotechnical conditions) during past earthquakes. This check may involve review of the earthquake history of an area and review of published post-earthquake reconnaissance reports. If there is evidence that liquefaction has previously occurred at the site, then it must be given further consideration regardless of what screening criteria indicate.

6.3.2 Liquefaction Strengths: Laboratory and In-situ Tests

Undrained cyclic stress controlled triaxial tests on saturated sands to simulate liquefaction were first studied by Seed and Lee (1966). Subsequently, to better simulate earthquake induced cyclic stress conditions in the field, cyclic simple shear tests were conducted by Finn et al. (1971) and Seed and Peacock (1971). Cyclic torsional shear tests (a special case of simple shear testing) have also been conducted to simulate earthquake induced cyclic loading of liquefiable soil. Representative strain controlled cyclic torsional shear tests showing degradation in stiffness and strength with number of cycles are shown in Figure 6-9 (Figueroa et al. (1994)). In denser soils, an increase in post liquefaction stiffness of the soil due to dilation may occur, as shown in Figure 6-10. Degradation in stiffness and strength of liquefied soil has also been demonstrated by back analysis of acceleration records at sites which have liquefied, as illustrated in Figure 6-11.

Most laboratory liquefaction tests are uniform cyclic loading tests. Typically, when displaying the results of uniform cyclic loading liquefaction tests, the cyclic stress ratio (CSR) that causes liquefaction is plotted against number of cycles of loading it took to cause liquefaction, as shown in Figure 6-12, where the $CSR = \tau_c / \sigma_v'$, τ_c = horizontal cyclic shear stress, and σ_v' is the initial vertical effective stress. The resulting curves are sometimes referred to as cyclic strength curves.

While there are procedures to use laboratory test results such as those shown in Figure 6-12 to evaluate liquefaction potential, the use of laboratory tests to evaluate liquefaction strengths for design has major disadvantages. These disadvantages primarily relate to sample disturbance, simulation of the multi-directional shaking which occurs in the field, and replication of the stress history to which the soil has been subjected in the field. Consequently, in the 1980's, correlations between values of the earthquake-induced CSR that caused liquefaction in the field (termed the cyclic resistance ratio, or CRR) started to be established by studies at sites which had or had not liquefied during past earthquakes. CRR correlations based on site characterization using SPT or CPT methods or shear wave velocity are now the standard of practice for evaluating liquefaction potential, as described in Section 6.3.3.

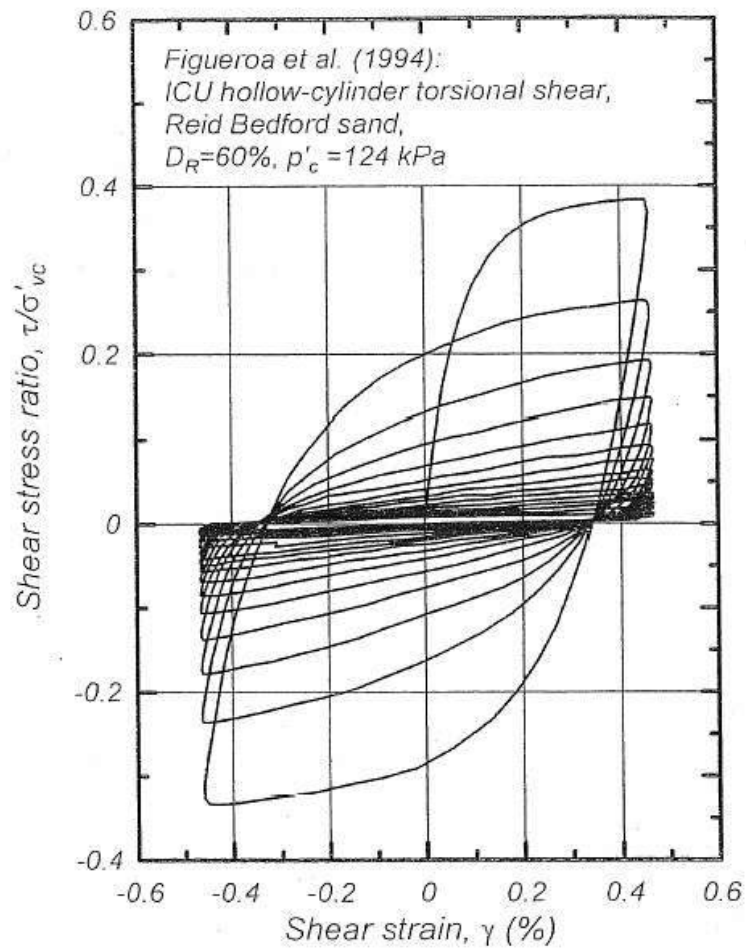


Figure 6-9 Strength Degradation in Cyclic Torsional Shear tests (Figueroa et al. 1994)

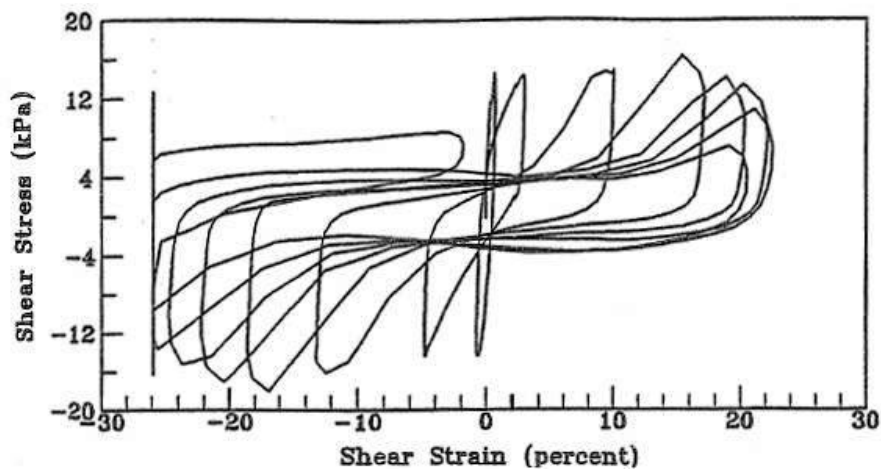


Figure 6-10 Undrained Cyclic Simple Shear Test Results Nevada Sand, $D_r = 40\%$ (Arulmoli et al., 1992)

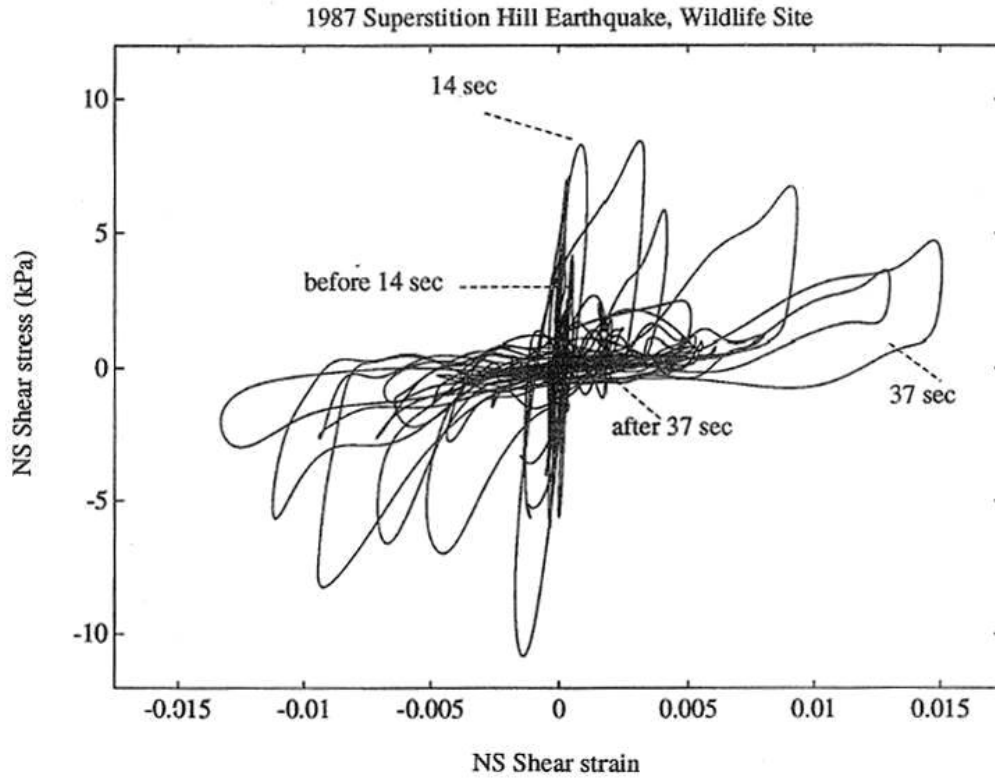


Figure 6-11 Shear Stress Strain History at the Wildlife Refuge Site during Liquefaction (Elgamal and Zeghal 1992, Zeghal and Elgamal 1994)

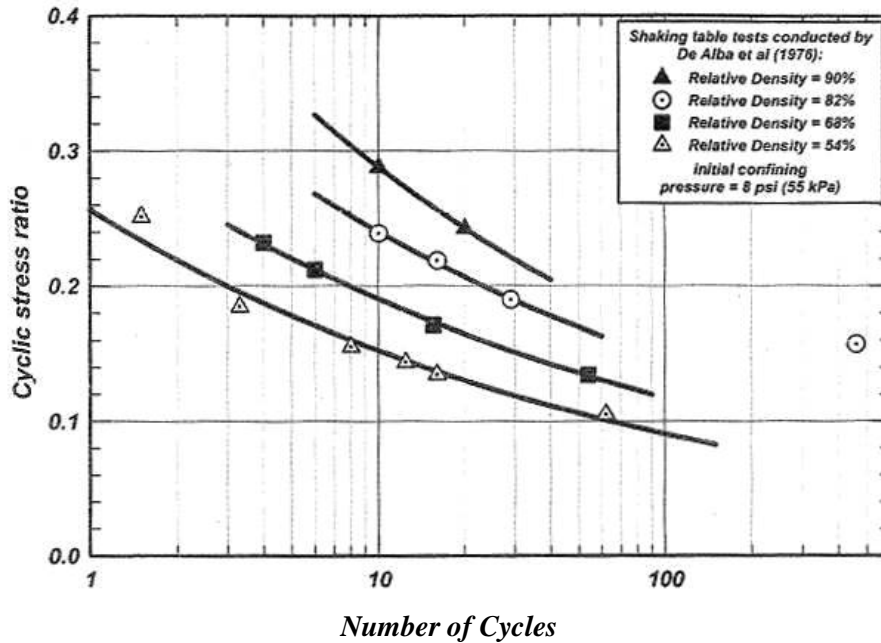


Figure 6-12 The CSR Required to Reach Initial Liquefaction ($r_u = 100\%$), from Shaking Table Tests by De Alba et al. (1976)

Detailed descriptions of SPT and CPT tests and shear wave velocity measurements for site characterization are provided in Chapter 4. The use of the data from such tests to establish liquefaction strengths at a given site and the associated liquefaction potential are described in the next section.

6.3.3 Empirical and Numerical Evaluation Procedures for Liquefaction Potential

The procedures given below for the evaluation of liquefaction are based on the following source documents:

1. Proceedings of the 1996 NCEER Workshop (now MCEER) on evaluating liquefaction resistance (Youd and Idriss, 1997; Youd et al., 2001).
2. Recommended LRFD Guidelines for the Seismic Design of Highway Bridges (ATC/MCEER, 2003), and the AASHTO Guide Specifications for LRFD Seismic Bridge Design (AASHTO, 2009)
3. Seismic Retrofitting Manual for Highway Structures: Part 1- Bridges (FHWA, 2006).
4. Procedures for Implementing Guidelines for Analyzing and Mitigating Liquefaction in California (SEEC, 1999).

A number of factors must be considered during the planning and execution of the field exploration phase of a liquefaction investigation. These include:

1. Location of Liquefiable soils.
2. Location of groundwater level.
3. Maximum anticipated depth of liquefaction.

During the field investigation, the limits of unconsolidated deposits with liquefaction potential should be mapped within and beyond the footprint of the bridge or transportation structure. Typically, this will include an investigation at each bridge pier location and at a sufficient number of locations away from approach fills to establish the spatial extent of liquefiable material. The investigation should establish the

thickness and consistency of liquefiable deposits from the ground surface to the depth at which liquefaction is not expected to occur.

The permanent groundwater level should be established during the exploration program. If uncertainty exists in the location of the groundwater level, piezometers should be installed during the exploration program. The location of the groundwater level should be monitored in the piezometers over a sufficient duration to establish seasonal fluctuations that may be due to rainfall, river runoff, or irrigation. If the groundwater level fluctuates due to tidal action or seasonal river fluctuations, then the zone of fluctuation will often have a lower degree of saturation, making the soil more resistant to liquefaction. Unless the high water table elevation due to seasonal fluctuation is expected to remain in place for an extended period of time (e.g. on the order of weeks) at the higher level, it is usually acceptable to use a long-term groundwater level as a basis for design.

Field exploration should be conducted to the maximum depth of liquefiable soil. A depth of about 15 m has often been used as the depth of analysis for the evaluation of liquefaction. However, liquefaction is now believed to have occurred to depths in excess of 80 ft during the 1964 Alaska earthquake. For this reason it is recommended that a minimum depth of 80 ft below the existing ground surface or lowest proposed finished grade (whichever is lower) be investigated for liquefaction potential. For deep foundations (e.g. shafts or piles), the depth of investigation should extend to a depth that is a minimum of 20 ft below the lowest expected foundation level (e.g. shaft bottom or pile tip) or 80 ft below the existing ground surface or lowest proposed finished grade, whichever is deeper. However, an investigation need not extend below a depth at which geologic deposits that are liquefiable are clearly no longer present.

As discussed in Chapter 4 and Section 6.3.2, three field exploration methods are normally used for evaluation of liquefaction potential: the Standard Penetration Test (SPT) method, and the Cone Penetrometer Test (CPT) method. Other methods may also be used as required if CPT or SPT testing is not feasible. For example, shear wave velocity measurements or the Becker Hammer Test (BHT) method may be used for assessments of liquefaction potential in gravelly soils (e.g. where SPT and CPT cannot be conducted). A geologic reconnaissance and review of the available geotechnical information for the site should supplement any field investigation.

Information presented in Youd and Idriss (1997), Youd et al. (2001) and SCEC (1999) indicate that the results of SPT explorations are affected by small changes in measurement method. Primarily because of their inherent variability, sensitivity to test procedure, and uncertainty, SPT N-values have the potential to provide misleading assessments of liquefaction hazard if the tests are not performed carefully. Because

of the sensitivity of SPT results to test procedure, the relative reliability of CPT test results, and the continuous soil profile provided by CPT soundings, the CPT method is gaining recognition as the preferred method for evaluating liquefaction potential in many locations. Methods for assessing liquefaction potential from CPT results are given in Youd and Idriss (1997) and Youd et al. (2001). The primary advantages of the CPT method are:

- It provides an almost continuous penetration resistance profile that can be used for stratigraphic interpretation, which is particularly important in determining the potential for lateral spreading, lateral flow slides, and significant earthquake induced total and differential action settlements.
- The repeatability of the test is very good.
- The test is fast and economical and less sensitive to field procedures compared to either the SPT or drilling and laboratory testing of soil samples.

However, the CPT method does have some limitations. The limitations of the CPT method are:

- It does not provide soil samples for visual classification or laboratory tests.
- It provides interpreted soil behavior types and not the actual soil type according to ASTM Test Methods D 2488 (Visual Classification) or D 2487 (USCS Classification) [ASTM, 1998].
- Tests cannot be performed in gravelly soils and sometimes the presence of hard/dense crusts or cemented layers at shallow depths makes penetration to desired depths difficult.

In cases where neither the SPT nor the CPT method can be employed (e.g. gravelly soil or soils where a hard crust hinders penetration), measurement of shear wave velocity provides an alternative means of evaluating liquefaction potential.

6.3.4 Evaluation of Liquefaction Potential

Two basic procedures are used to evaluate the potential for liquefaction at a site. These are:

- A simplified procedure that is based on empirical correlations to observations of liquefaction.
- More rigorous numerical modeling.

For most projects, the simplified procedure will be acceptable. However, for some projects, more rigorous numerical modeling using advanced codes may be appropriate. Conditions warranting the use of more rigorous numerical methods include:

- Sites where potentially liquefiable soils extend to depths greater than 25 m.
- Sites that have significant interlaying, particularly where interlayers comprise highly permeable soils or low permeability layers.
- Sites where the cost of ground improvement methods to mitigate the impact of liquefaction is great.

One potential benefit of using a rigorous numerical method to evaluate liquefaction potential is that the results of these methods generally provide an acceleration response spectrum that includes the effect of pore pressure softening. As noted in Chapter 5, considering earthquake induced pore pressure generation may result in lower estimates for earthquake ground motions at the ground surface (as well as within the soil profile) and AASHTO seismic provisions allow the design engineer to take advantage of the reductions in spectral acceleration due to pore pressure generation (up to a limiting reduction of 33% from the non-liquefaction values).

The most basic procedure used in engineering practice for assessment of soil liquefaction potential is the ‘Simplified Procedure’. This procedure, originally developed by Seed and Idriss (1971), compares the cyclic resistance ratio (CRR, the cyclic stress ratio required to induce liquefaction at a given depth) to the earthquake-induced cyclic stress ratio (CSR) at that depth from the design earthquake (generally defined by a peak ground surface acceleration and an associated earthquake magnitude). The CRR and CSR are both expressed as a ratio of cyclic shear stress to the initial (pre-earthquake) effective overburden pressure on a horizontal plane at the specified depth in the soil deposit. Values of CRR for the Simplified Procedure were originally established from data on the normalized SPT value, $(N_1)_{60}$, at sites that did or did not liquefy during past earthquakes, independent of earthquake magnitude and the fines content (percent by weight passing the #200 sieve) of the soil. The current version of this baseline chart, defining values of CRR as a function of $(N_1)_{60}$ and fines content for magnitude 7.5 earthquakes, is shown in Figure 6-13. This chart was established by consensus at a 1996 workshop organized by the Multi-Disciplinary Center for Earthquake Engineering (MCEER) (Youd and Idriss, 1997; Youd et al., 2001). As suggested by the form of this chart, the determination of CRR must consider the fines content of the soil, the efficiency (delivered energy) of the SPT hammer, the effective overburden pressure at the depth at which the SPT was conducted, and the magnitude of the earthquake (Youd and Idriss, 1997; Youd et al., 2001) as well as peak ground acceleration at the site due to the earthquake.

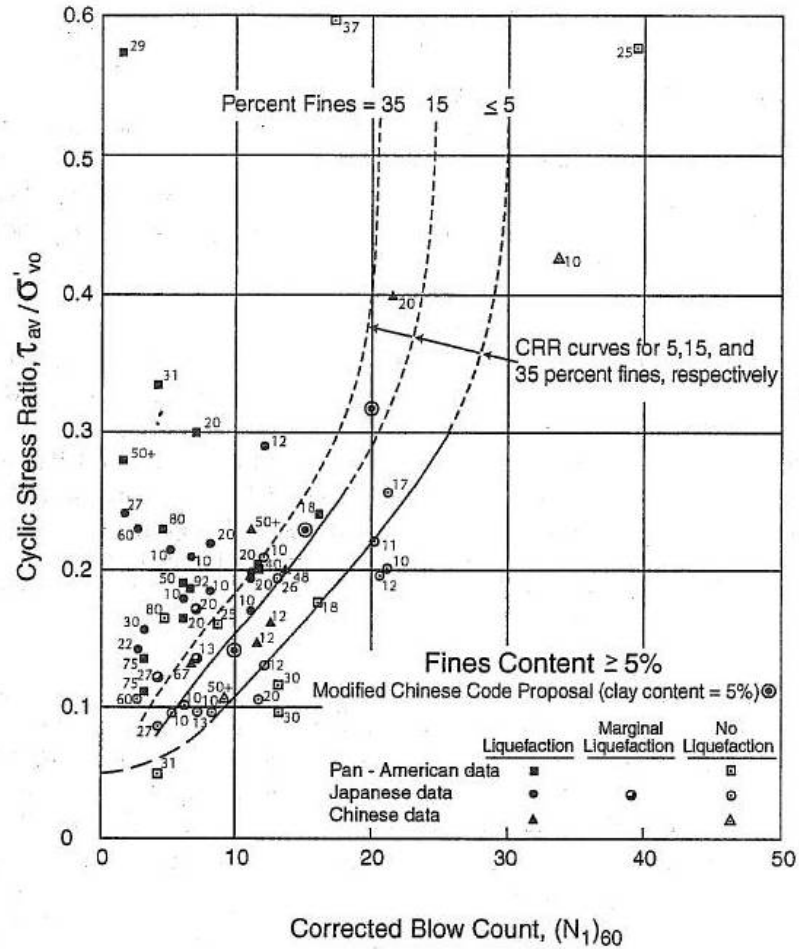


Figure 6-13 Simplified Base Curve Recommended for Determination of CRR from SPT Data for Magnitude 7.5 Along with Empirical Liquefaction Data (Youd and Idriss, 1997)

The effect of earthquake magnitude on CRR (i.e. the effect of magnitude other than 7.5 on the ordinates of Figure 6-13) is generally taken into account using a magnitude scaling factor, MSR, as follows:

$$CRR = MSF \cdot CRR_{M=7.5} \quad 6-10$$

The value of MSF was one of the more contentious issues considered during the 1996 MCEER Workshop (Youd and Idriss, 1997; Youd et al., 2001). The range of magnitude scaling factors recommended by various investigators is shown in Figure 6-14. The consensus recommendation from the workshop was that the magnitude factors defined by the curve at the lower-bound of the recommended range (cross-hatched area) in Figure 6-14 should be used unless different factors can be justified. Note that for magnitudes greater than 7.5, the corresponding recommended curve is the second highest curve shown in Figure 6-14.

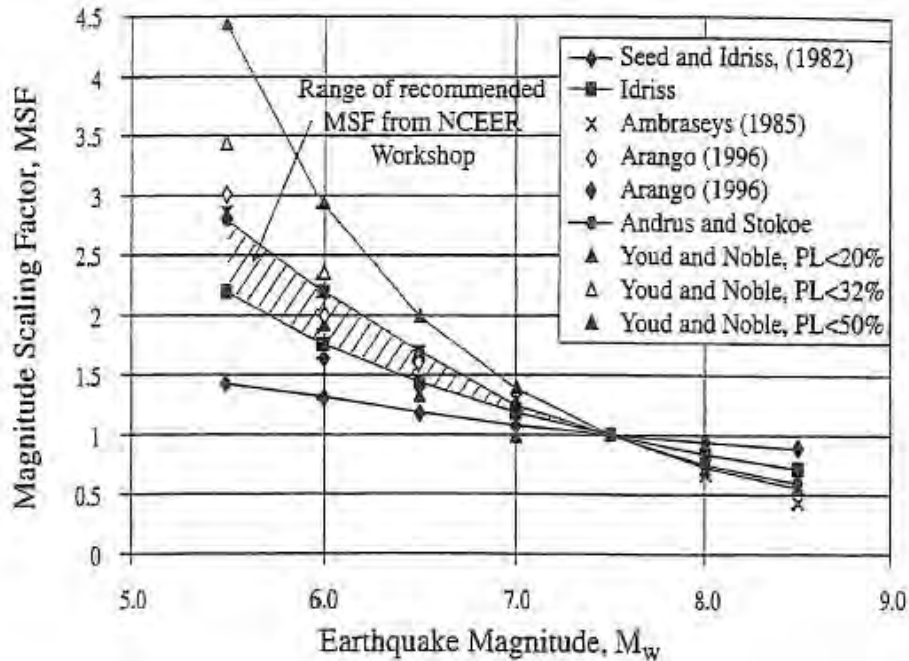


Figure 6-14 Magnitude Scaling Factors Derived by Various Investigators (Youd and Idriss, 1997)

Adjustments for changes in water table and overburden condition at the time of investigation may have to be made during a simplified analysis. The following guidance is provided for making these adjustments.

- Overburden Corrections for Differing Water Table Conditions To perform analyses of liquefaction potential, liquefaction settlement, seismically induced settlement, and lateral spreading, it is necessary to develop a profile of SPT blow counts that have been normalized to N_1 , the blow count at an effective overburden pressure of 1 TSF, using the effective overburden pressure at the time of the investigation. Normalization factors for N_1 are presented in Chapter 4.

Note that this normalization should always be performed using the effective stress profile that existed at the time the SPT testing was performed, as this reflects the condition under which the blow count was recorded. These normalized blow count values are then held constant throughout the remainder of the analyses, regardless of whether or not the analyses are performed using higher or lower water-table conditions. Although in some soils softening soil moistening can influence SPT results if the water table fluctuates, this is, in general, not a concern in soils prone to liquefaction it is commonly assumed that the only effect that changes in the water table have on the SPT blow count is due to changes in the effective overburden stress.

- Overburden Corrections for Differing Fill Conditions Approach fills, and other increases in overburden pressure, should be handled similarly to that described above for changes in groundwater location. The profile of normalized SPT blow counts that were established in the investigation before the fill is placed is held constant throughout the remainder of the analyses, regardless of whether or not the analyses are performed using a higher fill condition.
- Figure 6-15 shows the Robertson and Wride (1998) chart for determining liquefaction strength (CRR) for clean sands (fines content, FC, less than or equal to 5 percent) from CPT data. This chart, which is only valid for magnitude 7.5 earthquakes, shows calculated cyclic stress ratios plotted as a function of corrected and normalized CPT resistance q_{c1N} . Similar to the SPT CRR plot in Figure 6-13, Figure 6-15 is based upon CPT data obtained at liquefied and non-liquefied sites in earthquakes. The solid-line CRR curve separates regions of liquefaction from regions of non-liquefaction. Dashed curves showing approximate cyclic shear strain potential as a function of q_{c1N} are also shown on this plot to emphasize that the cyclic shear strain and ground deformation potential of liquefied soils decrease as penetration resistance increases.

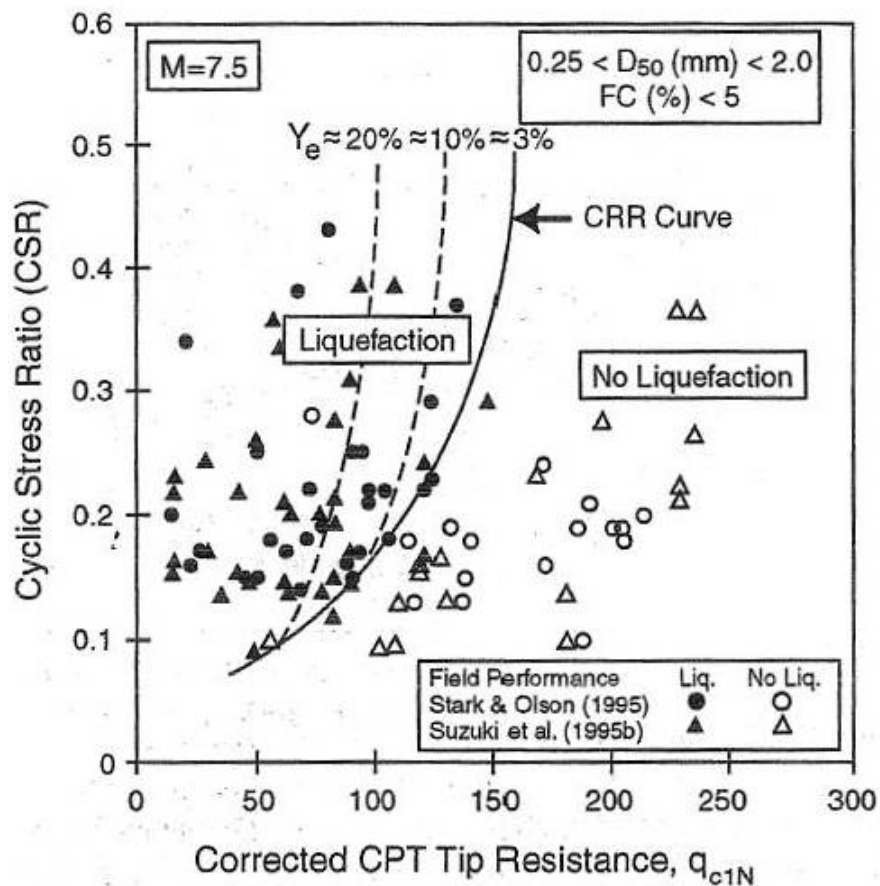


Figure 6-15 CPT-Liquefaction Resistance Correlation Chart (Robertson and Wride, 1998)

As in the SPT method, the determination of CRR using the CPT method must account for the fines content of the soil, the effective overburden pressure, and the magnitude of the earthquake. To account for these factors, the normalized clean sand CPT resistance, $(q_{cIN})_{CS}$, is used with Figure 6-15. According to Youd et. al (2001), $(q_{cIN})_{CS}$, is calculated as shown in Equation 6-11:

$$(q_{cIN})_{CS} = \left(\frac{p_a}{\sigma'_{vo}} \right)^n \cdot \left(\frac{q_c}{p_a} \right) K_c \quad 6-11$$

where p_a = atmospheric pressure (in the same units as q_c), the exponent n is equal to 0.5 for sand, 0.7 for silty sand, 0.8 for silt, and 1.0 for clay, and K_c is a CPT grain size correction factor. The value of K_c can be evaluated from Figure 6-16 as a function of the soil behavior type index, I_c , which can be calculated using Equation 6-12:

$$I_c = \left[(3.47 - \log Q)^2 + (1.22 + \log F)^2 \right]^{0.5} \quad 6-12$$

where Q and F are evaluated using Equations 6-13 and 6-14, respectively, as:

$$Q = \left[\frac{(q_c - \sigma_{vo})}{p_a} \right] \cdot \left[\frac{p_a}{\sigma'_{vo}} \right]^n \quad 6-13$$

and

$$F = \left[\frac{f_s}{(q_c - \sigma_{vo})} \right] \cdot 100\% \quad 6-14$$

Note that if I_c is greater than 2.6, the soil is considered to be non-liquefiable.

The comments given in the previous section regarding use of normalized (for effective overburden pressure) SPT blow counts in liquefaction analyses (e.g. use the water table depth and total and effective overburden pressures at the time of the site investigation to calculate CRR) are also valid for use of normalized CPT data. The recommended magnitude scaling factors for the CRR based upon CPT resistance are the same as those for the SPT-based CRR and are shown in Figure 6-14.

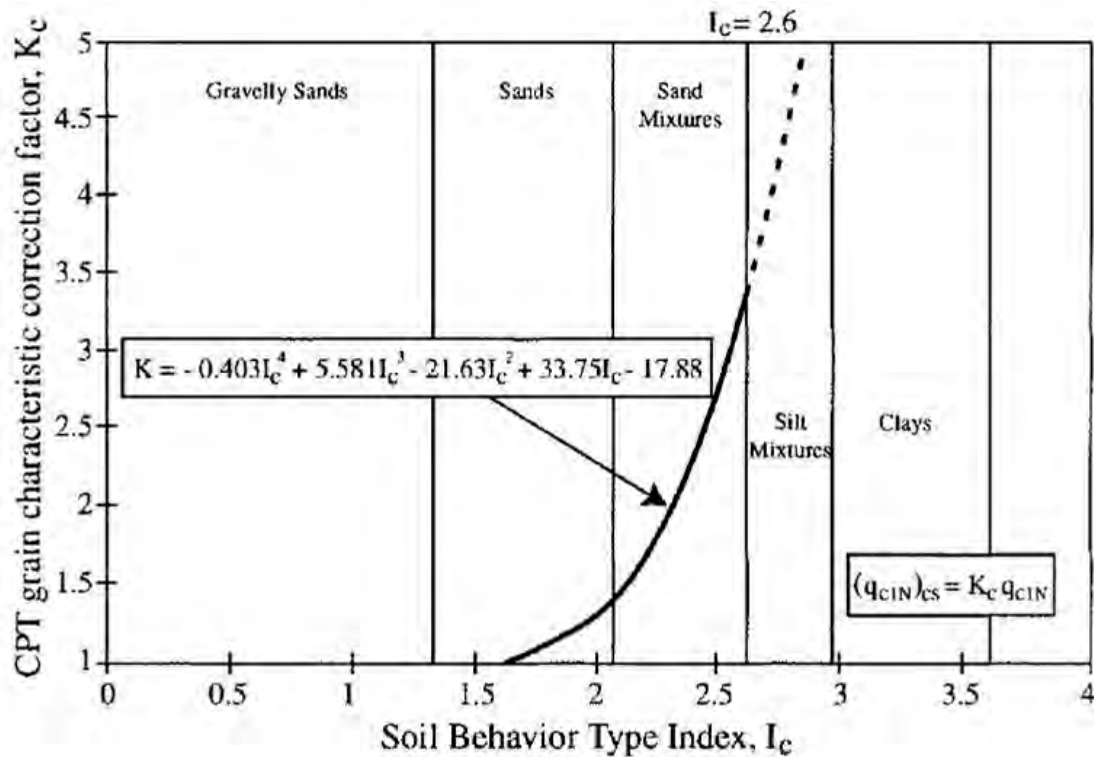


Figure 6-16 CPT Grain Size Characteristic Correction Factor (Robertson and Wride, 1998)

Figure 6-17 shows the basic plot from Andrus and Stokoe (2000) for determining the liquefaction strength (CRR) of Holocene-aged sands with fines contents of less than 5%, 20%, and greater than 35% in an earthquake of M_w 7.5 using shear wave velocity.

Figure 6-17 uses the shear wave velocity normalized to an overburden pressure of 1 TSF, V_{s1} , to characterize the soil. V_{s1} is evaluated as:

$$V_{s1} = V_s \left(\frac{p_a}{\sigma'_{vo}} \right)^{0.25} \quad 6-15$$

The CRR can also be obtained Becker Hammer Test (BHT) data, as discussed in Youd and Idriss (1997) and Youd et al. (2001). However, the use of the BHT for evaluating liquefaction resistance is not considered as reliable as the use of shear wave velocity due to the uncertainties and variability associated with Becker Hammer data.

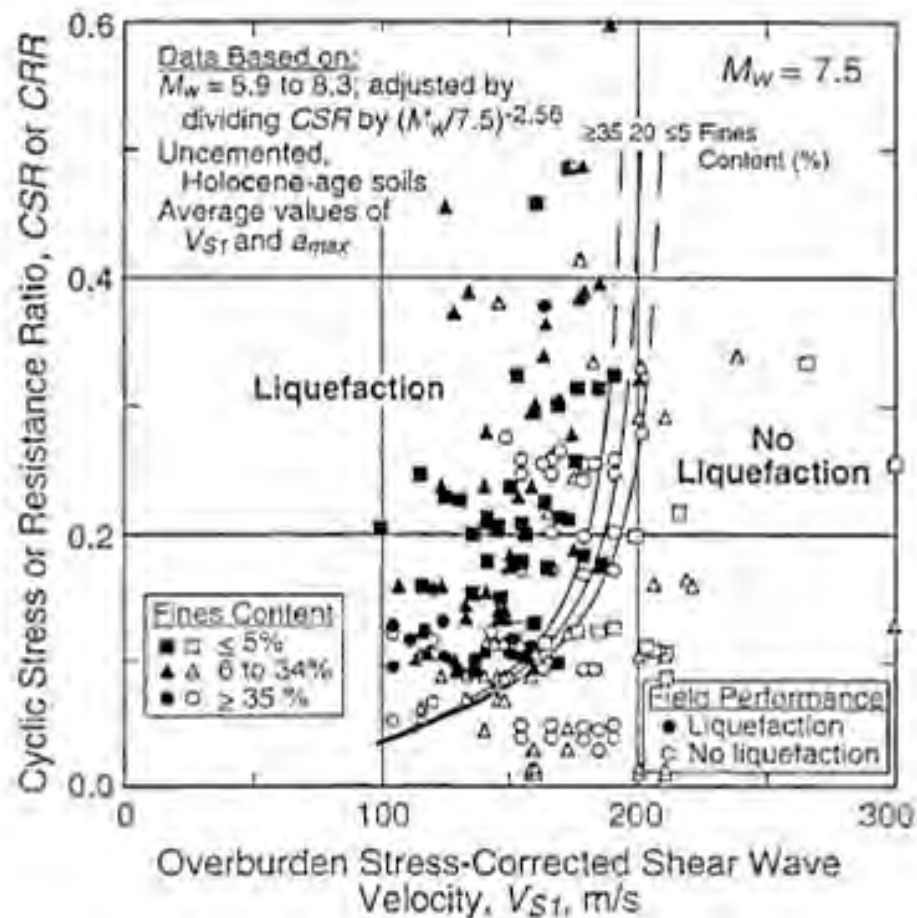


Figure 6-17 Shear Wave Velocity – Liquefaction Resistance Correlation Chart (Andrus and Stokoe, 2000)

To estimate values of the earthquake-induced cyclic shearing stress ratio, CSR, the MCEER workshop (Youd and Idriss, 1997; Youd et al., 2001) recommended essentially no change to the original simplified procedure developed by Seed and Idriss (1971). In this procedure, a magnitude-independent soil flexibility factor, r_d , shown in Figure 6-18, is used to define the reduction in CSR with depth (from the CRR value at the ground surface). Since the MCEER workshop, several investigators have provided alternative recommendations for assessing r_d . For instance, Idriss (1999) proposed that r_d be expressed as a function of earthquake magnitude. However, none of these alternative recommendations have achieved general acceptance in the geotechnical community. A more rigorous alternative to using r_d charts is to conduct a site-specific seismic response analysis of the ground motions, as discussed below.

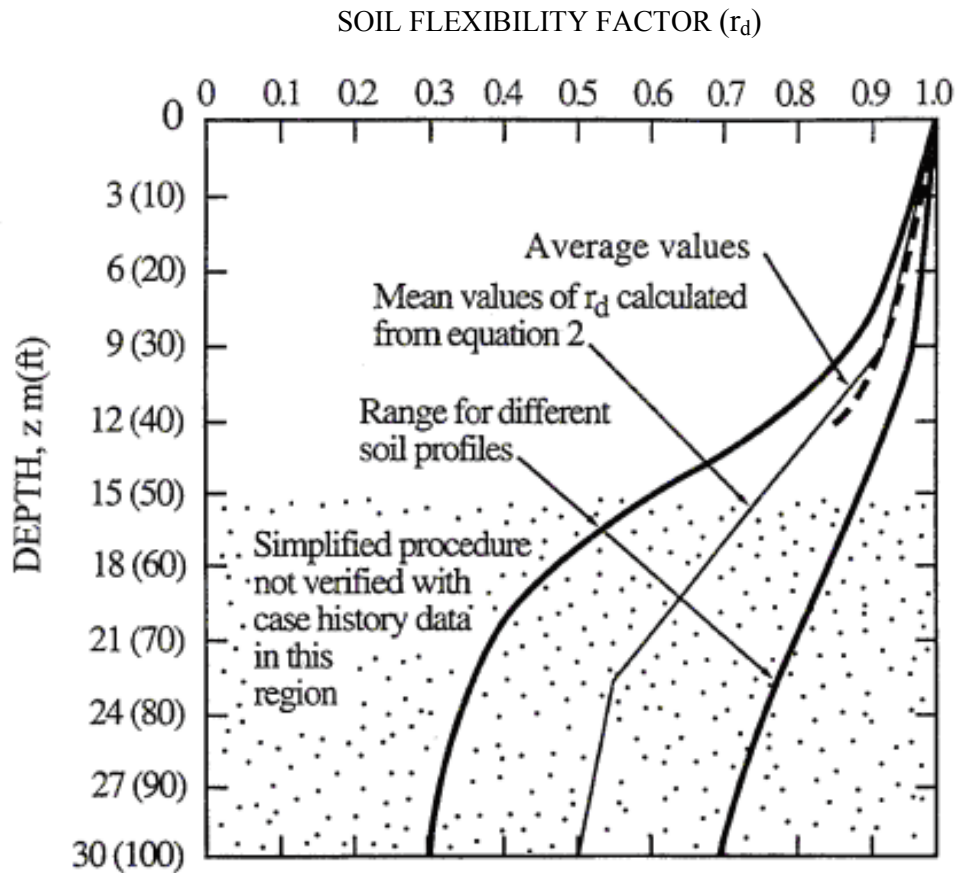


Figure 6-18 Soil Flexibility Factor (r_d) Versus Depth Curves Developed by Seed and Idriss (1971) (with added Mean Value line)

With the Simplified Procedure, the CSR is calculated using the following equation:

$$CSR = \left(\frac{\tau_{av}}{\sigma'_{vo}} \right) = 0.65 \cdot \left(\frac{a_{max}}{g} \right) \cdot \left(\frac{\sigma_{vo}}{\sigma'_{vo}} \right) \gamma_d \quad 6-16$$

where τ_{av} / σ'_{vo} is the representative earthquake induced cyclic shearing stress divided by the initial (pre-earthquake) effective overburden stress, a_{max} is the peak ground acceleration in units of g (the acceleration due to gravity), $\sigma_{vo} / \sigma'_{vo}$ is the ratio of the initial total overburden stress to the initial effective overburden stress, and r_d is the soil flexibility factor.

After values of CRR and CSR are established for a soil stratum at a given depth, the C/D ratio for liquefaction (i.e. the ratio CRR/CSR) can be computed. The C/D ratio should be greater than 1.1 to preclude the development of liquefaction. If the C/D ratio drops below 1.1, the potential for liquefaction must be considered in assessing the seismic performance of the site. An example of the summary plots from a liquefaction triggering analysis for a single SPT boring is shown in Figure 6-19.

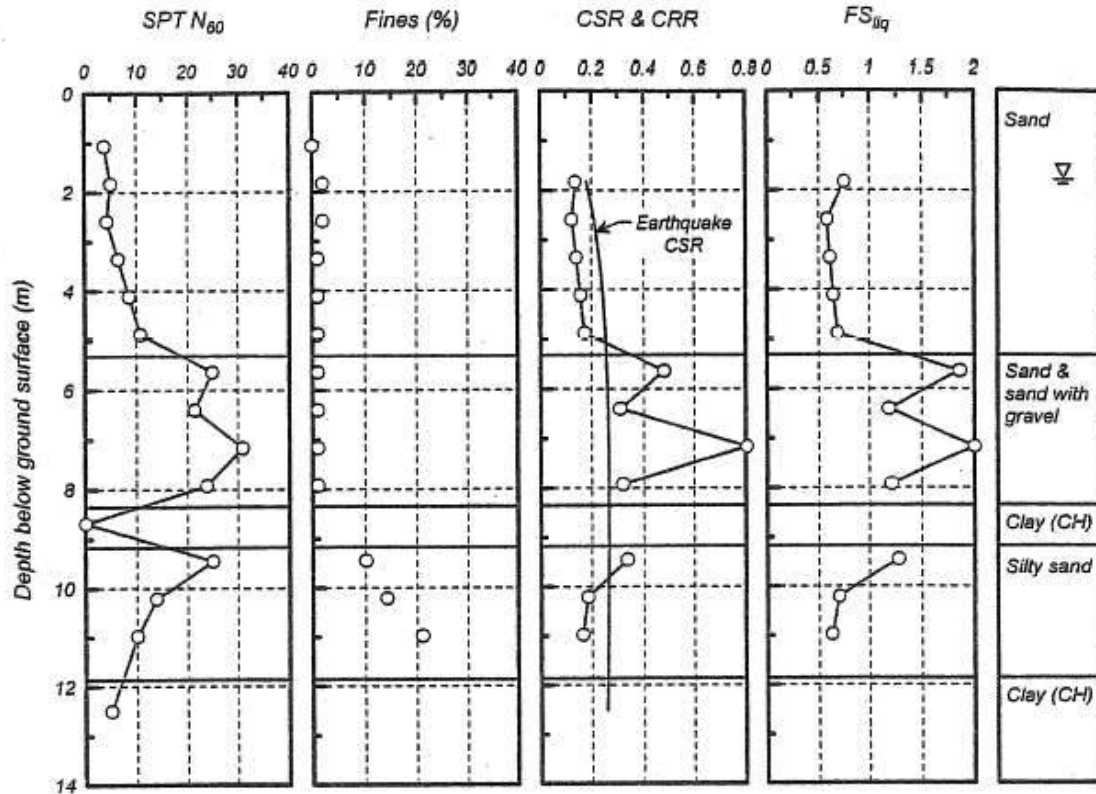


Figure 6-19 Example of a Liquefaction Triggering Analysis for a Single SPT Boring (Idriss and Boulanger, 2008)

6.3.5 Use of Site-Specific response Analyses

For important projects, the use of site-specific equivalent linear or nonlinear one-dimensional site response analyses may be warranted to assess the liquefaction potential at a site. These types of analyses were discussed in Chapter 5. The most common approach to site-specific site response analysis for liquefaction evaluation is to use an equivalent linear total stress analysis, e.g. a SHAKE analysis, to

determine the maximum earthquake-induced shearing stresses at depth, τ_{\max} , for use with the simplified procedure described above, in lieu of using Equation 6-16. Note that, as suggested by Equation 6-16, τ_{\max} from a site-specific analysis should be multiplied by a factor of 0.65 to obtain τ_{av} for calculating representative values of CSR for comparison with CRR values. An alternative numerical modeling approach involves the use of nonlinear effective stress site response analyses to directly determine developed pore water pressures, as discussed in Chapter 5.

As discussed in Chapter 3, numerical analyses of site response should never be based upon a single ground motion time history. A minimum of three time histories should be used in any site response analysis and if only three time histories are used the maximum response is to be used in the analysis. However, if at least seven time histories are used the average response from the analyses may be used in the liquefaction analyses. Furthermore, in general, as ground shaking levels increase to values greater than about 0.4 g or where maximum shearing strain amplitudes exceed 1 to 2 percent equivalent linear analyses become suspect due to the accumulation of non-linear effects in the soil response. For these cases, nonlinear effective stress site response analysis should be considered. Non-linear effective stress analysis of site response is discussed in Chapter 5. In the discussion of non-linear analysis in Chapter 5, it was recommended that analyses conducted for the purpose of evaluating the effect of pore pressure generation on the acceleration response spectrum also consider pore pressure dissipation to mitigate the potential for an unconservative result with respect to the resulting response spectra. However, in evaluating liquefaction potential, it is recommended to ignore pore pressure dissipation during the earthquake, as this is the more conservative approach.

6.4 LIQUEFACTION INDUCED GROUND DEFORMATIONS

6.4.1 Post Liquefaction Residual Strength

Perhaps the most serious consequence of liquefaction occurs when the post-liquefaction residual undrained shear strength of the soil is insufficient to maintain stability of a slope or supported embankment under the post-earthquake static load. In this case a flow slide will occur, leading to uncontrolled large deformations that will continue until the deformed geometry is statically stable. Therefore, establishing the post-earthquake residual shear strength of a liquefied soil is an important factor in liquefaction analysis.

As discussed in Chapter 4, empirical approaches for estimating values of the in situ undrained post liquefaction residual strength, S_r , have been developed by back-analyses of liquefaction induced flow slides. As discussed in Chapter 4, the two approaches currently used in practice today are the Idriss and Boulanger (2007) approach based upon SPT blow count and the Olsen and Johnson approach (2008) based on either SPT blow count or CPT tip resistance.

One question that arises in evaluating the post liquefaction residual strength is whether residual strengths mobilized during limited deformation lateral spreading displacements are consistent with residual shear strengths mobilized in flow slides. This concern due in part to the observation that in cyclic laboratory tests apparent low residual strength values in a liquefied soil may be arrested at larger strains due to dilation. However, it can be argued that most of the “ratcheting” incremental permanent deformations that lead to the accumulation of displacement during a lateral spread will occur during the time residual strength is mobilized. Olsen and Johnson (2008) back analyzed 39 well documented liquefaction induced lateral spreading case histories in terms of a mobilized undrained residual strength ratio S_r / σ_v' using the Newmark sliding block method. Based on analysis results, they found that the back calculated mobilized strength ratios from these lateral spreading cases essentially coincided with the strength ratios back calculated from flow failures.

6.4.2 Flow Failures

Flow failures are the most catastrophic form of ground failure that may be triggered when liquefaction occurs. Large translational or rotational flow failures are produced when the average static (gravity) shearing stresses on potential failure surfaces exceed the average residual strength of the liquefied soil.

To assess the potential for flow failure, the static strength properties of the soil in liquefied layer are replaced with the residual strength (S_r) of the liquefied soil and a conventional limit equilibrium static slope stability analysis is conducted. No seismic coefficient is used during this evaluation, thus representing conditions after completion of earthquake shaking. The resulting C/D ratio defines the potential for flow failures. If the C/D ratio is less than 1.0, a lateral flow failure is predicted.

The estimation of the displacements associated with a lateral flow failure cannot be easily made. The deformations can be on the order of tens of feet, depending on the geometry of the flowing ground and the types and layering of the soil. In the absence of the reliable methods for predicting deformations, it is usually necessary to assume that the soil will undergo unlimited deformations. If the loads imposed by

these deformations exceed those that can be tolerated by a structure, some type of ground remediation will likely be required. This situation should be brought to the attention of the owner and a strategy for dealing with the flow problem agreed upon.

6.4.3 Lateral Spreading Displacement Evaluations

The vulnerability of highway bridges to earthquake-induced ground failures arising from liquefaction has been clearly demonstrated by the extensive damage observed in past earthquakes. This damage has often been associated with translational slides and related embankment deformations due to progressive but limited lateral spreading deformations of the order of feet, driven by earthquake ground shaking subsequent to liquefaction, with deformations ceasing at the end of the earthquake. Damage modes associated with such lateral deformations are related to displacement demands on abutments and piers leading to possible pile damage and/or span collapse. Representative damage in the 1964 Alaska and Niigata earthquakes and the 1991 Costa Rica earthquake has been documented by Youd (1993). Damage of the 1995 Kobe earthquake is described by Tokimatsu and Asaka (1998). Specific examples of lateral spreading pile damage are provided in Chapter 7.

The evaluation of the mode and magnitude of liquefaction induced lateral ground deformations involves considerable uncertainty and is the subject of on-going research. Therefore, geotechnical specialist must stay apprised of recent developments in this area. The current state of the practice for evaluating lateral spreading displacements employs the Newmark sliding block approach on an assumed dominant failure plane at the base of a liquefied zone. The liquefaction-induced displacements are defined by the estimated lateral displacement on this dominant failure surface, as shown in Figure 6-20. In this type of analysis, the yield acceleration of the slide mass is evaluated using the post-earthquake undrained residual shear strength of the soil and then the lateral displacement is calculated using this yield acceleration in a conventional Newmark analysis (Newmark analysis was discussed previously in this chapter).

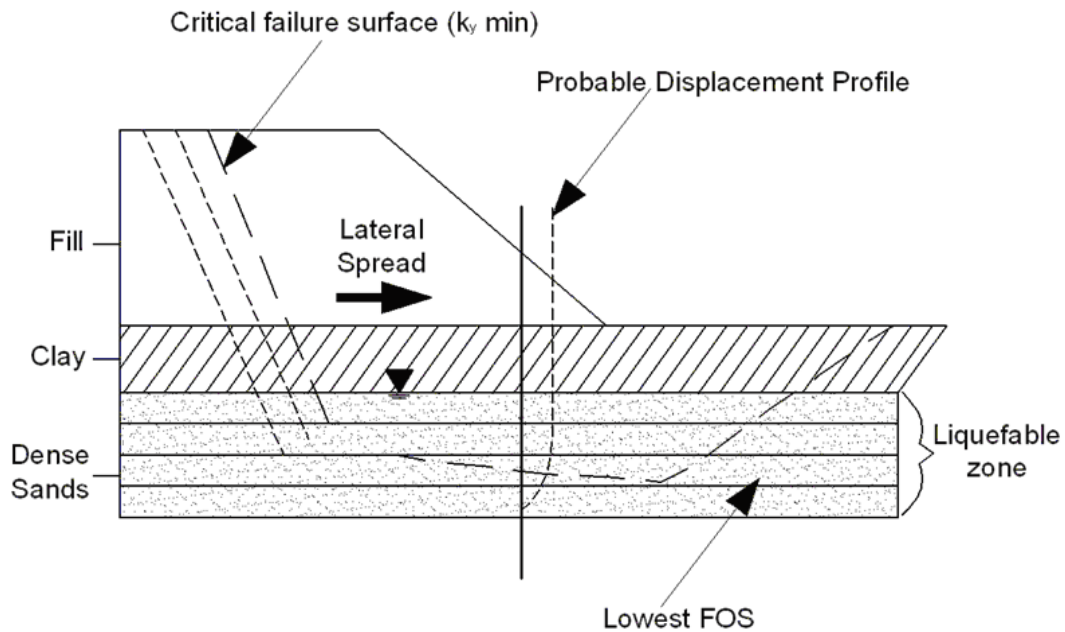


Figure 6-20 Newmark Sliding Block Analysis in Liquefied Soil (NCHRP 12-49, 2003)

Despite the limitations of applying the Newmark method to calculate the deformations induced by liquefaction-induced lateral spreading (e.g. assumptions of a constant yield acceleration based on the residual strength, a concentrated sliding surface, and a rigid sliding block), it provides a consistent and simple framework for analysis. Further, because lateral spreading occurs at relatively shallow depths and due to the base isolation effect created by relatively low undrained residual shear strengths, the dynamic effects within the sliding mass are likely to be minimal and can be neglected. Hence the Newmark displacement relationships described in Section 6.2.2 may be used directly (without slope height adjustments to k_{max}) to calculate lateral spread displacement values.

6.5 SOIL SETTLEMENT HAZARD

6.5.1 Settlement of Unsaturated Cohesionless Soils

Observations in past earthquakes have indicated that earthquake induced ground shaking can induce significant settlement in dry or unsaturated cohesionless soil deposits. In the 1971 San Fernando earthquake for example, settlements of 4 to 6 inches were reported under a building on spread footings on a 40 ft. deep sand fill (Seed and Silver, 1972). Laboratory tests to study the settlement of dry sands under

cyclic loading were first initiated by Silver and Seed (1971) and led to the widely used design procedure developed by Tokimatsu and Seed (1987). This procedure is reproduced below as a series of steps.

- Step 1: From borings and soundings, in situ testing and laboratory index tests, develop a detailed understanding of the project site subsurface conditions, including stratigraphy, layer geometry, material properties and their variability, and the areal extent of potential problem zones. Establish the zones to be analyzed and develop idealized, representative sections amenable to analysis. The subsurface data used to develop the representative sections should include normalized standardized SPT blow counts, $(N_1)_{60}$ (or results of some other test, e.g., the CPT from which $(N_1)_{60}$ can be inferred) and the unit weight of the soil.
- Step 2: Evaluate the total vertical stress, σ_v and the mean normal total stress, $\sigma_m \approx 0.65 \cdot \sigma_v$, at several layers within the deposit at the time of exploration and for design. The design values should include stresses resulting from highway facility construction. Outside of the highway facility footprint, the exploration and design values are generally the same.
- Step 3: Evaluate the stress reduction factor, r_d , using one of the approaches presented in Section 6.3.3.
- Step 4: Evaluate the normalized effective stress using $\gamma_{\text{eff}}(G_{\text{eff}}/G_{\text{max}}$ the Tokimatsu and Seed (1987) equation:

$$\gamma_{\text{eff}}\left(\frac{G_{\text{eff}}}{G_{\text{max}}}\right) = \left(\frac{0.65 \cdot \alpha_{\text{max}} \cdot \sigma_v \cdot \gamma_d}{g \cdot G_{\text{max}}} \right) \quad 6-17$$

where $\gamma_{\text{eff}}(G_{\text{eff}}/G_{\text{max}})$ is a hypothetical effective shear stress factor. Note that G_{max} can be evaluated from the shear wave velocity (V_s) and the mass density (ρ) of the soil (i.e. $G_{\text{max}} = \rho \cdot V_s^2$). Alternatively, G_{max} (in kPa) can be evaluated from one of the correlations in Chapter 4.

For unsaturated sand, σ'_m can be based upon an estimated value of the lateral earth pressure coefficient, K_o . However, for most practical purposes, the approximation $\sigma'_m = 0.65 \sigma'_v$ (which assumes $K_o = 0.475$) will suffice.

- Step 5: Evaluate γ_{eff} as a function of σ'_m and $\gamma_{\text{eff}}(G_{\text{eff}}/G_{\text{max}})$ using the chart reproduced in Figure 6-21.
- Step 6: Assuming that $\gamma_{\text{eff}} \approx \gamma_c$, where γ_c is the cyclic shear strain, evaluate the volumetric strain due to compaction, ε_c , as a function of γ_c and $(N_1)_{60}$ for an earthquake of magnitude 7.5 (15 cycles) using the chart reproduced in Figure 6-22.
- Step 7: Correct for earthquake (moment) magnitude other than M_w 7.5 using the correction factors reproduced in Table 6-3.
- Step 8: Multiply the volumetric strain due to compaction for each layer by two to correct for the multidirectional shaking effect, as recommended by Tokimatsu and Seed (1987), to get the representative volumetric strain for each layer.
- Step 9: Calculate seismic settlements of each layer by multiplying the layer thickness by the representative volumetric strain evaluated in Step 8. Sum up the layer settlements to obtain the total seismic settlement for the analyzed profile.

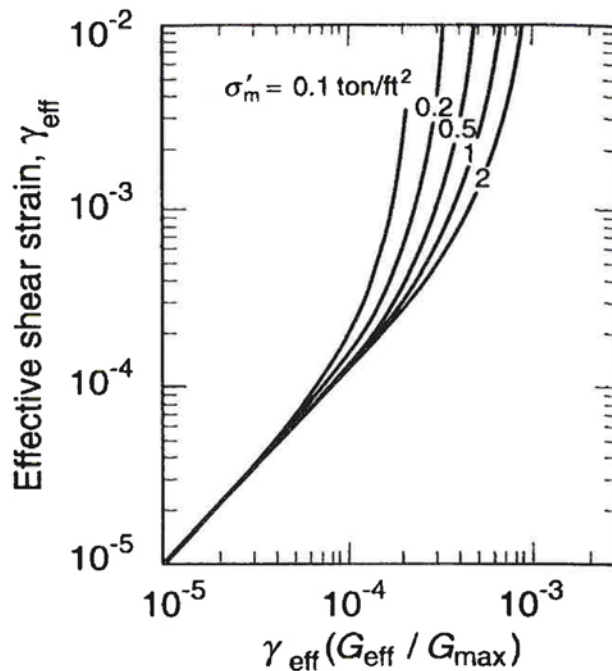


Figure 6-21 Plot for Determination of Earthquake-induced Shear Strain in Sand Deposits (Tokimatsu and Seed, 1987)

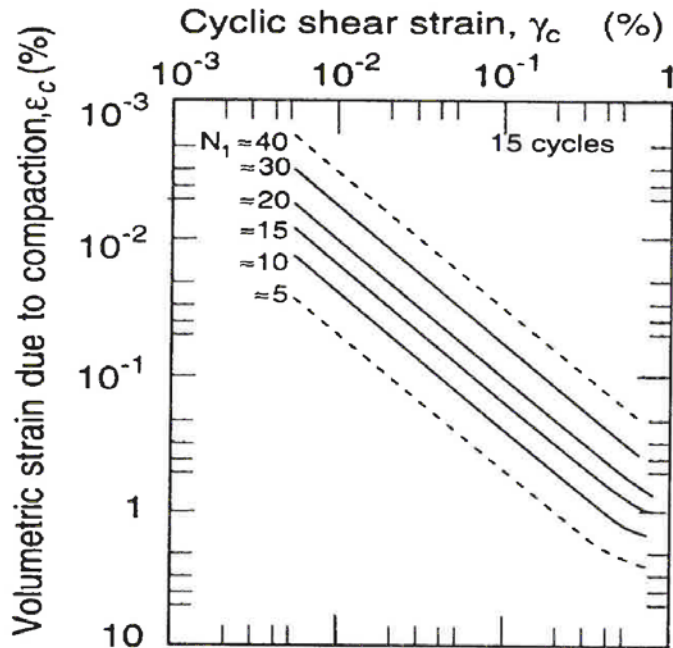


Figure 6-22 Relationship between Volumetric Strain, Cyclic Shear Strain, and Penetration Resistance for Unsaturated Sands (Tokimatsu and Seed, 1987)

TABLE 6-3 INFLUENCE OF EARTHQUAKE MAGNITUDE ON VOLUMETRIC STRAIN RATIO FOR DRY SANDS (after Tokimatsu and Seed, 1987)

Earthquake Magnitude	Number of Representative Cycles at $0.65 \tau_{\max}$	Volumetric Strain Ratio $\varepsilon_{C,N} / \varepsilon_{C,N} = 15$
8.5	26	1.25
7.5	15	1.0
6.75	10	0.85
6.0	5	0.6
5.25	2-3	0.4

Seed and Silver (1972) computed the settlement in a 50-ft thick deposit of sand with a relative density of 45%, which was subjected to a maximum surface acceleration of 0.45 g. They concluded that the computed settlement of 2.5 in. was in fairly good agreement with the observed settlement during the 1971 San Fernando earthquake. The same soil profile has been evaluated using the simplified method above. The results of the analysis are shown in Table 6-4, and the results are compared with those by Seed and Silver (1972) in Figure 6-23. It may be noted that the strain distribution determined by the approximate

method is in good agreement with the values computed by Seed and Silver and that the settlement estimated by the simplified procedure is in reasonable accordance with that determined previously.

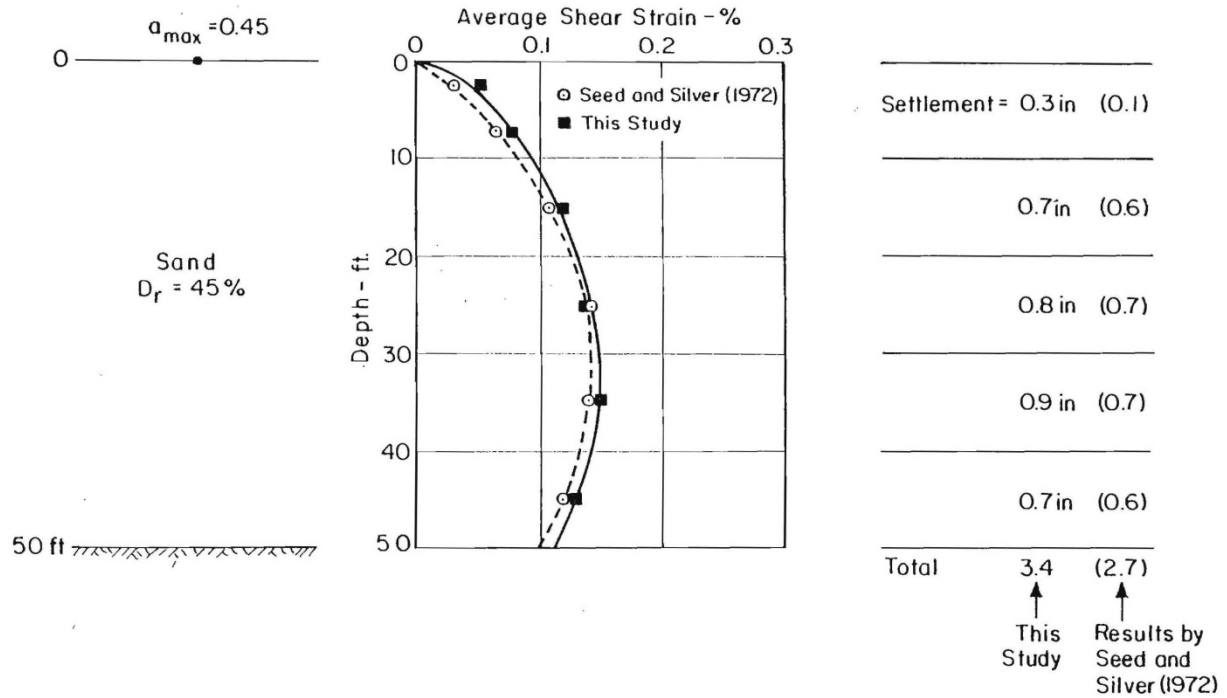


Figure 6-23 Computation of Settlement for 50-ft Deep Sand Layer (Seed and Silver, 1972)

TABLE 6-4 COMPUTATION OF SETTLEMENT FOR DEPOSIT OF DRY SAND

Layer number (1)	Thickness (ft) (2)	$\sigma_p = \sigma'_p$ (psf) (3)	D_r (%) (4)	N_1 (5)	G_{max}^a (ksf) (6)	γ_{eff} (G_{eff}/G_{max}) (7)	γ_{eff} (8)	$\epsilon_{C,M=7.5}$ (%) (9)	$\epsilon_{C,M=6.6}^b$ (%) (10)	$2\epsilon_{C,M=6.6}^c$ (%) (11)	Settlement (in) (12)
1	5	240	45	9	520	1.3×10^{-4}	5×10^{-4}	0.14	0.11	0.22	0.13
2	5	714	45	9	900	2.3	8	0.23	0.18	0.36	0.22
3	10	1,425	45	9	1,270	3.2	12	0.35	0.28	0.56	0.67
4	10	2,375	45	9	1,630	4	14	0.4	0.32	0.64	0.77
5	10	3,325	45	9	1,930	4.5	15	0.45	0.36	0.72	0.86
6	10	4,275	45	9	2,190	4.6	13	0.38	0.3	0.6	0.72
Total											3.37

^a $G_{max} = K_2 \cdot 1,000(\sigma'_m)^{\frac{1}{2}} = 20N_1^{\frac{1}{3}}(\sigma'_m)^{\frac{1}{2}} \times 1,000$

^b $\epsilon_{C,M=6.6}/\epsilon_{C,M=7.5}=8.0$

^cMultidirectional effect

6.5.2 Post Earthquake Settlement of Liquefied Soils

Another consequence of earthquake induced liquefaction is the subsequent post earthquake dissipation of excess pore-water pressures, leading to settlement. Based on experimental studies, Tokimatsu and Seed (1987) developed a simple chart based procedure for estimating post liquefaction settlement at level ground sites. The Tokimatsu and Seed (1987) chart for a magnitude 7.5 earthquake is shown in Figure 6-24. The volumetric strains corresponding to the blow counts $(N_1)_{60}$ and cyclic stress ratios (CSR) for each liquefied layer should be multiplied by layer thickness to estimate settlement. Note that these settlement estimates are valid for level-ground sites that have no potential for lateral spreading. For lateral spreading sites, settlement estimates are likely to be larger than those for level ground sites.

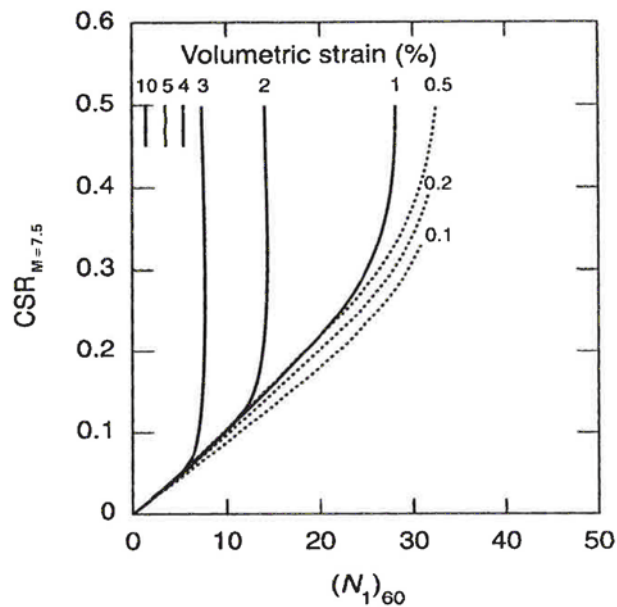


Figure 6-24 Curves for Estimation of Post-liquefaction Volumetric Strain Using SPT Data and Cyclic Stress Ratio for M_w 7.5 Earthquakes (Tokimatsu and Seed, 1987)

During the 1995 Kobe (Hyogoken-Nanbu) earthquake, total settlements in liquefied soils in the range of 0.5m to 0.7m were observed. However, in the case of these observations, the differential settlements were small as evidenced from the limited cracks in the paved areas (Bardet et al., 1997). Similar observations made during the 1994 Northridge earthquake suggest that the differential settlements due to pore pressure increases are only a fraction of the total settlement. Except for liquefaction occurrences with lateral spreading, the observed liquefaction-induced settlements during the Northridge earthquake were less than those observed in Kobe. In various observations in the San Fernando Valley, particularly

in the Woodland Hills area, the ground settlements were found to be relatively uniform. This phenomenon may be attributable to the following conditions: (1) presence of deep alluvial sediments; (2) relatively horizontal layering; (3) significant fines content in the soils.

Based on the above observations, it can be concluded that the differential settlements at level-ground sites with natural soils are expected to be small even if the total settlement is large compared to the total settlement for conditions that typically exist in Southern California. However, in the absence of extensive site investigation, it is suggested that the minimum differential settlement on the order of one-half of the total settlement be used in the design. The actual differential settlement value used is dependent upon factors such as the type of structure, bearing elevation of the foundation, subsurface conditions (relatively uniform versus highly variable laterally), number of borings/CPTs, etc.

6.6 SURFACE FAULT RUPTURE HAZARD

6.6.1 Fault Types and Field Identification

Surface fault rupture refers to the ground displacements that occur along an active fault trace when movement on the fault extends to the ground surface, or to the depth of a bridge foundation. Displacements can range from inches to tens of feet, depending on the magnitude of the earthquake. Because surface fault displacements tend to occur abruptly, often across a narrow zone, fault rupture can be very damaging to a bridge, particularly if it occurs directly below the structure. It is also difficult and often cost-prohibitive to mitigate. In the central and eastern United States, east of the Rocky Mountains, very few active faults with surface traces have been identified and the hazard of surface fault rupture is generally low in comparison to the western United States.

Surface fault ruptures generally are expected to occur along existing traces of active faults. Therefore, it can be assumed that a significant hazard of surface fault rupture does not exist if it can be established that either:

- There is no evidence of a fault trace traversing the bridge site, or
- If a fault trace does cross the bridge site but it has been established that the fault is not an active fault. Faults are generally considered to be active faults with a significant potential for future

earthquakes and displacements if they have experienced displacement during the past approximately 11,000 years (Holocene time).

Hazard screening for fault rupture should involve, as a minimum, the following steps:

- 1) Review of geologic maps as well as discussions with geologists in government agencies who are knowledgeable about the geology of the area, and
- 2) Site reconnaissance and review of aerial photographs, looking for geomorphic expression of faulting. If there is uncertainty in the fault location or its activity, the screening criteria should be applied conservatively.

If a surface fault rupture hazard cannot be screened out, the owner may decide to accept the risk or evaluate the hazard and consequences in detail. If detailed evaluations are carried out, they should be oriented toward:

- 1) Establishing the fault or fault zone location relative to a bridge site if it is not clearly established in the screening stage,
- 2) Establishing the activity of the fault if it traverses a bridge, and
- 3) Evaluating fault rupture characteristics; i.e., amount of fault displacement, width of zone of displacement, and distribution of slip across the zone for horizontal and vertical components of displacement. A probabilistic assessment of the likelihood of different magnitudes of fault displacement during the life of the bridge may also be useful in decision-making.

After a site has been evaluated by the screening criteria presented above and either there is insufficient information to rule out a surface fault rupture hazard or there is seismic, geomorphic, and/or geologic data that suggests an active fault(s) might be present at or near the site, the following information is required to define the fault rupture hazard:

- 1) The location of fault traces (if any) with respect to the site.
- 2) The timing of most recent slip activity on the fault.
- 3) The ground rupture characteristics for a design earthquake on the fault (e.g. type of faulting from Figure 6-25), amount of slip and distribution into strike-slip and dip-slip components, and width of the zone of ground deformation.

Survey (USGS), U.S. Department of Agriculture (Natural Resources Conservation Service), Bureau of Land Management, and the Forest Service. The USGS maintains the repository for federal photographic resources at its EROS Data Center, Sioux Falls, South Dakota 57198.

2) Contacting Knowledgeable Geologists

Geologists and other earth scientists familiar with geologic and tectonic conditions in the site vicinity may be willing to share their knowledge. These geologists might work for governmental agencies (federal, state, and local), teach and conduct research at nearby colleges and universities, or practice as consultants.

3) Ground Reconnaissance of Site and Vicinity

A walk-down of the site and its vicinity should be conducted to observe unusual topographic conditions and evaluate any geologic relationships visible in cuts, channels, or other exposures. Features requiring a field assessment might have been previously identified during the geologic and topographic map review, aerial photography interpretation, and/or during conversations with geologists.

4) Surface Exploration

Faults obscured by overburden soils, site grading, and/or structures can potentially be located by one or more techniques. Geophysical techniques such as seismic refraction surveying provide a remote means of identifying the location of steps in a buried bedrock surface and the juxtaposition of earth materials with different elastic properties. Geophysical surveys require specialized equipment and expertise, and their results may sometimes be difficult to interpret. Trenching investigations are commonly used to expose subsurface conditions to a depth of 4.5 to 6 m. While expensive, trenches have the potential to locate faults precisely and provide exposures for assessing their slip geometry and slip history. Borings can also be used to assess the nature of subsurface materials and to identify discontinuities in material type or elevation that might indicate the presence of faults.

If it is determined that faults pass beneath the site, it is essential to assess their activity by determining the timing of the most recent slip(s) as discussed below. If it is determined, based on the procedures outlined below, that the faults are not active faults, further assessments are not required.

1) Assess Fault Relationship to Young Deposits/Surfaces

The most definitive assessment of the recent history of fault slip can be made in natural or artificial exposures of the fault where it is in contact with earth materials and/or surfaces of Quaternary age (last 1.8 million years). Candidate deposits might include native soils, glacial sediments like till and loess, alluvium, colluvium, beach and dune sands, and other poorly consolidated surficial materials. Quaternary age surfaces might include marine, lake, and stream terraces, and other erosional and depositional surfaces. A variety of age-dating techniques, including radiocarbon analysis and soil profile development, can be used to estimate the timing of the most recent fault slip.

2) Evaluate Local Seismicity

If stratigraphic data are not available for assessment of fault activity, historical seismicity patterns might provide useful information. Maps and up-to-date plots depicting historical seismicity surrounding the site and vicinity can be obtained from the USGS at its National Earthquake Information Center in Golden, Colorado. Additional seismicity information may be obtained from state geologic agencies and from colleges and universities that maintain a network of seismographs (e.g. California Institute of Technology, University of California, Berkeley, University of Nevada, Reno, University of Washington, and the Multidisciplinary Center for Earthquake Engineering Research, Buffalo, New York). If the fault(s) that pass beneath the site are spatially associated with historical seismicity, and particularly if the seismicity and fault trends are coincident, the faults should probably be considered active.

3) Evaluate Structural Relationships

In the absence of both stratigraphic and seismological data, an assessment of the geometric/structural relationships between faults at the site and faults of known activity in the region could be useful. Although less definitive than the two prior criteria, the probability that the site fault is active increases if it is structurally associated with another active fault, and if it is favorably oriented relative to stresses in the current tectonic environment.

6.6.2 Fault Rupture Characteristics and Displacement Estimates

If the fault activity evaluation indicates one or more active faults are present beneath the site, the characteristics of future slip on the faults must be estimated. Several methods can be used to estimate the size of future displacements. These methods include:

- 1) Observations of the amount of displacement during past surface-faulting earthquakes.
- 2) Empirical relationships between fault displacement and earthquake magnitude or fault rupture length.
- 3) Calculated values based on the assumed recurrence rate for earthquakes along the fault and cumulative fault displacement over a long period of time encompassing numerous fault ruptures (i.e. fault slip rate).

The most reliable displacement assessments are based on the displacement in past events. Observations of historical surface ruptures and geologic evidence of paleoseismic events provide the most useful indication of the location, nature, and size of the future events. Where the geologic conditions do not permit a direct assessment of the size of past fault ruptures, the amount of displacement must be estimated using indirect methods. Empirical relations between displacement and earthquake magnitude based on historical surface-faulting earthquakes (e.g. Wells and Coppersmith, 1994) provide a convenient means for assessing the amount of fault displacement. An example of such a relationship is shown in Figure 6-26.

In Figure 6-26, the maximum displacement along the length of a fault rupture is correlated with earthquake magnitude. Maximum displacement typically occurs along a very limited section of the fault rupture length. Relationships are also available for the average displacement along the rupture length. Data from well-documented historical earthquakes indicate that the ratio of the average displacement to the maximum displacement ranges between 0.2 and 0.8 and averages 0.5 (Wells and Coppersmith, 1994). Other methods for calculating the average size of past displacements include dividing the cumulative displacement by the number of events that produced the displacement, and multiplying the geologic slip rate by the recurrence interval.

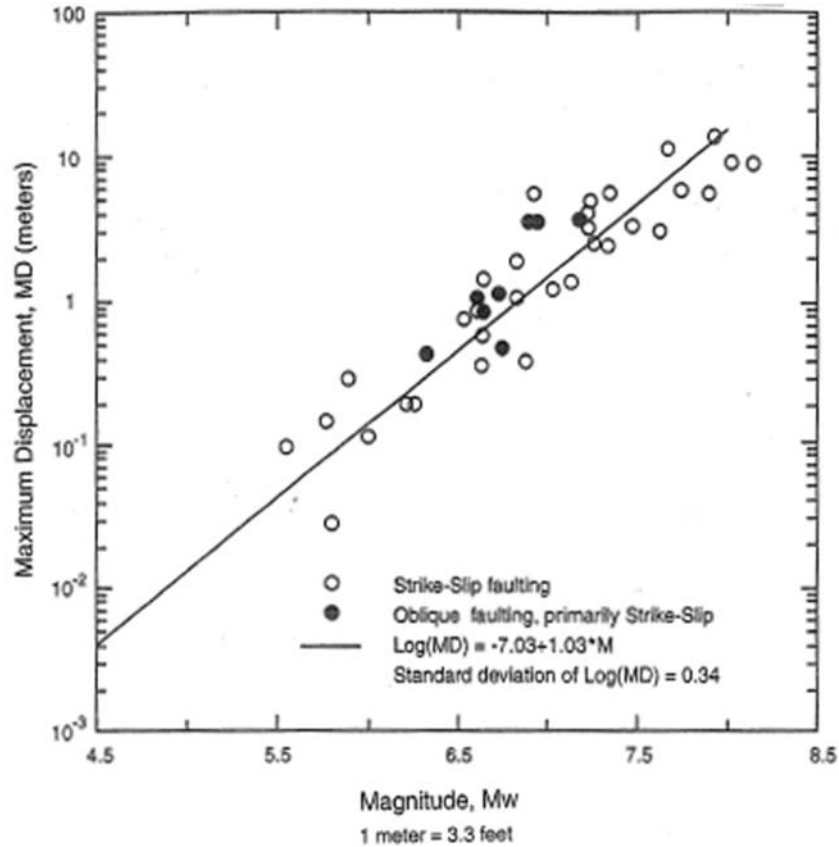


Figure 6-26 Relationship between Maximum Surface Fault Displacement and Earthquake Moment Magnitude for Strike-Slip Faulting (after Wells and Coppersmith, 1994)

Predicting the width of the zone and the distribution of slip across the zone of surface deformation associated with a surface faulting event is more difficult than predicting the total displacement. The best means for assessing the width of faulting is site-specific trenching that crosses the entire zone. Historical records indicate that the width of the zone of deformation is highly variable along the length of a fault. No empirical relationships having general applicability have been developed that relate the size of the earthquake or the amount of displacement on the primary fault trace to the width of the zone or to the amount of secondary deformation. The historical record indicates, and fault modeling shows that the width of the zone of deformation and the amount of secondary deformation tend to vary as a function of the dip of the fault and the sense of slip. Steeply dipping faults, such as vertical strike-slip faults, tend to have narrower zones of surface deformation than shallow-dipping faults. For dipping faults, the zone of deformation is generally much wider on the hanging wall side than on the foot wall side. Low-angle reverse faults (thrust faults) tend to have the widest zones of deformation.

Probabilistic methods for assessing the hazard of fault rupture have been developed that are similar to the probabilistic seismic hazard analysis (PSHA) methods used to assess earthquake ground motions (e.g. Coppersmith and Youngs, 1990, 2000). A PSHA for fault rupture defines the likelihood that various amounts of displacement will be exceeded at a site during a specified time period. For critical bridges, such analyses could be considered to assess whether the likelihood of surface fault rupture is high enough to warrant design for hazard and to aid in quantifying design values of displacement.

6.7 SUMMARY

This chapter presents an overview of geotechnical seismic hazards related to slope stability, liquefaction, seismic settlement and fault rupture. In the case of slope stability hazards, both pseudo-static limit equilibrium and displacement based slope stability are described for both soil and rock slopes. Development of the seismic coefficient for pseudo-static analyses is discussed in light on recent findings from the NCHRP 12-70 project. Newmark displacement based stability analyses are presented in the form of displacement design equations, which have been developed using the results of parametric time history analyses.

Liquefaction hazard or the potential for seismically generated pore pressure leading to reduced soil shear strength, slope failures and associated ground deformations, is discussed in detail. Laboratory and site investigation methods to determine the liquefaction strength of site soils (including SPT and CPT methods) are discussed leading to empirical evaluation procedures commonly used to determine the potential for triggering liquefaction. Screening approaches to assess the need for such evaluations in regions of low seismicity are also described. Liquefaction induced ground deformations are a significant source of damage in earthquakes. The various methods for the determination of post liquefaction residual undrained strength are reviewed.

The potential for post liquefaction flow failure under static loads is addressed along with a discussion of earthquake induced lateral spreading displacement. Both empirical and numerical methods for determining lateral spreading displacement potential are reviewed with particular emphasis on Newmark sliding block approaches. The soil settlement hazard includes both the post-liquefaction settlement of saturated cohesionless soil and the settlement of unsaturated cohesionless soil subject to seismic loading. Emphasis is placed on the commonly used Tokimatsu and Seed analysis approach for evaluating these

settlements. The final section of the Chapter briefly reviews fault types and field identification approaches, together with rupture characteristics and estimates of fault displacement.

The methods for analyzing the slope stability, liquefaction, and seismic settlement hazards presented in this chapter provide the basis for Chapter 7, Geotechnical Design of Earthwork Features, including discussions on performance based design concepts for slopes and embankments. The liquefaction hazard evaluation techniques for lateral spread deformations and post liquefaction settlement provide the basis for the discussion on mitigation measures in Chapter 7. The liquefaction hazard concepts will also be an issue in discussions on Shallow Foundation and Deep Foundation design presented in Chapters 10 and 11, respectively.

CHAPTER 7

GEOTECHNICAL DESIGN OF EARTHWORK FEATURES

7.1 GENERAL

This chapter describes the seismic analysis and geotechnical design of earthwork features associated with transportation systems. These features include embankment fills supporting a roadway or for a bridge approach and natural or cut slopes associated with a highway or bridge, including very gentle slopes of just a few degrees that may be subject to lateral spreading or flow failure in earthquakes. Evaluation of the performance of these features when subject to strong ground motions, including overall stability and permanent seismic deformation including liquefaction induced deformations, is discussed in this chapter. Permanent seismic displacement analyses including slope deformation, lateral spreading, and seismic settlement are presented. Performance based design criteria are discussed for each type of analysis, together with mitigation measures.

Section 7.2 presents selected case histories of earthquake induced landslides and slope or embankment deformations that have resulted in extensive damage to highway systems in past earthquakes. These case histories are presented to illustrate typical earthquake-induced damage modes and the need for seismic design. The case histories highlight the need for displacement (or performance) based design methods that address the development of unacceptable slope deformations in unstable slopes.

Section 7.3 describes performance based design criteria for the two most commonly used seismic slope stability design procedures (pseudo static limit equilibrium analysis and displacement based design) for both constructed embankments and natural or cut slopes. Screening criteria to identify when slopes designed using accepted static analysis procedures do not require seismic design checks are also presented. Strategies for establishing owner-approved criteria for acceptable seismic displacements of slopes and embankments are described based on the NCHRP 12-70 study (NCHRP 2008).

Section 7.4 summarizes mitigation measures that may be employed where a slope stability evaluation (for both soil and rock slopes) does not meet established seismic performance criteria. Methods described include the use of toe buttress structures, piles, ground anchors, and retaining structures. Lastly, Section 7.5 addresses performance based design concepts related to liquefaction induced embankment lateral spreading deformations and lateral spreading interaction with pile foundations. Design procedures for

accommodating lateral spreading effects are discussed. Liquefaction mitigation ground improvement techniques that can be employed when the liquefaction hazard is unacceptable are presented. Ground improvement techniques discussed in this section include densification methods such as dynamic compaction and stone column installation and deep soil mixing methods that are finding increasing application in the United States.

7.2 SEISMIC PERFORMANCE OF SLOPES AND EMBANKMENTS

Earthquake induced slope instability in the form of slope or embankment fill deformations and liquefaction induced deformations or lateral spreading have caused extensive damage to highways in past earthquakes. This section describes selected case histories of slope instability to illustrate damage modes and associated displacement potential. The case histories are divided into three groups (1.) natural slopes, (2.) embankment fills and (3.) liquefaction induced deformations and lateral spreads. These case histories illustrate that, from a highway geotechnical design standpoint, the potential for such instability needs to be evaluated when assessing the seismic design of cut slopes, embankments, and approach fills. The two seismic stability design procedures most commonly used in practice, pseudo static limit equilibrium and displacement based design, were introduced in Chapter 6 and are discussed more detail in Section 7.3.

7.2.1 Natural Slopes

Ground instability in major earthquakes is often characterized by significant landslides or rockfalls in natural slopes. The instability can take the form of catastrophic ground displacements (for slopes with marginal static stability or where strain softening leads to low residual strength as in the case of ancient landslides) or limited ground movements (of the order of inches) that are still potentially disruptive to associated highways or bridge foundations. Selected illustrative case histories of ground instability in earthquakes are described in the subsequent paragraphs of this section.

In the 1989 Loma Prieta Earthquake in California (Mw 7.1), over 1000 landslides and rockfalls were documented in the Santa Cruz Mountains (EERI 1990). Many of the landslides were associated with reactivation of old landslides (USGS 1998b), including the Ditullio landslide shown in Figure 7-1. The Ditullio landslide had a cumulative displacement of the order of about 20 in. As described in Section 7.3, Newmark displacement analyses may be applied to evaluate the potential for such displacements.

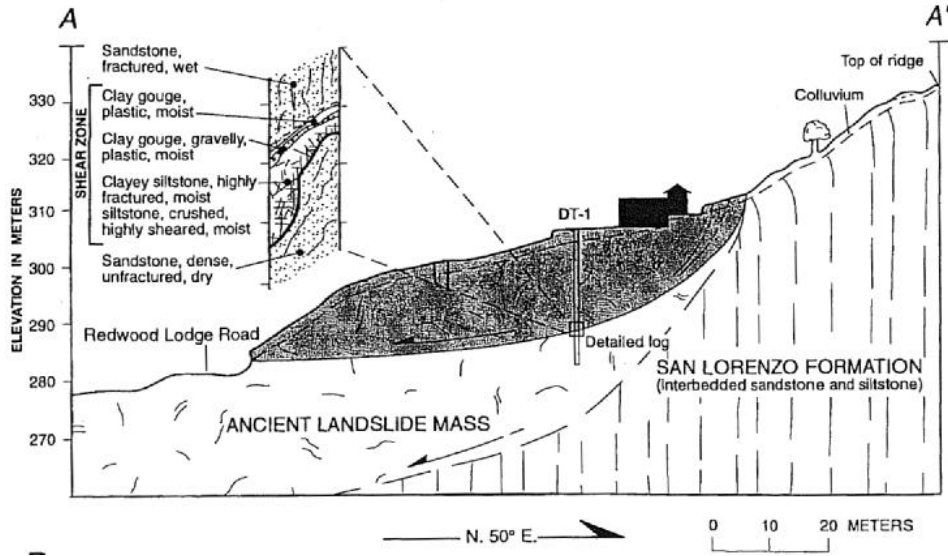


Figure 7-1 Ditullio Landslide, Loma Prieta Earthquake (after USGS, 1998c)

An example of a rockfall during the same earthquake is shown in Figure 7-2. This rockfall occurred on State Highway 17 in the Santa Cruz Mountains.



Figure 7-2 Route 17 landslide, Loma Prieta Earthquake (after USGS, 1998a)

Similar rockfalls closed the Rt 17 highway, the primary transportation corridor from the San Francisco Bay area into the epicentral region of the earthquake, for 12 miles over a period of 32 days (USGS 1998a).

Hundreds of landslides were also caused by the 1988 Spitak Earthquake (M_w 6.8) in Armenia, mostly occurring as rockfalls. Figure 7-3 shows a rock slide that occurred in this event along the main road near Spitak. This is an example of a planar failure which occurred along joint sets, striking parallel to and dipping 50° toward the road.

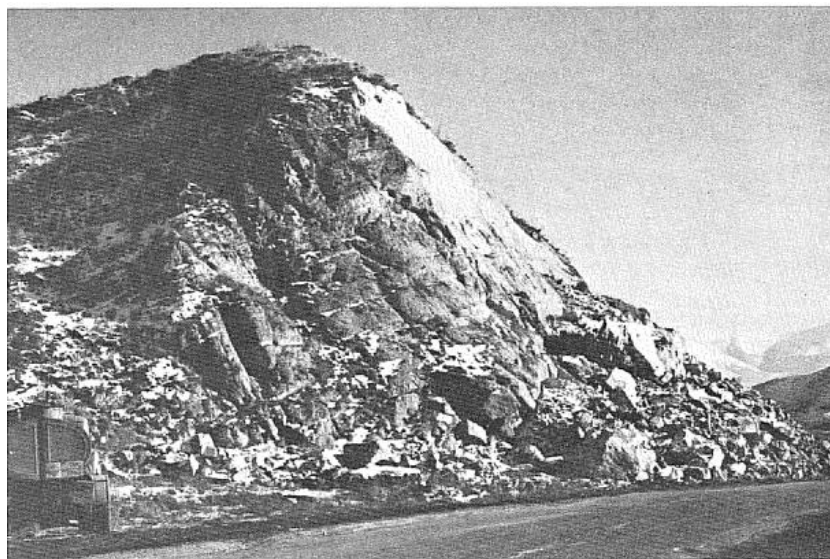


Figure 7-3 Planar Rock Slide in Volcanic Tuff 1989 Armenia Earthquake (after EERI, 1989)



Figure 7-4 Slope Failure with Ground Cracking along Mulholland Drive, 1994 Northridge Earthquake (after EERI, 1995)

7.2.2 Embankment Fills

In the absence of deformation or displacement of foundation soils or poorly compacted embankment materials, even the most intense seismic shaking has not caused significant damage to roads on properly compacted embankment fills. For example, numerous stable Interstate, primary arterial, and secondary roadways were strongly shaken during the 1971 San Fernando, 1989 Loma Prieta and 1994 Northridge earthquake without damage. Damage occurred only at localities susceptible to some form of permanent foundation deformation or displacement or where embankment soils did not meet current standards of practice for compaction. Based on past performance, pavements supported by embankments and foundations not susceptible to ground deformation or failure have also performed well, although some cases of buckling of pavement have been observed in epicentral regions of major earthquakes. Embankment and foundation failure modes that have caused damage to highway pavements are summarized in the FHWA Seismic Retrofitting Manual for Highway Structures (MCEER 2006) and are described below. The special case of embankment fills on liquefiable soils which has resulted in the most significant earthquake-induced damage to highway fills is discussed in Section 7.2.3.

Differential settlements induced by seismic compaction of embankment and/or foundation soils may be disruptive to pavements. The breadth of the zone across which the differential settlement occurs is generally as important to pavement damage as the amount of settlement. Where settlements are small,

uniform, or distributed across wide zones, little damage occurs. Rigid pavements are generally able to bridge areas of small differential settlement and flexible pavements are usually sufficiently ductile to absorb small differential movements without significant damage. Where large differential settlements have occurred across narrow zones, both rigid and flexible pavements have fractured and separated, disrupting traffic operations and requiring repairs.

Seismic compaction of approach fills adjacent to bridge abutments has been a major cause of damaging differential settlement in earthquakes. The stronger and longer the earthquake shaking, the thicker the fill, and the poorer the state of compaction, the greater the amount of seismically-induced differential settlement and pavement damage. Figure 7-5 shows about 600 mm of differential settlement that offset the paved surface and blocked traffic at the easterly approach to Bridge 53-199R during the 1971 San Fernando Earthquake (M_w 6.6). That bridge was part of a connector from northbound I-5 to eastbound I-210 in Sylmar, California. The highway was still under construction at the time of the earthquake. This settlement was caused by seismic compaction and perhaps some lateral spreading of the approach embankment.



Figure 7-5 Differential Settlement Induced by Seismic Compaction at the Easterly Approach to Bridge 53-1991R in I-5 to I-210 Interchange During 1971 San Fernando Earthquake

Backfills placed against bridge abutments have been particularly vulnerable to seismic settlement due to poor compaction. The difficulty in operating mechanized compaction equipment near walls is one reason for the poor compaction at these localities. The rigidity of the abutment wall also tends to concentrate and accentuate differential settlement.

Contacts between cuts and fills are also locations where differential settlements commonly occur. Materials in the cut section are usually more rigid and less compressible than material in the fill. Also, the cut-fill contact may impede the maneuvering of compaction equipment, leaving a poorly compacted section adjacent to the cut-fill line. For example, Figure 7-6 shows pavement disruption due to 100 mm to 200 mm of differential settlement and offset between pavement slabs at a cut-fill contact. This damage occurred on I-5 east of Van Norman Lake and about 1650 ft (500 m) north of the junction of I-5 and I-405 during the 1971 San Fernando Earthquake.

Pavements supported by poorly compacted embankment materials and/or loose or collapsible foundation soils are also vulnerable to large settlements. Such conditions are more likely to occur beneath sections of older highways than under highways built in accordance with modern codes and construction practices.



Figure 7-6 Differential Settlement across Pavement Joints Near Cut-fill Boundary on I-5 north of I-405 Separation. The Settlement is due to Seismic Compaction of Fill during the 1971 San Fernando Earthquake.

7.2.3 Liquefaction Induced Deformations and Lateral Spreading

As described in the FHWA Seismic Retrofitting Manual for Highway Structures (MCEER 2006), liquefaction of soils has been a major cause of highway embankment damage. Liquefaction may lead to a variety of types of ground deformation or ground failure, as discussed below, depending on geometric and soil conditions at the site. The types and amounts of displacement accompanying liquefaction depends on several factors including the height and steepness of embankments, the ground slope, and the depth, thickness and continuity of liquefiable layers. The following descriptions are extracted from the Retrofitting Manual cited above.

Where highways are underlain by low embankments and flat terrain, liquefaction induced ground settlement commonly mimics the thickness of underlying liquefiable layers in the foundation soils.

Figure 7-7 shows a section of Highway 5 south of Oshamanbe, Japan that settled differentially during the 1993 Hokkaido-Nansei-Oki Earthquake (M_w 7.8). In this instance, differential settlement generated waves in the highway that gave the flexible pavement a roller coaster appearance. Differential vertical displacements were as great as 2 ft (0.6 m) between crests and troughs of the induced waves (Youd, 1995).



Kiso-Jiban Consultants Co., Inc., Tokyo, reproduced from Youd et al., 1995

Figure 7-7 Wavy Pavement due to Differential Settlement Enhanced by Liquefaction during the 1993 Hokkaido-Nansei-Oki, Japan Earthquake.

Liquefaction of soils beneath embankments may also lead to penetration of the embankment into the liquefied soil, creating a bearing capacity type of failure as illustrated in Figure 7-8. During penetration, the embankment usually fractures longitudinally and may spread laterally, generating long open fissures oriented roughly along the centerline of the embankment. In some instances, one or both sides of the embankment may subside and rotate forming a rotational slump. For example, Figure 7-9 shows a segment of Highway 36, along the Caribbean coast in eastern Costa Rica that split longitudinally during the 1991 Limon Province Costa Rica Earthquake (M_w 7.5).

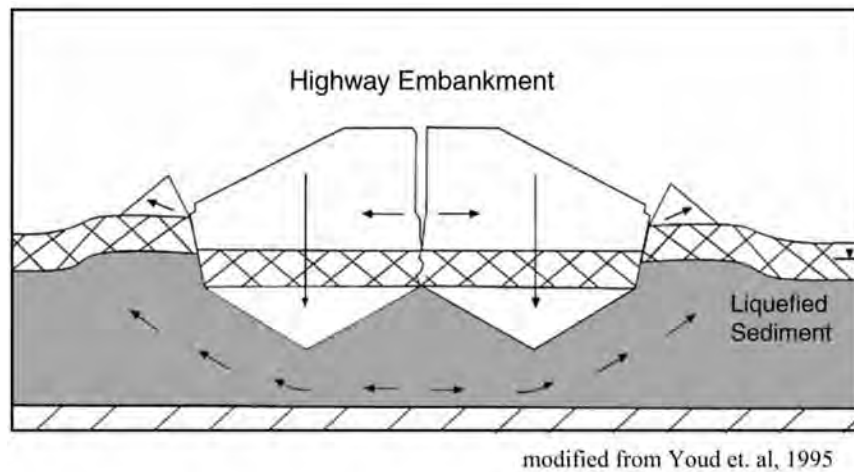


Figure 7-8 Failure Mechanism for an Embankment Founded Upon Liquefied Soil



Figure 7-9 Segment of Highway 36 Near Caribbean Coast in Costa Rica that Split Longitudinally, Settled and Spread Laterally during 1991 Earthquake by Mechanism

Embankment penetration and disruption due to liquefaction of the underlying soil is also illustrated in Figure 7-10 for the Highway 36 approach to the Rio Estrella Bridge in eastern Costa Rica. This approach fill subsided about 6.5 ft (2 m) and spread laterally due to a combination of soil compaction within the embankment, embankment penetration into the liquefied foundation soil, and embankment spreading. These actions severely disrupted the embankment and paved surface. In total, about 30 percent of all highways pavements in the lowlands of eastern Costa Rica were disrupted by the effects of liquefaction, primarily embankment penetration and spreading, during the 1991 earthquake.



Figure 7-10 Disrupted Fill and Pavement due to Liquefaction at the Approach to the Highway 36 bridge Over Rio Estrella, Costa Rica, during 1991 Earthquake.

Where lateral spreading occurs, the surface of the mobilized ground is commonly disturbed by a variety of ground deformation features, including open fissures, differential settlement, scarps, lateral shear zones, and pressure ridges. Structures built over or within lateral spreading zones, including highways, are commonly disrupted and displaced along with the underlying ground. Lateral spreading soil generally moves down gentle slopes or toward a free face such as an incised river channel. Horizontal displacements of laterally spreading soil commonly range up to a few meters in large earthquakes, but where shaking is particularly intense or of long duration and ground conditions are extremely vulnerable larger displacements have occurred. Figure 7-11 shows a section of the Golden State Freeway (I-5) that translated laterally by as much as 6.5 ft (2 m) due to a large lateral spread (called the Juvenile Hall slide) during the 1971 San Fernando Earthquake. Sheared and buckled pavement marked both margins of the failure zone. Between these margins, the highway shifted as much as 6.5 ft (2 m) westward.



Figure 7-11 Rigid pavement on I-5 south of I-5/I-210 interchange that sheared and buckled at two localities during the 1971 San Fernando earthquake due to 6.5 ft (2 m) of lateral spread displacement.

Where a highway is aligned parallel to the direction of lateral spreading movement, lateral spreading usually induces extensional features such as open fissures and pulled apart pavement slabs at the head of the slide and compressional features such as pressure ridges and buckled pavement at the toe. Figure 7-12 shows a section of Highway 36 in Costa Rica that crossed the head of a lateral spread and shifted toward the Rio Viscaya. The spreading movement generated deep open fissures in the ground and overlying highway embankment and pavement. Extensional movement at the head of the spread was compensated for by compression at the toe, beneath the Rio Viscaya Bridge. The displacement beneath the bridge sheared bearings and connections, causing the superstructure to collapse into the river.



M.J.N. Priestly, reproduced from Priestly et al., 1991

Figure 7-12 Extensional Fissures in Flexible Pavement Caused by Lateral Spread of Floodplain Deposits Toward Rio Viscaya during the 1991 Costa Rica Earthquake

Flow failure is the most catastrophic form of ground dislocation associated with liquefaction. Flow failures occur on relatively steep (typically greater than 6 percent) slopes or embankments that are underlain by loose saturated granular materials. Under these adverse conditions, seismic shaking generates large reductions in soil strength within the liquefied layers (causing static factors of safety against slope failure to drop below 1.0 because of the low residual shear strength) and resulting in massive ground displacements deformations. Substantial internal deformation usually occurs within the mobilized soil mass and overlaying structures. Pavements on such failures are nearly always displaced and destroyed. Figure 7-13 shows a flow failure that occurred in a highway fill along the western edge of Lake Merced in San Francisco during the 1957 Daly City, California Earthquake (M_w 5.2). This failure dislodged a section of the highway embankment that flowed into the lake, severing the roadway and blocking traffic.

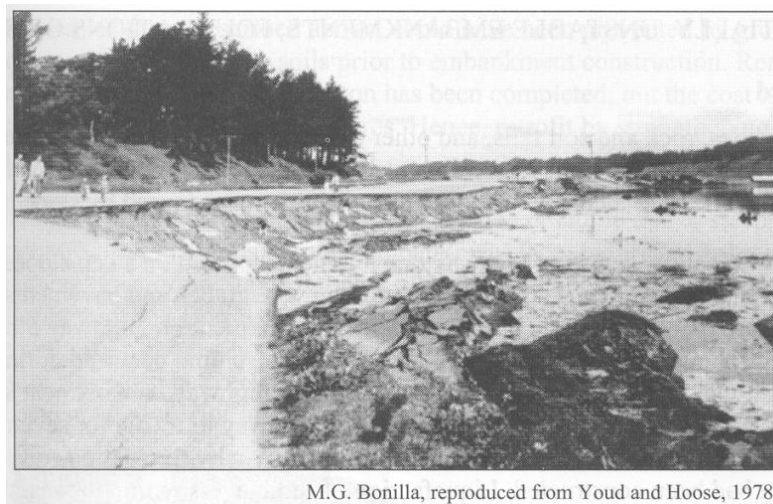


Figure 7-13 Liquefaction-induced Flow Failure of Roadway Embankment into Lake Merced during 1957 Daly City, California Earthquake

The vulnerability of highway bridges to earthquake-induced ground failures arising from liquefaction is clearly evidenced by the extensive damage observed in past earthquakes. Damage has been primarily associated with large translational flow slides and related embankment deformations (when static factors of safety against slope failure drop below 1.0 due to low residual undrained strengths of liquefied soil layers) or progressive but limited lateral spread embankment deformations of the order of feet, driven by earthquake ground shaking subsequent to liquefaction, with deformations ceasing at the end of the earthquake.

Damage modes associated with such lateral deformations are related to displacement demands on abutments and piers leading to possible pile damage and/or span collapse. Representative damage in the 1964 Alaska and Niigata Earthquakes and the 1991 Costa Rica Earthquake has been documented by Youd, (1993). Damage in the 1995 Kobe Earthquake is described by Tokimatsu and Asaka (1998). Specific examples of lateral spread pile damage are described below.

Hamada (1992) summarized the destructive effect of lateral spreading on two bridges during the 1964 Niigata Earthquake in Japan, an event that caused extensive damage due to soil liquefaction. Figure 7-14 illustrates the damage to the abutment and piers of the Yachiyo Bridge. The foundations of the abutments and piers were reinforced concrete piles, 1 ft (30 cm) in diameter and about 33 ft (10 m) in length. Pier No. 2 broke at the ground surface level and displayed a permanent deformation of 1.2 ft (1.1 m) between top and bottom. Once extracted, the piles showed severe damage in locations corresponding to the bottom of the liquefied layer, damage that was clearly caused by the 6.5 – 16.5 ft (2-5 m) of free field lateral spreading toward the river.

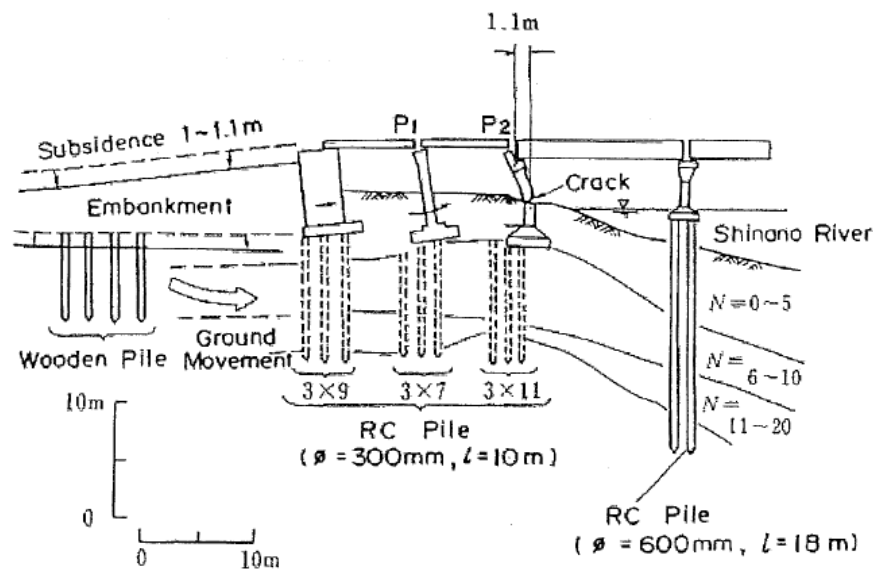


Figure 7-14 Damage to the Abutments and Piers of Yachiyo Bridge on the Left Bank (Hamada, 1992)

Figure 7-15 shows the collapse of the Showa Bridge during the 1964 Niigata Earthquake. Lateral spreading pushed the piers toward the river, causing five simply supported spans to fall off of their seats. The bridge was founded on 2 ft (60 cm) diameter steel piles driven through a 33 ft (10 m) layer of loose to

medium sand and 20 ft (6 m) into an underlying layer of dense fine sand. The 33 ft (10 m) layer is believed to have liquefied from the level of the riverbed down through its full depth. Figure 7-16 schematically illustrates a pile for this bridge that was extracted after the earthquake, evidencing a permanent lateral displacement of approximately 3 ft (1 m) and a maximum curvature close to the depth at which the strata made a transition from loose to medium dense sand.



Figure 7-15 Showa Bridge Collapse (Hamada, 1992)

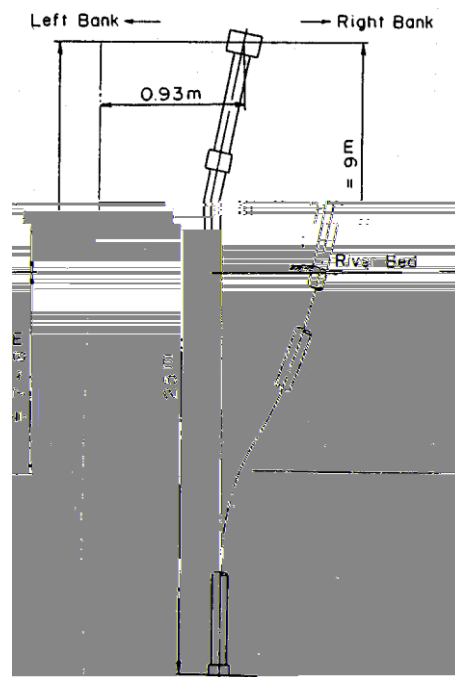


Figure 7-16 Deformation of a Steel Pipe pile for the Showa Bridge (Hamada, 1992)

An important case history of shallow non-liquefied soil layers riding on top of spreading liquefied soils is the lateral spreading that occurred at the site of the Landing Road Bridge during the 1987 M_w 6.3 Edgecumbe (New Zealand) Earthquake, shown in Figure 7-17. A liquefied 13 ft (4 m) thick loose sand layer moved about 6.5 ft (2 m) toward the river, carrying along a non-liquefied 5 ft (1.5 m) thick clayey silt layer. The movement was resisted by the five piers of the on-land spans of the bridge, which consisted on eight 16 in. (400 mm) square battered pre-stressed concrete piles connected by a pile cap and slab pier, as shown in Figure 7-18. After the earthquake, soil was mounded up behind the piers in what was apparently a passive failure. Subsequent trenching found failure surfaces and disturbed failure masses of soil confirming the occurrence of passive failure in the non-liquefied crust as it was driven against the buried piers and pile cap. The passive forces were found to be of the order of 10 times the estimated drag force exerted on the pile group by the liquefied sand (Berrill et al., 1997). Observations from the excavations and back analyses indicated that the piles successfully resisted the passive pressures mobilized against the piers. Cracks in the piles suggested plastic hinges in the piles were on the verge of forming, as shown schematically in Figure 7-19.

In the 1995 Kobe earthquake, field investigations using borehole cameras and slope indicators showed that failures of piles in lateral spreading zones concentrated at the interfaces between liquefied and non-liquefied layers as well as near pile heads. Also lateral pile analyses using p-y interface springs subject to the estimated ground displacement profiles were consistent with observed pile performance in this earthquake, as shown in Figure 7-20 from Tokimatsu and Asaka (1998).

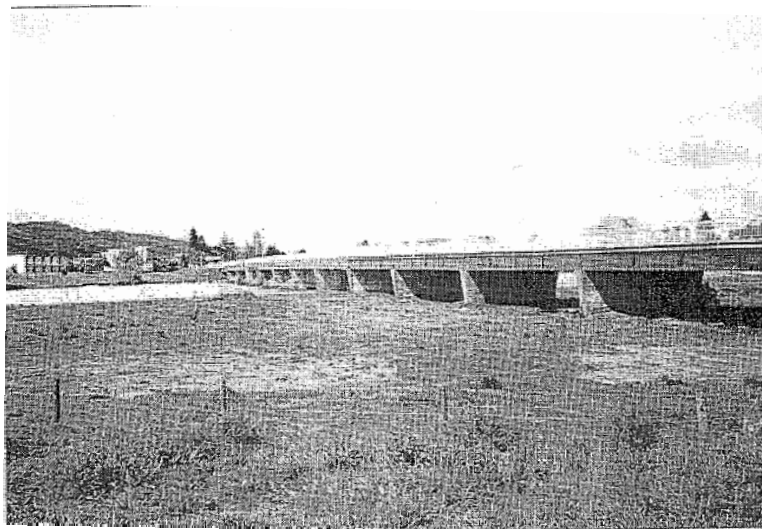


Figure 7-17 Landing Road Bridge, Whakatane, New Zealand (Keenan, 1996)

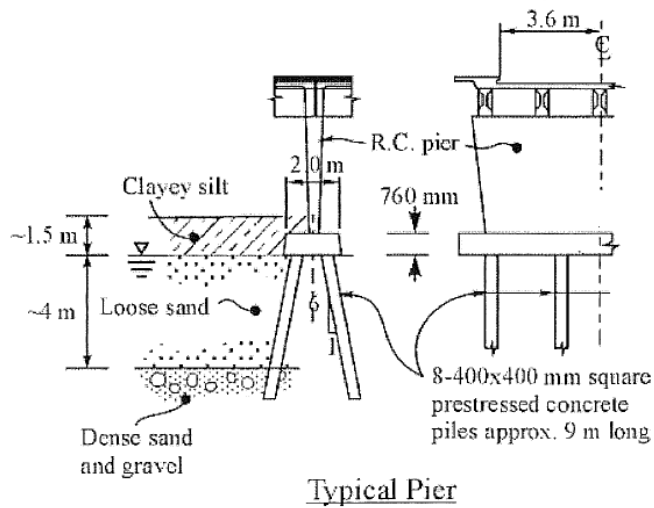


Figure 7-18 Schematic of the Raked-pile Foundation at the Landing Road Bridge (Berrill and Yasuda, 2002)

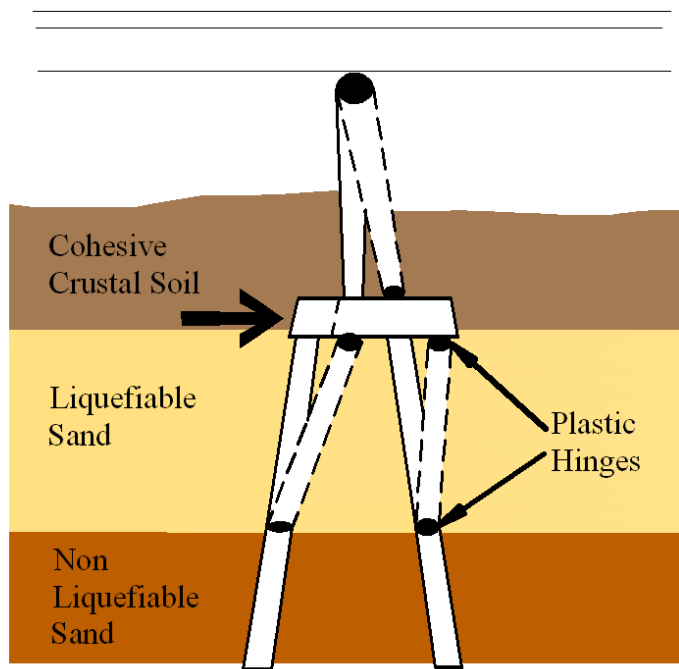


Figure 7-19 Potential Collapse Mechanism for Landing Load Bridge (Keenan, 1996)

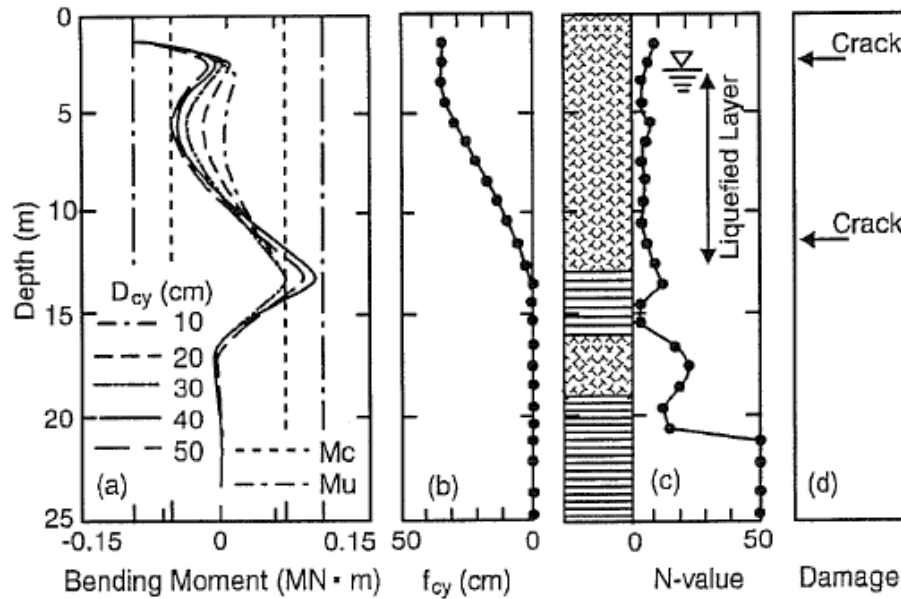


Figure 7-20 Site and Damage Characteristics for a Precast Concrete Pile Subjected to Lateral Spread in the Kobe Earthquake (after Tokimatsu and Asaka, 1998)

The above case histories illustrate important aspects of pile foundation response to lateral spreading. While in some cases the top of the pile foundation displaced laterally a distance similar to that in the free field, in other cases it moved much less due to the lateral stiffness of the foundation and/or constraining effect of the superstructure. Foundations may be exposed to large lateral soil pressures due to lateral spreading, including passive pressures from non-liquefied soil layers riding on top of the liquefied soil. In some cases the soil fails before the foundation, with negligible pile bending distress and small deformation of the piles. In other cases, foundations fail first, experiencing large permanent deformation and rotation. The observed damage and cracking of piles is often concentrated at the upper and lower boundaries of the liquefied soil layer where there is a sudden change in soil properties. More damage tends to occur to piles when the lateral movement is forced by a strong non-liquefied soil.

The above observations are reflected in the simplified design concepts discussed in Section 7.5, wherein the lateral resistance provided by piles and the associated foundations is incorporated into a lateral spreading analysis. These observations are also reflected in the analysis procedures for deep foundations in liquefied soils presented in Chapter 10. Clearly, lateral spreading deformations of the order of several feet can cause significant pile damage. However, analyses described in Section 7.5 suggest damage

related to plastic hinge formation could be acceptable if displacements are less than about 1 ft, depending on pile type or liquefied layer thickness.

7.3 SLOPE STABILITY DESIGN APPROACHES

The two basic analysis methods for evaluating seismic stability of slopes, the pseudo static analysis approach and the displacement based analysis approach, were described in detail in Chapter 6. In this section emphasis is placed on illustrating the displacement based approach and the basis for developing performance based criteria for evaluating slope stability using this approach. Screening criteria to identify situations in regions of low or moderate seismic exposure where seismic analysis would not be required are also presented in this chapter. Strategies for developing performance criteria that depend on the facilities or structures associated with the slope are discussed in detail. Mitigation measures for cases where the calculated seismic displacement exceeds the allowable value are presented in Section 7.4. Design issues related to liquefaction problems are addressed in Section 7.5.

In developing slope stability design approaches, two general classes of slopes need to be considered: constructed or engineered slopes and natural slopes. The general characteristics of these two categories of slopes vary significantly in terms of geometry, material properties, and groundwater conditions. In most cases constructed fill and embankment slopes will be relatively uniform in soil conditions, though the constructed material can vary from sands and gravels to fill that has a high fines content (that is, cohesive soil). Furthermore, the groundwater level will generally be below the base of the fill or embankment. On the other hand natural slopes, including soil slopes and jointed or weathered rock slopes, will usually be highly variable (e.g. with layers in soil slopes that range from gravels to clays) and often groundwater will be located within the slope.

7.3.1 Constructed Fill Slopes and Embankments

Fill and embankment slopes generally will be constructed from an imported material. Depending on the geographic area, the imported materials can be predominantly sands or gravels or they can have a high percentage of cohesive soil. These slopes are generally well compacted and will usually exhibit good strength characteristics. Slope angles often will range from 2H:1V (horizontal to vertical) to flatter than 3H:1V. The height of the slope can vary from a few feet to over 50 feet. A common example of these

slopes would be the approach fill used at either end of a bridge. These approach fill slopes are often on the order of 30 feet in height.

Constructed fill and embankment slopes are perhaps the easiest to evaluate from the standpoint that the soil type and density of the fill is generally well defined and therefore determination of material properties is generally straight-forward. If the fill is cohesionless, the friction angle will normally be on the order of 35 degrees or higher. If the fill has appreciable fines content, the compacted shear strength often will be in excess of 2,000 psf. The groundwater location for most of these slopes will be at some distance below the base of the fill. However, the design of these slopes become problematic if the embankment fill is being placed on a soft or liquefiable foundation material. In these cases the determination of the strength of the foundation material under static and seismic loading becomes a key consideration during the analysis, as discussed in Section 7.5 for liquefiable foundation soils.

The geotechnical investigation for an engineered fill will often be limited to investigating the characteristics of the foundation material. Exploration typically is conducted to a depth equal to twice the slope height to define the strength and compressibility of the soil layers upon which the embankment is, or will be, constructed. The geometry and properties of the fill is constrained by right-of-way widths and the cost of importing fill material.

From a seismic design perspective these types of slopes are routinely encountered in design of new roadways or where existing roadways are modified. Performance of well compacted fill or embankment slopes during seismic loading generally has been very good, even when subject to sever earthquake loading (as illustrated in the example below), except where liquefaction of the foundation material occurs.

The following example demonstrates the application of the NCHRP 12-70 (TRB 2008) procedure outlined in Chapter 6 for the seismic design of embankment slopes. The example considers embankments constructed with three slope heights (15, 30 and 45 feet) at two slope angles: 2:1 and 1.5:1 (typical of constructed embankment slopes). The two angles and three slope heights examined as shown on Figure 7-21.

The foundation soil below the embankment fill is assumed to be cohesive soil with a friction angle of 10° and cohesion of 4,000 psf. Therefore, deep failure planes through the foundation material were not a design consideration.

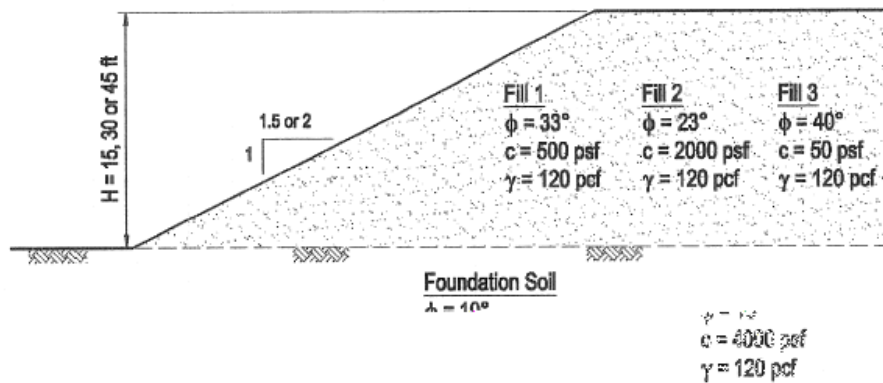


Figure 7-21 Slope Geometry

Three different fill materials were considered in the analysis. The properties for these fills are as follows:

- Fill 1: $\phi = 33^\circ$ and $c = 500 \text{ psf}$ (silty sand borrow)
- Fill 2: $\phi = 23^\circ$ and $c = 2,000 \text{ psf}$ (clayey sand borrow)
- Fill 3: $\phi = 40^\circ$ and $c = 50 \text{ psf}$ (gravel borrow)

The above fill properties represent a range of conditions that can be expected in different areas of the country. In areas with wet climates, the fill would likely be primarily cohesionless and exhibit low cohesion values. Embankment construction in areas with drier climates often will use soils with higher fines content and a higher cohesion value. The effects of the cohesion component of the shear strength (whether it be true cohesion or apparent cohesion due to capillarity acting at the time of the earthquake) are significant during seismic loading. Apparent cohesion due to capillarity may well be part of the reason compacted fill slopes have performed so well during seismic events.

Three sites with different levels of seismic activity were considered in the analysis. Two of the sites are located in the Western United States (WUS), one in the Los Angeles area and the other one in Seattle. The third site is located in Central and Eastern United State region (CEUS), in Charleston, South Carolina. The Peak Ground Acceleration (PGA) for each site was determined in accordance with the AASHTO seismic design specifications for 7.5% probability of being exceeded in 75 years (approximately a 1000 year return period). PGA values were initially determined for bedrock (Soil Type

B) and modified for Site Class D foundation soil. A summary of the site locations and seismicity data for this example is given in Table 7-1.

TABLE 7-1 SITE COORDINATES AND SEISMICITY DATA

Site Coordinates		Region	Soil Type B (Bedrock)		Soil Type D	
Longitude	Latitude		PGA	S_1^1	F_{pga} PGA	$F_v S_1^1$
-117.9750	34.0500	WUS (Los Angeles)	0.60	0.52	0.60	0.78
-122.2500	47.2700	WUS (Seattle)	0.40	0.30	0.46	0.54
-79.2370	33.1000	CEUS (Charleston)	0.20	0.10	0.30	0.24

1. Spectral acceleration coefficient at 1.0 second period

A common commercial limit equilibrium computer program was used in the analyses. Only circular failure planes were examined through the fill. The PGA was adjusted for slope-height effects when the maximum depth of the failure plane below the ground surface was greater than 20 feet (as discussed in Section 6). As the critical circular failure surfaces all were tangential to the underlying foundation soil, the height factor used to adjust the PGA was taken as the slope height H. Based on the NCHRP 12-70 procedure, the seismic acceleration was adjusted using Equation 6-2:

$$k_{av} = \alpha \cdot k_{max}$$

The height correction factor α was calculated from Equation 6-3:

$$\alpha = 1 + 0.01 \cdot H \cdot (0.5 \cdot \beta - 1)$$

where H is the slope height in feet and β is calculated from Equation 6-4:

$$\beta = F_v \cdot S_1^1 / k_{max}$$

where $F_v S_1^1$ is the spectral acceleration coefficient of a period at one second adjusted for site conditions.

A seismic coefficient equal to $k_{av}/2$ was used in pseudo-static seismic slope stability analyses, consistent with an acceptable seismic slope deformation of 1-2 inches, as described in Section 6. The values of k_{av} used in the analyses are shown in Table 7-2.

TABLE 7-2 HEIGHT-ADJUSTED SEISMIC COEFFICIENTS FOR SITE CLASS D, COMPACTED FILL SLOPE EXAMPLE

Longitude	Latitude	Region	$F_{pga}PGA$	$F_V S_1$	β	H [ft]	α	k_{av}
-117.9750	34.0500	WUS (Los Angeles)	0.60	0.78	1.30	15	0.95	0.569
						30	0.90	0.537
						45	0.84	0.506
-122.2500	47.2700	WUS (Seattle)	0.46	0.54	1.16	15	0.94	0.431
						30	0.87	0.402
						45	0.81	0.373
-79.2370	33.1000	CEUS (Charleston)	0.30	0.24	0.80	15	0.91	0.271
						30	0.82	0.244
						45	0.73	0.217

The Newmark displacement correlation equations from the NCHRP 12-70 study were used to estimate the slope movement during seismic loading for those cases where the Capacity to Demand (C/D) ratio (i.e., factor of safety) using a seismic coefficient equal to $k_{av}/2$ was less than 1.0. The seismic slope deformation was estimated from Equation 6-6:

$$\log(d) = -1.51 - 0.74 \cdot \log(k_y / k_{av}) + 3.27 \cdot \log(1 - k_y / k_{av}) - 0.8 \cdot \log(k_{max}) + 1.50 \cdot \log(PGV)$$

where the PGV was estimated as the value at the mean plus one standard deviation, given by $PGV = 55F_V S_1$. The yield acceleration (k_y) for each case was calculated using the limit equilibrium computer program (the yield acceleration is the horizontal seismic coefficient that results in a C/D ratio, or factor of safety, of 1.0). Note that in this manual, use of the mean value of the PGV, given by $PGV = 38F_V S_1$, and not the mean plus one standard deviation value as used in this example, is recommended for consistency with LRFD principles. Use of the mean value for the PGV instead of the mean plus one standard deviation value reduces the calculated displacement value by approximately 30 percent.

The pseudo static C/D ratios for each analysis using $0.5 k_{av}$ are reported in Table 7-3. Yield acceleration values are shown in Table 7-4. Permanent displacements are only expected for cases where k_{av} is larger than the yield acceleration (k_y). As discussed in Chapter 6, the NCHRP 12-70 design approach involves using half the k_{av} value and confirming that the C/D is greater than 1.0, assuming that some amount of deformation (1 to 2 inches) is acceptable. As shown in Table 7-3, the C/D ratios are less than 1.0 only for the steepest slopes and for the higher values of PGA. Newmark displacement estimates were made for these cases.

TABLE 7-3 PSEUDO-STATIC STABILITY ANALYSES CAPACITY TO DEMAND RATIO (FACTOR OF SAFETY) FOR A SEISMIC COEFFICIENT EQUAL TO 0.5 K_{AV} , COMPACTED FILL SLOPE EXAMPLE

Site 1: Soil Type D ($k_{max} = 0.6$)				
Slope Angles [H:V]	Slope Height [ft]	C/D Ratio (Spencer)		
		c = 500 psf / $\phi = 33^\circ$	c = 2000 psf / $\phi = 23^\circ$	c = 500 psf / $\phi = 40^\circ$
2:1	15	2.40	5.59	1.28
	30	1.73	3.31	1.17
	45	1.53	2.55	1.16
1.5:1	15	2.19	5.28	1.09
	30	1.58	3.09	0.98
	45	1.36	2.44	0.94
Site 2: Soil Type D ($k_{max} = 0.46$)				
Slope Angles [H:V]	Slope Height [ft]	C/D Ratio (Spencer)		
		c = 500 psf / $\phi = 33^\circ$	c = 2000 psf / $\phi = 23^\circ$	c = 500 psf / $\phi = 40^\circ$
2:1	15	2.68	6.39	1.43
	30	1.94	3.76	1.32
	45	1.72	2.89	1.31
1.5:1	15	2.43	5.96	1.21
	30	1.75	3.48	1.10
	45	1.50	2.72	1.05
Site 3: Soil Type D ($k_{max} = 0.298$)				
Slope Angles [H:V]	Slope Height [ft]	C/D Ratio (Spencer)		
		c = 500 psf / $\phi = 33^\circ$	c = 2000 psf / $\phi = 23^\circ$	c = 500 psf / $\phi = 40^\circ$
2:1	15	3.10	7.55	1.66
	30	2.26	4.43	1.54
	45	1.99	3.39	1.52
1.5:1	15	2.78	6.91	1.38
	30	1.97	4.01	1.26
	45	1.71	3.14	1.21

TABLE 7-4 YIELD ACCELERATION, K_Y , FOR COMPACTED FILL SLOPE EXAMPLE

Slope Angles [H:V]	Slope Height [ft]	Yield Acceleration		
		c = 500 psf / $\phi = 33^\circ$	c = 2000 psf / $\phi = 23^\circ$	c = 500 psf / $\phi = 40^\circ$
2:1	15	> 0.6	> 0.6	0.44
	30	> 0.6	> 0.6	0.37
	45	0.55	> 0.6	0.34
1.5:1	15	> 0.6	> 0.6	0.34
	30	> 0.6	> 0.6	0.26
	45	0.48	> 0.6	0.22

Results of the analyses are summarized in Table 7-5. These results show that embankments constructed at slopes varying from 2:1 to 1.5:1 using common types of embankment fill will perform very well during ground motions that might be encountered in seismically active areas of southern California, the Pacific Northwest, and the central and southeastern United States. Another conclusion that can be reached from these results is that the level at which seismic analyses are required will be relatively high for engineered slopes as long as some permanent slope displacement is acceptable.

TABLE 7-5 NEWMARK DISPLACEMENTS FOR COMPACTED FILL SLOPE EXAMPLE

Site 1: Soil Type D ($k_{max} = 0.60$)				
Slope Angles [H:V]	Slope Height [ft]	Newmark Displacement [in]		
		$c = 500 \text{ psf} / \phi = 33^\circ$	$c = 2000 \text{ psf} / \phi = 23^\circ$	$c = 500 \text{ psf} / \phi = 40^\circ$
2:1	15	0	0	< 1
	30	0	0	< 1
	45	0	0	< 1
1.5:1	15	0	0	1-2
	30	0	0	4
	45	0	0	6
Site 2: Soil Type D ($k_{max} = 0.46$)				
Slope Angles [H:V]	Slope Height [ft]	Newmark Displacement [in]		
		$c = 500 \text{ psf} / \phi = 33^\circ$	$c = 2000 \text{ psf} / \phi = 23^\circ$	$c = 500 \text{ psf} / \phi = 40^\circ$
2:1	15	0	0	0
	30	0	0	0
	45	0	0	0
1.5:1	15	0	0	< 1
	30	0	0	1
	45	0	0	1
Site 3: Soil Type D ($k_{max} = 0.298$)				
Slope Angles [H:V]	Slope Height [ft]	Newmark Displacement [in]		
		$c = 500 \text{ psf} / \phi = 33^\circ$	$c = 2000 \text{ psf} / \phi = 23^\circ$	$c = 500 \text{ psf} / \phi = 40^\circ$
2:1	15	0	0	0
	30	0	0	0
	45	0	0	0
1.5:1	15	0	0	0
	30	0	0	0
	45	0	0	0

7.3.2 Natural Slopes

Natural slopes present more difficulties than fill slopes because of the wide range of conditions that occur within these slopes, ranging from soil to weathered rocks to jointed rocks. While relatively uniform conditions can sometimes exist within a natural slope, most often a natural slope involves layers of different geologic materials and these materials often change from cohesionless to cohesive in characteristics. Groundwater often is found within the slope, and sometimes the water is intermittently perched on less permeable layers within the slope.

Further complicating the evaluation of a natural soil slope is the geometry. In areas where soils have been overconsolidated from glaciation stable natural slope angles can be steeper than 1H:1V, even where the fines content is minimal. In some areas the natural slopes can be marginally stable in their existing state. In other areas natural slopes that are relatively flat can have thin bedding planes characterized by very low friction angles for long-term loading. Where located adversely to a planned slope cut, the removal of materials buttressing these slopes can initiate large slides under gravity loading and reactivate slides during seismic events

Natural slopes are often the most difficult to characterize in terms of layering and material characteristics. Access to conduct site exploration can be difficult, particularly where steep slopes exist. The variability of natural deposits forming the slope often makes it difficult to locate or adequately model soil layers critical to the evaluation of slope stability, either under gravity or seismic loading.

From a seismic perspective, natural slopes are where most slope failures have been observed. Although there is no single cause of these past seismic failures, many of these failures have occurred where slopes are over steepened, i.e. where the slope is barely stable under gravity loading. The size of the failure can range from small slides of a few yards of soil or rock to movements involving thousands of yards of material. In highly seismic areas of the western US, the potential for seismic instability becomes a key consideration in some areas, particularly where critical lifeline transportation routes pass over mountain terrain.

The displacement-based slope design methodology applied to natural slopes is illustrated by considering the following slope conditions representative of glacial till slopes found in the State of Washington. The example is discussed in more detail in the NCHRP Report 611 (TRB 2008)

The glacial till at the site is primary silty sand with gravels. Blow counts from Standard Penetration Tests (SPTs) are generally very high, indicating a dense condition. With some slopes standing as steep as 1H to 1V, the friction angle of the granular soil could be as high as 45 degrees. However, common practice in the area is to assign the glacial till one of two strengths: (1) $\phi = 42$ degrees and $c = 0$ pounds per square foot, or (2) $\phi = 38$ degrees and $c = 200$ pounds per square foot. A lower bound till strength of $\phi = 36$ degrees and $c = 0$ pounds per square foot has also been used. Natural slope angles in the area ranged from 2H to 1V up to 1H to 1V. The firm-ground (Site Class B) values of PGA, S_s , and S_1 , for the site were determined to be 0.41g, 0.92 g, and 0.30g, respectively, for the 1,000-year return period design earthquake based on the AASHTO seismic hazard maps. Soil conditions at the site were representative of Site Class C. The objective of the seismic stability study was to evaluate the displacements that would be expected for the design earthquake. The owner was also interested in the risk of widening the roadway facility on the slope and therefore stability also was evaluated for a 10 percent probability of exceedance in 50 years (a 475-year event) and for a 2 percent probability of exceedance in 50 years (a 2,475-year event). Each of the common alternatives for the strength of the glacial till was evaluated in the analysis.

A commercially available limit equilibrium computer program was used to determine the static factor of safety and the yield accelerations for the various cases involved in this example. The yield acceleration, site-adjusted PGV, and site-and slope height-adjusted PGA were employed with the equations from Chapter 6 to estimate permanent seismic displacement. The estimated displacements from the analyses are summarized in Table 7-6. The summary indicates that the calculated displacements ranged from zero to a maximum of 44 inches, depending on assumptions made for soil properties and the design earthquake.

7.3.3 Screening Criteria

From the previous examples and based on additional examples from design practice, it is clear that from a displacement based perspective simple screening criteria can be established for slopes not requiring seismic analysis at sites not susceptible to liquefaction or that are not compromised by sensitive soil conditions. The screening criteria in Table 7-7 were established in the NCHRP 12-70 project (NCHRP, 2008). Seismic analysis of a cut or fill is not required if the site adjusted peak ground acceleration coefficient (i.e., F_{pga} PGA) at the ground surface for the site is less than the values listed in Table 7-7, unless allowed or required otherwise by the Owner.

TABLE 7-6 SEISMIC DISPLACEMENT ESTIMATES, NATURAL SLOPE EXAMPLE

Parameter	Slope Angle	Static C/D Ratio	Yield Acceleration k_v	Ground Motion Displacement (inches)		
				7% in 75 Years	10% in 50 Years	2% in 50 Years
Upper Bound Till ($\phi = 42$ degrees)						
Case 1	1H to 1V	0.9	NA	NA	NA	NA
Case 2	1.5H to 1V	1.3	0.13	6-9	3-5	14-18
Case 3	2H to 1V	1.7	0.25	< 1	< 1	3-4
Upper Bound Till ($\phi = 38$ degrees, $c = 200$ psf)						
Case 1	1H to 1V	1.2	0.09	12-19	7-11	26-32
Case 2	1.5H to 1V	1.6	0.26	< 1	0	3
Case 3	2H to 1V	2	0.32	0	0	< 1
Upper Bound Till ($\phi = 36$ degrees)						
Case 1	1H to 1V	0.8	NA	NA	NA	NA
Case 2	1.5H to 1V	1.2	0.07	18-27	11-17	36-44
Case 3	2H to 1V	1.5	0.17	3-5	1-2	8-11

Note: (1) NA indicates no analysis conducted. Static factor of safety was less than 1.0
 (2) Upper bound of range based on 84% confidence interval.

TABLE 7-7 NO SEISMIC ANALYSIS SCREENING CRITERION FOR STABILITY OF SLOPES NOT SUSCEPTIBLE TO LIQUEFACTION

Slope Angle	F_{pga} PGA
3H:1V	0.3
2H:1V	0.2

If liquefiable or sensitive soils exist within or support the slope, the minimum acceptable acceleration without requiring a stability analysis shall be 0.15g, as long as the SPT blow count measured in the field at an efficiency of 60% (N_{60}) is greater than 5 blows per foot (bpf). The slope angle used in screening criteria refers to the average angle of the slope above the retaining wall. If the slope is characterized by a non-uniform slope condition, the average angle of the slope should be used. Linear interpolation can be used when determining the need for a seismic analysis for slopes between those given in the table.

7.3.4 Strategies for Developing Acceptable Displacement

In many practical situations some small-to-moderate amount of permanent displacement is acceptable after the design seismic event. The Specifications and Commentaries prepared for the NCHRP 12-70 Project include provisions that allow for seismically-induced permanent displacements of slopes and embankments. These permanent displacements are generally associated with global stability, where the entire soil mass moves. Small permanent displacements are not likely to be life threatening and can be repaired by removing or placing earth. However, there are locations where even small slope or embankment movements may affect nearby structures or present a risk to public safety. In such cases, even a few inches of movement may not be acceptable.

If permanent movement of the slope is acceptable, there are significant benefits to the Owner:

- The seismic coefficient used in design may be reduced by 50% if 1 to 2 inches of permanent movement are acceptable.
- In many cases the slope or embankment can undergo more than 1-2 inches of displacement and not affect the function of the adjacent roadway, facilities, or public safety. In these cases a reduction in the seismic coefficient of greater than 50% may be acceptable.

Chapter 6 provided a methodology for estimating the amount of deformation in situations where deformations larger than the 1-2 inches associated with the 50% reduction in seismic coefficient are acceptable and where the capacity-to-demand (C/D) ratio does not meet the target of 1.0 with the 50% reduction. Rather than regrading the slope or introducing expensive mitigation measures to achieve a C/D ratio of 1.0 or more, the amount of permanent displacement can be calculated. If the amount of displacement is within reasonable limits, the seismic performance of the slope may be acceptable even though the C/D ratio is less than desired.

An overriding question in any approach that involves permanent deformations is the amount of deformation that is acceptable. Ultimately, that decision belongs to the Owner, who must weigh a number of factors in reaching this decision. Factors that should be considered when deciding on acceptable levels of permanent displacement include the implications of the movement and the likely mode of slope movement. When considering these factors, the Owner should evaluate both the relative consequences of movement and, as appropriate, the cost of designing to avoid the movement.

One of the main factors for deciding on the acceptable level of movement involves the location and function of the slope. The considerations associated with this factor can be summarized as follows:

- Slopes located in urban locations usually can tolerate less movement than slopes located in the countryside. Part of this relates to effects of slope movement on utilities and other nearby facilities, and part relates to aesthetics. After a design seismic event a slope that has moved 24 inches or more in the countryside may be completely functional and acceptable, but this same level of slope deformation may not be acceptable in an urban environment.
- Slopes that support a heavily traveled roadway should usually be designed for smaller displacements than slopes that are part of a less traveled roadway. This relates to loss of function if there is damage associated with slope movement. Generally, less traveled roadways can remain unusable for a longer period of time and, therefore, large amounts of permanent movement are acceptable. On the other hand, damage to roadways with heavy use may result in significant traffic and economic disruption if the roadways are out of service for even a few hours. For this situation it may be very important to limit displacement to levels that will have minimal disruption to service.
- Slopes the movement of which may pose a large risk to public safety should be designed for less movement than slopes the movement of which poses a low risk. Generally, the risk to the public increases as the amount of soil movement increases. The volume and rate of movement can also become considerations in this assessment. If there is a large risk associated with soil-mass movement, then the Owner is obligated to take a more conservative approach to design, which often will mean minimizing acceptable movements.

The type of soil at a site also should be considered when establishing displacement limits. This consideration is related to both the type of failure mechanism and the response of the slope to loads.

- Seismically-induced slope failures in some slopes will be primarily surface sloughing, while other slopes may undergo deep rotational failures. The former type of failure often involves simply a maintenance cleanup, while the latter can involve a significant rebuilding effort. The form of the failure usually is controlled by the types of soil making up the slope – with granular soils being involved in more surficial failures while cohesive soils are more often involved in deeper rotational failures.

- Displacement of slopes that are characterized by brittle soils or soils that decrease in strength with deformation will have a lower acceptable displacement threshold than soils that do not soften with strain. It is usually very hard to estimate how much cyclic strain will result in strength softening during the earthquake, making the prediction of deformations difficult and requiring more conservatism in establishing acceptable displacement limits.
- Finer-grained granular soils (e.g. fine sands) may often have some apparent cohesion due to capillarity. If this apparent cohesion has not been considered in design, it provides an unquantified inherent level of conservatism to the displacement estimates.
- The confidence in displacement predictions for liquefiable soils is often relatively low. If liquefaction is predicted at a slope location, it is generally better to mitigate the liquefaction condition. While it is possible to make estimates of slope displacement using residual strengths, the possibility of performance being different than expected increases for this situation.

Perhaps the easiest consideration to understand is the effects that slope movement will have on other facilities in proximity to the slope. Examples of these effects are summarized below.

- Utilities, sidewalks, and pavements located in front of, within, or behind the slope could be affected by permanent movement of the soil. The amount of displacement of the utility, sidewalk, or pavement can be approximated by the amount of permanent displacement being estimated.
- Slope aesthetics may also be affected by permanent displacements, as noted previously. Generally, as the amount of movement increases, the amount of distortion becomes more noticeable to the public. The slope movement can also alter drainage within the slope and adversely affect the vegetation growing on the slope.

7.3.5 Approach for Defining Acceptable Displacements

As summarized above, there are many factors that must be considered when deciding on the acceptable level of displacement for slopes and embankments. These factors make the development of a simple strategy for establishing the permanent displacement difficult. If displacements of more than 1 to 2 inches are being considered, a rigorous review of the possible consequences of movement of the slope or

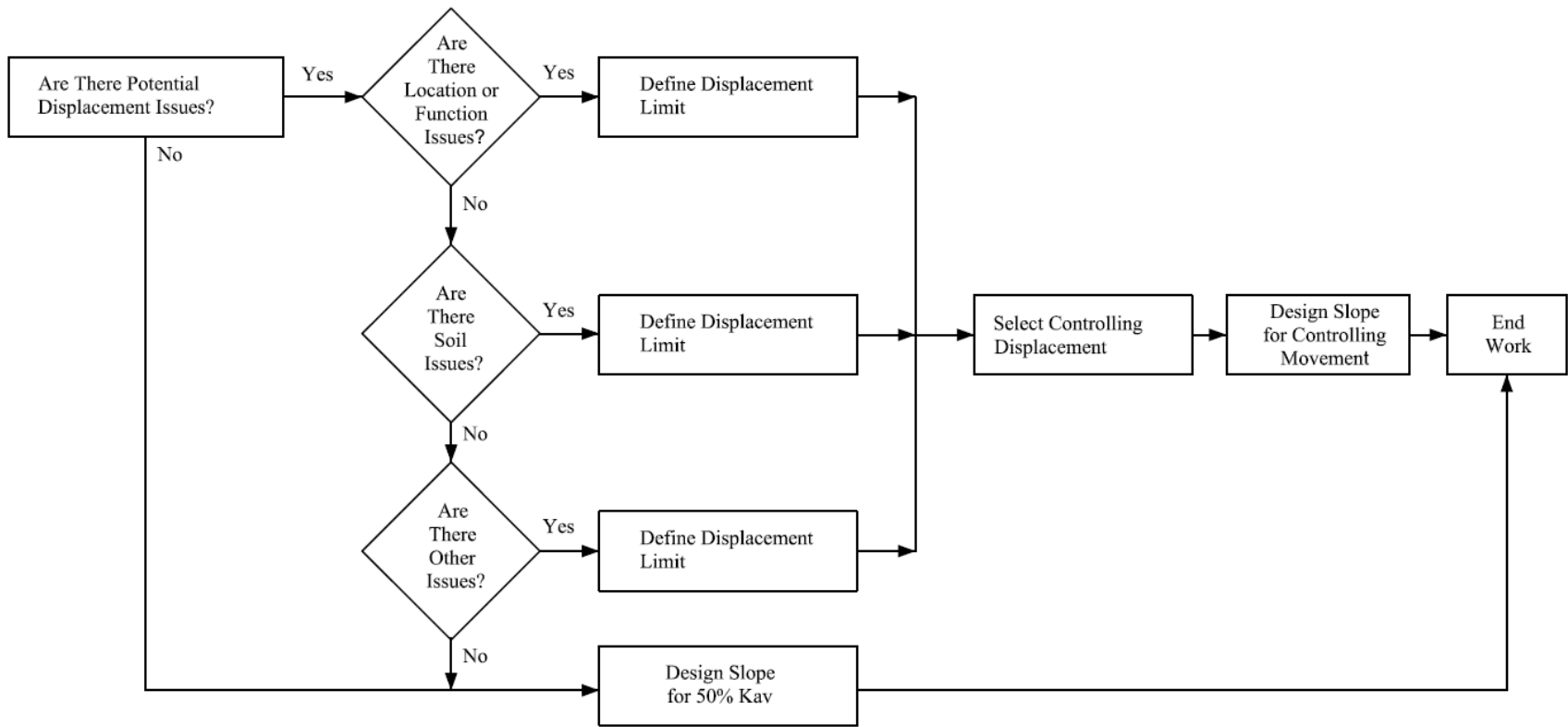


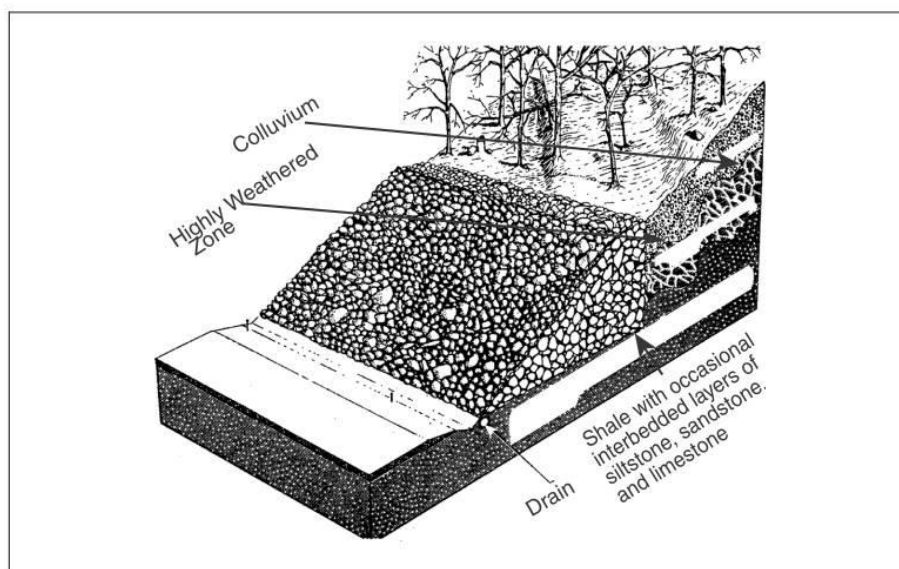
Figure 7-22 Procedure to Establish Acceptable Slope Movement

Drainage of surface water and groundwater is a widely used method for slope stabilization. Proper drainage will both reduce the weight of the sliding mass and increase the strength of the material in the slope. Lightweight backfill materials have been used in embankment construction to reduce driving forces tending to cause instability.

- **Increase in Resisting Forces**

Increasing the resisting forces on a potential or existing landslide can be achieved by applying an external load or a resisting force at the toe of the landslide, or increasing the internal strength of the soils in the failure zone so that the slope would remain stable.

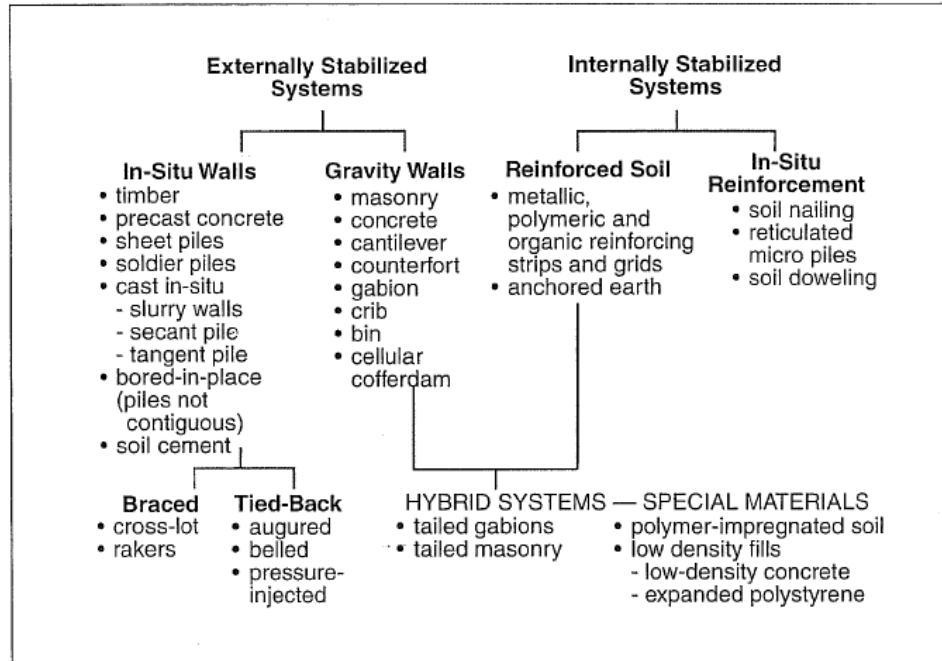
Procedures that have been used to increase the resisting force at the toe of a potential sliding mass include buttress fills and structural retention systems. Buttresses are often constructed of quarry rock, boulders, cobbles, and coarse gravel fill. An example of a rock fill buttress is shown in Figure 7-23. Notice in this figure that a toe drain was installed to further stabilize the slope by facilitating drainage.



Gedney and Weber, 1978

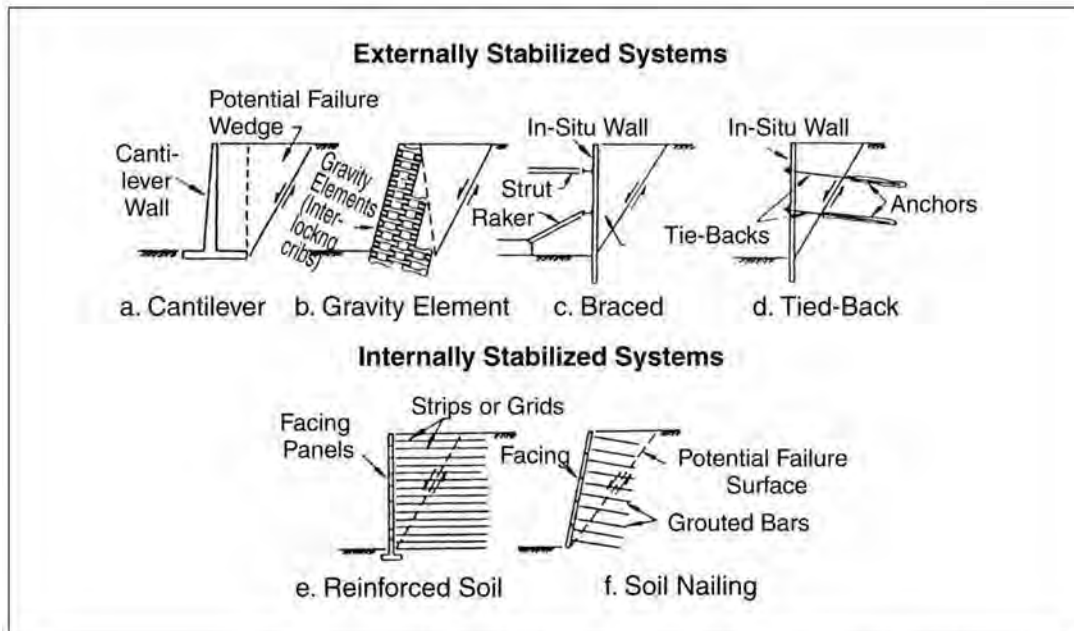
Figure 7-23 Rock Buttress Used to Increase Forces Resisting Slope Failure

In situations where buttress fills are not feasible because of geometry, cost, or space limitations, conventional retaining structures, piles, and mechanically stabilized earth slopes and walls may be used as for stabilization. These methods are summarized in Figure 7-24. The methods are divided into two groups, depending on whether they provide external or internal support. Both types of systems are illustrated in Figure 7-25.



Holtz and Schuster, 1996; modified from O'Rourke and Jones, 1990

Figure 7-24 Classification Scheme for Earth Retention Systems



Holtz and Schuster, 1996; modified from O'Rourke and Jones, 1990

Figure 7-25 Examples of Externally and Internally Stabilized Earth Retention Systems

Techniques that are commonly used to increase the internal strength of potentially unstable soil include subsurface drainage and soil reinforcing systems. Subsurface drainage is used to lower the groundwater table and usually consists of the following procedures: (a) drainage blankets and trenches; (b) drainage wells, galleries, and tunnels; and (c) horizontal and vertical drains. Types of vertical and horizontal drainage methods used in natural slopes are shown in Figure 7-26.

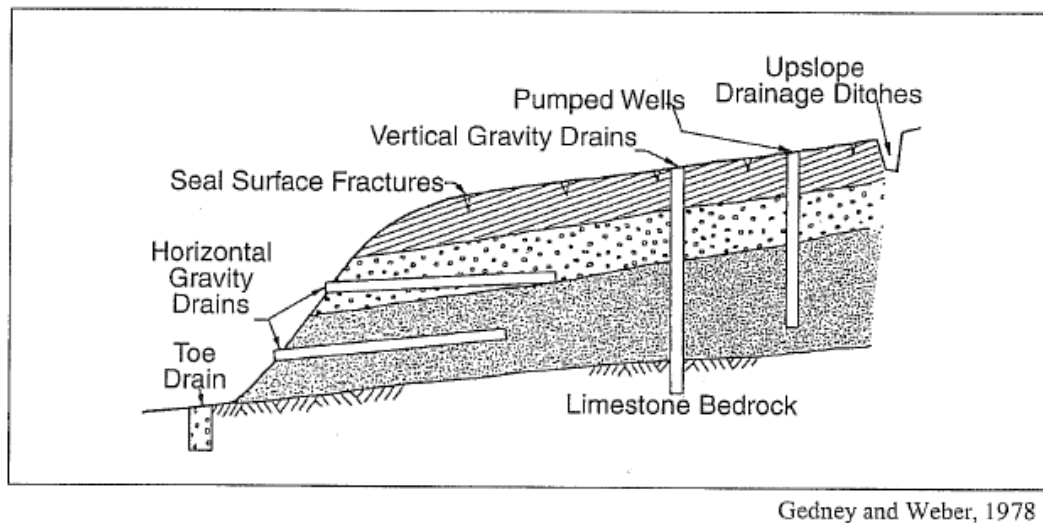


Figure 7-26 Types of Vertical and Horizontal Drains used to Lower the Groundwater in Natural Slopes

Geosynthetic products such as reinforcing geotextile and drainage geocomposites have been used for slope stabilization in several of the situations described above. Geotextiles have also been used as replacements of graded granular filters. Geocomposites are commonly installed for drainage in areas where access is difficult, behind retaining structures, and in other places where interception of seepage is desired.

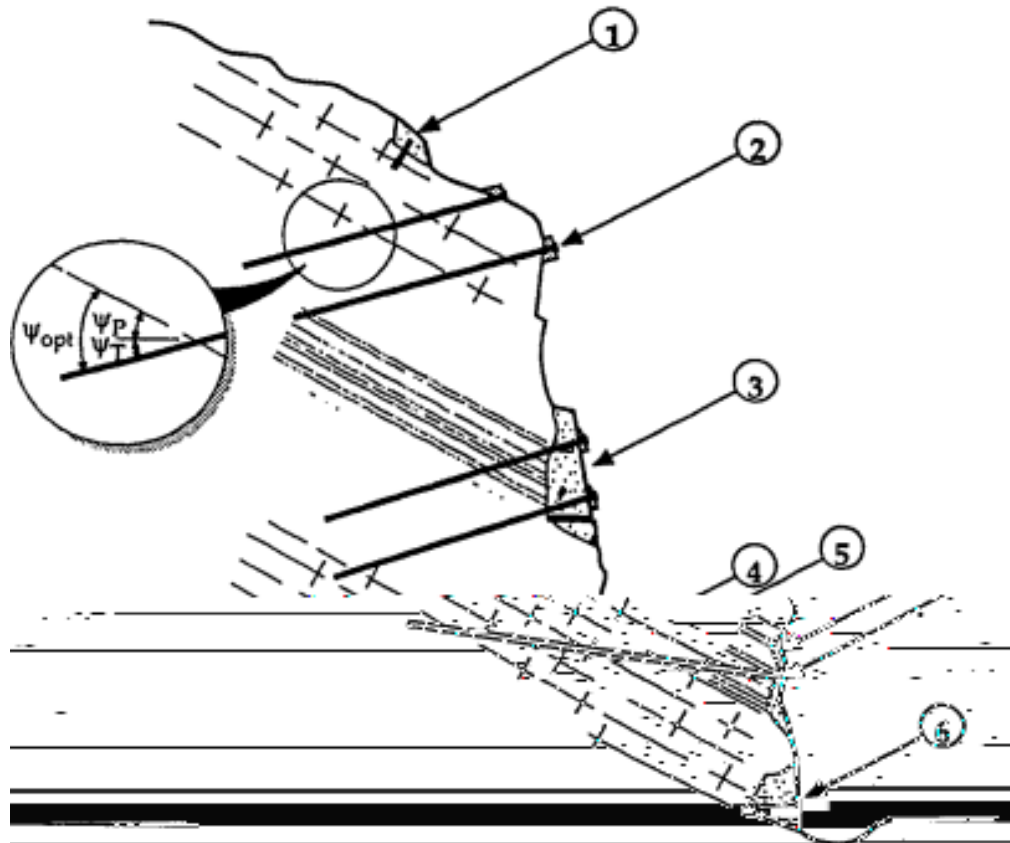
7.4.3 Rock Slopes

Wyllie and Norrish (1996) describe three categories of stabilization and protection of rock slopes: (1) reinforcement; (2) rock removal; and (3) protection. Engineering measures in these three categories are listed in Figure 7-27. Selecting the appropriate stabilization system is dependent on several issues that are usually site-specific. These issues include service life, importance of the highway structure, environmental concerns, construction time, economics and others.

Figure 7-27 Categories of Rock Slope Stabilization Measures (FHWA 1998a)

A number of different techniques are used for rock slope reinforcement. These techniques are shown schematically in Figure 7-28. These methods include reinforced concrete dowels, tensioned rock anchors, tie-back walls to prevent sliding on potential fault zones, shotcrete to prevent raveling of fractured rock, drain holes for reduction of pore pressures; and concrete buttresses to fill rock cavities. Potential rock toppling failures also may be stabilized through rock reinforcement. A feature common to many of these methods is that they minimize the relaxation and loosening of the rock mass that may take place as a result of excavation and/or seismic loading.

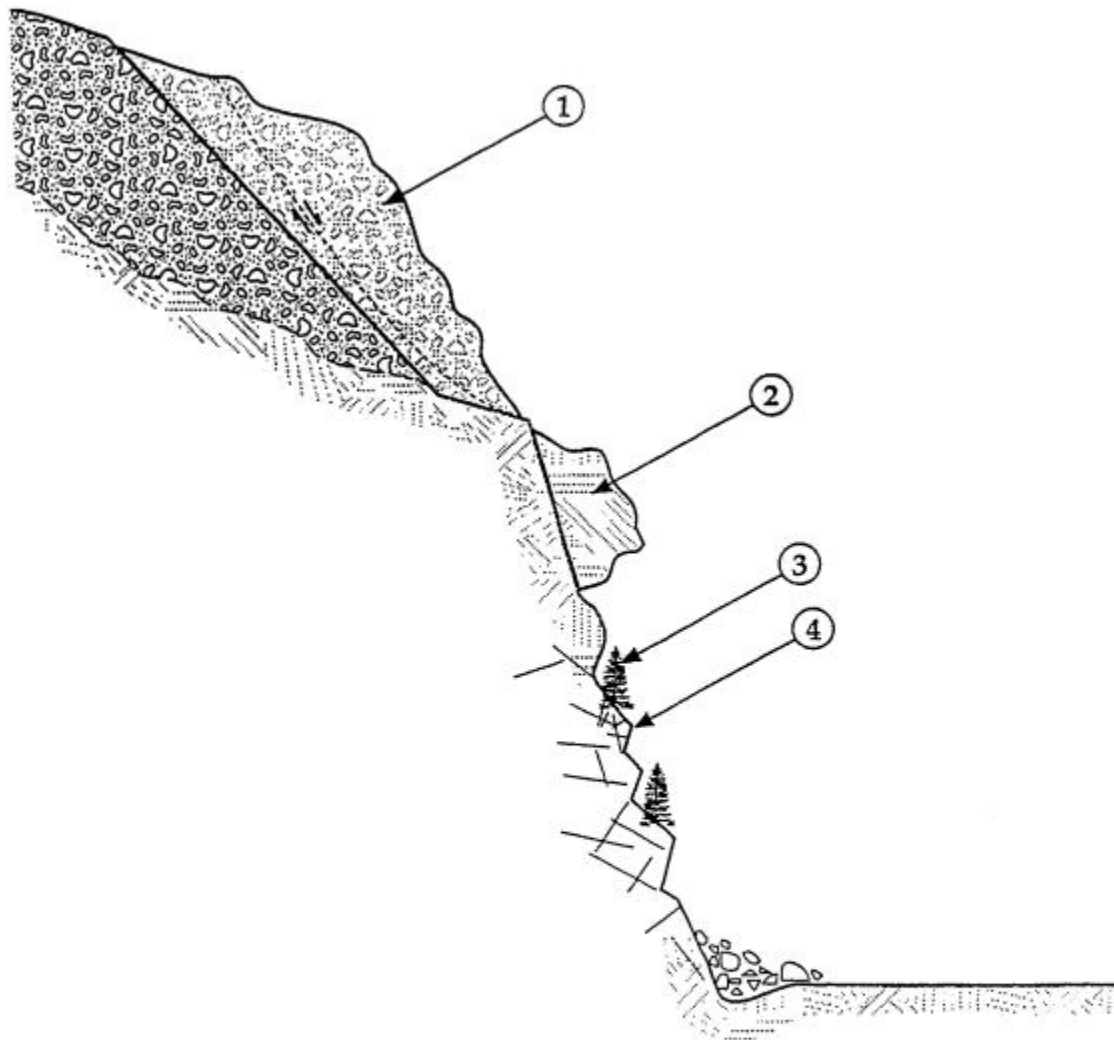
Cement grout anchors are commonly used for rock reinforcement because they provide a long service life at a reasonable cost. The grout usually contains non-shrink cement and/or admixtures for high strength, maximum viscosity, and reducing shrinkage. Rock removal is an effective method for stabilization of potentially unstable rock slopes because it eliminates the hazard, without the requirement of future maintenance. Rock removal includes resloping zones of unstable rock, trimming overhangs, and scaling of loose individual blocks of shattered rock. Examples of these methods are illustrated in Figure 7-29.



7' slab at crest.
 ong crest
 re
 rock

- ① Reinforced concrete shear key to prevent loosening of
- ② Tensioned rock anchors to secure sliding failure al
- ③ Tieback wall to prevent sliding failure on fault zon
- ④ Shotcrete to prevent raveling of zone of fractured
- ⑤ Drain hole to reduce water pressure within slope
- ⑥ Concrete buttress to support rock above cavity

Figure 7-28 Rock Slope Reinforcement Methods (FHWA 1998a)

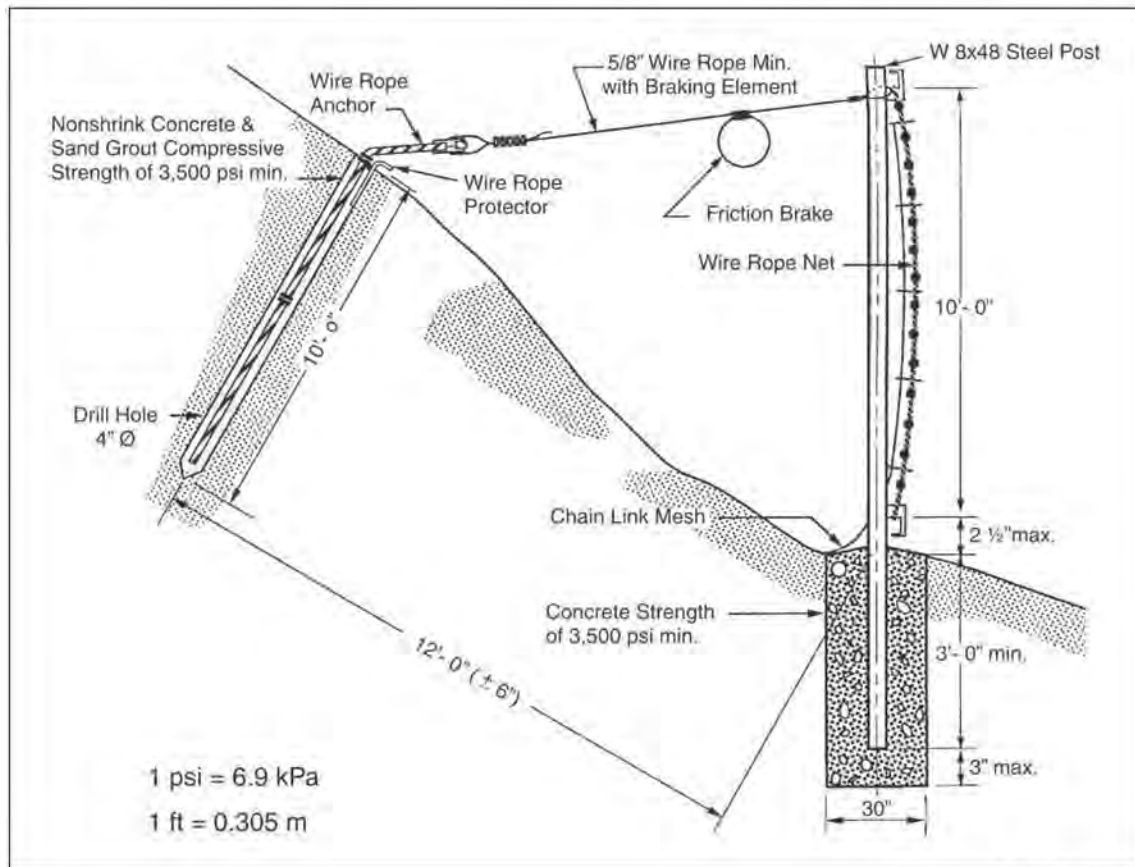


- ① Resloping of unstable weathered material in upper part of slope
- ② Removal of rock overhang by trim blasting
- ③ Removal of trees with roots growing in cracks
- ④ Hand scaling of loose blocks in shattered rock

Figure 7-29 Rock-removal Methods for Slope Stabilization (FHWA 1998a)

Another effective method of protection against the hazards of rockfalls is to let the rockfalls occur and control the distance and direction of travel of the falling rock. These methods include catchment ditches and barriers, wire mesh fences, mesh lining on the face of the slope, and rock sheds. All these methods rely on the energy-absorbing characteristics of the rockfall barrier, which is designed to either stop the rockfall over some distance or deflect it away from the facility being protected.

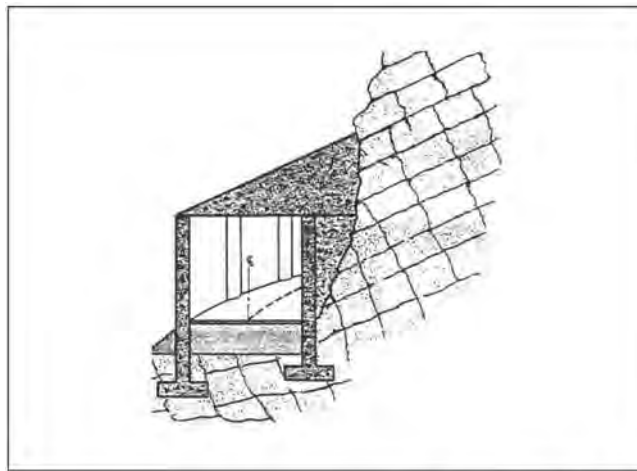
Details of various types of rockfall barriers are provided by Willie and Norrish (1996). Examples of these types of barriers include gabions and concrete blocks and geofabric-reinforced soil barriers. Flexible rockfall catch fences and attenuators also are commonly used for rockfall protection. These types of barriers include woven wire-rope nets, flex-post rockfall fences, and draped wire mesh. Figure 7-30 details the main components of a rockfall retaining net system used by the California Department of Transportation (Smith and Duffy, 1990).



Smith and Duffy, 1990

Figure 7-30 Side View of Rock Fall Restraint Net System with Fully Embedded Posts and Anchor Support

In areas of extreme rockfall hazards where stabilization work may be very costly, construction of rock sheds may be used to protect the highway. The sheds are built with roofs that are inclined at a shallow angle to direct the falling rocks over the highway rather than to withstand a direct impact. Figure 7-31, from McCauley et al. (1985) illustrates the rock shed concept. Design of such structures is based on the energy required to redirect the falling rocks and boulders.



McCauley et al., 1985

Figure 7-31 Example of a Rock Shed

The California Department of Transportation (Caltrans) report on rockfall mitigation (McCauley et al., 1985) provides a summary of the mitigation methods used by 14 selected states that responded to a survey. The results of the survey are summarized in Figure 7-32. Based upon this survey, mesh fences, catch ditches, rock bolts and dowels, controlled blasting, and flattening and scaling slope are the most widely applied rock slope mitigation methods.

States	AK	AZ	CO	HI	ID	MT	NV	NH	NM	OR	UT	VT	WA	WY
Flatten Slope		X				X	X	X	X	X				
Scale or Trim	X	X	X		X	X	X	X			X			
Skewed, Multiple Angle Slopes									X					
Slope Designed to Geology	X											X		
Controlled Blasting	X			X	X				X			X	X	X
Sub-Surface Drainage	X													
Rockbolt or Dowels	X		X				X	X	X	X		X		X
Shotcrete or Gunnite			X						X	X			X	X
Anchored Wire Mesh			X					X	X	X			X	X
Cable Lashing							X							
Retaining Wall		X										X		
Slope at Max. Steepness	X										X			
Highway Relocation		X				X								
Bench		X	X				X			X	X			
Standard Guard Rail							X	X					X	
Metal Barrier						X				X				
PCC Jersey Barrier					X	X	X		X	X				
Gabion	X								X				X	
Earth Berm										X				
Intercepting Slope Ditch								X						
Shaped Ditch at Grade	X		X		X		X	X	X	X	X		X	X
"Telephone Pole" Retainer									X					
Draped Wire Mesh	X		X	X	X		X		X	X	X		X	
Aggregate in Ditch Line								X						
Metal Bin Wall			X											
Wire Mesh Fence		X		X	X		X		X	X	X		X	

Note:
Chart prepared from the responses sent to Caltrans from other states, other methods may also be used by listed states. Combinations of mitigation measures are also used.

McCauley et al., 1985

Figure 7-32 Rock Slope Mitigation Methods Used by Selected States

7.5 LIQUEFACTION INDUCED LATERAL SPREADS: DESIGN APPROACH AND REMEDIATION

7.5.1 Background

As noted in Chapter 6 and illustrated by the case histories in Section 7.2, the vulnerability of transportation facilities to liquefaction-induced ground failure has been clearly demonstrated in past earthquakes (e.g. 1964 Niigata, 1964 Alaska, 1990 Luzon, 1991 Costa Rica, 1995 Kobe).

Based on past experience, three liquefaction-related hazards need to be considered in highway design:

1. Flow slides (large translational or rotational movements) mobilized by existing static stresses.
2. Limited lateral spreads (displacements) triggered and sustained by the earthquake's ground motion.
3. Post-liquefaction ground settlement.

Each of these hazards can cause major damage and should be considered during the development of bridge design or retrofit as well as in highway design. Damage modes for a typical highway structure such as the one illustrated in Figure 7-23 include:

- Lateral deformation of abutments and piers due to liquefaction-induced flow or lateral spreads, leading to pile damage and potential span collapse.
- Differential settlement of footings and abutments leading to damage in continuous superstructures and pile damage due to downdrag.

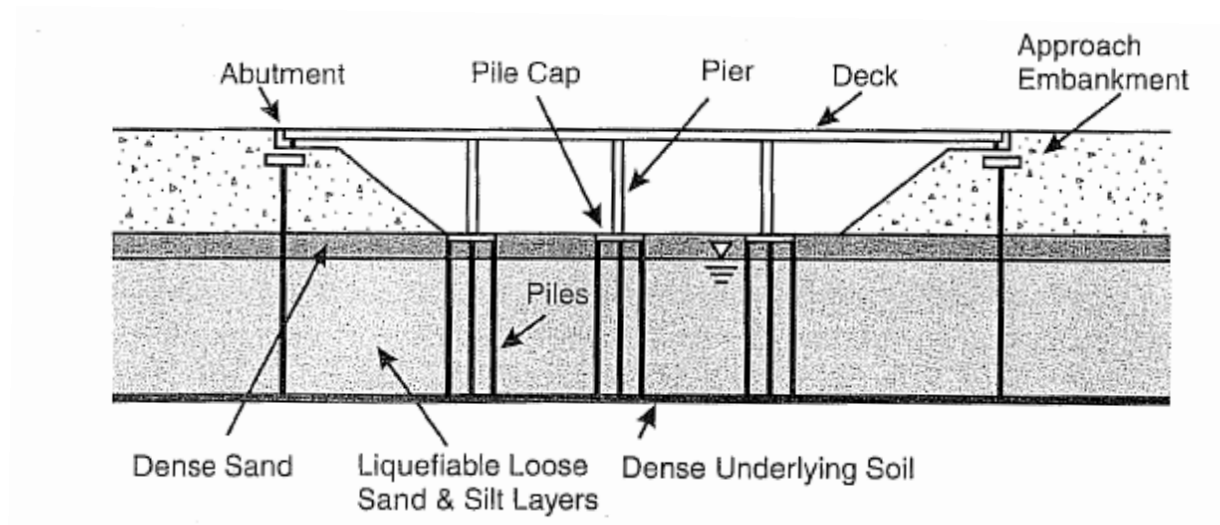


Figure 7-33 Elevation View of a Representative Bridge on a Liquefiable Stratum
 Liquefaction-induced lateral spreading, flow sliding, and differential settlement of the running length of the highway must also be considered.

Methods to assess the potential for liquefaction are discussed in Chapter 6 together with recommended procedures to estimate post-liquefaction settlement. The calculation of the amount of lateral spreading ground deformation to be expected in the free-field is also described in Chapter 6. The calculation of liquefaction-induced ground displacements, which uses the Newmark sliding block approach on an assumed dominant failure plane within the liquefied zone, involves considerable uncertainty and is the subject of ongoing research. The free-field displacements calculated in this manner are defined by an estimated lateral displacement on a failure surface, with the displacement linearly distributed over the failure zone, as shown in Figure 7-34 and discussed in Chapter 6.

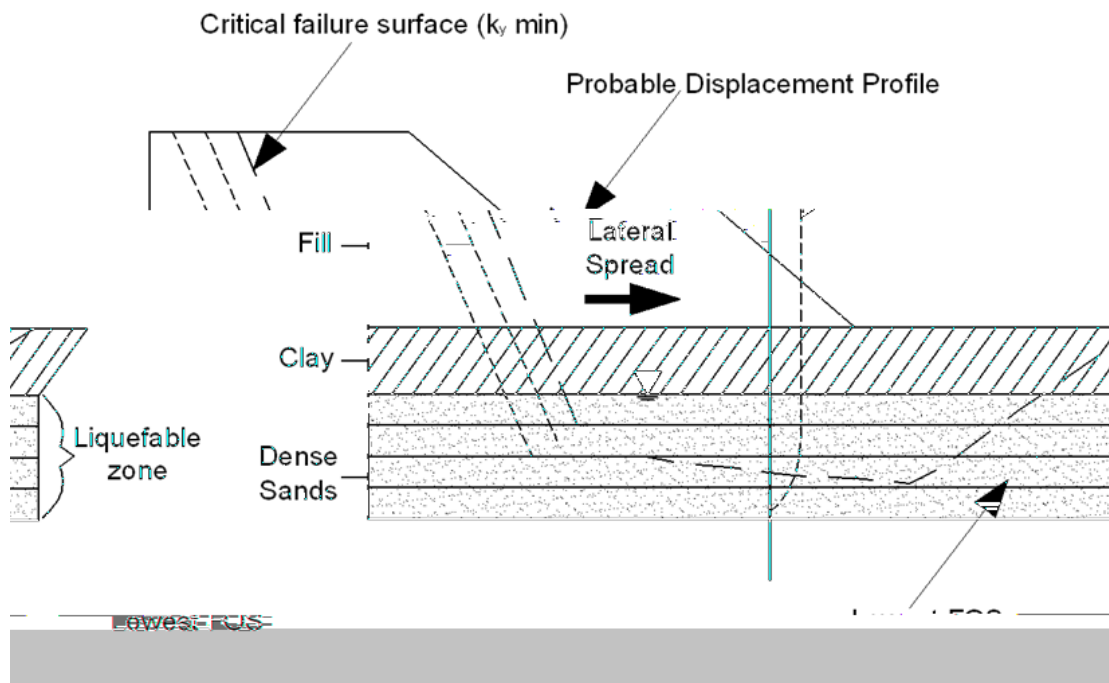


Figure 7-34 Pseudo-static Stability Analysis

Mitigation methods can be considered when damaging liquefaction-induced ground displacements are likely to occur. Aside from relocating the highway (or bridge) to a less vulnerable site, two basic mitigation options are available:

- 1) Structural design or retrofit to accommodate liquefaction and related ground displacement demands. This could entail construction of a bridge or viaduct to span over liquefiable ground or, if a structure on deep foundations is involved, an analysis of soil-foundation-structure interaction to determine if the deformation and load capacity of the foundation system can accommodate the ground deformation demands without collapse, or can meet other prescribed performance criteria. Evaluation methods that may be used in this approach are discussed briefly in paragraph 7.5.2 and in detail with respect to deep foundation performance in Chapter 10.
- 2) Site remediation to stabilize the soil and prevent or inhibit liquefaction and thereby minimize ground displacement demand. Remediation methods that can reduce ground deformations to tolerable levels include:
 - In-situ densification of liquefiable soils in zones surrounding bridge piers and underneath the highway and the toe of approach fills;
 - Deep soil mixing using cement, which creates stabilizing zones in the soil similar to those developed by ground densification techniques; and
 - Dewatering, installation of gravel drains or permeation grouting, and similar techniques.

Site remediation methods are discussed in detail in Section 7.5.3.

7.5.2 Structural Design to Accommodate Liquefaction-Induced Deformations

Structural design to accommodate liquefaction-induced ground deformations is a complex soil-foundation-structure interaction design problem. While in many cases the geotechnical specialist merely passes the displacement demand on to the structural specialist, design of deep foundations to resist lateral spreading and seismic settlement is a geotechnical problem and is the subject of ongoing research. Analysis of the performance of deep foundations in liquefied ground is discussed in detail in Chapter 10. However, besides consideration of the impact of foundation performance on the overlying structure, deep foundations may also mitigate lateral spreading. Simplified concepts to address the impact of deep foundations on lateral spreading were addressed in the NCHRP 12-49 project (NCHRP, 2003 and ATC/MCEER, 2003) and are described in the FHWA Seismic Retrofitting Manual (FHWA, 2006). These concepts are summarized below.

Initial design of pile foundations would normally be based on the LRFD design procedures for static loading, using both of the following configurations:

- 1) Non-liquefied configuration – using the appropriate acceleration response spectrum for the non-liquefied site soil conditions.
- 2) Liquefied configuration – using a softened pile-foundation stiffness within the liquefied layer and the non-liquefied site soil spectrum (unless special studies are undertaken).

If liquefaction-induced lateral flow sliding or spreading of the ground is predicted during a seismic event, structures that would be loaded by the deforming ground need to be checked and possibly re-designed to withstand the loads from the moving soil. The recommended approach for evaluating this condition involves the following four basic steps:

- 1) Slope stability analyses are conducted for the liquefied state using the residual shear strength to determine the post-liquefaction yield acceleration and the associated failure surface (normally associated with the deepest soil layer showing liquefaction potential). This step may include consideration of the pinning effects of the piles and/or the increased resistance of soil that has provided by some type of ground improvement method.
- 2) Newmark sliding block analyses are performed using the post-liquefaction yield acceleration to estimate the post-liquefaction displacements of the soil-pile system.
- 3) Forces on the structure and its foundation due to the lateral spreading movements are calculated.
- 4) Plastic hinge mechanisms that are likely to develop in foundation elements are determined.

In the above procedures, it is assumed that the effects of ground displacement can be decoupled from the effects of structural inertial loading. In most cases, this is a reasonable assumption, as peak vibration response is likely to occur in advance of the maximum ground displacement and displacement-induced maximum moment and shear on a foundation element will generally occur at deeper depths than those from inertial loading. The rationale behind the proposed procedure is to assess the ability of the structure to both accommodate the anticipated movement and/or potentially limit the movement.

The concept of considering a plastic mechanism in the foundation under the action of the lateral spreading forces is tantamount to accepting damage in the foundation. The justification for this is that it is unlikely that the formation of a hinge mechanism in the foundation will lead to structure collapse. The reasoning behind this is that lateral spreading is essentially a displacement-controlled process. Thus the estimated soil displacement represents a limit on the structure displacement excluding the phenomenon of buckling of the piles or shafts below grade and the continued displacement that could be produced by large $P-\Delta$

effects. This is an important concept, as analyses suggest that the moments induced in a deep foundation element for a structure subject to significant liquefaction-induced displacement demand can be very large at the interface between the liquefied zone and an underlying non-liquefied layer. Buckling should be also be checked using methods that include the residual soil resistance. O'Rourke et al. (1994) provides a method for checking buckling of deep foundation elements in liquefied soil.

The magnitudes of the moment and shear induced in pile foundations by ground displacements may be computed using soil-pile interaction programs. The assumed displacement field is as a support displacement to soil springs whose properties are represented by p-y curves. In the liquefied zone, these p-y curves must be adjusted for liquefaction effects. Examples of such analysis are given by O'Rourke et al. (1994), Soydemir et al. (1997), and Ishihara and Cubrinovski (1998). In the liquefied zone, the soil is can be treated as a soft cohesive soil with p-y curves computed using the undrained residual strength of liquefied soil as the cohesion.

The largest loads on foundations at sites where lateral spreading or flow sliding is expected occurs in cases where a non-liquefied crust slides on a liquefied layer. In such case, the ground deformations may exert full passive pressures on the foundation in the non-liquefied zone. The loads in these cases may be very large, as the passive pressure will typically be generated over a width equal to 2 times the width of the foundation element in cohesive soil and 3 times the width of the foundation element in cohesionless soil. The passive pressure against a pile cap in a laterally spreading non-liquefied crust may be assumed to be applied over the width of the pile cap plus twice the depth of the base of the cap below grade. In the liquefied zone, the passive pressure calculated using the residual shear strength may be assumed to apply over the width of the foundation element or pile cap. An analysis conducted using these assumptions will generally result in extremely large forces on the foundation and the formation of plastic hinges in the foundation elements. However, the foundations may still remain intact without failure in a state of limiting equilibrium, as in the case history of the Landing Road Bridge described in Section 7.2.3.

The reinforcing or pinning effects a piles or pile group has on the lateral displacements may then be considered by representing the pile shear forces at the location of the failure plane as an equivalent shear strength in the calculation of the yield acceleration of the sliding mass, which is subsequently used in the displacement analysis. This requires an iterative approach, as shear forces are a function of displacements which, in turn, are reduced as shear forces increase.

In the event that the pile foundations cannot accommodate the displacement demands from spreading ground, one option is to install additional foundation piles (using a pile cap overlay in a retrofit case) to increase the pinning action and, hence, reduce the displacement demands. Another option is the use of passive piles driven through the liquefiable layer and failure surface to provide additional pinning action without physically attaching the piles to the bridge structure (such piles are sometimes referred to as “pinch” piles). Installing additional foundation piles may be particularly relevant if additional piles are also required to accommodate high overturning moments or to minimize down drag effects. Where additional piles are required, the costs of mitigation should be compared with the costs of ground remediation to reduce lateral spreading displacements.

The framework of the simplified approach to design for the impact of soil liquefaction on a bridge structure using the above concepts and presented in the NCHRP 12-49 Guidelines is outlined in the flow chart shown in Figure 7-35. The steps involved are described as follows:

- Step 1: Identify the soil layers that are likely to liquefy

- Step 2: Assign residual undrained strengths to layers that liquefy. Conduct pseudo-static seismic stability analyses to determine the minimum yield acceleration k_y . This defines the depth of soil likely to spread laterally and the extent of the likely-soil failure block. If the yield acceleration is equal to (or less than) zero, the site is subject to uncontrolled flow failures and unlimited deformation in the liquefied zone must be assumed.

- Step 3: Estimate the maximum lateral spreading displacement of the soil. This may be accomplished using the displacement equations presented in Chapter 6 or a site-specific Newmark time history analysis.

- Step 4: Assess whether the soil will continue to displace or flow around a stable foundation or whether movement of the foundation will occur in concert with the soil. This assessment requires a comparison between the estimated passive soil forces that can be exerted on the foundation and the ultimate structural resistance that can be developed by the structure. In cases where a crust of non-liquefied material may exist at the ground surface, the full structural resistance may be less than the displacement-induced passive forces and the foundation is likely to continue to move with the soil. In many cases, it may be immediately obvious which condition is more likely to occur. Schematic illustrations of the two cases are shown in Figure 7-36.

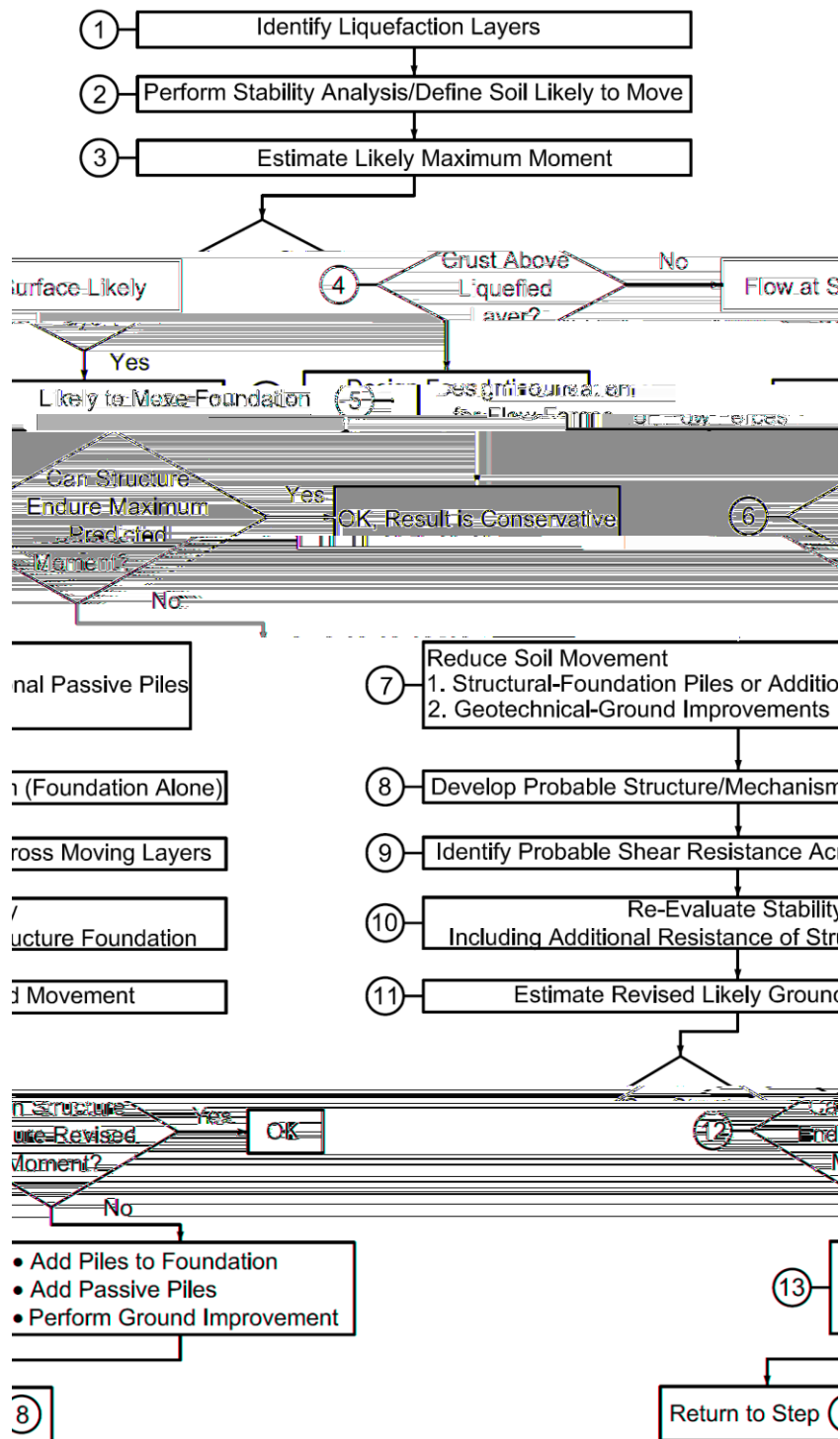


Figure 7-35 Design Flowchart

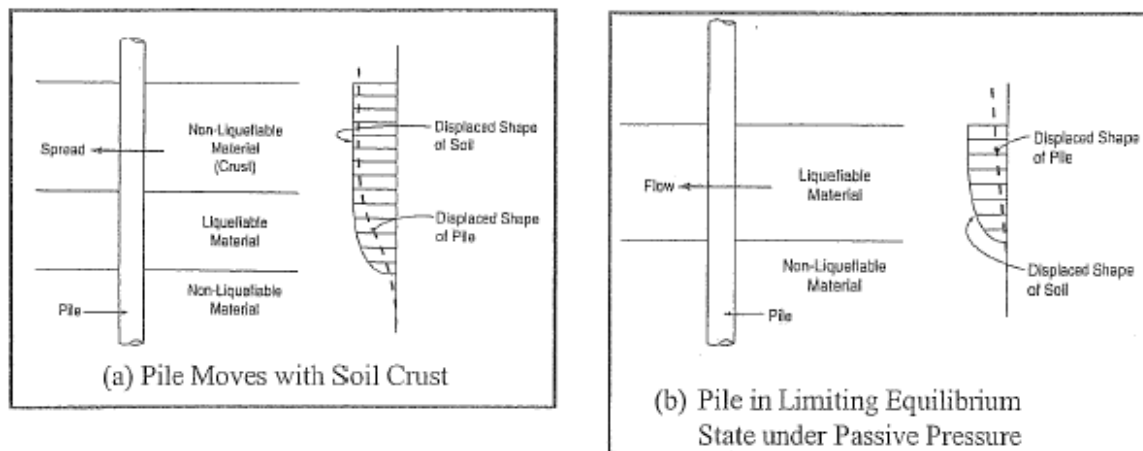


Figure 7-36 Deformation Models for Piles at Lateral Spreading Sites

Step 5: If the soil continues to displace around a stable foundation, the foundation is designed to withstand the passive pressures created by the flowing soil. The induced forces are effectively the largest forces that the structure will experience and, for this reason, it is conservative to design a structure for such forces.

Step 6: If the assessment indicates that movement of the foundations is likely to occur in concert with the soil, then the structure must be evaluated for adequacy at the maximum expected displacement. The implication of this assessment is that for relatively large ground movements, soil displacements are likely to induce similar magnitude movements of the foundation. In this context, “large” is taken relative to the structural yield resistance. The resulting induced movements of the foundations may produce substantial plasticity or hinge zones in the foundations, and may induce relatively large reactions in the superstructure. For an upper level event, a maximum plastic rotation of 0.05 radians is the recommended acceptance criteria, although values determined by rational cross section analyses are also acceptable and preferred in many cases.

Step 7: If the deformations determined in Step 6 are not acceptable, two ways to restrict the foundation and substructure forces to values less than yield can be considered. The first method is to design or retrofit the foundations to resist the forces that would accompany passive flow of the soil around the foundations. The second method would be to limit the ground movement by

providing either ground or structural remediation. It is the structural option that provides a potential first path, and this makes use of the “pinning” or dowel action that pile or shaft foundations contribute as they cross the potential failure plane of the moving soil mass. This can effectively reduce the magnitude of lateral displacement.

- Step 8: Determine the plastic mechanism that is likely to occur in the presence of lateral spreading. This should be done in a reasonable manner. Due to the range of inherent uncertainties, great precision in the determination may not produce more accuracy. Simple estimates of the mechanism and its corresponding lateral resistance capability may be adequate. Such estimates could be based on hinge development in stable or firm soil zones above and below (by say 2 pile diameters) the liquefiable layer. Maximum “pinning” shear could then be assumed equal to $2M_p/L$, where M_p is the plastic moment and L is the distance between hinges – this assumes that the load transfer in the liquefied zone is negligible. The lateral shear that produces the plastic mechanism can be adjusted downward to account for the driving influence of the P- Δ effect. A more precise method of determining the plastic mechanism would be to use an approach that ensures compatibility of deformations between the soil and piles (e.g., one that uses a p-y analysis) and which accounts for plastic deformations in the piles themselves.
- Step 9: Assess the system for the calculated displacement field from the lateral spreading analysis. From this analysis, an estimate of the likely shear resistance that the foundation will provide is determined, which can then be incorporated back into the stability analysis.
- Step 10: If substantial resistance is provided by the foundation system, then its effect on limiting the instability driven movement of the soil block should be accounted for.
- Step 11: Recalculate the overall displacement on the basis the revised resistance levels.
- Step 12: Once a realistic displacement is calculated, the foundation and structural system can be assessed for this movement. It is at this point that more permissive displacements than those allowed for substructure design can be relied upon. This implies that plastic and potentially large rotations may be allowed to occur in the foundation under such conditions.
- Step 13: If the structure’s behavior is acceptable, then the liquefaction design is complete. If not, assess whether or not adequate behavior can be achieved by providing ground remediation or

additional piles or shafts. Note that additional piles or shafts may not need to connect to the foundation (passive piles) or the cap. Ground improvement approaches may be considered include stone columns, deep soil mixing, and grouting. The selection of a preferred structural or geotechnical method is based on the relative economies of the systems being considered.

An example of the application of this procedure is provided by the analysis of a Washington State Department of Transportation (WSDOT) bridge site (Site Class E) at the site whose abutment fill subsurface profile is shown in Figure 7-37. Seismic hazard analyses for the site (assumed located near Olympia) generated a site-specific peak horizontal ground acceleration of 0.42 g for a 2475 year return period and a 6.5 mean magnitude for the design event. For a 475 year return period. The design magnitude was still 6.5 and the peak horizontal ground acceleration was 0.24 g.

The 500 ft long box girder bridge structure at the site is continuous between the overhanging stub abutments. The intermediate piers are two column bents supported on pile caps and concrete-filled 24 in. steel pipe piles, embedded in till at elevation -200 ft. Soils between elevations of 0 to -100 ft comprise interlayered medium-dense sands and soft clays (shear strength 1000 psf). Stiff clays (shear strength 2000 psf) were assumed between elevations -100 to -200 ft.

Evaluations of liquefaction potential (step 1 of the design procedure) for the 2475 year event, show liquefaction in all sands without overlying fill, and with overlying fill for layers at elevations -10 to -15 ft, -30 to -35 ft and 045 to -50 ft and below. For the 475 year event, liquefaction occurs in sands at elevations -30 to -35 ft and -45 to -50 with overlying fill, but does not occur for sands below the fill.

One dimensional nonlinear effective stress site response analyses were also conducted to evaluate the time history of pore pressure increase and site liquefaction characteristics. Acceleration time histories were developed from records consistent with the hazard levels and site conditions and modified to match design response spectra. The results of the nonlinear effective stress site response analysis were generally consistent with the liquefaction calculations. However, a key conclusion from these studies was the strong likelihood that lateral spreading deformations would be controlled by a failure zone in the layer at elevations of between -45 ft to -55 ft. In general, the effective stress site response analyses showed that the post-liquefaction shear strains focused on the deepest layer susceptible to liquefaction.

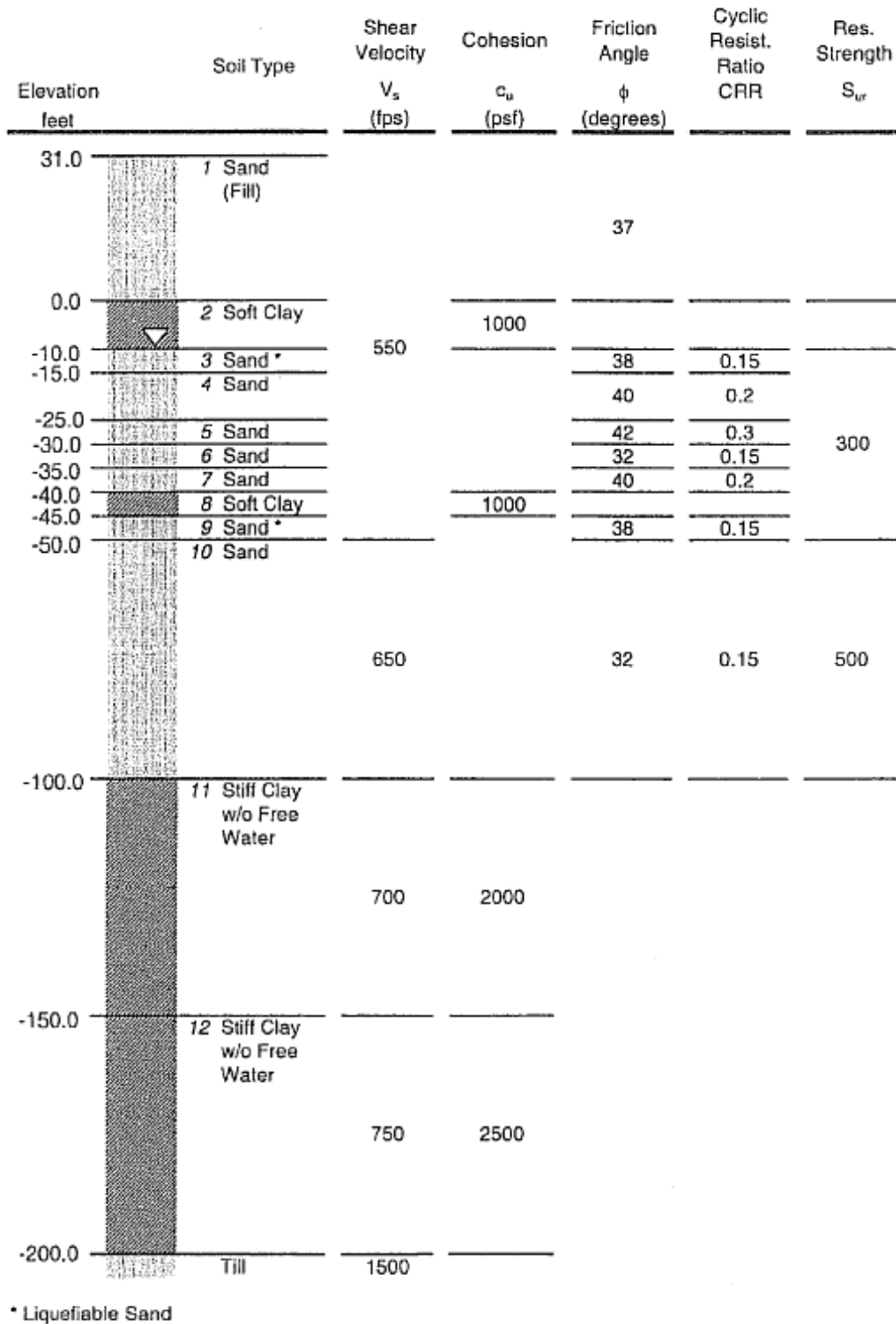


Figure 7-37 Site profile, Washington Bridge

Once it was established that liquefaction and lateral spreading was likely to occur, a post-liquefaction stability analysis of the abutment fill was performed as indicated in Step 2 of the design procedure. Pre-liquefaction analyses indicated static C/D values for the embankment slopes were greater than 1.5. However, when post liquefaction residual undrained strengths of 300 psf were assigned to the sand layer at elevations -45 to -55 ft, C/D values dropped to a minimum of approximately 0.8, as shown in Figure 7-38, indicating the potential for an unconstrained flow failure.

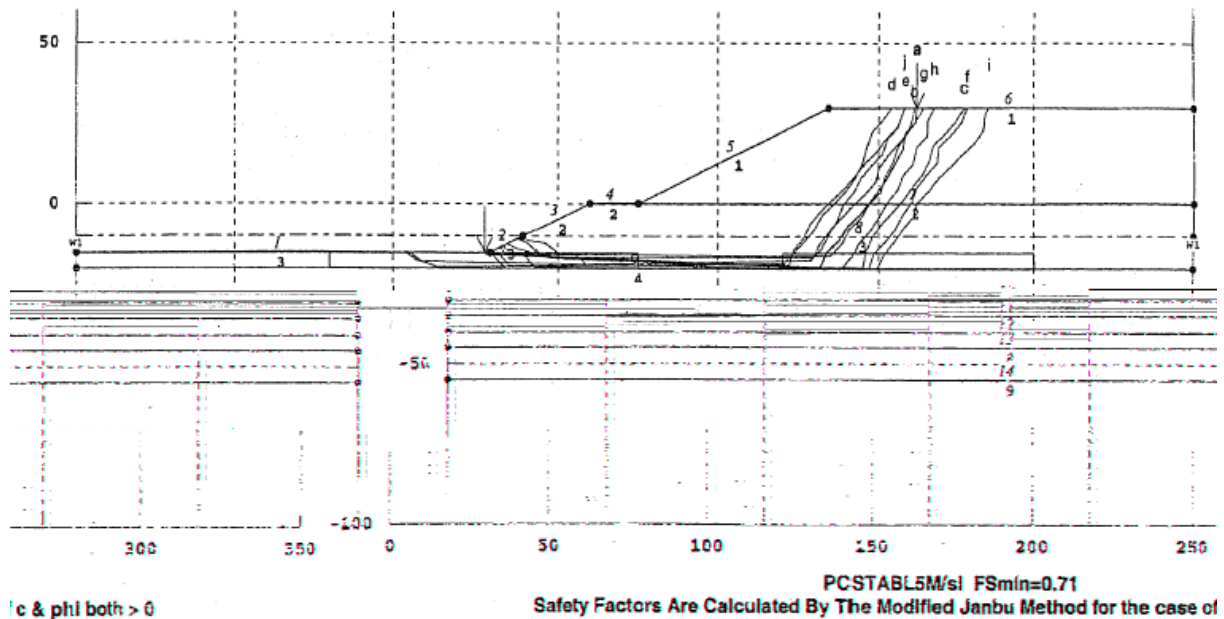


Figure 7-38 Typical Sliding Mechanism for Flow Failure

Given the potential for large unconstrained lateral spreading, the next step (step 7) was to evaluate the beneficial pinning action of the pile foundations. The deep failure mechanism for lateral spreading at the right abutment shown in Figure 7-39 is example f this step of the analysis. Given the high passive pressure forces which could be generated by the embankment moving against the abutment and piles, it was clear in this case that a limiting equilibrium condition associated with flow around the foundations would not develop and that the foundation would move with the soil.

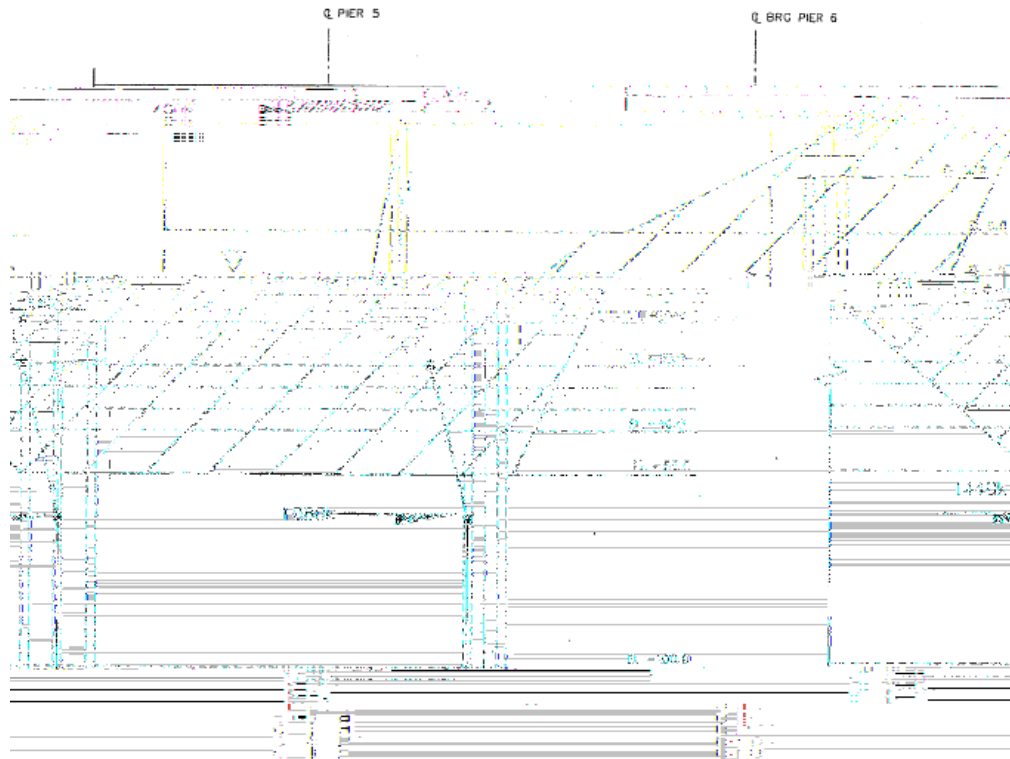


Figure 7-39 Forces Provided by Bridge and Foundation Piles for Resisting Lateral Spread

The maximum pinning forces that could be developed were then considered to see if they were sufficient to provide post-earthquake static stability. Figure 7-39 illustrates the pinning forces acting on a soil block sliding on the lower liquefiable layer. In this case, the abutment itself provides about 400 kips of shear resistance (through passive resistance provided by backfill acting against end diaphragm), and the columns at Pier 5 provide about 420 kips of shear resistance. The total abutment pile resistance is 1080 kips and the total resistance of the Pier 5 piles is 1440 kips. The pile resistance corresponds to the approximate plastic mechanism shear force with 30 ft between points of assumed fixity in piles. The 30 ft between points of fixity is comprised of 10 feet of liquefiable material and a conservatively assumed distance of 5D (D = pile diameter) to the point of fixity above and below that layer. This conservatism allows for softening in adjacent layers. The upper portion of the soil block is assumed to move essentially as a rigid body, and therefore the piles are assumed to be restrained by the integrity of this upper block.

The sum of these forces (3360 kips total) represents the maximum shear resistance provided by the bridge foundation system and occurs only after significant plasticity develops. In the case of Pier 5, the approximate displacement limit is 22 in., which is comprised of 4 inches to yield and 18 inches of plastic

drift. The plastic drift limit for this case was taken as 0.05 radians, which is reasonable for well detailed ductile piles. Because the abutment piles (Pier 6) are the same as the piles at Pier 5, their displacement limit was also 22 in.

The total 3360 kip resistance calculated above represents 70 kips/ft of width of the abutment and was introduced into the slope stability analysis as an equivalent shear strength (530 psf) along the shear plane in the liquefied zone. This increase in shear resistance was sufficient to increase the post-earthquake C/D ratio to greater than 1.0, hence negating the potential for an uncontrolled flow failure. Similar pinning analyses for the upper failure surface led to a C/D ratio of 1.0, indicating the potential for an uncontrolled flow failure was still a concern.

For the lower failure surface, the lateral spreading displacement due to inertial forces imposed during the earthquake remained to be evaluated (step 3). These displacements were evaluated by calculating the yield acceleration and estimating the resulting lateral displacements using the Newmark sliding block method. For the calculated yield acceleration of 0.02g, a displacement of about 22 in. was calculated for the 475 year event and a displacement of 36 in. was calculated for the 2475 year event. The 22 in. displacement is within the plastic capacity of the piles, whereas for the 2475 year event, either additional “pinch” piles could be added or ground remediation could be implemented. Subsequent analyses showed that the installation of a 30 ft wide stone column toe buttress extending through the liquefied zones to an elevation of -55 ft leads to a yield acceleration of 0.12g and reduced the estimated lateral displacement to less than 5 in. for the 475 year event and 8 in. for the 2475 year event. The 30 ft wide stone column buttress was estimated to cost about \$120,000 for both sides of the embankment, or about 4% of the likely bridge cost.

The case history above shows that the beneficial effects of considering the resistance that the bridge substructure offers to lateral displacements of soil via “pinning” action can be significant and should be considered in predictions of lateral soil movements. In addition, the benefit of allowing inelastic behavior of pile foundations under the action of lateral ground spreading is that relatively large displacements of the ground may be accommodated by the structure without collapse. If pile foundations cannot tolerate the predicted displacements (including pile pinning effects), then either structural or ground improvement remediation options should be used.

7.5.3 Liquefaction Mitigation Ground Improvement Methods

To prevent or inhibit liquefaction and reduce lateral ground deformations and settlements to acceptable performance levels, site remediation using one or more ground improvement options may be deployed. Remediation methods include:

- In-situ densification of liquefiable soils in zones beneath embankments, underneath the toe of approach fills or surrounding bridge piers; this will reduce ground deformations to tolerable levels.
- Deep soil mixing using cement, which creates stabilizing zones in the soil similar to those developed by ground densification techniques.
- Dewatering or installation of gravel drains to prevent pore water pressure build up.
- Grouting techniques.

Such remediation methods are also applicable to embankments on liquefiable soils in the absence of bridge abutments, where lateral spread deformations are not acceptable.

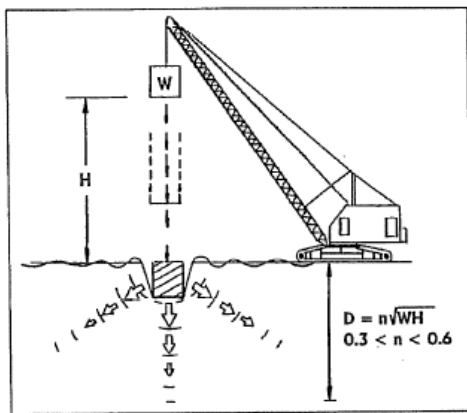
Overviews of the state-of-practice for site remediation are documented in several publications (ASCE, 1997; Andrus and Chung, 1995, Elias et al., 2006). A comprehensive report on ground remediation measures for liquefaction at existing bridge sites was published by Cooke and Mitchell (1999). A summary of several ground improvement methods for liquefaction remediation is given in Table 7-8, extracted from the Cooke and Mitchell (1999) report. Brief summaries of several of the remediation methods are given below.

TABLE 7-8 GROUND IMPROVEMENT METHODS (after Cooke and Mitchell, 1999)

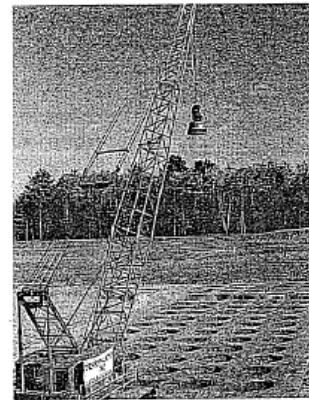
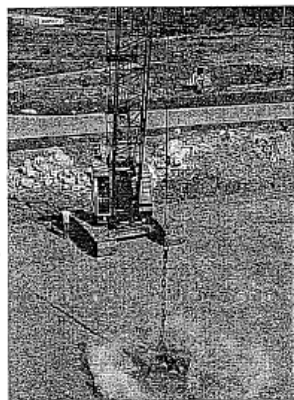
Method	Principle	Suitable Soil Types	Treated Soil Properties	Relative Costs
Compaction Grout	Highly viscous grout acts as spherical hydraulic jack when pumped under high pressure resulting in densification.	Compressible soils with some fines	Increased D_r <u>SPT</u> : $(N_1)_{60}$ 25 to 30 <u>CPT</u> : $q_{cl}=80$ To 150 tsf (Kg/cm ²)	Low material cost; high injection cost.
Particulate Grouting	Penetration grouting: fill soil pores with cement, soil and/or clay.	Clean, medium to coarse sand and gravel	Cement-grouted soil: high strength	Lowest of grouting systems
Chemical Grouting	Solutions of two or more chemicals react in soil pores to form a gel or solid precipitate.	Silts and sands	Low to high strength	High to very high
Jet Grouting	High speed jets at depth excavate, inject and mix stabilizer with soil to form column or panels	Sands, silts and clays	Solidified columns and walls	High
Vibro-Compaction	Densification by vibration and compaction of backfill at depth.	Sand (<20% passing No. 200 sieve)	D_r : up to 85+% <u>SPT</u> : $(N_1)_{60}$ 25 to 30 <u>CPT</u> : $q_{cl}=80$ To 150 tsf (Kg/cm ²)	Moderate
Vibro-replacement/ Stone Columns	Densely compacted gravel columns provide densification, reinforcement, and drainage	Sands and silts	Increased D_r <u>SPT</u> : $(N_1)_{60}$ 25 to 30 <u>CPT</u> : $q_{cl}=80$ To 150 tsf (Kg/cm ²)	Moderate to high
Drains: Gravel Sand Wick	Relief if excess pore water pressure to prevent liquefaction. Intercept and dissipate excess pore water pressure plumes from adjacent liquefied soil.	Sands, Silts	Improved drainage	Low to moderate
Mini-Piles	Provide piles to carry loads through liquefiable soils to firm stratum.	All soils	-	High

For new construction, particularly in open areas some distance from existing structures, in situ densification using vibratory techniques or dynamic compaction are the most commonly deployed methods for improving the density, and hence strength and stiffness, of loose cohesionless soils. For saturated cohesionless soils, vibratory methods have been widely used to increase liquefaction resistance under earthquake loading. However, these methods would in most cases, not be suitable for use in improving soils around existing foundations, embankments, or roadways. Each method has its own technology, effectiveness and suitability for different soil types. Experience indicates that vibratory techniques can increase relative densities to values greater than 80%.

Deep dynamic compaction (shown schematically in Figure 7-40) entails dropping weights of 10-40 tons from heights of 50-100 feet over impact grids ranging from 7x7 feet to 25x25 feet. The depth that can be effectively improved is a function of the size of weight, height of drop, and the soil type. The effective depth of improvement is limited to about 35 feet using conventional equipment and is controlled by the soil type, degree of saturation, permeability, and initial relative density. Levels of ground vibration are an important environmental constraint with this method, and areas treated using this method will probably need to be a minimum of 100 feet from existing structures. A detailed description of applications of dynamic compaction and associated ground response is given by Mayne et al. (1984), ASCE (1994), ASCE (1997), and FHWA (2004).



The dynamic compaction process



Typical dynamic compaction equipment

Figure 7-40 Dynamic Deep Compaction

Vibro-compaction methods, the most common of which is known as vibroflotation (shown schematically in Figure 7-41), involves the repeated insertion and withdrawal of a large vibrating probe to the desired depth of densification. In some cases granular backfill soil is added and densified during withdrawal of

the probe. The procedure is repeated over the site using a grid spacing ranging between 6 and 11 feet with typical depths of improvement ranging from 10 to 50 ft. The method is more suited to clean sands. For silty sands, the vibro-replacement method described below is more widely used. The effectiveness of vibro-compaction in saturated cohesionless soils depends on the initiation of localized liquefaction followed by pore pressure dissipation and settlement. Brown (1977) provides general background information on the technique. Dobson (1987) describes several case histories where vibro-systems have been used to minimize liquefaction.



Figure 7-41 The Vibro Compaction Process

The most widely used densification method is the vibro-replacement technique, which has been shown to be effective in remediating potentially liquefiable soil in past earthquakes (Mitchell et al., 1995). This method involves the replacement or displacement of the liquefiable soil with a column of dense granular soil formed by repeated insertion and withdrawal of a large vibrating probe into the soil to the desired depth of improvement, as shown in Figure 7-42. As the vibrating probe is plunged up and down, crushed stone backfill is placed around the vibrator, leading to the development of a dense stone column that is approximately 1 m (3 ft) in diameter. The procedure is repeated at a grid spacing of 2.4 to 3.7 m (8 to 12 ft) to form an improved zone.

Vibro-replacement includes wet methods where the insertion of the probe is aided by jetting and dry methods where the probe is penetrated into the ground typically using a vibrating hammer of some sort.

The wet methods rely more on replacement than displacement and are more suitable for ground improvement at non-liquefiable soft soil sites. Dry methods displace the soil, densifying the adjacent soil and providing liquefaction mitigation by densification as well as through reinforcement and enhanced drainage.

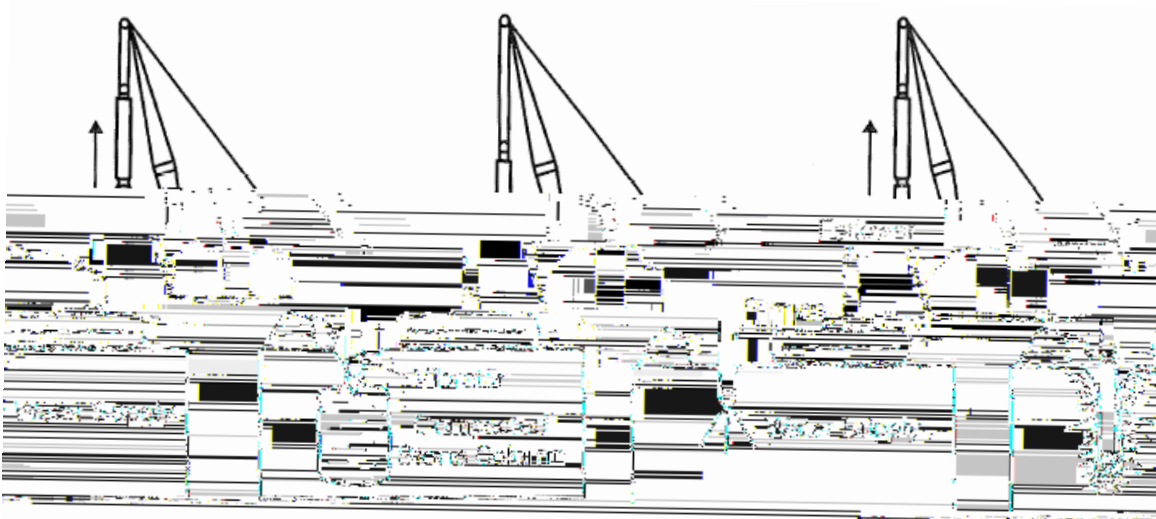
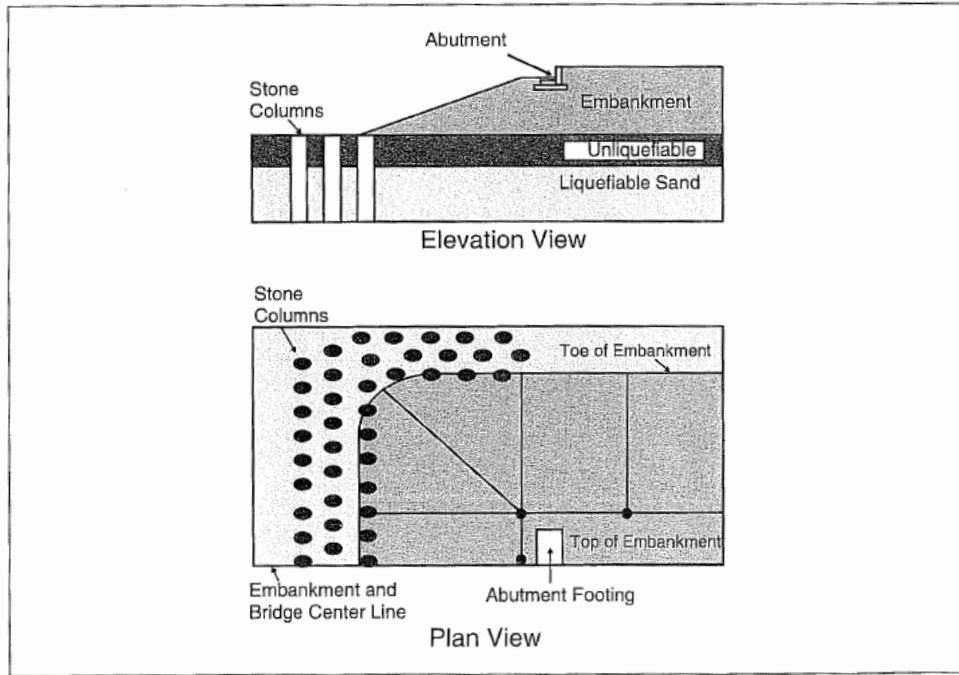


Figure 7-42 Vibro-replacement Equipment and Process

Vibro-replacement is effective if the sands to be densified contain less than 15 to 20 percent fines.

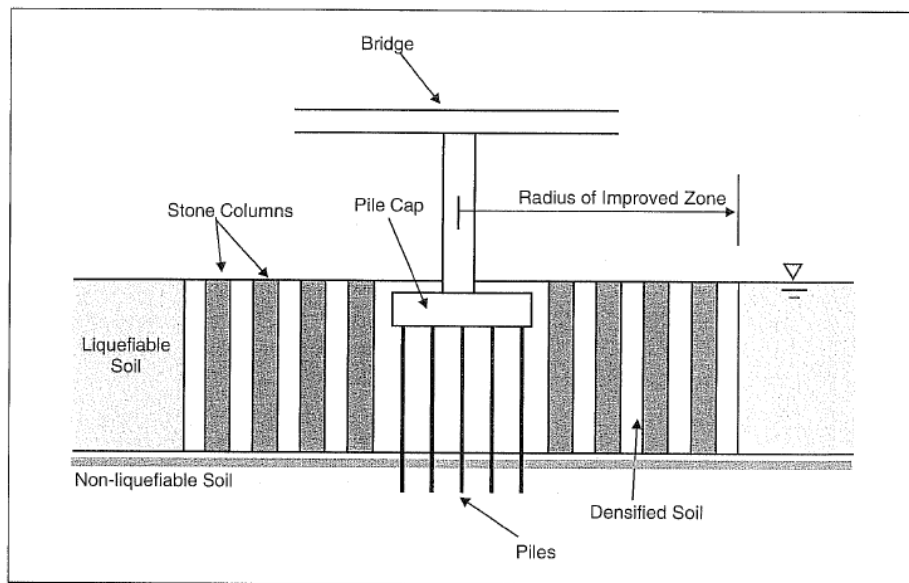
A representative application of vibro-replacement is shown in Figure 7-43, where a densified stone column buttress has been constructed at the toe of an embankment. The buttress increases the yield acceleration through the reinforcement provided by the columns and the densification of the soil in between the columns. This, in turn, reduces lateral spreading. The enhanced drainage provided by the stone columns is an unquantified additional benefit of the buttress. An example of this approach is described by Egan et al. (1992).

Another example of the application of stone columns for liquefaction remediation is shown in Figure 7-44, where a densified soil zone has been placed around a pile-supported bridge pier. The placement of such a zone (normally within a radius of 150 to 200 percent of the thickness of the liquefiable layer) would be designed to eliminate post-liquefaction downdrag on the piles as well as to reduce the potential for liquefaction induced lurching or lateral spreading of the ground..



Cooke and Mitchell, 1999

Figure 7-43 Vibro-system (stone column) Treatment at Toe of Approach Embankment

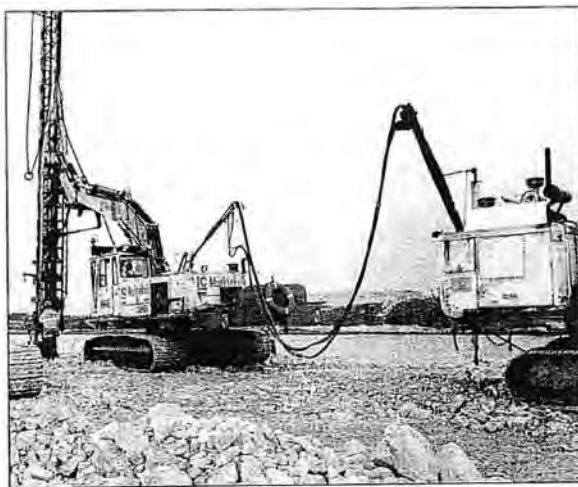


Jackura and Abghari, 1994

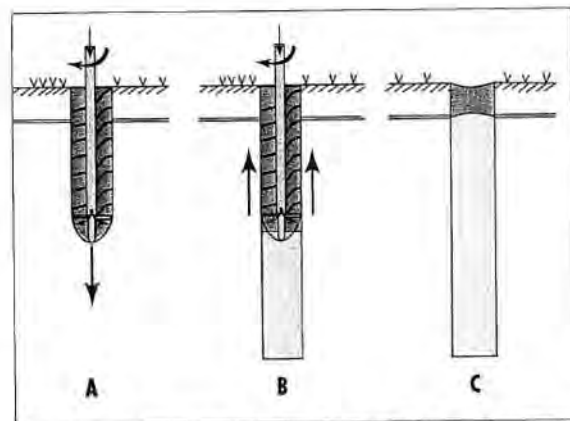
Figure 7-44 Vibro-system (stone column) Treatment Around a Pile-supported Bridge Pier

For sites where vibratory techniques may be impractical, compaction grouting can be used. Shown schematically in Figure 7-45, compaction grouting involves pumping a stiff mix of soil, cement, and water into the ground under high pressure to compress or densify the soil. A very stiff soil-cement and water mixture is injected into the soil forming a grout bulb, which displaces and potentially densifies the surrounding ground, without penetrating the soil pores. A grid or network of grout columns that is formed by grouting from the bottom up results in improved liquefaction resistance over the required surface area, similar to a network of stone columns (Boulanger and Hayden 1995). A theoretical study of the mechanics of ground improvement in sands (Mace and Martin, 2000) has shown that increased liquefaction resistance arises primarily from increased lateral stresses rather than from densification. Consequently, increases in liquefaction strength are best measured using cone penetration test (CPT) correlations (Salgado et al., 1997). However, there are uncertainties as to the permanence of increases in the lateral stress. Furthermore, compaction grouting is one of the more expensive liquefaction ground remediation options.

The deep soil mixing method encompasses a group of technologies where cementitious material (usually cement or lime) is introduced and blended into the soil through a hollow rotating shaft or shafts equipped with cutting tools and mixing paddles or augers. The materials may be injected under pressure in either slurry (wet) or dry form.



Dry Soil Mixing rig with mobile powder silo.



(A) Mixing tool is inserted to prepare the soil. (B) Lime and cement are injected and mixed as tool is rotated and raised. (C) Depths of completed columns are predetermined and controlled by on-board computer.

Figure 7-46 shows a typical rig used for the dry mixing method with a schematic diagram of the mixing process. The process leads to vertical stabilized columns of about 1 m diameter. Multiple augers are often used in the wet methods. For dry methods (used beneath the water table or in high moisture content

clays), typically 50-150 lb (100-300 kg) of cementitious material is injected per cubic meter of soil, while for wet methods, 50-250 lb (100-500 kg) is injected. The strength gain of the soil depends on the physical properties of the soil and the quantity of cementitious material injected. Typically, values of unconfined compressive strengths of 5-50 tsf are achieved in treated granular soils and 2-20 tsf in cohesive soils

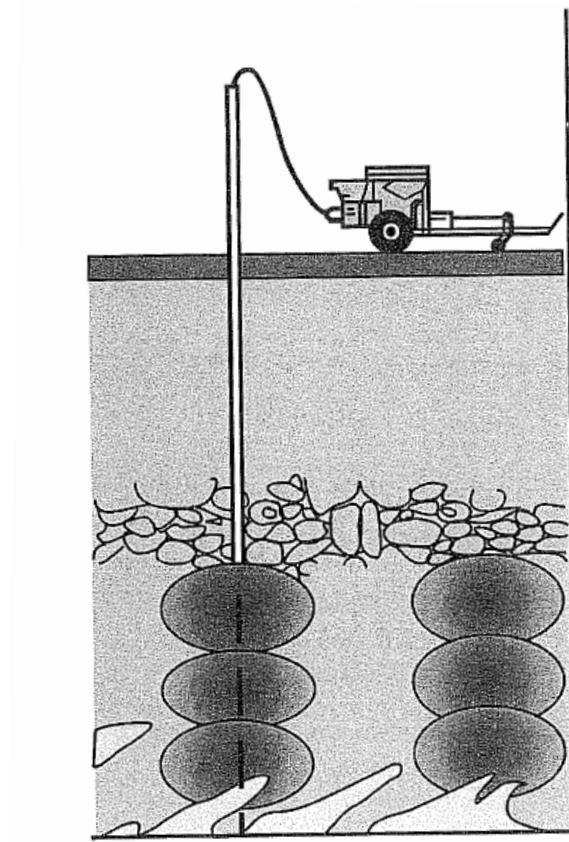
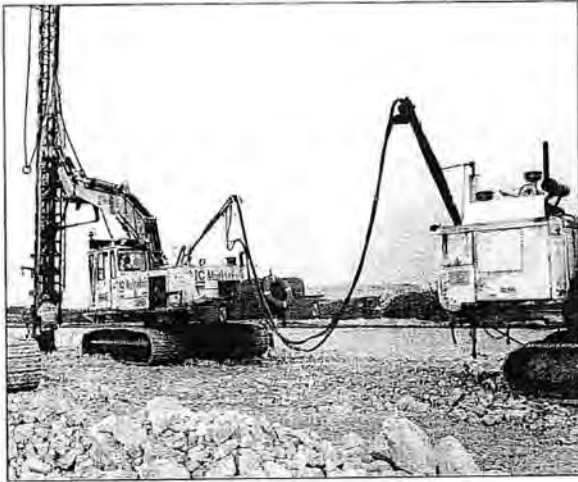
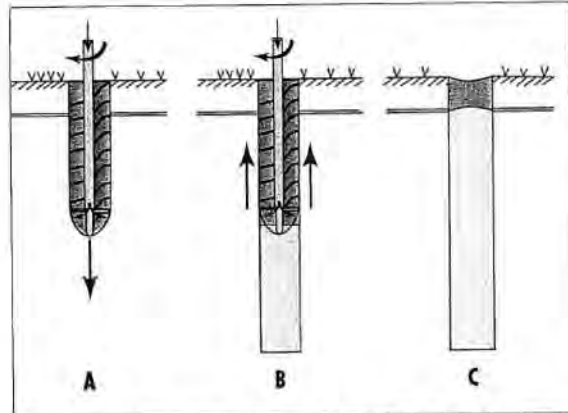


Figure 7-45 Compaction Grout Bulb Construction



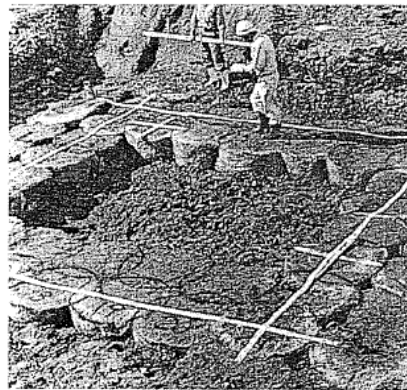
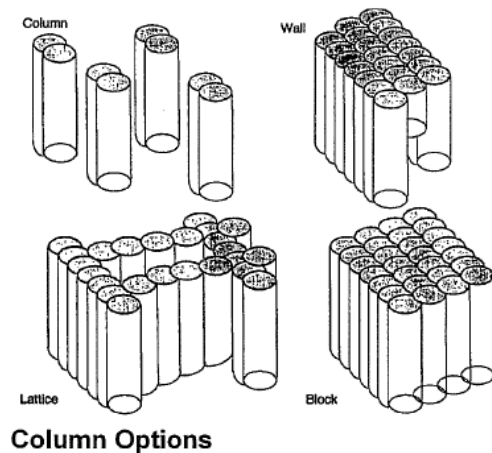
Dry Soil Mixing rig with mobile powder silo.



(A) Mixing tool is inserted to prepare the soil. (B) Lime and cement are injected and mixed as tool is rotated and raised. (C) Depths of completed columns are predetermined and controlled by on-board computer.

Figure 7-46 Dry Method Column Installation

The versatility of the deep mixing construction technique allows columns to overlap to form blocks, walls, or lattice configurations, as shown in Figure 7-47. The choice of pattern depends on the specific application as illustrated in Figure 7-48. Structural walls are typically used for resisting lateral earth pressures in construction of deep excavations while solid blocks may be used to strengthen large volumes of weak soil. Lattice or cellular structures may be used to support lightly loaded structures or to control embankment stability.



Installed Lattice or Cellular Configuration

Figure 7-47 Deep Mixing Column Patterns (after Porbaha et al., 1999)

An example of the use of a lattice type deep mixing columns to mitigate liquefaction is illustrated by a Kobe earthquake case history. The lattice-type deep mixing method was applied to enhance the lateral resistance of the pile foundation of a fourteen story hotel building on the foreshore of the Port of Kobe as shown in Figure 7-49. The building was supported on concrete piles 2.5 m in diameter and 33 m long. The deep mixed walls were installed to encapsulate the piles to a depth of 15.8 m to mitigate liquefaction in the liquefiable fill and prevent lateral spread. During the great Hanshin earthquake (January 17, 1995, magnitude of 7.2 Richter), the quay walls on the west, south and east of the building moved horizontally by 1 m, 2 m, and 0.5-0.6 m, settling by 0.4-0.6 m, 0.5-0.7 m, and 0.2-0.3 m, respectively. This building, nevertheless, survived without damage to its pile foundation. Excavation of the foundation after the earthquake indicated no sign of liquefaction or lateral spread. In concept, the cellular wall structure reduced levels of shear strain in the fill by absorbing the shear loading, thereby mitigating the liquefaction potential.

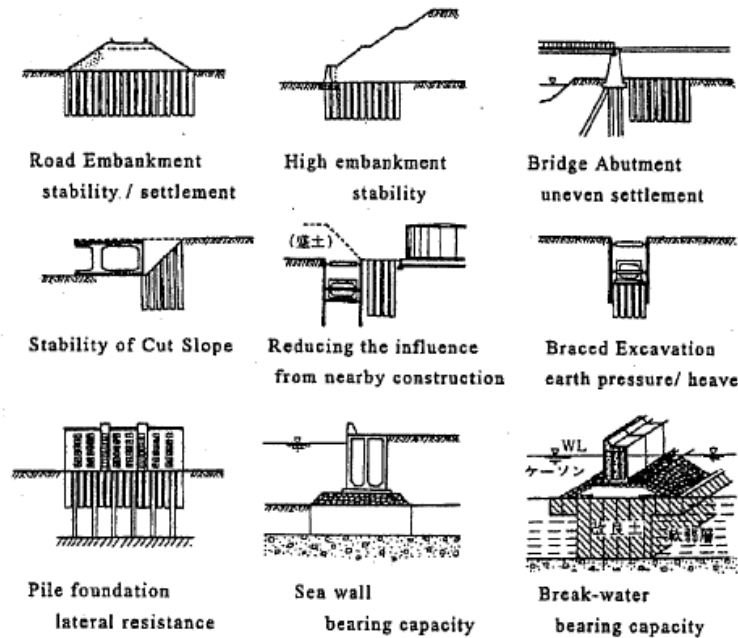


Figure 7-48 Deep Mixing Applications in Japan (after Terashi and Juran, 2000)

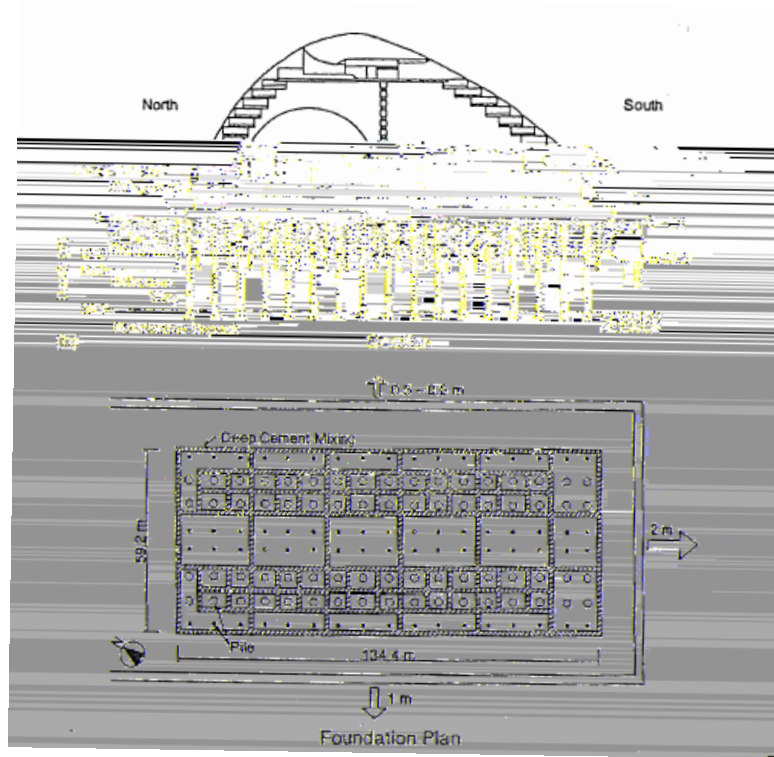


Figure 7-49 Kobe Hotel Foundation Plan

7.6 SUMMARY

This chapter presents an overview of approaches to the seismic analysis and geotechnical design of earthwork features associated with transportation systems. These features are primarily associated with embankment fill and natural and/or cut slopes, where seismic design issues of concern include slope stability and/or earthquake induced deformations, settlement, and liquefaction induced lateral spreads.

Case histories of damages to highways from the above failure modes in past earthquakes are reviewed to illustrate the need for design methods to address deformation performance criteria. Both pseudo-static and displacement based design procedures for slope stability analyses are described and illustrated leading to screening procedures to define conditions where deformation based design checks are not needed. Criteria for establishing acceptable slope displacements are discussed, and mitigation measures to employ where slopes do not meet performance criteria are reviewed. Such measures include toe buttresses, piles, ground anchors, and retaining structures.

The special case of liquefaction included embankment lateral spread deformations are discussed in detail including analysis and design procedures, and illustrative examples. Liquefaction mitigation ground improvement techniques are described including dynamic compaction, stone column installation and deep soil mixing.

CHAPTER 8

GEOTECHNICAL SEISMIC DESIGN FOR TRANSPORTATION STRUCTURES AND SOIL-FOUNDATION-STRUCTURE INTERACTION

8.1 GENERAL

This chapter discusses geotechnical aspects of seismic design for transportation structures, including the importance of interaction between the structural designers and geotechnical specialists, the principles of capacity design, and soil-structure interaction. The following topics are discussed in this chapter:

- The need for collaboration between structural designers and geotechnical specialists in seismic design of transportation structures.
- The seismic design process, including the need for interaction between structural designers and geotechnical specialists in this process.
- How seismic design demand is established for both force-based design and displacement-based design and the principle of capacity protection of foundation elements.
- The desired characteristics of earthquake resisting systems for transportation structures;
- The unintended and potentially adverse consequences on the seismic performance of the overall structure of the intentional incorporation of what is often perceived as conservatism to accommodate uncertainties in soil properties.
- The proper way to account for uncertainties in geotechnical earthquake engineering, including uncertainties associated with the earthquake motion characteristics and soil properties in a practical manner.
- General aspects of geotechnical design for good seismic performance.
- Inertial and kinematic soil-structure-foundation interaction analyses.

8.2 INTERACTION BETWEEN STRUCTURAL DESIGNERS AND GEOTECHNICAL SPECIALISTS IN THE SEISMIC DESIGN PROCESS

Interaction between structural designers and geotechnical specialists during the design of transportation structures is essential, particularly in the context of seismic design, in order to ensure that the resultant design functions as intended when subjected to the design loads. Reasons why interaction between structural designers and geotechnical specialists is necessary in the seismic design process include:

- There are many complexities involved in defining the design earthquake load. The characteristics of the earthquake load (e.g. amplitude, frequency content, duration) depends on three major parameters: (1) the ground motion characteristics, (2) the inertial mass of the structural system, and (3) the overall stiffness of the superstructure and the foundation system. The characteristics of the earthquake ground motion are generally the purview of the geotechnical specialist and the inertial mass of the structure is generally controlled by the structural engineer. However, design decisions from both the structural designer and geotechnical specialist can affect the overall stiffness of the structure.
- Complexities in establishing the earthquake demand often necessitate further interaction between the structural designers and geotechnical specialists. Complexities in the interpretation of the design load associated with the earthquake load include the use of force reduction factors (reduction factors applied to forces established from an elastic response modal analysis in the force based seismic design method). Furthermore, it is often necessary and appropriate to treat the earthquake load as a displacement demand (i.e. to employ the displacement based seismic method) and design strategies for providing force based capacity (which often result in a stiffer system) can be counter-productive to the need for providing displacement capacity (i.e. ductility) to the overall system. These complexities associated with earthquake resistant design require a high degree of interaction between structural designers and geotechnical specialists so that design decisions from either party are not counter-productive to the desired performance of the resultant structure.
- Since some of the required soil properties are difficult to assess and can change significantly during the earthquake, there is a high degree of uncertainty in soil properties as well as an inherent uncertainty in the earthquake loading condition. As such, there is a greater need to properly account for basic uncertainties in the design process for earthquake design than in non-seismic design. This increased uncertainty requires a higher degree of interaction between the structural designers and geotechnical specialists in the earthquake design process.

8.3 GLOBAL DYNAMIC RESPONSE MODEL

Development of a global structural model is usually the first step in the seismic design process for a transportation structure. Typically, a dynamic response analysis using a global structural model is used to develop the seismic demand (load) on individual components of the structure. The dynamic response

analysis is then followed by the determination of the capacity of the structure (e.g., using a pushover analysis to determine the displacement capacity of the structure in the displacement based method). Integrity of the structural system is then established by comparing the capacity to the demand. The three fundamental parameters in the dynamic response analysis of the global structural model, depicted in an idealized manner in Figure 8-1, include:

- 1) Design ground motion characteristics are usually provided by the geotechnical specialist. Chapter 3 in this report provides further details on ground motion characterization. Either a response spectrum or a suite of acceleration time histories usually form the basis for ground motion characterization. In most design applications the design ground motion is characterized by an acceleration response spectrum.
- 2) The inertial mass of the structure. The inertial mass is usually defined by the structural designer.
- 3) The overall stiffness of the structural system. Both the structural designer (who defines the stiffness of the superstructure) and the geotechnical specialist (who defines the stiffness of the foundation) affect the resultant overall stiffness.

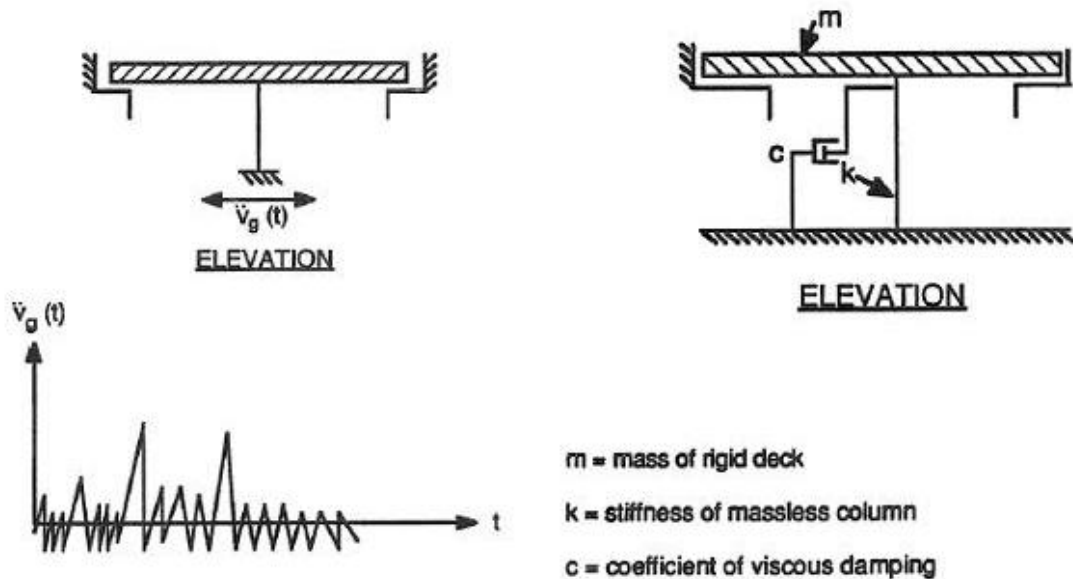


Figure 8-1 Global Structural Model for Seismic Design

Upon developing the global dynamic response model of the structural system, the fundamental period of the structure, T , can be estimated. The earthquake load demand can then be determined from the response spectrum for the fundamental period of the structure. The fundamental period of the structure T is related to the ratio of the overall (lumped) mass and stiffness of the structural system as shown in Equation 8-1:

$$T = 2\pi\sqrt{\frac{M}{K}} \quad 8-1$$

where M is the inertial mass of the structure and K is the overall stiffness (the structure and the foundation) of the system.

Equation 8-1 described the fundamental period, or first mode of vibration, of the structure. In many cases, higher modes of response are also considered in design.

8.4 MEASURES FOR SEISMIC DEMAND IN DESIGN

Figure 8-2 presents a typical generic elastic acceleration response spectrum for use in seismic design. For an analysis where only the first mode of vibration is considered, the fundamental period of the structural system, T, is used along with the design response spectrum to estimate the peak force-based seismic design load, F, in accordance with Newton's second law of motion, $F = M \cdot A$, where A is the spectral acceleration from the design response spectrum corresponding to the fundamental period T. In addition to the force-based design defined by the peak inertial load F (subject to force modification via the use of response modification factor), the system also has a displacement demand defined by the spectral displacement corresponding to the fundamental period, T. The spectral displacement, D, is defined by Equation 8-2:

$$D = \frac{T^2 \cdot A}{(2\pi)^2} \quad 8-2$$

Therefore, in addition to the conventional acceleration response spectrum established for design, there is a corresponding displacement response spectrum defined by Equation 8-2.

Figure 8-2 shows both the acceleration and the displacement response spectra. The acceleration response spectra are denoted by the solid line and the displacement response spectra are shown by the dashed line in this figure.

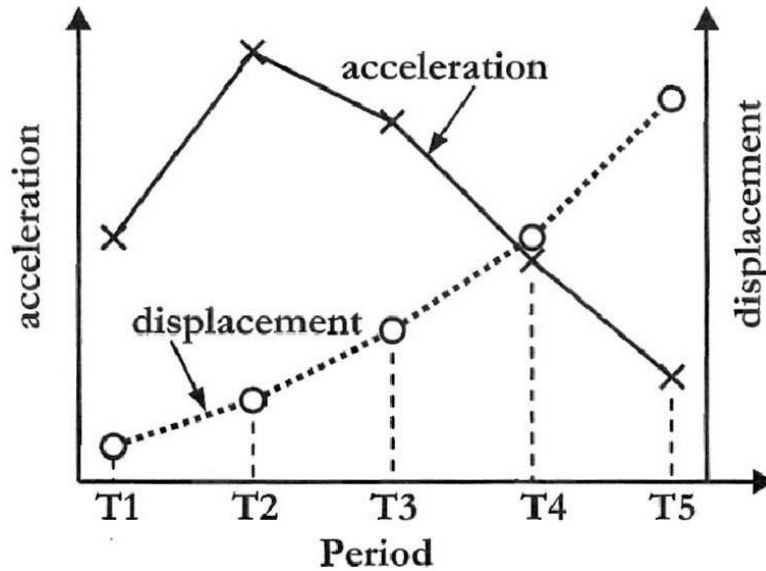


Figure 8-2 Acceleration and Displacement Design Spectra

Figure 8-2 can be used to establish the seismic demand in terms of both the force demand (proportional to the spectral acceleration) and the displacement demand (proportional to the spectral displacement) on the structure for the specified damping ratio (usually assumed to be at 5% in most common design applications). The relationship between spectral acceleration and spectral displacement shown in Figure 8-2 is valid as long as the structure behaves within the linear elastic range. However, in most situations, it would be uneconomical to design a structure for elastic response (implying no damage) in a major earthquake (except in some geographic locations where the seismicity may be low enough that elastic response is all that is expected and required). Modern seismic design in the U.S. is often predicated upon a structure responding inelastically to the design earthquake, provided that life safety is not threatened. When a structure performs inelastically, a force reduction factor, R , is applied to the force demand based upon the elastic response spectrum to determine the actual force level for design.

Figure 8-3 illustrates some of the assumptions implicit in applying a force reduction factor to the peak load based upon the elastic response spectrum to account for inelastic behavior in seismic design. The force demand developed from the elastic design response spectrum. The corresponding elastic displacement demand (from the elastic displacement spectrum) is designated as Δ_u . The force level V_D in Figure 8-3 corresponds to the force at which the member is expected to yield corresponds to an elastic displacement Δ_y .

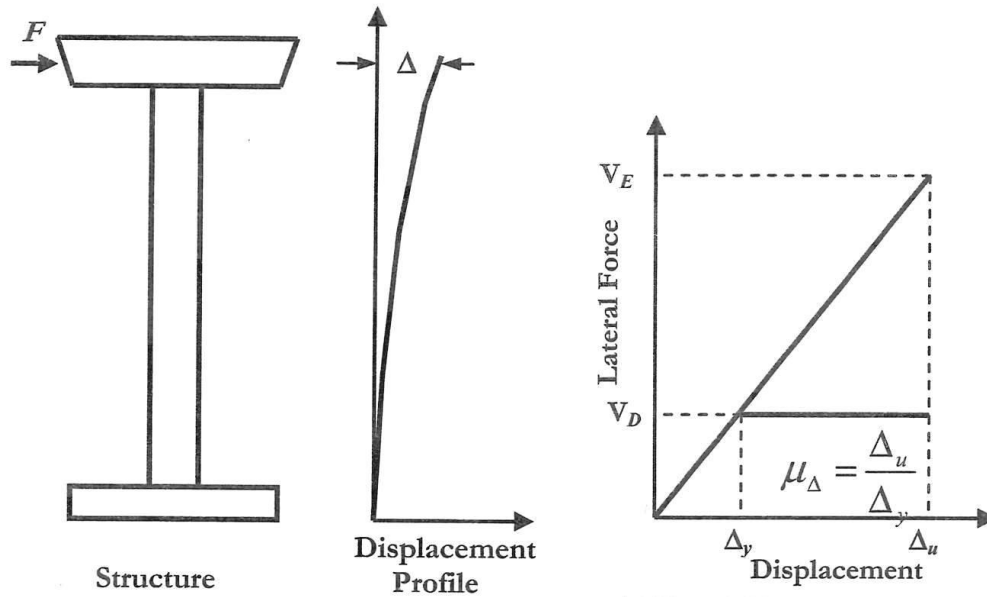


Figure 8-3 Elastic and Inelastic Force and Displacement Demand and the Ductility Ratio

Table 8-1 presents the force reduction factors for bridge substructures from the AASHTO LRFD Bridge Design Specifications. Note that the value of the force reduction factor depends upon the importance category of the bridge. Critical and essential bridges are designed using smaller force reduction factors and thus higher loads (loads closer to the force demand from an elastic response spectra analysis).

TABLE 8-1 FORCE REDUCTION FACTORS, R, FOR BRIDGE SUBSTRUCTURES (Table 3.10.7.1-1, AASHTO LRFD Bridge Design Specifications, 2008 Interim Revisions)

Substructure	Importance Category		
	Critical	Essential	Other
Wall-type piers-larger dimension	1.5	1.5	2.0
Reinforced concrete pile bents	1.5	2.0	3.0
• Vertical piles only	1.5	1.5	2.0
• With batter piles			
Single columns	1.5	2.0	3.0
Steel or composite steel and concrete pile bents			
• Vertical pile only	1.5	3.5	5.0
• With batter piles	1.5	2.0	3.0
Multiple column bents	1.5	3.5	5.0

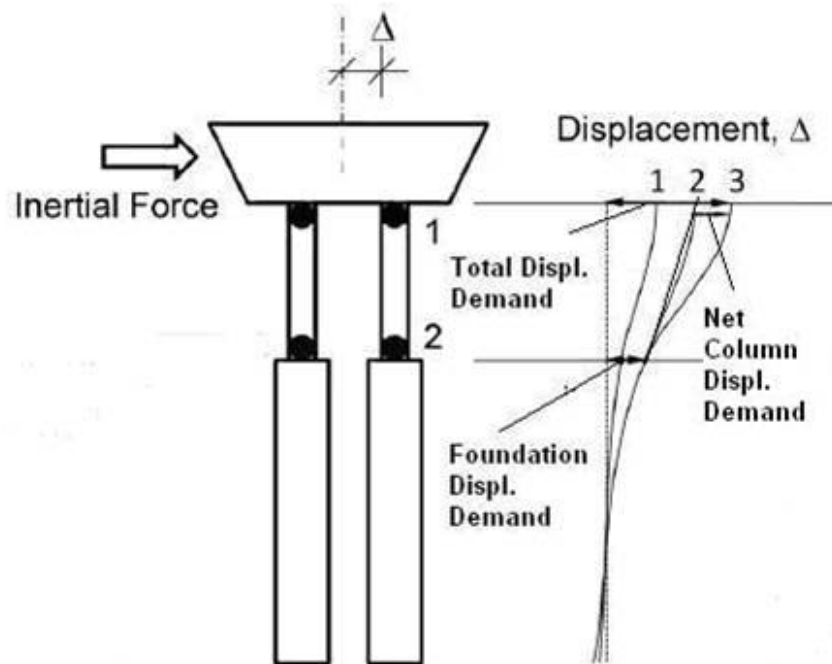
A common assumption in seismic design is the “equal displacement principle” which states that, whereas the actual force demand on the structural system will be much lower than the elastic force demand (V_D is much lower than V_E in Figure 8-3), the displacement demand for the yielding structural system can be approximated by the elastic displacement demand (Δ_u in the Figure 8-3). The ratio of Δ_u (the elastic displacement demand, assumed equal to the displacement demand for the yielding structure) to Δ_y (the displacement at yield) is defined as the ductility demand, μ , from the design earthquake (i.e. $\mu = \Delta_u/\Delta_y$) and is used as an indicator of the anticipated performance of the structure. The ductility ratio μ is related to the degree of damage expected for the structure for various limit states. A ductility ratio μ_1 might represent minimal damage for the serviceability limit state while a larger ductility ratio μ_2 would represent repairable damage for the controlled damage limit state and an even larger ductility ratio μ_3 would represent the non-collapse but significant damage for the life safety limit state.

Once the seismic demand has been established, the next step in the design process is the capacity analysis. The structure capacity may also be force based or displacement based. The capacity analysis in the displacement based method typically consists of a pushover analysis in which the lateral load on the structure is increasing until the lateral displacement from the demand analysis is reached, as illustrated in Figure 8-4. As the structure is displaced laterally the overall displacement demand is distributed into the various components within the structural system. Part of the displacement demand is accommodated by the deformation of the superstructure (e.g. by deformation of the column) and part of the displacement demand is distributed to the foundation system. Theoretically the portion of the displacement demand distributed to the foundation corresponds to the seismic demand on the foundation and the foundation should be checked for the stress corresponding to this demand (superimposed on top of the initial static load). However, very often the foundation is designed to a higher level of performance than the load induced by the superstructure in a pushover analysis (i.e. to keep the behavior of the foundation in the elastic range even when subject to the forces from yielding of the superstructure). This technique, intended protect the foundation from yielding, is referred to as capacity protecting the foundation system (described further in the next section).

An appreciation of the concept of displacement demand in seismic design, as opposed to a conventional force based demand, is important when furnishing geotechnical recommendations to the structural designer. The conventional notion that a lower soil stiffness and foundation capacity is conservative is invalid in a displacement based design framework. Projecting a lower soil stiffness and foundation capacity into the global seismic response model may be counter-productive with respect to the seismic performance of the overall structure due to the following reasons:

- An overly soft soil stiffness may lead to lower stresses in the structural components of both the superstructure and the foundation in a displacement based capacity pushover analysis.
- An overly soft foundation capacity will lead to distribution of a larger proportion of the displacement deformation to the foundation, and hence can lead to an unconservative proportion of the displacement demand being assigned to the superstructure (usually at the bridge column).

Depending on the response characteristics (global stiffness) of the structure and the frequency content of the ground motion, a lower stiffness may also move the overall response of the structure towards resonance (towards the peak or the acceleration response spectrum), thereby increasing the seismic demand. Additional discussions on this topic will be presented in later sections of this chapter when recommendations on accounting for uncertainties in design and on design practice for good seismic performances are provided.



Stages: 1 – First Plastic Hinges Form; 2 – Second Hinges Form; 3 – Deformation Capacity Reached.

Figure 8-4 Pushover Analysis for Displacement Demand Distribution

8.5 CAPACITY PROTECTED DESIGN FOR FOUNDATIONS

The previous section summarized the steps in developing the earthquake force and displacement demand of the overall structure. In a force-based analysis, the force-based demand is compared to the elastic

capacity (capacity at yield) of the structural element. However, displacement based design analysis has increasingly become the general practice for seismic design in areas of high seismicity, especially in the design of the bridge columns. In displacement based design, design of foundation systems can be more complicated than simply providing adequate displacement capacity. In addition to accommodating the portion of the overall displacement demand distributed to the foundation system from the pushover analysis, modern seismic design usually also calls for capacity protection of the foundation. Under capacity protected design, the foundation is provided with an elastic capacity greater than the capacity required to accommodate the applied displacement in order to force inelastic behavior into the bridge columns, where it can be detected and repaired. Figure 8-5 illustrates the concept of capacity protecting the foundation for earthquake loading.

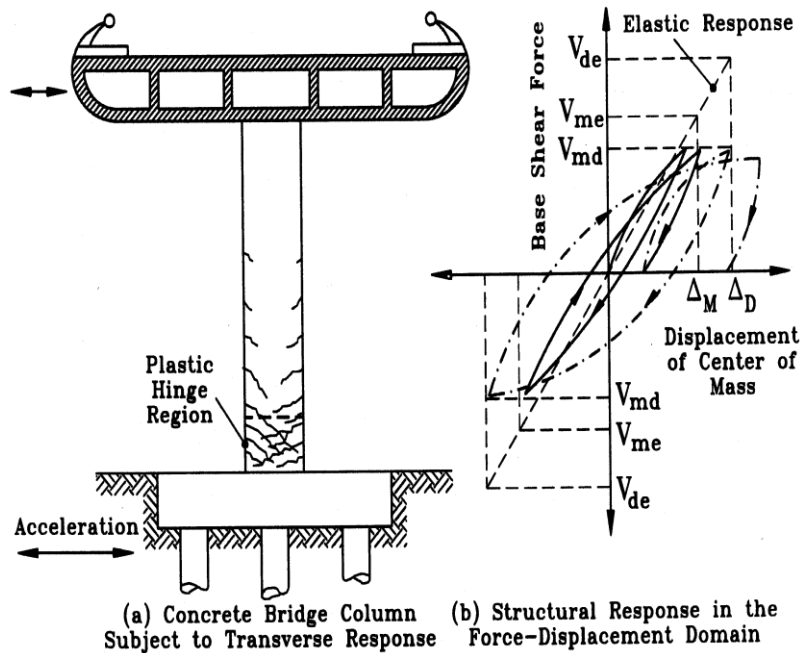


Figure 8-5 Concept for Capacity Protecting the Foundation

Because it is difficult to inspect damage below ground and because there are large inherent uncertainties in the geotechnical elements of the design, capacity protection of the foundation calls for confining potential damage to above ground elements of the structure, typically at the bridge column. For instance, a typical seismic design strategy would be to allow a plastic hinge to form at the base of the column, as illustrated in Figure 8-5. The capacity of the plastic hinge limits the moment and shear that can be transferred to the foundation and the foundation is designed to perform elastically under these limiting

loads (i.e. after the plastic hinge formed). Because the plastic hinge limits the transmission of lateral load to the foundation, it is often referred to a load fuse. In general, the foundation is designed with forces that are greater than the forces required to form the plastic hinge in the column. The AASHTO seismic design procedures are, in general, intended to ensure that yielding is confined above the foundation.

In many situations, capacity protection may not be achievable due to economic constraints and structural forms. Figure 8-6 presents various deep foundation structural forms.

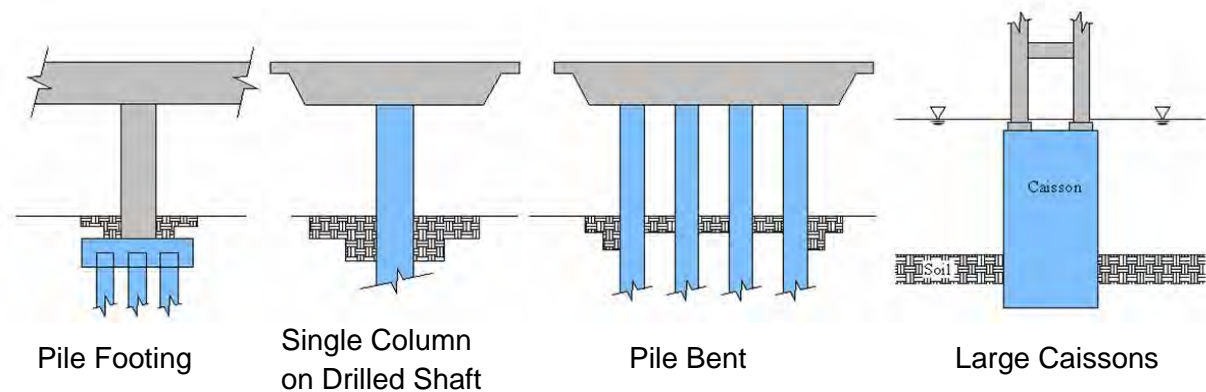


Figure 8-6 Typical Structural Forms for Bridge Foundation Systems

Among the various foundation systems depicted in Figure 8-6, only the classical case of a pile group supported on a column footing readily lends itself to design of a capacity protected foundation. For all the other cases, including for pier walls (in transverse direction), there are practical difficulties in implementing a capacity protected foundation strategy. These difficulties include:

- 1) It is difficult to detail a pier wall for satisfactory ductility behavior in the transverse direction. Hence, it is difficult to ensure for a load fuse above ground for the transverse loading direction.
- 2) For single column drilled shafts, and especially for the multiple column pile extensions, it is difficult to enforce a plastic hinge zone above ground because the maximum moment will usually be below ground. In some cases, structural designers might have the option of enlarging the portion of the shaft or pile extension below ground (relative to the section above ground) to achieve a plastic hinge zone above ground. However, such an approach may complicate construction and lead to a more costly design. Therefore, this approach is employed only in special situations (usually only in seismically active states for important structures).

- 3) It is difficult to achieve capacity protection for large caissons (often used for support of major water crossing structures). For such foundations, most of the inertial mass occurs in the caissons themselves, which are normally very rigid and difficult to detail for ductile behavior. For large caissons, the weak link is often in the soil-caisson interface below the caisson, even though it is possible to design for plastic hinges in the tower leg above the caisson.

In addition to the inherent difficulties in designing various structural forms to achieve a capacity protected foundation system, there are other difficulties in applying this strategy. The concept of foundation capacity protection is a relatively new concept, introduced after the 1971 San Fernando earthquake. Therefore, it is usually very costly to retrofit the older vintage designs often encountered on seismic retrofit projects. On these retrofit projects, the foundations are generally not capacity protected. Instead, there is an emphasis on evaluating the actual performance of the foundation subject to the displacement demand for the design earthquake.

Capacity protection may be extended to elements of the structural system beyond the foundation. The process of applying capacity protection to the entire structure may be generically referred to as capacity design. Capacity design may be summarized by the following three principles:

- 1) Select the locations where damage to the structure is preferred.
- 2) Design those elements of the structure to be ductile.
- 3) Suppress the failure in all other elements.

In force-based design, capacity protection is implicit (based upon the variations in the R factors applied to the elastic demand forces) while in displacement-based design capacity protection is an explicit component of the design process in areas of high seismicity.

8.6 FORCE VERSUS DISPLACEMENT BASED SEISMIC DESIGN

While the trend in practice is towards use of the displacement based method, particularly in areas of high seismicity, force-based design is still used in some jurisdictions and, even if a displacement-based design methodology is used the design of foundations (and some other structural components) may need to be based on force-based criteria to achieve capacity protection. In general, designing the foundation using the capacity protection method implies a higher performance goal, and hence implies an additional cost for the foundation compared to a foundation designed using displacement-based capacity criteria. The

cost differential between force and displacement based design may be especially significant in the less seismically active states, where column sizes are normally dictated by conventional gravity load cases.

It should be recognized that design analysis using a force-based capacity approach implies designing the structural system to resist the peak earthquake load. Such criteria is generally very conservative as it does not consider the transient nature of the earthquake force and the limited amount of time the peak load is applied to the structure compared to sustained gravity load cases (the exception being for very brittle designs). In reality, there can generally be substantial yielding in a ductile structure subject to extreme loads. Yielding will generally modify the dynamic behavior of the structural system such that a reduction in force demand from the assumed elastic response will occur.

One of the consequences of yielding behavior is an increase in the fundamental period of the structure. As the fundamental period lengthens, the forces in the structure will usually be reduced and the displacement will progressively increase. Figure 8-2 can be used to illustrate this point. Assume that the initial period estimated for the structure is equal to T_1 . From the elastic response spectrum depicted in Figure 8-2, the force demand would correspond to spectral acceleration coefficient A_1 and the displacement demand would be Δ_1 . However, as yielding occurs, the initial stiffness would decrease. Assuming the stiffness decreased progressively to a stiffness corresponding to fundamental periods T_2 , T_3 , and T_4 , the force demand would initially increase to correspond to spectral acceleration A_2 but then would decrease to values corresponding to spectral accelerations A_3 and A_4 . At the same time, the displacement demand on the structure will progressively increase to values corresponding to Δ_2 , Δ_3 , and Δ_4 .

8.7 THE EARTHQUAKE RESISTING SYSTEM

One of the beneficial requirements of displacement-based design is that, in areas of high seismicity, the earthquake resisting system of the structure must be explicitly defined, facilitating rational and economic seismic design. Although it is not required, the earthquake resisting system can also be explicitly defined in a displacement based design, and probably should be as a matter of good design practice. The earthquake resisting system defines the path through which the lateral inertial force from the earthquake is transmitted from the superstructure to the foundation. The earthquake resisting system is a “building block” approach for organizing the earthquake load path – it is a tool that focuses the designer on providing a rational load path. The basic requirements for the earthquake resisting system include:

- Simplicity: the load path should be clear and designable;
- Symmetry: the design should provide balanced stiffness, mass, and strength; and
- Integrity: there should be adequate connectivity between elements along the load path.

With respect to design of the foundation, the general principles employed in developing the earthquake resisting system for a displacement-based design include:

- Preventing damage, if possible, by allowing yielding in the structure above the foundation and designing the foundation to withstand forces from the yielding structure times an overstrength factor; and
- If foundation damage is unavoidable, avoid brittle failure modes and limit ductility demands on the foundation elements.

Bridge abutments do not necessarily need to be included in the earthquake resisting system for a bridge. However, abutment design must consider the forces mobilized during the earthquake, should protect damage intolerant parts of the abutment, and prevent brittle modes of failure and limit ductility demands where damage is allowed.

Section 3.3 of the 2009 AASHTO Guide Specifications for LRFD Seismic Bridge Design defines three classes of earthquake resisting system elements: elements that are unconditionally permissible, elements that are permissible with the owner's approval, and elements that are not recommended. With respect to bridge foundations, permissible earthquake resisting system elements include:

- Capacity protected footings, pile caps, and piles that behave elastically;
- Piles or footings with pinned head connections;
- Plastic hinges below cap beams;
- Spread footings that meet eccentricity criteria; and
- Abutment walls that rely on no more than 70% of the presumptive seismic passive earth pressure.

Earthquake resisting elements in the foundation that are permissible with the owner's approval include:

- Batter piles that fail geotechnically (as opposed to structurally);
- Spread footings that slide and rock;
- Pile groups in which more than the outer piles plunge or uplift; and
- Abutment walls that mobilize the full seismic passive resistance.

8.8 SOIL-FOUNDATION-STRUCTURE INTERACTION ANALYSIS

The presence of a constructed facility alters the motion at the base of the structure in a manner that usually tends to reduce it compared to the free field ground motion. The source of the modification of the free field ground motion by the presence of a structure is referred to as soil-structure interaction (SSI). Considering that the structure interacts with the foundation and the foundation interacts with the ground, this phenomenon is perhaps more properly referred to as Soil-Foundation-Structure interaction. There are two sources of soil-foundation-structure interaction:

- Modification of the support motion due to the compliance (stiffness) of the foundation, referred to as inertial interaction; and
- Modification of the free-field ground motions by the presence of the foundations, referred to as kinematic interaction.

Inertial interaction effects depend upon the fundamental period of the structure and the frequency content of the ground motions. Kinematic interaction is generally negligible for shallow foundations and for flexible piles in competent soils and tends to reduce the support motion for stiff piles.

There are various approaches for solving a SSI problem. The most comprehensive approach involves using the finite element or finite difference method to discretize the foundation soils and the structure, including the superstructure, embedded elements of the foundation system, and the surrounding soils. Input motions are applied to the boundary of the model and then propagated through the discretized model. However, such an approach generally leads to extremely large numerical models and is not feasible for most practical applications. If kinematic interaction can be ignored or can be accommodated using an approximation to adjust the free-field ground motion for kinematic interaction effects (which is the case for most situations encountered in practice), simplified approaches such as an equivalent cantilever or the spring and dashpot model shown in Figure 8-7 are often used in practice to model SSI effects. In the simplest case, SSI can be ignored and the free-field motions can be applied to the base of the structure as the design input motions. Such a model ignores the tendency for ground shaking to decrease with depth and hence will generally be conservative and in some cases overly conservative.

The spring and dashpot models illustrated in Figure 8-7 can employ uncoupled or coupled springs. The uncoupled spring models are simple and easy to use but cannot represent the cross-coupling of moment and shear (e.g., coupled rocking and sliding) in foundation behavior. Uncoupled models are generally adequate for shallow foundations and can also be used to model pile groups if proper care is taken to

account of connection details. They are, however, inappropriate for single-column drilled shaft foundations. Coupled springs, including p-y and t-z deep foundation models, can, in general, rigorously account for all types of foundation and abutment systems. However, more parameters are required to describe foundation response and they require more work to develop. Equivalent cantilever models are simple and generally accepted by all bridge design computer codes. They allow for some degree of cross-coupling and may be used to model the dynamic response of single-column drilled shafts foundations. However, they cannot account for the moment distribution in the deep foundation element and the equivalent cantilever may have a different length for each of the five relevant degrees of freedom (3 translational and 2 rotational degrees of freedom) of the foundation

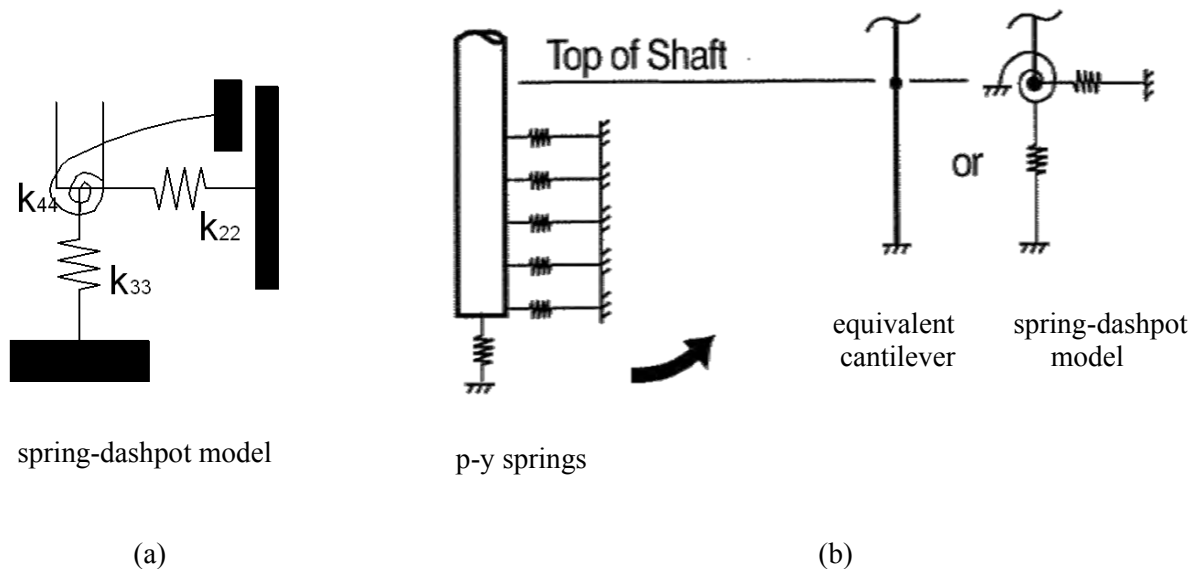


Figure 8-7 Inertial Interaction Models; a) Shallow Foundation Model and b) Deep Foundation Model

The kinematic interaction of a deep foundation system can be modeled using the approach illustrated in Figure 8-8. This model makes use of linear or nonlinear spring elements to model the soil and beam column elements to model the structural components. Depth-varying free field motions from a site response analyses are input at the free ends of the soil spring elements. This type of soil-structure interaction model, representing the entire pile foundation all the way to the pile tips, is referred to as a direct (or total) soil-structure interaction model.

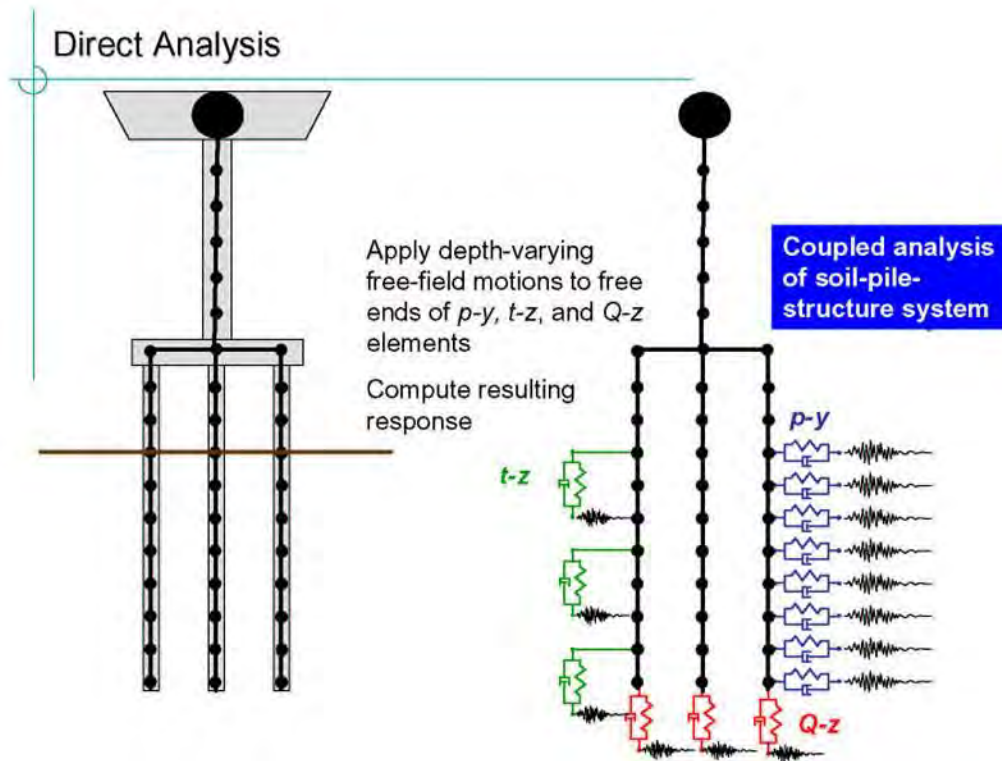


Figure 8-8 Direct (or Total) Soil-Structure Kinematic Interaction Model

The degree of conservatism implicit in designing for the free field ground surface motion, i.e. in ignoring kinematic interaction, depends on several factors, including the stiffness of the soil profile. Using the free field ground surface shaking motion as the design motion is particularly conservative for soft soil sites, where there is generally a significant decrease in ground shaking intensity at depth, even for a moderate depth below ground surface. For such soft soil sites, there may be a significant benefit for conducting more advanced kinematic soil-structure interaction analyses to minimize the conservatism associated with using the free field ground surface motion as the input motion. In these cases, the SSI analysis can be conducted employing the direct SSI model shown in Figure 8-8. However, on many projects a more economical substructuring analysis technique is used to reduce the size of the foundation model. A common way to develop a foundation substructure would be to statically condense the pile foundation and the depth-varying free field motions to the pile cap node. In this manner, the many degrees of freedom of a pile group foundation can be reduced to a six degree of freedom system (3 translational and 3 rotational degrees of freedom) at the pile cap node, as shown in Figure 8-9. Static condensation of the depth-varying input motion is accomplished by taking the dot product of the input ground displacement and the soil spring stiffnesses. The resulting kinematic motion time history can be used as the input

motion for a time history response analysis of the structural substructure or to develop a response spectrum for a response spectrum analysis of the bridge. This methodology has been discussed in detail by Lam and Law (2000).

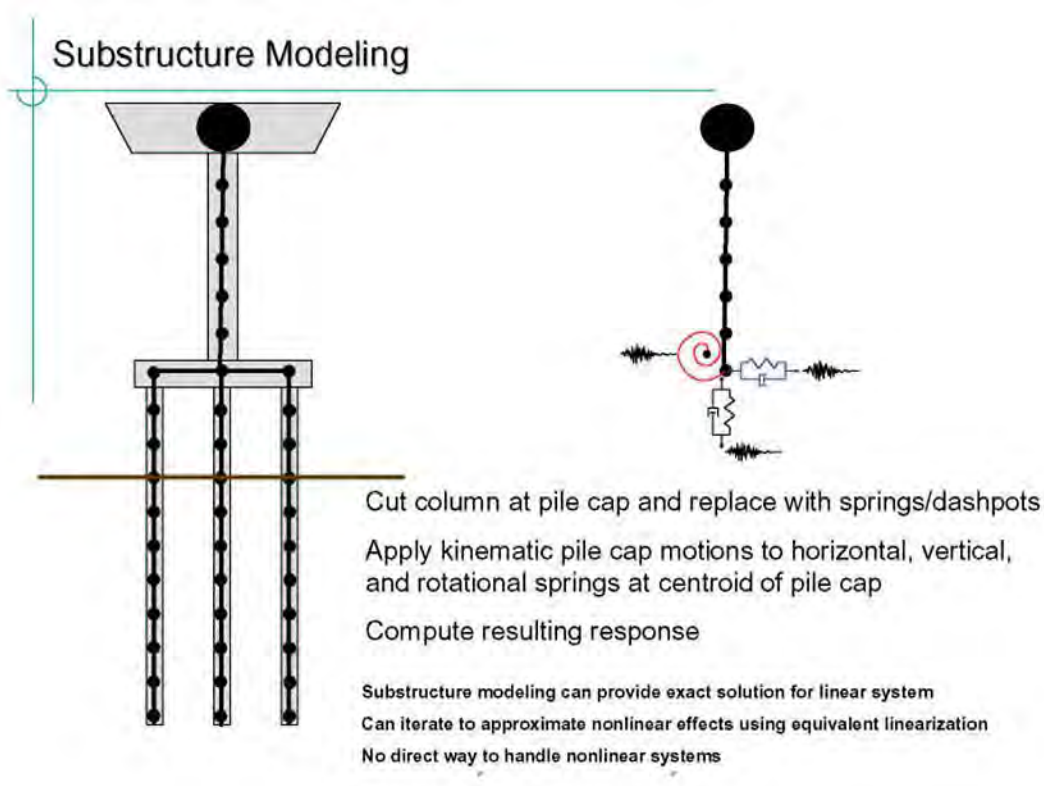


Figure 8-9 Foundation Substructuring Model for Kinematic Analysis

Kinematic interaction can also be addressed in an approximate manner by empirically adjusting the free-field ground motion to account for kinematic interaction effects. Figure 8-10 presents ground shaking versus depth (in terms of acceleration and displacement response spectra) from a site response analysis conducted for the San Francisco-Oakland Bay Bridge East Span Replacement Project. A response spectrum developed from the kinematic pile cap motion (shown as the thick dark green spectrum) from substructure static condensation has also been presented in this figure for comparison. Comparison of the kinematic pile cap response spectrum to the free field ground surface response spectrum (shown in red) shows that the intensity of the kinematic motion is about 50% of the intensity of the free field ground surface motion. However, as shown in the figure, the kinematic pile cap spectrum corresponds roughly to the free field motion at about 46 ft depth (between 5.5 and 6 times pile diameter).

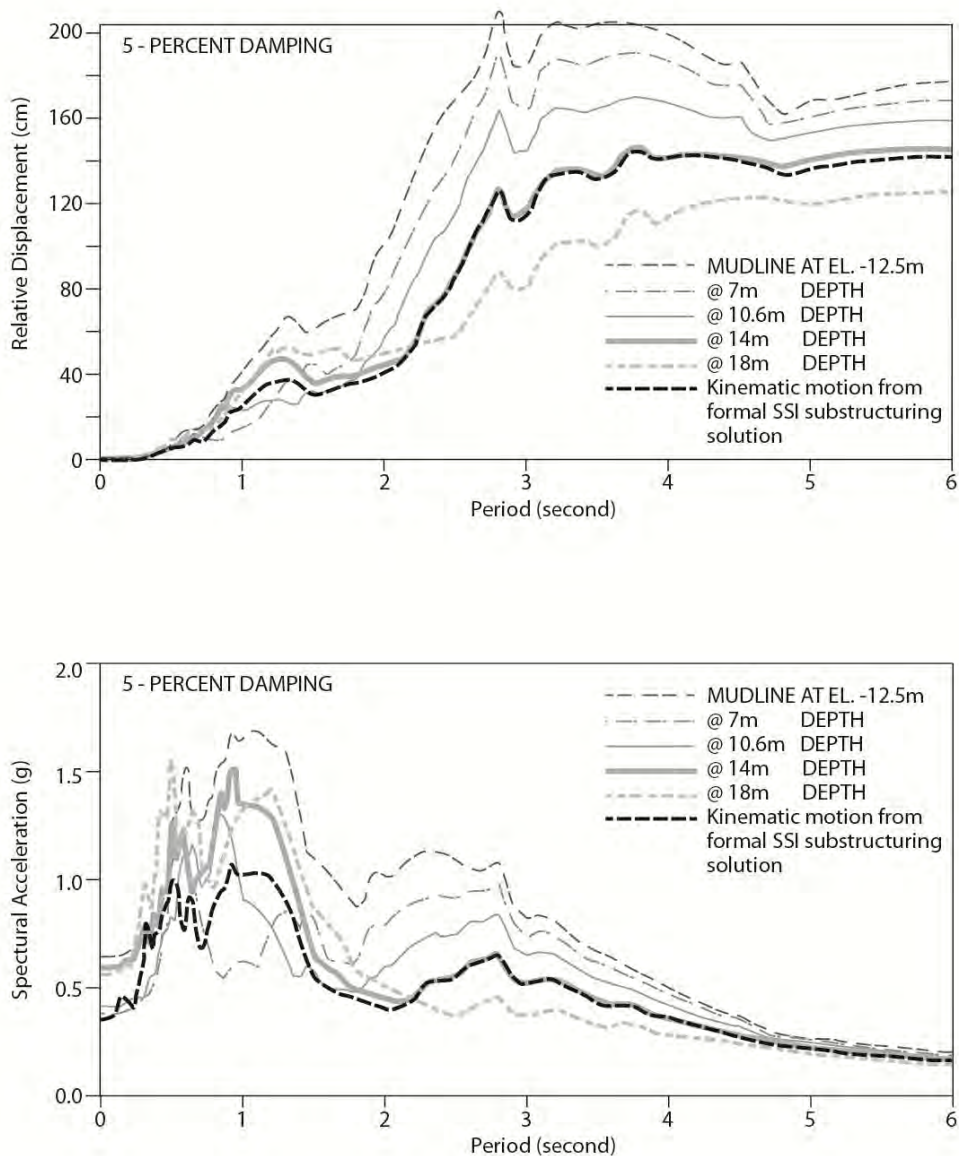


Figure 8-10 Comparison of Kinematic Motion from SSI to Free field Depth Varying Motions

From the Bay Bridge example, it can be deduced that, for soft soil sites and large diameter pile foundations (8 ft diameter piles were used for the Bay Bridge project), soil-structure interaction analyses can lead to a significant cost saving by minimizing undue conservatism associated with the use of the free field ground surface motion as the input motion for structural design. Developing a mathematically rigorous substructure model for the kinematic pile cap motion may be beyond the scope of many projects. However, experience with SSI analysis suggests that a pile foundation may be designed for the ground motion at equal to approximately 4 to 6 times pile diameter beneath the pile cap. The validity of this

approximate method to account for kinematic interaction has been verified by independent checks conducted by structural designers on numerous projects (e.g. by Ingham et al.1999).

8.9 AASHTO SEISMIC DESIGN REQUIREMENTS

AASHTO bridge design specifications include provisions for both force-based design and displacement-based design. The 2008 Interim Revisions to the 2007 LRFD Bridge Design Specifications (the Interim Revisions) address force-based design. The 2009 Guide Specification for LRFD Seismic Bridge Design (the Guide Specifications) addresses displacement-based design. In both the force- and displacement-based design provisions of AASHTO, bridge seismic design requirements depend upon the value of S_{D1} , the site class-adjusted value of the design spectral acceleration coefficient at 1 second. AASHTO defines four seismic design levels, referred to as Seismic Zones in the Interim Revisions and Seismic Design Categories in the Guide Specifications, based upon, S_{D1} . Table 8-2 presents the four AASHTO Seismic Zones (Table 3.10.6-1 in the Interim Revisions) and Seismic Design Categories (Table 3.5-1 in the Guide Specifications).

TABLE 8-2 AASHTO SEISMIC DESIGN CATEGORIES

Value of $S_{D1}=F_v S_1$	Seismic Zone	SDC
$S_{D1} < 0.15$	1	A
$0.15 \leq S_{D1} < 0.30$	2	B
$0.30 \leq S_{D1} < 0.50$	3	C
$0.50 \leq S_{D1}$	4	D

Both seismic design requirements and foundation modeling requirements in AASHTO depend upon the seismic design zone or category.

8.9.1 Interim Revisions

The AASHTO Interim Revisions employ force based design. Design requirements are based upon the Seismic Zone as briefly outlined in Table 8-2. Table 8-3 (Table 4.7.4.3.1-1 from the Interim Revisions) presents a summary of the minimum analysis requirements for seismic design of bridges in accordance with the Interim Revisions. Table 8-4 summarizes seismic design requirements from Section 3.10 of the Interim Specifications.

TABLE 8-3 SEISMIC ANALYSIS REQUIREMENTS FOR BRIDGES FROM THE INTERIM REVISIONS

Seismic Zone	Single-Span Bridges	Multispan Bridges					
		Other Bridges		Essential Bridges		Critical Bridges	
		regular	irregular	regular	irregular	regular	irregular
1	No seismic analysis required	*	*	*	*	*	*
2		SM/UL	SM	SM/UL	MM	MM	MM
3		SM/UL	MM	MM	MM	MM	TH
4		SM/UL	MM	MM	MM	TH	TH

UL = uniform load elastic
 SM = single-mode elastic
 MM = multimode elastic
 TH = time history method

TABLE 8-4 SEISMIC DESIGN REQUIREMENTS FOR BRIDGES FROM THE INTERIM REVISIONS

Seismic Zone	Summary of Seismic Design Requirements
1	Horizontal connection forces based upon prescribed horizontal force coefficient and minimum support lengths
2	Design for elastic seismic forces divided by R-factors except for foundation elements other than pile bents and retaining wall, where R/2 (but not less than R=1) shall be used. Prescriptive detailing and minimum support lengths are also required.
3 and 4	Design for the lesser of: Elastic seismic forces divided by R-factors, with R = 1 for foundation elements; or The force effects resulting from inelastic hinging with prescribed overstrength factors for columns and piers Prescriptive detailing and minimum support lengths are also required.

8.9.2 Guide Specifications

Table 8-5 presents a summary of the minimum seismic design requirements from Section 2.5 of the 2009 AASHTO Guide Specifications for LRFD Seismic Bridge Design. For SDC A, explicit identification of the Earthquake Resisting System is not required, no demand analysis or capacity check is needed, and capacity design is not required. Furthermore, in the AASHTO Guide Specifications a liquefaction analysis is not required for SDC A. The only seismic design requirements for SDC A are minimum detailing, connection force, and support length requirements.

For SDC B, identification of the ERS is optional, a demand analysis is required, a capacity check is performed using implicit formulae. The ERS should be identified to avoid weak links in the ERS, capacity design should be considered for column shear, and a liquefaction check should be considered. For SDC C, identification of the ERS, demand analysis, capacity design, and liquefaction evaluation are

required. For SDC D, in addition to the requirements for SDC C, a displacement capacity evaluation using a pushover analysis is required as is a member ductility demand limit check. In SDC D, the implicit displacement capacity check may be used in lieu of the pushover analysis, but the limits provided by that check are conservative. There are also specific detailing requirements for each SDC.

TABLE 8-5 SEISMIC DESIGN REQUIREMENTS FROM THE 2009 AASHTO GUIDE SPECIFICATIONS

SDC	ERS	<i>Demand Analysis</i>	<i>Capacity Check</i>	<i>Capacity Design</i>
A	No	No	No	No
B	Optional	Yes	Implicit	Optional
C	Yes	Yes	Implicit	Yes
D	Yes	Yes	Yes	Yes

Table 8-6 presents the AASHTO requirements for foundation modeling from Section 5.3.1 of the 2009 AASHTO Guide Specifications for LRFD Seismic Bridge Design. Modeling methods are divided into two categories for each of three foundation types. The recommended modeling method depends upon both Seismic Design Category and Site Class. Modeling Method I includes modeling foundations as rigid supports and modeling foundations using an equivalent depth to fixity. Method II includes rigid modeling for rock-supported foundations and modeling using foundation springs and p-y curves for soil-supported foundations. For SDC A, no modeling is required. For SDC B and C, foundations for bridges in Site Class A through D may be modeled as rigid foundations or using the depth of fixity, i.e., using Method I. For SDC B and C and Site Classes E and F, Modeling Method II is required. For SDC D, Modeling Method II is required for all site classes.

TABLE 8-6 FOUNDATION MODELING REQUIREMENTS FROM THE 2009 AASHTO GUIDE SPECIFICATIONS

Foundation Type	Modeling Method I	Modeling Method II
Spread Footing	Rigid	Rigid for Site Classes A and B. For other soil types, foundations springs required if footing flexibility contributes more than 20% to pier displacement.
Pile Footing with Pile Cap	Rigid	Foundation springs required if footing flexibility contributes more than 20% to pier displacement.
Pile Bent/Drilled Shaft	Estimated depth to fixity	Estimated depth to fixity or soil springs based on P-y curves.

8.10 COORDINATION BETWEEN STRUCTURAL DESIGNERS AND GEOTECHNICAL SPECIALISTS

There are a variety of design issues on which coordination is required between geotechnical specialists and structural designers. These issues include:

- 1) How do the structural designers intend to use the foundation stiffness parameters (e.g. soil springs) provided by the geotechnical specialists. Are the foundation stiffness parameters to be used solely for determining the fundamental period of the overall structure, or will they also be used for determining the seismic demand of the overall structural system? Is the primary measure of seismic demand for the overall structure to be measured in terms of the displacement or force demand?
- 2) Are the foundation springs to be used in capacity pushover analyses for assessing the integrity of the superstructure (e.g. at the column)? Will the drift of the column be reduced by the foundation displacement, in which case an overly soft foundation stiffness could result in under-estimating the column demand and hence be unconservative for designing the superstructure (e.g. the bridge columns)?
- 3) Following the integrity evaluation of the superstructure (e.g. bridge columns), how will the foundation integrity evaluation be conducted? Is the measure of foundation demand in terms of displacement (e.g. the displacement demand distributed to the foundation in a pushover analysis), or is it a force based demand from a plastic hinge in the column? Clarifying this issue is important in recommending soil spring stiffness parameters so as not to mislead the structural designers in a manner counter-productive to good design. If the foundation demand is displacement based (e.g. in terms of pile cap displacement demand), an overly soft soil spring can lead to an unconservative pile stress in addition to an unconservative column drift.
- 4) Is the project a new design as opposed to a retrofit design? It is generally economically feasible to design a new foundation system based on the capacity protected foundation approach because one can design the column based on more modern ductility design procedures. However, in a retrofit project, it may not be economically feasible to achieve a capacity protected foundation system. In such cases, it is usually necessary to evaluate the actual performance of the structure, including the foundation system, based on a displacement based procedure.

- 5) Realizing that there are significant uncertainties in the soil properties used in seismic design, it is generally desirable to evaluate the design considering some degree of variation in the soil parameters. Additional comments on incorporation of uncertainties in soil properties into the design are presented in the next section.

8.11 TREATMENT OF UNCERTAINTY IN SEISMIC DESIGN

As discussed in the preceding section, good seismic design practice often requires consideration of a range of soil parameters to account for uncertainty in their values. Consideration of soil property uncertainty is particularly important due to the difficulty in determining the impact of soil spring stiffness on design. The impact of soil spring stiffness on design depends upon (1) the specific structural component being designed (e.g. the column in the superstructure or the foundation element), (2) whether the demand is measured in terms of force or displacement, and (3) where the fundamental period of the structure lies with respect to the predominant period of the design ground motion

Experience shows that a large degree of uncertainty can be accommodated in soil stiffness with only a very modest cost impact on the designed structure. One of the most important aspects in considering the impact of soil spring stiffness on seismic design is the need to be consistent in the assumed soil stiffness throughout the design analysis process. Seismic design is usually conducted in a two step procedure, starting with a response analysis using a linear elastic model for establishing the seismic demand and then employing a capacity analysis involving a nonlinear structural model (when displacement based method is adopted). Due to a different analytical frameworks in the two step procedure, an incompatible soil spring representation is often introduced into the two models. This practice usually leads to undue conservatism in the design process.

Figure 8-11 illustrates the need for consistency in analysis and the potential for undue conservatism if inconsistent soil spring stiffness is adopted between the demand analysis and the capacity assessment. This figure presents the results of a sensitivity study that employed three soil spring stiffness scenarios: (1) the best estimate case, (2) a stiffer case in which the soil stiffness is multiplied by 2.0, and (3) a softer case in which the soil stiffness is reduced by a factor of 0.3. The figure presents the pile load versus deflection and corresponding pile load versus pile moment curves for the three different soil stiffness cases for a 24-inch reinforced concrete pile. The load-deflection plots for the 660% in soil stiffness show about a 300% difference in the overall pile stiffness.

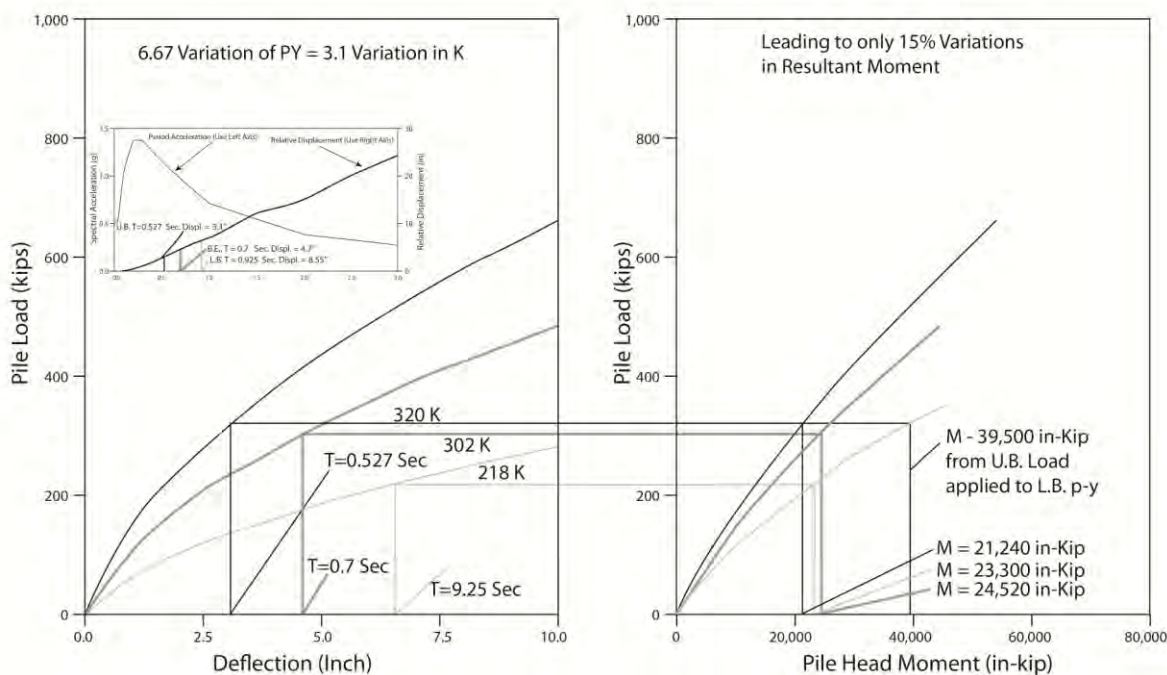


Figure 8-11 Effect of Soil Stiffness on Performance of 24-inch Reinforced Concrete Pile

The variation in pile stiffness leads to a change in the fundamental period for the bridge from 0.7 second for the best-estimate stiffness to 0.53 second for the stiffer case and 0.93 second for the softer case.

The bridge that employed the piles modeled in Figure 8-11 was designed using the response spectra shown at the top of Figure 8-11. The variation in the fundamental period for the three cases of soil stiffness led to a displacement demand varying from 3.1 to 6.6 inches. Thus the 660% variation in soil stiffness led to a 300% variation in overall pile stiffness and a 210% variation in the corresponding displacement demand. However, the associated pile maximum moment changes from 21,240 in-kip to 24,520 in-kip over this displacement demand range, a variation of only about 15%! The 15% variation in pile moment will have a relatively modest impact on the reinforcing requirement for the pile foundation and therefore will impact the cost of the constructed structure by a very modest amount. The 210% variation in the displacement demand may only affect the design of the expansion joints and therefore would also have a modest cost impact on the constructed bridge. It is also interesting to note that the governing pile moment arises from the best-estimate soil stiffness, illustrating the difficulty in predetermining which design scenario would be most conservative in seismic design. This sensitivity

study suggests that even if one employs a 660% variation in soil stiffness to account for uncertainty, it may not have a significant cost impact to the design. This is consistent with feedback from experienced structural designers on past projects.

Figure 8-11 can also be used to illustrate the impact of designing the bridge using inconsistent soil stiffness between the demand and the capacity models. For example, if the seismic demand is developed based on the stiffer soil stiffness, it would imply a shear load of 320 kips per pile. If this shear load is then used in a separate laterally loaded pile analysis based on the softer stiffness, the pile moment would become 39,500 in-kip, which is much higher than the 24,520 in-kip maximum obtained when consistent in soil stiffness is used in the demand and capacity model, even when this stiffness is allowed to vary by 660%.

8.12 FOUNDATION DESIGN STRATEGY FOR GOOD SEISMIC PERFORMANCE

Keys to good seismic performance include simplicity, integrity and symmetry in the structural system. AASHTO strongly encourages balanced stiffness among various frames in a bridge system. Design guidelines suggest the difference in stiffness between any two bents within a frame or between any two columns in a bent should be no more than 50 percent. Furthermore, the variation in stiffness between adjacent bents within a frame or between adjacent columns within a bent should not differ by more than 25 percent. Balanced frame geometry provisions strongly encourage that adjacent frames (i.e. structural units on either side of an articulation joint, such as an in-span hinge) have fundamental vibration periods that are within 30 percent of one another.

The concept of minimizing the variation in the overall structural stiffness may also be extended to the foundation system. The foundation designer should strive to minimize the variation in foundation stiffness from bent to bent and from footing to footing where feasible. One of the primary contributors to the variation in foundation stiffness, especially between adjacent bents, is the variation in soil conditions. Variable soil stiffness is particularly important in the surficial soil layers. Surficial soil layers tend to have the greatest impact on the lateral stiffness of the foundation as well as a tendency for a larger degree of variation than soil layers at depth. The structural stiffness of a deep foundation element (i.e. the bending stiffness EI) also influences the overall stiffness of the foundation. Employing a pile with a larger EI can therefore reduce the degree of variation in foundation stiffness due to variations in surficial soil stiffness at the site. Also, because the variation in surficial soil stiffness has a more profound influence on the lateral foundation stiffness than the axial pile stiffness, the use of battered piles to carry

the lateral load can sometimes be an effective strategy for reducing the degree in variation in the lateral stiffness among bents. However battered pile systems can introduce additional complexity in design (especially when there is significant potential for kinematic earth pressure loading on the pile due to permanent ground movements), as discussed in the next paragraph.

The preceding paragraphs have concentrated on designing for seismic inertial loads. However, there is another seismic load case, the kinematic ground displacement load case. The kinematic ground displacement load case refers to the loads due to seismically induced permanent ground displacement on the foundation, and was discussed in detail in Chapter 7. The kinematic ground displacement load case is important at sites prone to liquefaction induced lateral spreading ground displacement as well as sites where there is downslope movement due to embankment instability (e.g. at banks of river crossings). These permanent ground displacements can induce passive earth pressures on the foundation system, resulting in distress to the structural elements of the foundation, or cause excessive movement of the bridge resulting in the bridge deck falling off the bridge seats (and other forms of structural distress). These forms of bridge damage have been the cause for a significant proportion of the recorded bridge damage during earthquakes, e.g. in the 1964 Alaskan earthquake and the 1964 Niigata earthquake in Japan. These forms of damage also have been the prevalent form of earthquake induced damage to pile supported wharf structures at port facilities.

Kinematic ground displacement loading tends to involve massive movement of the ground and hence it is generally not feasible to resist this movement with foundation elements on a brute force basis. A better option in case of kinematic loading is to employ a compliant foundation system that can move and deform with the ground. Because they are relatively non-compliant, battered pile groups have performed poorly when subject to kinematic loading (e.g. battered concrete pile damage beneath Port of Oakland wharf structures during the 1989 Loma Prieta earthquake). Either steel piles, due to their ductility, or specially fabricated concrete piles or drilled shafts that are designed to accommodate ground deformation would be the preferred foundation system for cases of kinematic loading.

Kinematic loading due to permanent ground displacement may also be important for embedded structures (including retaining walls, culverts and tunnels). For an embedded structure, the kinematic ground deformation induced earth pressure may far exceed the magnitude of loading due to inertial effects. Hence, a good strategy in seismic design of an embedded structure is to provide the structure with an ability to deform with the ground movement, as oppose to hardening the structure to resist it.

8.13 SUMMARY

In summary, this chapter presents a discussion of several seismic design issues, including the need for collaboration between structural designers and geotechnical specialists, force- and displacement-based methods for seismic demand and capacity evaluation, the principles of capacity protection and earthquake resisting system design, and soil-structure interaction. Interaction between structural designers and geotechnical specialists is needed to deal with conflicting requirements for earthquake design. Seismic design of foundation systems may employ both displacement-based and force-based design procedures. The displacement-based design procedure is particularly useful in areas of high seismicity as it has the capacity to account for the inelastic response of modern structures in the design earthquake. The force based approach, especially the use of capacity protected foundation systems, is designed to provide adequate seismic performance of the structural system but is not necessarily expected to predict its actual performance. The force based approach is generally a more conservative approach suitable for designing new structures where one can implement an appropriate ductility mechanism in the intended locations. The displacement based approach, however, would generally be more appropriate in the context of retrofitting existing structural systems. It is generally too costly to retrofit existing structures to achieve the goal of a capacity protected foundation system. The geotechnical specialist should discuss with the structural designer the appropriate foundation evaluation approach in order to develop a workable overall design approach.

A description of advanced soil-structure interaction topics was also presented in this chapter. The need for revision of the free-field ground surface motion to account for kinematic interaction effects was discussed. Previous project experience showed that significant reduction in free field ground surface motion may be realized in soft soil sites when proper SSI effects are taken into consideration.

This chapter also provides a discussion on practical ways to treat uncertainty in the seismic design process. It was demonstrated that, when properly handled, the foundation design can account for a very large degree of uncertainty in soil properties with only very modest impact on the cost of the structural system. It was also demonstrated that it is dangerous to design based on the conventional assumption that a softer soil stiffness and lower soil strength is conservative.

Strategies for selecting the appropriate foundation system for good seismic performance of the overall structure were also presented in this chapter. In addition to the basic inertial load case, the issue of seismic loads due to kinematic ground displacement (deformation) was discussed.

CHAPTER 9

SHALLOW FOUNDATIONS

9.1 GENERAL TYPES OF SHALLOW FOUNDATIONS

This section outlines seismic analysis and design procedures for shallow foundations. As the name implies, in a shallow foundation the base of the foundation where the loads from the structure are transferred to the underlying soil is at relatively shallow depth, close to the ground surface. This geometric configuration lends itself to modeling as a rigid footing resting on the surface of an infinite soil mass. Classical solutions for rigid surface footings, including solutions for capacity and stiffness, can be evaluated independent of the coupling between moment and shear loads. This is fundamentally different from deep foundations, where it is important to account for the coupling effects between the moment and shear load.

The assumption of a rigid footing at a shallow depth is implicit for most design equations and charts in the literature for shallow foundations (spread footings). When analyzing the performance of a shallow foundation, the engineer should examine the validity of the two parts of this implicit assumption (rigidity and shallow depth), as foundations that do not conform to these two conditions may require special treatment. Further comments regarding the validity of these conditions will be provided subsequent sections of this Chapter.

Figure 9-1 presents typical configurations employed for shallow foundations. The most common types of shallow foundations for transportation facilities are rectangular footings (for circular or rectangular columns) and strip footings for pier walls. Mat foundations are relatively rare for transportation facilities. Shallow foundations are suitable at rock sites or when firm soils are found at shallow depth provided the potential for landslide induced displacements is fairly low and the risk of liquefaction is very low or non-existent. In areas where deposits of compressible, expansive, or collapsible soils are found at depth below the ground surface, shallow foundations may not be suitable. Where soil conditions are not suitable for the use of shallow foundations, deep foundations are used.

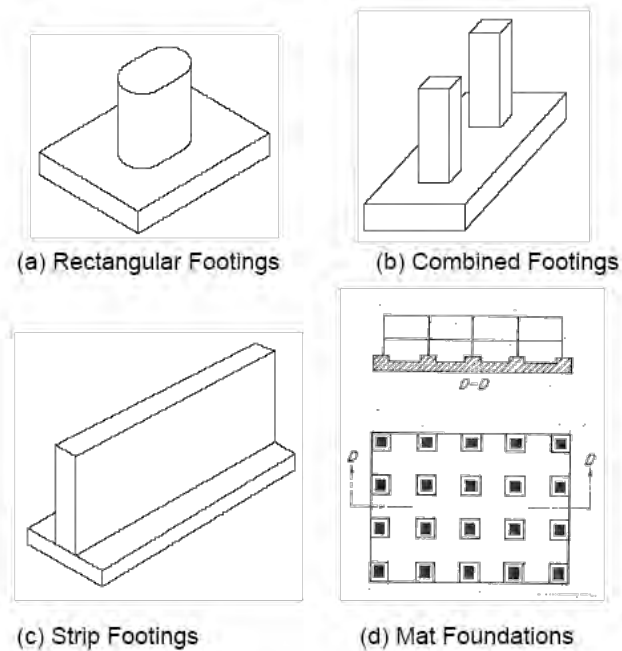


Figure 9-1 Types of Shallow Foundations

9.2 SEISMIC PERFORMANCE AND VULNERABILITY OF SHALLOW FOUNDATIONS

Iwasaki et al. (1972) provided a comprehensive review of the seismic performance of highway bridges. Although their review was triggered by the 1971 San Fernando Earthquake, these investigators compiled observations of damage to highway bridges from 14 major earthquakes around the world, including earthquakes in U.S., Japan and in South America. The report documented a wide range of bridge damage, including the role played by foundation in the observed damage. These investigators observed apparent distinct differences in case histories for highway bridge damage as far as foundation behavior was concerned. For example, bridge damage from the 1964 Alaskan earthquake and many of the Japanese earthquakes, including the 1964 Niigata Earthquake, were typically due to foundation failure triggered by ground failure (often from liquefaction). There is little evidence in those case histories that excessive inertial force from dynamic bridge response led to the observed damage of the bridge. The bridge deck commonly remained intact for such case histories, but the excessive foundation movement often led to the bridge deck falling off its seat support.

Bridge damage observed in the 1971 San Fernando Earthquake was very different from the damage observed in Japan and Alaska in 1964. The most common type of bridge damage observed in the 1971 San Fernando Earthquake, as well as in other more recent California earthquakes (including the 1989 Loma Prieta Earthquake and the 1994 Northridge Earthquake), was associated with excessive inertial loading induced by the earthquake. However, most of the damage in these case histories was confined to the structural components of the bridge. There is relatively little evidence of seismically-induced damage to bridges on shallow foundations due to inadequate geotechnical foundation capacity that does not involve liquefaction ground failure. Shallow foundations generally perform satisfactorily when subject to earthquake-induced inertial loads in the absence of liquefaction largely because a relatively large margin of safety is provided for the bearing capacity under static loads. Therefore, vertical bearing failure under seismic loads is unlikely. The primary impacts of seismic loads on a shallow foundation are likely to be limited lateral and vertical displacements and perhaps yielding of structural components of the footing, impacts that are not likely to threaten life safety or lead to collapse.

The inertial loading on the bridge structure (including the loading on the foundation elements) is dependent upon is the response characteristics (stiffness) of the foundation due to soil-foundation-structure interaction effects, as discussed in Chapter 8. Thus, characterizing the stiffness of a shallow foundation subject to earthquake loading is an important seismic design consideration. Despite the paucity of case histories of earthquake-induced damage due to exceeding the geotechnical capacity of a shallow foundation, geotechnical capacity evaluation of a shallow foundation is also an important design task, along with evaluation of the structural capacity of the foundation elements.

9.3 STATIC VERSUS SEISMIC LOADS ON SHALLOW FOUNDATIONS

The most common seismic analysis procedure in bridge design is the response spectrum method, in which evaluation of the seismic loads are based upon the assumption that the bridge structure behaves in a linear elastic manner. Non-linear behavior, including yielding of structural components, yielding of the soil, and geometric nonlinearity such as rocking or uplifting of the footing, tends to reduce the calculated earthquake load for most bridge structures. Hence, relatively large load reduction factors (2 to 4) are commonly applied to the force calculated from a response spectrum analysis. Actually, as discussed in Chapter 8, earthquake design analyses are progressively trending toward the displacement based approach, leading to the need to design bridge components to accommodate the displacement demands from the earthquake (described by the displacement response spectrum) as opposed to the force demand

(from the acceleration response spectrum). In a displacement-based capacity analysis, a pushover analysis is conducted to model various forms of nonlinearity in the bridge system and to evaluate the force levels for design. Forces determined from these nonlinear structural pushover analyses are, in general, more realistic than the elastic forces from an elastic response spectrum analysis reduced by gross force reduction factors in a bridge designed to yield but not collapse. Furthermore, as discussed in Chapter 8, in areas of high seismicity foundations are often capacity protected, with force demands controlled by fuses in the system such as a plastic hinge at the base of the column. The designer of the foundation should be clear about the design approach being used by the structural designer to determine the foundation demand in order to provide appropriate recommendations for design.

9.4 SOIL-FOUNDATION-STRUCTURE INTERACTION

9.4.1 Foundation Substructuring

Foundation design often employs the concept of substructuring the overall bridge structure-foundation-and soil mass system so that the foundation can be considered independently of the superstructure. A global bridge model generally involves a very large number of elements in order to model the entire superstructure, all of the piers or columns, and the foundation supports at each pier or bent along the alignment. Because of the size of the overall model, generally it is not feasible to analyze the overall bridge structure-foundation-soil mass system as a total complete model in a single step solution. Hence, substructuring is generally employed to condense each of the foundation supports and its supporting soil mass into a foundation substructure to reduce the resultant global bridge model to a manageable size. Available methods for substructuring foundation systems are discussed by Lam and Law (2000). One of the most common ways involves substructuring the foundation to a single node at the base of each pier.

One of the limitations of the substructuring approach is that in a response spectrum analysis it invokes the principle of superposition and therefore cannot explicitly model nonlinearity in the foundation substructure system. However, if the dynamic (inertial) response analysis of the bridge superstructure model is conducted in the time domain, nonlinearity in the superstructure can be treated in the inertial interaction problem. State-of-the-art dynamic response analyses for seismic design have been moving toward time-domain solution approaches (particularly for major long-span bridge projects). The need for substructuring to reduce the size of the global bridge model has also been progressively relaxed in favor of the superior complete total model (i.e. incorporating the foundation into the global structural model

without the need of substructuring) as computational capabilities increase. However, for a shallow foundation the substructuring approach can generally adequately capture the dynamic response characteristics of the foundation and their impact on the seismic performance of the bridge system.

9.4.2 Kinematic and Inertial Interaction

As discussed in Chapter 8, soil-foundation-structure interaction effects include kinematic interaction (modification of the foundation support motion by the presence of the foundation) and inertial interaction (modification of the structure motion due to the compliance of the foundation). Lam and Law (2000) concluded that, even for very large foundations (caisson foundations for long-span bridge), as long as the site soil is competent the free field outcrop motion will be modified by kinematic interaction only in the high frequency range (spectral periods less than 0.5 second period). Furthermore, it has been shown that ignoring the effect of kinematic interaction and designing for the free field outcrop motion tends to be conservative, especially for high frequency motions. Kinematic interaction effects can be significant at very soft soil sites, but these sites typically require the use of deep foundations. Therefore, for spread footings (i.e. for foundations in competent soil conditions) kinematic interaction is not important for practical problems and only inertial interaction needs to be considered for seismic design of the foundation and superstructure.

Figure 9-2 outlines the two steps involved in a rigorous inertial interaction analysis. The first step involves conducting a forced vibration analysis of the foundation-soil mass system (Figure 9-2a) to solve for the frequency dependent foundation impedance (stiffness and damping) function. The second step involves inputting the frequency dependent foundation impedance function developed in Step-1 to the global structural model and conducting the inertial response analysis of the structure (Figure 9-2b). As shown in Figure 9-2, the impedance function can be visualized as a dynamic spring of stiffness K in parallel with a viscous dashpot with a damping coefficient C . When this impedance function is used in the inertial response analysis, it accounts for both the soil mass stiffness and the energy dissipation mechanism referred to as radiation damping (the dissipation of energy due to seismic waves radiating away from the foundation).

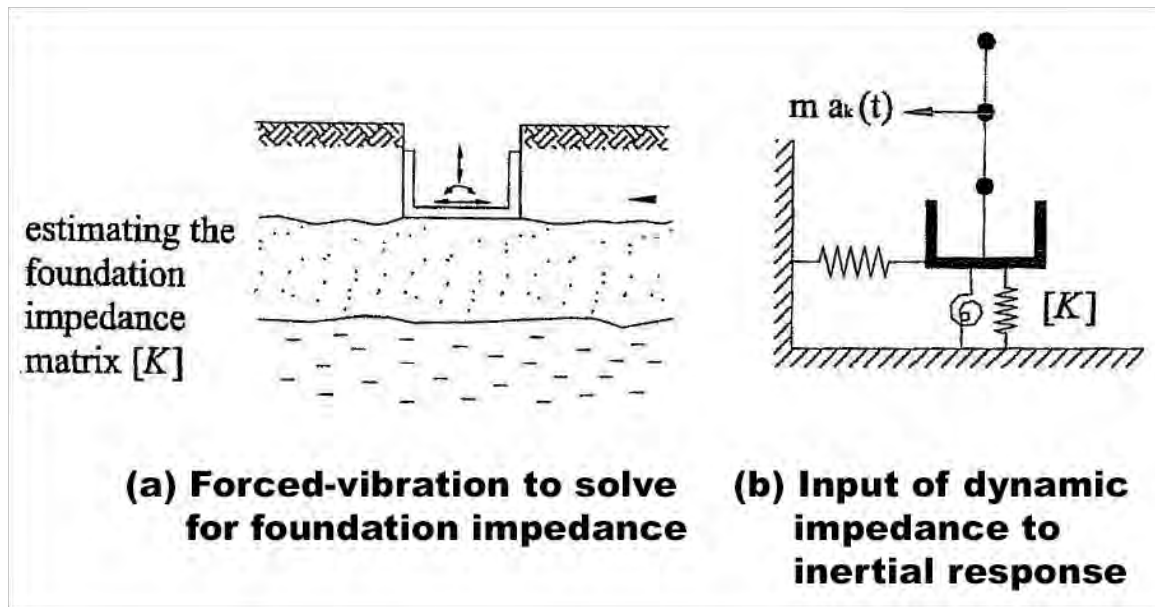


Figure 9-2 Two Step Rigorous Inertial Response Solution Incorporating Frequency Dependent Foundation Impedance

Figure 9-3, from Mylonakis and Gazetas (2002), shows the dynamic stiffness factor (the ratio of the dynamic stiffness to the static stiffness) for the impedance function for the rocking mode of a rigid rectangular footing on the ground surface (assuming an elastic semi-infinite half space). Figure 9-3 shows that the dynamic stiffness approaches the static foundation stiffness (i.e. the dynamic stiffness factor becomes unity) when the normalized frequency of loading ($\omega B/V_s$) approaches zero (i.e. at long periods) and when the length, L , of the footing divided by its width, B , is equal to or less than 4. In fact, for the range of spectral periods and L/B ratios generally applicable to the seismic design of bridges, the dynamic stiffness factor is close to 1. Therefore, for response spectrum analysis (the analysis most often used for ordinary highway bridges), the static foundation stiffness is generally employed in design. The frequency dependent stiffness only becomes important for problems involving high frequency response such as foundation vibration problems and nuclear power plant containment structures.

Even in a major bridge project employing time history response analyses, it is not possible to implement the frequency dependent foundation impedance function. Instead, the engineer can select one characteristic frequency relevant to the overall response of the global structural system. However, in virtually all cases where this has been done, the period of interest was sufficiently long that the foundation stiffness was based on the static stiffness

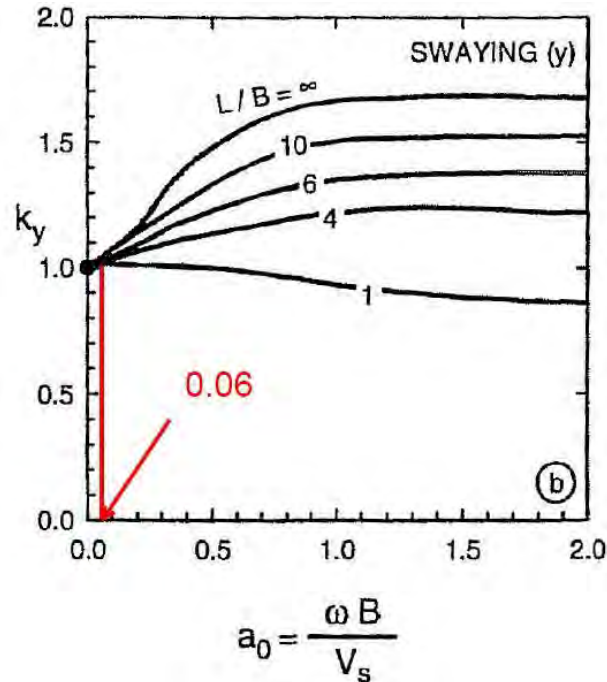


Figure 9-3 Frequency Dependent Dynamic Stiffness Factor for a Surface Footing (Gazetas, 2002)

It also should be noted that there is a lack of experimental data to support the validity of the frequency dependent solution. In fact, data presented by Gadre and Dobry (1998) showed that footing stiffness and damping exhibit very strong displacement amplitude dependent tendencies, as opposed to being frequency dependent. The trend of softening in stiffness and an increase in energy dissipation with increasing amplitude of footing displacement observed by Gadre and Dobry suggests nonlinear material governs footing response behavior rather than frequency dependent behavior of a rigid footing on an elastic medium.

Gadre and Dobry also conducted forced vibration experiments at frequencies ranging from 0.5 to 0.0167 hertz and concluded that radiation damping was negligible and that the observed damping can be largely attributable to internal (material) damping. Gadre and Dobry also compared the shear modulus back calculated from the response measured in their experiments with the small strain shear modulus, G_{max} , for their foundation material (75% relative density dry Nevada sand). The shear modulus deduced from their testing was approximately 1.73 MPa (36,200 psf) at the smallest displacement level that could be measured in their experiments. This shear modulus is much lower than small strain modulus for the Nevada sand. In fact, the modulus reduction factor, G/G_{max} , implied by the experiment for the foundation soil is smaller than 0.05. This observation emphasizes the need to be focused on the near field large strain

behavior as opposed to the far field smaller strain behavior relevant to a free field wave propagation problem.

9.5 FOUNDATION STIFFNESS FORMULATION

9.5.1 Spring Constants

Procedures for evaluating soil-footing-structure interaction problems have evolved over time from the theory of continuum mechanics. As noted above, frequency dependent stiffness and damping (or foundation impedance functions) applicable to low amplitude, high frequency machine vibration problems and very rigid site nuclear power plant containment buildings founded on very competent soil are not applicable to earthquake soil-foundation-structure interaction problems for bridges. The frequency dependence of the dynamic stiffness of the foundation can be ignored and it is adequate to employ the static foundation stiffness for seismic design of bridges.

9.5.2 Equivalent Stiffness Matrix for Shallow Footing

The general form of the 6 x 6 shallow footing stiffness matrix is shown in Figure 9-4. As shown in the figure, off diagonal terms in the stiffness matrix for shallow footings are generally assumed to be zero (i.e. the cross-coupling terms are ignored). However, this assumption may become invalid when the depth of embedment becomes large. Additional discussion is provided in Section 9.5.3 on this point.

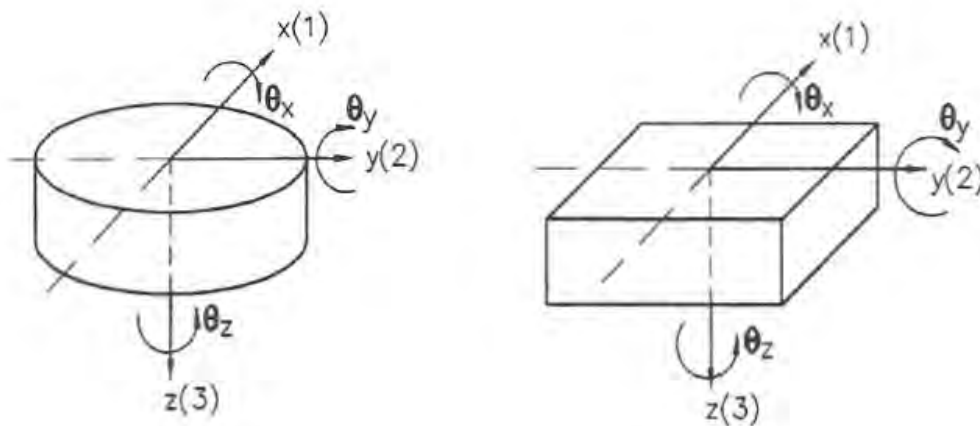
The uncoupled stiffness coefficients (i.e. the diagonal terms) in the 6 x 6 stiffness matrix may be based upon theoretical solutions from elasticity theory. Solutions for the stiffness of a rectangular rigid plate of dimensions L and B resting on the surface of an elastic half space from Gazetas (1991) are presented in Figure 9-5. The stiffness matrix coefficients shown in Figure 9-5 can be adjusted to account for embedment, as discussed in the next section.

In some cases, when the size of the footing becomes large the rigid footing assumption may no longer be valid and the footing stiffness developed from Figure 9-5 and Figure 9-6 may over estimate the stiffness of the foundation. Hytenyi (1946) used beam on elastic subgrade theory to check whether a large footing can be assumed to be rigid. Hytenyi classified beam and subgrade combinations into (1) short beam, (2) intermediate beam and (3) infinitely long beam problems. A rigid footing assumption must satisfy the short beam classification.

Hytényi defined a short beam in terms of the following condition:

$$\lambda L < 6 \quad \text{for } \lambda = \sqrt[4]{\frac{E_s}{4EI}} \quad 9-1$$

where E_s is the subgrade modulus (dimension of FL^{-2}); and EI is the bending stiffness of the footing (dimension of FL^2).



$$\begin{matrix}
 \delta_x & \delta_y & \delta_z & \theta_x & \theta_y & \theta_z \\
 \left[\begin{array}{cccccc}
 K_{11} & 0 & 0 & 0 & -K_{15} & 0 \\
 0 & K_{22} & 0 & K_{24} & 0 & 0 \\
 0 & 0 & K_{33} & 0 & 0 & 0 \\
 0 & K_{42} & 0 & K_{44} & 0 & 0 \\
 -K_{51} & 0 & 0 & 0 & K_{55} & 0 \\
 0 & 0 & 0 & 0 & 0 & K_{66}
 \end{array} \right]
 \end{matrix}$$

Figure 9-4 Form of the Shallow Foundation Stiffness Matrix

9.5.3 Footing Embedment Effects

The surface footing stiffness terms discussed above can be modified for embedment effects by multiplying the stiffness coefficients for the surface footing shown in Figure 9-5 by the embedment factors e_i presented in Figure 9-6. However, the assumption that the off-diagonal stiffness terms are small and can be ignored becomes questionable when the thickness of the footing, d , becomes large with respect to the footing width. The embedment factors in Figure 9-5 should not be used when $d > B$ (i.e. when the footing thickness is greater than the smaller plan dimension of the footing).

Stiffness Parameter	Rigid Plate Stiffness at Surface, K_i'
Vertical Translation, K_z'	$\frac{GL}{(1-\nu)} \left[0.73 + 1.54 \left(\frac{B}{L} \right)^{0.75} \right]$
Horizontal Translation, K_y' (toward long side)	$\frac{GL}{(2-\nu)} \left[2 + 2.5 \left(\frac{B}{L} \right)^{0.65} \right]$
Horizontal Translation, K_x' (toward short side)	$\frac{GL}{(2-\nu)} \left[2 + 2.5 \left(\frac{B}{L} \right)^{0.65} \right] - \frac{GL}{(0.75-\nu)} \left[0.1 \left(1 - \frac{B}{L} \right) \right]$
Rotation, K_{θ_x}' (about x axis)	$\frac{G}{(1-\nu)} I_x^{0.75} \left(\frac{L}{B} \right)^{0.25} \left[2.4 + 0.5 \frac{B}{L} \right]$
Rotation, K_{θ_y}' (about y axis)	$\frac{G}{(1-\nu)} I_y^{0.75} \left[3 \left(\frac{L}{B} \right)^{0.15} \right]$
<div style="display: flex; justify-content: space-between;"> <div style="width: 45%;"> <p style="text-align: center;">Plan</p> <p style="text-align: center;">Section</p> </div> <div style="width: 45%;"> <ol style="list-style-type: none"> Determine the uncoupled total surface stiffnesses, K_i', of the foundation element by assuming it to be a rigid plate bearing at the surface of a semi-infinite elastic half-space (see above). Adjust the uncoupled total surface stiffnesses, K_i', for the effect of the depth of bearing by multiplying by embedment factors (see Table 6-2), e_i, to generate the uncoupled total embedded stiffnesses, K_i $K_i = e_i K_i'$ </div> </div>	
<p>Note: I_x, I_y are moments of inertia of the footing about the x- and y-axes, respectively.</p>	

adapted from Gazetas, 1991

Figure 9-5 Stiffnesses for a Rigid Surface Footing on a Semi-Infinite Half Space

Stiffness Parameter	Embedment Factors, e_i
Vertical Translation, e_z	$\left[1 + 0.095 \frac{D}{B} \left(1 + 13 \frac{B}{L} \right) \right] \left[1 + 0.2 \left(\frac{(2L + 2B)}{LB} d \right)^{0.67} \right]$
Horizontal Translation, e_y (toward long side)	$\left[1 + 0.15 \left(\frac{2D}{B} \right)^{0.5} \right] \left\{ 1 + 0.52 \left[\frac{\left(D - \frac{d}{2} \right) 16(L+B)d}{BL^2} \right]^{0.4} \right\}$
Horizontal Translation, e_x (toward short side)	$\left[1 + 0.15 \left(\frac{2D}{L} \right)^{0.5} \right] \left\{ 1 + 0.52 \left[\frac{\left(D - \frac{d}{2} \right) 16(L+B)d}{LB^2} \right]^{0.4} \right\}$
Rotation, $e_{\theta x}$ (about x axis)	$1 + 2.52 \frac{d}{B} \left(1 + \frac{2d}{B} \left(\frac{d}{D} \right)^{-0.20} \left(\frac{B}{L} \right)^{0.50} \right)$
Rotation, $e_{\theta y}$ (about y axis)	$1 + 0.92 \left(\frac{2d}{L} \right)^{0.60} \left(1.5 + \left(\frac{2d}{L} \right)^{1.9} \left(\frac{d}{D} \right)^{-0.60} \right)$

adapted from Gazetas, 1991

Figure 9-6 Embedment Factors for a Rigid Footing on a Semi-Infinite Half Space

Design charts for adjusting for the embedment effect for rectangular footings, developed by Lam et al. (1986), are presented in Figure 9-7. The advantage of these charts is that they employ a single parameter, D , to characterize the embedment effect instead of the two parameters, D and d , employed in Figure 9-6. It should be noted that the embedment adjustment factor appears to become unrealistically large at large embedment, possibly due to the idealistic no slippage at the interface and the no soil failure assumption inherent to the elastic half space solution.

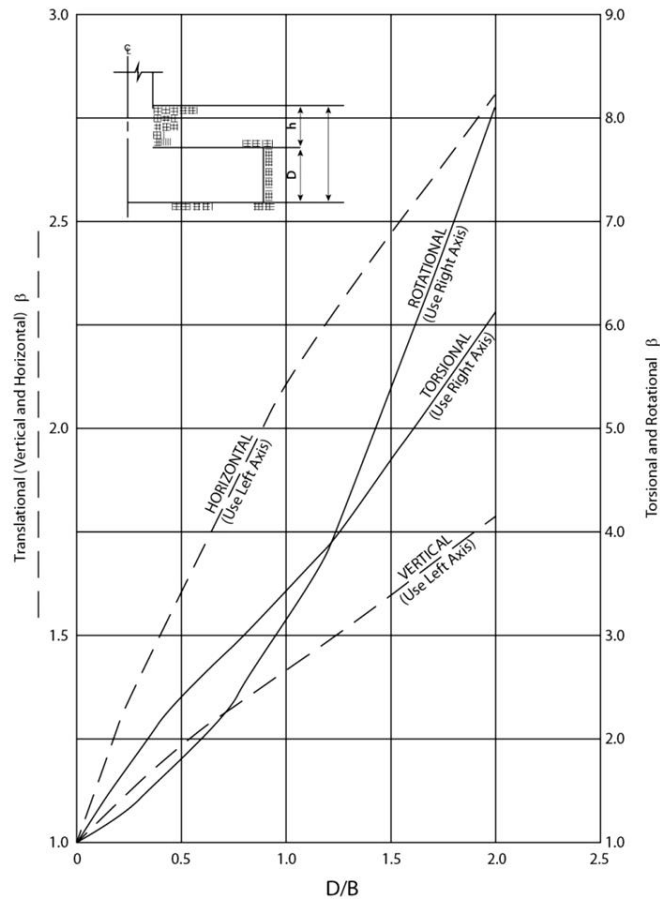


Figure 9-7 Embedment Factor in Graphical Format from Lam and Martin (1986)

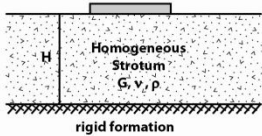
9.5.4 Soil Modulus for Foundation Stiffness

As noted previously, soil modulus values based upon the shear wave velocity of the soil (i.e. the small strain modulus of the soil) must be reduced to account for softening at the strain levels relevant to foundation response. For practical purposes, modulus softening can be related to the intensity of the earthquake ground motions. In NCHRP 12-49 (NCHRP 2002), modulus softening was related to the site class-adjusted spectral acceleration at a period of 1 second for the free field motion. For relatively strong motions, e.g. $F_v S_1 > 0.5g$, it was recommended that the small strain modulus be reduced by a factor of 0.25. For weak motions, e.g. $F_v S_1 < 0.3g$, it was recommended that the shear modulus be reduced to 50 percent of the small strain value. For in between values of ground motions, interpolation was recommended. However, it is also recommended that the sensitivity of the results of the seismic analysis to

the foundation stiffness be evaluated using stiffness values varied from half of the best estimate value to twice the best estimate value.

9.5.5 Effects of Limited Depth to Hard Layer

Natural soil deposits are frequently underlain by stiffer soil layers or bedrock. If the stiffer or bedrock layer is at a sufficiently shallow depth, it may be appropriate to adjust the foundation stiffness for the effect of the underlying stiffer layer. Figure 9-8, from Mylonakis and Gazetas (2002), presents the solution for the stiffness coefficients for a finite soil layer overlying a rigid base for use in design.



Foundation Shape		Circular Foundation of Radius $B = R$	Rectangular Foundation $2B$ by $2L$ ($L > B$)	Strip Foundation $2L \rightarrow \infty$
Static stiffness K	Vertical, z	$K_z = \frac{4GR}{1-\nu} (1 + 1.3 \frac{B}{H})$	$K_z = \frac{2GL}{1-\nu} [0.73 + 1.54 (\frac{B}{L})^{3/4}] (1 + \frac{7.7}{0.5+8L})$	$\frac{K_z}{2L} = \frac{0.73B}{1-\nu} (1 + 3.5 \frac{B}{H})$
	Horizontal, y	$K_y = \frac{8GR}{2-\nu} (1 + 0.5 \frac{B}{H})$	•	$\frac{K_y}{2L} = \frac{2G}{2-\nu} (1 + 2 \frac{B}{H})$
	Horizontal, x	$K_x = K_y$	•	—
	Rocking, rx	$K_{\alpha} = \frac{8GR}{3(1-\nu)} (1 + 0.17 \frac{B}{H})$	•	$\frac{K_{\alpha}}{2L} = \frac{xGD}{2(1-\nu)} (1 + 0.2 \frac{B}{H})$
	Rocking, ry	$K_{\alpha} = K_{ry}$	•	—
	Torsional, t	$K_t = \frac{10GR}{3} (1 + 0.10 \frac{B}{H})$	•	—

Figure 9-8 Footing Stiffness for a Finite Soil Layer above Rigid Base

9.5.6 Advanced Numerical Analysis

As noted above, the stiffness coefficients for the 6 x 6 stiffness matrix, i.e. stiffness coefficients developed using Figure 9-6 though Figure 9-8, represent the static elastic stiffness of the footing. Therefore, another way to develop these stiffness coefficients is to conduct a linear elastic analysis using a finite element method or other advanced numerical model. This type of analysis could be used to model irregular foundation geometry and complex soil profiles that cannot be accounted for using the closed form solutions discussed above.

9.5.7 Incorporation of Foundation Model into Bridge Response Model

The stiffness matrix developed using Figure 9-6 through Figure 9-8 implicitly represents the stiffness matrix for a point at the centroid of the bottom of the footing. However, very often the superstructure model stops at the bottom of the bridge pier or the column, i.e. at the top of the footing, as illustrated in Figure 9-9. In addition to the difference in elevation of the interface nodes between the foundation and superstructure models, the column may not always be positioned at the centroid of the footing and the local axes of the footing (i.e. its long and short directions) may not be aligned with the column axes (i.e. the longitudinal and transverse axes of the bridge pier) or the longitudinal and transverse axes of the superstructure. All these geometric aspects must be reconciled in order to properly implement the foundation stiffness matrix defined in the prior section in the global bridge model. This aspect of foundation modeling is often neglected and can lead to significant error in the design analysis. For instance, if the centroid of the footing is not aligned with the point of structural loading (e.g. the bottom bridge column), the stiffness matrix must be transformed to a different loading position (the point of structural loading) and, will become more complex, including off-diagonal stiffness terms.

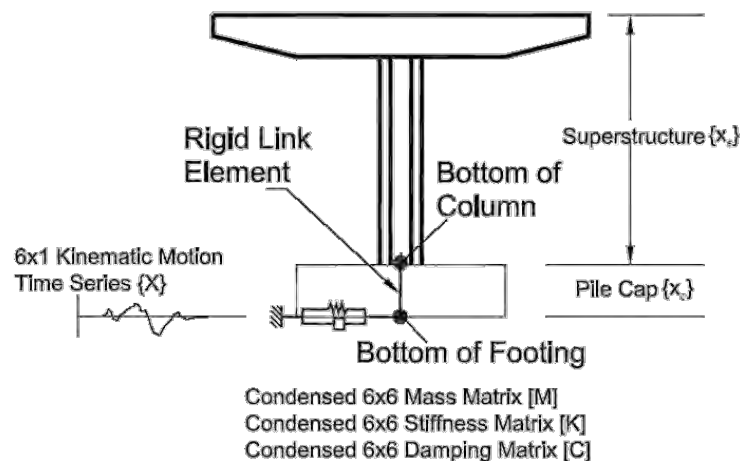


Figure 9-9 Implementation of Foundation Submodel in the Global Structural Model

There are two ways to reconcile the difference in the nodal positions between the two models (the foundation model for the bottom of the footing and a superstructure model that ends at the bottom of the column or pier). The foundation stiffness matrix can be transformed to a different position. As noted above, this normally will lead to a more complex form for the stiffness matrix and will generally involve the use of a computer program. A simpler approach to reconcile the difference is to define two nodes at

the base of the superstructure model: one node at the point of structural loading application point (e.g. the base of the column) and another node at the foundation stiffness reaction point (i.e., at the centroid of the bottom of the footing). The foundation stiffness matrix can be input to this superstructure model in terms of the local axes of the footing (which can be different from both the global coordinate system and the local axes of the pier or the column). After defining the two nodes, a rigid link element between the two nodes can be assigned to the model, as illustrated in Figure 9-9. This rigid link element will essentially take care of the proper transformation of the foundation stiffness matrix to other loading application points and will also reconcile the transformation of different coordinate axes (i.e. transforming the stiffness matrix for the footing to the appropriate global coordinate system).

If an advanced numerical model (e.g. a finite element model) is used to develop the stiffness matrix for the foundation system, the footing can be explicitly included in the model and the stiffness coefficient can be developed for the point of load application at the top of the footing.

9.6 GEOTECHNICAL CAPACITY

Geotechnical capacity analyses for shallow foundations subject to seismic loading include overturning, bearing capacity, and sliding resistance. These analyses are essentially the same as the analyses employed for static design of the foundation except that the Extreme Event 1 load combinations are employed in the analysis. The complete details of these analyses are covered elsewhere (e.g. NHI Course 132037 on Shallow Foundations). This section only addresses those aspects of evaluation of the geotechnical capacity of shallow foundations that is unique or particularly relevant to seismic design.

9.6.1 Pseudo-Static Seismic Loads

As in the case of retaining wall design and slope stability, the geotechnical capacity analysis of a shallow foundation is a pseudo-static analysis. The effect of the earthquake is modeled by applying static loads to the foundation that represent the inertial loads applied to the foundation by the superstructure. However, unlike slope stability and retaining wall design, vertical and moment loads induced by the earthquake must be considered in the geotechnical capacity evaluation of the foundation.

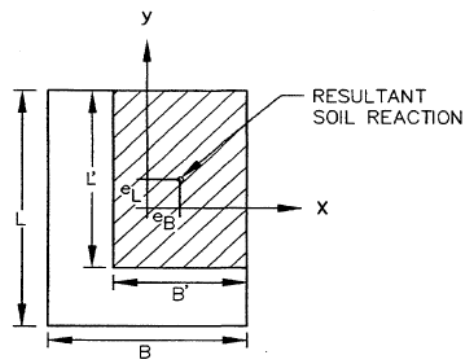
The loads employed in the geotechnical capacity evaluation are based upon the peak loads from the inertial response analysis of the superstructure. However, similar to slope stability and retaining wall

design, consideration should be given to reducing these loads to account for permissible displacements of the foundation. Furthermore, the appropriate combination of loads must be considered, as it would be overly conservative to superimpose the peak moment on top of the peak vertical load if they did not occur at the same time. With respect to load combinations, it is suggested that load cases include peak loads for each type of load (e.g. moment, vertical force, horizontal force) in combination with the other loads that occur at the same time as the peak load. However, in the case of the vertical load it may be necessary to include both the upwards and downwards vertical load if it not be clear *a priori* which load case is critical.

Load reductions may be applied due to acceptable lateral (sliding) displacement based upon the logic employed in retaining wall and slope design. Using this logic, a reduction factor of 0.5 may be applied to the loads if sliding displacements on the order of 1-2 inches are acceptable. However, criteria for overturning and bearing capacity implicitly account for acceptable displacements and thus no reduction factor should be applied to these loads.

9.6.2 Effective Footing Dimensions

Geotechnical capacity analyses for shallow foundation do not, in general, explicitly consider moment loading of the footing. Instead, the bearing capacity and overturning analyses consider the performance of a footing with reduced dimensions subject to only the applied normal and shear forces. These reduced, or effective, dimensions are based upon the eccentricity induced by the moment load, as illustrated in Figure 9-10 and as discussed in Section 10.1.6.3 of the AASHTO LRFD Bridge Design Specifications (AASHTO 2007).



$$e_B = M_y / V, \quad e_L = M_x / V$$

$$B' = B - 2e_B, \quad L' = 2e_L$$

Figure 9-10 Equivalent Footing Dimensions (FHWA 1998)

9.6.3 Overturning

The overturning capacity of a shallow foundation subject to seismic loading is based upon the eccentricity of the applied load. The AASHTO Guide Specifications for LRFD Seismic Bridge Design allow for an eccentricity of B/4 for a shallow foundation on soil and 3B/4 for a shallow foundation on rock without the owner's approval. Larger values of eccentricity are allowed with the owner's approval and, in fact, there can be substantial benefit to allowing larger eccentricity, as this can limit the load transferred to the footing from the bridge structure. There is little evidence of bridge foundation failure due to overturning (rocking) under seismic loads and some owners (e.g. Caltrans) allow for complete uplift (eccentricity equal to B/2) under the peak seismic load. Appendix A of the AASHTO Guide Specifications for LRFD Seismic Bridge Design provides a detailed discussion on rocking limits for shallow foundations.

9.6.4 Bearing Capacity

For foundations on soil, bearing capacity is evaluated using the effective footing width (the footing width adjusted for eccentricity per Figure 9-10) and the equivalent uniform load (the vertical load divided by the effective footing width). For foundations on soil designed for loads from an elastic response analysis, bearing capacity is evaluated by comparing the bearing stress from the linear elastic seismic response analysis to the nominal bearing resistance (i.e. using load and resistance factors of 1.0). Nominal bearing resistance is evaluated using the effective footing dimensions and the general bearing capacity equation given in Section 10.6.3 of the AASHTO LRFD Bridge Design Specifications. For footings on loose sand, the a resistance factor of 0.67 should be applied to the strength parameter (c' and $\tan\phi'$) to account for general shear failure, as described in AASHTO.

In displacement-based design, capacity-protected shallow foundations are evaluated based upon the plastic moment capacity and associated shear demand of the column or pier wall using the following equation:

$$M_{po} + V_{po} H_f < \phi P_u [(L-a)/2] \quad 9-2$$

where: M_{po} = overstrength plastic moment capacity of footing
 V_{po} = overstrength plastic shear demand
 P_u = axial force in column (including force from overstrength plastic hinging)
 a = $P_u / (q_n B)$ where q_n = nominal bearing capacity

- H_f = depth of footing
- L = length of the footing in the direction of loading
- B = width of footing
- ϕ = resistance factor for overturning of the footing = 1.0

The overstrength plastic moment, M_{po} , in Equation 9-2 is 1.2 times the idealized plastic moment if ASTM A 706 reinforcement is used in the column and 1.4 times the plastic moment if ASTM A 615 grade reinforcing steel is used. Nominal bearing capacity is evaluated as described previously.

For footings on rock, the maximum bearing stress on the base of the footing is compared to the unconfined compressive strength of the rock. The maximum bearing stress is evaluated using either a trapezoidal or triangular distribution, depending upon the magnitude of the applied moment, in accordance with Section 10.6.1.4 of the AASHTO LRFD Bridge Design Specifications.

9.6.5 Sliding Capacity

The capacity check for sliding of a shallow foundation subject to seismic loading, like bearing capacity, depends upon whether the foundation has been designed using a force-based approach or a displacement-based approach as follows.

If the forces on the foundation are from a linear elastic analysis (force-based design):

$$\gamma P_h > \phi_t R_t + \phi_{ep} R_{ep} \quad 9-3$$

If the forces on the foundation are based upon the plastic moment analysis (displacement-based design):

$$V_{po} \leq \phi R_n \quad 9-4$$

- where: P_h = shear demand from linear elastic response analysis
- R_t = nominal shear resistance
- R_{ep} = nominal passive resistance
- V_{po} = overstrength plastic shear demand of column or wall
- R_n = nominal shear resistance against sliding = $R_t + R_{ep}$

ϕ_t, ϕ_{ep} = resistance factors for sliding and earth pressure = 1.0
 γ = load factor for seismic loading = 1

Components of the sliding capacity of a shallow foundation in Equation 9-4 include both the frictional resistance to sliding and the lateral earth pressure. If evaluating the friction sliding resistance, the shear strength parameters for the soil-concrete interface (c_B and $\tan\phi_B$) are typically assumed to be 70% of the shear strength parameters for the underlying soil (c' and $\tan\phi'$). In evaluating the earth pressure, the active thrust on the back for the footing should be subtracted from the passive resistance against the face of the footing.

9.7 STRUCTURAL CAPACITY

Shallow foundation design must also consider the structural capacity of the footing. Structural capacity checks include checks for flexure, shear, and, for Seismic Design Categories C and D, joint shear. The flexure capacity check may be conducted in accordance with Equation 9-5:

$$\phi M_n \geq M_u \quad 9-5$$

where: M_u = factored ultimate moment demand in footing
 ϕ = resistance factor for concrete in bending
 M_n = nominal moment capacity of the footing at the critical section based upon effective width, $b_{eff} = B_c + 2H_f \leq B$,
 B_c = diameter or width of column or wall normal to direction of loading.

The capacity check for shear may be done in accordance with Equation 9-6:

$$\phi V_n \geq V_u \quad 9-6$$

where: V_u = factored ultimate shear demand in footing at the face of the column or wall
 f = resistance factor for concrete in shear
 V_n = nominal shear capacity of the footing at the face of the column or wall

The capacity check for joint shear may be done by checking the principal stress ratio in accordance with Equation 9-7:

$$p_c \leq 0.25 f_c' \quad (\text{Compression}) \quad 9-7$$

$$|p_t| \leq 0.38 (f_c')^{0.5} \quad (\text{Tension}) \quad 9-8$$

where: p_c = principal compression stress
 $|p_t|$ = principal tensile stress
 f_c' = uniaxial compressive strength of concrete

The principal compression stress, p_c , and the principal tensile stress, p_t , are evaluated in accordance with the provisions of Section 6.4.5 of the AASHTO Guide Specifications for LRFD Seismic Bridge Design.

9.8 PERMANENT FOUNDATION DISPLACEMENT

Assuming that the structural components of the bridge system have been designed to perform satisfactorily when subject to the peak earthquake load (in terms of either force or displacement basis), then it is relevant to consider the capacity of the foundation to accommodate permanent foundation displacements induced by the earthquake. Permanent foundation displacement may place a displacement demand on the superstructure or on the foundation itself. Damage to the foundation caused by permanent displacement may be difficult, or impractical, to repair. The desire to avoid foundation damage leads to the concept of capacity protecting the foundation system, as discussed in Chapter 8. However, as discussed in Chapter 8, capacity protection of the foundation may not always be possible due to economic considerations (especially at poor soil sites) or limitation on structural forms (e.g. limitations on implementing a structural load fuse), particularly on retrofit projects. Experience has shown that it can be both difficult and costly in a retrofit project to capacity protect the foundation system. Because of these difficulties, the permissible permanent foundation displacements for a bridge subject to seismic loading must sometimes be addressed (Lam, 1994; Fenves and Chung, 1996 and Martin and Lam, 2000).

The impact of permanent ground displacement on foundation and bridge performance is generally considered on a project-specific basis. In the recent Washington State Tacoma Narrows Bridge Second Crossing design-build contract, WSDOT's specifications for designing the caisson foundation called for the permanent displacement of the caisson at the end of the earthquake to be less than 2-ft at the top of the caisson. The Bay Bridge East Span replacement design scope of work also included analyses of the amplitude of permanent pile footing settlement after the design earthquake and its impact on bridge performance.

Experience shows that the permanent displacement of the foundation can be highly sensitive to the earthquake time history characteristics. Near-field earthquake ground motion records with high velocity pulses, which can be highly directional, may be particularly problematic. Lam (1994) and Martin and Lam (2000) showed that unacceptable permanent foundation displacements (especially permanent settlement) generally occur under seismic loading when there is inadequate reserve capacity for static loading. Therefore, a practical way to mitigate the potential for permanent foundation displacement (especially for settlement) in a seismic event may be to provide an adequate static capacity. Martin and Lam concluded that, in the absence of liquefaction, if the static factor safety (capacity/demand ratio) for the foundation is higher than 2.5, permanent seismic settlement will be minimal, even in major earthquake.

9.8.1 Liquefaction-Induced Lateral Spreading and Settlement

In general, shallow foundations are not a viable foundation type for sites that are prone to liquefaction unless ground improvement is employed to mitigate liquefaction potential. However, occasionally an existing bridge may have a shallow foundation that is located on top of a liquefiable soil layer. In this case, the methods presented in Chapter 6 may be used to evaluate the seismic settlement and lateral spreading associated with the design earthquake. The ground deformations calculated in these analyses may then be applied to the bridge structure as a displacement demand. Seismic settlement of dry cohesionless soils beneath the foundation may also be addressed in this manner.

9.9 SUMMARY

This section outlines seismic analysis and design procedures for shallow foundations. Shallow foundations are suitable at rock sites or when firm soils are found at shallow depth provided the potential for landslide induced displacements is fairly low and the risk of liquefaction is very low or non-existent. There is relatively little evidence of seismically-induced damage to bridges on shallow foundations due to inadequate geotechnical foundation capacity that does not involve liquefaction ground failure. The primary impacts of seismic loads on a shallow foundation are likely to be limited lateral and vertical displacements and perhaps yielding of structural components of the footing, impacts that are not likely to threaten life safety or lead to collapse. Classical solutions for the capacity and stiffness of rigid surface footings at a shallow depth are employed in shallow foundation design independent of any coupling between moment and shear loads.

The most common seismic analysis procedure in bridge design is the response spectrum method, in which evaluation of the seismic loads are based upon the assumption that the bridge structure behaves in a linear elastic manner. As the inertial loading on the bridge structure (including the loading on the foundation elements) is dependent upon the response characteristics (stiffness) of the foundation due to soil-foundation-structure interaction effects, characterizing the stiffness of a shallow foundation subject to earthquake loading is an important seismic design consideration. In areas of high seismicity, shallow foundations are often capacity protected, with force demands controlled by fuses in the system such as a plastic hinge at the base of the column.

For shallow foundations, kinematic interaction is not important for practical problems and only inertial interaction needs to be considered for seismic design. It is common to represent the foundation as a single node at the base of each pier. Linear springs are then attached to this node to represent foundation compliance for each degree of freedom included in the response analysis, with the spring stiffness based upon the static stiffness of the foundation. These stiffness values may be based upon theoretical solutions from elasticity theory or may be derived using numerical methods, e.g. finite element analysis. Soil modulus values based upon the small strain modulus of the soil must be reduced to account for softening at the strain levels relevant to foundation response. For relatively strong motions, e.g. $F_v S_1 > 0.5g$, it is recommended that the small strain modulus be reduced by a factor of 0.25. For weak motions, e.g. $F_v S_1 < 0.3g$, it is recommended that the shear modulus be reduced to 50 percent of the small strain value. However, it is also recommended that the sensitivity of the results of the seismic analysis to the foundation

stiffness be evaluated using stiffness values varied from half of the best estimate value to twice the best estimate value.

Geotechnical capacity analyses for shallow foundations subject to seismic loading include overturning, bearing capacity, and sliding resistance. These analyses are essentially the same as the analyses employed for static design of the foundation except that the Extreme Event 1 load combinations are employed in the analysis. The loads employed in the geotechnical capacity evaluation are based upon the peak loads from the inertial response analysis of the superstructure. However, a reduction factor of 0.5 may be applied to the loads if sliding displacements on the order of 1-2 inches are acceptable. The bearing capacity and overturning analyses consider the performance of a footing with reduced dimensions based upon the eccentricity induced by the moment load. Structural capacity may be evaluated using either force or displacement based design methods.

CHAPTER 10

DEEP FOUNDATIONS

10.1 TYPES OF DEEP FOUNDATIONS

Compared to shallow foundations, deep foundations are usually more costly and therefore are generally used when soil conditions are not suitable for shallow foundations, e.g. at site with compressible soils in order to minimize potential settlement problems. Deep foundations can be categorized into pile foundations (including drilled shafts in the context of this document) and caisson foundations. Pile foundations can be subdivided into various sub categories in terms of the pile sizes (i.e. pile diameters), number of piles in a group (large groups, small groups), types (e.g. reinforced concrete, steel, timber), installation method (e.g. drilled, driven), and how they are connected to the superstructure (e.g. embedded pile footings, pile extensions, pile footings cantilevered above the mudline).

One main difference between modeling caissons and pile foundation is that caissons are relatively rigid and they can be regarded as a rigid foundation. However, piles are relatively flexible and it is necessary to account for the deformability of piles. Furthermore, as opposed to shallow foundations, a deep embedment configuration for a pile foundation and caisson design require consideration of the coupling of moment and shear loads when modeling the stiffness of these foundations.

10.2 SEISMIC VULNERABILITY OF DEEP FOUNDATIONS

There have been numerous reports of damage to deep foundations in earthquakes. Perhaps the most recognized case history of pile damage from earthquakes in the United States is the extensive damage to battered piles at the Seventh Street Pier at the Port of Oakland from the 1989 Loma Prieta Earthquake (Serventi et al., 2004). Lateral spreading of a rockfill dike on top of the liquefied soil at Seventh Street placed large demands upon battered piles driven through the dike. Figure 10-1 shows damage to the head of one of the battered piles at Seventh Street. Gerwick and Fotinos (1990) reported that “Almost all the inshore-leading batter piles of the 6 marginal wharves on the Seventh Street Pier were broken. Piles crushed and sheared near their top, and in many cases pulled out from the bottom of the deck slab. The failure appeared to be due to a combination of high compression, shear and bending at the top of the pile,

caused not only by the lateral forces imparted to the deck slab and its overlying fill and pavement, but by the subsidence of the rock dike around the pile. Several marginal wharves have been constructed recently in Oakland, using all-vertical piles. The inner row (or rows) of piles is given additional ductility through incorporation of additional unstressed reinforcement along with very heavy confining spiral. These structures all performed well with no damage.” This case history suggests that battered piles are particularly vulnerable to liquefaction-induced lateral spreading but that well designed pile foundations can perform satisfactorily, even at liquefied sites.



Figure 10-1 Damage to the head of battered piles at the Port of Oakland (after Serventi, 2004)

Most of the case histories of pile damage from earthquakes in the United States have involved damage to the pile head, as shown in Figure 10-1. Other modes of earthquake-induced damage to pile foundations includes shear failure and punching shear failure of the deck or pile cap at the pile head connection point, as shown in Figure 10-2 through Figure 10-4 for the Struve Slough Bridge following the Loma Prieta Earthquake. As observed in Figure 10-1 through Figure 10-4, pile head damage in earthquakes is often due to deficiencies in confinement (spiral reinforcement) or inadequacies in detailing for ductile behavior at the pile head. Furthermore, in both the Port of Oakland and the Struve Slough Bridge case histories, the observed damage appeared to have been induced by liquefaction-induced permanent lateral ground displacement, as opposed to the inertial loading.

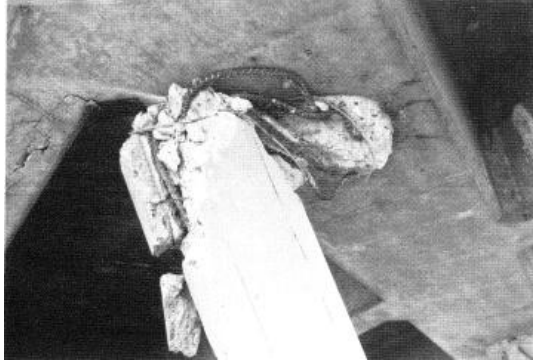


Figure 10-2 Shear Failure in the Cap Beam Connection of the Struve Slough Pile Bent (EERI, 1990)



Figure 10-3 Piles Punched-Through the Deck Slab in the Collapsed Struve Slough Bridge (EERI, 1990)



Figure 10-4 Large Lateral Displacements Imposed on Adjacent Piles, Struve Slough Bridge (EERI, 1990)

Pile head damage similar to that shown in Figure 10-1 through Figure 10-4 has been observed in earthquakes around the world, including to piles supporting bridges in several earthquakes in Japan and New Zealand and piles supporting harbor structures in India in the recent 2004 Sumatra earthquake (Current Science, 2006). These case histories clearly illustrate the need for attention to the design of the vulnerable pile head connection.

Piles in liquefied ground have also been found to be damaged at depth, typically at the interfaces between liquefied and non-liquefied soil layers. Hamada and O'Rourke (1992) compiled case histories of liquefaction and lifeline performance during earthquakes from a number of Japanese earthquakes. Several of these case histories clearly showed that permanent displacements induced by liquefaction can lead to significant pile damage at depth at the boundaries of liquefied soil layers (in addition to damage at the pile head location). A noteworthy aspect of these case histories is that in many cases the damaged piles continued to adequately support the overlying structure. The damage to the piles in these cases was not uncovered until many years after the earthquake, when the piles were excavated during building reconstruction. Figures 10-5 through 10-8 illustrates the phenomenon of liquefaction-induced pile damage below the ground surface from the case histories of Hamada and O'Rourke (1992), as discussed in the following paragraphs.

The Niigata Court House The Niigata Family Court House, a four-story reinforced concrete building, was located in the Hakusan area on the left bank of the Shinano River. It was founded upon concrete pile foundations, each with a diameter of 35 cm and a length of 6 to 9 m. After the earthquake, the building inclined about 1 degree due to the differential settlement of the ground. There was some conjecture following the earthquake that the foundation piles were damaged. However, after minor repairs were made to the inclined floors, the building was used without additional modifications for 25 years. When the building was reconstructed, two foundation piles were excavated. Figure 10-5 illustrates observed damage in the excavated piles.

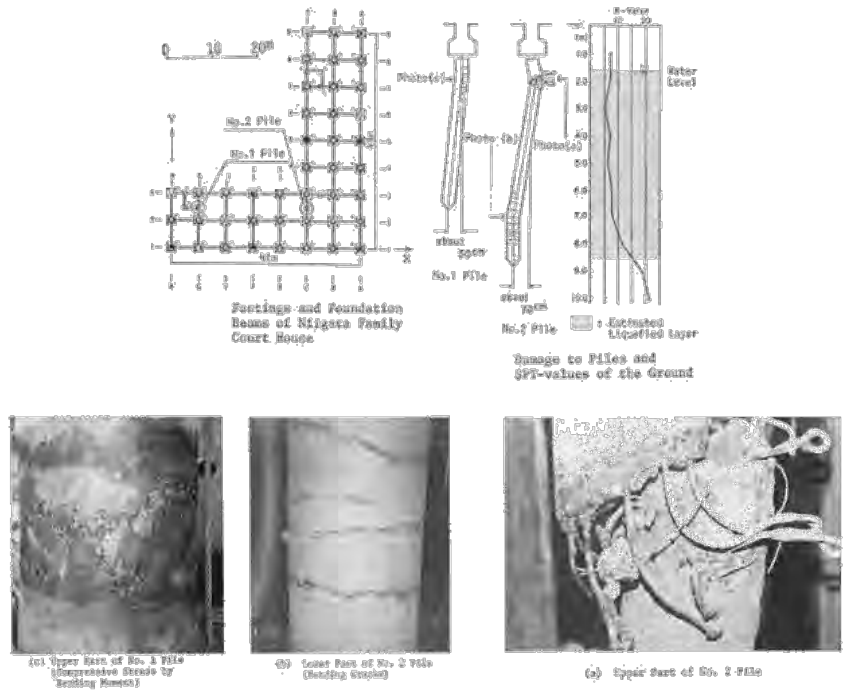


Figure 10-5 Damage to Excavated Pile from the Niigata Court House (Hamada and O'Rourke, 1992)

S-Building The S-building was a three-story reinforced concrete building constructed on reinforced-concrete friction piles with a 25 cm outer diameter and a 13 cm inner diameter. Three piles were extracted during reconstruction of the building 24 years after the earthquake. Figure 10-6 shows the a photo of the extracted piles and a sketch of the crack patterns in these piles

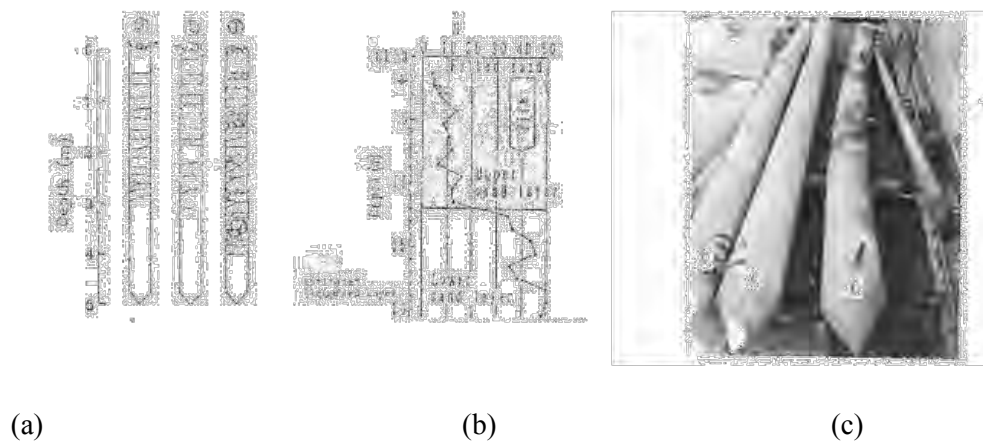


Figure 10-6 Pile Damage Observed from S Building (Hamanda and O'Rourke, 1992); (a) Damage to Foundation Pile; (b) SPT Value; (c) Photos of Damage

NHK Building. The NHK Building was a four-story reinforced concrete building founded upon reinforced concrete piles 35 cm in diameter and 11 to 12 m in length. When the foundations of the building was excavated for reconstruction in 1985, about twenty years after the earthquake, the reinforced concrete piles were found to be completely fractured, as shown in Figure 10-7. This building had been return to use after the earthquake following basic repairs to the floors without any awareness of damage to the pile. From the observed pile damage suggested horizontal ground displacement on the order of about 1.0 to 1.2 m beneath the building compared to about 2 m lateral displacement away from the building.

Hotel Niigata. Figure 10-8 shows damage to the 35 cm diameter reinforced concrete piles of the Hotel Niigata. The damage was discovered during reconstruction of the building 23 years after the earthquake.

Hokuriku Building. The 10-storey Hokuriku building is in the same neighborhood as the NHK building. The Hokuriku building was founded on reinforced concrete piles 40 cm in diameter and 12 m long. No damage was reported to the superstructure after the earthquake. The number of piles supporting the 10-story Hokuriku-Building was significantly greater than for the four-story NHK building. There was little evidence of lateral spreading beneath the Hokuriku building, despite evidence of 2-m ground displacement close to the building. It has been suggested that densification of the soil due to the large number of driven piles beneath contributed to limiting the lateral displacement beneath the building.

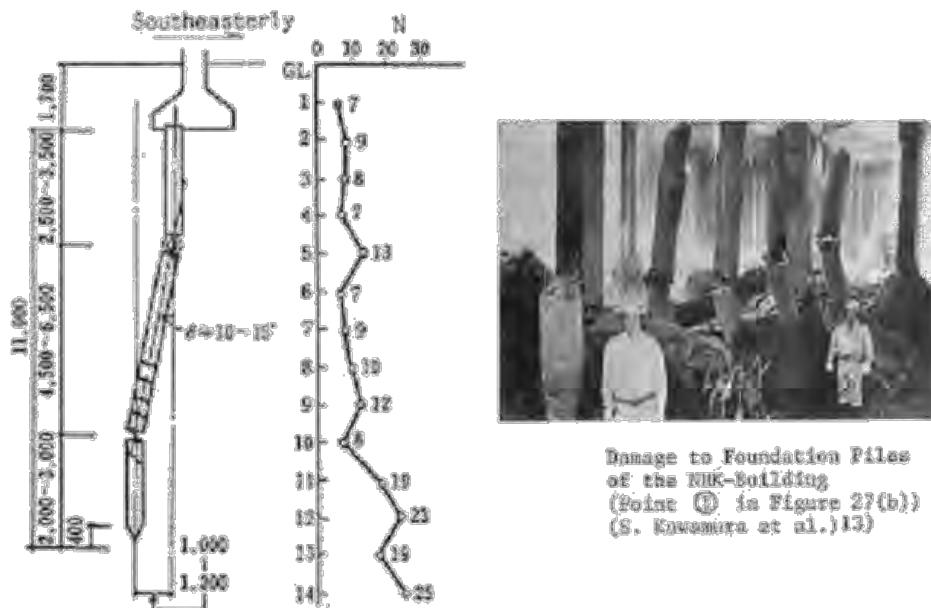
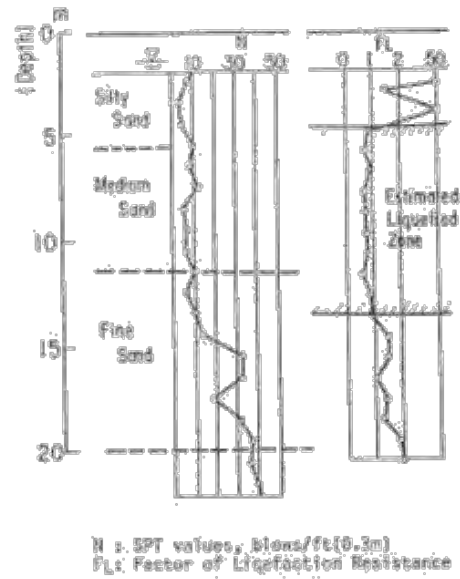


Figure 10-7 Pile Damage Observed from NHK Building (Hamanda and O'Rourke, 1992)



Damage to Foundation Piles of the Hotel Niigata Building



Soil Conditions at the Hotel Niigata Site

Figure 10-8 Pile Damage Observed from Hotel Niigata (Hamanda and O'Rourke, 1992)

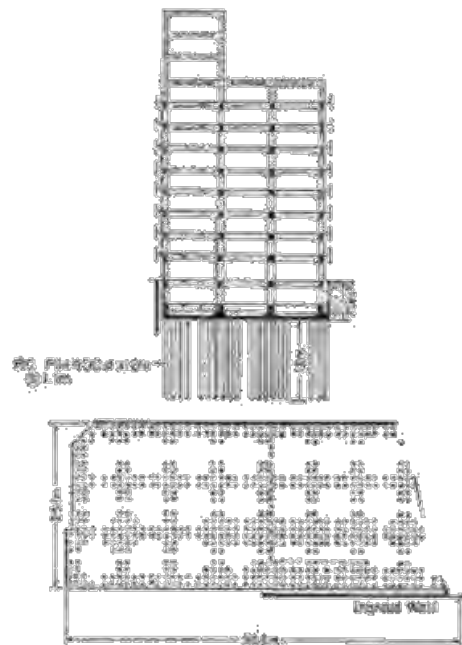


Figure 10-9 Pile Layout of Hokuriku Building (Hamanda and O'Rourke, 1992)

In addition to the case histories presented above, there are many other cases of damage to bridges due to large ground displacements at liquefied soil sites. In particular, these are several notable cases of bridge decks falling off their bearings (seats) due to lateral spreading of the bridge piers.

The case histories reported above all damage involve liquefaction-induced lateral spreading. Piles at sites that have not liquefied have generally been reported to have performed well in earthquakes. However, as evidenced by the case histories from O'Rourke and Hamada, the lack of reported pile damage might be due to the fact that the damage was hidden below the ground surface.

10.3 SEISMIC LOADS ON DEEP FOUNDATIONS

Many structures on piles that have performed well in earthquakes were designed either without consideration of earthquake loads or based on very low lateral design loads (e.g. 10% of the gravity load) by today's standards. What the foundations for these structures have in common is that they generally had an adequate static factor of safety (capacity). Therefore, the static capacity of the foundation remains an important benchmark, as it affects the reserve capacity available to accommodate extreme loads, e.g. the design earthquake load.

10.3.1 Soil-Foundation-Structure Interaction

Figure 10-10, from Gazetas et al. (1992), provides an overview of the earthquake design process for a pile foundation from a rigorous theoretical perspective. Similar to the seismic design of shallow foundations, the overall design uses the substructuring technique to separate the foundation response from the response of the superstructure. The foundation response can then be separated into two problems: (1) the kinematic response problem, with the objective of developing the appropriate earthquake ground motion for design of the superstructure, and (2) the inertial structure response problem, for evaluating the performance of the structural system, including the foundation elements, subject to the design ground motion.

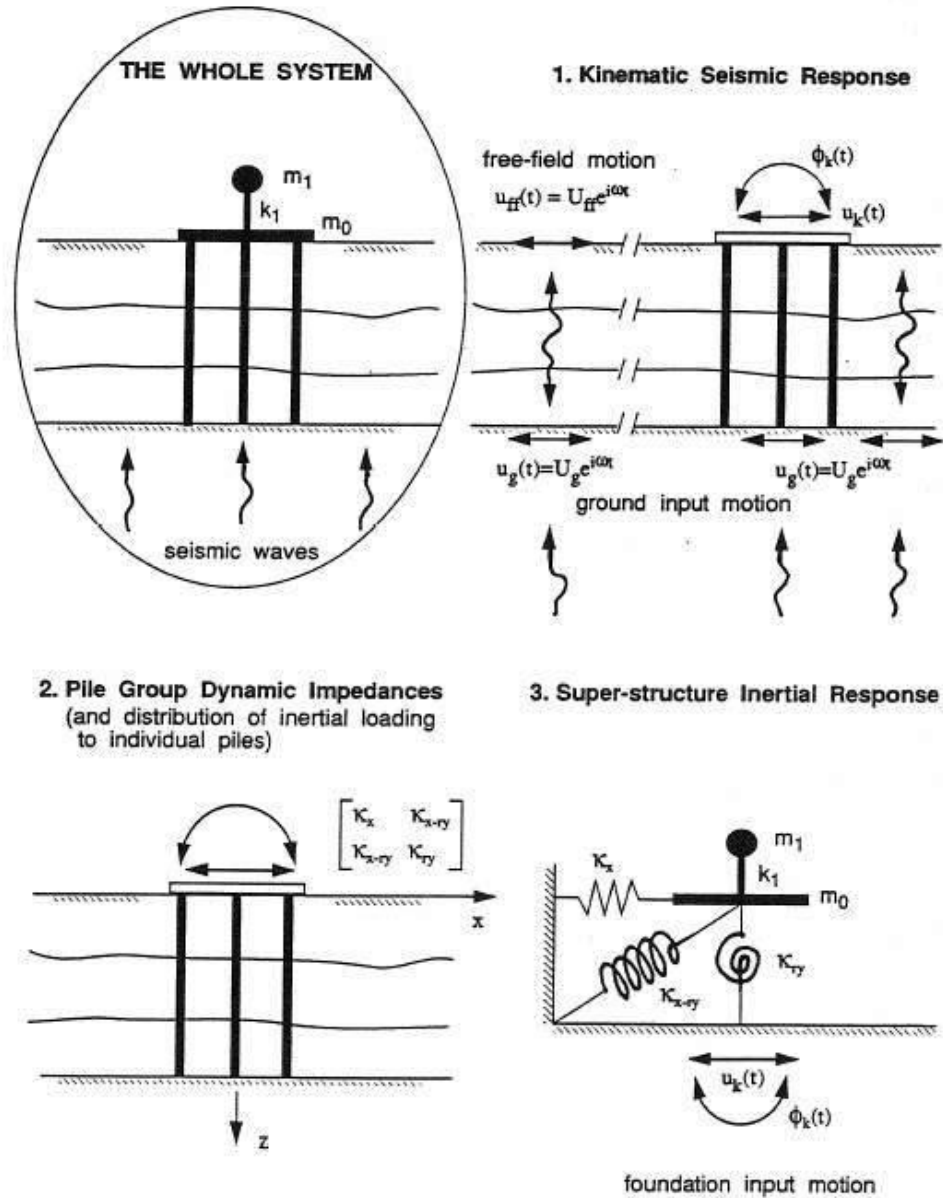


Figure 10-10 Seismic Design of Pile Foundations (Gazetas et al., 1992)

In Chapter 9 it was established that kinematic interaction can be ignored for shallow foundations built upon competent soils. However, pile foundations are often used at soft soil sites with low shear wave velocity. At soft soil sites, kinematic interaction can create a ground motion at the base of the structure that differs significantly from the free field ground surface motion and that should be accounted for in design.

Similar to the design of shallow foundations, the inertial response problem involves developing the impedance function for the pile foundation and then applying this impedance function in the global structural model to calculate the seismic response of the superstructure. In a manner also similar to shallow foundation design, the frequency dependent impedance function can be simplified by adopting the static foundation stiffness and ignoring the radiation damping radiation damping in the foundation model. It is common practice to develop the pile foundation stiffness based on p-y and t-z solutions for pile response, which directly the near field nonlinear soil-structure interaction behavior of the piles.

The displacement of the foundation interface node can then be used as input back into the p-y and t-z analyses to evaluate the stresses and displacements of the piles.

Detailed discussions of the theory of substructuring techniques for bridge foundations are presented by Lam and Law (2000). The transformation of the original problem into an inertial response structural system involving only the superstructure and the foundation interface pile-cap node and can be developed based on classical static condensation techniques (e.g., Cook, et al., 1989). Reduction of the pile foundation pile group and its supporting soil mass into a 6 x 6 condensed stiffness matrix is well understood and accepted in design practice. The design ground motion is input to the superstructure model through a foundation node that is represented by the stiffness matrix.

10.3.2 Kinematic Loading

As observed from the case histories of damage to pile foundations in earthquakes, permanent ground displacement is an important load case. The response of a pile foundation to permanent ground deformation is unrelated to the mechanism of inertial loading. Therefore, it is necessary to formulate an additional load case for design of pile foundations subject to earthquake-induced permanent ground displacement. This load case is generally referred as kinematic loading. However, this kinematic load case should not be confused with the classical kinematic interaction problem shown in Figure 10-10.

10.4 EFFECTIVE SUPPORT MOTIONS FOR DEEP FOUNDATIONS IN SOFT SOIL SITES

In cases where the foundation is located in soft soil, the designer may wish to take advantage of kinematic interaction, as it usually reduces the amplitude of the input motion. A rigorous kinematic interaction analysis would require very large and complex three-dimensional numerical models (even without

modeling of the superstructure). Hence, the simplified (but not necessarily simple) modeling approach illustrated in Figure 10-11(b) is often used. The simplified modeling approach involves conducting wave propagation site response analyses to develop the depth-dependent free field motions. Then, the free field input motions are applied to the support nodes of the horizontal soil springs attached below the ground surface to the pile, as shown in Figure 10-11b. The wave propagation analysis may be conducted using any of the site response analysis methods described in Chapter 5, including the equivalent linear method. The soil springs may be developed using conventional p-y analyses. The resultant displacement time history at the defined foundation substructure interface node may then be used as the kinematic input motion for the inertial response problem.

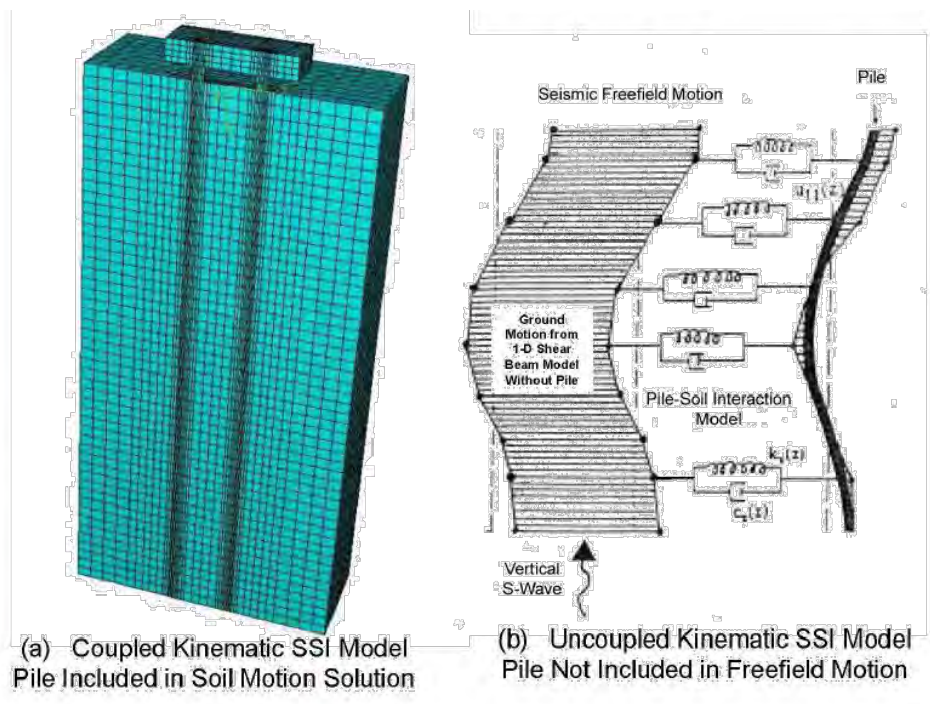


Figure 10-11 Modeling Approaches to Solve for the Kinematic Interaction

For many practical problems, the simplified kinematic interaction analysis described above is still overly complex. An even more simplified approach is needed to account for kinematic interaction effects for these problems. Figure 10-12 presents a typical bent from the skyway for the San Francisco-Oakland Bay Bridge East Span replacement structure along with the soil condition. The simplified kinematic soil-structure interaction method described above was employed to derive the kinematic motion to be used in the global model response analysis. The site response analyses were conducted using conventional 1-D

equivalent linear site response analyses. Figure 10-13 presents the acceleration response spectra developed from the free field motions from the site response analysis at various depths. The acceleration response from the kinematic interaction analysis is also shown in this figure by the thick green line. Comparison of the kinematic motion with free field motions shown in Figure 10-13 suggests that the kinematic motion corresponds reasonably with the free field motion at a depth of about 14-m, or 5.6 pile diameters, below the mudline, especially in the long period range of the response. The comparison also shows that designing for the ground surface outcrop motion is rather conservative for this site. Therefore, this example suggests that the engineer can use the free field motion at a depth of between 5 and 6 pile diameters as the input motion for an inertial interaction analysis in order to account for the effect of kinematic interaction. This simple approach can be easily implemented within the context of a site specific response analysis.

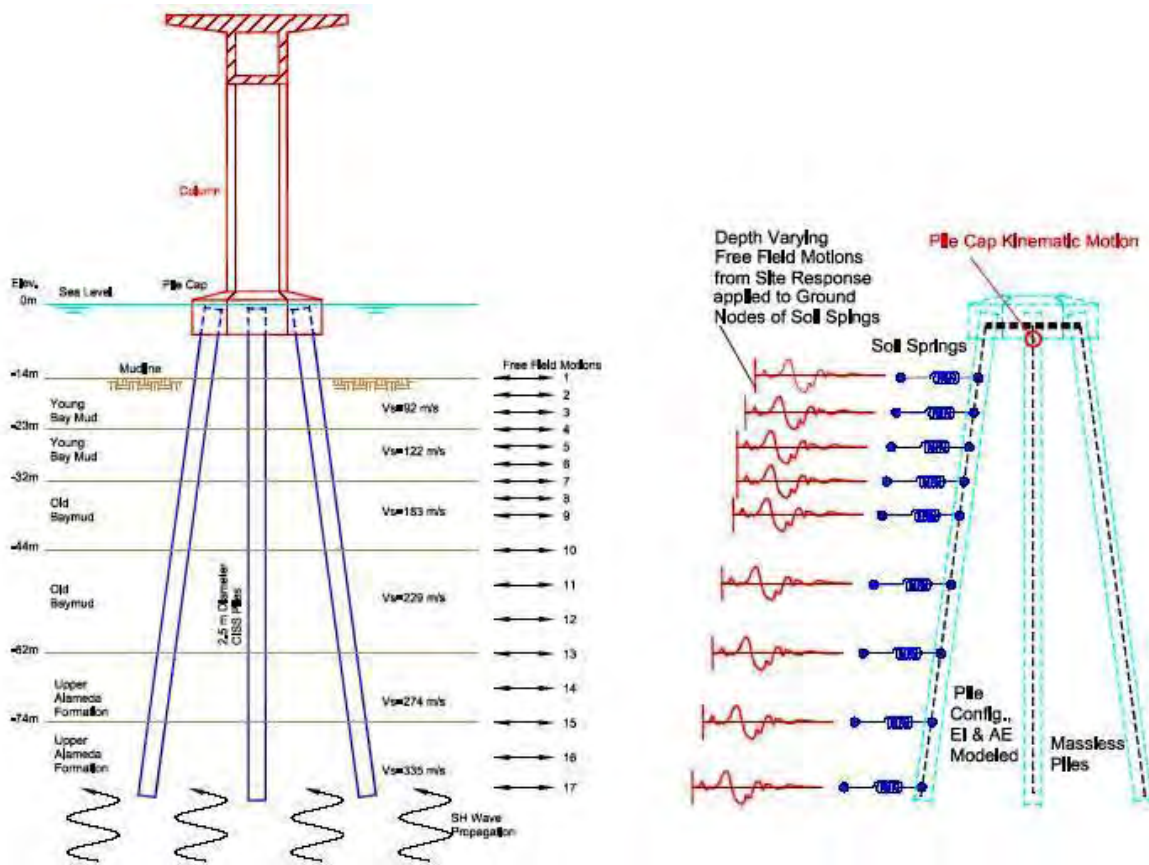


Figure 10-12 Pile Group Layout and Kinematic Interaction Model, San Francisco East Bay Bridge Replacement Structure Skyway

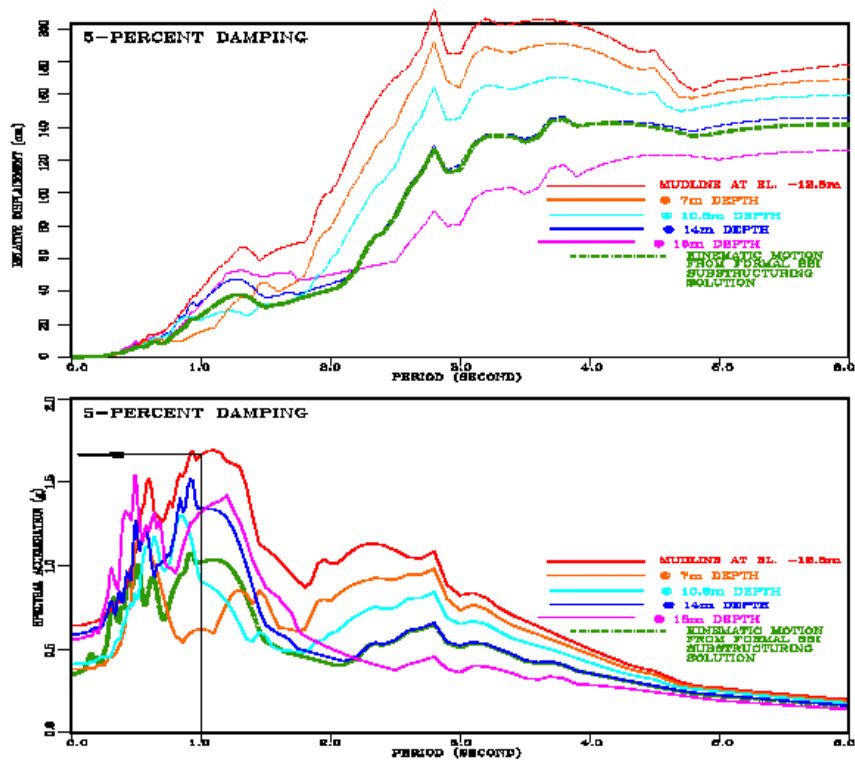


Figure 10-13 Comparison of Ground Motions from 1-D Site Response Analysis to Kinematic Motion

10.5 SOIL-FOUNDATION INTERACTION SPRINGS

10.5.1 Two-Springs-in-Series Model

Traditionally, p-y and t-z analyses are used to develop the soil springs for a soil-foundation-structure interaction analysis. Recently, some investigators have suggested modifications to this approach to account for the rate of dynamic loading and other earthquake related response issues (e.g. liquefaction effects). Wang et al. (1998) showed that, while analyses based upon traditional p-y and t-z curves gave reasonable agreement with the results of centrifuge tests of dynamic loading of pile groups, enhanced accuracy could be obtained by using two horizontal springs in series at each node on the pile: a near-field spring modeled using the conventional p-y approach and a much stiffer spring representing the far-field soil response. Figure 10-14 illustrates this model. In such a model, the far-field spring (based on soil modulus at smaller strain amplitude at far-field associated with wave propagation loading) will usually be over 10 times the stiffness of the near-field spring (as the near field motions involve a much higher degree of soil nonlinearity due to the large strains adjacent to the pile). Due to the significantly greater stiffness

of the far-field spring, the resultant overall behavior of the composite element is dominated by the near field spring response. Hence, for practical purposes, the far-field spring can be ignored without significantly altering the resultant behavior. Furthermore, as the global model for a major bridge is inherently complicated due to the need to model many bents and many structural components, the added complexity of the two-springs-in-series approach does not appear to be warranted even on major bridge projects.

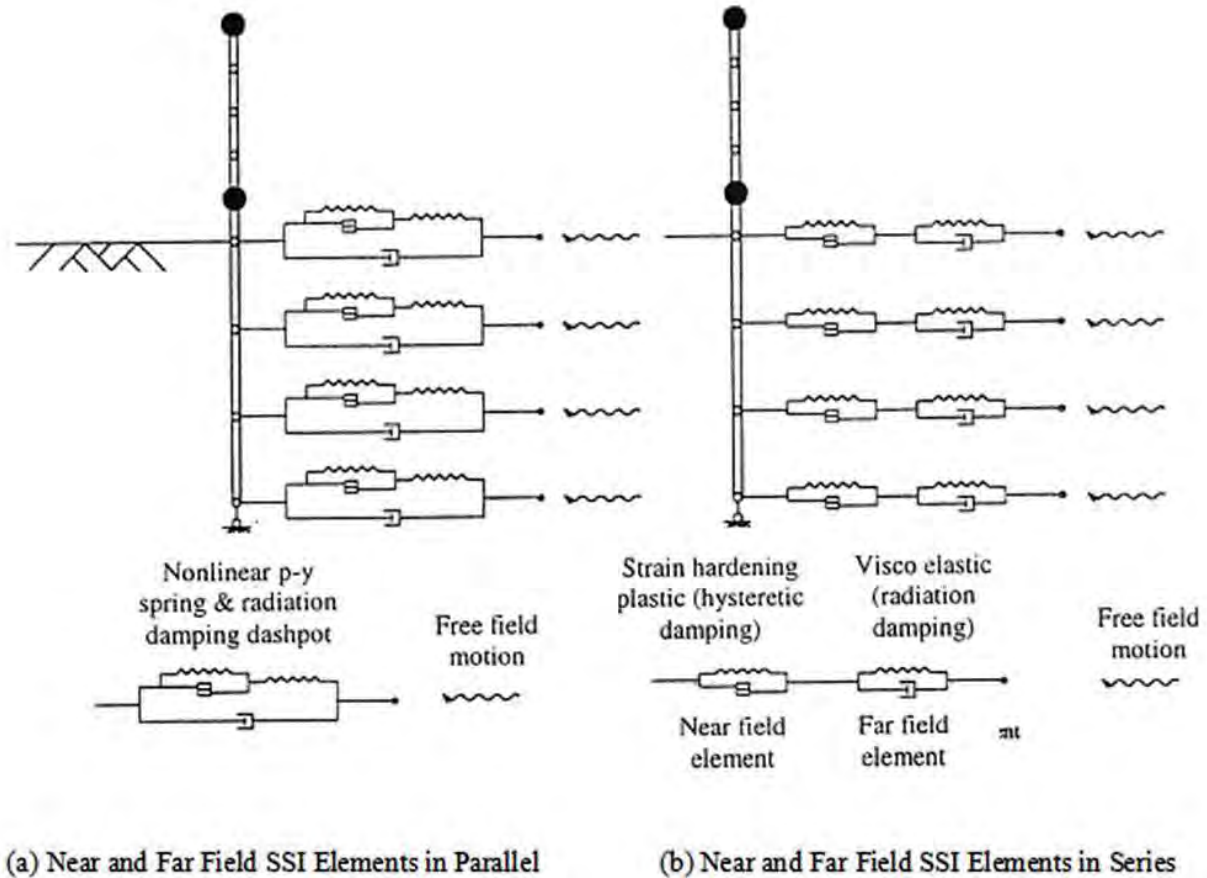


Figure 10-14 Two-Springs-in Series Soil-Pile Interaction Model (Wang et al., 1998)

10.5.2 p-y and t-z Curves for Soil-Pile Interaction Analyses

The state-of-practice for design of piles subject to lateral loading is a beam-column model employing nonlinear discrete Winkler spring foundations. This approach, commonly referred to as a p-y analysis, is widely accepted by both structural and geotechnical specialists and the nonlinear support curves characterizing the lateral soil reaction are usually referred to as p-y curves. For analysis of a pile subject

to vertical loading, the corresponding nonlinear curves for the soil reaction on the side of the pile are usually referred to as t-z curves. Recommendations for p-y, t-z and Q-z curves are generally embedded in the computer programs used to conduct the soil-pile interaction analyses and will not be covered herein. Lam and Martin (1986), Lam (1994), Lam and Cheang (1995), Lam and Law (1996), and Lam et al. (1998) provide a thorough discussion on p-y curves for earthquake design applications.

10.6 FOUNDATION STIFFNESS EVALUATION

Development of the stiffness matrix for an inertial response analysis is generally accomplished by first evaluating the stiffness of a single pile and then, if necessary, adjusting that stiffness for pile group effects. Evaluation of the stiffness of an individual pile must consider the response of the pile head to vertical and lateral loads and to moments applied about a horizontal axis. The stiffness of an individual pile subject to moment loading about a vertical axis is generally assume equal to the structural torsional stiffness of the pile, with no contribution from the surrounding soil. As noted above, evaluation of pile stiffness due to lateral loads and moments applied about a horizontal axis are often accomplished using p-y computer programs. Evaluation of pile response to vertical loads may be accomplished using t-z/Q-z computer programs. The non-linear load-deformation response provided by these programs must be linearized to develop the stiffness coefficients for the 6 x6 stiffness matrix. Ideally, the stiffness matrix coefficients should be developed in an iterative manner, with initial stiffness based upon assumed deformation levels adjusted in subsequent iterations based upon foundation displacements obtained from the inertial interaction model. However, as the foundation response can be relatively linear up to the point where a plastic moment forms in the pile and as results of the global analysis may be relatively insensitive to foundation stiffness for many problems, sensitivity analyses may be used instead of an iterative procedure as a practical way to develop a robust design while minimizing the need for overly complex analysis procedures. Furthermore, estimates of the stiffness coefficients for a single pile can be obtained from simple design charts based upon linear elasticity that employ the pile stiffness and the coefficient of subgrade reaction for the near-surface soil.

Both the more sophisticated p-y approach to developing pile lateral stiffness and the simple chart solutions assume typically assume either that the pile head is free to rotate or is fixed against rotation, though a rotational stiffness can be input to the p-y solutions. However, the free-head and fixed-head conditions represent end cases for pile head restraint and the lateral stiffness of most piles can be reasonably modeled using one of these assumptions.

10.6.1 Pile Head Stiffness for Lateral Loading

Various authors have developed recommendations for p-y curves for piles in sand and clays based on small-diameter pile load tests that can be used in a p-y program to estimate the lateral stiffness of the head of a pile subjected to seismic loading. The most commonly used p-y curves are those by Reese et al. (1974) and O'Neill et al. (1983) for sands and by Matlock (1970) and O'Neil et al. (1984) for clays. A variety of commercially available p-y programs have these relationships built in to them.

Given the many uncertainties in site conditions, a simplified procedure to develop a linear stiffness for a laterally loaded pile based on typical working loads can be used to eliminate the need for iteration to find appropriate p-y stiffness. Lam and Martin (1986) found that lateral load-deflection characteristics representing the overall stiffness of the soil-pile system is only mildly nonlinear because the relatively stiff elastic response of the pile usually dominates pile response. Furthermore, the significant soil-pile interaction zone for lateral loading is usually confined to a depth equal to 5 to 10 pile diameters. Therefore, simplified single-layer pile-head stiffness design charts are appropriate practical design applications provided that sensitivity studies are conducted to ensure that the designed foundation is sufficiently robust to allow for uncertainty in soil stiffness.

Single-layer linear design charts for the lateral and rotational stiffness of fixed head and free head piles with the pile head at the ground surface are presented in Figure 10-15 to Figure 10-18 (FHWA, 2006). These charts assume a soil stiffness which increases linearly with depth, starting from zero at grade. Figure 10-19 through Figure 10-21 give stiffness coefficients for piles with their head embedded to depths of 1.5 m and 3 m (5 and 10 ft), also based on a subgrade modulus that increases linearly with depth.

The soil stiffness in these solutions is defined by a subgrade modulus, E_s , and the coefficient of variation of the subgrade modulus, f , with depth, z , in accordance with Equation 10-1:

$$f = \frac{E_s}{z} \quad 10-1$$

Values of the coefficient f , which has units of force/unit volume, are provided for sands in Figure 10-22 as a function of the friction angle or relative density and in Figure 10-23 for clays as a function of cohesion (undrained shear strength) or normalized and standardized Standard Penetration Test blow

count, $(N_1)_{60}$. Average soil conditions for the upper five pile diameters should be used when using these charts, which are strictly applicable only for piles up to 0.6 m (24 in) in diameter.

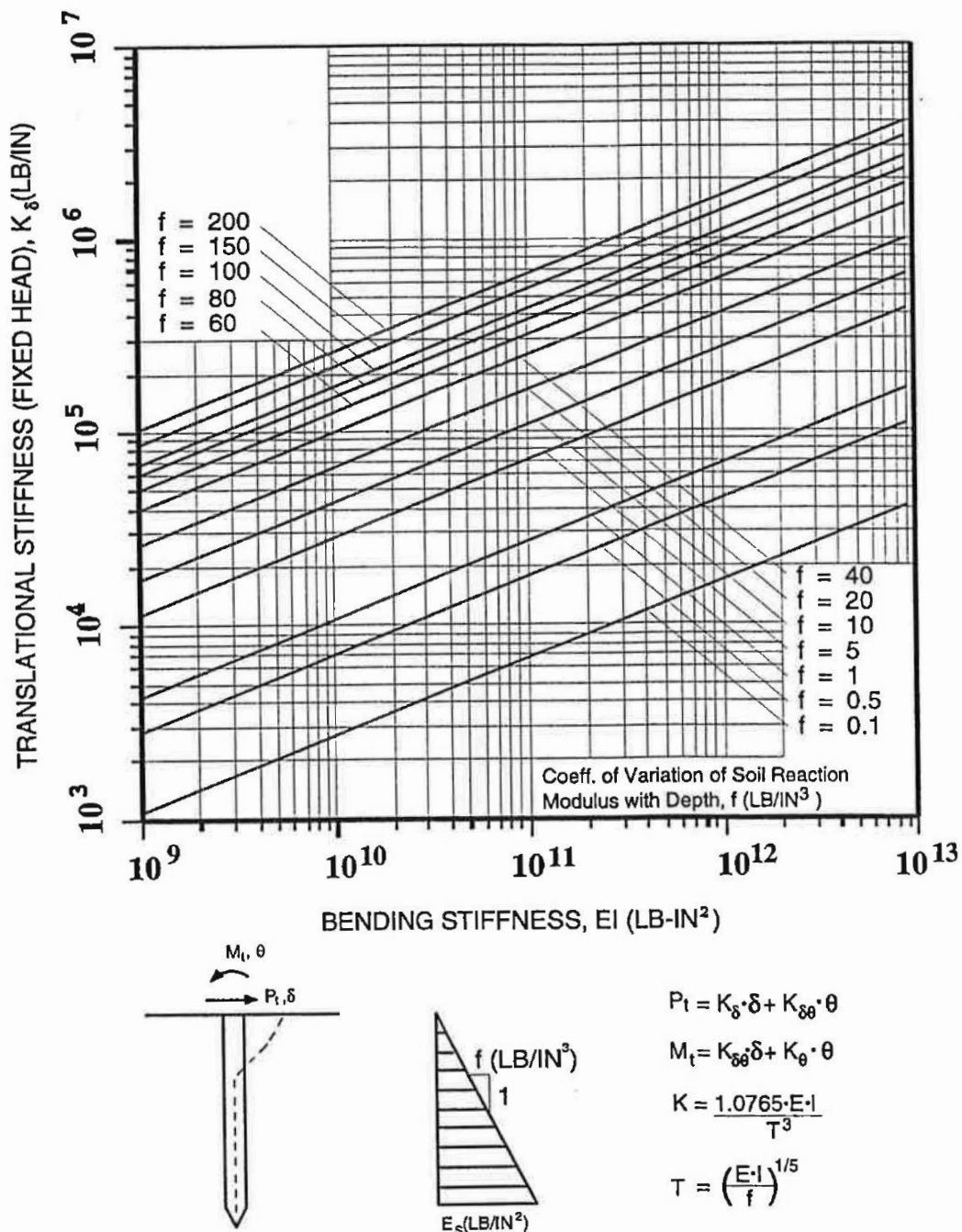
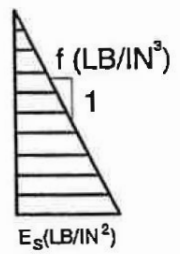
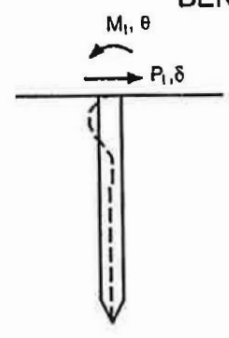
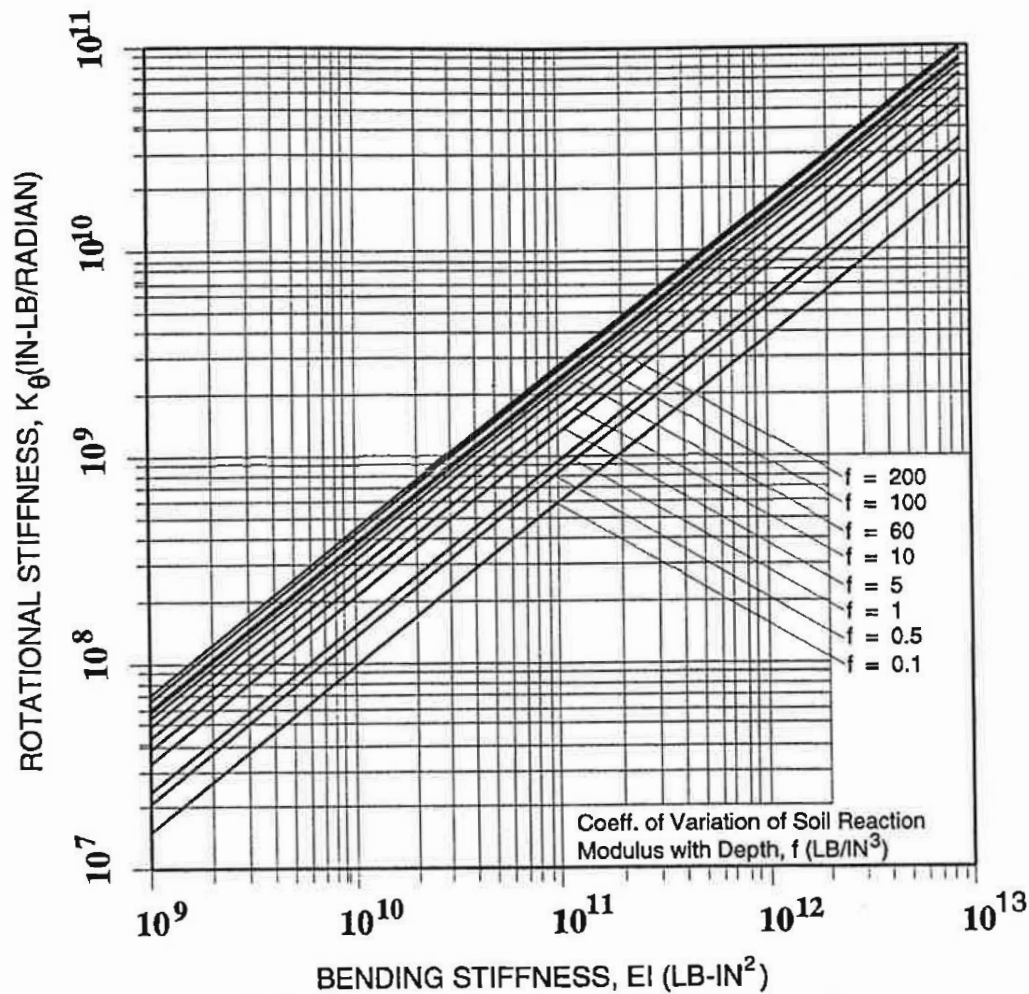


Figure 10-15 Lateral Translational Diagonal Stiffness Coefficient (Same as Fixed Head Stiffness)



$$P_t = K_\delta \cdot \delta + K_{\theta\theta} \cdot \theta$$

$$M_t = K_{\delta\theta} \cdot \delta + K_\theta \cdot \theta$$

$$K = \frac{1.499 \cdot E \cdot I}{T^3}$$

$$T = \left(\frac{E \cdot I}{f} \right)^{1/5}$$

Figure 10-16 Rotational Diagonal Stiffness Coefficient

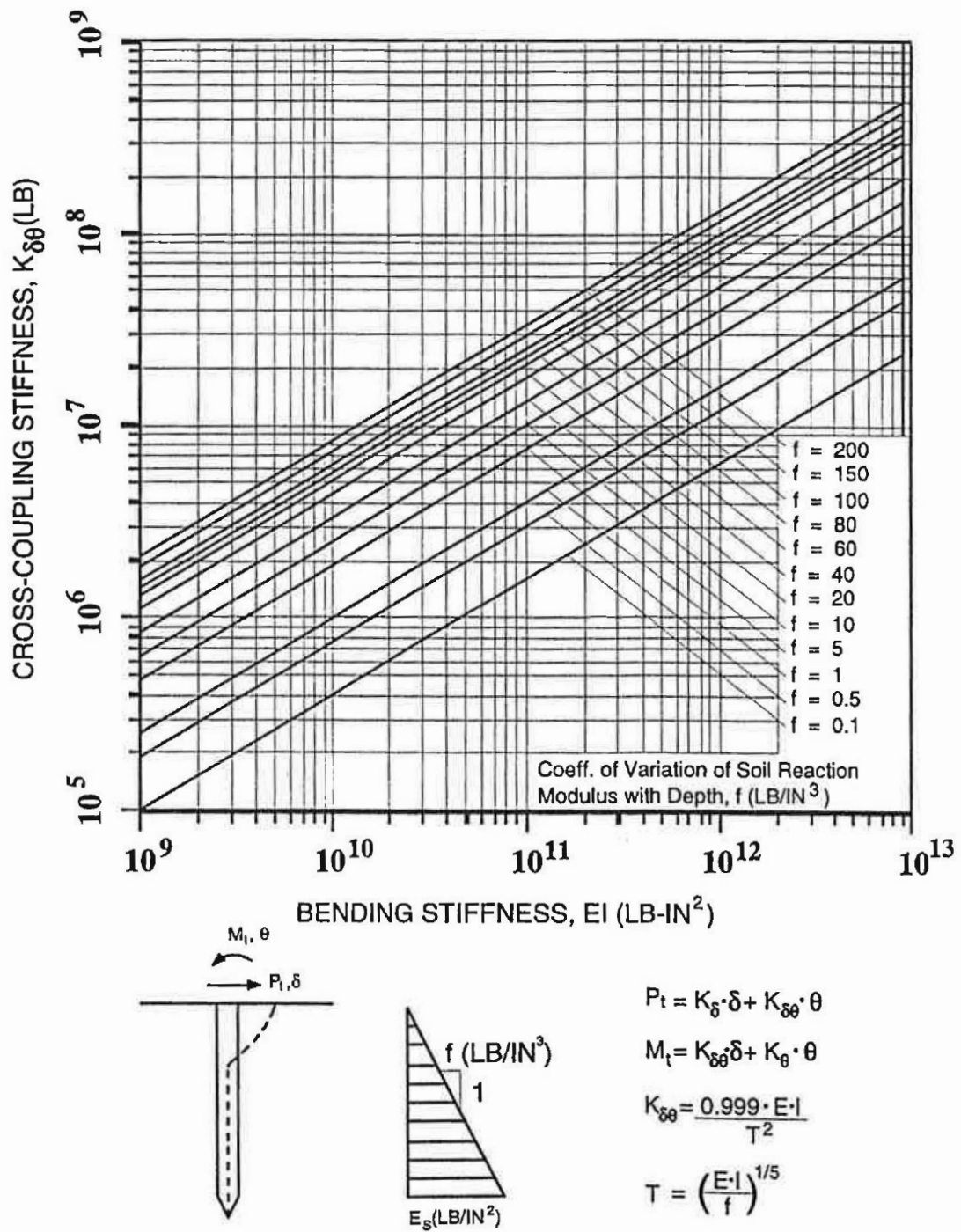


Figure 10-17 Cross Coupling of Diagonal Stiffness Coefficient

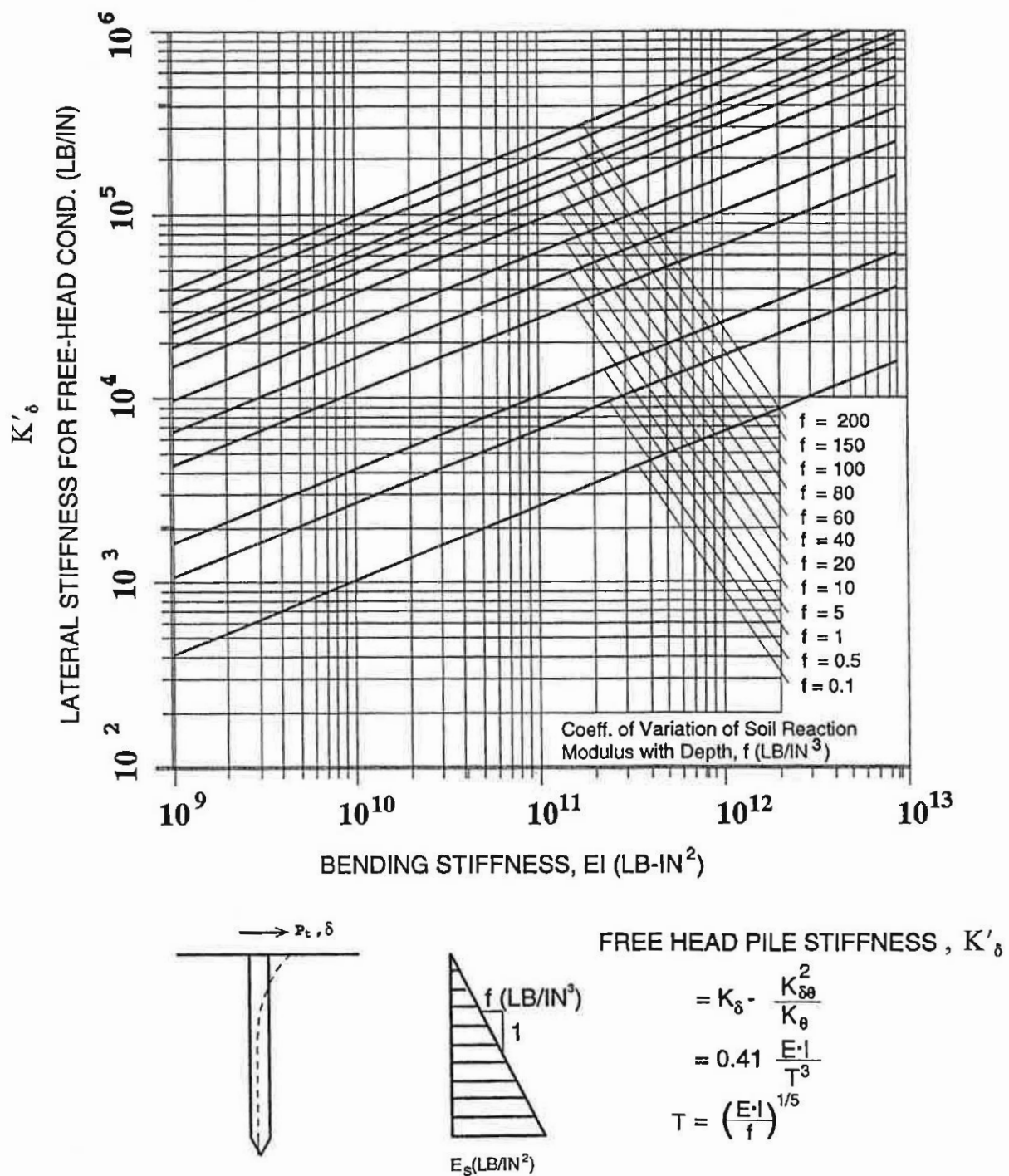
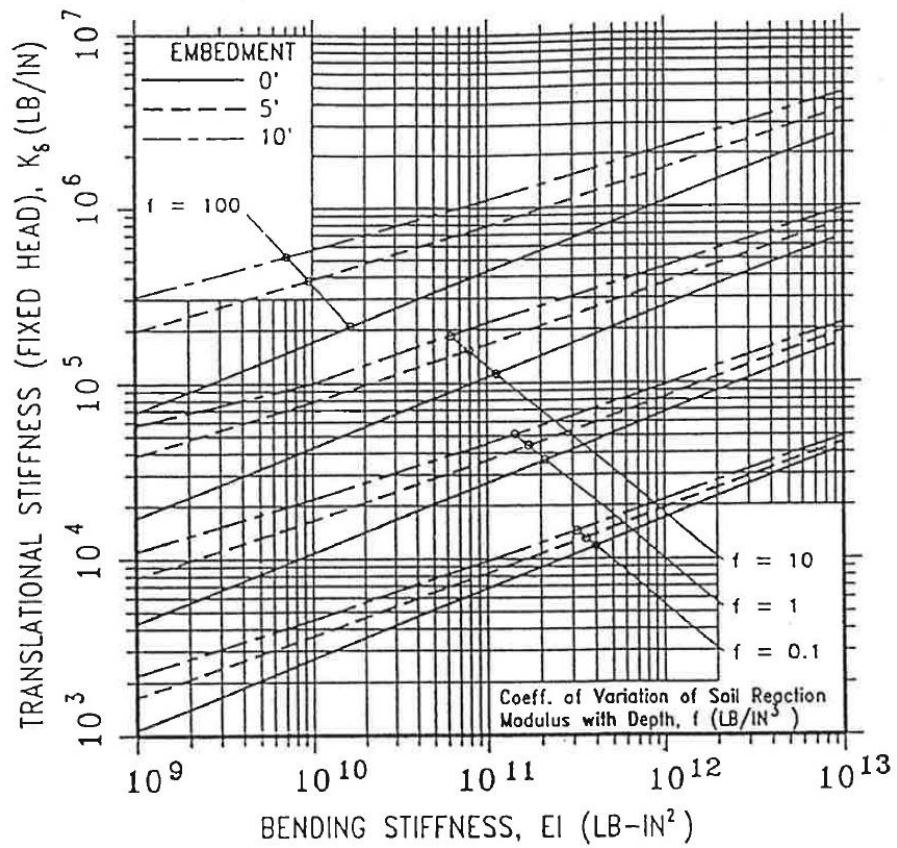


Figure 10-18 Lateral Free Head Stiffness Coefficient



$$P_t = K_b \cdot \delta + K_{s0} \cdot \theta$$

$$M_t = K_{t0} \cdot \delta + K_\theta \cdot \theta$$

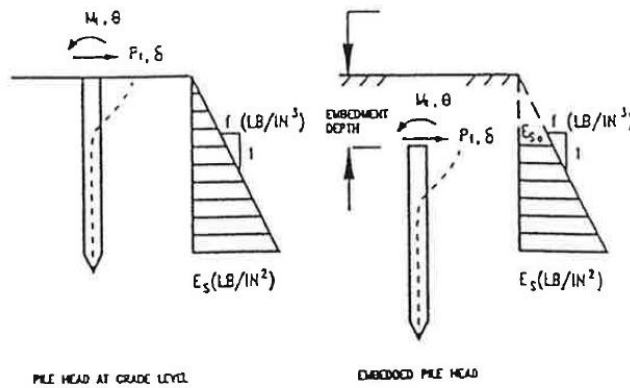
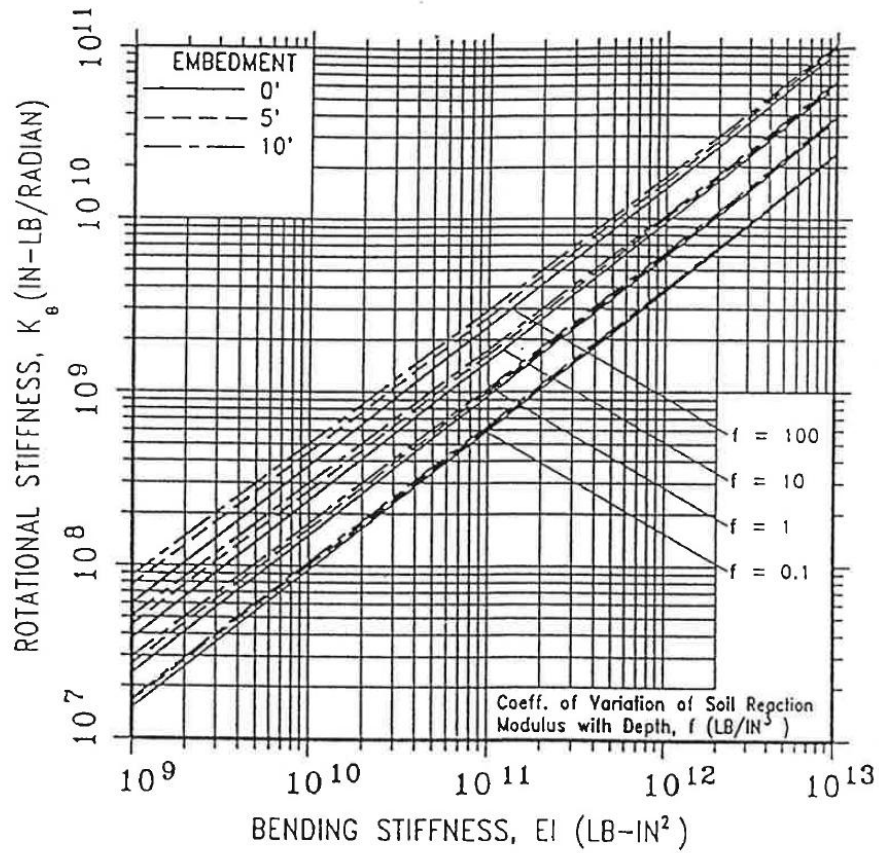


Figure 10-19 Lateral Translational Diagonal Stiffness Coefficient (Same as Fixed Head Stiffness) for Embedded Pile Head



$$P_t = K_s \cdot \delta + K_{s\theta} \cdot \theta$$

$$M = K_{s\theta} \cdot \delta + K_\theta \cdot \theta$$

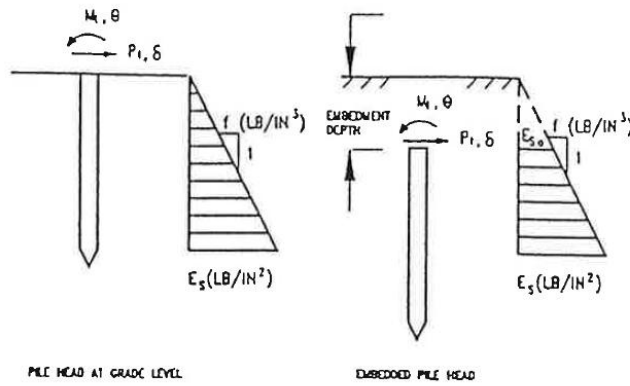
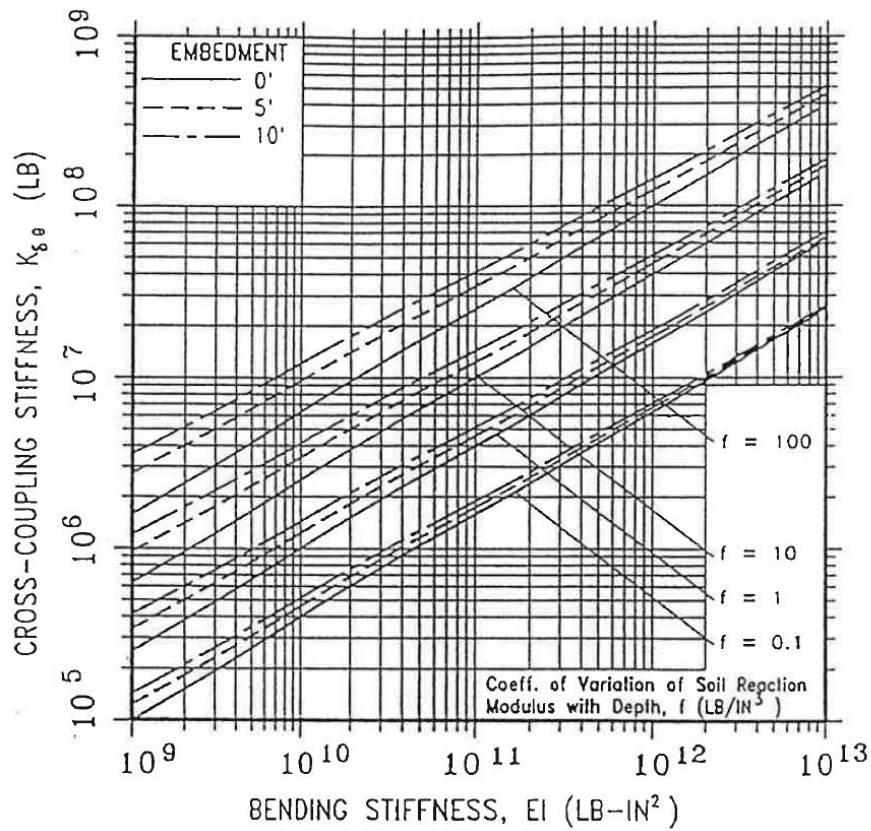


Figure 10-20 Rotational Diagonal Stiffness Coefficient for Embedded Pile Head



$$P_i = K_{\delta} \cdot \delta + K_{g\theta} \cdot \theta$$

$$M_i = K_{\theta} \cdot \theta + K_{\delta} \cdot \delta$$

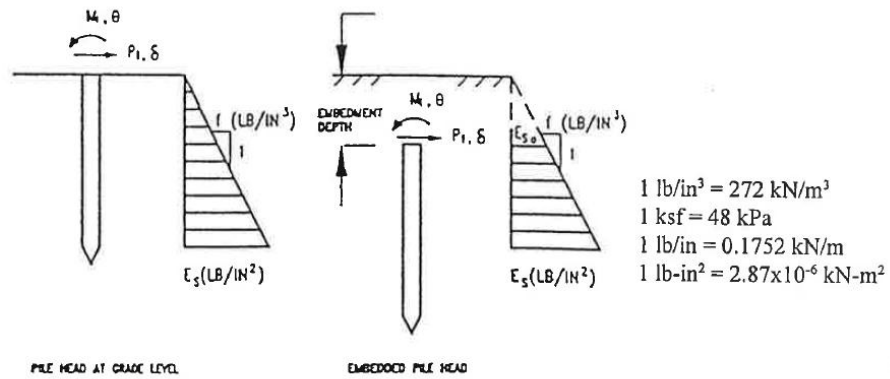


Figure 10-21 Cross Coupling of Diagonal Stiffness Coefficient for Embedded Pile Head

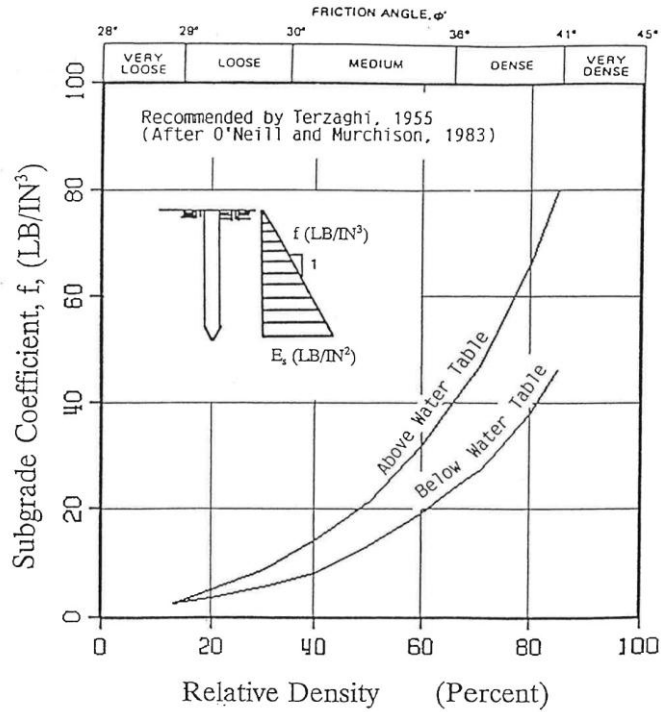


Figure 10-22 Recommended Coefficient of Variation in Subgrade Stiffness with Depth for Sands

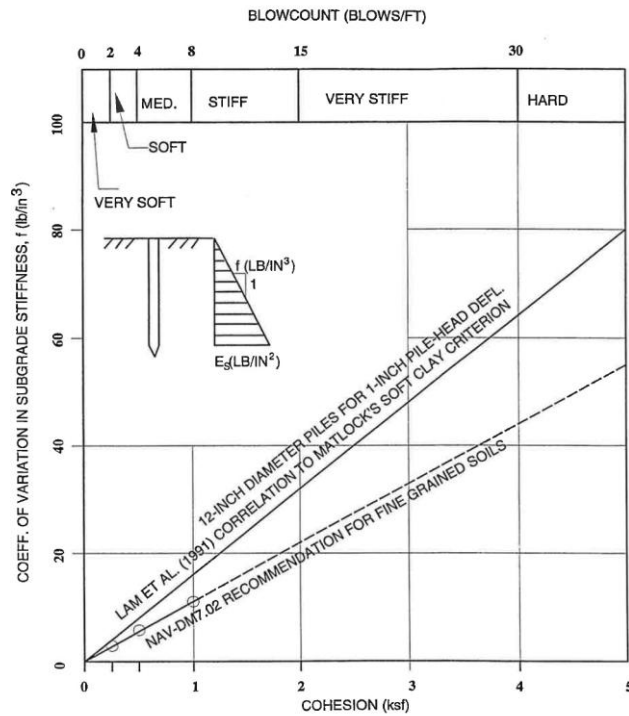


Figure 10-23 Recommended Coefficient of Variation in Subgrade Stiffness with Depth for Clays

10.6.2 Pile Head Stiffness for Axial Loading

The axial stiffness of a pile head is generally assumed to be uncoupled from the stiffnesses in the lateral and rotational directions. One reason why axial load-displacement characteristics may be assumed to be uncoupled from the lateral load-displacement behavior is because much of the soil resistance to axial loading comes from relatively deep depths. A realistic determination of axial pile stiffness should account for heterogeneous soil layering as well as slippage along the sides of the pile. Therefore, linear, homogeneous analytical solutions should not be used for axial stiffness calculations. Instead, methods that account for both soil layering and plastic slippage at the soil-pile interface should be used.

A graphical procedure that gives the axial stiffness coefficient for a single pile and includes layering and slippage at the pile soil interface proposed by Lam and Martin (1986) is illustrated in Figure 10-24 and described as follows:

- Step 1: *Ultimate compressive capacity.* Calculate the ultimate pile capacity from a site-specific pile capacity analysis using conventional procedures for skin-friction and end-bearing capacities for the different soil layers. When assigning values to the skin-friction and end-bearing capacities, make allowances for the construction method (e.g., pre-drilling, driving), special conditions (e.g., consolidation due to surcharging, corrosion), and dynamic soil behavior (e.g., cyclic strength degradation, soil liquefaction).
- Step 2: *Rigid pile load-displacement curve.* Develop the pile load-displacement curve based on the estimated ultimate capacity and published skin-friction and end-bearing pile displacement relationships (e.g. the relationships in Section 10.8.2.2.2 of the AASHTO LRFD Bridge Design Specifications (AASHTO 2007)). The resulting load-displacement curve, illustrated in Figure 10-24, is obtained from the sum of the skin friction and end-bearing capacities at each axial displacement, provides a pile-head load-displacement relationship for a pile that is axially-rigid. This curve is a lower bound on the actual pile displacements.

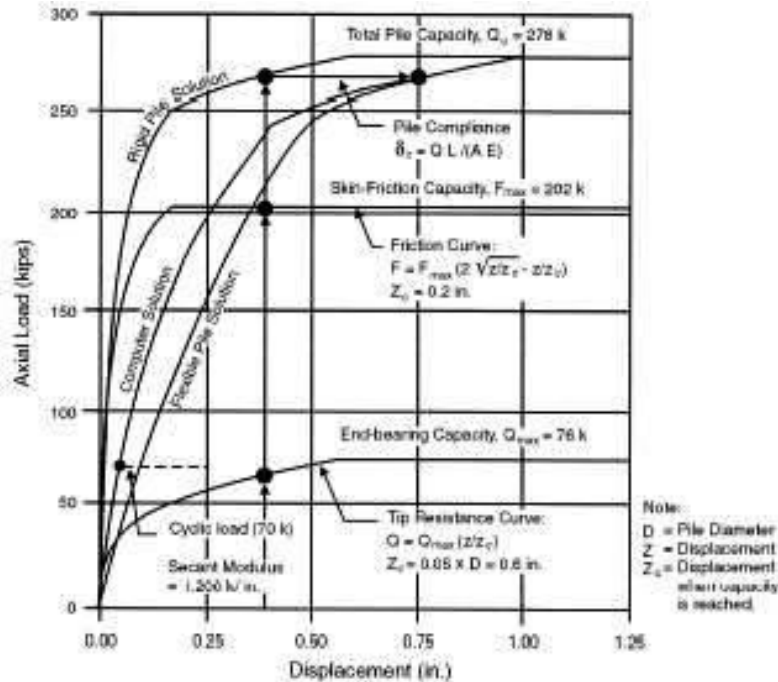


Figure 10-24 Graphical Solution for Developing Axial Pile Stiffness

Step 3: *Flexible pile load-displacement curve.* Calculate the axial displacement at the pile head due to the compression of the pile under axial load but neglecting the surrounding soil. This displacement is given by:

$$\delta_c = \frac{QL}{AE} \tag{10-2}$$

where Q is the axial load, L is the length, and AE is the axial rigidity of pile.

Obtain the flexible pile solution by adding the displacement from Equation 10-2 to the rigid-pile load-displacement curve in Figure 10-24 at pile loads that correspond to the rigid pile load-displacement curve. This curve is an upper bound on the actual pile displacements.

Step 4: *Actual load-displacement curve.* As a first approximation, obtain the actual axial load-displacement curve by averaging the curves from steps 2 and 3. The actual solution is bounded by the rigid and flexible load-displacement solutions derived in steps 2 and 3 and depends on the nature of the soil-pile system. Averaging the results is a good place to start.

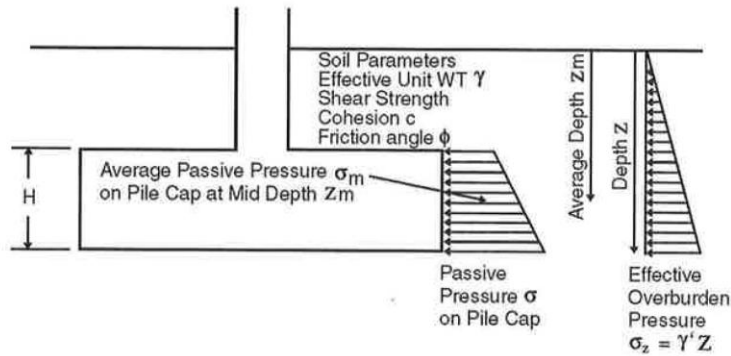
For an end-bearing pile, the actual curve may be closer to the flexible-pile solution. For a friction pile at small load levels, the upper portion of the pile is compressed first and thus the load-displacement curve will be closer to the rigid-pile curve. At higher loads, slippage occurs along most of the pile and the solution moves towards the flexible-pile curve.

Step 5: *Axial pile stiffness.* Calculate a value for the pile secant stiffness from the load-displacement curve over the range of expected displacements and use it to find the equivalent axial stiffness coefficient for inclusion in the pile stiffness matrix. Expected displacements may be found from the expected range of axial loads, which for a regular highway bridge foundation would be in the range of 50 to 70 percent of the ultimate pile capacity.

The above procedure may be used to obtain the corresponding uplift load-displacement curve by ignoring end-bearing and using only skin-friction to evaluate capacity.

10.6.3 Lateral Stiffness of Pile Cap

Because most pile footings are embedded, the pile cap stiffness should be superimposed on the pile stiffness to develop the pile footing stiffness. The centrifuge tests conducted by Gadre and Dobry (1998) confirmed the concept that the stiffness of the piles and the pile cap are additive as well as that the passive pressure acting on the pile cap constitutes the bulk of the pile cap stiffness. Because of the possibility of soil settlement and the uncertainties concerning the interaction between the footing and the piles, contributions to the pile cap stiffness as well as to foundation capacity from the footing's base and from side shear are neglected. Hence the primary source of lateral resistance is the mobilization of passive pressure on the vertical face of the pile cap. Maximum passive pressures can be computed using the approach illustrated in Figure 10-25 (FHWA, 2006) or the approach used for earth retaining structure design (discussed in Chapter 11). The mobilized passive pressure and the associated deformation depend upon the displacement of the pile cap and may be calculated using the method described for calculating the stiffness of bridge abutments in Chapter 12.



Recommended Method for Passive Pressure Capacity

- (I) For Frictional Soil (ϕ only):
Average Passive Pressure Capacity = $K_p \gamma' Z_m$
 K_p Based on Caquot & Kerisel for
Interface Friction Angle $\delta = 0.5 \phi$
- (II) For Cohesive Soil (c only):
Based on Rankine Pressure Theory
Average Passive Pressure Capacity = $\gamma' Z_m + 2c$
- (III) For c and ϕ Soils:
Average Passive Pressure Capacity = $K_p \gamma' Z_m + 2c \tan(45^\circ + \phi/2)$

Total Force Capacity on Pile Cap Per Unit Width
= Average Passive Pressure Capacity x Thickness of Cap (H)

Figure 10-25 Method for Passive Pressure Capacity of Pile Cap (FHWA, 2006)

10.6.4 Group Effects for Typical Pile Footings

The single pile stiffness must be adjusted for group effects if the foundation is supported by a pile group. In general, if the center to center spacing of the piles in a group is less than five pile diameters, interactions between the piles (i.e. pile group effects) must be considered in evaluating pile stiffness. In the p-y approach, this interaction is defined using what is referred to as a p-multiplier, a factor by which the p ordinate of the p-y curve is multiplied to account for group effects. However, as group effects reduce pile stiffness the p-multiplier is always less than 1. Experimental data on p-y curves for closely spaced piles show that the load distribution varies depending on the position of the pile. Table 10-1 presents recommendations for the p-multiplier for piles in a 3 x 3 group spaced at 3 diameters subject to

monotonic unidirectional loading. Table 10-2 shows the effect of pile spacing on the p-multiplier of piles subjected to monotonic unidirectional loading.

TABLE 10-1 P-MULTIPLIERS FOR PILES IN A 3 X 3 GROUP AT 3 DIAMETER SPACING SUBJECT TO MONOTONIC LOADING

Pile Test, Soil Description, Reference	p-multiplier on single-pile p-y curves		
	Front Row	Middle Row	Back Row
Free-Head, Medium Dense Sand, $D_r = 50\%$ Brown et al. (1988)	0.8	0.4	0.3
Fixed-Head, Medium Dense Sand, $D_r = 55\%$ McVay Centrifuge (1995)	0.8	0.45	0.3
Fixed-Head, Medium Dense Sand, $D_r = 33\%$ McVay Centrifuge (1995)	0.65	0.45	0.35
Free-Head, Soft to Medium Clays and Silts Rollins et al. (1997)	0.6	0.38	0.43

TABLE 10-2 INFLUENCE OF PILE SPACING ON P-MULTIPLIERS FOR PILE SUBJECT TO MONOTONIC LOADING

Row Spacing	Front Row	2nd Row	3rd & More Rows
3D	0.8	0.45	0.35
4D	0.9	0.65	0.55
5D	1	0.85	0.75

Piles subjected to earthquake loading are generally subjected to reversing (cyclic) loads, as opposed to the monotonic loading used to develop Table 10-1 and Table 10-2. Under cyclic loading condition, the front row pile will become the back row pile when the load direction reverses. For simplicity, Lam et al. (1998) recommend use a 0.5 p-multiplier on all the piles for design analyses. This recommendation is supported by full scale pile load test data reported by Matlock et al. (1980) that shows that the load tends to become uniformly distributed among all the piles in a pile group during cyclic loading. The value of 0.5 is approximately the mean value for the p-multiplier of piles a 3-diameter spacing subject to monotonic loads. If we assume that under two way loading a constant p-multiplier equal to the mean p-multiplier for one-way loading should be used, the p-multiplier values in Figure 10-26 can be derived.

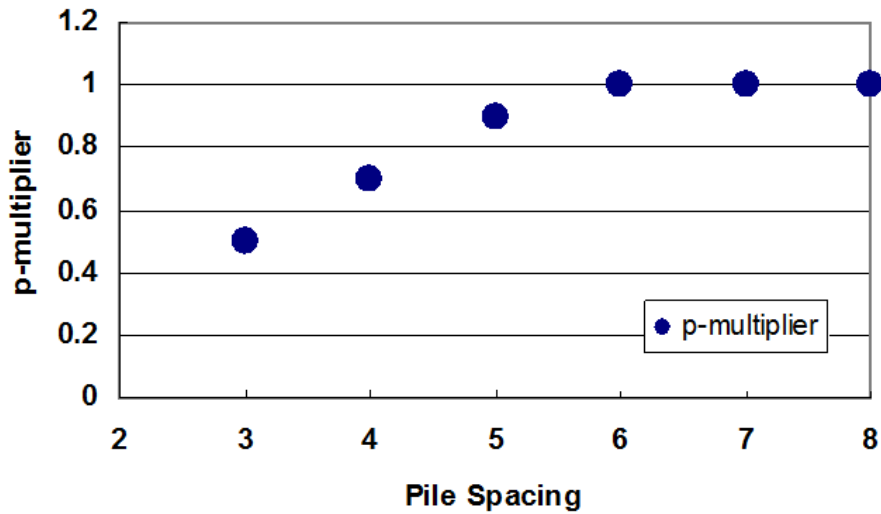


Figure 10-26 P-Multipliers for Two-Way Seismic Loading

10.6.5 Group Effects for Very Large Pile Groups

The pile group effects discussed above are from pile load tests on relatively small pile groups involving either 9 or 16 piles in the pile groups. Foundations for major water crossings may involve extremely large piers supported by several hundred piles. In these cases, the horizontal dimension of the footing can easily be greater than the length of the piles, in contrast to small groups where the pile length is usually several times the size of the pile cap. The pile-soil system in these configurations may be thought of as a reinforced soil mass. A full-scale experiment for such a huge pile group would be impossible. Therefore, engineers must rely upon numerical analyses to evaluate group effects for this problem. Dodds (2005) developed the recommendations shown in Table 10-3 for the p-multiplier for piles in large groups as a function of pile spacing.

TABLE 10-3 P-MULTIPLIERS FOR LARGE PILE GROUPS (DODDS 2005)

Soil Condition	3D Spacing	6D Spacing
Soft Clay	0.1	0.5
Medium Dense Sand	0.2	0.7

10.6.6 p-y Curves for Liquefied Sand

Liu and Dobry (1995) conducted centrifuge tests to evaluate the reduction in the p-y resistance of a soil as a function of the cyclically generated excess pore pressure in sandy soils. Figure 10-27 presents a plot obtained from these experiments showing the reduction in pile resistance (i.e. the p-multiplier), termed C_u in this figure, versus the excess pore pressure ratio. Note that at a pore pressure ratio of 1, representative of liquefaction, the p-multiplier is approximately 0.1, so the lateral resistance of the liquefied soil is approximately 10% of its initial value. However, it may not be appropriate to assign this reduced p-y resistance to the pile during shaking, as pore pressure generally builds up gradually during the earthquake and the reduction in p-y resistance does not exceed 0.5 until the pore pressure ratio equals 70%.

The centrifuge experiment discussed above was conducted on loose, clean Nevada sand with a relative density D_r of 40%. Evidence of a higher residual strength of liquefied soil has been observed in parallel centrifuge experiments conducted at the University of California at Davis in which p-multipliers for liquefied soil as high as 0.25 have been reported.

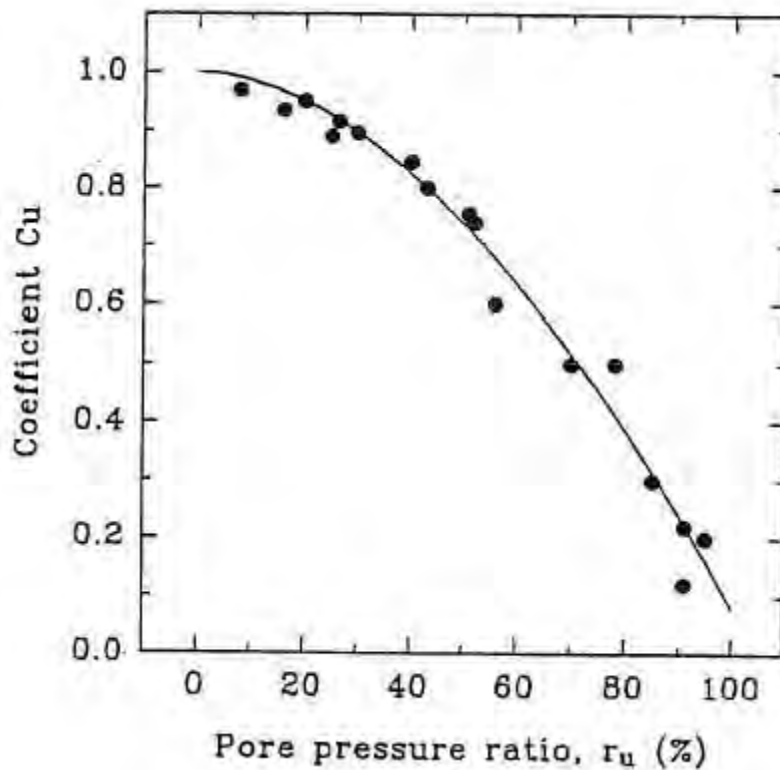


Figure 10-27 Scaling Factor to Reese's static p-y Curves from the 1995 Liu and Dobry Centrifuge Test

Another approach to characterizing the lateral resistance of a pile in liquefied soil is to assign the liquefied soil a representative undrained shear strength, S_u . Based upon back analysis of centrifuge test results, Abdoun (1997) found that the lateral resistance of a pile in liquefied loose sand could be represented by assigning an undrained shear strength of 21 psf to the liquefied soil. The ultimate passive pressure on the side of a pile in cohesive soil (i.e. the p in a p - y curve) was been found to increase from $3S_u D$ at mudline to $9S_u D$ at depth (Matlock, 1970). Therefore, the p value corresponding to an undrained shear strength of 21 psf could vary from 63 psf to 189 psf depending on the depth along the pile.

10.6.7 Stiffness Matrix of a Pile Group

The stiffness of the individual piles must be integrated with the stiffness of the pile cap to develop the stiffness matrix for a pile group. For complex pile group configurations, and particularly for pile groups that include battered piles, developing a linear 6 x 6 pile group stiffness matrix involves the use of a computer program (see Lam and Martin 1986). However, many pile groups encountered in practice have relatively simple configurations and involve only plumb (vertical) piles. For such situations, it is practical to develop the pile group stiffness matrix by hand calculations. The vertical and translational stiffness are simply the sum of the stiffness of the individual piles (plus the stiffness of the cap for the translational mode). The rotational stiffness for moment loading about a horizontal axis (rocking) is coupled to the vertical stiffness of the piles in the group as follows:

$$(k_q)_{cap} = S k_{qi} + S(k_{di} R_i^2) \quad 10-3$$

where $(k_q)_{cap}$ = rotational stiffness of cap
 k_{qi} = rotational stiffness of pile i
 k_{di} = translation stiffness of pile i
 R_i = distance from pile i to center of group

The torsional stiffness is evaluated in a similar manner using the vertical stiffness of the piles and the passive resistance against the pile cap.

10.6.8 Pile Head Rotational Stiffness

A fixed head (or rigid) pile-pile cap connection is probably the most widely adopted assumption in pile design analysis. This assumption is adopted for convenience, as it is difficult to characterize the

rotational stiffness of a pile embedded in a pile cap. However, as real pile-pile cap connections generally do allow some rotation, the assumption of a rigid connection can have a profound impact on design. The assumption of a rigid connection can result in significant under-estimation of the shear capacity of the pile due to exaggeration of the bending moment at the pile head.

The impact of the rotational stiffness of the pile-pile cap connection on the performance of a pile was investigated as part of the Pier 400 Project for the Port of Los Angeles. The performance of a pile supported wharf structure subject to seismic loading using a bi-linear rotational spring to model the pile-pile cap connection. The bi-linear pile rotational spring was developed based on a full-scale pile load in which the pile head moment-rotational characteristics were evaluated. Figure 10-28 compares the observed pile head rotational behavior (Blandon, 2007) to the behavior predicted using the pile head rotational spring.

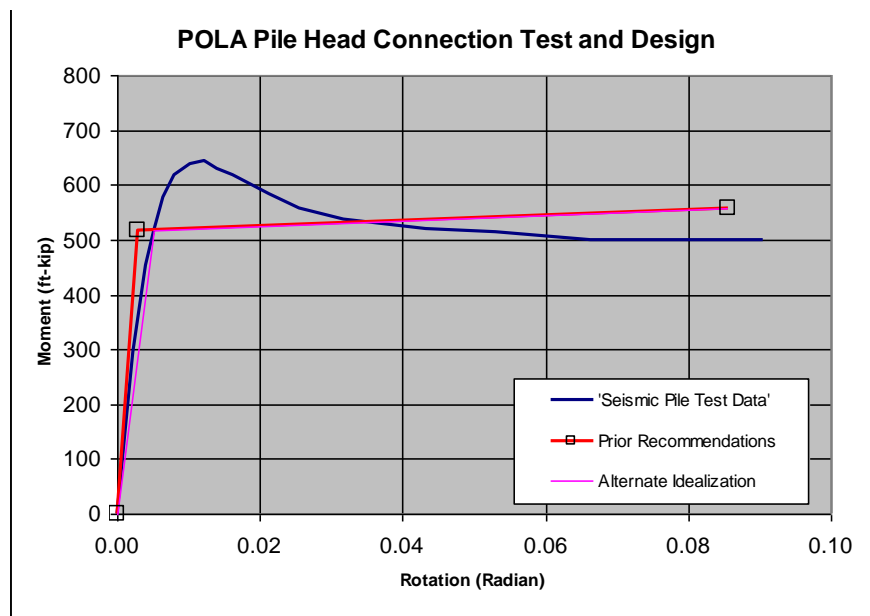


Figure 10-28 Measured versus Predicted Pile Head Rotation

Figure 10-29 presents the results of pile pushover analyses that illustrate the benefit of modeling the pile head with the rotational spring as opposed to employing the traditional assumption of a fixed head. The moment capacity for the pile at the pile-pile deck connection point was found to be 6,692 in-kips. At this moment capacity, the pile would have a displacement capacity of only about 0.7 inch for the conventional fixed-head assumption. However, the displacement capacity of the pile increased to almost 10 inches for

the recommended safety level criterion of 0.0855 radian rotation when the bi-linear moment-rotation spring was employed. Even under a no damage criterion (no inelastic action at the pile head), the displacement capacity using the bi-linear moment-rotation spring increased to approximately 1.4, essentially twice the 0.7 inch capacity from the fixed head assumption.

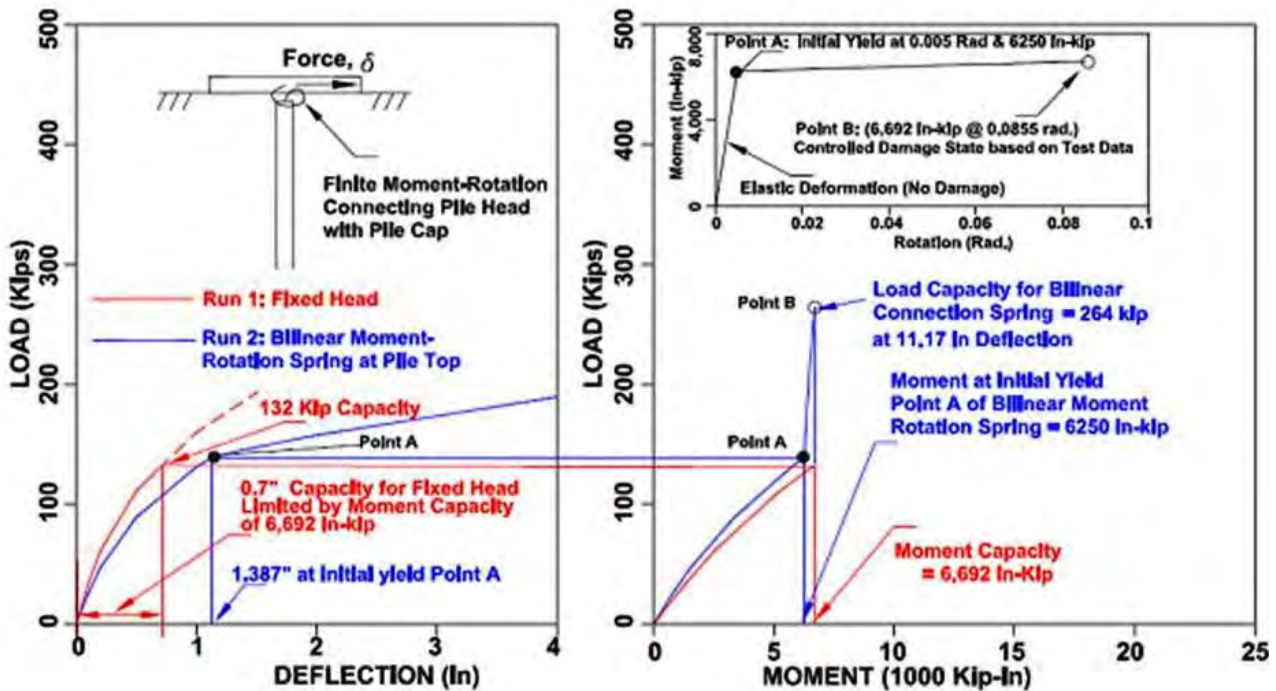


Figure 10-29 Shear vs. Moment Load Solution

The rotational spring also increased the shear capacity of the pile head connection. With the bi-linear spring, a lateral shear load capacity of 264 kips mobilized at the 11.17 inch limiting deflection compared to the 132 kips shear load capacity for the fixed head assumption. The rotational spring also resulted in a more evenly distributed moment along the entire pile at failure, as the pile becomes more efficient in mobilizing soil capacity at deeper depths without overstressing the pile top region.

10.7 MOMENT CAPACITY OF PILE GROUPS

Moment capacity of a pile group is typically governed by the axial pile uplift and compression capacities. The ultimate moment capacity of a pile group is often evaluated based upon first yield of any pile in the group. However, unrestrained deformation cannot occur until multiple piles in the group (typically all but

one pile or row of piles, about which the group will rotate) yield. Figure 10-30 shows calculations of the moment capacity of a 4 x 3 pile group using both assumptions. The ultimate compression and uplift capacity of the piles are 180 kips and 90 kips, respectively. If the cap is assumed to fail upon first yield of one of the outer piles in the group, the moment capacity of the group is 2,700 ft-kips. However, if it is assumed the cap does not fail until three of the four piles yield geotechnically (as required for unrestrained rotation of the cap), the moment capacity of the cap is 4,050 ft-kips. Note that the pile cap must be designed to sustain a tension load equal to the uplift capacity of the pile to realize this capacity.

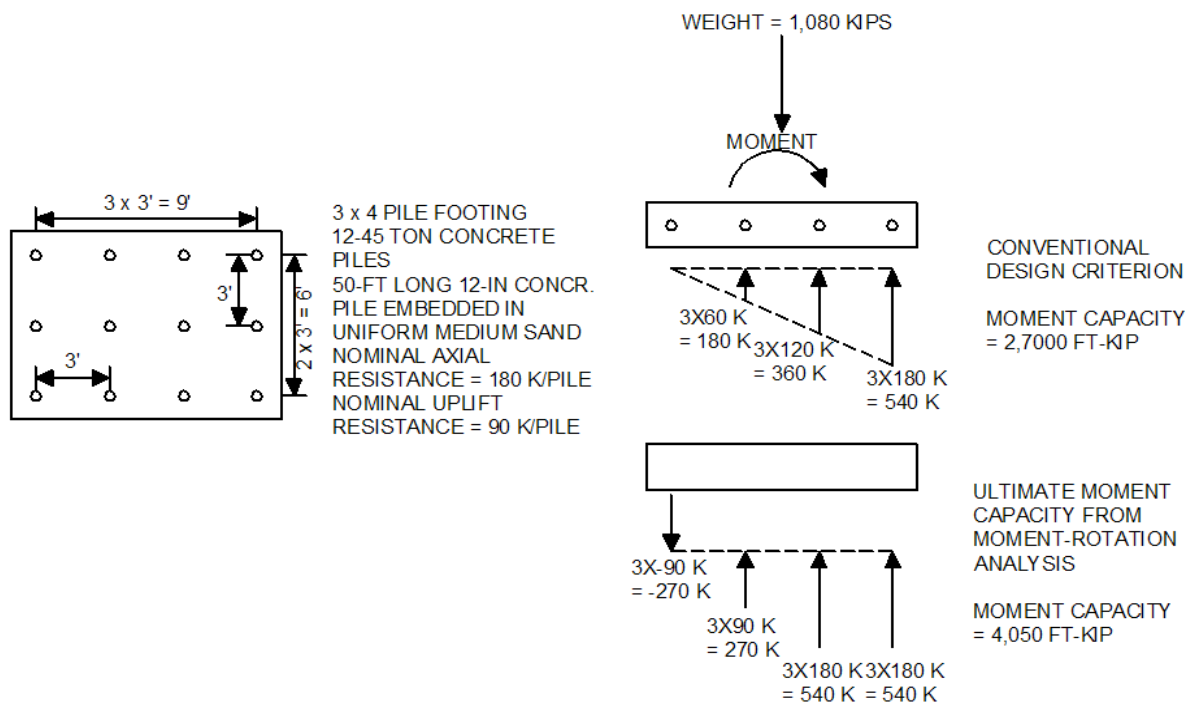


Figure 10-30 Moment Capacity of a Pile Group

It is recommended that the pile head connection be designed so that its capacity in tension exceeds the geotechnical uplift capacity of the pile, forcing the failure of the system under moment loading into the soil, rather than at the connection. Again, using this design philosophy it can be counter-productive if geotechnical engineer is overly conservative in evaluating the uplift capacity of the pile, as underestimating the uplift capacity could be counter-productive to the goal of forcing the failure into the soil.

Following the 1989 Loma Prieta earthquake, Caltrans embarked on a very aggressive program to retrofit existing bridges in California. Many of the foundations were concluded to be inadequate in terms of their capacity to resist the earthquake loading. A particular concern was the lack of moment capacity due to exceeding the uplift capacity of the piles in conventional force-based demand analyses. However, it was also recognized that there was a lack of any evidence of inadequate moment capacity in past earthquakes (e.g. from overturning failure of bridge piers). A series of research projects were organized under the auspices of MCEER to investigate this apparent discrepancy. The following paragraphs summarize the overall conclusions from the studies conducted by Fenves (1998) as part of this effort:

- In terms of the moment-rotation ductility demand on the column, an overly strong footing results in a higher potential for damage to the column. A softer foundation (i.e. lower moment capacity of the footing), especially where there are good connection details to enforce the energy dissipation mechanism in the soil, results in lower inelastic demand on the column.
- A lower static factor of safety implies a higher degree of peak and permanent footing rotation. A higher static factor of safety leads to significantly lower peak and residual rotations.
- In the case of a connection detail failure (zero uplift pile capacity), the inelastic demand on the column is actually reduced significantly. As connection detail failure takes place, the superstructure becomes isolated from the earthquake ground motion and hence a lower amount of earthquake force is transmitted to the superstructure. However, connection detail failure implies a higher degree of global instability.
- The force-based design approach is an extremely conservative approach with respect to global stability.

10.8 DESIGNING FOR UNCERTAINTY

Figure 10-31 presents the results of a series of pushover analyses for a 16-inch drilled shaft at a medium dense sand site. The pile is represented as a linear elastic material and the pile head is modeled using the typical fixed head pile top boundary condition. The figure presents the results of a sensitivity study using three p-y curves (1) benchmark p-y curves developed based on a 35-degree friction angle, (2) a set of

stiffer p-y curves developed by using a p-multiplier of 2 on the benchmark p-y curves, and (3) a set of softer p-y curves developed using a p-multiplier of 0.5 on the benchmark p-y curves.

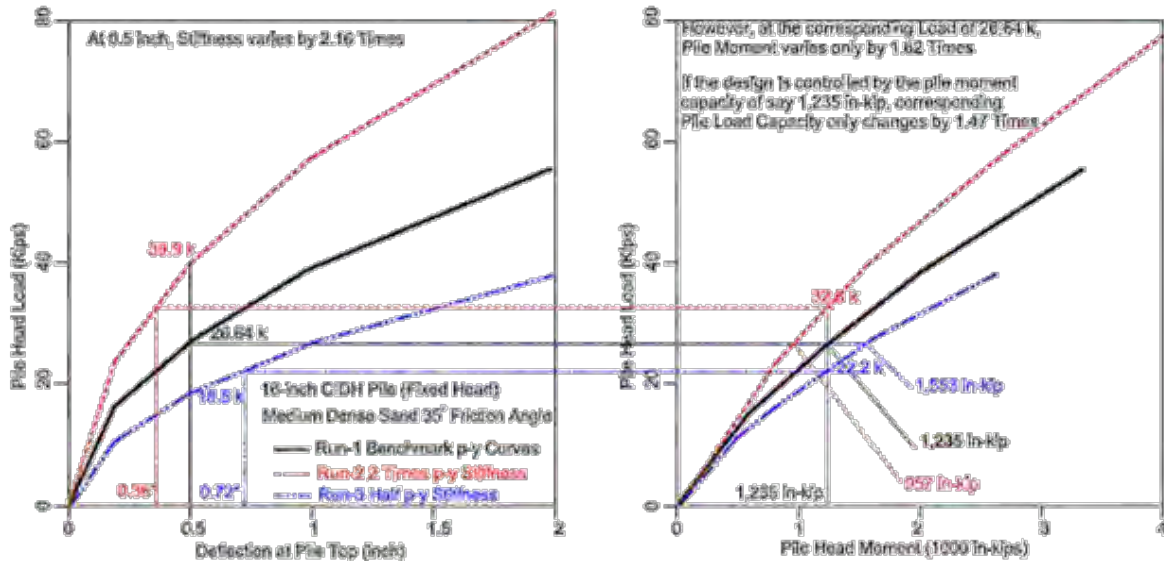


Figure 10-31 Sensitivity of a 16-inch Drilled Shaft to Variations in p-y Curve Stiffness

For the variation of a factor of 4 in the p-y curve stiffness, the mobilized pile resistance at 0.5-inch deflection changes from 18.5 to 39.9 kips, or a variation by a factor of approximately 2. The right side of Figure 10-31 presents the moment versus pile shear relationship, which is often of more importance than the pile load-deflection relationship shown on the left side. For a pile head load of 26.64 kips, the pile moment varies from 957 to 1,553 in-kips, or a variation by a factor of 1.6, which is even smaller than the variation in the pile stiffness. Furthermore, from the right side of Figure 10-31 it can be seen that for a moment of 1,235 in-kips the shear load on the pile varies from 22.2 to 32.8 kips, a variation by a factor of approximately 1.5 times. In summary, a 4 times variation in the stiffness of the p-y curve implies about a 2 times variation in the foundation stiffness, about a 1.62 times variation in the pile moment for a specified shear load, and a 1.5 variation in the shear load for a specified moment capacity. This example highlights the fact that the behavior of pile foundations is usually relatively insensitive to relative small variations in p-y curve stiffnesses, especially when designing for displacement capacity.

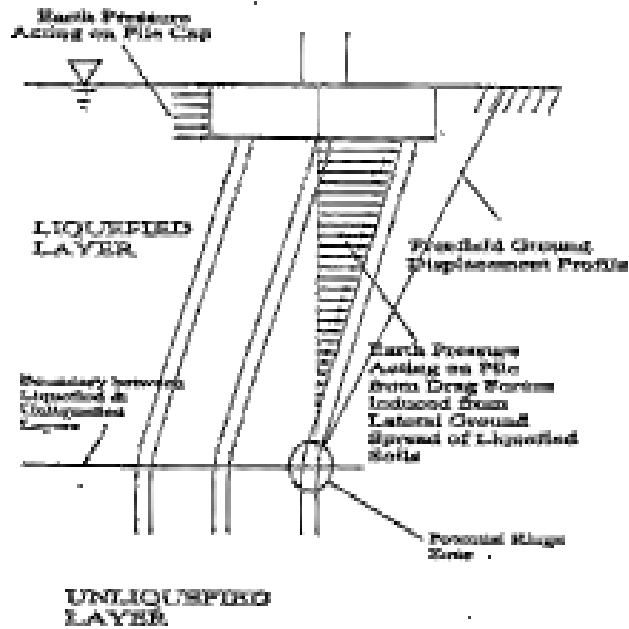
If the earthquake demand is assumed to be a displacement based demand, at a moment capacity of 1,235 in-kips the corresponding displacement capacity of the foundation would be 0.72 inch and 0.36 inch,

respectively, for the soft p-y and stiff p-y cases. Therefore, the softer p-y curve results in a higher displacement capacity for the foundation. This notion is supported by case histories that show that stiffer structural components are actually more vulnerable to earthquake damage than softer components. Actually, it is difficult to predetermine whether softer or stiffer p-y curves would be conservative in the overall design of the structure. Therefore, good design practice calls for analyzing the foundation and the structural system for a wide range of p-y curve stiffness assumptions to account for the basic uncertainty in p-y curve characterization. In addition to varying p-y curve stiffness, the designer often needs to allow for uncertainty in other aspects of the design, including the assumed pile cap embedment depth and pile head fixity assumptions. Often, these issues are of more significance to the design than p-y curve stiffness. Designing the foundation for large variations in p-y curve stiffness is also a practical way to deal with design issues such as pile group effects and the stiffness of piles in liquefiable ground.

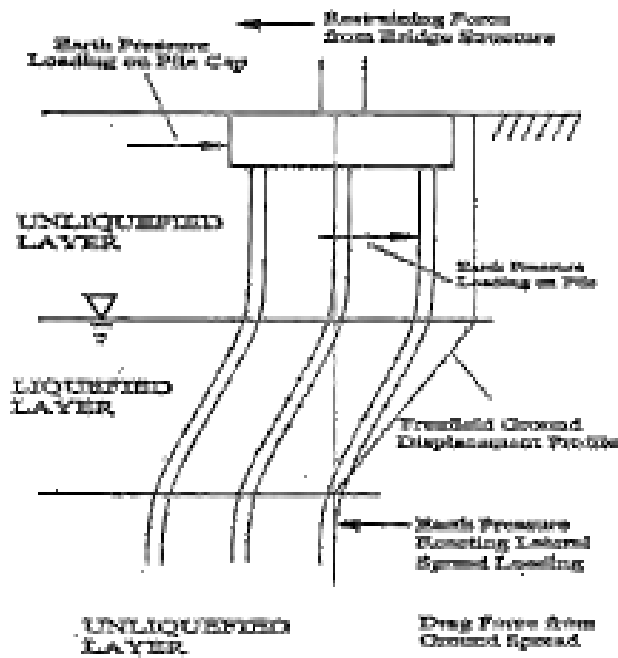
10.9 DESIGNING FOR KINEMATIC DISPLACEMENT DEMAND IN LIQUEFIED SOILS

Analysis of ability of a deep foundation to withstand the kinematic displacement demand from laterally spreading soil can be into two categories: (1) cases where the liquefied soil layer extends all the way to the ground surface; and (2) cases where the liquefied soil layer is overlain by a nonliquefied layer. These two categories of the lateral spreading problem are shown schematically in Figure 10-32.

Conceptually, cases where the liquefied soil extends all the way to the ground surface can be analyzed simply by applying the appropriate p-y curves to the liquefied soil. Recommendations for liquefied soil p-multipliers are on the order of 0.1 to 0.25, as previously discussed. However, p-y curves back calculated from the performance of laterally loaded piles in soil liquefied by blasting reported by Rollins et al (2005) and presented in Figure 10-33 show stiffening at large deflections as well as a different backbone curve shape than conventionally assumed for p-y curves. At the present time there is no consensus on the proper approach to modeling the p-y behavior of liquefied soils, suggesting a need for sensitivity studies to account for this uncertainty, as discussed above.



(a) Lateral Spread Loading Problem for Liquefied Layer above Unliquefied Layer



(b) Lateral Spread Loading Problem for Unliquefied Layer above Liquefied Layer

Figure 10-32 The Two Cases for Pile Design in Lateral Spreading Liquefied Soils

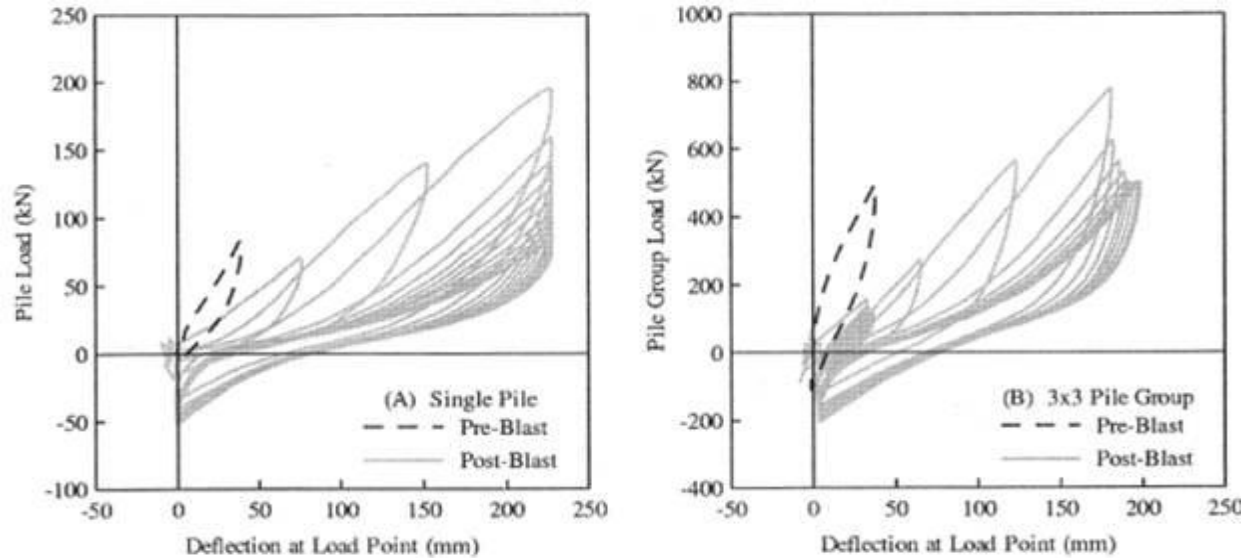


Figure 10-33 p-y Curves Back calculated from Soil Liquefied by Blasting (Rollins et al 2005)

A review of the case histories of piles damaged by lateral spreading of liquefied ground suggests that all of the cases in which pile damage is reported are associated with a non-liquefiable crust sliding on a liquefied layer. This loading mechanism is generally considered to be unrelated to the inertial response of the foundation.

In an attempt to address the problem of a non-liquefied soil layer sliding on liquefied soil, Lam et al. (2007) conducted a series of 3-dimensional finite element analyses, illustrated in Figure 10-34. The studies included analyses for a large range of pile types and pile diameters with a large range of EI values, three sets of liquefied layer thicknesses, and also a sufficiently large range of soil properties. The resultant solutions were used to develop a set of non-dimensional charts for simplified design analysis. The pile is modeled using linear elastic properties and therefore the design charts will only be valid prior to pile yielding. Furthermore, the solution is for the basic single solitary pile problem (i.e. without pile group effect).

The steps involved in the simplified pile design analyses are outlined below:

Step-1: Estimating the Relative Slippage Displacement Amplitude, D , between the upper crust and the lower stable nonliquefied layer: Any of the commonly used approaches for evaluating the

magnitude of lateral spreading, including the Newmark sliding block approach discussed in Chapter 6, can be used to estimate the basic displacement amplitude demand value for design.

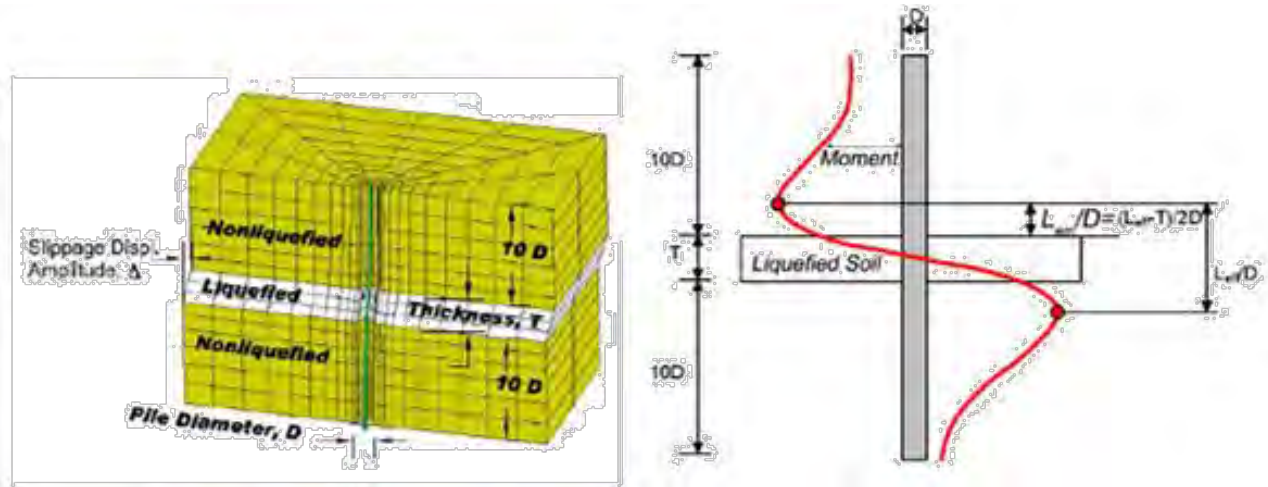


Figure 10-34 3-D Finite Element Model of a Pile in Laterally Spreading Ground with a Nonliquefied Crust

Step-2: Estimating the Locations of the Maximum Pile Moment Above and Below the Liquefied Soil layer: Lam et al (2007) found a rational non-dimensional parameter encompassing a very wide range of pile types, liquefied layer thickness and soil properties (the solution is only sensitive to the soil modulus, E_s of the nonliquefied upper and lower crust adjacent to the liquefied soil layer) to accomplish this task. This dimensionless characteristic parameter β , referred to as the soil-pile-liquefied thickness interaction parameter, is defined by the equation shown below.

$$\beta = \frac{E_s T^2 D^2}{EI} \quad 10-4$$

where: E_s is the modulus of elasticity of the stiff soil layer
 EI the bending stiffness of the pile
 T is the thickness of the liquefiable layer
 D is the (outer) diameter of the pile.

After determining the β parameter, Figure 10-35 can be used to establish the location of the maximum pile moment, Figure 10-36 can be used to estimate the maximum moment, Figure 10-37 can be used to estimate the maximum shear.

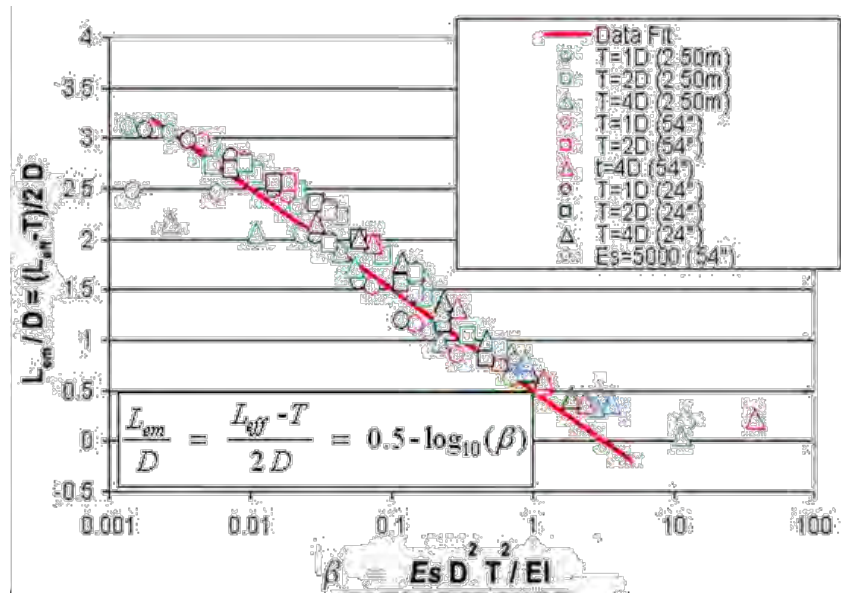


Figure 10-35 Maximum Pile Moment Location

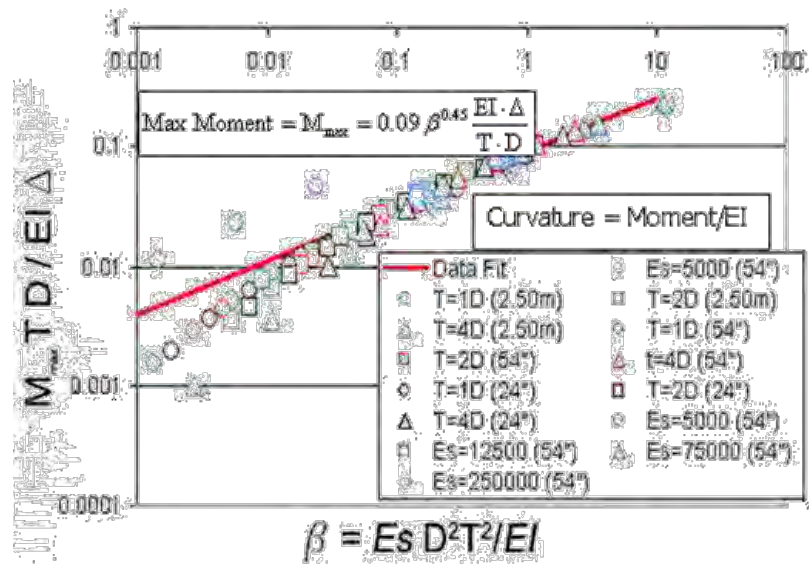


Figure 10-36 Maximum Pile Moment Solution

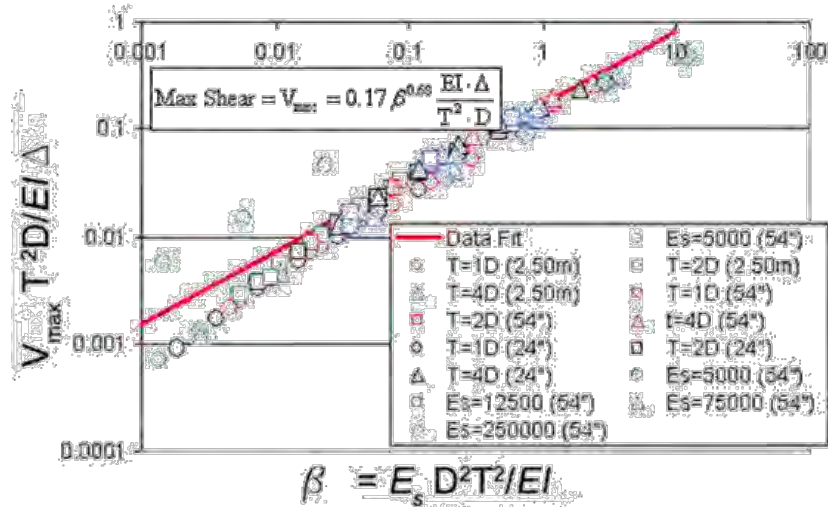


Figure 10-37 Maximum Pile Shear Solution

10.10 DESIGN PROCEDURES FOR LARGE DIAMETER DRILLED SHAFTS

The question of whether p-y curves should be diameter dependent has been debated for a long time and there have been various proposals for adjustments to the Reese and Matlock p-y curve procedures to better account for diameter effects (Stevens and Audibert, 1979 and Penders 1993, and Ling, 1988). Ashford and Juirnarongrit (2003) presented evidence that the initial tangent modulus of the p-y curves appeared to be independent of pile diameters, confirming the hypothesis of Terzaghi (1955) that p-y resistance should be independent of pile diameter. This is still a subject of active research. But, at the present time there is no reason to consider p-y curves as being diameter dependent.

10.11 CAISSONS DESIGN

Caissons foundations are typically used for over-water bridges. They are typically sunk to significant depths (varying from tens of feet to over 100 feet) and hence are classified as deep foundations. Because of their large embedment depth, the coupling effects between the lateral shear and overturning moment can be an important consideration in caisson design. However, caissons such as the caissons for the west span of the San Francisco-Oakland Bay Bridge that rest directly on rock can be treated as shallow foundations without consideration of coupling.

Because of the large dimensions involved in typical caissons (usually over 50-ft for the shorter dimensions), elastic charts are rarely applicable because of the need to account for the inhomogeneous soil profile over the embedment depth. Also, because caissons are used for major bridges, there is usually room in the design process to conduct more complex finite element analyses for developing the appropriate soil springs for caisson design. Figure 10-38 depicts the various soil-foundation-structure interaction modeling approaches for caissons. The nonlinear lumped springs approach is shown in Figure 10-38 (b), where uncoupled nonlinear springs are assigned to some appropriate point of support (e.g. the base of the caisson) for various modes of displacements. Nonlinear soil springs are usually necessary for caisson design, even if the caisson is resting on stiff soils (such as the west span of the San Francisco-Oakland Bay Bridge), because of the likelihood of uplift of the base under moment loading. Due to the potential for base uplift, a nonlinear moment-rotational spring will be necessary to capture this geometric nonlinearity, as shown in Figure 10-38b. However, it needs to be recognized that under cyclic loading a geometric nonlinearity will behave very different from a material nonlinearity. For geometric nonlinearity, even though the moment-rotation backbone curve is nonlinear, there is little or no material yielding and the hysteretic behavior should be modeled as nonlinear but elastic for both the loading and unloading paths (i.e. loading and unloading will follow the same backbone curve). The conventional Masing type of hysteretic cyclic load-displacement loading and unloading rules can over-exaggerate the damping effect when modeling caisson type foundations using the lumped springs approach.

Because of the potential for geometric nonlinearity (i.e. base separation and gapping) interacting with material nonlinearity, present day caisson modeling normally employs nonlinear distributed springs, as depicted in Figure 10-38d (MCEER,2007). This approach entails the use of Winkler springs distributed over the bottom and the sides of the embedded portion of the caisson foundation. The soil springs are normally modeled as nonlinear and hysteretic springs for consideration of yielding of the adjacent soils. However, gapping elements are usually implemented in series with the nonlinear hysteretic soil springs to allow for the base uplift and gapping behavior. These springs are included as part of the global bridge model.

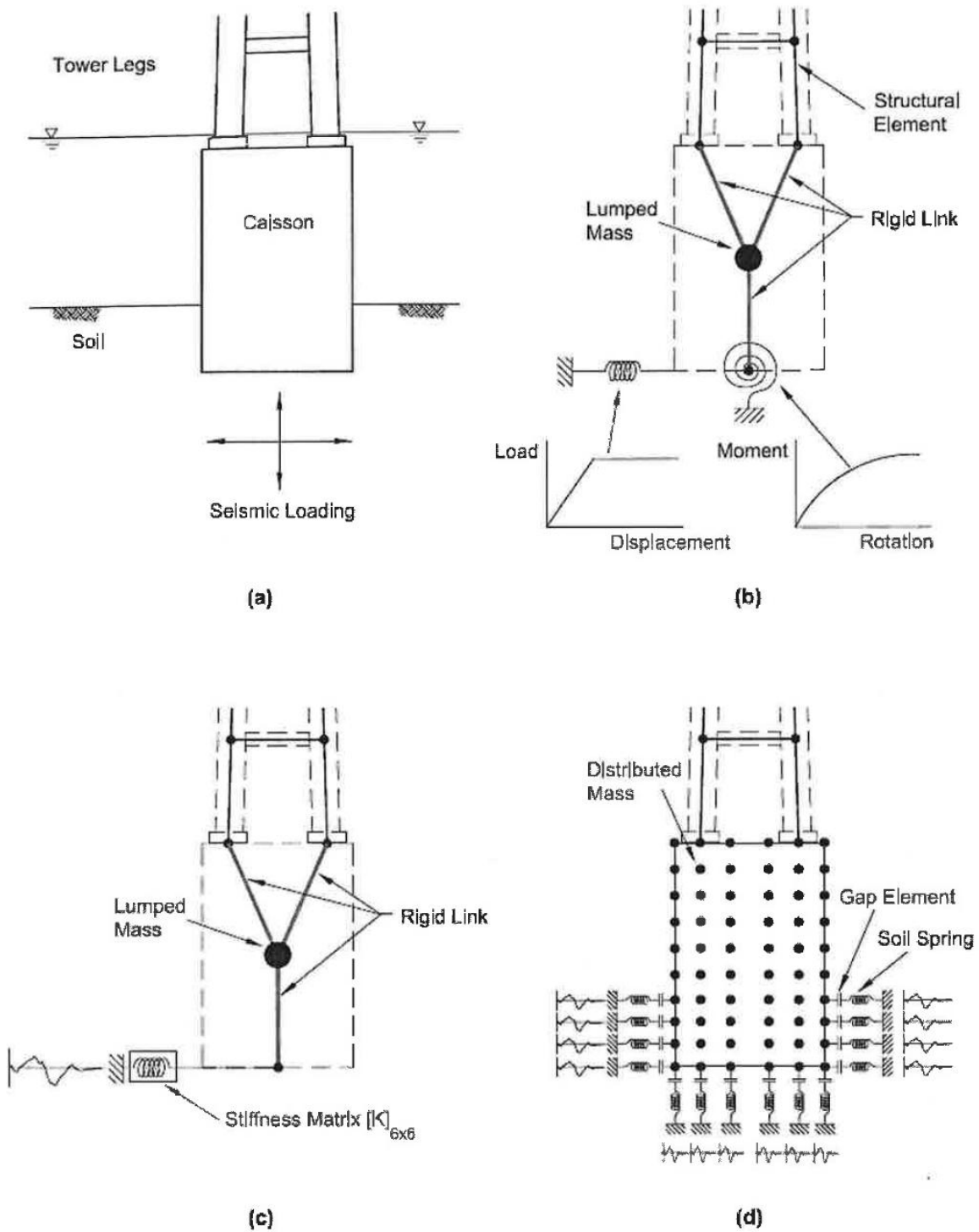


Figure 10-38 Various SSI Modeling Approaches for Caissons

Establishment of the proper distributed soil springs is a key to successful modeling of the caisson using the distributed spring approach. A pushover analysis of the caisson using the finite element method can be conducted to extract the appropriate soil springs for use in the global bridge model. It should be noted that the load-displacement solution from the finite element analysis will be dependent on the loading condition employed in the analysis. Therefore, the appropriate pushover loading condition needs to be carefully considered, especially the proportion of the shear versus moment load.

Input seismic excitation to the distributed spring model is accomplished by applying multiple ground motions at each layer of the soil strata. This provides a mechanism that could potentially be used to consider incoherent motions that occur as a result of wave scattering. However, Lam et al. (2007) showed that wave scattering generally will alter only the high frequency motions, and these motions are not particularly important with respect to caisson response. Therefore, it is generally valid to use the free field motions for input to caisson analyses.

10.12 SUMMARY

This chapter presents approaches to the design of deep foundations. Case histories of pile foundation damage in earthquakes are reviewed. Lessons from these case histories formed the basis for emphasis in the recommended procedures and design approaches (e.g. characterization of the pile head connections and design against liquefaction).

Experience with design of deep foundations shows that, similar to the design of shallow foundations, frequency dependent stiffness models are not required and the static stiffness can be used in seismic analysis to assemble the 6 x 6 stiffness matrix. However, unlike shallow foundations, there are situations where kinematic interaction must be considered in seismic design of deep foundations.

Both rigorous and simplified (but not simple) procedures for conducting a kinematic interaction analysis are described. The benefit of considering kinematic interaction at soft soil sites is illustrated and an approximate method to consider the effects of kinematic interaction using the results of a one-dimensional site response analysis is presented.

The use of both p-t-z analyses and simple design charts to evaluate the stiffness coefficients for a single pile are described. Considerations in the analysis of pile groups, including pile interaction effects,

evaluation of the contribution of the pile cap to group stiffness, and calculating the group stiffness coefficients are presented. The impact of pile stiffness on design is discussed and illustrated with an example. In the context of moment capacity of the pile group, the importance in designing the pile connection to prevent uplift pull out at the pile head is discussed.

The importance and benefits of conducting sensitivity analyses by varying the p-y stiffness of the piles is illustrated with an example. Results from pushover analyses are presented to provide an appreciation of how p-y curves affect the pile foundation in various aspects, including foundation stiffness, pile moment and shear load capacity as well as displacement capacity of the pile foundation.

Recommendations for developing p-y curves in liquefied soils are reviewed. A new procedure to analyze the piles subject to lateral spreading in soils with a nonliquefied surface layer is presented.

The issue of the diameter-dependence of p-y curves is briefly addressed, with the conclusion that no adjustment is warranted at this time. Design methodologies for large caissons are presented.

CHAPTER 11

EARTH RETAINING STRUCTURES

11.1 INTRODUCTION

11.1.1 Design Criteria

This chapter describes the seismic design procedure for earth retaining systems (as opposed to bridge abutments, which are addressed in the next Chapter). The current AASHTO LRFD specifications do discuss the seismic design of earth retaining structures. Furthermore, additional information and recommendations on design of earth retaining structures is provided in FHWA-NHI-07-071, Earth Retaining Structures. However, NCHRP Report 611 (NCHRP, 2008), developed under NCHRP Project 12-70, provides enhanced recommendations for LRFD seismic design of these types of structures and forms the basis of the recommendations provided herein.

In accordance with the AASHTO LRFD specifications for bridge design, seismic LRFD design requirements for earth retaining structures should be done in general compliance with requirements for Extreme Event I. Under these requirements, presented in Table 1.1, seismic LRFD design of free standing retaining walls shall include the earthquake load, the friction load, and the water and stream pressure load with a load factor of 1.0, and the factored permanent (dead) load and live load. AASHTO LRFD permanent load factors, presented in Table 1.2, provide maximum and minimum values for components, wearing surfaces, vertical earth pressures, and earth surcharge loads and call for using the values that produce the most critical design load combination for design. However, as discussed in Chapter 1 and consistent with the recommendations in NCHRP Report 611, it is recommended herein to use a load factor of 1.0 for all permanent loads for LRFD seismic design of free standing earth retaining structures. Furthermore, as discussed in Chapter 1, a load factor of 0.5 applied to the average daily truck traffic (ADTT) load is recommended for the earthquake live load. However, no inertial component of the live load is considered in seismic design.

In addition to the above considerations, seismic design of earth retaining systems requires consideration of the tolerable lateral deformation of the wall system. Displacement-based seismic design of earth retaining structures is addressed in this chapter. However, criteria for the tolerable level of lateral wall deformations are controlled by the surrounding facilities and are set by the owner (though often based

upon input from the engineer). An Appendix in Volume 2 of NCHRP Report 611 discusses the considerations involved in establishing such criteria.

11.1.2 Types of Earth Retaining Structures

Retaining walls can be broadly classified as walls that retain fills and walls that retain cuts. Walls that retain fill include gravity, semi-gravity, prefabricated modular, and mechanically stabilized earth (MSE) walls. The gravity, semi-gravity, and prefabricated modular walls are considered to be externally stabilized walls while MSE walls are considered to be internally stabilized walls. Walls that retain cuts include non-gravity cantilever, anchored, soil nail, and micro-pile walls. Non-gravity cantilever and anchored walls are considered to be externally stabilized while soil nail and micro-pile walls are considered to be internally stabilized.

11.1.3 Gravity and Semi-Gravity Walls

Gravity walls derive their capacity to resist lateral loads through dead weight of the wall. Semi-gravity walls are similar to gravity walls, except they rely on their structural components to mobilize the dead weight of backfill to derive their capacity to resist lateral loads. While gravity and semi-gravity walls are classified as fill walls, they can also be used in cut applications.

Gravity walls may be constructed of stone masonry, un-reinforced concrete, or reinforced concrete as shown in Figure 11-1. However, reinforcement in these walls is usually nominal and is provided primarily to resist temperature loads. They have relatively narrow base widths. They are generally not used when deep foundations are required and are most economical at low wall heights.

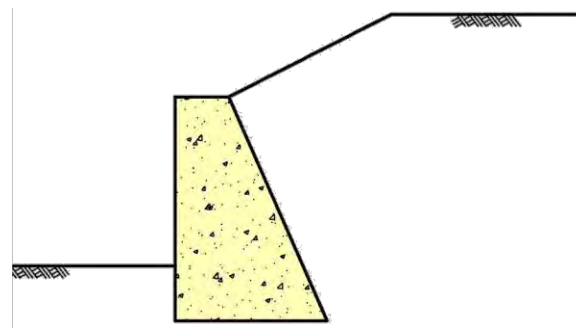


Figure 11-1 Mass Concrete Gravity Wall

Semi-gravity walls are sometimes referred to as stem walls. As shown in Figure 11-2, semi-gravity walls may be supported on deep or shallow foundations. Semi-gravity cantilever walls include counterfort and buttress walls, as shown in Figure 11-3, and Figure 11-4. Semi-gravity cantilever walls are constructed of reinforced concrete. Classified as fill walls, they can also be used in cut applications. They have relatively narrow base widths. The position of the wall stem relative to the footing can be varied to accommodate right-of-way constraints. These walls can support soundwalls, sign structures, and other highway features. They are most economical at low to medium wall heights.

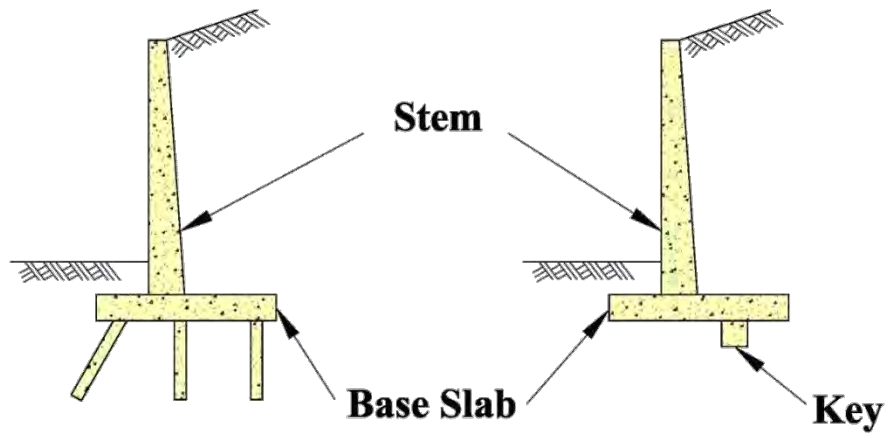


Figure 11-2 Semi-Gravity Cantilever Retaining Walls

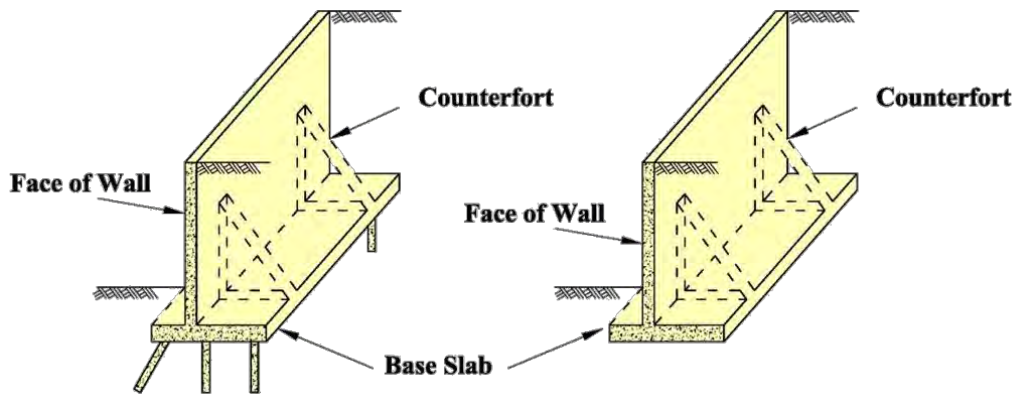


Figure 11-3 Counterfort Retaining Walls

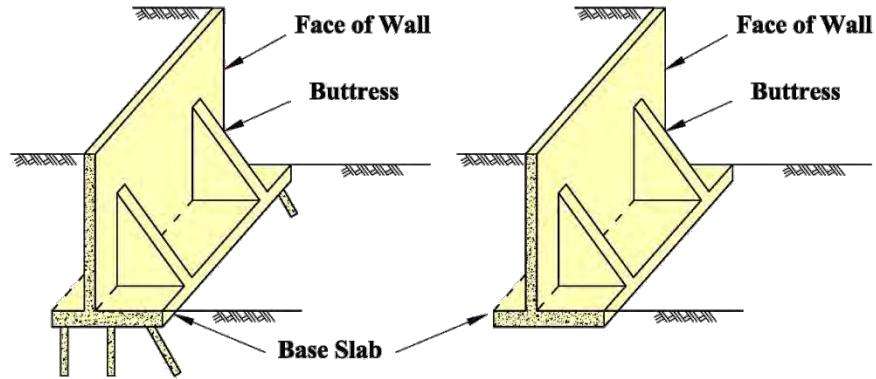


Figure 11-4 Buttressed Retaining Walls

11.1.4 Non-Gravity Cantilevered Walls

Non-gravity cantilevered walls are constructed of vertical structural members consisting of partially embedded soldier piles or continuous sheet piles, as shown in Figure 11-5. Non-gravity cantilevered walls rely on the structural components of the wall that are embedded in the foundation material to resist lateral loads.

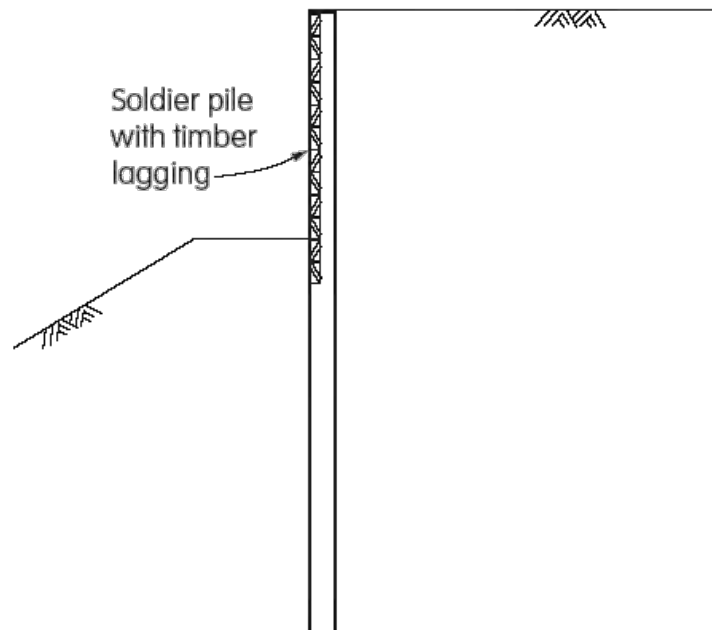


Figure 11-5 Non-Gravity Cantilever Wall

Soldier piles may be constructed with driven steel piles, treated timber, precast concrete or steel piles placed in drilled holes and backfilled with concrete or cast-in-place reinforced concrete. Continuous sheet piles are typically driven steel sheet piles but precast prestressed concrete sheet piles may also be used. Soldier piles may be faced with treated-timber, reinforced shotcrete, reinforced cast-in-place concrete, precast concrete or metal elements. This type wall depends on both the resistance of the foundation material and the moment resisting capacity of the vertical structural members for stability, therefore its maximum height is limited by the competence of the foundation material and the moment resisting capacity of the vertical structural members. The economical height of this type wall is generally limited to a maximum value of around 18 feet.

11.1.5 Non-Gravity Anchored Walls

Non-gravity anchored walls derive their capacity to resist lateral loads by their structural components, including tension elements connected to anchors and sometimes by embedment of their structural components into foundation material. Non-gravity anchored walls are typically composed of the same elements as non-gravity cantilevered walls plus one or more levels of anchors as shown in Figure 11-6. The additional lateral resistance provided by the anchors allows these walls to overcome the height limitations of non-gravity cantilever walls. For transportation applications, the anchors are typically ground anchors (tiebacks) consisting of drilled holes with grouted prestressing steel tendons extending from the wall face to an anchor zone located behind potential failure planes in the retained soil or rock mass. Anchored walls are typically constructed in cut situations. Anchored walls may be used to stabilize unstable slopes. Provided adequate foundation material exists at the site for the anchors, wall heights up to 80 feet are feasible for anchored walls.

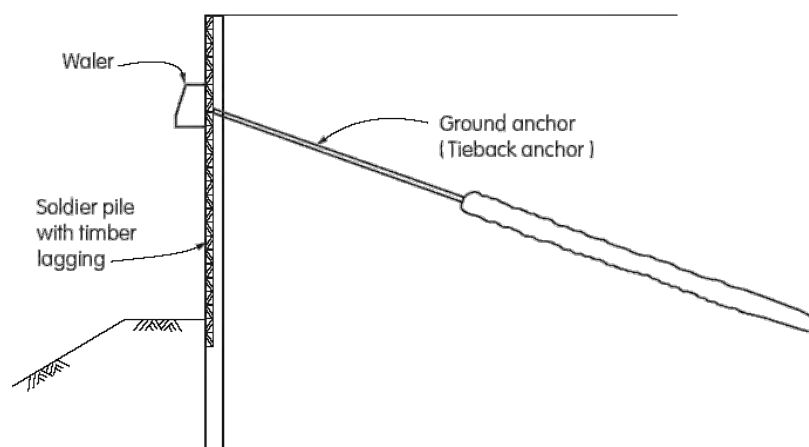


Figure 11-6 Single Tieback System

11.1.6 Mechanically Stabilized Earth Walls

Mechanically stabilized earth (MSE) walls use either metallic (inextensible) or geosynthetic (extensible) soil reinforcement embedded within the wall backfill and attached to vertical or near vertical facing elements, as shown in Figure 11-7, to mobilize the shear strength of the soil for support of the wall system. MSE walls behave as a gravity wall in that they derive their lateral resistance through the dead weight of the mechanically stabilized backfill. MSE walls are typically used for fill walls and are employed in the same types of situations where conventional gravity and semi-gravity retaining walls are employed. The practical height of an MSE wall may be limited only the competence of the foundation material at a given site: tiered MSE walls with stepped-back faces have been used for wall height of over 100 ft. MSE walls are particularly well suited for sites where substantial total and differential settlements are anticipated. The allowable differential settlement is limited by the deformability of the wall facing elements within the plane of the wall face.

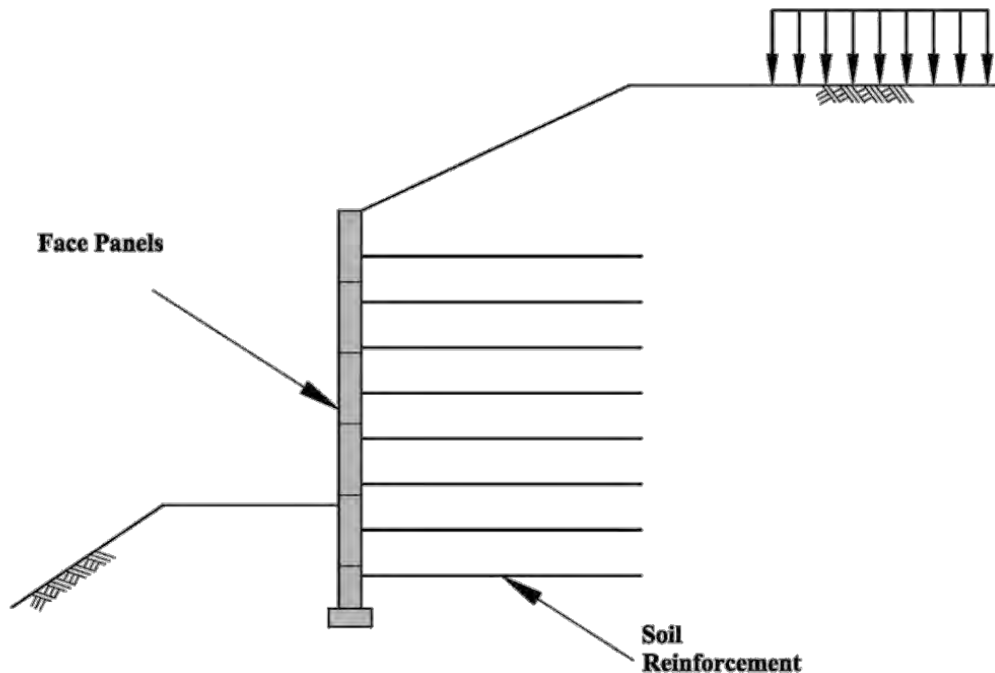


Figure 11-7 MSE Wall with Precast Concrete Face Panels

11.1.7 Soil Nail Wall

Soil nailing is an economical technique for stabilizing cut slopes and for constructing retaining walls in cuts from the top down. Soil nail walls are similar to MSE walls in that they rely on reinforcing elements that extend into the soil or rock behind the wall to mobilize the shear strength of the ground to support the wall. The reinforcing elements in a soil nail wall are generally steel tendons which are drilled and grouted into the soil or rock, as shown in Figure 11-8. The soil nails are typically spaced about 4 to 6 feet apart in both the horizontal and vertical direction, and usually vary in length from 0.7 to 1.2 times the wall height. In permanent soil nail walls, the soil nail bars have an additional layer of corrosion protection (usually epoxy coating). A wire mesh and shotcrete facing is typically employed for soil nail walls, though many architectural options such as precast panels or "green" vegetated cells are available for permanent wall facings. Prefabricated drainage panels are often placed against the cut slope behind the facing before the shotcrete is applied.

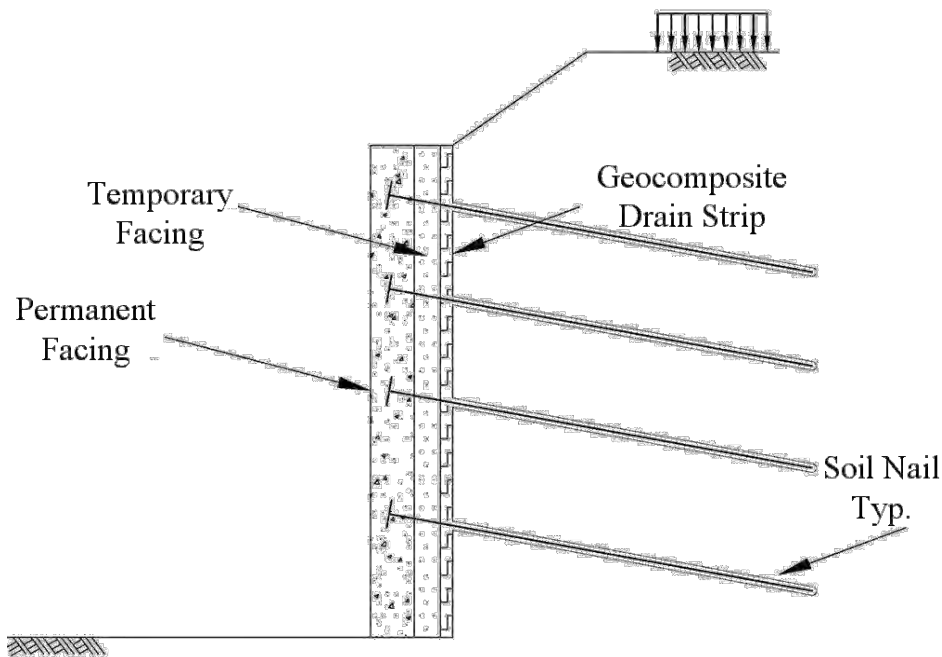


Figure 11-8 Soil Nail Wall

11.1.8 Prefabricated Modular Walls

Prefabricated modular walls use stacked or interconnected structural elements filled with soil or rock to resist lateral earth pressures, as shown in Figure 11-9, acting essentially as gravity retaining walls. Prefabricated modular block walls include crib walls, bin walls, gabion walls, and modular block walls. Structural elements consisting of treated timber, or precast reinforced concrete may be used to form a cellular system which is filled with the backfill material to construct a crib wall. Steel modules bolted together in similar manner are also used to construct a bin wall. Rock filled wire gabion baskets may be used to construct a gabion wall. Solid precast concrete units or segmental concrete masonry units are stacked to form a modular block wall. The aesthetic appearance of some of these type walls is governed by the nature of the structural elements used. Those elements consisting of precast concrete may incorporate various aesthetic treatments. This type wall is most economical for low to medium height walls.

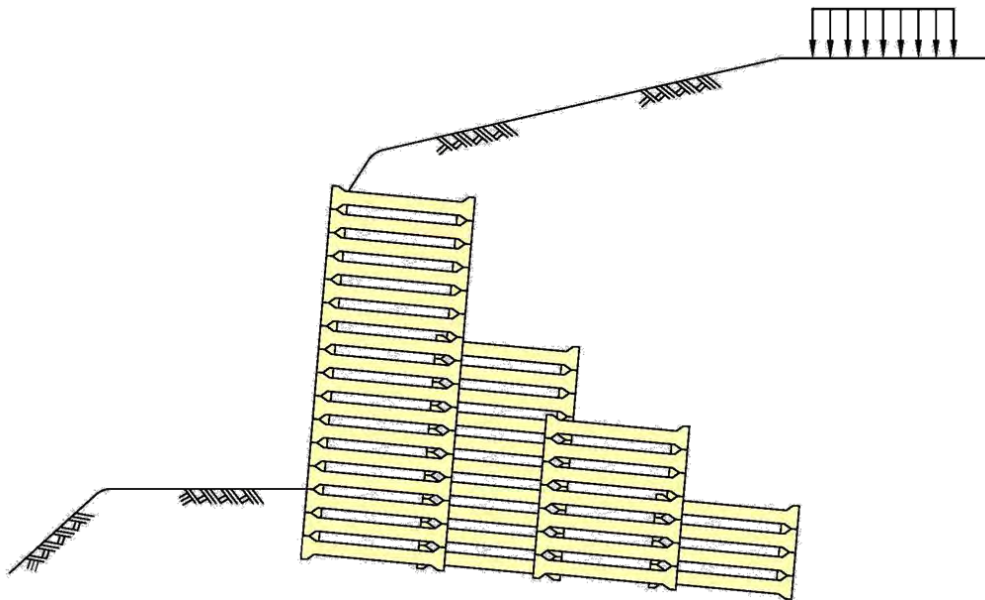


Figure 11-9 Precast Concrete Crib Walls

11.2 SEISMIC FORCES ON EARTH RETAINING STRUCTURES

11.2.1 Seismic Load and Resistance

The seismic demand on retaining walls includes the seismic active thrust from the soil behind the wall and the inertial loading on the wall itself. Surcharge loads may also contribute to the demand. Sources of resistance for retaining wall systems include seismic passive resistance in front of the wall, the frictional sliding resistance of the base of the wall and the bearing resistance of the foundation soil for walls that rely on the base to serve as a spread footing, e.g. gravity, semi-gravity, and MSE walls, the axial and lateral geotechnical capacity of the deep foundation elements for retaining walls supported on deep foundations, and the structural resistance of the wall system.

Figure 11-10 shows the forces acting on a semi-gravity cast-in-place retaining wall during a seismic event. As described subsequently, the active seismic thrust, P_{AE} , and the seismic passive earth pressure, P_{PE} , are functions of backfill properties, the wall and backfill geometry, and the seismic coefficient, k_h , which in turn depends upon the site adjusted peak ground acceleration, $F_{PGA}PGA$. In the absence of other information, P_{AE} and P_{PE} may be assumed to act at the midpoint of the wall height (NCHRP Report 611). Note that the NCHRP Report recommends that the total active pressure under seismic loading P_{AE} may be assumed uniformly distributed. The procedures described to determine P_{AE} in subsequent sections are detailed in the NCHRP 2008 Report, and are recommended to replace the current AASHTO procedures. The inertia loads acting on the wall, $k_h \times W_c$, and the inertia force acting on the soil above the heel of the wall, $k_h \times W_s$, are also a function of seismic coefficient, k_h . The resistance force of the base of the wall, H_R , is a function of total normal load on the base of the wall, N , and the frictional coefficient between the base of the wall and the underlying foundation, μ . In the absence of adhesion between the wall and the foundation soil, μ is equal to $\tan\phi_w$, where ϕ_w is the interface friction angle between the wall foundation and the soil underneath the foundation.

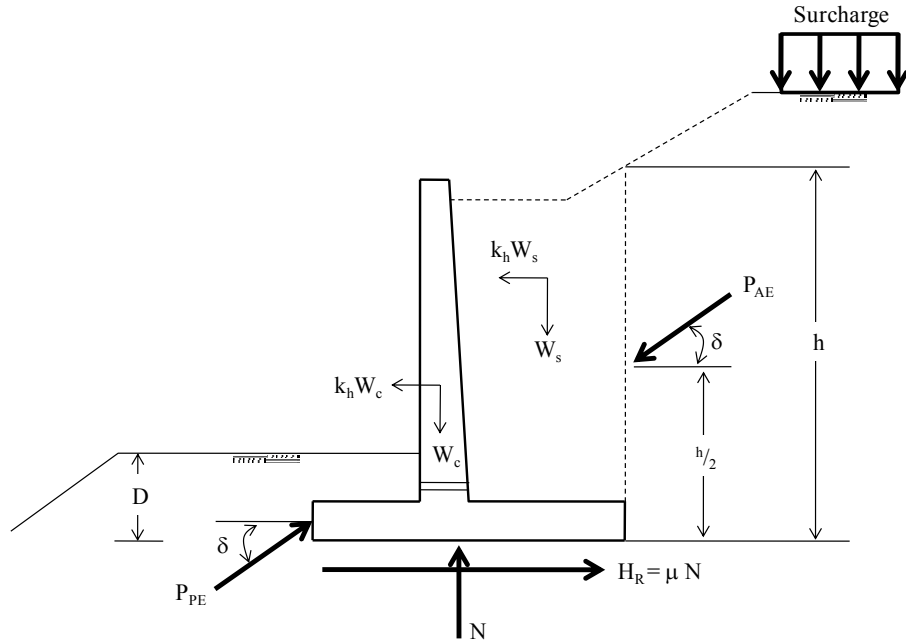


Figure 11-10 Seismic Forces on a Semi-gravity Retaining Wall

11.2.2 No Analysis Provisions

Not all walls need be analyzed for seismic loading. The NCHRP Project 12-70 recommendations indicate that the site-adjusted peak ground acceleration, $F_{PGA}PGA$, is less than 0.3 g and the backfill behind the wall is flat, no seismic analysis is necessary unless the foundation is susceptible to liquefaction. Similarly, no analysis is necessary if the site-adjusted PGA is less than 0.2 g and the backfill slope is flatter than 3H:1V or if the site adjusted PGA is less than 0.1 g and the backfill slope is flatter than 2H:1 V and liquefaction is not anticipated. Table 11-1 (NCHRP, 2008) summarizes these conditions under which no seismic analysis is necessary for free standing earth retaining structures.

TABLE 11-1 CONDITIONS UNDER WHICH SEISMIC ANALYSIS IS NOT REQUIRED FOR A FREE STANDING EARTH RETAINING WALL (NCHRP, 2008)

Slope Angle Above Wall	$F_{PGA}PGA$
Flat	0.3 g
3H:1V	0.2 g
2H:1V	0.1 g

11.3 SEISMIC LATERAL EARTH PRESSURES

11.3.1 Mononobe-Okabe Seismic Earth Pressure Theory

The most common means of calculating seismic active thrust used in practice today is Mononobe-Okabe earth pressure theory. Mononobe-Okabe theory is an extension of basic Coulomb earth pressure theory to include a lateral force on the backfill soil to represent the effect of seismic loading. The forces acting on a Coulomb wedge due to horizontal and vertical ground acceleration are shown in Figure 11-11.

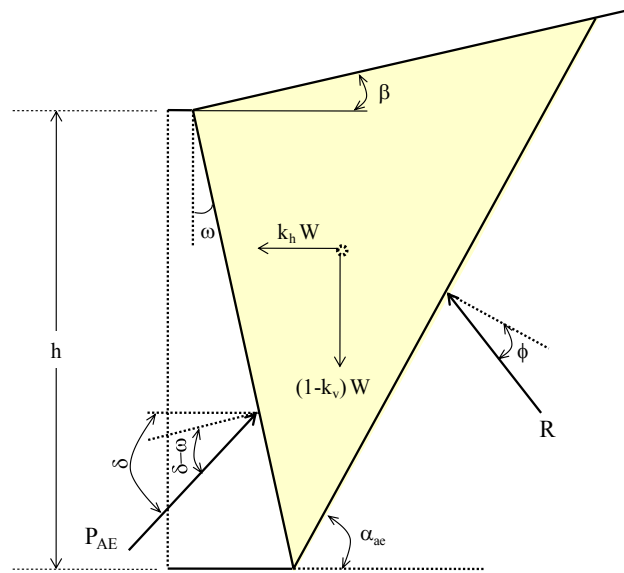


Figure 11-11 Free Body Diagram for Mononobe-Okabe Active Earth Pressure Theory

In practice, the effect of the vertical acceleration on the seismic earth pressure is usually ignored. Reasons for ignoring the vertical acceleration include that:

- the vertical acceleration is generally out of phase with and has different frequency characteristics than the horizontal acceleration, and thus is as likely to be acting in a manner that reduces the earth pressure (upwards) as it is to be acting in a manner that increases the earth pressure (downwards);
- the peak vertical acceleration generally does not occur at the same time as the peak horizontal acceleration, thus it does not make sense to superimpose a vertical seismic coefficient on top of a horizontal seismic coefficient that is based upon the peak ground acceleration; and

- the tendency of a downward vertical acceleration to increase the seismic earth pressure is counteracted by the associated increase in the sliding and overturning resistance due to a downward vertical acceleration.

Ignoring the vertical acceleration, in a uniform soil the seismic active earth pressure on a wall of height H is given by:

$$P_{AE} = \frac{1}{2} \gamma H^2 k_{AE} \quad 11-1$$

where k_{AE} is the seismic active earth pressure coefficient. In Mononobe-Okabe theory, k_{AE} can be expressed as a function of the friction angle of the backfill, ϕ , the wall batter, ω , the backfill slope, β , the wall-backfill interface friction angle, δ , and the seismic coefficient, k_h , by the following equation:

$$k_{AE} = \frac{\cos^2(\phi - \theta - \omega)}{\cos \theta \cos^2 \omega \cos(\theta + \omega + \beta) \left(1 + \sqrt{\frac{\sin(\phi + \delta) \sin(\phi - \theta - \omega)}{\cos(\delta + \theta + \omega) \cos(\beta - \omega)}} \right)^2} \quad 11-2$$

where θ is the seismic inertial angle and is given by:

$$\theta = \tan^{-1}[k_h] \quad 11-3$$

Mononobe-Okabe theory can also be used to calculate a seismic passive earth pressure coefficient. However, as discussed subsequently, the use of Mononobe-Okabe theory to predict seismic passive earth pressure is not recommended. Hence, the Mononobe-Okabe equation for seismic passive earth pressures is not presented herein.

11.3.1.1 Limitations of Mononobe-Okabe Theory

The use of the Mononobe-Okabe theory to evaluate seismic earth pressures is subject to a number of significant limitations. As noted above, Mononobe-Okabe theory should not be used to calculate seismic passive earth pressure under any conditions. The use of the Mononobe-Okabe theory to evaluate seismic active earth pressure assumes that the soil within the seismic active wedge is a uniform free draining

cohesionless material and that the backfill slope is uniform. However, the seismic active wedge can be significantly flatter than the active wedge for static conditions, particularly at high values for the seismic coefficient, k_h . Figure 11-12 presents the inclination (to horizontal) of the seismic active wedge, α_{AE} , versus seismic coefficient, k_h , for backslope inclinations varying from horizontal to 2H:1V for a friction angle of 35° .

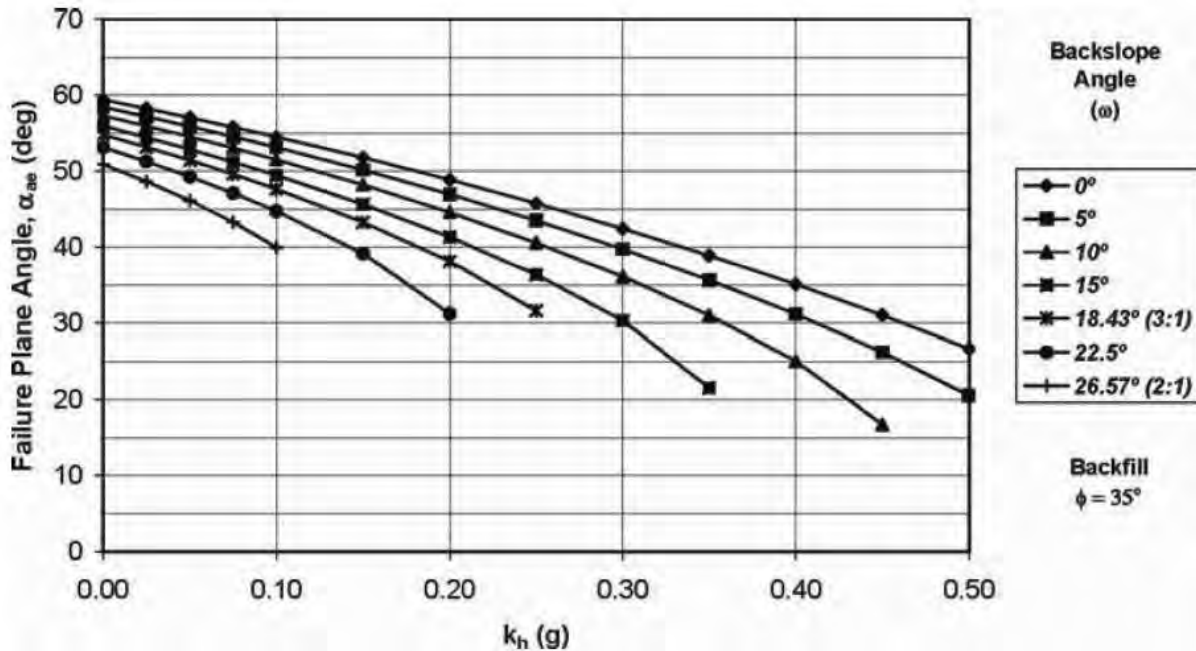


Figure 11-12 Inclination of the Seismic Active Wedge for $\phi = 35^\circ$ (NCHRP, 2008)

In practice the soil within the active wedge under seismic conditions is unlikely to be cohesionless or even uniform, except for small values of H and/or k_h . In fact, the Mononobe-Okabe equation tends to “blow up” (give very large values of k_h) for soils with steep backslope angles and/or high seismic coefficients. Furthermore, the backslope within the seismic active zone may not be uniform (even if the backfill composition is uniform) and the soil behind the wall may often have some cohesion (even if it is apparent cohesion). In these instances, earthquake-induced active pressure should be determined using either the Coulomb wedge method or the general equilibrium method as described subsequently.

11.3.2 Trial Wedge Method

The trial wedge method provides an alternate means of calculating seismic active earth pressures in cases where the Mononobe-Okabe equation does not apply. This includes cases where the soil within the active wedge is non-uniform or contains some cohesion or where the backslope angle is not uniform. The trial

wedge method is essentially the Coulomb active wedge method with a horizontal force equal to $k_h \times W_s$, where W_s is the weight of the soil within the wedge, applied at the centroid of the wedge to simulate the effect of seismic loading. For the conditions assumed by the Mononobe-Okabe method (uniform cohesionless soil with a constant backslope), the trial wedge method gives the same result as the Mononobe-Okabe equation. Trial wedge method solutions can be used for any wall adhesion and interface friction angle regardless of irregularity of the backfill and surcharges. Figure 11-13 shows the generalized geometry employed in the trial wedge method.

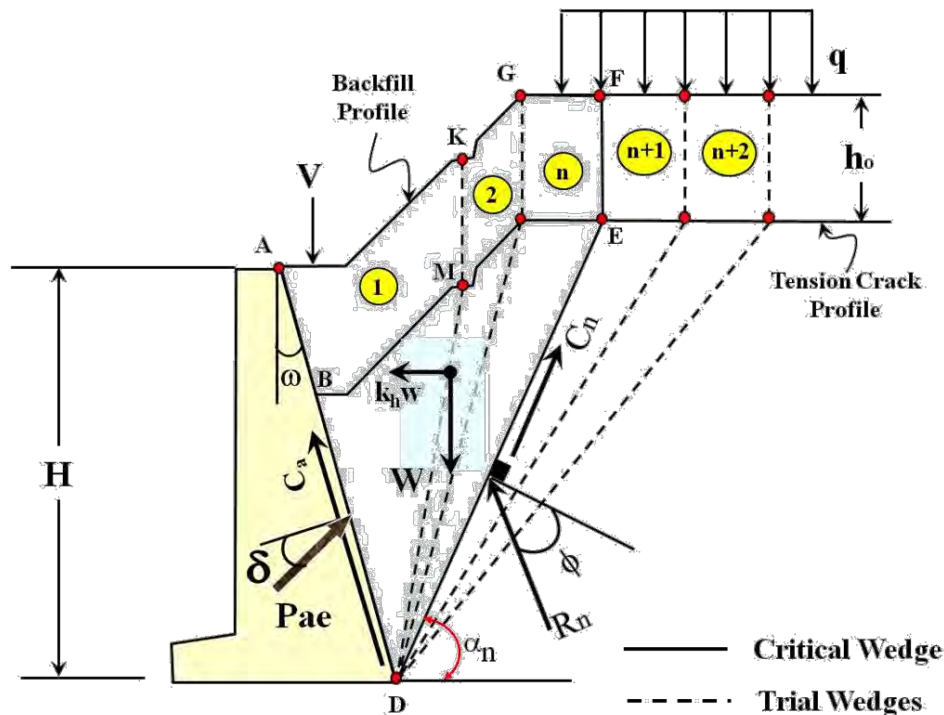


Figure 11-13 Active Trial Wedge

In Equation 11-4, the equations of force equilibrium have been solved for the trial wedge geometry shown in Figure 11-13 to develop an equation for P_{AE} as a function of the angle of the trial wedge, α_n . The soil in Figure 11-13 is assumed to have a shear strength characterized by a friction angle ϕ and a cohesion c and interface shear strength between the wall and the backfill is characterized by a wall-backfill interface friction angle δ and an adhesion c_a .

$$P_{AE} = \frac{WT - COH - ADH}{[1 + \tan(\delta + \omega)\tan(\alpha - \phi)]\cos(\delta + \omega)} \quad 11-4$$

where WT is the seismic earth pressure due to the weight of the wedge, COH is the reduction in seismic earth pressure due to soil cohesion, and ADH is the reduction in seismic earth pressure due to wall-backfill adhesion. WT is given by:

$$WT = W[\tan(\alpha - \phi) + k_h] \quad 11-5$$

where W is the weight of the soil in the wedge. COH is given by:

$$COH = c L_n [\sin \alpha \tan(\alpha - \phi) + \cos \alpha] \quad 11-6$$

where L_n is the length of the surface upon which the cohesion acts (chord DE in Figure 11-13). ADH is given by:

$$ADH = c_a L_a [\tan(\alpha - \phi)\cos(-\omega) + \sin \omega] \quad 11-7$$

where L_a is the length of the surface upon which the adhesion acts (chord DB in Figure 11-13). For a vertical wall face without adhesion, Equation 11-4 reduces to:

$$P_{AE} = \frac{W[\tan(\phi - \alpha) + k_h] - c * L[\tan(\phi - \alpha)\sin \alpha + \cos \alpha]}{[1 + \tan \delta \tan(\phi + \alpha)] * \cos \delta} \quad 11-8$$

The trial wedge method is an iterative process. The failure plane angle, α_n , for the trial wedge is varied until the maximum value of the active earth pressure is computed using Equation 11-4 or 11-8.

11.3.2.1 Influence of Cohesion on Seismic Active Earth Pressure

One of the primary shortcomings of the Mononobe-Okabe method is that it cannot consider the effect of cohesion in the backfill on the seismic active earth pressure. Even relatively small amounts of cohesion in the backfill can significantly reduce the seismic active earth pressure. Sources of cohesion in backfill soils include both true cohesion due to inter-particle bonding and apparent cohesion due to capillary forces in the backfill. The influence of cohesion on the seismic active earth pressure is a function of the normalizing parameter $c/\gamma H$, where γ is the unit weight of the backfill soil. Figure 11-14 presents a plot of the seismic active earth pressure coefficient, K_{AE} , as a function of the normalizing parameter $c/\gamma H$ and the seismic coefficient, k_h , for a friction angle of 35° and for a uniform level backfill. An Appendix in NCHRP Report 611 presents additional plots for friction angles of 30° and 40° .

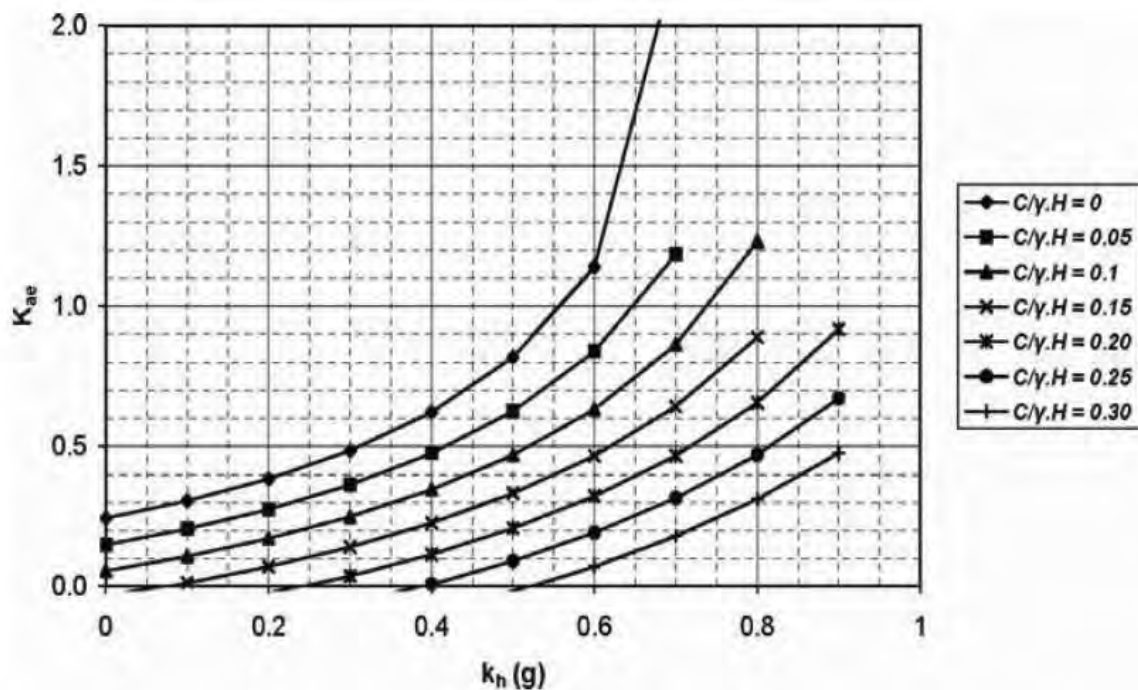


Figure 11-14 Effect of cohesion on the seismic active earth pressure coefficient for $\phi = 35^\circ$ (NCHRP, 2008)

NCHRP Report 611 provides recommendations for the maximum amount of apparent cohesion that should be assumed for backfill soil as a function of the fines content of the soil. These recommendations are presented in Table 11-2.

TABLE 11-2 MAXIMUM AMOUNT OF APPARENT COHESION THAT SHOULD BE ASSUMED FOR BACKFILL SOILS (NCHRP, 2008)

% (by weight) passing #200 sieve	maximum apparent cohesion
----------------------------------	---------------------------

5 - 15	50 psf
15 - 25	100 psf
25-50	200 psf

11.3.3 Log Spiral Earth Pressure Theory

The Mononobe-Okabe and Trial Wedge methods for calculating earth pressure assume that the failure surface in the backfill is planar. It has been long recognized that when there is a significant soil-wall friction angle, the assumption of the planar failure surface is incorrect. Instead, in a homogeneous soil a logarithmic surface gives the critical values for the active and passive earth pressure in a limit equilibrium analysis. Note, however, that when there is no wall friction the logarithmic surface degenerates to a planar surface. As illustrated in Figure 11-15, or the active case the difference between the critical log spiral surface and the critical planar surface is small enough that it can be ignored, even when there is wall friction. However, as illustrated in Figure 11-15, the critical log spiral surface for the passive case differs significantly from the critical planar surface when the wall friction angle is more than one-third the value of the backfill friction angle. In these cases it is essential to consider the logarithmic surface: failure to do so can result in an unconservative assessment of the seismic passive earth pressure.

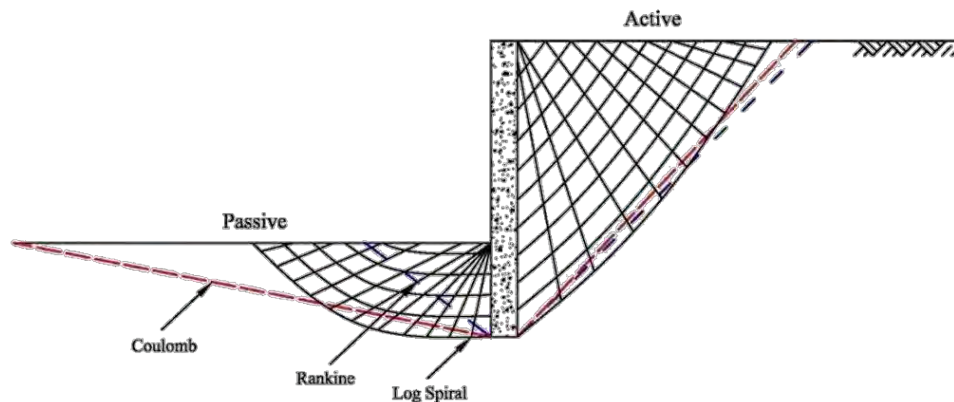


Figure 11-15 Critical Log Spiral Surfaces Compared to Planar Critical Surfaces

The log spiral method can be used to evaluate seismic passive earth pressures accounting for backfill friction and cohesion, soil-wall interface friction angle, and backslope angle. Shamsabadi et al. (2007) describe the general method that can be used to do this. The soil-wall interface friction angle is a key parameter in this approach. The soil-wall interface friction angle for static loading is often assumed to

range from 50% to 80% of the soil friction angle. In the absence of any specific guidance or research results for seismic loading, NCHRP Report 611 suggests that a wall interface friction equal to $2/3^{\text{rds}}$ of the soil friction angle be used to evaluate the seismic passive earth pressure.

Figure 11-16 presents a plot of the seismic passive earth pressure coefficient versus seismic coefficient derived using the log spiral method for friction angles from 20° to 40° for cohesionless soil and a wall friction angle (δ) equal to $2/3^{\text{rds}}$ of the friction angle of the soil in the passive wedge.

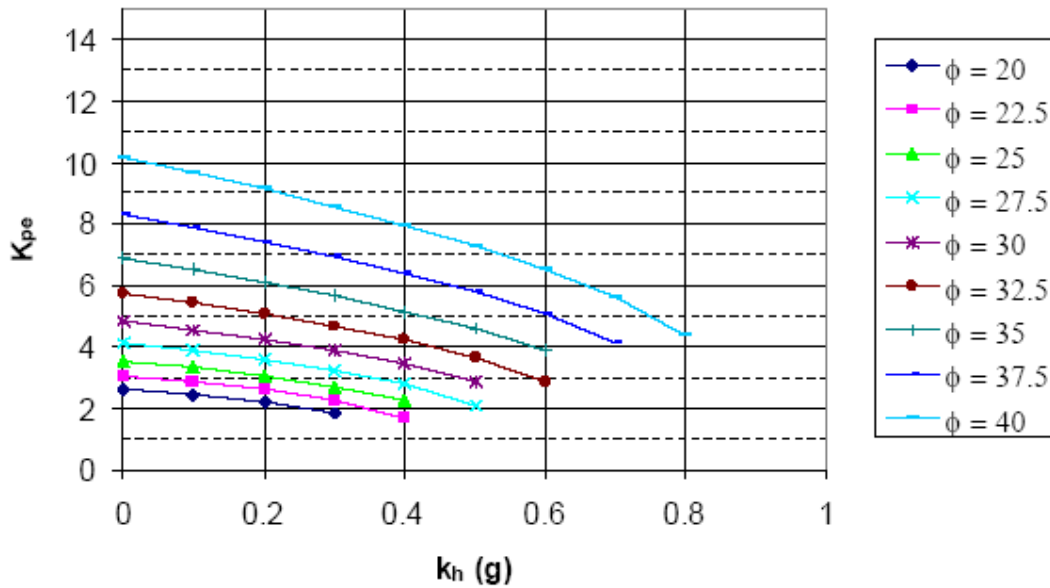


Figure 11-16 Passive Seismic Earth Pressure Coefficient from the Log Spiral Method for Cohesionless Soil and $\delta = 0.67\phi$ (NCHRP, 2008)

Like the seismic active earth pressure, the effect of cohesion on the seismic passive earth pressure can be described using the normalizing parameter $c\gamma/H$. The Appendix of NCHRP Report 611 presents charts similar to Figure 11-16 for values of $c\gamma/H$ equal to 0.05 through 0.25.

Another important consideration when using the seismic passive earth pressure is the amount of deformation required to mobilize this force. The deformation required to mobilize the passive earth pressure during static loading is usually assumed to be 3% to 10% of the wall height (Shamsabadi et al 2007). Similar guidance is not available for seismic loading and therefore the normal approach during design for seismic passive earth pressures is to assume that the displacement required to mobilize the

seismic passive earth pressure is the same as for static loading. Shamsabadi et al. (2007) suggest that 5% of the wall height to be used for granular backfill and 10% of the wall height to be used for cohesive backfill.

11.3.4 General Limit Equilibrium Method

Another alternative for evaluating seismic earth pressure is to use the general limit equilibrium (GLE) method. Any conventional slope stability program can be used to evaluate the seismic active earth pressure using this type of analysis. As illustrated in Figure 11-17, to evaluate the seismic active earth pressure for a specified seismic coefficient, the seismic coefficient is assigned to the backfill and an external force is applied at mid-height of the face of the backfill at an angle equal to the wall/backfill interface friction angle. The value of the external force is then increased until the factor of safety is equal to 1 to find the seismic active thrust. The method is described in more detail in NCHRP Report 611 (NCHRP, 2008).

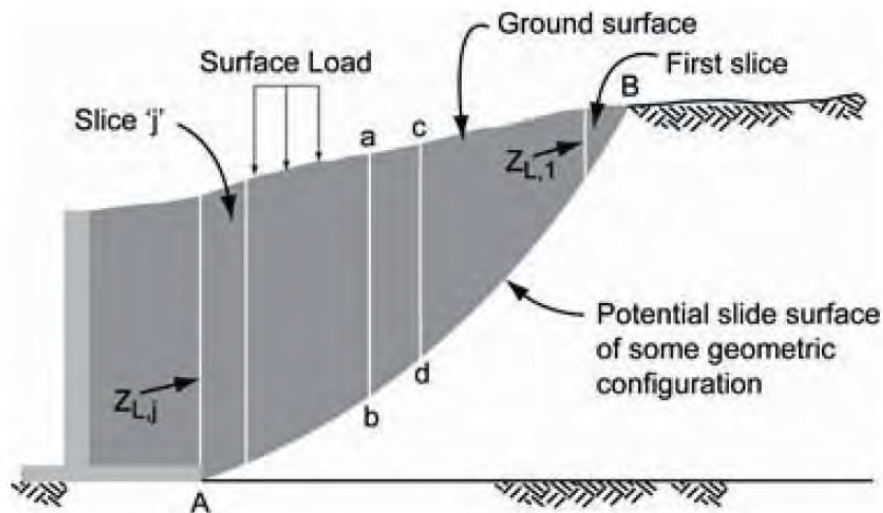


Figure 11-17 General Limit Equilibrium Method for Evaluating the Seismic Active Earth Pressure (Chugh, et. al, 1995)

In applying the GLE method, the engineer must make sure the geometry of the problem is set up appropriately, as some programs have a preferred direction in which failure is assumed to occur. In Figure 11-17, the failure is assumed to occur from right to left.

The seismic passive earth pressure may also be evaluated using the GLE method. However, in applying this method, the engineer must make sure the geometry of the problem is set up appropriately to force a

passive failure in the soil. To determine the passive resistance for the slope shown in Figure 11-17, the slope geometry would have to be turned around so that the backfill was on the left hand side of the wall and the force applied to the face of the backfill was oriented from right to left. Again, the seismic coefficient is assigned as a pseudo-static load on the backfill and an external force is applied to the face of the backfill at an angle equal to the wall/backfill interface friction angle. The value of the external force is increased until the factor of safety is equal to 1, to find the seismic passive thrust, P_{PE} . The height of the external force is varied between 0.3H and 0.6H from the base of the wall. The minimum value of P_{PE} for the different application heights is used for design.

11.4 SEISMIC EARTH PRESSURE COEFFICIENT

11.4.1 Maximum Seismic Coefficients for Design

The maximum seismic coefficient (k_{max}) for computation of seismic earth pressure shall be determined on the basis of the site class adjusted peak acceleration at the ground surface, $F_{PGA}PGA$, as shown in Equation 11-9:

$$k_{max} = F_{PGA} * PGA \quad 11-9$$

where F_{pga} is the site factor for the PGA, discussed in Chapter 4.

For the walls founded on AASHTO Site Class A and B, k_{max} shall be based on 1.2 times the site-adjusted peak ground acceleration coefficient as shown in Equation 11-10.

$$k_{max} = 1.2 * F_{PGA} * PGA \quad 11-10$$

However, the values of k_{max} in Equations 11-9 and 11-10 are the maximum possible values and only apply to walls of less than 20 ft in height that cannot accommodate lateral displacement on the order of 1-2 inches in the design earthquake. For walls 20 ft tall or higher, the value of k_{max} can be reduced to account for spatial incoherence (also referred to as wave scattering), or averaging of the ground acceleration over the active (or passive) wedge. For walls that can accommodate at least 1-2 inches of lateral displacement in the design earthquake, another reduction for system ductility (allowable lateral displacement) can be

applied. These adjustments can be applied to the maximum seismic coefficient to evaluate the design seismic coefficient, k_h , in accordance with Equation 11-11:

$$k_h = r * \alpha * k_{Max} \quad 11-11$$

where r is the ductility (allowable lateral displacement) reduction factor and α is the height adjustment factor.

11.4.1.1 Wall Height Adjustment Factor

For values of H greater than 20 feet but less than 70 feet, the value of height adjustment factor, α , can be determined from Figure 11-18 for walls founded upon AASHTO Site Class C, D, and E soils. For retaining walls with AASHTO Site Class A and B foundations (rock sites), values from Figure 11-18 must be multiplied by 1.2. Figure 11-18 is essentially the same figure used to develop the height-dependent seismic coefficient for slope stability analysis discussed in Chapter 6. β is a parameter related to the seismic environment and is related to the site adjusted values of the peak ground acceleration and spectral acceleration at 1 second. Values of β less than 1.0 would be typically associated with seismic conditions in the East, firm ground conditions and lower acceleration levels, while values of β greater than 1.0 would be associated with the Western U.S., higher accelerations, and C or D site conditions. The curved lines in Figure 11-18 represent the results of numerical analyses while the straight lines represent engineering simplifications.

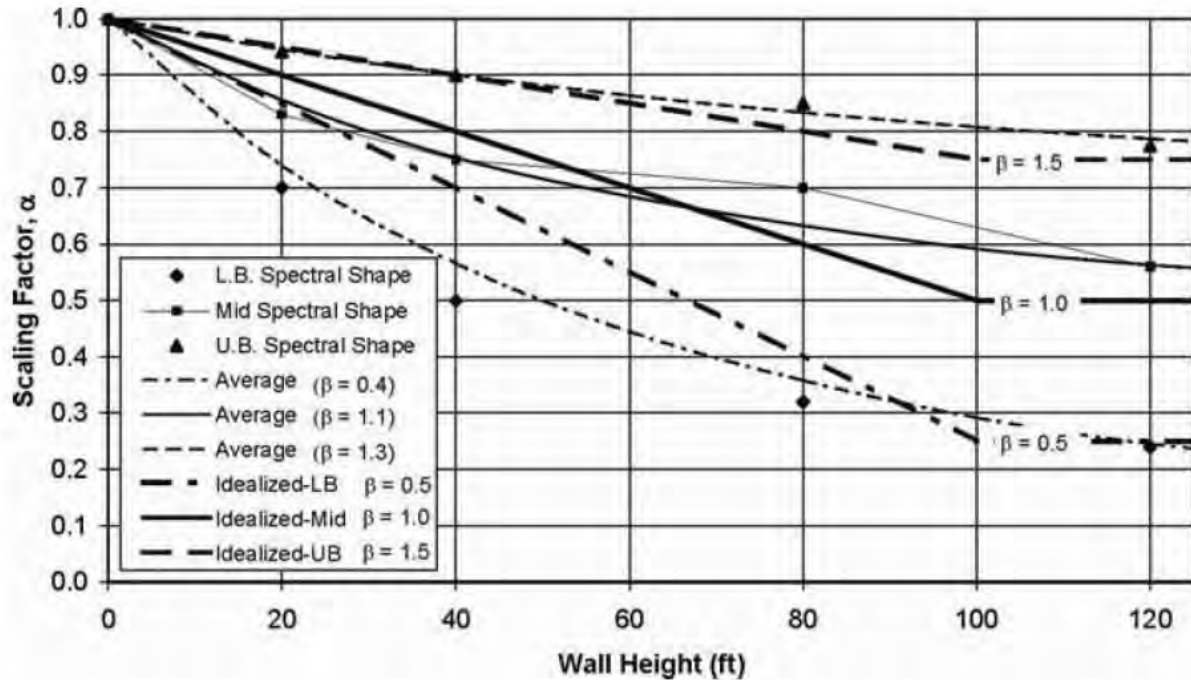


Figure 11-18 Wall height adjustment factor, α , vs. wall height (NCHRP, 2008)

As reported in Chapter 6, the straight line simplifications for the wall height adjustment factor can be represented by the following equations: or site Category C, D, and E

$$\alpha = 1 + 0.01H(0.5\beta - 1) \quad 11-12$$

where H = slope height (feet)

$$\beta = F_v S_1 / k_{\max} \quad 11-13$$

where F_v = site adjustment factor for 1 second spectral ordinates

S_1 = USGS mapped 1 second spectral ordinate for site class B.

For site categories A and B (hard and soft rock foundation soils) the values of α from Equation 11-12 should be increased by a factor of 1.2.

11.4.2 Displacement-Based Seismic Coefficient

If the earth retention system can be allowed to translate laterally, the seismic coefficient can be reduced to account for the ductility of the wall system. In the current AASHTO specifications, the allowable reduction is based upon the 1979 Richard and Elms displacement equation. This equation was based upon a rather limited number of model tests and numerical analyses. As discussed in Chapter 6 with respect to seismically-induced slope displacements, in NCHRP project 12-70 (as described in NCHRP Report 611) a pair of new seismic displacement equations were developed using a large database of strong motion records. These two equations (one for rock sites in the Eastern and Central US and one for the rest of the US) were developed using the Newmark method to calculate the permanent seismic displacement for each record and regression analyses. As discussed in Chapter 6, in the Newmark method permanent seismic displacement is a function of the yield acceleration, the acceleration at which seismic displacement is initiated. For a retaining wall, the yield acceleration is the seismic coefficient at which the horizontal forces (the demand) on the wall system equal the lateral resisting forces (its capacity). For instance, for the semi-gravity wall in Figure 11-12 the horizontal forces include the horizontal component of the seismic active earth pressure ($P_{AE}\cos\delta$) and the inertia forces on the wall itself ($k_h W_c$) and the backfill over the heel of the wall ($k_h W_s$), while the resisting forces include the frictional sliding resistance of the wall (H_R) and the horizontal component of the seismic passive pressure on the toe of the wall ($P_{PE}\cos\delta$). The yield acceleration would be the seismic coefficient at which ($P_{AE}\cos\delta + k_h W_c + k_h W_s$) was equal to ($H_R + P_{PE}\cos\delta$).

The NCHRP 12-70 displacement equations reported in Chapter 6 are repeated here for the sake of completeness. For all sites except Central and Eastern United State (CEUS) rock sites (i.e. except for CEUS Site Class A and B), displacement (in inches) can be estimated by:

$$\log(d) = -1.51 - 0.74 \log\left(\frac{k_y}{k_{\max}}\right) + 3.27 \log\left(1 - \frac{k_y}{k_{\max}}\right) - 0.8 \log(k_{\max}) + 1.59 \log(PGV) \quad 11-14$$

For CEUS rock sites (i.e. for CEUS Site Class A and B), displacement (in inches) can be estimated by:

$$\log(d) = -1.31 - 0.93 \log\left(\frac{k_y}{k_{\max}}\right) + 4.52 \log\left(1 - \frac{k_y}{k_{\max}}\right) - 0.46 \log(k_{\max}) + 1.12 \log(PGV) \quad 11-15$$

where:

$k_y =$ Yield acceleration
 $PGV =$ Peak ground velocity

When using Equation 11-14 or 11-15, it is necessary to estimate the peak ground velocity (PGV). Values of PGV in inch per second may be estimated using the following correlation between the PGV and spectral ordinates at one second (S_1) for Site Class B.

$$PGV = 38F_v S_1 \quad 11-16$$

Note that the above displacement equations represent mean values and can be multiplied by 2 to obtain an 84 percent confidence level.

11.4.2.1 Displacement Ductility Adjustment Factor

For rigid retaining wall systems that are not able to accommodate any lateral displacement in the design earthquake, and for wall systems in which critical displacement-sensitive facilities are located within the active wedge, no reduction in the seismic coefficient for wall displacement ductility is recommended (i.e. $r = 1$). However, many free standing retaining wall systems can accommodate lateral displacements in the design earthquake on the order of several inches, particularly if the performance standard is life safety. Extensive analyses conducted for the NCHRP 12-70 project using Equation 11-14 and 11-15 show that when the seismic coefficient is greater than or equal to 50% of k_{max} , the calculated seismic displacement is less than 1 inch. Therefore, for earth retention systems that are able to accommodate 1-2 inch of lateral displacement, it is recommended that the ductility reduction factor, r , be set equal to 0.5. For retaining wall systems that can accommodate more than 2 inches of lateral displacement in the design earthquake, a ductility reduction factor less than 0.5 may be used. To summarize these recommendations:

- For rigid retaining wall systems that cannot accommodate any lateral displacement in the design earthquake and for retaining walls in which critical displacement facilities are located in the active wedge:

$$k_h = \alpha * k_{max} \quad 11-17$$

- For retaining wall systems able to accommodate 1-2 inches of lateral displacement in the design earthquake:

$$k_h = 0.5 * \alpha * k_{\max} \quad 11-18$$

- For retaining wall systems able to accommodate more than 2 inches of lateral displacement in the design earthquake, the recommended approach is to evaluate the yield acceleration for a design that meets all static design requirements and then calculate the seismic displacement using Equation 11-14 or 11-15. If this calculated seismic displacement is less than the established acceptable value (i.e. to the design criterion):

$$k_h = r * \alpha * k_{\max} \quad 11-19$$

and

$$r = k_y / k_{\max} \quad 11-20$$

For cases where the retaining wall system can accommodate more than 2 inches of lateral displacement in the design earthquake (Equations 11-19), if the calculated displacement is significantly less than the acceptable value, the ductility reduction factor may be even greater than calculated using Equation 11-20. In this case, the engineer may wish to iteratively reduce the value of r until the calculated displacement equals the acceptable displacement.

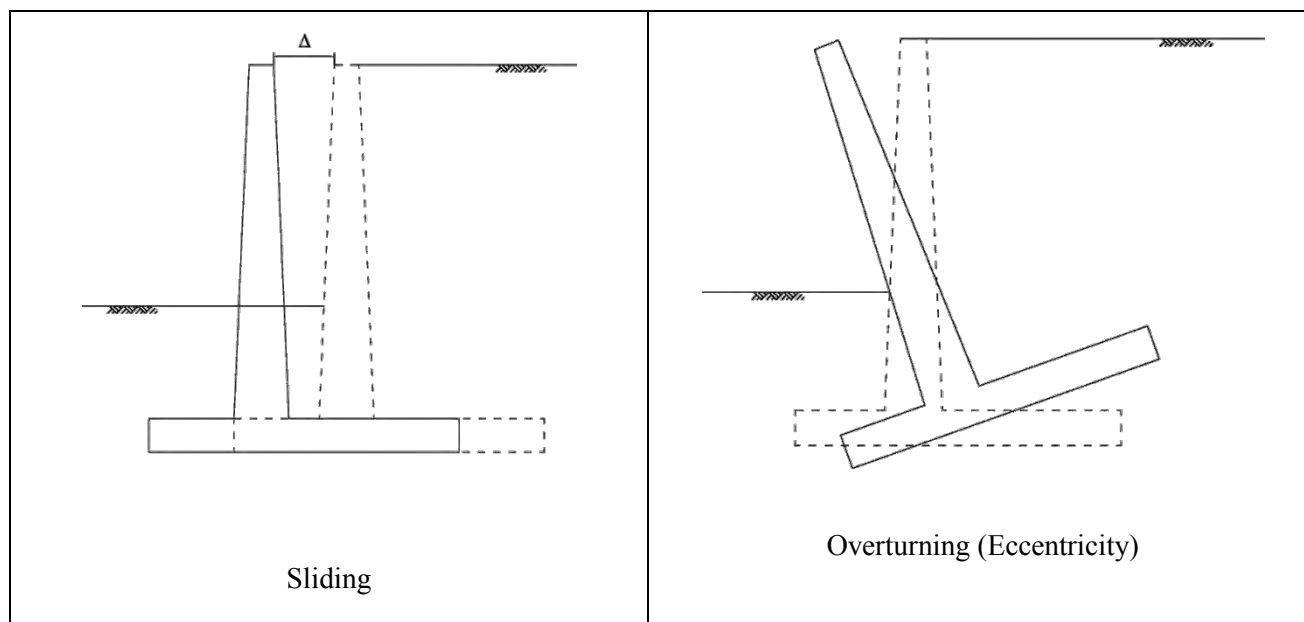
11.4.3 Walls with Backfill of Limited Extent

There are many situations such as walls constructed in front of natural slopes where the existing ground is stable and stands without sliding and/ or caving where the backfill for a gravity or semi-gravity retaining wall is limited to a zone of lesser extent than the seismic active wedge. In these cases, either the trial wedge method or Equations 11-4 through 11-7, with α_n (the inclination of the trial wedge) equal to the angle between the stable natural slope and the horizontal, may be used to estimate the seismic active earth pressure imposed from the limited backfill zone on the wall. Further discussion of these cases is provided in NHCPR Report 611 (NCRHP, 2008).

11.5 GRAVITY AND SEMI-GRAVITY EARTH RETAINING STRUCTURE DESIGN

Design of gravity walls must satisfy both external stability as well as internal stability. External stability modes include sliding, overturning (eccentricity), and bearing capacity. Internal and external stability modes of the failure for a semi-gravity earth retaining wall supported on a shallow foundation are shown in Figure 11-19.

Sliding of the wall is simply due to the lateral thrust exceeding the lateral resistance. Most gravity and semi-gravity retaining structures can withstand substantial amounts of sliding displacement unless there are displacement-sensitive facilities (e.g. structures, utilities) located within the seismic active wedge behind or the seismic passive wedge in front of the wall. Overturning is of particular concern for tall walls with narrow footings. Excessive lateral thrust loads can induce unacceptable tilting and or rotation of the wall during a seismic event.



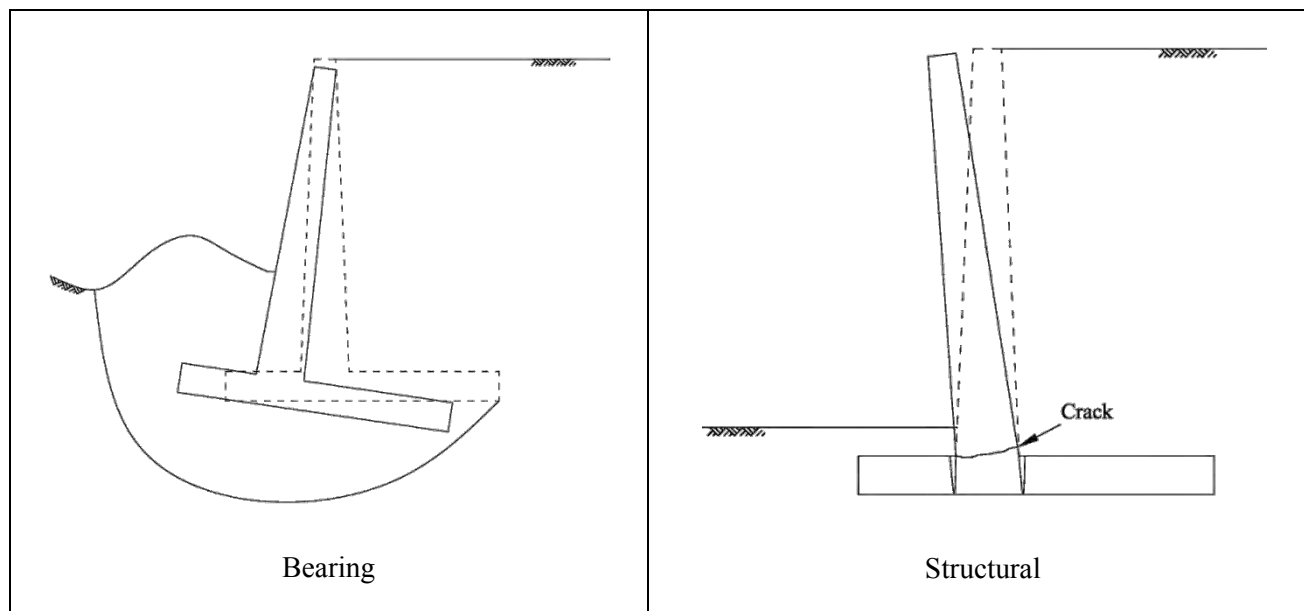


Figure 11-19 Modes of Failure for a Semi-Gravity Earth Retaining Structure

Bearing capacity failure is due excessive vertical loads but can be exacerbated by the increase is vertical stress at the toe of the wall due to the overturning moment induced by the lateral thrust on the wall. Loss of bearing capacity can also lead to overturning and or excessive tilting and settlement of the wall.

Internal failure is generally not a concern with a gravity wall. Internal failure of a semi-gravity wall is due overstressing of the structural components of either the stem or base of the wall. Seismic loading has a twofold effect on the lateral earth pressure applied to the stem and foundation of the earth retaining system. In addition to the seismic load, the height above the base of the lateral earth pressure resultant (the lateral thrust) increases with respect to the base of the wall. This increase in the height of the resultant can lead to significant increases in bending moments within the stem of the wall and the toe and heel of the wall foundation.

11.5.1 External Stability for Walls Supported on a Shallow Foundation

The procedure for external stability evaluation is essentially the same for gravity and semi-gravity retaining walls. The only difference between these two wall types with respect to external stability is that the soil above the heel of a semi-gravity wall is considered to be part of the wall for external stability evaluation purposes. The procedure for external stability evaluation of gravity and semi-gravity walls is as follows:

- 1) Calculate seismic load and resistance as a function of backfill properties, PGA, and AASHTO Site Class (for the foundation material).
- 2) Evaluate sliding.
- 3) Evaluate eccentricity.
- 4) Evaluate bearing capacity.
- 5) Evaluate global stability.
- 6) Evaluate maximum wall displacement and settlement.

Sliding of the wall is due to excessive horizontal driving horizontal forces. The driving force is a result of horizontal seismic thrust load from the backfill ($P_{AE}\cos\delta$) and the horizontal seismic inertial loads from the wall itself ($k_h W_c$) and, for a semi-gravity wall, from the soil above the heel of the wall ($k_h W_s$). The resisting force is provided by the passive pressure in front of the wall ($P_{PE}\cos\delta$) and the shear resistance between the foundation base and foundation soil (H_R). The seismic active thrust and passive resistance and the wall and soil inertial forces are a function of k_h , which, in turn, depends upon the acceptable lateral displacement, as discussed in the previous section. For the wall to be stable, the summation of the factored driving force must be less than summation of factored resisting forces as shown in Equation 11-21:

$$\sum \gamma Q = \sum \phi R_n \quad 11-21$$

where

- γ = Load Factors
- Q = Driving Forces
- ϕ = Resistance Factors
- R_n = Nominal Resisting Forces

The resistance against sliding can be written as:

$$H_R = \varphi R_n = \varphi_\tau R_\tau + \varphi_{ep} R_{ep} \quad 11-22$$

- Where R_n = nominal sliding resistance against failure by sliding
 φ_τ = resistance factor for shear resistance between soil and foundation
 R_τ = nominal sliding resistance between soil and foundation
 φ_{ep} = resistance factor for passive resistance
 R_{ep} = nominal passive resistance of soil in front of the toe (equal to $P_{PE}\cos\delta$)

For seismic loading, the load and resistance factors for sliding evaluation are all 1.0. If the soil beneath the footing is cohesionless, the nominal sliding resistance between soil and foundation is given as:

$$R_\tau = N \tan\phi_b \quad 11-23$$

where N = Summation of the normal forces acting on the base of the footing, including the vertical components of P_{AE} and P_{PE} ; and
 ϕ_b = Interface friction angle between the footing and soil

For a wall system in which there is adhesion between the base and the foundation, an adhesion term must be added to Equation 11-23 for the nominal sliding resistance between the soil and the foundation. Furthermore, when the lateral thrust load on the wall is large, a shear key may be added to stabilize the wall against sliding, adding additional active thrust and passive resistance terms to the equation. However, the passive resistance in front of the wall may be neglected unless the wall extends well below the depth of frost penetration, scour or other types of disturbance.

Eccentricity (wall rotation) is a particular concern for tall walls with narrow footings. The rotational stability of the wall depends upon the driving moment, M_D , that tends to rotate the earth retaining system and the resisting moment, M_R , that tends to resist wall rotation. M_D is a function primarily of the driving seismic thrust and its line of action while M_R depends to a large extent upon wall geometry. Whether or not the eccentricity of the wall system is acceptable is evaluated based upon the location of the resultant force, N , at the base of the footing (which depends upon both M_D and M_R). For the seismic case, the location of the resultant force, N , should be within $B/4$ of the foundation centroid for foundations on soil,

and within $3B/8$ of the foundation centroid for foundations on rock. Equation 11-24 may be used to calculate wall eccentricity.

$$e = \frac{B}{2} - \frac{M_R - M_{R'}}{N} \quad 11-24$$

For a wall founded on soil, bearing capacity is evaluated by comparing the factored maximum bearing stress at the toe of the wall to the factored nominal foundation material bearing resistance. The procedure for evaluating the nominal bearing resistance, q_n , is given in AASHTO (2007) Section 10.6.3.1 and 10.6.3.2.

The maximum bearing stress shall be calculated assuming a linearly distributed pressure over an effective base area. If $e < B/6$, the resultant vertical force is within the middle one-third of the wall base and the bearing stress distribution on the bottom of the footing is trapezoidal. In this case, the maximum bearing stress $\sigma_{v \max}$ can be found as:

$$\sigma_{v \max} = \frac{N}{B} \left(1 + \frac{6e}{B} \right) \quad 11-25$$

If $e \geq B/6$, the resultant vertical force is outside the middle one-third of the wall base and the bearing stress distribution is triangular. In this case, the maximum bearing stress $\sigma_{v \max}$ can be found as:

$$\sigma_{v \max} = \frac{4N}{3(B - 2e)} \quad 11-26$$

Equation 11-21 is also the governing equation for bearing capacity evaluation, except that the seismic load, Q , is the maximum bearing stress, $\sigma_{v \max}$, the load factor for bearing stress is 0.67, and the nominal seismic resistance, R_n , is the nominal bearing resistance, q_n . Therefore, employing a load factor of 1 for the seismic case, the bearing capacity criterion can be written as:

$$0.67 q_n \geq \sigma_{v \max} \quad 11-27$$

The use of a resistance factor of 0.67 for the nominal bearing stress, recommended in NCHRP Report 611, is intended to provide reserve resistance against permanent rotation or tilt of the wall in the design earthquake.

Global stability refers to the stability of the entire earth retaining wall system, including the soil behind the wall and below wall footing. Global stability analysis is typically performed using a commercially available slope stability computer program.

The lateral displacement limits for the retaining wall system is implicit in the selection of the seismic coefficient, k_h . For most gravity and semi-gravity walls, a ductility factor, r , equal to 0.5 can be used as this type of wall can easily accommodate 1-2 inches of lateral displacement. However, if critical facilities are located in front of or behind the wall it may be prudent to use a ductility factor of 1.0 and ductility factors of less than 0.5 may be appropriate for wall systems that can accommodate more than 2 inches of lateral displacement. Vertical settlement of both the backfill and the foundation soil due to seismic loading must be evaluated using the methods discussed in Chapter 6 and compared to allowable values to complete the external stability assessment.

11.5.2 Internal Stability Assessment of Semi-Gravity Cantilever Retaining Walls

Semi-gravity cantilever retaining walls must also be designed to satisfy two internal failure criteria. This type of wall consists of two structural elements: the stem and the footing. The footing must be wide and thick enough to provide adequate external and internal stability for the wall. The thickness of the stem and footing must be sufficient to resist the shears and moments due to the seismic loads.

The lateral thrust load on the stem can create a tensile force on the back face of the stem and a compressive force on the front of the stem, causing the stem to bend away from the backfill. The exaggerated deformed shape of the wall as a result of thrust loads is shown in Figure 11-20. The heel of the footing supports a large amount of backfill weight as well as the vertical component of the thrust loads, while the soil bearing pressure acting at the bottom of the heel is very small due to the eccentricity of the normal force on the base induced by the seismic thrust. This will cause the footing to bend concave downward, creating a tensile stress at the top surface and a compressive stress at the bottom surface of the heel. The bearing pressure at the bottom surface of the toe is relatively large compared to the weight of the soil resting at the top surface of the toe. This causes the toe to bend concave upward, creating a tensile stress at the bottom surface of the toe and a compressive stress at the top surface of the toe.

Since the concrete has low tensile strength, reinforcement is required on the tension sides of all the wall components. Thus, reinforcement is required at the backfill face of the stem, the top of the heel and bottom face of the toe. In wall design, it is assumed that the stem, the heel and the toe all behave like a cantilever beam with fixed ends located at sections ac, ab and cd in Figure 11-20.

The thickness and the required reinforcement of the stem, the heel and the toe is controlled by the induced shear and moment from the lateral thrust loads, the backfill vertical weight and vertical component of the lateral thrust loads and the bearing pressure, respectively.

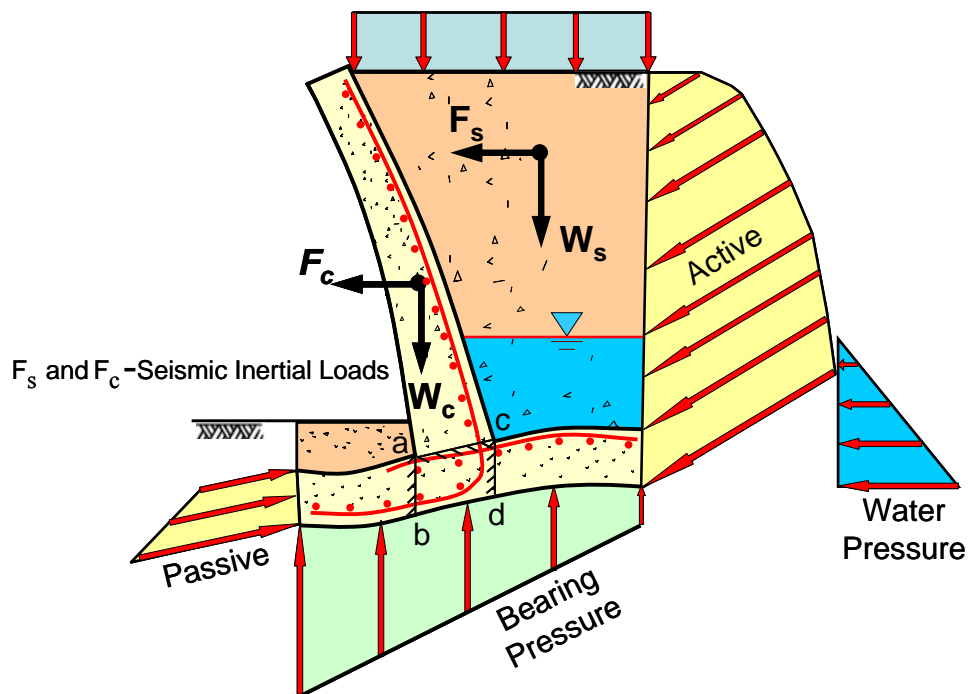


Figure 11-20 Combined Thrust Loads and Deformed Shape of Cantilever Wall

In structural design of the wall, the factored seismically induced shear forces and bending moments computed at the critical sections of the wall are compared to the factored seismic resistance of these elements. The seismically induced inertia forces applied to the stem, footing and the soil above the heel must be included in the calculation of maximum shear forces and moment. The critical sections for a cast-in-place concrete wall are shown in Figure 11-21.

Since the horizontal inertia load, F_s , of the soil above the heel reduces the moment at section cd of the heel, it is generally not considered in the heel design.

The reinforcement for a semi-gravity retaining wall is generally detailed by a structural specialist.

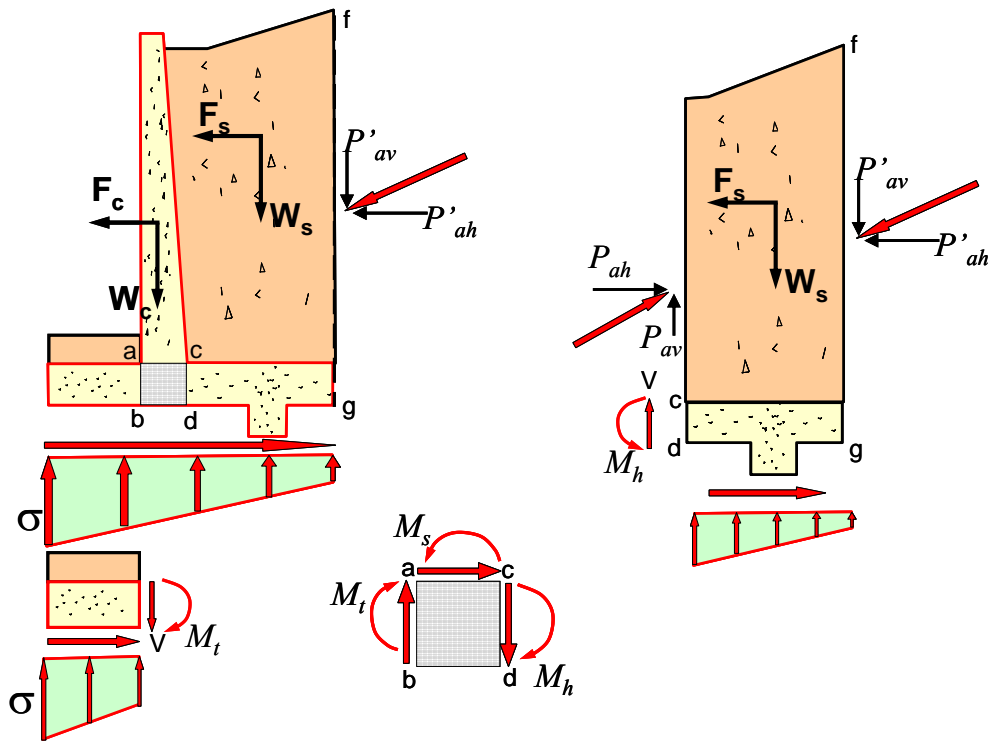


Figure 11-21 Forces Acting at the Critical Sections of the Wall

11.5.3 Gravity and Semi-Gravity Retaining Walls on Piles

Retaining structures may be constructed on pile foundations when the soil for a considerable depth beneath the base of the wall is too weak or compressible to provide adequate support for the wall. A pile-supported retaining wall is illustrated in Figure 11-22. Note that for the wall illustrated in Figure 11-22, the piles in the front two rows are battered to resist the horizontal components of the lateral earth pressure. If battered piles are employed to support the wall, most of the lateral loads are carried as axial loads in the batter piles (due to the much greater stiffness of batter piles in axial loading compared to vertical piles subject to a lateral load). However, the heads of the batter piles still must be designed to

resist the moments induced in these piles by lateral loading. The moment induced on the footing by seismic loading is also assumed to be carried by the foundation piles as axial loads.

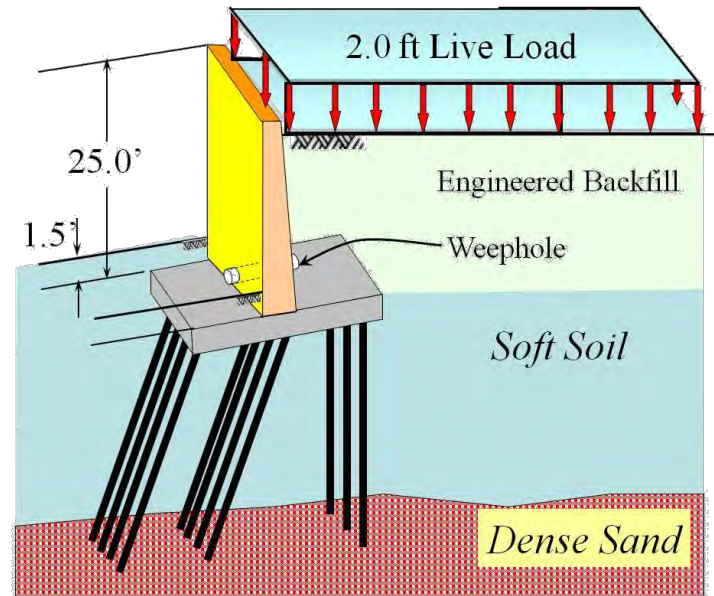


Figure 11-22 Pile Supported Retaining Wall

Because of the rigidity of pile supported foundations, a ductility factor of 1.0 is recommended for design of gravity retaining walls supported on piles unless a deformation analysis is conducted to determine the associated seismic displacement of the system. If a displacement analysis is conducted, an iterative analysis: seismic loads based upon an initial estimated ductility factor of 0.5 are applied to the wall system and the resulting lateral displacement of the pile-supported wall system is calculated. If this displacement is not between 1- 2 inches, the ductility reduction factor should be changed (increased if the calculated displacement is less than 1 inch, decreased if it is greater than 2 inch) and the seismic loads and displacements re-calculated. The new displacement should be compared to a displacement calculated using Equation 11-14 or 11-15 a yield acceleration k_y equal to $(r \times F_{PGA} \text{PGA})$ for compatibility with the displacement calculated based upon the seismic forces. This process continues until convergence.

11.6 DESIGN OF CANTILEVER AND ANCHORED EARTH RETAINING STRUCTURES

Cantilevered and anchored earth retaining systems are constructed of vertical structural members with an above-ground height, H and an embedded depth D . The vertical support members may be soldier piles spaced at a distance, S , or continuous sheet piles. Both types of systems are illustrated in Figure 11-23.

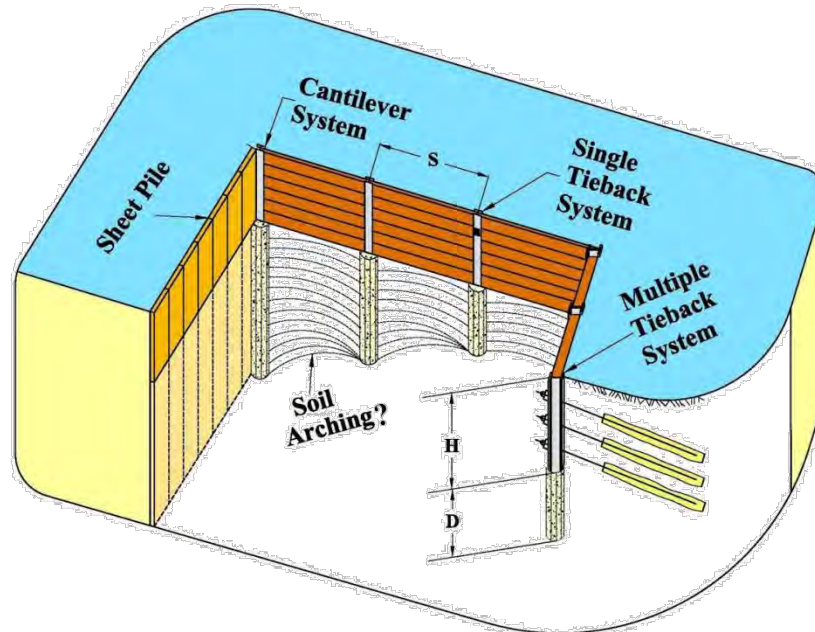


Figure 11-23 Cantilevered and Anchored Earth Retaining Systems

11.6.1 Non-Gravity Cantilevered Earth Retaining System

Non-gravity cantilevered walls include both soldier pile and sheet pile wall systems. Soldier piles may be constructed with driven steel piles, cast-in-place reinforced concrete drilled piers, or treated timber, precast concrete, or steel piles placed in drilled holes and backfilled with concrete. Soldier pile walls are faced with either treated-timber, reinforced shotcrete, reinforced cast-in-place concrete, precast concrete panels, or metal panels. Continuous sheet pile walls may be constructed with driven precast pre-stressed concrete sheet piles or steel sheet piles. Non-gravity cantilevered walls depend on the passive resistance of the foundation material against the embedded portion of the wall and the moment resisting capacity of the vertical structural members for stability. Therefore, the maximum height of these walls is limited by the competence of the foundation material and the moment resisting capacity of the vertical structural members. The economical height of this type wall is generally limited to a maximum height of 18 feet.

The simplified seismic lateral earth pressure distribution shown in Figure 11-24 may be used for design of cantilever earth retaining systems (NCHRP Report 611). The seismic active earth pressure is distributed uniformly above the excavation line (NCHRP Report 611). The hydrostatic water pressure is assumed to be zero. Furthermore, the active lateral earth pressure acting over the wall height (H) shall not be less than 0.25 times the effective overburden pressure at any depth, or 0.035 KSF/FT of wall height, whichever is greater.

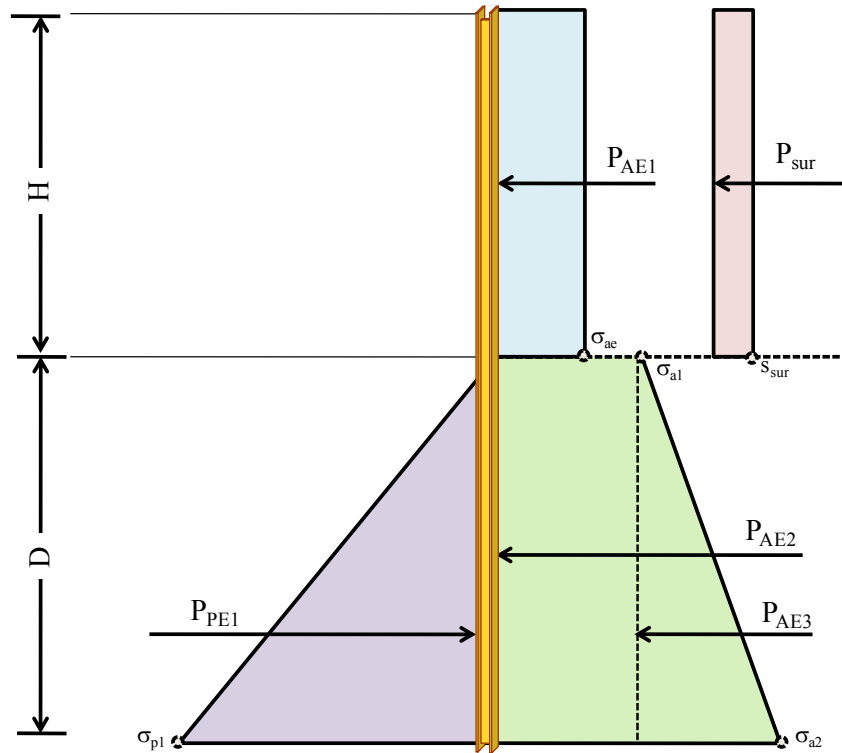


Figure 11-24 Seismic Load Distribution for Non-Gravity Cantilever Retaining Walls

For a sheet pile wall, the load distribution shown in Figure 11-24 can be used directly to design the wall. For a soldier pile wall, the load diagram must take into account the spacing between the soldier piles and the effective width of the embedded soldier piles. For the above-ground section of the soldier pile, the earth pressure and water pressure diagrams are multiplied by the soldier pile spacing, S , to get the load on each soldier pile. Below grade, the active soil pressure acts only on the width of the soldier pile but the passive pressure is assumed to act on an effective width that is greater than the actual soldier pile width.

The width of the soldier pile maybe taken as the diameter of the drilled-hole when structural concrete is used.

Arching of the soil between soldier piles can increase the effective width of a soldier pile to as much as 3 times the width of the element (AASHTO, 3.11.5.6). In competent cohesionless soil, a factor of three is used to calculate the effective width in the passive zone as long as the center-to-center spacing of the soldier piles exceeds 3.75 feet (for spacing less than 3.75 feet, the factor is 0.8 times the spacing). However, if the soldier pile is embedded in stiff clay, the factor used to develop the effective width is 2 and for soft clay (clay in which the undrained shear strength greater than 3 times the in situ vertical normal stress), soil arching will not occur and the actual width shall be used as the effective width for passive resistance. Where a vertical element is embedded in rock (AASHTO, Figure 3.11.5.6-2) the passive resistance of the rock is assumed to develop through the shear failure of a rock wedge equal in width to the vertical element, b , and defined by a plane extending upward from the base of the element at an angle of 45° .

A ductility reduction factor of 1.0 is recommended for design of non-gravity cantilever walls unless a demonstration of the ability of the wall to sustain displacement is provided and the owners' permission is obtained. With a demonstration of the ability to sustain displacement and the owner's permission, a displacement-based ductility reduction factor may be used for the seismic active pressure above the ground surface in front of the wall. Furthermore, due to the deformation required to mobilize the passive resistance, it is recommended that a passive resistance equal to $P_{PE}/1.5$ be used in design.

The following procedure is used for the seismic design of a cantilever retaining wall:

- 1) Calculate the surcharge loads above the excavation line and the Active/Passive earth pressures to some arbitrary point depth below the excavation line.
- 2) Find the embedment depth D_O at which the moment due to the seismic passive earth pressure on the left hand side of the wall (P_{PE1}) is balanced by the moments due to the seismic active earth pressures and surcharge pressures on the left hand side of the wall (P_{AE1} , P_{AE2} , P_{AE3} , and PS_{UR}), i.e. where the sum of the moments due to the earth pressures is zero..
- 3) Increase D_O by 20 percent ($D = 1.2D_O$)
- 4) Calculate the resultant force on the wall, R , by summation of all of the forces in horizontal direction: if R is larger than zero, increase D until $R = 0$.

- 5) Use the resulting pressure diagram to calculate the Maximum Bending Moment (M_{MAX}) and Maximum Shear Force (V_{MAX}) for design of the vertical structural member and lagging.

11.6.2 Anchored Walls

Anchored walls are typically composed of the same elements as non-gravity cantilevered walls but derive additional lateral resistance from one or more levels of anchors. The anchors are typically ground anchors (tiebacks) consisting of drilled holes with prestressing steel tendons extending from the wall face to an anchor zone located behind potential failure plane (i.e. behind the active wedge) in the retained soil or rock mass, as illustrated in Figure 11-25. The tendons are typically grouted over the section of the hole in the active zone (the bonded length), then prestressed, and then grouted over the balance of the hole for corrosion protection (the unbonded length). Other support systems include deadman anchors and, in rare instances for permanent walls, external bracing. An anchored wall includes an exposed design height (H) over which the soil is retained, as well as, an embedded depth (D) which provides vertical and lateral support.

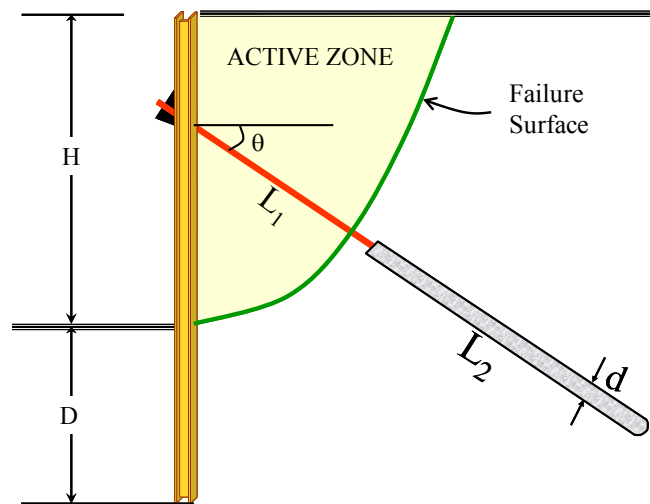


Figure 11-25 Lateral Earth Pressure for Anchored/Braced Walls

where

- L_1 = Unbonded Length
- L_2 = Bonded Length
- d = Diameter of Drill Hole
- D = Wall Embedment Depth
- H = Wall Height

θ = Tieback Inclination Angle

The lateral earth pressure distribution for seismic design of a single level braced/tieback wall, developed in accordance with the recommendations in NCHRP Report 611, is shown in Figure 11-26. The maximum ordinate (σ_a) of the trapezoidal seismic pressure diagram is determined as follows:

$$\sigma_a = \frac{P}{\frac{2}{3}H} \quad 11-28$$

where the total active earth pressure, P, is found as:

$$P = 1.3 P_{AE} \quad 11-29$$

The active earth pressure P_{AE} above the excavation line is best determined using the generalized equilibrium method as soil conditions are likely to be c - phi materials and stratified.

A ductility reduction factor of 1.0 is recommended for design of single anchor walls. Use of a displacement-based ductility reduction factor is not recommended. As recommended for non-gravity cantilever walls, due to the deformation required to mobilize the passive resistance, it is recommended that a passive resistance equal to $P_{PE}/1.5$ be used in design. The following procedure can be used for the design of a Single Tieback/Brace System wall:

- 1) Determine the seismic active and passive earth pressure coefficients using the methods described in Section 11.3. Reduce the passive coefficient by 1.5 to account for the large displacement required to fully mobilize passive resistance.
- 2) Convert the seismic active earth pressure above the excavation line to a trapezoidal pressure distribution
- 3) Take a moment about the tieback to calculate embedment depth, D.
- 4) Apply force equilibrium in the horizontal direction (set the sum of the horizontal forces equal to zero) to calculate tieback/brace force, T.
- 5) Calculate Maximum Bending Moment (M_{MAX}) and Maximum Shear Force (V_{MAX}) for design of the vertical structural member and lagging.

The bonded length of the tieback should be located behind the actual failure surface.

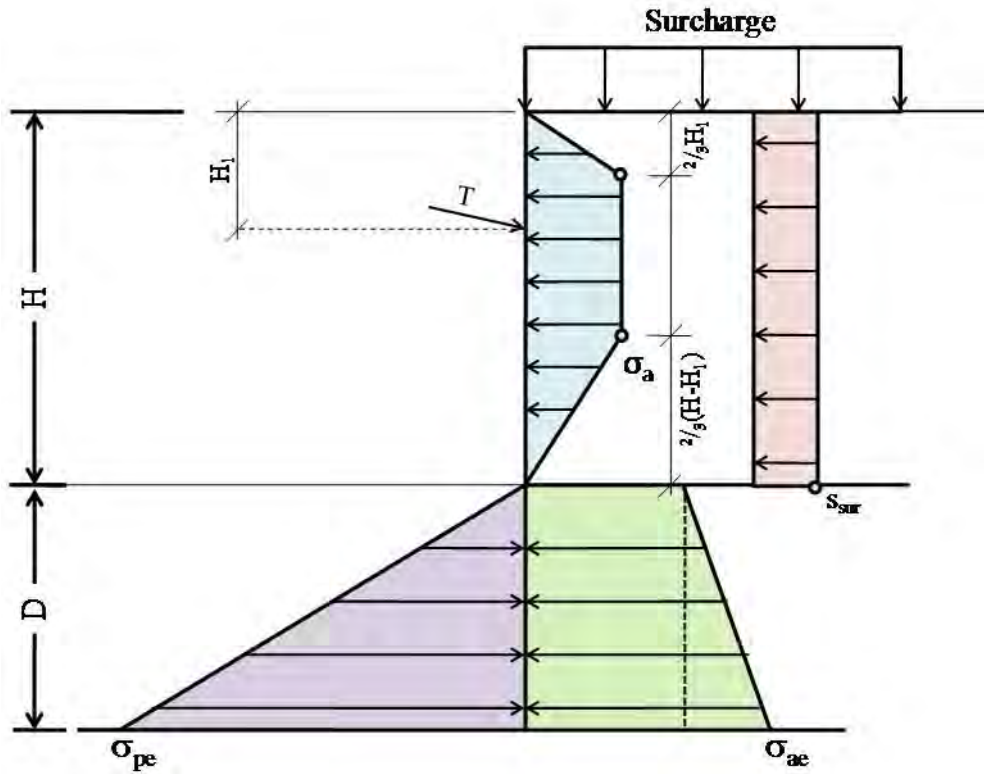


Figure 11-26 Single Tieback System

The lateral active horizontal earth pressure for a multilevel anchored wall, developed in accordance with the recommendations in NCHRP Report 611, is shown in Figure 11-27. The maximum ordinate of the trapezoidal seismic pressure distribution for a multiple tieback wall may be calculated as follows.

$$\sigma_a = \frac{P}{\left[H - \frac{1}{3}(H_1 + H_{n+1}) \right]} \quad 11-30$$

where P is again evaluated in accordance with Equation 11-29 as 1.3 times the seismic active earth pressure.

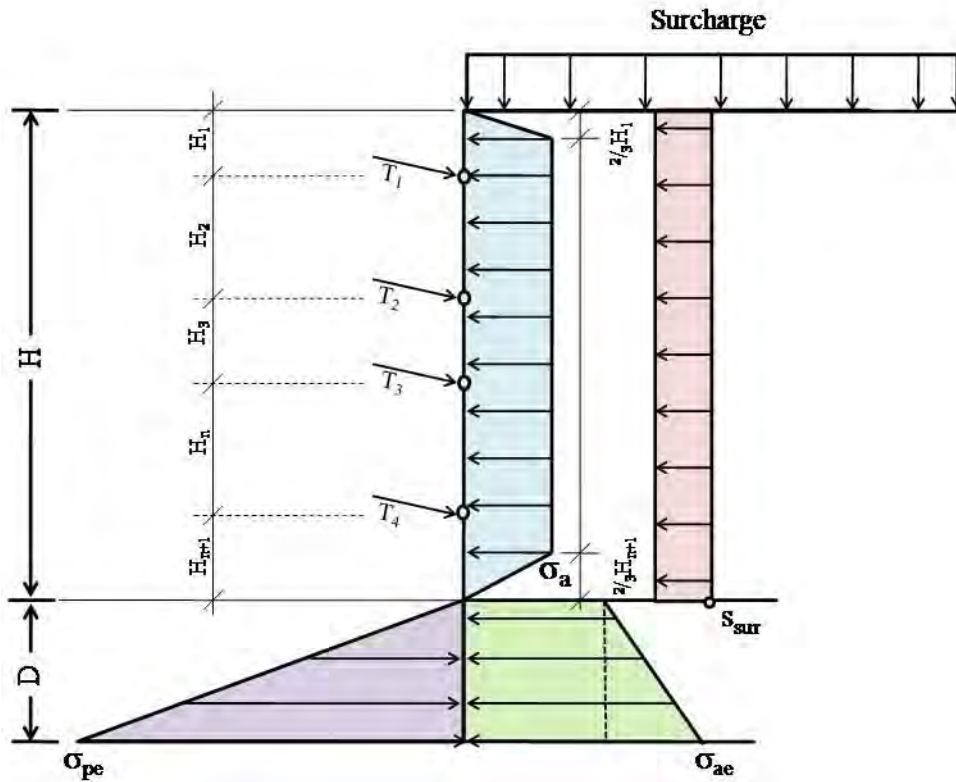


Figure 11-27 General Pressure Distribution for Tieback Retaining Walls

Similar to single anchor walls, a ductility reduction factor of 1.0 is recommended for design of multiple anchor walls. Use of a displacement-based ductility reduction factor is not recommended. As recommended for non-gravity cantilever and single anchor walls, due to the deformation required to mobilize the passive resistance, it is recommended that a passive resistance equal to $P_{PE}/1.5$ be used in design.

Figure 11-28 shows a simple trapezoidal pressure diagram for a multiple tieback system. The vertical wall element is divided into three types of spans.

- Starting Cantilever Span S_1
- Interior Spans S_n
- Embedment Span S_D

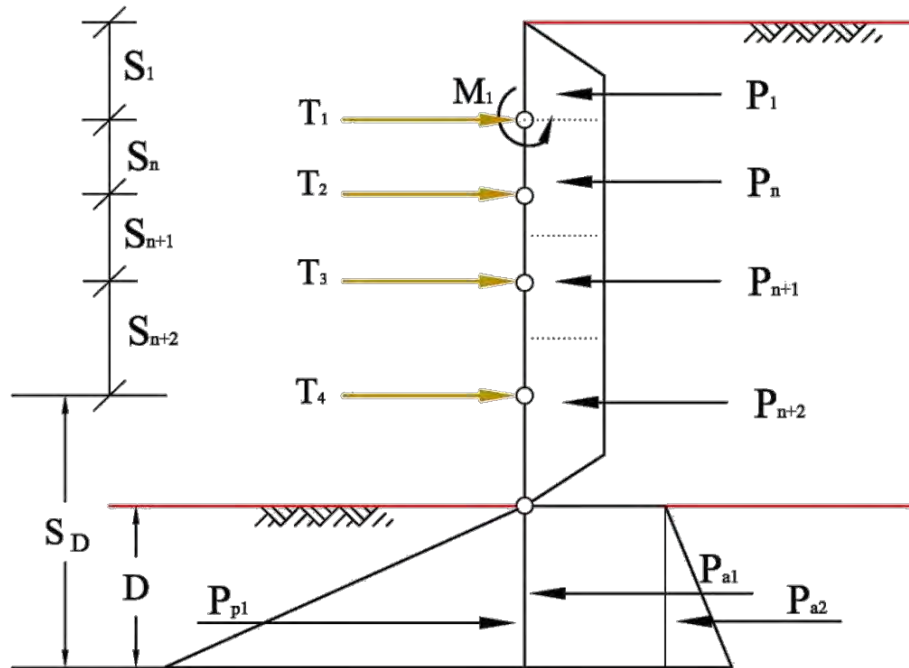


Figure 11-28 Simple Seismic Pressure Distribution for a Multiple Tieback System

The hinge method illustrated in Figure 11-29 is used to design multiple Tieback/Brace wall systems. The procedure may be described as follows:

1. Take a moment M_1 about the upper level tieback due to cantilever action of the soil pressure above the upper tieback
2. Use combination of the moment, M_1 , and tributary area to calculate the remaining tieback loads except the last tieback load
3. Take a moment about the last tieback to calculate embedment depth, D using a factor of safety of 1.0
4. Set summation of forces equal to zero in horizontal direction to calculate the last tieback force, T_{n+1}
5. Calculate Maximum Bending Moment (M_{MAX}) and Maximum Shear Force (V_{MAX}) for structural design of the vertical structural member and lagging.

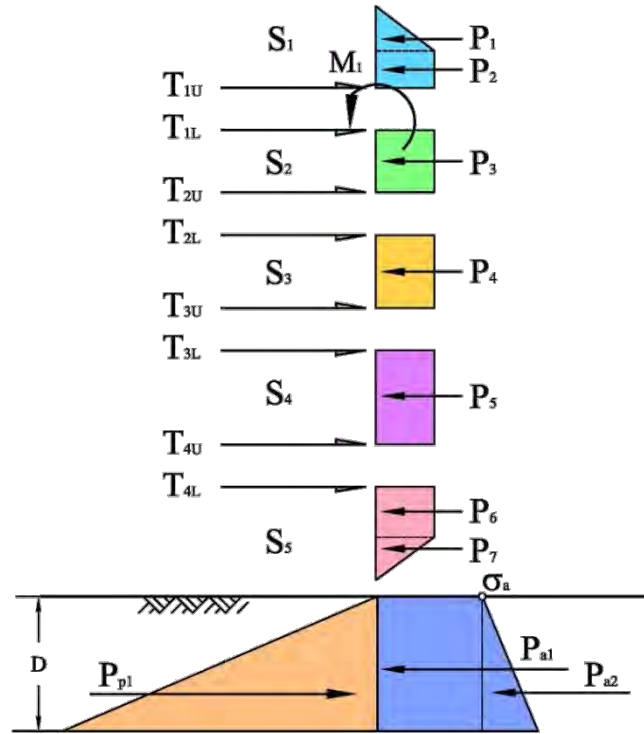


Figure 11-29 Hinge Method for Tieback Design

11.7 MECHANICALLY STABILIZED WALLS

Mechanically stabilized earth (MSE) walls are composed of either metallic (inextensible) or geosynthetic (extensible) soil reinforcement in the soil mass and vertical or near vertical discrete modular precast concrete facing elements. Various aesthetic treatments can be incorporated in the precast concrete face panels. MSE walls behave as a gravity wall, deriving their lateral resistance through the dead weight of the reinforced soil mass behind the facing.

MSE walls are typically used where conventional reinforced concrete retaining walls are considered, and are particularly well suited for sites where substantial total and differential settlements are anticipated. MSE walls can be used in both cut and fill applications. Because their base width is greater than that of conventional reinforced concrete walls they are most cost effective in fill applications. The practical height of MSE walls is limited by the competence of the foundation material at a given site. Due to the inherent flexibility of MSE walls they have performed exceptionally well during past earthquakes.

MSE walls are designed for both external stability and internal stability of the reinforced soil mass. Structural design of the wall facing may also be required. However, only external stability of MSE walls is addressed in this manual. Internal stability and facing design are discussed in a separate NHI document dedicated entirely to MSE wall design.

The current method for seismic design of MSE walls in the AASHTO LRFD Bridge Design Specifications is based on pseudo-static analysis procedures. Relevant modes of external failure for MSE wall are shown in Figure 11-30. These modes of failure include:

- Sliding
- Eccentricity
- Bearing Capacity
- Global Stability

The global stability of the wall, including vertical settlement, will not be discussed in this manual.

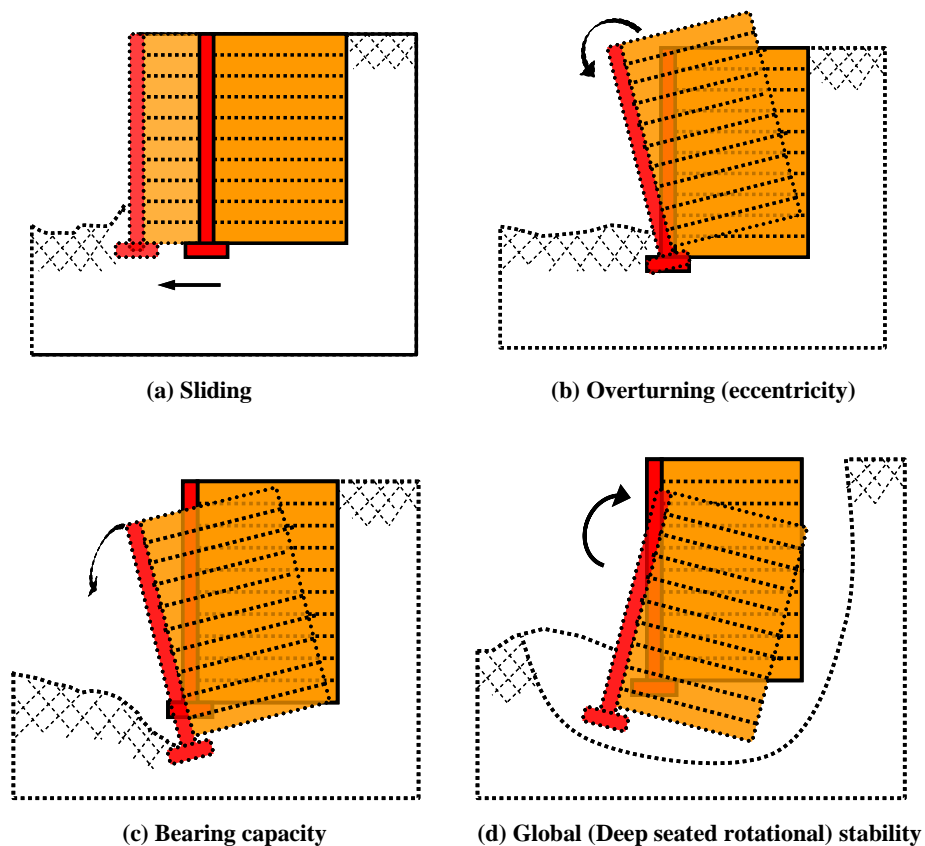


Figure 11-30 Potential External Failure Mechanisms for MSE Walls

The design procedure for external stability of MSE walls may be described as follows:

- 1) Calculate seismic loads
- 2) Evaluate Sliding
- 3) Evaluate Eccentricity
- 4) Evaluate Bearing Capacity
- 5) Evaluate Wall Displacement

The design height of the MSE wall (for external stability computations) is the sum of the wall embedment depth and the wall height. Similar to the gravity retaining walls, for the design and analysis of MSE walls lateral seismic earth pressure, as well as, lateral inertial load of the reinforced soil mass must be considered. Figure 11-31 shows the forces acting on a MSE wall during a seismic event.

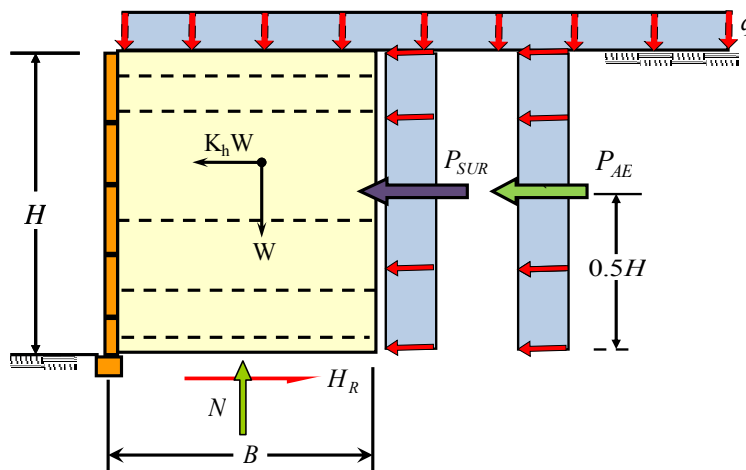


Figure 11-31 Pressure Diagram for MSE wall with Seismic Force

Figure 11-32 shows the seismic active earth pressure acting on the back of the reinforced zone for the case of a sloping backslope. The procedures described in Section 11.3 are recommended to be used to determine the seismic active earth pressure on the backfill of a MSE wall, in place of the current AASHTO procedure. As MSE walls are inherently ductile structures, a ductility reduction factor of 0.5 (for acceptable lateral displacements of 1-2 inches) or less (for acceptable displacements greater than 2 inches) may be used to calculate the seismic coefficient for MSE wall design unless critical structures or facilities are located in front of or behind the wall.

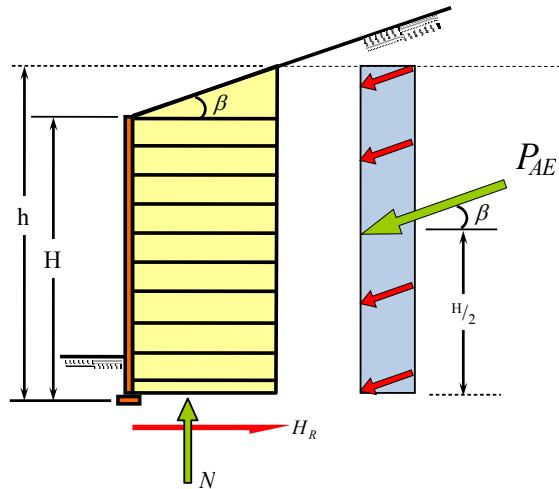


Figure 11-32 Pressure Diagram for MSE Walls with Sloping Backslope

The sliding resistance of a MSE wall is evaluated in the same way as it is evaluated for a gravity earth retaining structure.

The eccentricity, e_b , of an MSE wall can be calculated as shown in the equation below:

$$e_b = \frac{B}{2} - X_o \quad 11-31$$

where

B = base width (length of reinforcement elements) and

X_o = location of the resultant from the toe of the wall.

The parameter X_o is calculated as:

$$X_o = \frac{(M_{RE} - M_{DR})}{N} \quad 11-32$$

where M_{RE} = resisting moment due to vertical component earth pressure calculated about the toe of the wall;

M_{DR} = driving moment due to seismic horizontal earth pressure from ground and from live load surcharge calculated about the toe of the wall;

N = vertical weight of the reinforced soil mass and vertical component of the seismic earth pressure

It should be noted that the effect of external loadings on the MSE mass, which increases sliding resistance, should only be included if the loadings are permanent (with the exception of traffic live loads, where a surcharge equal to 0.5 times the average daily truck traffic load is recommended (as discussed in Chapter 1). For eccentricity to be considered acceptable, the calculated location of the resultant vertical force should be within the middle half of the base (i.e., $e_{b \text{ max}} = B/4$).

Due to the flexibility of MSE walls and the inability of the flexible reinforcement to transmit moment, a uniform base pressure distribution is generally assumed beneath the base of the MSE wall over an equivalent footing width, B' , equal to the actual footing width, B , minus twice the eccentricity, e_b (i.e. $B' = B - 2e_b$).

Assuming a load factor of 1 for seismic loading, the design criterion for the bearing resistance (q_R) for an MSE wall is given as:

$$q_{uniform} \geq \phi q_n \quad 11-33$$

where:

- ϕ = resistance factor = 0.67 per recommendations in NCHRP Report 611
- q_n = nominal bearing resistance
- $q_{uniform}$ = uniform bearing pressure

11.8 SUMMARY

This chapter describes the seismic design procedure for earth retaining systems. NCHRP Report 611 (NCHRP, 2008) forms the basis of the recommendations provided herein. Seismic LRFD design for earth retaining structures should be done in general compliance with requirements for Extreme Event I. However, it is recommended herein to use a load factor of 1.0 for all permanent loads for LRFD seismic design of free standing earth retaining structures. Furthermore, it is recommended that a load factor of 0.5 be applied to the average daily truck traffic (ADTT) load the earthquake live load but that no inertial component of the live load is considered in seismic design.

The seismic demand on retaining walls includes the seismic active thrust from the soil behind the wall and the inertial loading on the wall itself. Surcharge loads may also contribute to the demand. Sources of seismic resistance for retaining wall systems include seismic passive resistance in front of the wall, the frictional sliding resistance of the base of the wall, and the bearing resistance of the foundation soil for walls that rely on the base to serve as a spread footing, the axial and lateral geotechnical capacity of the deep foundation elements for retaining walls supported on deep foundations, and the structural resistance of the wall system. The active seismic thrust, P_{AE} , and the seismic passive earth pressure, P_{PE} , are functions of backfill properties, the wall and backfill geometry, and the seismic coefficient, k_h , which in turn depends upon the site adjusted peak ground acceleration, $F_{PGA}PGA$. In the absence of other information, P_{AE} and P_{PE} may be assumed to act at the midpoint of the wall height (NCHRP Report 611). The inertia loads acting on the wall, $k_h \times W_c$, and the inertia force acting on the soil above the heel of the wall, $k_h \times W_s$, are also a function of seismic coefficient, k_h . Not all walls need be analyzed for seismic loading. Table 11-1 summarizes these conditions under which no seismic analysis is necessary for free standing earth retaining structures.

The most common means of calculating seismic active thrust used in practice today is Mononobe-Okabe earth pressure theory. While Mononobe-Okabe theory can sometimes be used to calculate the seismic active pressure coefficient, the use of Mononobe-Okabe theory to predict seismic passive earth pressure is not recommended. Shortcomings of the Mononobe-Okabe method for calculating the seismic active earth pressure coefficient include inability to consider cases where the soil within the active wedge is non-uniform or contains some cohesion or where the backslope angle is not uniform. The trial wedge method provides an alternate means of calculating seismic active earth pressures in cases where the Mononobe-Okabe equation does not apply, including

Even relatively small amounts of cohesion in the backfill can significantly reduce the seismic active earth pressure. Sources of cohesion in backfill soils include both true cohesion due to inter-particle bonding and apparent cohesion due to capillary forces in the backfill. Charts are available for a uniform backfill that include the influence of cohesion on the seismic active earth pressure as a function of the normalizing parameter $c\gamma/H$, where c is the backfill cohesion, H is the wall height, and γ is the unit weight of the backfill soil, for values of $c\gamma/H$ equal to 0.05 through 0.25. Recommendations are provided in Table 11-2 for the maximum amount of apparent cohesion that should be assumed for backfill soil as a function of the fines content of the soil. There are many situations such as walls constructed in front of natural slopes where the existing ground is stable and stands without sliding and/ or caving where the backfill for a gravity or semi-gravity retaining wall is limited to a zone of lesser extent than the seismic active wedge.

In these cases, either the trial wedge method or Equations 11-4 through 11-7, with α_n (the inclination of the trial wedge) equal to the angle between the stable natural slope and the horizontal, may be used to estimate the seismic active earth pressure.

The log spiral method can be used to evaluate seismic passive earth. The soil-wall interface friction angle is a key parameter in this approach. Charts are available for a uniform backfill to evaluate the seismic passive earth pressure coefficient for a wall interface friction equal to $2/3^{\text{rds}}$ of the soil friction for values of $c\gamma/H$ equal to 0.05 through 0.25.

Another alternative for evaluating seismic earth pressure is to use the general limit equilibrium (GLE) method. Any conventional slope stability program can be used to evaluate the seismic active and passive earth pressure using this type of analysis.

The maximum possible seismic coefficient (k_{max}) for computation of seismic earth pressure is equal to the site class adjusted peak acceleration at the ground surface, $F_{\text{PGA}}\text{PGA}$. For walls 20 ft tall or higher, the value of k_{max} can be reduced to account for spatial incoherence (also referred to as wave scattering), or averaging of the ground acceleration over the active (or passive) wedge and for walls that can accommodate at least 1-2 inches of lateral displacement in the design earthquake another reduction for system ductility (allowable lateral displacement) can be applied to evaluate the design seismic coefficient, k_h . The same pair of seismic displacement equations used in seismic slope deformation analysis, one for rock sites in the Eastern and Central US and one all other cases, can be used to calculate the permanent seismic displacement is a function of the yield acceleration of the all system, the acceleration at which seismic displacement is initiated. Based upon these equations, a ductility reduction factor, r , equal to 0.5 is recommended for earth retention systems that are able to accommodate 1-2 inch of lateral displacement. For retaining wall systems that can accommodate more than 2 inches of lateral displacement in the design earthquake, a ductility reduction factor less than 0.5 may be used

Design of retaining walls must satisfy both external and internal stability criteria. Global stability of the wall system must also be considered. External stability modes include sliding, overturning (eccentricity), and bearing capacity. Internal stability includes consideration of shear and moment capacity of the structural elements of the wall system. While it is generally recommended to use load and resistance factors of 1.0 in seismic design, the use of a resistance factor of 0.67 for the nominal bearing stress and of 0.8 for the lateral and uplift resistance of piles is recommended for LRFD seismic design.

Gravity and semi-gravity retaining walls and non-gravity cantilever walls may often be able to accommodate more than 1-2 inch of lateral displacement and thus may be designed using ductility reduction factors smaller than 0.5. However, anchored wall systems are relatively rigid and should be designed for a ductility reduction factor of 1.0 unless it can be demonstrated that the wall system (including the anchors) can tolerate displacements of 1-2 inch, in which case a ductility reduction factor of 0.5 may be used. While the seismic active earth pressure behind a gravity, semi-gravity wall, on non-gravity cantilever wall may be taken as uniformly distributed over the wall height, the seismic earth pressure above the excavation line behind an anchored wall should be distributed in the same manner as the static active earth pressure.

CHAPTER 12

BRIDGE ABUTMENTS

12.1 INTRODUCTION

In current practice, LRFD seismic design of bridge abutments is often based on a displacement performance philosophy. This type of design necessitates that the geotechnical engineer predict the resistance of the abutment backfill soils to large displacements. Characterization of the inherently non-linear stiffness of the abutment-backfill system is also necessary if the designer wishes to consider the interaction between the bridge superstructure and the abutments in the global bridge model. Note that the abutment wingwalls are usually designed as conventional retaining walls to retain the abutment backfills and are expected to yield or fail during a major seismic event (i.e. they do not contribute to the capacity of the bridge structure). The transverse capacity of the abutment is provided by the abutment shear keys.

The displacement-based design philosophy in the AASHTO Guide Specifications for LRFD Seismic Bridge Design (AASHTO 2009) involves the design of ductile bridge structures that will resist earthquake loads in a predictable and quantifiable manner. While force-based design also generally involves the design of ductile bridge structures, ductility demand is not explicitly quantified in the force-based approach. Bridge designs with ductile columns will impose large displacements on abutments and this may cause more damage to the abutments than the damage levels that have been observed in the past earthquakes. Furthermore, in many cases, bridge engineers ignore the contributions of the abutment resistance in seismic design of bridge structures due to the complexity of the abutment soil-structure interaction problem. However, proper evaluation and design of the contribution of the bridge abutments to the global response of the bridge can reduce the column displacement demand during earthquake shaking, thus leading to a more efficient and economical design.

Measurements from instrumented bridges and results of large-scale field tests have demonstrated that the stiffness of the abutment-backfill system is a function of the mobilized displacement of the abutment wall. The abutment-backfill can not only provide significant lateral resistance but is also a good source of energy dissipation during large deformations due to nonlinear hysteretic behavior of the abutment-soil system. The abutment force-displacement relationship exhibits significant stiffness degradation at large displacements. Therefore, it is important for practicing engineers to realistically represent the relationship

between the mobilized passive resistance (force) of the backfill on the abutment wall and the abutment wall movement (displacement) for dynamic analysis of bridge structures.

For modern highway bridges, backfill soils behind bridge abutments usually satisfy AASHTO (or State) specifications with regard to compaction and soil type. Therefore, abutment-backfill force-displacement models can be developed based upon typical backfill materials and material properties. AASHTO seismic design provisions provide simple bi-linear models for the abutment-backfill force-displacement relationship for typical backfill soils. Furthermore, data from recent field tests on bridge abutments with typical backfill soils discussed below provide an enhanced understanding of the characteristics of the force-displacement behavior of bridge abutment-backfill systems. This field data provides a basis for the development of a closed-form expression for the non-linear force-displacement behavior of bridge abutments.

12.1.1 Types of Abutment

A bridge abutment system consists of stem walls to support the bridge deck, wingwalls to retain the abutment-backfill, and footings or piles to support the stem wall and wingwalls. Abutments are basically classified into two types: (1) seat-type-abutments, and (2) monolithic abutments. A seat-type abutment is constructed separately from the bridge deck while a monolithic abutment is cast integrally with the superstructure. The bridge engineer is responsible for the selection of the bridge abutment type, taking into account the requirements for the service, strength, and extreme event limit states.

12.1.2 Seat Type Abutment

Seat-type-abutments are located at or near the top of approach fills and may be supported on piles or spread footings. As shown in Figure 12-1, seat-type abutments have a backwall with a depth sufficient to accommodate the bridge deck depth and the bridge deck rests on the abutment seat through bearings pads.

Seat-type abutments may be classified as a short seat abutment (stemwall height less than 8 feet) or as a high cantilever abutment (stemwall height greater than 8 feet), as shown in Figure 12-2.

During a seismic event, a bridge deck moves longitudinally and may collide with the abutment backwall. In an ordinary bridge designed to a life safety standard, the backwall may be designed to break off in the design earthquake in order to protect the foundation from inelastic action as a result of backwall

displacement. This type of abutment design allows the bridge engineers to control the amount force that is transferred to the abutment foundation (i.e. to capacity-protect the foundation).

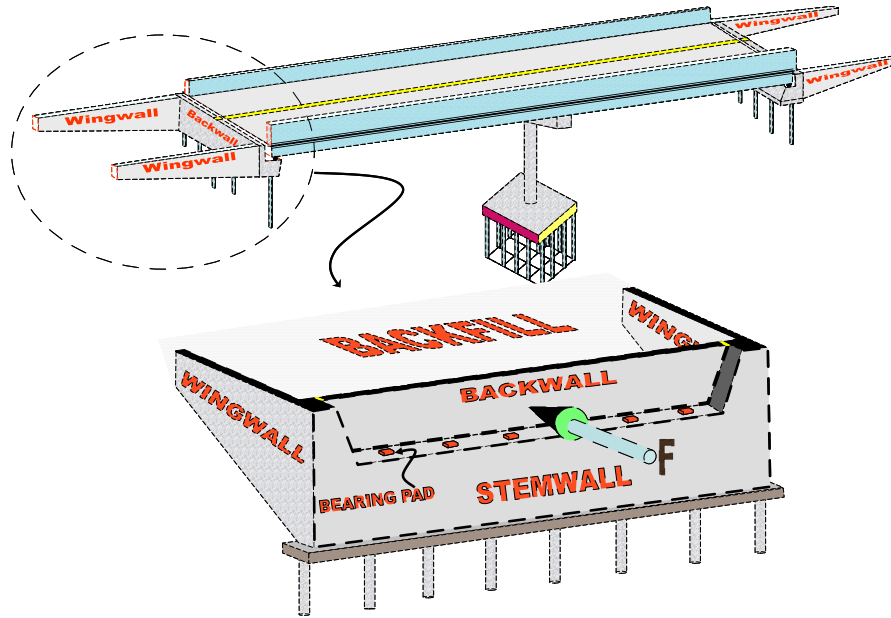


Figure 12-1 Seat-Type Abutment and Foundation System

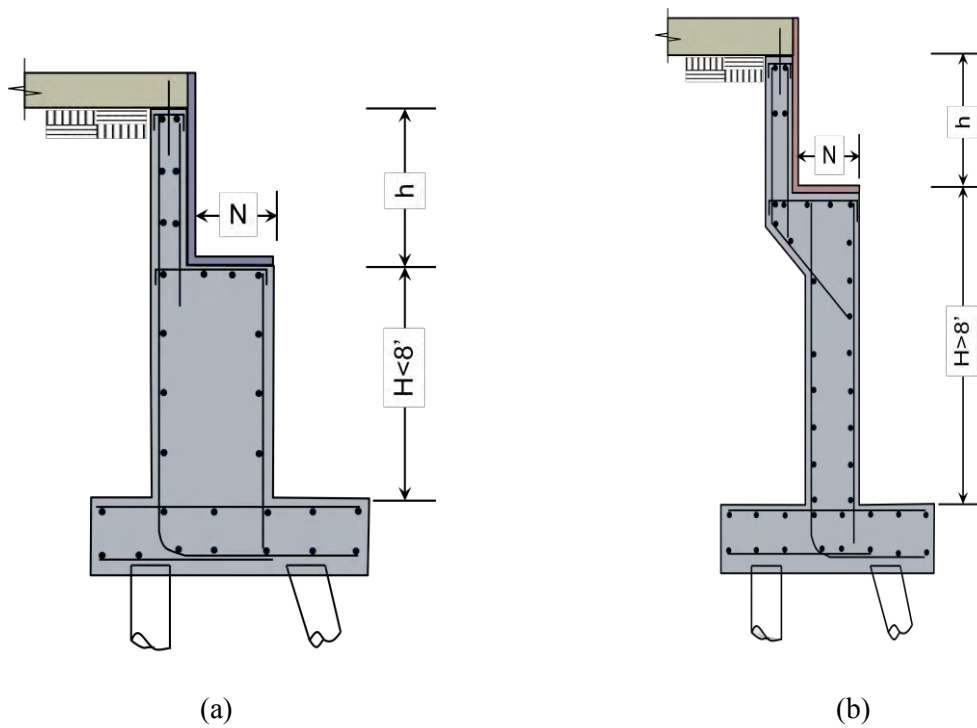


Figure 12-2 Seat Type Abutments; a) Short Seat and b) High Cantilever

Abutment capacity is provided by the passive resistance of the abutment backfill. A typical highway bridge usually has a moderate back wall height in comparison to its width. This height to width relationship makes the earth pressure problem a plane strain problem and two-dimensional passive earth pressure solutions such as those discussed in Chapter 9 are generally sufficient to characterize the abutment-backfill capacity.

12.1.3 Monolithic Abutment

Monolithic abutments are cast integrally with the superstructure and are supported on either spread footings or pile foundations. A pile-supported monolithic abutment is shown in Figure 12-3. For monolithic abutments, the backwall engages the backfill immediately when the bridge is displaced longitudinally. Monolithic bridge abutments are classified as either short stem (H less than 14 feet) or high stem (H greater than 14 feet) abutments, as shown in Figure 12-4.

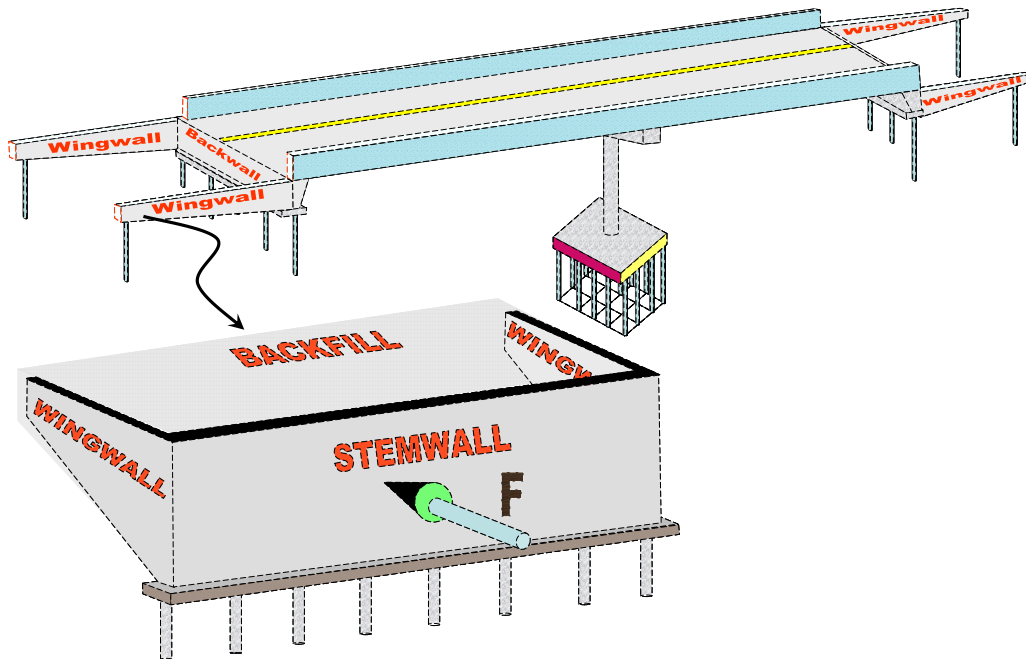


Figure 12-3 Monolithic Abutment and Foundation System

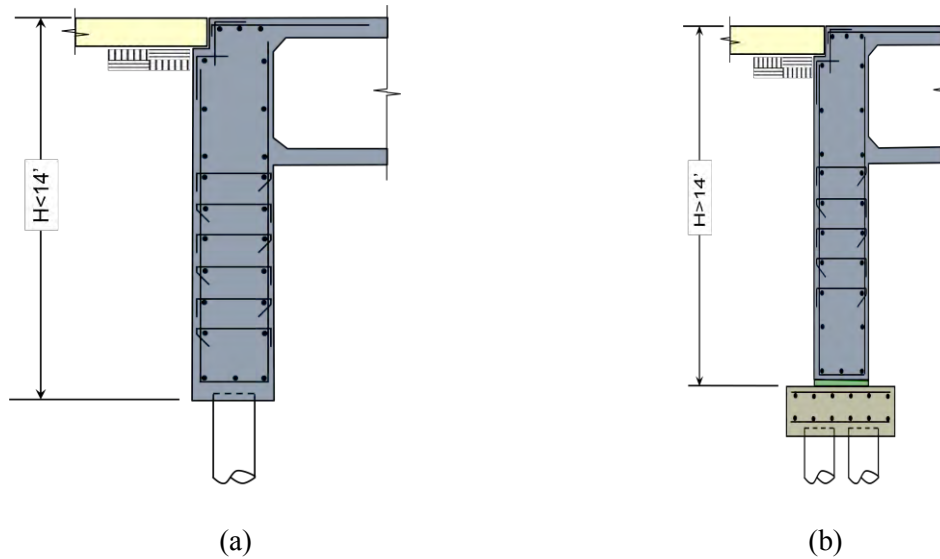
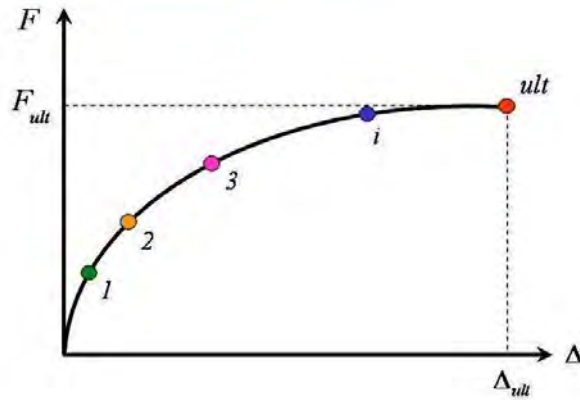
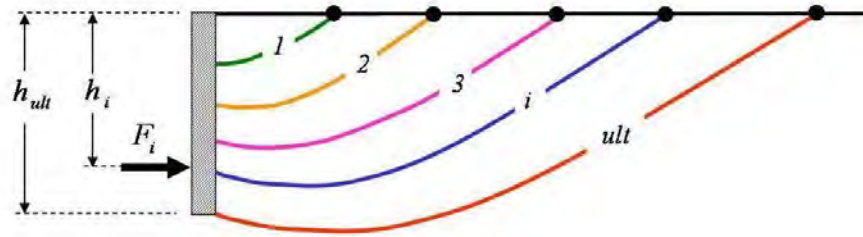


Figure 12-4 Monolithic Abutment Types; (a) Short Stem and (b) High Stem

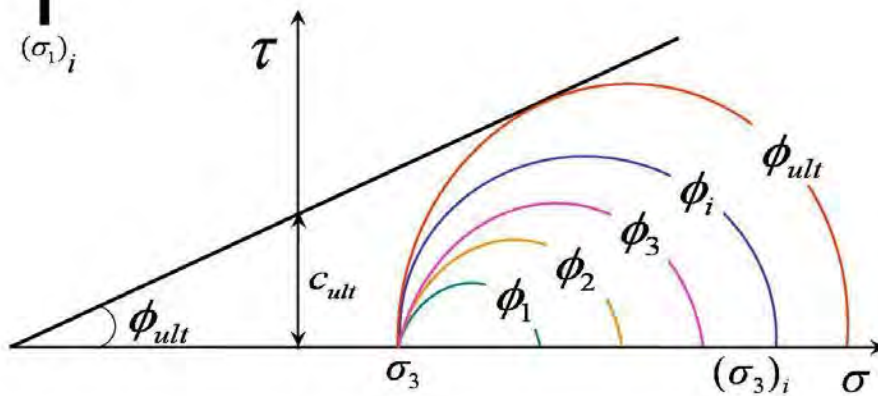
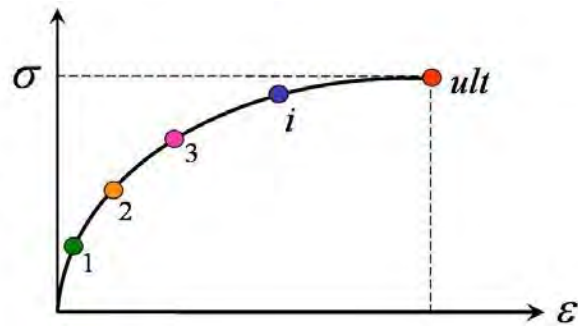
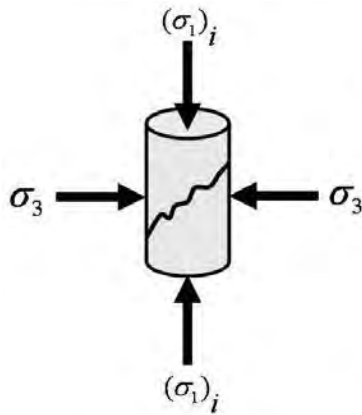
There is no relative displacement allowed between the superstructure and abutment. All the superstructure forces at the bridge ends are transferred to the abutment backwall and then to the abutment backfill and foundations. The lateral force-deformation capacity of a monolithic abutment is a function of abutment backfill properties as well as the foundation and structural capacity of the abutment backwall. As opposed to a seat-type abutment, a monolithic abutment wall may have to sustain large forces during a major seismic event if the backwall capacity is greater than the passive resistance of the backwall. However, if the backwall has been designed to be weaker than the passive earth pressure exerted by the abutment backfill, the effective abutment height is limited to the depth of the bridge deck and the resistance of the abutment is controlled by the passive resistance associated with this effective backfill height.

12.1.4 Mechanism of Abutment Backfill Failure

When an abutment wall is loaded by a horizontal force, F , the wall movement is resisted by the mobilized passive resistance of the abutment backfill. This mobilized passive resistance is a function of relative displacement Δ between the wall and the backfill, as illustrated in Figure 12-5. When the displacement becomes large enough ($\Delta = \Delta_{ult}$), the shear strength of the backfill will be fully mobilized and the ultimate passive backfill capacity F_{ult} develops. For intermediate levels of displacement ($\Delta < \Delta_{ult}$), the shear strength of the backfill is not be fully mobilized and therefore an intermediate passive resistance force F is developed.



(a) Force-Displacement Relationship



(b) Stress-Strain Relationship

Figure 12-5 Mobilization of Passive Resistance (Shamsabadi, 2007)

Post earthquake investigations and full scale field experiments have shown that during a major seismic event mobilized passive wedges will form within the abutment backfill. The effect of an actual earthquake pushing a bridge deck into the abutment-backfill is shown in Figure 12-6. Figure 12-6 shows surface cracks that developed in the roadway pavement behind the northern (77-foot wide, near-normal 5° skew) abutment of the Shiwei Bridge in Taiwan during the Chi-Chi earthquake (Kosa et al., 2001). This is an example of the mobilized passive wedge formation when a bridge superstructure has been pushed into the abutment-backfill due to longitudinal seismic excitation

Figure 12-7 shows another example of formations of mobilized passive wedges and the associated abutment damage from the June 2001 Attica earthquake in Peru. The north abutment of the Puente Los Banos Bridge (a three-span continuous RC box girder structure supported on two-column bents and seat-type abutments) experienced significant displacement and rotation in this event. The top of the abutment was pushed back by the impact from the superstructure. Since there was not sufficient lateral embankment resistance, the bottom of the abutment moved forward, pushing out the slope paving and imposing high flexural and shear demand on the abutment piles.



Figure 12-6 Formations of Mobilized Passive Wedges (Kosa et al., 2001)



Figure 12-7 Puente Los Banos Bridge

12.1.5 Typical Backfill Soil Behavior

As part of the California Department of Transportation (Caltrans) seismic safety research program, a state-wide research study on abutment backfill characterization was performed in 2004 (Kapuskar et al. 2005). The purpose of this study was to develop typical soil properties for bridge abutment backfills in California, with the ultimate goal of developing soil-specific abutment load-deformation relationships that could be used for improved bridge design. The study involved a review of 115 sets of bridge plans state-wide and geotechnical investigation of the abutment backfill at 11 typical bridges sites. The field investigations consisted of soil borings with sampling, CPT soundings with shear wave velocity measurement, pressuremeter testing, and data analysis.

Laboratory testing was conducted on soil samples from the 11 bridge sites and on samples provided by Caltrans from four additional bridge sites. Testing included in-place moisture and density, gradation, plasticity index, expansion potential, sand equivalent, modified Proctor compaction, direct shear, and cyclic triaxial testing. The data was grouped into 4 characteristic backfill soil types: clean sands, silty sands, clayey sands, and cohesive soils (the majority of backfills were found to be silty sands with gravels). Representative geotechnical properties were assigned to each soil type. Results from laboratory cyclic triaxial tests indicated that the stress-strain behavior was nonlinear from the very early stages of the loading and that stiffness decreased and irreversible plastic strain increased with increasing load amplitude for all the backfill soil types.

12.1.6 Full Scale Abutment Loading Tests

The behavior of typical bridge abutment-backfill systems have been studied experimentally on full-scale bridge abutments field tests conducted by the University of California at Los Angeles (UCLA) and the University of California at Davis (UCD) as part of the Caltrans seismic safety research program. These field tests provide insight on the performance of abutment-backfill systems as well as data for development of backfill-abutment force-displacement models.

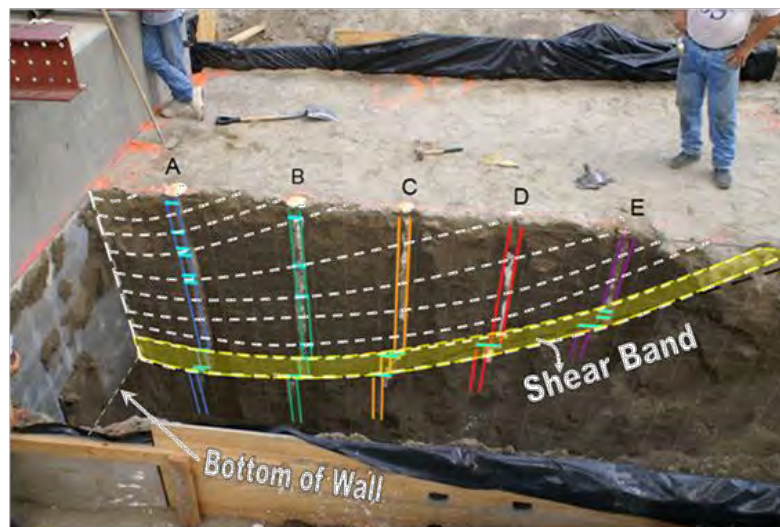
12.1.6.1 UCLA Abutment Experiment

A University of California, Los Angeles (UCLA) research team performed a full-scale cyclic load test on a 15 foot-wide seat-type abutment wall with a height of 5.5 feet and a silty sand backfill (Stewart et. al., 2007). The backfill was placed in layers and compacted to over 95% Modified Proctor dry density. The compacted backfill extended longitudinally about 3 times the backwall height. Before loading the abutment, 3-inch diameter vertical holes were drilled along the longitudinal centerline of abutment backfill and filled with the gypsum columns, as shown in and Figure 12-8. The abutment wingwalls were constructed using smooth plywood and plastic sheeting was placed at the interior face of the wingwalls to minimize friction and thereby simulate a plane strain condition.

In the load test, the backwall was pushed horizontally in between the abutment wingwalls without any vertical component. After the completion of the test, a longitudinal trench was excavated and the failure mechanism of the backfill was carefully mapped using the gypsum columns and cracks in the compacted soil to identify the local passive wedges mobilized along the abutment backfill. The observed crack patterns in within the abutment backfill are highlighted in Figure 12-8b. *En echelon* passive wedges start from near the top of the abutment wall and progress down to the base of the wall, breaking the ground surface progressively further away from the top. The final failure surface extended from the bottom of the abutment backwall and intersected the backfill surface at about 3 times the height of the backwall. The width of the surface rupture zone and displacement of the gypsum columns indicated that the final failure surface was manifested as a shear band, or zone of intense shearing, which formed a log spiral failure surface, as shown in Figure 12-8b. The ultimate capacity of the abutment backfill was measured to be approximately 480 kips at a lateral displacement of about 2.5 inches followed by a residual capacity of about 475 kips at a lateral displacement of about 3.5 inches (Stewart et. al 2007).



(a) Field Experiment



(b) Mapped Failure Wedges

Figure 12-8 Full Scale Abutment Experiment with Silty Sand Backfill

12.1.6.2 UCD Abutment Experiment

A full-scale abutment load test was conducted on a monolithic abutment at the University of California, Davis (UCD). Cyclic longitudinal loading of increasing amplitude was applied to the 5.5 foot-high pile – supported abutment wall until failure. Figure 12-9 shows the test abutment configuration and Figure 12-10 shows the loading ram (Romstad et al., 1995, Maroney et al., 1994). The backfill for this test consisted of compacted Yolo Loam clay.

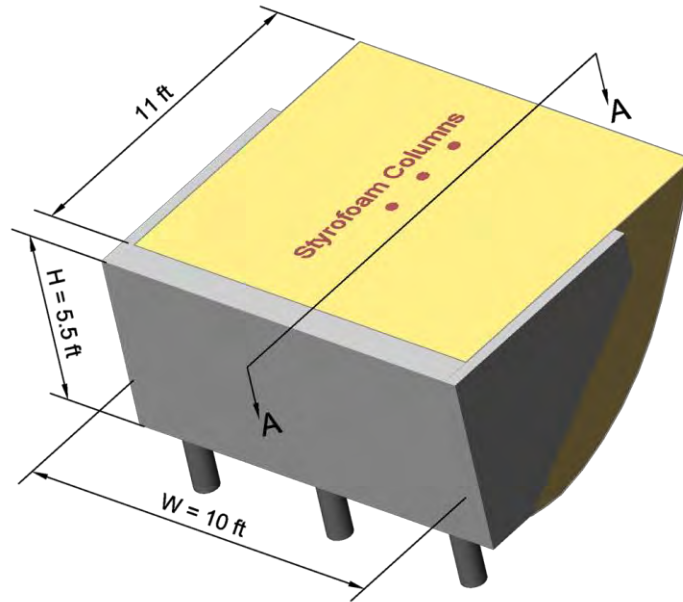


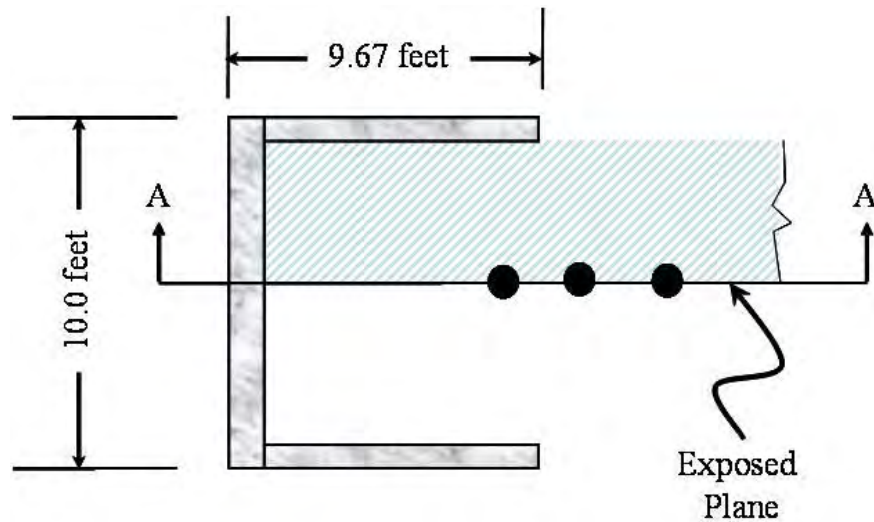
Figure 12-9 UCD Abutment Field Test



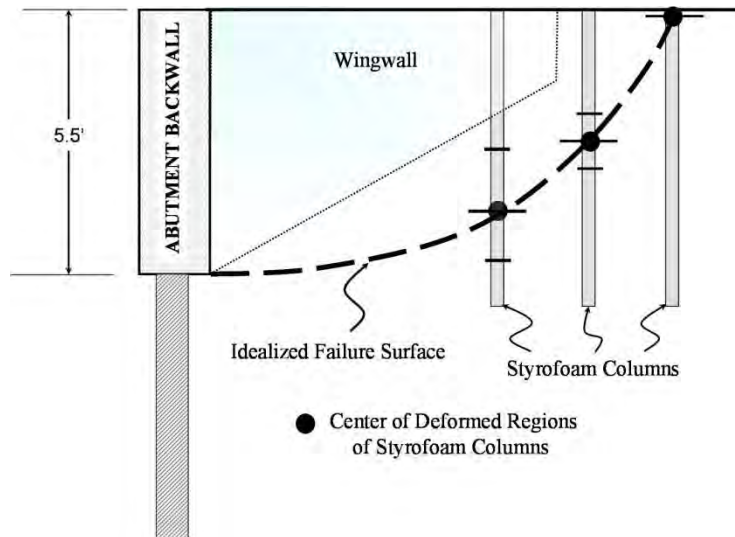
Figure 12-10 UCD Abutment Test Loading Setup

Before the loading the test abutment, 3-inch diameter vertical holes were drilled along the longitudinal centerline of the abutment backfill and filled with liquid Styrofoam, as illustrated in Figure 12-11. After the completion of the test, a longitudinal trench was excavated through the backfill and the backfill failure mechanism was carefully mapped using the displacement of the styrofoam columns as a guide (Romstad

et al., 1995). The approximate idealized failure surface mapped using the Styrofoam columns as a guide is shown in Figure 12-11. Maroney (1995) reported that the failure surface extended from the bottom of the abutment backwall at initially a zero slope upward to the embankment surface with increasing slope, intercepting embankment surface at a distance behind the wall approximately equal to twice the height of the backwall.



(a) Plan



(b) A-A Section

Figure 12-11 Failure Mechanism of the UCD Abutment Test

12.2 MODELING OF REGULAR (NON-SKEWED) ABUTMENTS

The complex nonlinear force-displacement response of bridge abutments subject to seismic loading is usually idealized using a simple, bi-linear relationship. Furthermore, presumptive values are often used to calculate this bi-linear relationship. The bi-linear relationship is then used to model the nonlinear behavior of the backfill as a set of independent horizontal springs, as illustrated in Figure 12-12. Various numerical simulations have been developed and calibrated using full-scale abutment experiments to develop simplified procedures for seismic analysis of bridge abutments. However, more realistic nonlinear force-displacement models have recently been developed to better characterize the seismic performance of abutment-backfill systems. Furthermore, advanced two- and three-dimensional models that employ the Finite Element (FE) method have been employed to investigate the mechanisms of backfill failure. Brief descriptions of each model are presented in the following sections.

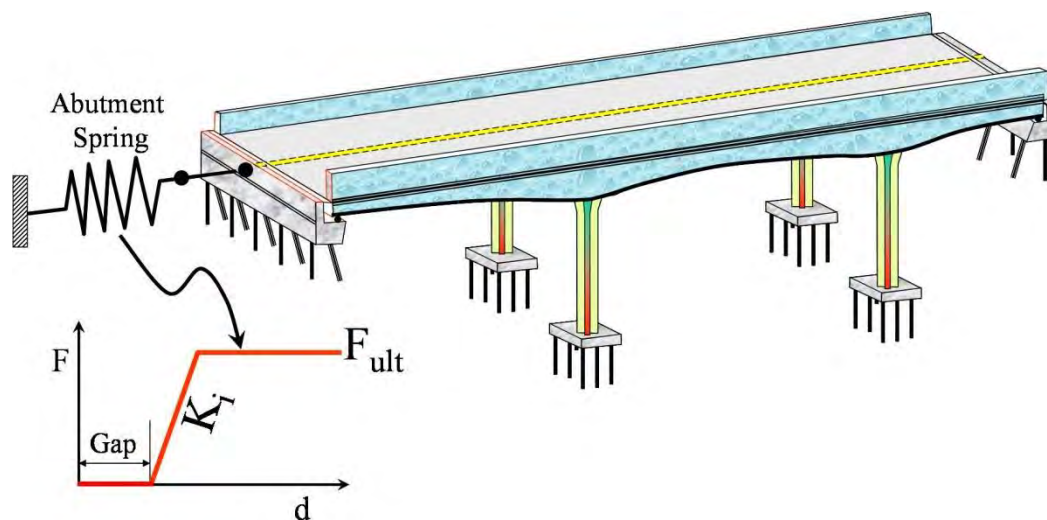


Figure 12-12 Bridge Model for Seat-Type Abutment with an Expansion Gap

12.2.1 Bi-linear Model

The bi-linear abutment force-deformation relationship assumes linear elastic stiffness, K_{Abut} , for all stress states below the backfill capacity (i.e. the passive resistance of the backfill). Once the backfill capacity, F_{Ult} , is reached, the abutment resistance remains constant with increasing displacement, d , as shown in Figure 12-13. For a seat-type abutment, an initial displacement equal to the gap between the bridge deck and the backwall, Δ_{gap} in Figure 12-13, is required to mobilize the backfill resistance. For design

purposes, the stiffness of seat-type abutment is then characterized by the effective abutment stiffness, K_{eff} , as illustrated in Figure 12-13.

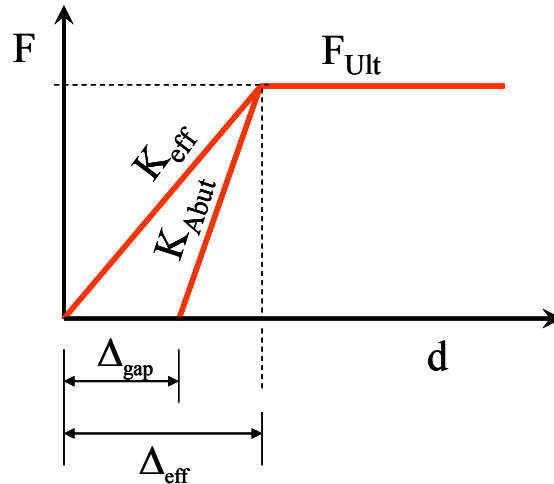


Figure 12-13 Bi-Linear Abutment Force-Deformation Relationship

The abutment passive capacity may be calculated using the methods for evaluating the passive resistance discussed in Chapter 9 (subject to certain limitations discussed subsequently). However, in bridge engineering practice, it is common to use a presumptive value to calculate the abutment capacity for seismic analysis and design. Section 5.2.3 of the AASHTO LRFD Guide Specification (AASHTO 2009) provides the following recommendations for the passive soil pressure, p_p , for backfill compacted to at least 95% of the modified Proctor maximum dry density:

- for cohesionless soil with less than 30%, by weight, passing the #200 sieve:

$$p_p = 2H/3 \text{ ksf} \quad 12-1a$$

where H is the wall height in feet; and

- for cohesive soil with greater than 15% clay-sized particles and an undrained shear strength of at least 4 ksf:

$$p_p = 5 \text{ ksf} \quad 12-1b$$

Note that p_p is the passive earth pressure and must be multiplied by the wall area to get the passive resistance, P_p . Also note that the AASHTO LRFD Guide Specifications state that owner's approval should be obtained if the engineer is going to rely upon a passive resistance greater than 70% of the presumptive passive resistance in seismic design (AASHTO 2009).

The abutment-backfill stiffness, K_{Abut} , is calculated by assuming that the passive resistance is mobilized at a deformation equal to the wall height, H , times the presumptive displacement factor F_w presented in Table 12-1. The abutment stiffness is therefore given by the following equation:

$$K_{Abut} = P_p/[H \times F_w] \quad 12-2$$

TABLE 12-1 PRESUMPTIVE DISPLACEMENT FACTORS, F_w (AASHTO 2009)

Soil Type	Dense Sand	Medium Dense Sand	Compacted Silt	Loose Sand	Compacted Clay
F_w	0.01	0.02	0.04	0.05	0.05

12.2.2 Non-Linear Hyperbolic Abutment Stiffness Relationship

Shamsabadi et al. (2007) summarized load-deflection test data from model tests and full-scale tests for a variety of structural backfills and concluded that the abutment- backfill load-displacement curve is approximately hyperbolic in shape, as shown in Figure 12-14. In the Shamsabadi et al. (2007) hyperbolic model illustrated in Figure 12-14, F_{ult} , the maximum abutment capacity, is developed at a maximum displacement y_{max} . The average soil stiffness, K , is defined at y_{ave} , the displacement corresponding to half of the maximum abutment force, $1/2F_{ult}$, by Equation 12-3:

$$K = \frac{\frac{1}{2} F_{ult}}{y_{ave}} \quad 12-3$$

The hyperbolic force-displacement relationship shown in Figure 12-14 can then be expressed as:

$$F(y) = \frac{Ay}{1 + By} \times H^n \quad 12-4$$

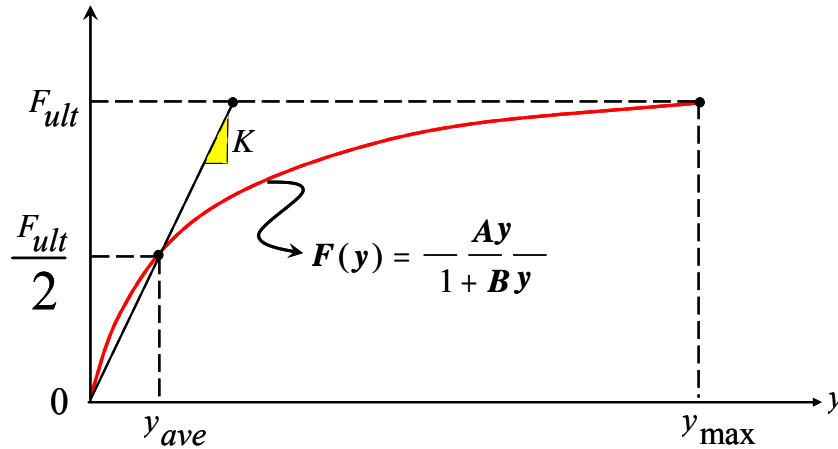


Figure 12-14 Closed-Form Solution

The constants A and B can be related to the key parameters ($K, F_{ult}, y_{max}, y_{ave}$) as follows:

$$A = \left(2K - \frac{F_{ult}}{y_{max}} \right) \quad 12-5$$

$$B = 2 \left(\frac{K}{F_{ult}} - \frac{1}{y_{max}} \right) \quad 12-6$$

The maximum wall displacement y_{max} in Equation 12-6 can be estimated from:

$$\begin{aligned} y_{max} &= 0.05H \text{ For Granular Backfill} \\ y_{max} &= 0.10H \text{ For Cohesive Backfill} \end{aligned} \quad 12-7$$

where H is the wall height. Based on experimental data and parametric studies, the exponent n can be assumed equal to 1.5 and the hyperbolic force-displacement relationships per foot of abutment-backwall for cohesionless and cohesive backfills, respectively, can be expressed as:

$$F(y) = \frac{8y}{1+3y} H^{1.5} \quad (\text{y in inches, } F \text{ in kips per ft of wall}) \quad 12-8$$

$$F(y) = \frac{8y}{1+1.3y} H^{1.5} \quad (\text{y in inches, } F \text{ in kips per ft of wall}) \quad 12-9$$

12.2.3 Advanced Numerical Analysis

The most common numerical method used in the geotechnical engineering to solve complicated soil-structure interaction problems is the finite element method (FEM). Numerical simulations for the full-scale Caltrans-UCLA abutment test were carried out using the FEM model to calculate the nonlinear backbone force-displacement curves and to investigate the failure mechanism of the abutment backfill (Shamsabadi et. al., 2009). The 2-D finite element mesh used in this analysis is shown in Figure 12-15.

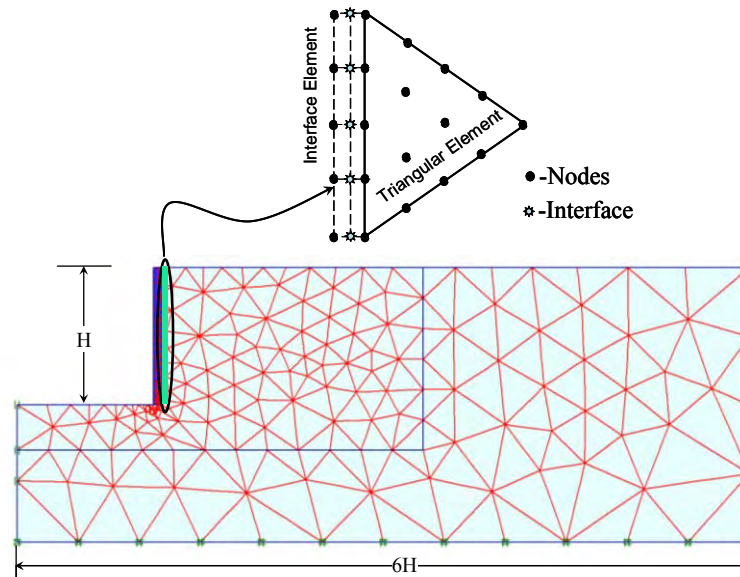


Figure 12-15 2-D finite Element Mesh of Bridge Abutment

The abutment backwall-backfill interaction was modeled in the FE analysis with interface elements. The shear strength of the interface was established by applying a suitable reduction factor to the shear strength of the backfill. The deformed mesh after loading of the wall to failure is presented in Figure 12-16.

Figure 12-16 clearly shows that the failure surface for the passive wedge behind the wall is a logarithmic spiral in shape.

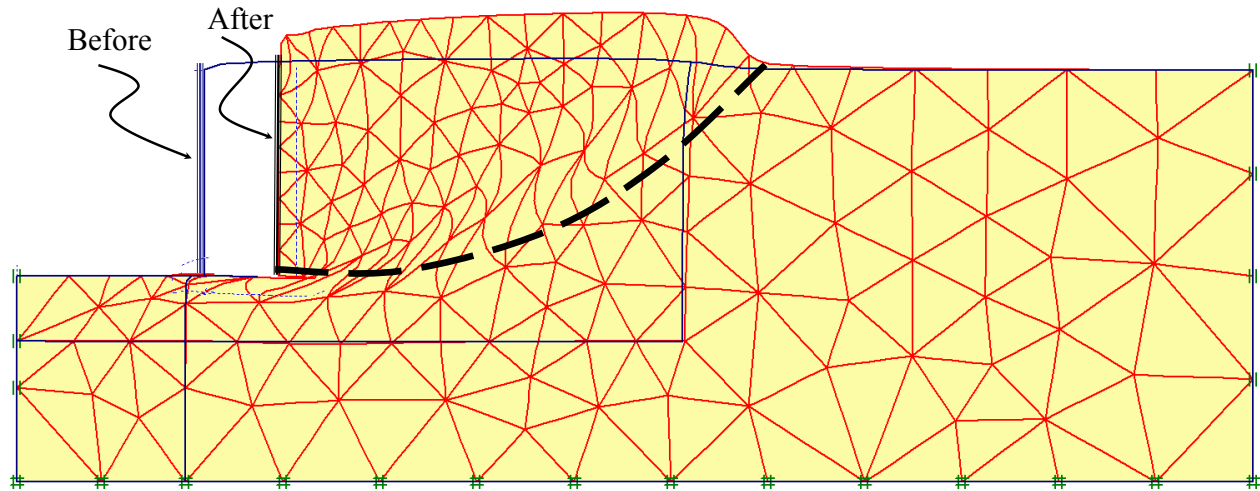


Figure 12-16 Deformed Shape of Abutment Backfill in Simulation by the 2-D FEM Model

12.2.4 Global Backwall-Backfill Longitudinal Response

To evaluate the interaction behavior of an abutment with the bridge superstructure, a global three-dimensional nonlinear dynamic analysis of the concrete box-girder bridge shown in Figure 12-17 was performed using a zero skew angle (Shamsabadi, 2007). The interaction between abutments and backfill was modeled by four nonlinear soil springs, denoted A, B, C and D, oriented normal to the backwall at each abutment. Each spring was modeled by a nonlinear plasticity link element. The model was excited by the near-field earthquake motion with a high-velocity pulse shown in Figure 12-18.

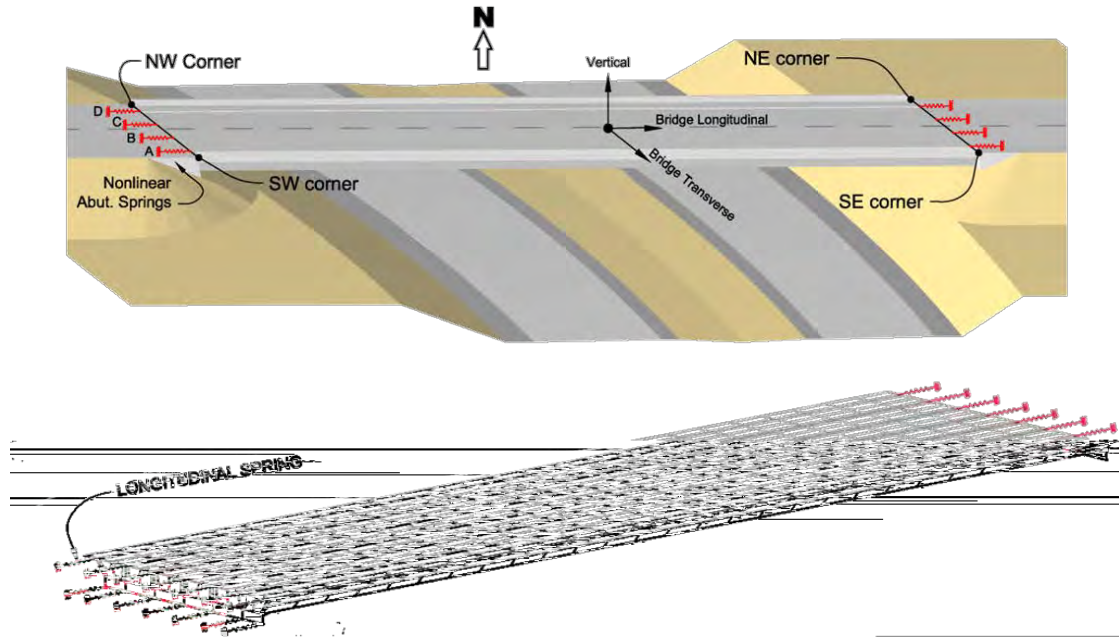


Figure 12-17 Bridge and Abutment Model

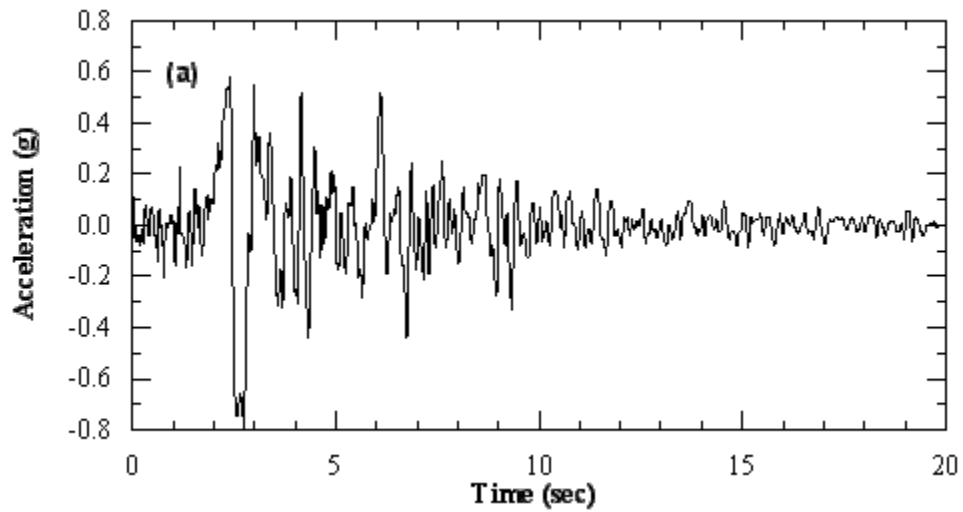


Figure 12-18 Near-field Ground Motion with High Velocity Pulse

Figure 12-19 shows the hysteretic abutment-backfill force-displacement response due to the input acceleration time history shown in Figure 12-18. It can be observed that the ultimate abutment passive force is fully developed at both abutments.

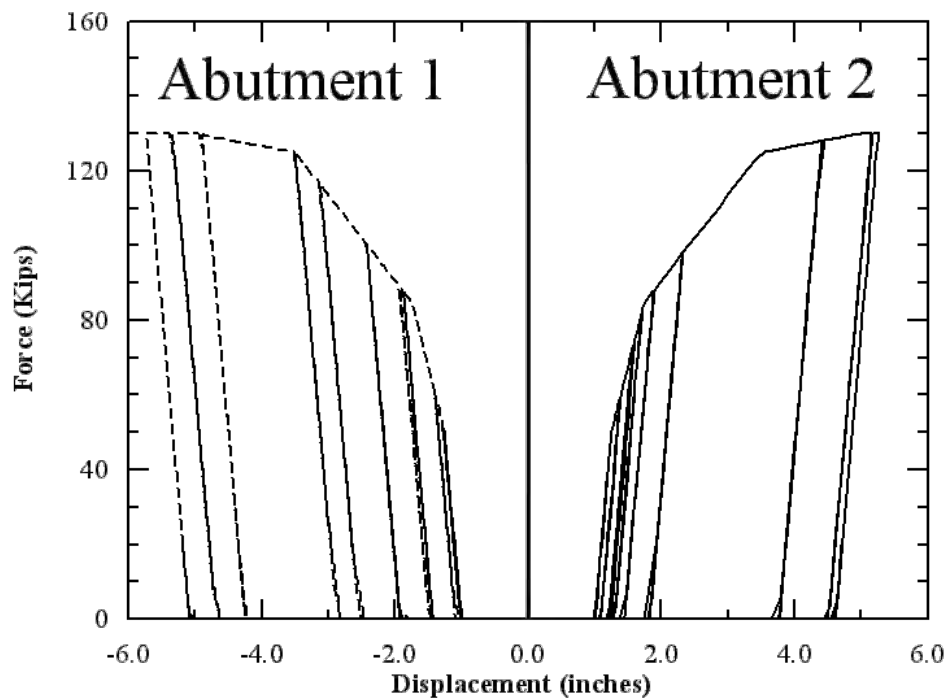


Figure 12-19 Longitudinal Hysteretic Behavior of a Single-Span Bridge Abutment

12.3 MODELING OF SKEWED ABUTMENTS

Due in part to the complexities of modeling skewed abutments, AASHTO recommends avoiding skewed abutments or minimizing the skew when it cannot be avoided. During seismic events, the bridge deck in a skewed abutment may experience significant rotational motions about its vertical axis, as illustrated in Figure 12-20. As a result, the opposite corners of the deck first “collide” with the abutment and then rotate away from the abutment, resulting in the separation of the deck from the abutment (for a seat-type abutment).

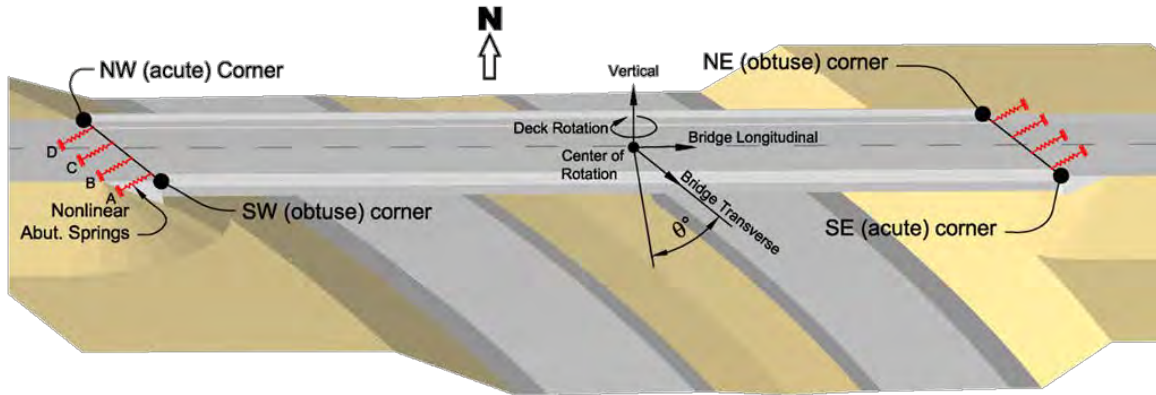


Figure 12-20 Deck Rotation in a Bridge with Skewed Abutments During a Seismic Event

Inspection of skewed abutments after recent earthquakes indicates that the passive wedges that form behind the skewed walls tend to be asymmetric along the abutment backwall due to deck rotation. Such behavior was observed at the northern abutment of the skewed Wushi highway bridge in Taiwan that was severely damaged during the recent Chi-Chi earthquake, as shown in Figure 12-21.

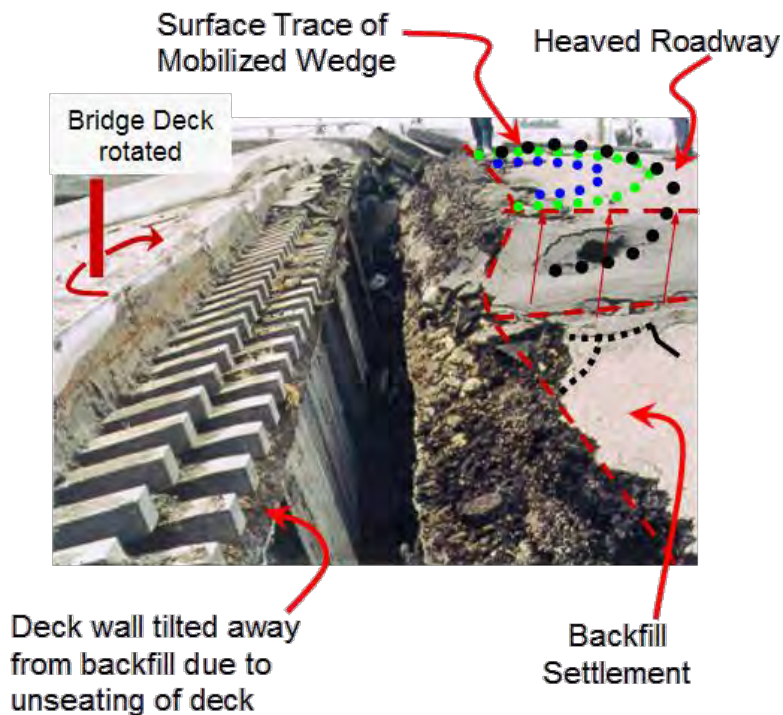


Figure 12-21 Non-Uniform Passive Wedge behind a Skewed Abutment

12.3.1 3-D Finite Element Model of the Abutment Backfill

A set of 3-D FE analyses was performed to evaluate the development of passive resistance behind a 75-foot wide abutment with a 5.5-foot high backwall of varying skew angles (Shamsabadi, 2007). First, a non-skewed abutment was loaded. The formation of a uniform mobilized passive wedge behind the abutment wall and the associated displacement contours are shown in Figure 12-22.

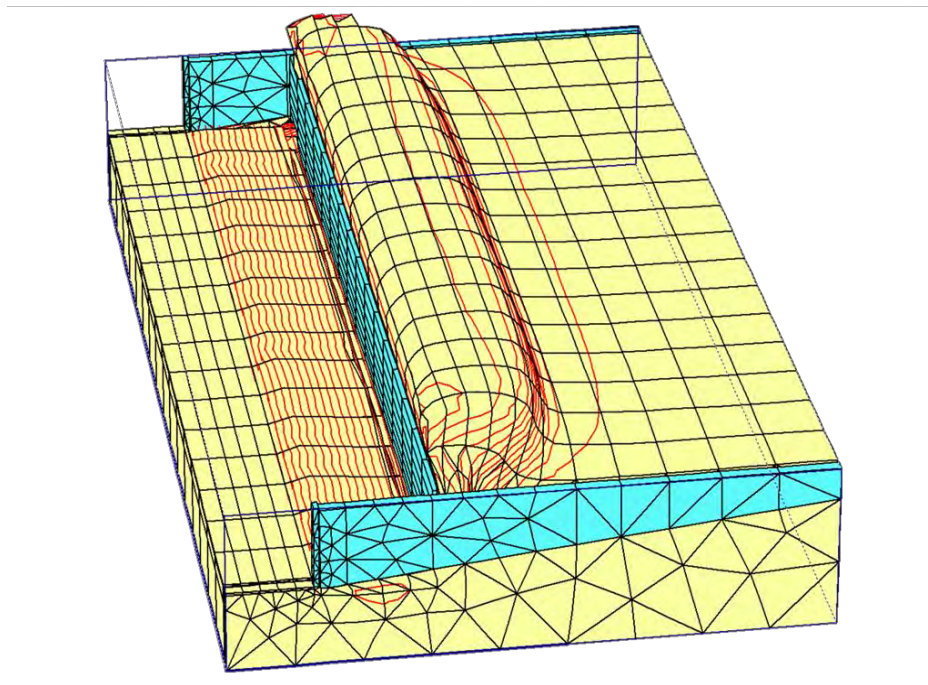


Figure 12-22 Passive Soil Wedge in a Non-Skewed Abutment

The same 3-D FE model was then used to investigate the failure mechanism of skewed-abutments with various skew angles. Figure 12-23 shows the shape of the 3-D passive wedge formed between the wingwalls of an abutment with 45° skew. The FE analyses showed that, as a result of deck clockwise rotation, the abutment backwalls tend to be pushed primarily into the obtuse corners of the deck, causing asymmetric passive wedges to form behind the abutment backwall. Furthermore, the non-uniform loading of the skewed abutment backwall can result in a reduced mobilized soil capacity compared to an ordinary non-skewed abutment. The ground heave at the far side of the wall in Figure 12-23 illustrates the overstress and breakdown of the passive wedge in a skewed abutment, resulting in reduction of soil resistance normal to the abutment backwall.

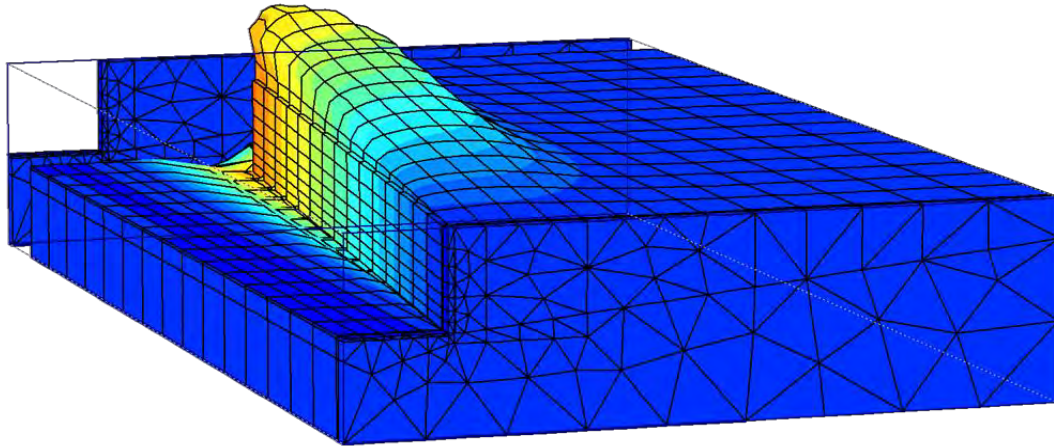


Figure 12-23 3-D FE Model of Passive Wedge Formation behind a Skewed Abutment

12.3.2 Load-Deformation Relationship

Due to the in-plane motions and compressive pounding forces of the bridge deck in a skewed abutment system, the abutment-backfill response consists of both normal and tangential passive resistance. Figure 12-24 shows an example of the nonlinear tangential and normal components of 30° skewed-abutment-backfill backbone curves. Therefore, in the global seismic analysis of the skew bridges both the tangential and normal components of the abutment backfill force should be considered. The tangential component of passive resistance for the abutment with 30° skewed-angle in this example was about one third of the normal component.

The normal components of the abutment passive resistance for various skew angles are shown in Figure 12-25. These results indicate that the mobilized passive capacity might decrease as a function of skew angles at large displacement levels.

From the computer simulations described above, it was found that the skewed abutment develop an asymmetric passive soil wedge that is less wide and generates less soil resistance than the passive wedge that forms behind a non-skewed abutment. The size (width) and capacity of the skew-affected passive wedge depends on abutment's backwall width and the skew angle, which influence the interaction of the bridge deck with the abutment. Soil resistance is not seen to increase with higher skew angles, as might be expected from a combination of passive resistance normal to the wall and the additional soil traction

developed along the back face of the abutment wall. These analyses indicate that the width and total resistance of the mobilized passive wedge is a maximum for zero skew and decreases as the magnitude of skew angles is increased. Full-scale field experiments at UCLA are planned by Caltrans to investigate the formation and force-displacement capacity of the soil backfill behind a skewed abutment wall.

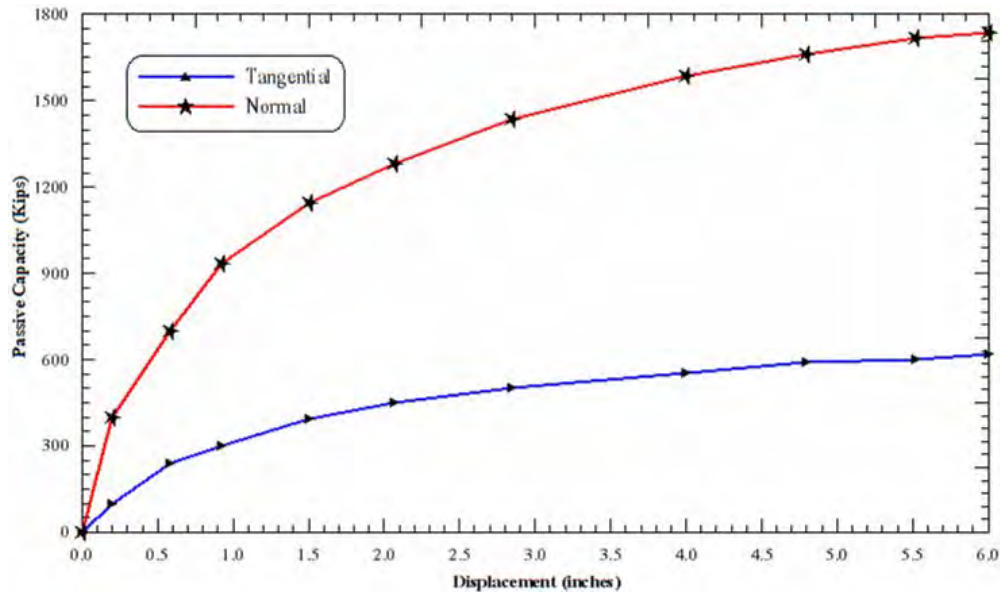


Figure 12-24 Nonlinear Normal and Tangential Components of Abutment-Backfill Resistance for a 30° Skew

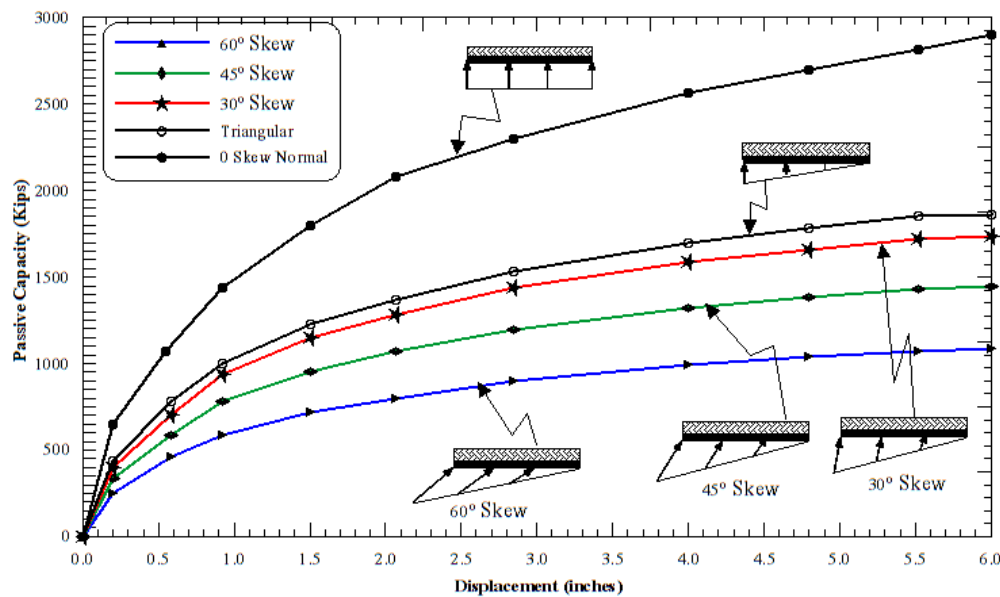


Figure 12-25 Impact of Skew Angles on Nonlinear Abutment Force-Deformation Relationship

12.3.3 Effects of Skew Angles on the Bridge Abutment Global Response

It has been long recognized that ground motions with asymmetrical and high amplitude velocity pulse characteristics have a tendency to produce a biased, one-sided response of the bridge structure. This tendency is exacerbated in a bridge with a skewed abutment, as the asymmetrical impulsive loading generates large displacements in one direction, leading to significant rotation and residual displacement of the bridge. To evaluate the interaction behavior of a skewed bridge deck with a skewed abutment, a global three-dimensional nonlinear dynamic model of the single span bridge shown in Figure 12-26 was performed using a 45 degree skew angle (Shamsabadi, 2007). The interaction between abutments and backfill was modeled by rows of four nonlinear soil springs, denoted A, B, C and D, oriented normal to the backwall at each abutment. The model was excited by the two horizontal components of the earthquake motion with a high-velocity pulse.

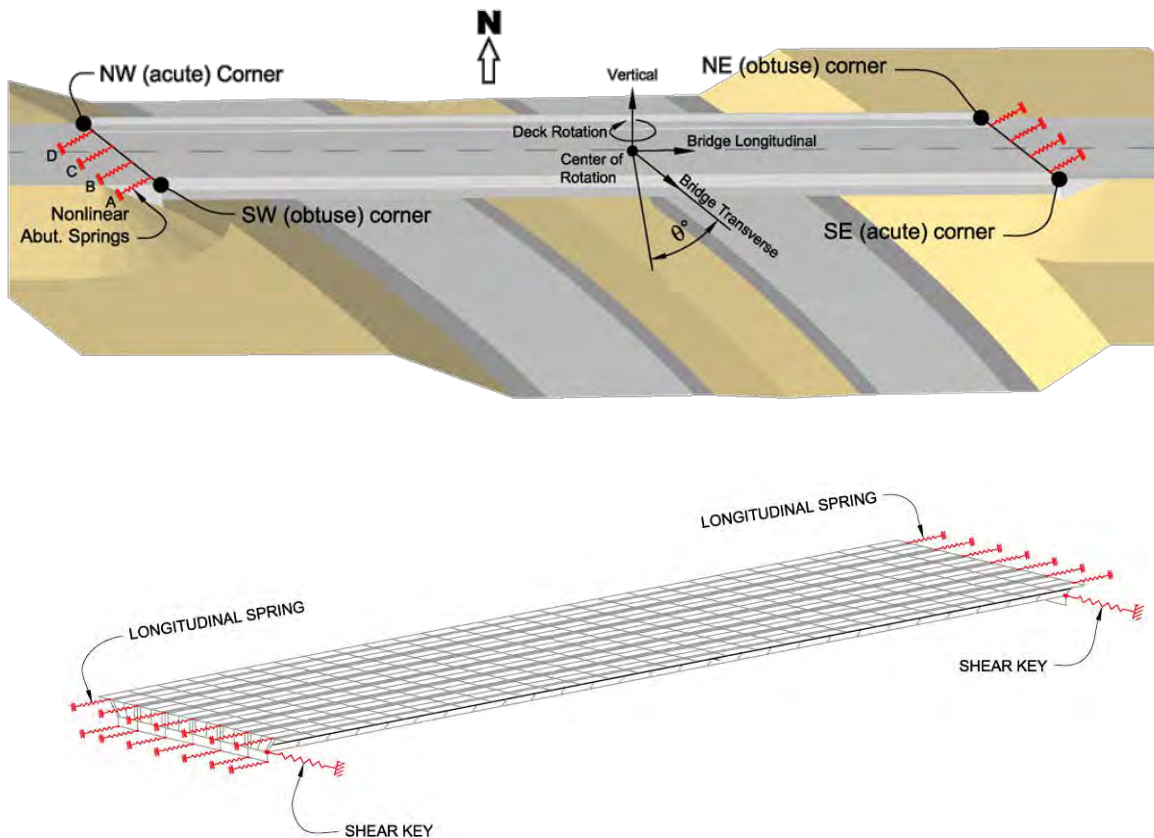


Figure 12-26 Single Span Bridge 45° Skew Angles

Figure 12-27 shows the hysteretic behavior of the abutment backfill at the obtuse corner (south west) and acute corner (south east) of the 45 degree skewed-bridge abutment due to the input motion. As the result of bridge rotation, the obtuse corners of the bridge deck have been pushed into the abutment backfill and the passive force is fully mobilized, while the acute corners have moved away from the abutment backfill and the passive wedge has been mobilized only partially.

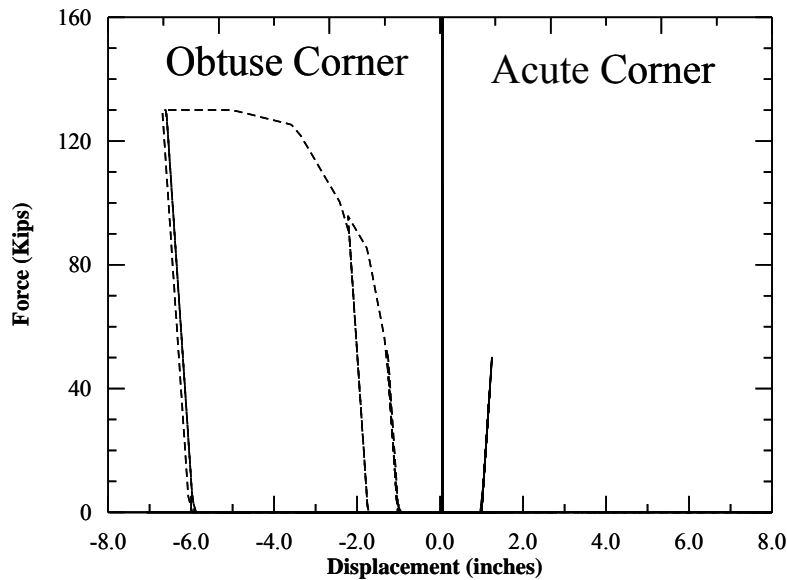


Figure 12-27 Hysteretic Abutment Response Obtuse and Acute Corner of the Single-Span Bridge with 45° Skew Angle

12.4 SUMMARY

LRFD seismic design of bridge abutments is often based on a displacement performance philosophy. This type of design necessitates that the geotechnical engineer predict the resistance of the abutment backfill soils to large displacements. Characterization of the inherently non-linear stiffness of the abutment-backfill system is also necessary if the designer wishes to consider the interaction between the bridge superstructure and the abutments in the global bridge model. The abutment-backfill can not only provide significant lateral resistance but is also a good source of energy dissipation at large deformation due to nonlinear hysteretic behavior of the abutment-soil system.

Abutment capacity is provided by the passive resistance of the abutment backfill. Seat-type abutments have a backwall with a depth sufficient to accommodate the bridge deck depth and the bridge deck rests on the abutment seat through bearings pads. In an ordinary bridge designed to a life safety standard, the

backwall may be designed to break off in the design earthquake in order to protect the foundation from inelastic action as a result of backwall displacement. Monolithic abutments are cast integrally with the superstructure and are supported on either spread footings or pile foundations. For monolithic abutments, the backwall engages the backfill immediately when the bridge is displaced longitudinally. The lateral force-deformation capacity of the monolithic abutment is a function of abutment backfill properties as well as foundation and structural capacity of the abutment backwall. Contrary to the seat-type abutment, a monolithic abutment wall may have to sustain large forces during a major seismic event if the backwall capacity is greater than the passive resistance of the backwall. However, if the backwall has been designed to be weaker than the passive earth pressure exerted by the abutment backfill, the effective abutment height is limited to the depth of the bridge deck and the resistance of the abutment is controlled by the passive resistance associated with this effective backfill height.

Post earthquake investigations and full scale field experiments have shown that during a major seismic event mobilized passive wedges will form within the abutment backfill. The force-displacement response of bridge abutments subject to seismic loading is usually idealized using a simple, bi-linear relationship. The bi-linear relationship is then used to model the nonlinear behavior of the backfill as a set of independent horizontal springs. The bi-linear abutment force-deformation relationship assumes linear elastic stiffness, K_{Abut} , for all stress states below the backfill capacity (i.e. the passive resistance of the backfill). Once the backfill capacity is reached, the abutment resistance remains constant with increasing displacement. For a seat-type abutment, an initial displacement equal to the gap between the bridge deck and the backwall is required to mobilize the backfill resistance. For design purposes, the stiffness of seat-type abutment is then characterized by the effective abutment stiffness, K_{eff} . The abutment passive capacity may be calculated using the methods for evaluating the passive resistance discussed in Chapter 9 (subject to certain limitations discussed subsequently). However, in bridge engineering practice, it is common to use a presumptive value to calculate the abutment capacity for seismic analysis and design.

Field data has provided a basis for the development of more realistic hyperbolic force-displacement models to better characterize the seismic performance of abutment-backfill systems. Furthermore, advanced two- and three-dimensional models that employ the Finite Element (FE) method have been employed to investigate the mechanisms of backfill failure.

Due in part to the complexities of modeling skewed abutments, skewed abutments should be avoided or the skew minimized when it cannot be avoided. Inspection of skewed abutments after recent earthquakes indicates that the passive wedges that form behind the skewed walls tend to be asymmetric along the

abutment backwall due to deck rotation. Furthermore, both the tangential and normal components of the abutment backfill force should be considered. For example, the tangential component of passive resistance for an abutment with 30° skewed-angle was about one third of the normal component in the example presented at the end of this chapter.

CHAPTER 13

BURIED STRUCTURES

13.1 GENERAL

This chapter presents rational procedures for seismic evaluation of buried structures that are used as part of highway facilities, including culverts and pipelines. Buried structures, in general, have performed better during earthquakes than have above ground structures such as bridges and buildings. Buried structures are constrained by the surrounding ground and, in general, cannot be excited independent of the ground or be subject to strong vibratory amplification, such as the inertial response of a bridge structure during earthquakes. Adequate design and construction of seismic resistant culvert/pipeline structures, however, should never be overlooked, as moderate to major damage has been experienced by many buried structures during earthquakes.

The general procedure for seismic design and analysis of buried structures should be based primarily on the ground deformation approach (as opposed to the inertial force approach); i.e., the structures should be designed to accommodate the deformations imposed by the ground. This chapter presents the deformation-based procedure for seismic design and analysis of buried structures. The following general subjects are discussed in this chapter: (1) seismic performance and vulnerability of buried structures, (2) general characteristics and properties of these structures, (3) potential failure modes when subject to seismic loading, (4) seismic loads on buried structures, (5) simplified procedure for ovaling of circular buried structures and racking of rectangular buried structures, (6) numerical modeling, and (7) a general design approach to permanent ground displacement (PGD).

13.2 SEISMIC PERFORMANCE OF CULVERTS AND PIPELINES

Damage to buried culverts and pipelines during earthquakes has been observed and documented by previous investigators (Davis and Bardet, 1999 and 2000; NCEER, 1996; O'Rourke, 1999; Youd and Beckman, 2003). In general, buried structures have performed better in past earthquakes than above-ground structures. Seismic performance records for culverts and pipelines have been very favorable, particularly when compared to reported damages to other highway/transportation structures such as bridges.

The main reason for the good performance of buried structures has been that buried structures are constrained by the surrounding ground. It is unlikely that they could move to any significant extent independent of the surrounding ground or be subjected to vibration amplification/resonance. Compared to surface structures, which are generally unsupported above their foundations, buried structures can be considered to display significantly greater degrees of redundancy thanks to the support from the ground. The good performance may also be partly associated with the design procedures used to construct the embankment and backfill specifications for the culverts and pipes. Typical specifications require close control on backfill placement to assure acceptable performance of the culvert or pipe under gravity loads and to avoid settlement of fill located above the pipe or culvert, and these strict requirements for static design lead to good seismic performance.

It is important that the ground surrounding the buried structure remains stable. If the ground is not stable and large permanent ground deformation (PGD) occur (for example, resulting from liquefaction, settlement, uplift, lateral spread, or slope instability/landslide) then significant damage to the culvert or pipe structures can be expected. Although transient ground deformation (TGD) due to shaking can also damage buried structures, compared to the effects of PGD, the damage is typically of a more limited extent.

13.3 CULVERT/PIPE CHARACTERISTICS

Culvert/pipe products are available over a large range in terms of material properties, geometric wall sections, sizes, and shapes. Pipe sizes as small as 1 foot and as large as culverts that span 40 feet and larger are used in highway applications. They can be composed of concrete, steel, aluminum, plastic, and other materials. Detailed information about their shapes, range of sizes, and common uses for each type of culvert or pipe are summarized by Ballinger and Drake (1995).

13.3.1 Flexible Culverts and Pipes

In general, culverts and pipes are divided into two major classes from the static design standpoints: flexible and rigid. Flexible culverts and pipes typically are composed of either metal (for example, corrugated metal pipe, CMP, made of steel or aluminum) or thermoplastic materials (for example, HDPE or PVC). Flexible culverts and pipes respond to loads differently than rigid culverts/pipes. Because their ovaling stiffness is small relative to the adjacent soil, flexible culverts and pipes rely on firm soil support

and depend upon a large strain capacity to interact with the surrounding soil to hold their shape while supporting the external pressures imposed upon them.

For static design, current AASHTO *LRFD Bridge Design Specifications* require as a minimum the following main design considerations (in addition to the seam failure) for flexible culverts and pipes: (1) buckling (general cross sectional collapse as well as local buckling of thin-walled section), and (2) flexibility limit for construction. Except for large box structures or other large spans with shapes other than circular (NCHRP Report No. 473, 2002), the flexural strength consideration (i.e., bending moment demand) is generally not required for flexible culverts and pipes.

Neither current AASHTO *LRFD Bridge Design Specifications* nor the NCHRP (2002) study has addressed seismic design concerns for culvert structures. From the seismic design standpoint, there are two main factors that should be considered:

- 1) Seismic loading is in general non-symmetric in nature and therefore may result in sizable bending in the culvert structures (even for circular shape culverts). Furthermore, the behavior of thin-walled conduits (such as for the flexible culverts and pipes) is vulnerable to buckling. This behavior differs somewhat from that of a rigid concrete culvert structure, for which bending moments are often the key factor by which to judge structural performance. For buckling, thrust (that is, hoop force) is the key factor and seismically induced thrust can be significant, particularly if the interface between the culvert or pipe structure and the surrounding soil is considered a non-slip condition (Wang, 1993). Therefore, it is important that both seismically induced bending and thrust be evaluated using published solutions for circular tube (Moore, 1989; Janson, 2003) as failure criteria for evaluating the seismic performance of CMP and polymeric conduits (for example, corrugated HDPE pipes).
- 2) Implicit in the current AASHTO design assumptions for flexible culverts is the existence of adequate soil support. This may happen to be the weakness of flexible culverts in case of earthquakes in that the soil support can be reduced or lost during liquefaction or other permanent ground failure mechanisms associated with seismic events. Significant distortion or collapse of the culvert cross section is likely if soil support is reduced or lost.

13.3.2 Rigid Culverts and Pipes

Rigid highway culverts and pipes consist primarily of reinforced concrete shapes that are either precast or cast-in-place. Unreinforced concrete culverts and pipe structures are not recommended for use in seismic regions. The sizes of reinforced concrete pipe (RCP) range (in diameter) from about 1 foot to 12 feet. Larger RCP can be precast on the site or constructed cast-in-place. Rectangular four-sided box culverts can be furnished precast in spans ranging from 3 feet to 12 feet. Larger spans can be constructed cast-in-place. Three-sided precast box culverts can be furnished in spans up to 40 feet.

Unlike the flexible culverts and pipes, the strain capacity of rigid culverts and pipes is much lower. Therefore, rigid culverts must develop significant ring stiffness and strength to support external pressures. Hence, they are not as dependent upon soil support as flexible culverts.

For static design the primary design methods used for precast concrete pipe, either reinforced or unreinforced, include: (1) the Indirect Design Method, based on the laboratory three-edge bearing strength test, (2) a more direct design procedure that accounts for bending moment, shear, thrust/tension, and crack width (buckling is generally not an issue with rigid culverts/pipes) around the periphery of the culvert wall, and (3) methods employing computerized numerical models accounting for the soil-structure interaction effects.

For box culverts the static design uses the same criteria as other reinforced concrete structures (for example, beams and columns). In general, the effect of surrounding soils is accounted for by applying the soil pressures (active or at-rest) directly against the wall in the model, instead of fully taking advantage of the soil-structure interaction effect. Most current commercially available computer software can perform the structural analysis required for this design. For other structural shapes, consideration of soil-structure interaction becomes important and therefore is generally accounted for by using computerized numerical models.

13.4 GENERAL EFFECTS OF EARTHQUAKES AND POTENTIAL FAILURE MODES

The general effects of earthquakes on culverts and pipe structures can be grouped into two broad categories – *ground shaking* and *ground failure*. The following sections discuss each of these categories. As it will be demonstrated, soil-structure interaction plays a critical role in the evaluation of the effect of

seismic loading for both flexible and rigid culverts and pipes. A unified evaluation procedure is developed in this chapter to provide a rational and reliable means for seismic evaluations as well as realistic design for buried culvert and pipe structures.

13.4.1 Ground Shaking

Ground shaking refers to the vibration of the ground produced by seismic waves propagating through the earth's crust. The area experiencing this shaking may cover hundreds of square miles in the vicinity of the fault rupture. The intensity of the shaking attenuates with distance from the fault rupture.

Ground shaking motions are composed of two different types of seismic waves, each with two subtypes:

- Body waves travel within the earth's material. They may be either longitudinal compressional (P-) waves or transverse shear (S-) waves, and they can travel in any direction in the ground.
- Surface waves travel along the earth's surface. They may be either Rayleigh waves or Love waves.

As a stable ground is deformed by the traveling waves, any culverts or pipelines in the ground will also be deformed. The shaking or wave traveling induced ground deformations are called transient ground deformations (TGD).

When subject to TGD, the response of a buried linear culvert or pipe structure can be described in terms of three principal types of deformations: (1) axial deformations, (2) curvature deformations (refer to Figure 13-1), and (3) ovaling (for circular cross section) or racking (for rectangular cross section) deformations (refer to Figure 13-2).

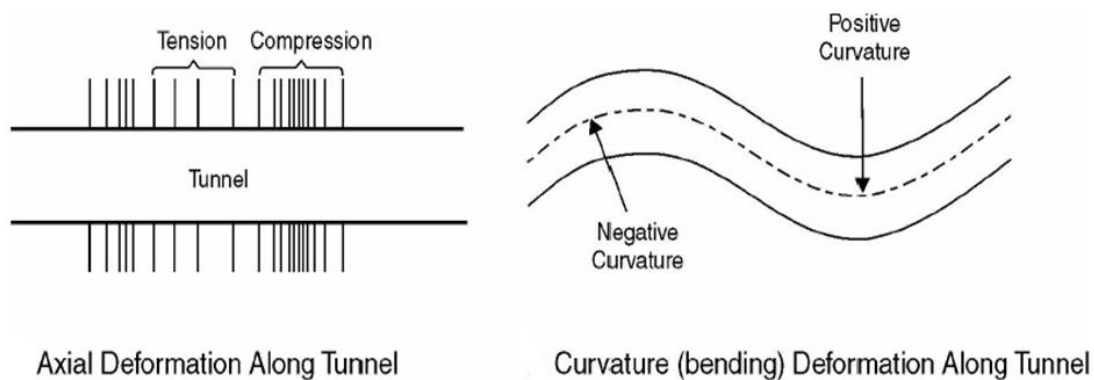


Figure 13-1 Longitudinal Axial and Curvature Response to Traveling Waves

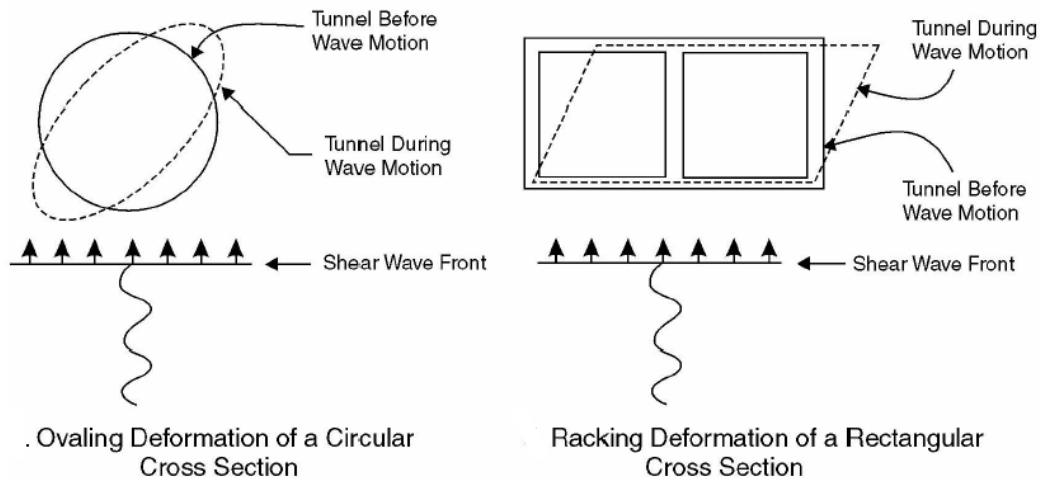


Figure 13-2 Transverse Ovaling and Racking Response to Vertically Propagating Shear Waves

The axial and curvature deformations are induced by components of seismic waves that propagate along the culvert or pipeline axis. Figure 13-1 shows the idealized representations of axial and curvature deformations. The general behavior of the linear structure is similar to that of an elastic beam subject to deformations or strains imposed by the surrounding ground.

Current design and analysis methodology for pipeline systems was developed typically for long, linear structures. The principal failure modes for long, continuous pipeline structures consist of (1) rupture due to axial tension (or pull out for jointed segmented pipelines), and (2) local buckling (wrinkling) due to axial compression and flexural failure. If the pipelines are buried at shallow depth, continuous pipelines in compression can also exhibit beam-buckling behavior (that is, global buckling with upward buckling deflections). If the axial stiffness of the structures is large (such as that for a large sectional concrete pipe), then the buckling potential in the longitudinal direction is small (for both local buckling and global buckling). The general failure criteria for the above-mentioned potential failure modes have been documented by previous studies (O'Rourke and Liu, 1996).

It should be noted, however, that typical culvert structures for transportation applications are generally of limited length. Therefore this condition is unlikely to develop significant transient axial/curvature deformations along the culvert structures. The potential failure modes mentioned above are not likely to take place during the earthquake. Important pipeline structures with a long length, such as gas, sewer, or

water pipeline, are generally not designed as a part of the highway facility. The main focus of this chapter therefore will not be on the effects of axial/curvature deformations. Instead, the scope of this chapter will concentrate on transverse deformations of culverts and pipes, as discussed below.

The ovaling or racking deformations of a buried culvert or pipe structure may develop when waves propagate in a direction perpendicular or nearly perpendicular to the longitudinal axis of the culvert or pipe, resulting in a distortion of the transverse cross-sectional shape of the structure. Figure 13-2 shows the ovaling distortion and racking deformation associated with a circular culvert or pipe and a rectangular culvert, respectively. In this figure, vertically propagating shear waves (with soil particles moving horizontally in back-and-forth motions) from the base of a soil column caused shear displacement in the ground which in turns caused the ovaling/racking displacements in the structure lining. The general behavior of the structure may be simulated as a buried structure subject to ground deformations under a two-dimensional, plane-strain condition.

Ovaling and racking deformations may be caused by vertically, horizontally, or obliquely propagating seismic waves of any type. Many previous studies have suggested, however, that the vertically propagating shear wave is the predominant form of earthquake loading that governs the ovaling/racking behavior for the following reason: (1) except possibly in the very near-source areas, ground motion in the vertical direction is generally considered less severe than its horizontal component, (2) vertical ground strains are generally much smaller than shearing strain because the value of confined modulus of compressibility is much higher than that of the shear modulus, and (3) the amplification of vertically propagating shear wave, particularly in the soft/weak soils, is much higher than vertically propagating compressional wave and any other type of waves traveling in the horizontal direction. Therefore the analysis and methodology presented in this chapter addresses mainly the effects of vertically propagating shear waves on ovaling/racking behavior of the buried culverts or pipes.

When subject to ovaling/racking deformations, a flexural type failure mode due to the combined effects of bending moment and thrust force must be checked. The flexural failure mode is typically the main concern for rigid culverts and pipes, such as those constructed with reinforced concrete. For flexible culverts and pipes (typically, thin-walled conduits constructed with steel, aluminum, or thermoplastic such as HDPE or PVC), they are likely to be controlled by buckling, which can occur in the elastic range of stresses. For buckling, thrust is the key factor and conservative assumption must be made regarding interface condition (slip or non-slip) between the exterior surface of the conduit and the surrounding

ground. An elastic buckling criterion for circular conduits in uniform soil was proposed by Moore (1989) and may be used for buckling potential evaluation purpose.

13.4.2 Ground Failure

Ground failure broadly includes various types of ground instability such as faulting, landslides, liquefaction (including liquefaction-induced lateral spread, settlement, floatation, etc.), and tectonic uplift and subsidence. These types of ground deformations are called Permanent Ground Deformations (PGD). Each of these PGDs may be potentially catastrophic to culvert or pipeline structures, although the damages are usually localized. To avoid such damage some sort of ground improvement is generally required, unless the design approach to this situation is to accept the displacement, localize the damage, and provide means to facilitate repairs.

The characteristics of PGD and its effects on culvert and pipes are extremely complex and must be dealt with on a case-by-case basis. It is unlikely that simple design procedures or solutions can be developed due to the complex nature of the problem. In this chapter, detailed study of problems associated with PGD will not be conducted. Instead, only general guidelines and recommendations on methodology for seismic evaluation under the effects of PGD will be provided.

13.5 CURRENT SEISMIC DESIGN PRACTICE FOR BURIED STRUCTURES

Currently there is no standard seismic design methodology or guidelines for the design of culvert structures, including Section 12 within the current AASHTO *LRFD Bridge Design Specifications*. The NCHRP Report 473 *Recommended Specifications for Large-Span Culverts*, (NCHRP, 2002) does not address issues related to seismic evaluation of long-span culverts.

In the past, design and analysis procedures have been proposed by some researchers and design engineers for pipelines (for example, gas and water) or tunnel (that is, transportation or water) systems. While some of these procedures can be used for the design and analysis of culvert and pipes (for example, the transverse ovaling/racking deformation of the section, Figure 13-2), others cannot be directly applied because they are only applicable for buried structures with a long length, or with a deep burial depth. Furthermore, significant disparity exists among engineers regarding the appropriate design philosophy and methods of analysis that is applicable to various types of culvert structures. The following paragraphs

provide a brief description of some procedures and methodologies proposed in the past for seismic evaluation of buried structures in general.

O'Rourke (1998) provides a general overview of lifeline earthquake engineering, including the treatment of seismic evaluation of pipelines. O'Rourke and Liu (1996) present a detailed methodology for evaluating response of buried pipelines subject to earthquake effects. Pipelines response to both TGD and PGD were addressed in these two studies. However, the focus of these studies was on pipeline behavior in the longitudinal direction which is more suitable for a long continuous buried pipeline structure. Although failure criteria for axial tension and axial compression (local buckling/wrinkling and beam buckling) were developed, there were no discussions related to the procedure for evaluating the transverse ovaling deformation of the pipe's cross-sectional behavior.

Based on the field performance of 61 corrugated metal pipes (CMP) that were shaken by the 1994 Northridge Earthquake, Davis and Bardet (2000) provided an updated approach to evaluating the seismic performance of CMP conduits. The focus of their study was on the ovaling and buckling (of the thin metal wall) of the transverse section behavior of the CMP. This approach involves the following general steps:

- 1) Estimating the initial condition of compressive strain in the conduit, which is related to depth of burial.
- 2) Estimating the compressive ground strain induced by a vertically propagating shear wave, which was calculated from the closed-form solution for transient shearing strain, as $\gamma_{\max} = V_s/C_{se}$, in which γ_{\max} is the maximum transient shearing strain of the ground, V_s is the horizontal peak particle velocity transverse to the conduit, and C_{se} is the average effective shear wave velocity of the surrounding ground.
- 3) Adding the static and transient compressive strains.
- 4) Comparing the strain so determined with the critical compressive strain that would cause the dynamic buckling (due to hoop force) of the CMP pipe. The critical buckling strain (or strength) was assumed to be dependent on the stiffness of the surrounding soil (Moore, 1989).

The methodology derived by Davis and Bardet, although more rational than most of the other procedures, has some drawbacks, including:

- The procedure is applicable for thin-walled pipes only. The failure mode considered by using this procedure is primarily for buckling and does not include flexural (that is, bending) demand and capacity evaluation. The latter is a very important failure mode that must be considered for rigid culvers and pipes (such as those constructed with reinforced concrete).
- The soil-structure interaction effect was considered in evaluating the buckling capacity, but not in the evaluation of the demand (that is, earthquake-induced ground strains).
- The method assumed that the strains in the pipe coincide with those in the surrounding ground (that is, pipe deforms in accordance with the ground deformation in the free-field), on the basis of the assumption that there is no slippage at the soil-pipe interface. This assumption was incorrect, as Wang (1993) pointed out in his study that the strains/deformations of a buried conduit can be greater, equal, or smaller than those of the surrounding ground in the free-field, depending on the relative stiffness of the conduit to the surrounding ground.

To account for the effects of TGD on tunnel structures, Wang (1993) developed closed-form and analytical solutions for the determination of seismically induced ovaling/racking deformations and the corresponding internal forces (such as moments and thrusts) for bored as well as cut-and-cover tunnel structures. The procedure presented by Wang for the bored tunnels was developed from a theory that is familiar to most mining/underground engineers (Peck et al., 1972). Simple and easy-to-use seismic design charts were presented. The design charts are expressed primarily as a function of relative stiffness between the structure and the ground. Solutions for both full-slip and no-slip conditions at the interface between soil and the exterior surface of the tunnel lining were developed. These solutions fully account for the interaction of the tunnel lining with the surrounding ground. The results were validated through a series of finite element/difference soil-structure interaction analyses.

For the cut-and-cover tunnels (with a rectangular shape), the design solutions were derived from an extensive study using dynamic finite-element, soil-structure interaction analyses. A wide range of structural, geotechnical, and ground motion parameters were considered by Wang in his study. Specifically, five different types of cut-and-cover tunnel geometry were studied, including one-barrel, one-over-one two-barrel, and one-by-one twin-barrel configurations. To quantify the effect of relative stiffness on tunnel lining response, varying ground profiles and soil properties were used in the parametric analyses. Based on the results of the parametric analyses, a deformation-based design chart was developed for cut-and-cover tunnels.

Although these solutions were intended originally for tunnel structures (considered a fairly rigid type of structure), the methodology is rational and comprehensive and provides a consistent and unified approach to solving the problem of buried conduits subject to ground shaking regardless of whether they are rigid or flexible structures. With some adjustments this approach is also applicable to the culvert and pipe structures typically used for highway construction. Therefore, a more detailed discussion of Wang's approach is given in the following section.

13.6 GENERAL METHODOLOGY AND RECOMMENDED PROCEDURES

The general methodology and recommended procedures are presented in the following sections for the ovaling of circular conduits and the racking of rectangular conduits.

13.6.1 Ovaling of Circular Conduits

This section provides methods for quantifying the seismic ovaling effect on circular conduits. The conventionally used simplified free-field deformation method, discussed first, ignores the soil-structure interaction effects. Therefore its use is limited to conditions where the buried structures can be reasonably assumed to deform according to the free-field displacements during earthquakes.

A refined method is then presented in Section 13.6.2 that is equally simple but capable of eliminating the drawbacks associated with the free-field deformation method. This refined method - built from a theory that is familiar to most mining/underground engineers - considers the soil-structure interaction effects. Based on this method, a series of design charts are developed to facilitate the design process.

Ovaling Effect: As mentioned earlier, ovaling of a circular lining is primarily caused by seismic waves propagating in planes perpendicular to the axis of the buried structure. The results are cycles of additional stress concentrations with alternating compressive and tensile stresses in the lining. These dynamic stresses are superimposed on the existing static state of stress in the lining.

Free-Field Shear Deformations: As mentioned previously, the shear distortion of ground caused by vertically propagating shear waves is probably the most critical and predominant mode of seismic motions. It causes a circular buried structure to oval and a rectangular buried structure to rack (sideways motion), as shown in Figure 13-2. Analytical procedures by numerical methods are often required to

arrive at a reasonable estimate of the free-field shear distortion, particularly for a soil site with variable stratigraphy. Many computer codes with variable degree of sophistication are available (e.g., SHAKE, FLUSH, FLAC, PLAXIS, et al.). The most widely used approach is to simplify the site geology into a horizontally layered system and to derive a solution using one-dimensional wave propagation theory (Schnabel, Lysmer, and Seed, 1972). The resulting free-field shear distortion of the ground from this type of analysis can be expressed as a shear strain distribution or shear deformation profile versus depth.

For a deep buried structure located in relatively homogeneous soil or rock and in the absence of detailed site response analyses, the simplified procedure by Newmark (1965) may provide a reasonable estimate, noting, however, that this method tends to produce more conservative results particularly when the effect of ground motion attenuation with depth is ignored. Here, the maximum free-field shear strain, γ_{\max} , can be expressed as

$$\gamma_{\max} = \frac{V_s}{C_{se}} \quad 13-1$$

where V_s = Peak particle velocity
 C_{se} = Effective shear wave propagation velocity

The effective shear wave velocity of the vertically propagating shear wave, C_{se} , should be compatible with the level of the shear strain that may develop in the ground at the elevation of the buried structure under the design earthquake shaking. The values of C_{se} can be estimated by making proper reduction (to account for the strain-level dependent effect) from the small-strain shear wave velocity, C_s , obtained from in-situ testing (such as using the cross-hole, down-hole, and P-S logging techniques). For rock, the ratio of C_{se}/C_s can be assumed equal to 1.0. For stiff to very stiff soil, C_{se}/C_s may range from 0.6 to 0.9. Alternatively, site specific response analyses can be performed for estimating C_{se} .

An equation relating the effective propagation velocity of shear waves to effective shear modulus, G_m , is expressed as:

$$C_{se} = \sqrt{\frac{G_m}{\rho}} \quad 13-2$$

where ρ = Mass density of the ground

An alternative simplified method for calculating the free-field ground shear strain, γ_{\max} , is by dividing the earthquake-induced shear stresses (τ_{\max}) by the shear stiffness (i.e., the strain-compatible effective shear modulus, G_m). This method is especially suitable for buried structures with shallow burial depths.

In this simplified method the maximum free-field ground shear strain is calculated using the following equation:

$$\gamma_{\max} = \frac{\tau_{\max}}{G_m} \quad 13-3$$

$$\tau_{\max} = \left(\frac{\text{PGA}}{g} \right) \sigma_v R_d \quad 13-4$$

$$\sigma_v = \gamma_t (H + D) \quad 13-5$$

where G_m = Effective strain-compatible shear modulus of ground surrounding the buried structure (ksf)
 τ_{\max} = Maximum earthquake-induced shear stress (ksf)
 σ_v = Total vertical soil overburden pressure at invert elevation of buried structure (ksf)
 γ_t = Total soil unit weight (kcf)
 H = Soil cover thickness measured from ground surface to structure crown (ft)
 D = Height of structure (or diameter of circular structure) (ft)
 R_d = Depth dependent stress reduction factor; can be estimated using the following relationships:

$$\begin{aligned} R_d &= 1.0 - 0.00233z && \text{for } z < 30 \text{ ft} \\ R_d &= 1.174 - 0.00814z && \text{for } 30 \text{ ft} < z < 75 \text{ ft} \\ R_d &= 0.744 - 0.00244z && \text{for } 75 \text{ ft} < z < 100 \text{ ft} \\ R_d &= 0.5 && \text{for } z > 100 \text{ ft} \end{aligned}$$

where z = the depth (ft) from ground surface to the invert elevation of the structure and is represented by $z = (H+D)$.

Lining Conforming to Free-Field Shear Deformations: When a circular lining is assumed to oval in accordance with the deformations imposed by the surrounding ground (e.g., shear), the lining's transverse sectional stiffness is completely ignored. This assumption is probably reasonable for most circular structures in rock and in very stiff/hard ground, because the lining stiffness against distortion is low compared with that of the surrounding ground. Depending on the definition of "ground deformation of surrounding ground," however, a design based on this assumption may be overly conservative in some cases and non-conservative in others. This will be discussed further below.

Shear distortion of the surrounding ground, for this discussion, can be defined in two ways. If the non-perforated ground in the free-field is used to derive the shear distortion surrounding the structural lining, the lining is to be designed to conform to the maximum diameter change, $\Delta D_{\text{free-field}}$, shown in the top of Figure 13-3.

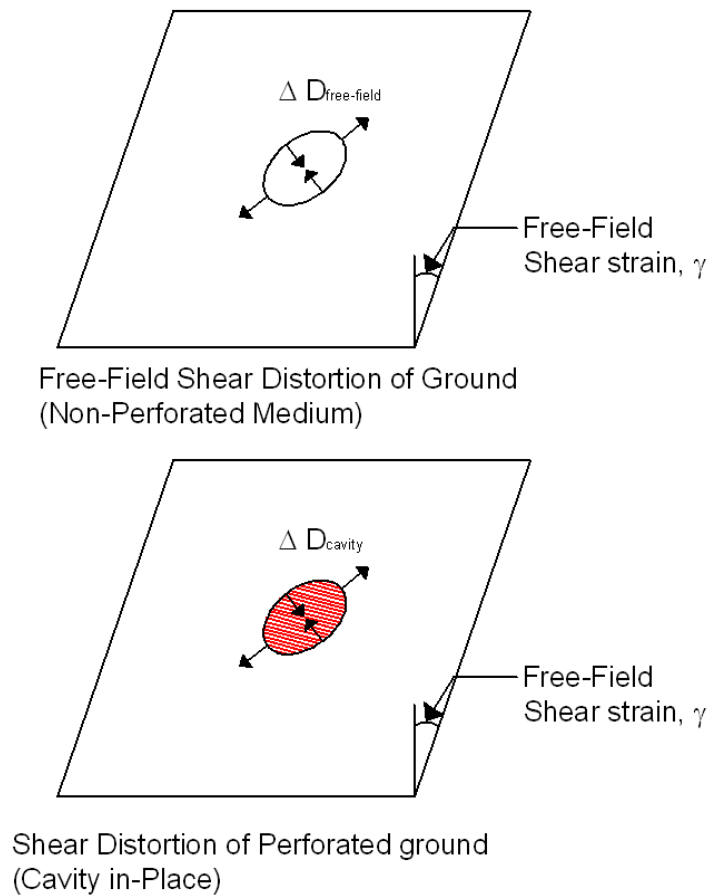


Figure 13-3 Shear Distortion of Ground – Free-Field Condition vs. Cavity In-Place Condition

The maximum diametric change of the lining for this case can be derived as:

$$\Delta D_{\text{free - field}} = \pm(\gamma_{\text{max}} / 2)D \quad 13-6$$

where

D = the diameter of the structure

γ_{max} = the maximum free-field shear strain

On the other hand, if the ground deformation is derived by assuming the presence of a cavity due to the excavation of the structure (bottom of Figure 13-3, for perforated ground), then the lining is to be designed according to the diametric strain expressed as:

$$\Delta D_{\text{cavity}} = \pm 2\gamma_{\text{max}} (1 - \nu_m)D \quad 13-7$$

where ν_m = the Poisson's Ratio of the surrounding ground

Equations 13-6 and 13-7 both assume the absence of the lining. In other words, lining-ground interaction is ignored.

Comparison between Equations 13-6 and 13-7 shows that the perforated ground deformation would yield a much greater distortion than the free-field case (non-perforated ground). For a typical ground medium, the difference could be as much as three times. Based on the assumptions made, some preliminary conclusions can be drawn as follows:

- Equation 13-7, for the perforated ground deformation, should provide a reasonable estimate for the deformation of a lining that has little stiffness (against distortion) in comparison to that of the surrounding ground.
- Equation 13-6, for the free-field ground deformation, on the other hand, should provide a reasonable result for a lining with a distortion stiffness close or equal to the surrounding ground.

Based on the discussions above, it can be further suggested that a lining with a greater distortion stiffness than the surrounding ground should experience a lining distortion even less than the free-field deformation. This latest case may occur when a structure is built in soft to very soft soils. It is therefore clear that the relative stiffness between the structure and the surrounding ground (i.e., soil-structure interaction effect) plays an important role in quantifying the response of a buried structure during the seismic loading condition. This effect will be discussed next.

Importance of Lining Stiffness- Compressibility and Flexibility Ratios: To quantify the relative stiffness between a circular lining and the surrounding ground, two ratios designated as the compressibility ratio, C, and the flexibility ratio, F (Hoeg, 1968, and Peck et al., 1972) are defined by the following equations:

Compressibility Ratio:

$$C = \frac{E_m(1 - \nu_1^2)R_1}{E_1 t_1(1 + \nu_m)(1 - 2\nu_m)} \quad 13-8$$

Flexibility Ratio:

$$F = \frac{E_m(1 - \nu_1^2)R_1^3}{6E_1 I_{1,1}(1 + \nu_m)} \quad 13-9$$

Where:

- E_m = Strain-compatible elastic modulus of the surrounding ground
- ν_m = Poisson's ratio of the surrounding ground
- R_1 = Nominal radius of the structure lining
- ν_1 = Poisson's ratio of the structure lining
- $I_{1,1}$ = Moment of inertia of lining per unit width of structure along the buried conduit axis.
- t_1 = The thickness of the lining

Of these two ratios, it often has been suggested that the flexibility ratio is the more important because it is related to the ability of the lining to resist distortion imposed by the ground. As will be discussed later, the compressibility ratio also has a significant effect on the lining thrust response, particularly in the case where buckling potential may be of concern for flexible culverts/pipes.

In the following section a refined procedure taking into account the lining-ground interaction effect is presented to provide a more accurate assessment of the seismic ovaling effect on a circular lining.

13.6.2 Lining-Ground Interaction Solutions for Ovaling Response of Circular Lining

Closed form analytical solutions have been proposed (Wang, 1993) for estimating ground-structure interaction for circular lining under the seismic loading conditions. These solutions are generally based on the assumptions that:

- The ground is an infinite, elastic, homogeneous, isotropic medium.
- The circular lining is generally an elastic, thin walled tube under plane strain conditions.
- Full-slip or no-slip conditions exist along the interface between the ground and the lining.

The expressions of these lining responses are functions of flexibility ratio and compressibility ratio as presented previously in Equations 13-8 and 13-9. The expressions for maximum thrust, T_{\max} , bending moment, M_{\max} , and diametric strain, $\Delta D/D$, can be presented in the following forms:

$$M_{\max} = \pm \frac{1}{6} K_1 \frac{E_m}{(1 + \nu_m)} R_1^2 \gamma_{\max} \quad 13-10$$

$$T_{\max} = \pm K_2 \frac{E_m}{2(1 + \nu_m)} R_1 \gamma_{\max} \quad 13-11$$

$$\Delta D_{\max}/D = \pm \frac{1}{3} K_1 F \gamma_{\max} \quad 13-12$$

$$K_1 = \frac{12(1 - \nu_m)}{2F + 5 - 6\nu_m} \quad 13-13$$

$$K_2 = 1 + \frac{F[(1 - 2\nu_m) - (1 - 2\nu_m)C] - \frac{1}{2}(1 - 2\nu_m)^2 C + 2}{F[(3 - 2\nu_m) + (1 - 2\nu_m)C] + C[\frac{5}{2} - 8\nu_m + 6\nu_m^2] + 6 - 8\nu_m} \quad 13-14$$

K_1 and K_2 are defined herein as lining response coefficients. The earthquake loading parameter is represented by the maximum shear strain induced in the ground (free-field), γ_{max} , which may be obtained through a simplified approach (such as Equations 13-1 or 13-3), or by performing a site-response analysis.

To ease the design process, Figure 13-4 shows the lining response coefficient, K_1 , as a function of flexibility ratio and Poisson's Ratio of the ground. The design charts showing the lining coefficient K_2 , primarily used for the thrust response evaluation, are presented in Figure 13-5, Figure 13-6 and Figure 13-7 for Poisson's Ratio values of 0.2, 0.35 and 0.5, respectively.

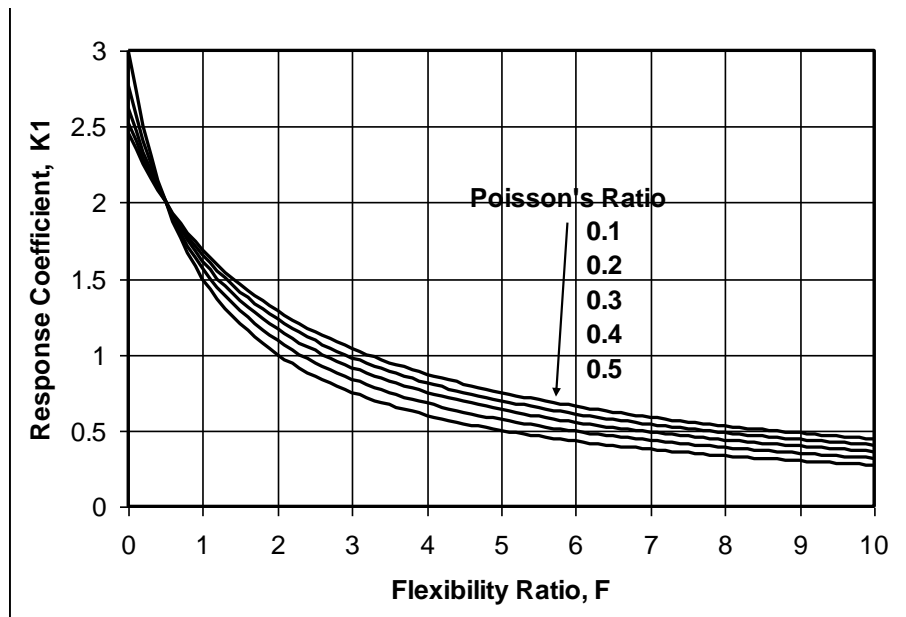


Figure 13-4 Lining Response Coefficient, K_1 (Full-Slip Interface Condition)

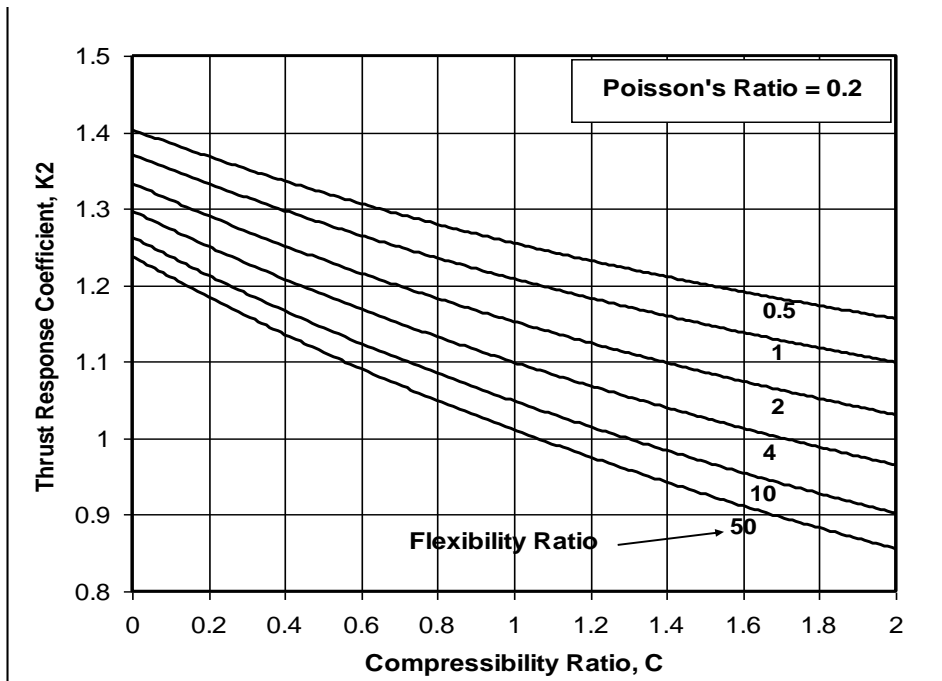


Figure 13-5 Lining Response Coefficient, K_2 , for Poisson's Ratio = 0.2 (No-Slip Interface Condition)

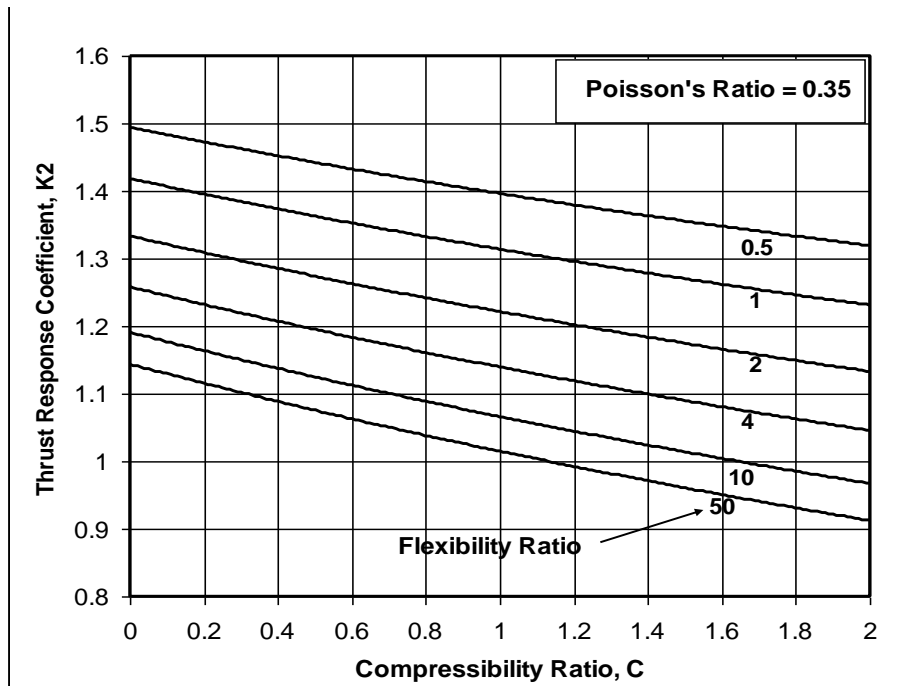


Figure 13-6 Lining Response Coefficient, K_2 , for Poisson's Ratio = 0.35 (No-Slip Interface Condition)

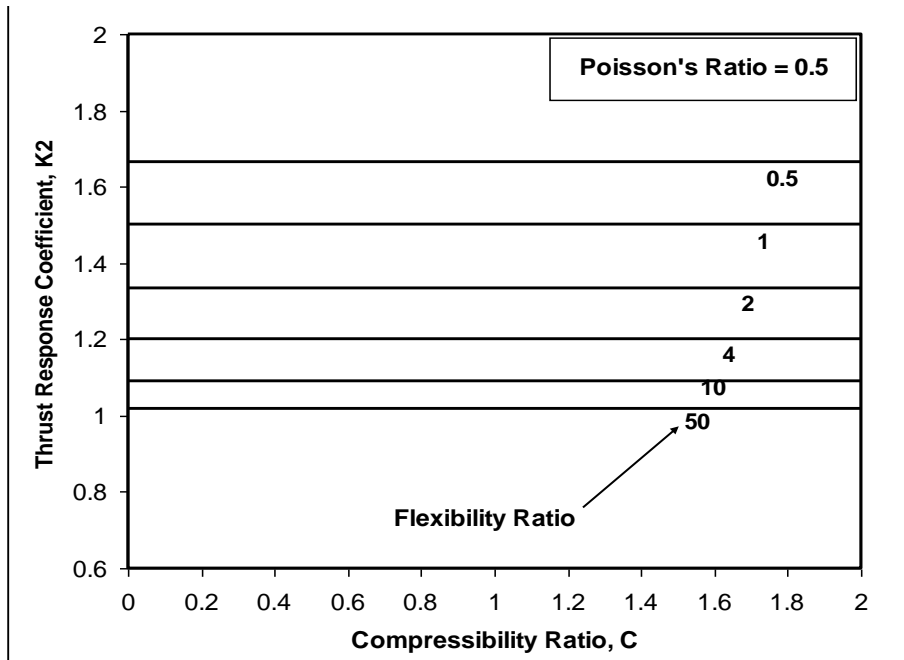


Figure 13-7 Lining Response Coefficient, K_2 , for Poisson's Ratio = 0.5 (No-Slip Interface Condition)

It should be noted that the solutions in terms of M_{max} , ΔD_{max} , and ϵ_m provided herein are based on the full-slip interface assumption. For the maximum thrust response T_{max} the interface conditions is assumed to be no-slip. These assumptions were adopted because full-slip condition produces more conservative results for M_{max} and ΔD_{max} , while no-slip condition is more conservative for T_{max} . During an earthquake, in general, slip at interface is a possibility only for structures in soft soils, or when seismic loading intensity is severe. For most buried structures, the condition at the interface is between full-slip and no-slip. In computing the forces and deformations in the lining, it is prudent to investigate both cases and the more critical one should be used in design.

The conservatism described above is desirable to offset the potential underestimation of lining forces resulting from the use of equivalent static model in lieu of the dynamic loading condition. Therefore, the full-slip model is recommended in evaluating the moment and deflection response (i.e., Figure 13-4 and Equations 13-10, 13-12 and 13-14) of a circular lining.

Using the full-slip condition, however, would significantly underestimate the maximum thrust, T_{max} , under the seismic simple shear condition. Therefore, it is recommended that the no-slip interface assumption be used in assessing the lining thrust response (Equations 13-11 and 13-14).

13.6.3 Lining-Ground Interaction Solutions for Racking Response of Rectangular Lining

During earthquakes a rectangular box structure in soil or in rock will experience transverse racking deformations (sideways motion) due to the shear distortions of the ground, in a manner similar to the ovaling of a circular structure discussed in Section 13.6.1. The racking effect on the structure is similar to that of an unbalanced loading condition.

The external forces the structure is subjected to are in the form of shear stresses and normal pressures all around the exterior surfaces of the box. The magnitude and distribution of these external earth forces are complex and difficult to assess. The end results, however, are cycles of additional internal forces and stresses with alternating direction in the structure members. These dynamic forces and stresses are superimposed on the existing static state of stress in the structure members. For rigid frame box structures, the most critical mode of potential damage due to the racking effect is the distress at the top and bottom joints.

Realizing that the overall effect of the seismically induced external earth loading is to cause the structure to rack, it is more reasonable to approach the problem by specifying the loading in terms of deformations. The structure design goal, therefore, is to ensure that the structure can adequately absorb the imposed racking deformation (i.e., the deformation method), rather than using a criterion of resisting a specified dynamic earth pressure (i.e., the force method).

Free-Field Racking Deformation Method It has been proposed in the past that a rectangular buried structure be designed by assuming that the amount of racking imposed on the structure is equal to the “free-field” shear distortions of the surrounding ground, as illustrated in Figure 13-8 (i.e., $\Delta_{free-field} = \Delta_s$). The racking stiffness of the structure is ignored with this assumption.

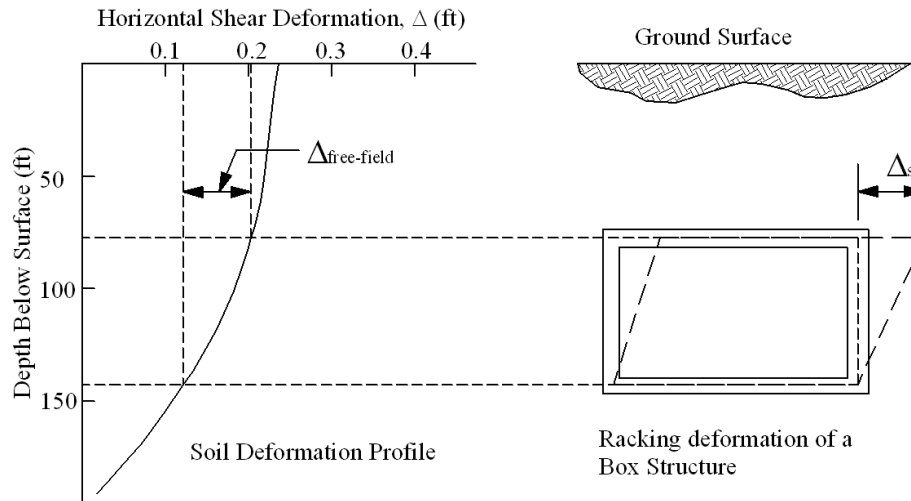


Figure 13-8 Soil Deformation Profile and Racking Deformation of a Box Structure

The free-field deformation method serves as a simple and effective design tool when the seismically induced ground distortion is small, for example when the shaking intensity is low or the ground is very stiff. Given these conditions, most practical structural configurations can easily absorb the ground distortion without being distressed. The method is also a realistic one when the racking stiffness of the structure is comparable to that of its surrounding medium.

It has been reported (Wang, 1993), however, that this simple procedure could lead to overly conservative design (i.e., when $\Delta_{\text{free-field}} > \Delta_s$) or un-conservative design (i.e., when $\Delta_{\text{free-field}} < \Delta_s$), depending on the relative stiffness between the ground and the structure. The overly conservative cases generally occur in soft soils. Seismically induced free-field ground distortions are generally large in soft soils, particularly when they are subjected to amplification effects. Ironically, rectangular box structures in soft soils are generally designed with stiff configurations to resist the static loads, making them less tolerant to racking distortions. Imposing free-field deformations on a structure in this situation is likely to result in unnecessary conservatism, as the stiff structure may deform less than the soft ground.

On the other hand, the un-conservative cases arise when the shear stiffness of the ground is greater than the racking stiffness of the structures – a behavior similar to that described for the ovaling of circular structures (Section 13.6.1). To more accurately quantify the racking response of rectangular structures a rational procedure accounting for the structure-ground interaction effect is presented in the following section.

Structure-Ground Interaction Analysis: Although closed-form solutions accounting for soil-structure interaction, such as those presented in Section 13.6.2, are available for circular lining, they are not readily available for rectangular structures due primarily to the highly variable geometrical characteristics typically associated with rectangular structures.

To develop a simple and practical design procedure, Wang (1993) performed a series of dynamic soil-structure interaction finite element analyses. In this study, the main factors that may potentially affect the dynamic racking response of rectangular structures were investigated. Additional parametric studies and evaluations were also conducted specifically for buried structures with properties and characteristics that are typical of culverts in the NCHRP 12-70 study (NCHRP Report No. 611, 2008). Based on the results of the analyses, a simplified procedure incorporating soil-structure interaction for the racking analysis of rectangular buried structures was developed. The step-by-step procedure is outlined below.

Step 1: Estimate the free-field ground strains γ_{\max} (at the structure elevation) caused by the vertically propagating shear waves of the design earthquakes, see Section 13.6.1 in deriving the free-field ground strain using various methods. Determine $\Delta_{\text{free-field}}$, the differential free-field relative displacements corresponding to the top and the bottom elevations of the box structure (see Figure 13-10) by using the following expression:

$$\Delta_{\text{free-field}} = H \cdot \gamma_{\max} \quad 13-15$$

Where: H = height of the box structure

Alternatively site-specific site response analysis may be performed to provide a more accurate assessment of $\Delta_{\text{free-field}}$.

Step 2: Determine the racking stiffness, K_s , of the box structure from a structural frame analysis. The racking stiffness should be computed using the displacement of the roof subjected to a unit lateral force applied at the roof level, while the base of the structure is restrained against translation, but with the joints free to rotate. The ratio of the applied force to the resulting lateral displacement yields K_s . In performing the structural frame analysis, appropriate moment of inertia values, taking into account the potential development of cracked section, should be used.

Step 3: Determine the flexibility ratio, F_r , of the box structure using the following equation:

$$F_r = \left(\frac{G_m}{K_s} \right) \cdot \left(\frac{W}{H} \right) \quad 13-16$$

Where:

- W = Width of the box structure
- H = Height of the box structure
- G_m = Average strain-compatible shear modulus of the surrounding ground between the top and bottom elevation of the structure
- K_s = Racking Stiffness of the box structure

The strain-compatible shear modulus can be derived from the strain-compatible effective shear wave velocity, C_{se} , see Equation 13-2).

Detailed derivation of the flexibility ratio, F_r , is given by Wang (1993).

Step 4: Based on the flexibility ratio obtained from Step 3 above, determine the racking coefficient, R_r , for the proposed structure. The racking coefficient, R_r , is the ratio of the racking distortion of the structure embedded in the soil, Δ_s , to that of the free-field soil, $\Delta_{\text{free-field}}$, over the height of the structure (see Figure 13-9):

$$R_r = \frac{\Delta_s}{\Delta_{\text{free-field}}} \quad 13-17$$

From a series of dynamic finite element analyses, Wang (1993) presented results showing the relationship between the structure racking and the flexibility ratio, F_r . The values of R_r vs. F_r obtained from the dynamic finite element analyses are shown in Figure 13-9a and Figure 13-9b. Also shown in these figures are curves from closed-form static solutions for circular lining (refer to Section 13.6.2). The solutions shown in the figures are from the full-slip solution presented by Wang (1993) and Penzien (2000) and the no-slip solution presented by Penzien (2000). As can be seen in the figures, the curves from the closed-form solutions provide a good approximation of the finite element analysis results. These curves can therefore be used to provide a good estimate of the racking of a rectangular structure as a function of the flexibility ratio defined by Equation 13-17. The analytical expressions for the curves in Figure 13-9 are:

For no-slip interface condition:

$$R_r = \frac{4(1 - \nu_m)F_r}{3 - 4\nu_m + F_r} \quad 13-18$$

For full-slip interface condition:

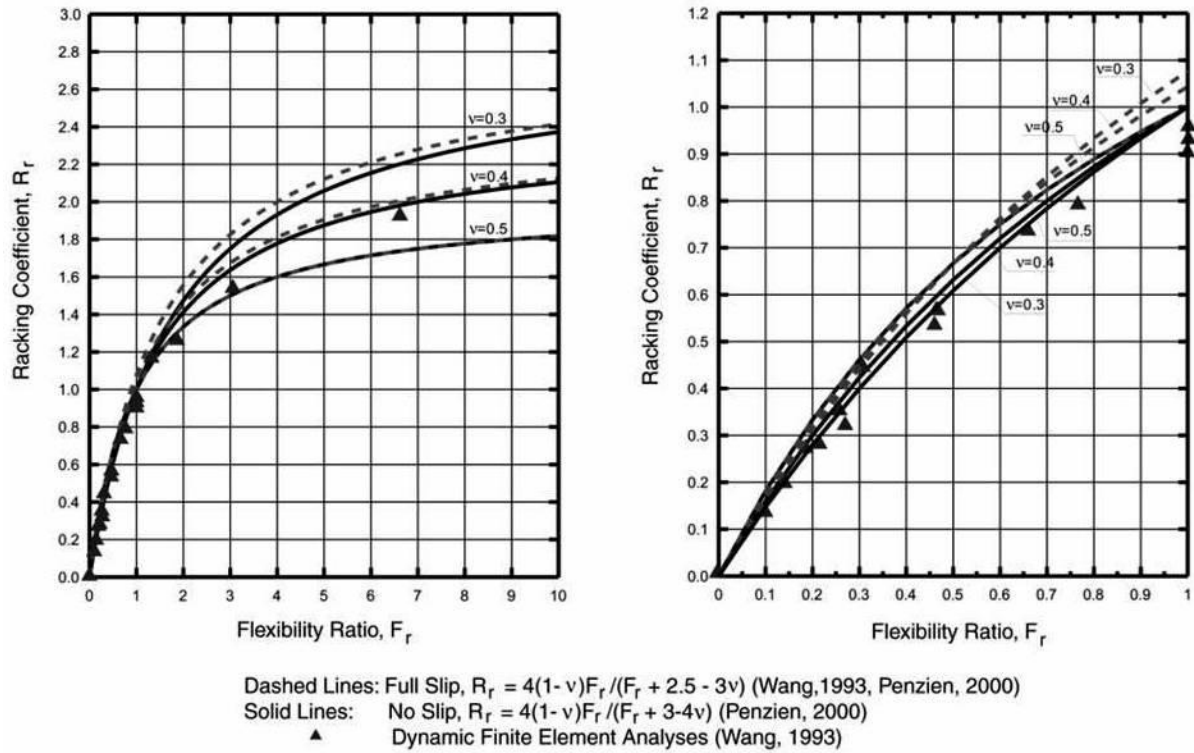
$$R_r = \frac{4(1 - \nu_m)F_r}{2.5 - 3\nu_m + F_r} \quad 13-19$$

Several observations can be made from Figure 13-9. When F_r is equal to zero, the structure is perfectly rigid, no racking distortion is induced, and the structure moves as a rigid body during earthquake loading. When F_r is equal to 1, the racking distortion of the structure is approximately the same as that of the surrounding soil (exactly equal to that of the soil for the no-slip interface condition). For a structure that is flexible relative to the surrounding ground, ($F_r > 1$), racking distortion of the structure is greater than that of the free-field. As noted by Penzien (2000), if the structure has no stiffness (i.e., $F_r \rightarrow \infty$), R_r is approximately equal to $4(1 - \nu_m)$, which is the case of an unlined cavity.

Step 5: Determine the racking deformation of the structure, Δ_s , using the following relationship:

$$\Delta_s = R_r \cdot \Delta_{\text{free-field}} \quad 13-20$$

Step 6: The seismic demand in terms of internal forces as well as material strains are calculated by imposing Δ_s upon the structure in a frame analysis as depicted in Figure 13-10. Results of the analysis can also be used to determine the detailing requirements.



a. Flexibility Ratios Between 0.0 and 10

b. Flexibility Ratios Between 0.0 and 1.0

Figure 13-9 Racking Coefficient R_r for Rectangular Structures (MCEER-06-SP11, Modified from Wang, 1993, and Penzien, 2000)

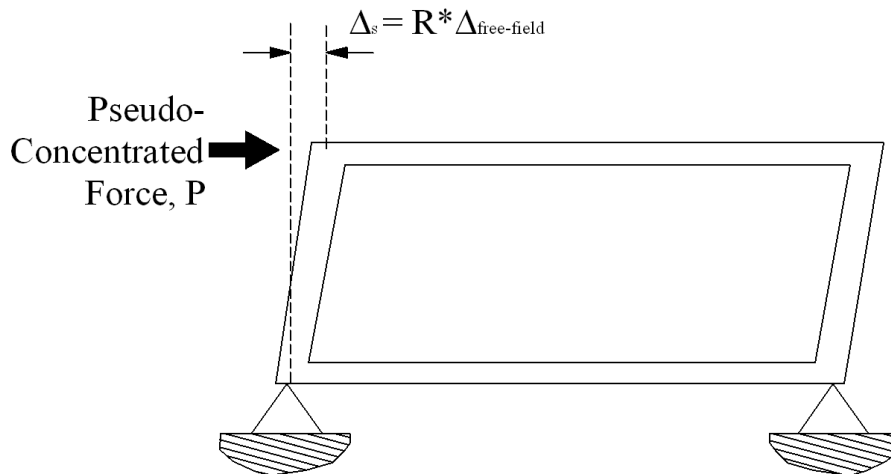


Figure 13-10 Simplified Racking Frame Analysis of a Rectangular Structure

It should be noted that the methodology developed above was intended to address the incremental effects due to earthquake-induced TGD only. The seismic effects of transient racking/ovaling deformations on culverts and pipes must be considered additional to the normal load effects from surcharge, pavement, and wheel loads, and then compared to the various failure criteria considered relevant for the type of culvert structure in question.

A load factor of 1.0 shall be used in conjunction with the methodology given in this chapter to determine the seismic loading effects discussed above. The current AASHTO *LRFD Bridge Design Specifications* require that the load factor for live load in combination with the seismic load should be determined on a project-specific basis. On a heavily traveled roadway where the buried structure is likely to be subjected to the live load on a nearly continuous basis, the load factor for live load shall be taken at least equal to 0.5.

13.7 NUMERICAL MODELING METHODS

In situations where the simplified methods for estimating seismic forces are inadequate, more rigorous 2-dimensional soil-structure interaction continuum numerical modeling methods should be used. There are a number of situations that may warrant the use of numerical modeling, including where (1) the geometry is too complex to be represented by a circular or box-type structure, (2) long-span culverts that may be sensitive to seismic loads are being used, (3) critical (important) structures are identified, (4) highly variable subsurface conditions occur, and (5) in high seismic areas.

For transverse ovaling/racking analysis, the model needs to be developed with the capability of capturing SSI effects as well as appropriate depth-variable representations of the earth medium and the associated free-field motions (or ground deformations) obtained from site-response analyses of representative soil profiles.

Two types of two-dimensional finite element (or finite difference) continuum numerical modeling methods have been used in practice and they are described in the following sections.

Pseudo-Static Seismic Coefficient Deformation Method: The pseudo-static seismic coefficient induced deformation method (the simpler of the two methods) is a generally accepted method of analysis for underground structures buried at shallow depths and is particularly suited for conventional highway

culverts/pipes where the burial depths are generally shallow (i.e., within 75 feet from ground surface). In this analysis it is assumed that ground stability is not of concern. The general procedure in using this method is outlined below:

- Perform one-dimensional free-field site response analysis (e.g., using SHAKE program). From the results of the analysis derive the maximum ground acceleration profile expressed as a function of depth from the ground surface.
- Develop the two-dimensional finite element (or finite difference) continuum model incorporating the entire excavation and soil-structure system, making sure the lateral extent of the domain (i.e., the horizontal distance to the side boundaries) is sufficiently far to avoid boundary effects. The side boundary conditions should be in such a manner that all horizontal displacements at the side boundaries are free to move and vertical displacements are prevented (i.e., fixed boundary condition in the vertical direction and free boundary condition in the horizontal direction). These side boundary conditions are considered adequate for a site with reasonably leveled ground surface subject to lateral shearing displacements due to horizontal excitations.
- The strain-compatible shear moduli of the soil strata computed from the one-dimensional site response analysis (e.g., using the SHAKE program) should be used in the two-dimensional continuum model.
- The maximum ground acceleration profile (expressed as a function of depth from the ground surface) derived from the one-dimensional site response analysis is applied to the entire soil-structure system in the horizontal direction in a pseudo-static manner.
- The analysis is executed with the culvert structure in place using the prescribed horizontal maximum acceleration profile and the strain-compatible shear moduli in the soil mass. It should be noted that this pseudo-static seismic coefficient approach is not a dynamic analysis and therefore does not involve displacement, velocity, or acceleration histories. Instead, it imposes ground shearing displacements throughout the entire soil-structure system (i.e., the two-dimensional continuum model) by applying pseudo-static horizontal shearing stresses in the ground. The pseudo-static horizontal shearing stresses increase with depth and are computed by analysis as the product of the total soil overburden pressures (representing the soil mass) and the horizontal seismic coefficients. The seismic coefficients represent the peak horizontal acceleration profile derived from the one-dimensional free-field site response analysis. As discussed above the lateral extent of the domain in

the two-dimension analysis system should be sufficiently far to avoid boundary effects. In this manner, the displacement profiles at the two side boundaries are expected to be very similar to that derived from the one-dimensional free-field site response analysis. However, in the focus area near the culvert construction the displacement distribution will be different from that of the free field, reflecting the effects of (1) soil-structure interaction, and (2) the earth mass removed for constructing the culvert.

Dynamic Time History Analysis: In a dynamic time history analysis, the entire soil-structure system is subject to *dynamic* excitations using ground motion time histories as input at the base of the soil-structure system. The ground motion time histories used for this purpose should be developed to match the target design response spectra and have characteristics that are representative of the seismic environment of the site and the site conditions.

13.8 GENERAL DESIGN METHODOLOGY FOR PERMANENT GROUND DISPLACEMENTS

As mentioned earlier, the greatest risk to buried structures is the potential for large ground movements as a result of unstable ground conditions (e.g., liquefaction and landslides) or fault displacements. In general, it is not feasible to design a buried structure to withstand large ground displacements. The proper design measures in dealing with the unstable ground conditions may consist of:

- Ground stabilization
- Removal and replacement of the problem soils
- Re-route to bypass the problem zone

With regard to the fault displacements, the best strategy is to avoid any potential crossing of active faults. If this is not possible, then the general design philosophy is to accept and accommodate the displacements by either employing an oversized excavation, perhaps backfilled with compressible/collapsible material, or using ductile lining to minimize the instability potential of the lining. In cases where the magnitude of the fault displacement is limited or the width of the sheared fault zone is considerable such that the displacement is dissipated gradually over a distance, design of a strong lining to resist the displacement may be technically feasible. The structures, however, may be subject to large axial, shear and bending forces. Many factors need to be considered in the evaluation, including the stiffness of the lining and the ground, the angle of the fault plane intersecting the structure, the width of the fault, the magnitude as well

as orientation of the fault movement. Analytical procedures are generally used for evaluating the effects of fault displacement on lining response. Some of these procedures were originally developed for buried pipelines (ASCE Committee on Gas and Liquid Fuel Lifelines, 1984). Continuum finite-element or finite-difference methods have also been used effectively for evaluating the structure-ground-faulting interaction effects.

The effects of liquefaction and liquefaction-induced ground deformations on buried structures should be evaluated and considered in the seismic design. These effects include the following: (1) uplift, buoyancy, and floatation of the buried structures, (2) large lateral displacement, and (3) post-liquefaction settlements and deformations, total as well as differential.

An initial screening study (NCEER, 1996) should be carried out, followed by more refined analyses and evaluations of the impact on the proposed structures, to assess the risk of liquefaction-related permanent ground displacement. If the liquefaction impact analyses yield unacceptable performance of the structures, mitigation measures should be incorporated into the design.

The evaluation for seismically induced landslides and slope instability, if identified, should also be conducted in accordance with the procedures discussed in Chapter 6, followed by an impact study. If the impact analyses yield unacceptable performance of the structures, mitigation measures should be incorporated into the design.

13.9 SUMMARY

Simplified seismic analysis procedures for evaluating culvert and pipe structures against ground shaking induced transient ground deformations (TGD) were discussed in this chapter. The analysis procedures use a deformation-based methodology that can provide a more reliable prediction of culvert/pipe performance. The approach focuses on the deformations in the transverse section of the structure (that is, ovaling/racking deformations) instead of the longitudinal axial/curvature deformations, due primarily to the general condition that typical culvert structures for transportation applications are of limited length, and as such it is in general unlikely to develop significant transient axial/curvature deformations along the longitudinal direction of the culvert structures.

For PGD, such as occurs with slope failures and liquefaction, a general deformation-based methodology for evaluating the impacts of PGD on culverts and pipe structures are briefly described. In this case conventional methods for assessing liquefaction potential (including spreads, settlement, and floatation) and the seismic stability of the slope, with or without liquefaction, can be used to derive the magnitude and distributions of the PGD, and where appropriate ground improvement can be implemented to mitigate the ground movement.

CHAPTER 14

REFERENCES

- Abdoun, T. H., (1997), —Modeling of Seismically Induced Lateral Spreading of Multi-Layer Soil Deposit and Its Effect on Pile Foundations”, Ph.D. Thesis, Dept. of Civil Engineering, Rensselaer Polytechnic Institute, Troy, NY.
- Abrahamson, N.A. (1992). —Generation of Spatially Incoherent Strong Motion Time Histories,” Proceedings of the Tenth World Conference on Earthquake Engineering, Madrid, Spain, July 19-24, pp. 845-850.
- Abrahamson, N.A. and Silva, W.J. (1997). —Empirical response spectral attenuation relations for shallow crustal earthquakes,” Seismological Research Letters, Vol. 68, No. 1, pp. 94–127.
- Abrahamson, N.A. (2000). —Effects of rupture directivity on probabilistic seismic hazard analysis”. Proceedings of the 6th International Conference on Seismic Zonation, Palm Springs, Earthquake Engineering Research Institute.
- Abrahamson, N.A. (2005). Personal Communications on PGV correlations.
- Abrahamson, N.A., G. Atkinson, D. Boore, Y. Bozorgnia, K. Campbell, B. Chiou, I. Idriss, W. Silva, and R. Youngs (2008). —Comparisons of the NGA Ground-Motion Relations”, EERI Earthquake Spectra, Vol. 24, No. 1, pp. 45-66, February, 2008.
- AASHTO (Association of State Highway and Transportation Officials) (2007). —LRFD Bridge Design Specifications, Customary U.S. Units” Fourth Edition with 2008 and 2009 Interims, AASHTO, Washington, D.C.
- AASHTO (Association of State Highway and Transportation Officials) (2009). —Guidelines Specifications for the LRFD Bridge Design,” American Association of State Highway and Transportation Officials, Washington, D.C.
- AASHTO (Association of State Highway and Transportation Officials) (2010) —Guidelines Specification for Seismic Isolation Design” Third Edition, American Association of State Highway and Transportation Officials, Washington, D.C.
- Andrus, R.D. and Chung, R.M., (1995), —Ground Improvement Techniques for Liquefaction Remediation Near Existing Lifelines”, National Institute of Standards and Technology Report NISTIR 5714, Gaithersburg, MD, 74 pp.
- Andrus, R.D., and Stokoe, K.H. II (2000) —Liquefaction resistance of soils from shear-wave velocity.” ASCE Journal of Geotechnical and Environmental Engineering, Vol. 126, No. 11, November, pp. 1015-1022
- ASCE (American Society of Civil Engineers) Committee on Gas and Liquid Fuel Lifelines, (1984), —Guidelines for the Seismic Design of Oil and Gas Pipeline Systems,” Technical Council on Lifeline Earthquake Engineering, ASCE, New York.

- ASCE (American Society of Civil Engineers) (1994). —*In situ Deep Soil Improvement*,” Geotechnical Special Publication No. 45 (Ed. Kyle Rollins).
- ASCE (American Society of Civil Engineers) (1997). —*Ground Improvement, Ground Reinforcement, Ground Treatment, Developments 1987-1997*,” Geotechnical Special Publication No. 69, ASCE, New York, 616 pp.
- ASTM (American Society for Testing and Materials) (1998). —*Soil and Rock*”, American Society for Testing and Materials, v.4.08, March.
- Arias, A. (1969), "A Measure of Earthquake Intensity," In: *Seismic Design for Nuclear Power Plants*, R. Hansen, Editor, Massachusetts Institute of Technology Press, Cambridge, Massachusetts.
- Arulmoli, K., Muraleetharan, K.K., Hossain, M.M. and Fruth, L.S. (1992). —*VELACS Laboratory Testing Program-Soil data Report*,” The Earth Technology Corporation, Project No. 90-0562.
- Ashford, Scott and Juirnarongrit, Teerawut, (2003), —*Evaluation of Pile Diameter Effect on Initial Modulus of Subgrade Reaction*”, *Journal of Geotechnical and Geoenvironmental Engineering*, ASCE. Vol. 129, No. 3, March, 2003.
- ATC/MCEER (2003) —*Recommended LRFD Guidelines for the Seismic Design of Highway Bridges, Specifications and Commentary*”, Applied Technology Council/Multidisciplinary Center for Earthquake Engineering Research Joint Venture, MCEER-ATC 49, University at Buffalo, Buffalo NY.
- Baldi, G., R., Bellotti, V. N., Ghionna, M., Jamiolkowski, and D.C.F. LoPresti, (1989) —*Modulus of Sands from CPTs and DMTs*”, *Proceedings, 12th International Conference on Soil Mechanics and Foundation Engineering*, Vol. 1, Rio de Janeiro, Brazil, Balkema, Rotterdam, The Netherlands, pp. 165–170.
- Ballard, R.F., Jr. (1964), "Determination of Soil Shear Moduli at Depth by In Situ Vibratory Techniques," *Miscellaneous Paper No. 4-691*, U.S. Army Waterways Experiment Station, Vicksburg, MS, USA.
- Ballinger, C.A. and Drake, P.G. (1995), —*Culvert Repair Practices Manual: Volumes I and II*”, Report No. FHWA-RD-94-096, Federal Highway Administration, Washington, DC.
- Bardet, J.P., Tobita, T., Mace, N. and Hu, J. (2002). —*Regional Modeling of Liquefaction-Induced Ground Deformation*”, *Earthquake Spectra*, EERI 18(1), 19-46.
- Bardet, J.P., Idriss, I.M., O'Rourke, T.D., Adachi, N., Hamada, M. and Ishihara, K. (1997). —*North America-Japan Workshop on the Geotechnical Aspects of the Kobe, Loma Prieta and Northridge Earthquakes*,” University of Southern California, February.
- Bartlett, S.F. and Youd, T.L. (1995). —*Empirical Prediction of Liquefaction-Induced Lateral Spread*”, *J. Geotechnical Eng.*, ASCE 121(4), 316-29.
- Barton, N.R. (1976). —*The Shear Strength of Rock and Rock Joints*.” *Engineering Geology*, Vol. 7, Elsevier Science Publishing Company, Inc., New York, N.Y., pp. 287-332.
- Barton, N.R. (1973). —*Review of a New Shear Strength Criteria for Rock Joints*.” *Engineering Geology*, Vol. 7, pp. 18-236.

- Barton, N., (2002), —Some new Q-value correlations to assist in Site Characterization and Tunnel Design”, ISRM, 39, p185-216, Pergamon.
- Berrill, J.B., Christensen, S.A., Keenan, R.J., Okada, W., and Pettinga, J.R. (1997). —Lateral-spreading Loads on a Piled Bridge Foundation,” Seismic Behavior of Ground and Geotechnical Structures, Proceedings, Special Technical Session on Earthquake Geotechnical Engineering, 14th ICSMFE, A.A. Balkema, Rotterdam, pp. 173-183.
- Berrill, J. and Yasuda, S (2002). —Liquefaction and Piled Foundations: Some Issues,” Journal of Earthquake Engineering, Vol. 6, pp 1-41.
- Blandon, C.A. (2007) —Seismic Analysis and Design of Pile Supported Wharfs”, Ph.D. Thesis, Rose School of Engineering, Pavia, Italy, October, 2007.
- Bolt, B.A. (1973), "Duration of Strong Ground Motion," Proc. 5th World Conference on Earthquake Engineering, Rome, Italy.
- Bolt, B.A. (1993) —Earthquakes”, W.H. Freeman and Company, New York
- Bonilla, M .G., Mark, R.K., and Lienkaemper, J. J. (1984), "Statistical Relations Among Earthquake Magnitude, Surface Rupture Length and Surface Fault Displacement," Journal of Geophysical Research, Vol. 74, Vol. B6, pp. 2379-2411.
- Boore, D. M., Joyner, W. B., and Fumal, T. E. (1997). —Equations for Estimating Horizontal Response Spectra and Peak Acceleration from Western North American Earthquakes: A summary of recent work”, Seism. Res. Letters, v. 68, p. 128-153.
- Borden, R.H., Shao. L., and Gupta, A. (1996), "Dynamic Properties of Piedmont Residual Soils," Journal of Geotechnical Engineering, ASCE, Vol. 122, No. 10, pp. 813-821.
- Bowles, J.E. (1988), "Foundation Analyses and Design," 4th Edition, McGraw-Hill Book Company, New York, 1004 p.
- Boulanger, R.W. and Hayden R.F. (1995). —Aspects of Compaction Grouting of Liquefiable Soils,” Journal of Geotechnical Engineering, Volume 1121, Number 12, pp. 844-855.
- Boulanger, R. W., Wilson, D. W., Kutter, B. L., and Abghari, A. (1997). "Soil-pile-Superstructure Interaction in Liquefiable Sand." Transportation Research Record No. 1569, TRB, National Research Council, National Academy Press, Washington, D.C. 55
- Brawner, C.O. and Wyllie, D.C. (1975). —Rockslope stability on railway projects.” Proc. American Railway Engineering Association, Regional Meeting, Vancouver, B.C.
- Bray, J.D., Augello, A.J., Leonards, G.A., Repetto, P.C. and Byrne, R.J. (1995), "Seismic Stability Procedures for Solid-Waste Landfills," Journal of Geotechnical Engineering, ASCE, Vol. 121, No. 2, pp. 139-151.
- Briggs, R. P., J. S. Pomeroy, and W. E. Davies (1975). —Landsliding in Allegheny County, Pennsylvania”, U.S. Geological Survey Circular 728, 18p.

- Brown, D. A., Morrison, C., and Reese, L. C. (1988). —“Lateral Load Behavior of Pile Group in Sand,” *Journal of Geotechnical Engineering*, Vol. 114, No. 11, November.
- Brown, D. A., Reese, L. C., and O’Neill, M. W. (1987). —“Behavior of Large-Scale Pile Group Subjected to Cyclic Lateral Loading,” *Journal of Geotechnical Engineering*, Vol. 113, No. 11, November, pp. 1326 - 1343.
- Brown, R.E. (1977). —“Vibroflotation Compaction of Cohesionless Soils.” *J. of Geotech. Eng. Div., ASCE*, Vol. 103, No. GT12, Dec., pp. 1435-1451.
- Bruce, D.A., Bruce, M.E. and DiMillio, A.F. (1998). —“Deep Mixing Method: A Global Perspective,” *Soil Improvements for Big Digs*, ASCE Geotechnical Special Publication No. 81, pp. 1-26.
- Buckle, I.G. (1994) —“The Northridge, California Earthquake of January 17, 1994: Performance of Highway Bridges”, Technical Report NCEER-94-0008, National Center for Earthquake Engineering Research, University at Buffalo, Buffalo, NY
- Buckle, I.G. Mayes, R.L. and Button, M.R.(1986) —“Seismic Design and Retrofit Manual for Highway Bridges”, Federal Highway Administration Report FHWA-IP-87-6, Washington, D.C., 290 pp.
- Caltrans, (1990), —“Seismic Design References”, California Department of Transportation, Sacramento, California, January.
- Chugh, A. K. (1995). —“A Unified Procedure for Earth Pressure Calculations.” *Proceedings: Third International Conference on Recent Advances in Geotechnical Earthquake Engineering and Soil Dynamics*, Volume III, St. Louis, Mo.
- Coduto, D.P. (2001), —“Foundation Design, Principles and Practice,” 2nd Edition, Prentice Hall Book Company, Saddle Hill, New Jersey
- Cook, R.D., Malkus, D.S. and Plesha, M.E. (1989), —“Concepts and Application of Finite Element Analysis”, John Wiley & Sons.
- Cooke, H.G., and Mitchell, J.K. (1999), —“Guide to Remedial Measures for Liquefaction Mitigation at Existing Highway Bridge Sites”, Technical Report MCEER-99-0015, Multidisciplinary Center for earthquake Engineering Research, University at Buffalo, 176 pp.
- Coppersmith, K.J. and Youngs, R.R., (1990) —“Earthquakes and Tectonics” *Demonstration of a Risk-Based Approach to High-Level Nuclear Waste Repository Evaluation*, Report EPRI NP-7057, Electric Power Research Institute, Palo Alto, CA
- Coppersmith, K.J. and Youngs, R.R., (2000) —“Data Needs for Probabilistic Fault Displacement Hazard Analysis” *Journal of Geodynamics*, Volume 29, pp. 329-343
- Current Science (2006), Vol. 91. No. 9, 10 November 2006.
- Darendeli, M. (2001). —“Development of a new family of normalized modulus reduction and material damping curves.” Ph.D. thesis, Dept. of Civil Engineering, Univ. of Texas, Austin, Tex.
- Davidson, H.L (1982), —“Laterally Loaded Drilled Pier Research,” Vol. 1: Design Methodology, Vol. 2: Research Documentation, Final Report by Gai Consultants, Inc., to Electric Power Research Institute

(EPRI), January.

Davis, C. A. and Bardet, J. P. (1999), —**S**ismic Analysis of Buried Flexible Pipes”, ASCE Geotechnical Special Publication No.75 – Geotechnical Earthquake Engineering and Soil Dynamics III, Vol. 2.

Davis, C. A. and Bardet, J. P. (2000) —**R**esponses of Buried Corrugated Metal Pipes to Earthquakes”, ASCE Journal Of Geotechnical and Environmental Engineering, Vol. 126, No. 1, January.

DeAlba, P., Seed, H.B. and Chan, C.K. (1976). —**S**and Liquefaction in Large Scale Simple Shear Tests”, J. Geotechnical Eng. Div., ASCE 102(GT9), 909-27.

Deere, D.U. and Miller, R.P. (1966). —**E**ngineering Classification and Index Properties of intact Rock.” Technical Report No. AFWL-TR-65-116, Air Force Weapons Laboratory, Kirkland Air Force Base, New Mexico.

dePolo. C.M. and Slemmons, D.B. (1990), "Estimation of Earthquake Size for Seismic Hazards," Krinitzsky, E.L. and Slemmons. D.B., Neotectonics in Earthquake Evaluation, Chapter 1, Geological Society of America, Vol . 8.

Dobson, T. (1987). —**C**as histories of the vibro systems to minimize the risk of liquefaction,” Soil Improvement – A Ten Year Update, Proceedings of a Symposium, Atlantic City, J.P. Welsh (ed.), Geotechnical Special Publication No. 12, ASCE.

Dodds, A. M. (2005). "A Numerical Study of Pile Behavior in Large Pile Groups Under Lateral Loading." Doctor of Philosophy Dissertation, University of Southern California, Los Angeles, California, 639 p.

EERI (Earthquake Engineering Research Institute) (1995). Earthquake Spectra, Supplement C to Vol. 11, Northridge Earthquake of January 17, 1994 Reconnaissance Report, Vol. 1, Publication 95-03.

EERI (Earthquake Engineering Research Institute) (1990), Earthquake Spectra, Supplement to Vol. 6, Loma Prieta Earthquake Reconnaissance Report, Publication 96-01.

EERI (Earthquake Engineering Research Institute) (1989). Earthquake Spectra, Special Supplement, Armenia Earthquake Reconnaissance Report, Publication 8-01.

Egan, J.A. and Wang, Z-L. (1991). —**I**quefaction-Related Ground Deformation and Effects on Facilities at Treasure Island, San Francisco, During the 17 October 1989 Loma Prieta Earthquake,” Proceedings of the 3rd Japan-U.S. Workshop on Earthquake Resistant Design of Lifeline Facilities and Countermeasures for Soil Liquefaction, San Francisco, California, December 17-19.

Egan, J.A. and Hayden, R.F., Scheibel, L.L., Otus, M. and Servanti, G.M., (1992), —**S**ismic Repair at Seventh Street Marine Terminal”, Proc. Of Grouting, Soil Improvement and Geosynthetics, ASCE Conference, New Orleans, R.H. Borden, R.D. Holtz, and I. Juran (eds), Geotechnical Special Publication No. 30, Vol. 2, pp. 867-878

Electric Power Research Institute, (1993), Guidelines for determining design basis ground motions, Report No. EPRI TR-102293, Electric Power Research Center, Palo Alto, California

Elgamal, A.W. and Zeghal. M. (1992), —**A**nlysis of Wildlife Site Liquefaction During the 1987 Superstition Hills Earthquake”, Proceedings of the 4th U.S.-Japan Workshop on Earthquake Resistant

Design of Lifeline Facilities and Countermeasures Against Soil Liquefaction.

Elias, V., Welsh, J., Warren, J., Lukas, R., Collin, J.G., and Berg, R.R., (2006), Ground Improvement Methods, Volumes I and II, FHWA NHI-06-019 and FHWA NHI-06-020, US Dept. of Transportation, Federal Highway Administration.

FHWA (Federal Highway Administration) (1997). —Geotechnical Engineering Circular No. 3 - Earthquake Engineering for Highways, Design Principles, Volume 1” FHWA-SA-97-076, FHWA, Washington DC, May.

FHWA (Federal Highway Administration) (1997a). —Geotechnical Engineering Circular No. 3 - Earthquake Engineering for Highways, Design Principles, Volume 2” FHWA-SA-97-077, FHWA, Washington DC, May.

FHWA (Federal Highway Administration) (1998). —Geotechnical Earthquake Engineering”, FHWA HI-99-012, FHWA, Washington, DC, December.

FHWA (Federal Highway Administration) (1998a). —Rock Slopes”, FHWAHI-99-007, FHWA, Washington, DC, October.

FHWA (Federal Highway Administration) (2002). —Geotechnical Engineering Circular No. 5 - Evaluation of Soil and Rock Properties”, FHWA-IF-02-034, FHWA, Washington, DC, April.

FHWA (Federal Highway Administration) (2002a). —Subsurface Investigations – Geotechnical Site Characterization – Reference Manual”, FHWA-NHI-01-031, Federal Highway Administration, Washington, D.C.

FHWA (Federal Highway Administration) (2004) —Ground Improvement Methods”, FHWA-NHI-04-001, Washington, D.C.

FHWA (Federal Highway Administration) (2004). Seismic Retrofitting Manual for Highway Structures: Part 2- Retaining Structures, Slopes, Tunnels, Culverts and Roadways”, FHWA-HRT-05-067, Federal Highway Administration, Turner-Fairbank Highway Research Center, McLean, VA, August.

FHWA (Federal Highway Administration) (2006) —Seismic Retrofitting Manual for Highway Structures: Part 1-Bridges”, FHWA-HRT-06-032, Federal Highway Administration, Turner-Fairbank Highway Research Center, McLean, VA, January.

Fenves, Gregory L. and Chung, Paul C., (1996) "Effects of Pile Footings on Inelastic Earthquake Response of Bridge Columns," 12th U.S.-Japan Bridge Engineering Workshop, UJNR Panel on Wind and Seismic Effects, Buffalo, October 1996, pp. 121-135.

Fenves, Gregory L. (1998) "Effects of Pile Footings on Inelastic Earthquake Response of Bridge Columns," Report to Earth Mechanics, Inc.

Figuroa, J.L., Saada, A.S., Liang, L. and Dahisaria, N.M. (1994). —Evaluation of Soil Liquefaction by energy Principles”, J. Geotechnical and Geoenvironmental Eng., ASCE 120(9), 1554-569.

Finn, W.D.L., Pickering, D.J. and Bransby, P.L. (1971). —Sand Liquefaction in Triaxial and Simple Shear Tests”, J. Soil Mechanics and Foundations Div., ASCE 97(SM4), 639-59.

- Gadre, A and Dobry, R., (1998), —lateral Cyclic Loading Centrifuge Tests on Square Embedded Footing”, ASCE Journal of Geotechnical and Environmental Engineering, November, 1998.
- Gazetas, G., (1991), —Foundation Vibrations,” Foundation Engineering Handbook, Second Edition, edited by Hsai-Yang Fang, Van Nostrand Reinhold.
- Gazetas, G., Fan, K., Tazoh, T., Shimizu, K., Cavadas, M., and Makriis N. (1992), —Sismic Pile-Group-Structure Interaction”, ASCE Geotechnical Special Publication No. 34.
- Gedney, D.S. and Weber, W.G. (1978). —Design and Construction of Soil Slopes,” Special Report 176: Landslides: Analysis and Control, Chapter 8, Transportation Research Board, National Research Council, Washington, D.C., pp. 172-191.
- GeoMotions, LLC (2007). —EMOD2000 User’s Manual.”
- Gere, J.M., and Shah, H.C. (1984), "Terra Non Firma," Stanford Alumni Association, Stanford, California.
- Gerwick, B.C. and Fotinos, G.C. (1990), —Design and Construction of Port Structures” Proceedings, Port of Los Angeles Seismic Workshop, March, 1990, San Pedro, California.
- Gohl, W.B. (1993), —Response of Pile Foundations to Earthquake Shaking- General Aspects of Behavior and Design Methodologies,” Seismic Soil-Structure Interaction Seminar, Canada Society for Civil Engineering/ Vancouver Structure Engineers Group, Vancouver, May.
- Gutenberg, B. and Richter, C.F. (1942), "Earthquake Magnitude, Intensity, Energy, and Acceleration," Seismological Society of America Bulletin, Vol. 32, pp. 163-191.
- Gutenberg, B. and Richter, C.F. (1944). —Frequency of Earthquakes in California,” Bulletin of Seismological Society of America Vol. 34, pp. 1985-1988.
- Gutenberg, B. and Richter, C.F. (1954). —Seismicity of the Earth”, 2nd Ed. Princeton, New Jersey: Princeton University Press.
- Hamada, M. (1992). —Large Ground Deformations and Their Effects on Lifelines: 1964 Niigata Earthquake,” Case Studies of Liquefaction and Lifeline Performance During Past Earthquakes, NCEER Technical Report 92-0001, Vol. 1.
- Hamada, M. and O’Rourke, T.D. (1992), —Case Studies of Liquefaction and Lifeline Performance During Past Earthquakes”, Volume 1, Japanese Case Studies. Technical Report NCEER-92-0001, February 17, 1992.
- Hanks TC, and Kanamori H (1979). "A Moment Magnitude Scale". Journal of Geophysical Research Vol. 84, No. B5, pp. 2348–50
- Harder, L.F., Jr. (1991), "Performance of Earth Dams During the Loma Prieta Earthquake," Proc. Second International Conference on Recent Advances in Geotechnical Earthquake Engineering and Soil Dynamics, University of Missouri, Rolla, pp. 11-15.

- Hart, E.W. (1980), "Fault-Rupture Hazard Zones in California," Alquist-Priolo Special Studies Zones Act of 1972 with index to Special Studies Zones Maps. In: California Division of Mines and Geology Special Publication 42 (Revised edition), 24 p.
- Hashash, Y. M. A., and Park, D. (2001) —"Nonlinear One-Dimensional Seismic Ground Motion Propagation in the Mississippi Embayment," *Engineering Geology*, Vol. 62, No. 1–3, pp. 185–206.
- Hashash, Y. M. A., and Park, D. (2002). "Viscous damping formulation and high frequency motion propagation in nonlinear site response analysis." *Soil Dynamics and Earthquake Engineering*, 22(7), pp. 611-624.
- HAZUS (1997) —"Earthquake Loss Estimation Methodology", Technical Manual, National Institute of Building Sciences for Federal Emergency Management Agency, Washington, DC.
- Heaton, T.H., Tajima, F. and Mori, A.W. (1986), "Estimating Ground Motions Using Recorded Accelerograms," *Surveys in Geophysics*, Vol. 8, pp. 23-83.
- Hoeg, K. (1968), —"Stresses Against Underground Structural Cylinders," *Journal of the Soil Mechanics and Foundation Division, ASCE*, Vol. 94, SM4.
- Hoek, E. (1994). —"Strength of Rock and Rock Masses." *News Journal, International Society of Rock Mechanics*, 2(2).
- Hoek, E. (1983). —"Strength of Jointed Rock masses." *Geotechnique*, Vol. 33, No. 3, pp. 187-223.
- Hoek, E., Carranza-Torres C., Corkum B. (2002) —"Hoek-Brown criterion – 2002 edition". *Proceeding NARMS-TAC Conference, Toronto, 2002, 1, 267-273*
- Hoek E. and Marinos P. (2000) —"Predicting Tunnel Squeezing". *Tunnels and Tunneling International*, Part 1, 32/11, 45-52 – November 2000, Part 2, 32/12, 33-36 – December 2000.
- Hoek, E. and Bray, J.W. (1977). —"Rock Slope Engineering". *Institution of Mining and Metallurgy, London, U.K.*
- Hoek, E. and Brown, E.T. (1997). —"Practical Estimates of Rock Mass Strength." *International Journal of Rock Mechanics and Mining Sciences*, (available at <http://www.roscience.com/>)
- Hoek, E. and Brown, E.T. (1988). —"The Hoek-Brown Failure Criterion – a 1988 Update." *Proceedings, 15th Canadian Rock Mechanics Symposium, Toronto, Canada.*
- Hoek, E., Kaiser, P.K. and Bawden. W.F. (1995). —"Support of underground excavations in hard rock", *Rotterdam: Balkema.*
- Holtz, R.D., Schuster R.L. (1996) —"Stabilization of Soil Slopes", *Landslides Investigation and Mitigation Special Report 247*, (Turner A.K. and Schuster R.L. eds.) *Transportation Research Board, National Academy of Sciences, Washington, D.C, Chapter 17, July.*

- Hudson, M., Idriss, I.M. and Beikae, M. (1994)¹, "QUAD4M - A Computer Program to Evaluate the Seismic Response of Soil Structures using Finite Element Procedures and Incorporating a Compliant Base," User's Manual, Center for Geotechnical Modeling, Department of Civil and Environmental Engineering, University of California, Davis, California, 27 p. (plus Appendices).
- Husid, R.L. (1969), "Análisis de Terremotos: Análisis General, " Revista del IDEM, No. 8, Santiago, Chile, pp. 21-42.
- Hynes, M.E. and Franklin, A.G. (1984). —Rationalizing the Seismic Coefficient Method," Miscellaneous Paper GL-84-13, U.S. Army Waterways Experiment Station, Vicksburg, MS, 21 pp.
- Hytenyi, M., (1946) —Bearing on Elastic Foundation", Ann Arbor: University of Michigan Press.
- Idriss, I.M. (1999). —An Update to the Seed-Idriss Simplified Procedure for Evaluating Liquefaction Potential", in Proceedings, TRB Workshop on New Approaches to Liquefaction, Publication No. FHWA-RD-99-165, Federal Highway Administration, January.
- Idriss, I.M., Lysmer, J., Hwang, R. and Seed, H.B. (1973), "QUAD4 - A Computer Program for Evaluating the Seismic Response of Soil Structures by Variable Damping Finite Element Procedures," Report No. EERC 73-16, Earthquake Engineering Research Center, University of California, Berkeley, California, 67 p.
- Idriss, I.M. (1990), "Response of Soft Soil Sites During Earthquakes," Proc. Memorial Symposium to Honor Professor H.B. Seed, Berkeley, California.
- Idriss, I. M. and Sun, J. I. (1992), —SHAKE91 - A computer Program for Conducting equivalent Linear Seismic Response Analyses of Horizontally Layered Soil Deposits," Center for Geotechnical Modeling, Department of Civil and Environmental Engineering, University of California at Davis, CA, 13p. (plus Appendices).
- Idriss, I. M., and Boulanger, R. W. (2007). "SPT- and CPT-based relationships for the residual shear strength of liquefied soils." Earthquake Geotechnical Engineering, 4th International Conference on Earthquake Geotechnical Engineering – Invited Lectures, K. D. Pitilakis, ed., Springer, The Netherlands, 1-22
- Idriss, I. M., and Boulanger, R. W. (2008) —Soil liquefaction during earthquakes" Monograph MNO-12, Earthquake Engineering Research Institute, Oakland, CA, 261 pp.
- Imai, T. and Tonouchi, K. (1982), "Correlation of N-Value with S-Wave Velocity and Shear Modulus," Proc. 2nd European Symposium on Penetration Testing, Amsterdam, The Netherlands, pp. 67-72.
- Ingham, T. J., Rodriguez, S., Donikian, R., and Chan, J., (1999), —Seismic Analysis of Bridges with Pile Foundations", Proceedings, ADINA conference, MIT
- Ishibashi, I. and Sherif, M.A. (1974), "Soil Liquefaction by Torsional Simple Shear Device," Journal of the Geotechnical Engineering Division, ASCE, Vol. 100, No. GT 8, pp. 871-888.

¹ Available through NISEE / Computer Applications, (510) 642-5113

- Ishihara, K. (1986), "Evaluation of Soil Properties for Use in Earthquake Response Analysis," In: Geomechanical Modelling in Engineering Practice, R. Dungar and J.A. Studer, Eds., A.A. Balkema, Rotterdam, the Netherlands, 241 - 275.
- Ishihara, K., Kokusho, T. and Silver, M.L. (1989), "Recent Developments in Evaluating Liquefaction Characteristics of Local Soils," State-of-the-Art Report, Proc. 12th International Conference on Soil Mechanics and Foundation Engineering, Rio de Janeiro, Brazil, Vol. 4, pp. 2719-2734.
- Ishihara, K., and Cubrinovski, M. (1998). —Problems Associated with Liquefaction and Lateral Spreading During Earthquakes," Geotechnical Earthquake Engineering and Soil Dynamic III, ASCE, Geotechnical Special Publication Number 75, Volume I, pp. 301-312.
- Ishihara (1993), "Liquefaction and Flow Failure During Earthquakes," Géotechnique, Vol. 43, No. 3., pp. 351-415.
- Itasca Consulting Group, Inc. (2006). —FLAC – Fast Lagrangian Analysis of Continua, User's Manual."
- Iwasaki, T.; Penzien, J. and Clough, R. (1972), —Literature Survey-Seismic Effects on Highway Bridges" (EERC 72-11).
- Iwasaki, T., Tatsuoka, F. and Takagi, Y. (1978), "Shear Moduli of Sands Under Cyclic Torsional Shear Loadings," Soils and Foundations, JSSMFE, Vol. 18, No. 1, pp. 39-56.
- Jamiolkowski, M., D.C.F. LoPresti, and M. Manassero (2001), —Evaluation of Relative Density and Shear Strength of Sands from Cone Penetration Test and Flat Dilatometer Test," Soil Behavior and Soft Ground Construction (GSP 119), American Society of Civil Engineers, Reston, Va., pp. 201–238.
- Janson, L-E. (2003), —Plastic Pipes for Water Supply and Sewage Disposal", 4th Ed. Borealis, Stockholm, Sweden.
- Johnston, A.C. and Nava, S.J. (1994), "Seismic Hazard Assessment in the Central United States," Proc. Seminar on New Developments in Earthquake Ground Motion Estimation and Implications for Engineering Design Practice, Applied Technology Council, AT C35-1, Redwood City, California, pp. 2-1 - 2-12.
- Jones, R. (1962), "Surface Wave Technique for Measuring Elastic Properties and Thickness of Roads: Theoretical Development," British Journal of Applied Physics, Vol. 13, pp. 21-29.
- Joyner, W.B. and Boore, D.M. (1988), "Measurement, Characterization, and Prediction of Strong Ground Motion. " In: Von Thun, J.L., Ed., Earthquake Engineering and Soil Dynamics 11, Recent Advances in Ground Motion Evaluation, ASCE Geotechnical Special Publication No. 20, pp. 43-102.
- Kapuskar, M. (2005), —Final Field Investigations Report for Abutment Backfill Characterization", Response Assessment of Bridge Systems - Seismic, Live, and Long Term Loads, Task 3, Research Technical Agreement Contract No. 59A0337, report to Dept. of Civil Eng., Univ. of Cal. at San Diego, and Office of Earthquake Engineering, Caltrans, Sacramento, Jan. 18, Earth Mechanics Inc.
- Keenan, Richard P. (1996). —Foundations Loads Due to Lateral Spreading at the Landing Road Bridge, Whakatane," University of Canterbury, Christchurch, New Zealand, Master of Engineering Thesis.

- Keever, M. (2008) —“Impact of Research on Seismic Design”, Seismic Performance of Bridge Systems with Conventional and Innovative Designs, NEES Webinar, National Science Foundation, Washington, DC.
- Kondner, R.L. and Zelasko, J.S. (1963), "A Hyperbolic Stress-Strain Formulation of Sands," Proc. 2nd Pan American Conference on Soil Mechanics and Foundation Engineering, Sao Paulo, Brazil, pp. 289-324.
- Kottke, A. and Rathje, E.M. (2008) —“A Semi-Automated Procedure for Selection and Scaling of Recorded Earthquake Motions for Dynamic Analysis,” accepted for publication, Earthquake Spectra, EERI.
- Kosa, K., Tazaki, K. and Yamaguchi, E. (2001). —“Mechanism of Damage to Shiwi Bridge caused by 1999 Chi-Chi Earthquake”. *Seismic Fault-induced Failures*, JSCE, 155-160.
- Krarnar, S. L. (1996), "Geotechnical Earthquake Engineering, " Prentice-Hall, Inc., Upper Saddle River, New Jersey, 653 p.
- Kulhawy, F.H. and P.W. Mayne, (1990) —“Manual on Estimating Soil Properties for Foundation Design”, Report EPRI EL-6800, Electric Power Research Institute, Palo Alto, Calif., 306 pp.
- Kwok, A.O.L. Stewart, J.P., Hashash, Y.M.A., Matasovic, N., Pyke, R., Wang, Z., and Yang, Z. (2006) —“Use of Exact Solutions of Wave Propagation Problems to Guide Implementation of Nonlinear Seismic Ground Response Analysis Procedures,” Journal of Geotechnical and Geoenvironmental Engineering, Vol. 133, No. 11, pp. 1385-1398.
- Lam, I. (1994) —“Soil-Structure Interaction Related to Piles and Footings”, Proceedings, Second International Workshop on Seismic Design and Retrofitting of Reinforced Concrete Bridges, Queenstown, New Zealand, August 9-12, 1994.
- Lam, I., and Martin, G., (1986), —“Seismic Design of Highway Bridge Foundations Vol. II Design Procedures and Guidelines”, FHWA Report No. FHWA/RD-86/102, McLean Virginia..
- Lam, I. P, Martin, G. R. and Imbsen, R (1991), —“Modeling Bridge Foundations for Seismic Design and Retrofitting”, Transportation Research Record 1290,
- Lam, I.P., Cheang, L. (1995), —“Dynamic Soil-Pile Interaction Behavior in Submerged Sands”, ASCE Geotechnical Special Publications No. 55.
- Lam and Law (1996) —“Soil-Foundation-Structure Interaction, Analytical Consideration by Empirical p-y Methods,” Proceedings of the Fourth Caltrans Seismic Research Workshop, Sacramento, CA, July 9th– 11th, 1996
- Lam, I.P., Kapuskar, M., and Chaudhuri, D., (1998), —“Modeling of Pile Footings and Drilled Shafts for Seismic Design”, MCEER-98-0018, December 21, 1998.
- Lam, I.P., and Law, H. (2000) —“Soil Structure Interaction of Bridges for Seismic Analysis”, Technical Report MCEER-00-0008, Multidisciplinary Center for Earthquake Engineering Research, University at Buffalo, Buffalo, NY, September 25, 2000

- Lam, I.P., Law, H., and Kapuskar, M. (2004), —Design For The New San Francisco-Oakland Bay Bridge East Span, Soil-Structure Interaction Problems’, Proceedings, Geo-Institute Conference on Geotechnical Engineering for Transportation Projects, UCLA, Los Angeles, July 27-31, 2004.
- Lam, I., Law, H. and Martin, G.R., (2007), —Bridge Foundations: Modeling Large Pile Groups and Caissons for Seismic Design”, MCEER-07-0018, December 1, 2007.
- Lam, I.P., Arduino, P. and Mackenzie, P., (2007b) —OENSEES Soil-Pile Interaction Study under Lateral Spread Loading”, Report to PEER, November 30, 2007, U.C. Berkeley Agreement No. SA5628-23584, Purchase Order No. 1291149.
- Lam, I.P., Arduino, P. and Mackenzie, P., (2009) —OENSEES Soil-Pile Interaction Study under Lateral Spread Loading”, ASCE Special Publication No. 186, pp. 206-213, Presented at the 2009 International Foundation Congress and Equipment Expo, Orlando, FL., March 15-19.
- Lee, M.K.W. and Finn, W.D.L. (1978), "DESRA-2, Dynamic Effective Stress Response Analysis of Soil Deposits with Energy Transmitting Boundary Including Assessment of Liquefaction Potential," Soil Mechanics Series No. 36, Department of Civil Engineering, University of British Columbia, Vancouver, Canada, 60 p.
- Li, A. J., Lyamin, A. V., Merifield, R. S. (2009), —Seismic Rock Slope Stability Charts based on Limit Analysis Methods,” Computers and Geotechnics, 36(1~2), 135-148.
- Li, A. J., Merifield, R. S., Lyamin, A. V. (2008), —Stability Charts for Rock Slopes based on the Hoek-Brown Failure Criterion,” International Journal of Rock Mechanics & Mining Sciences, 45(5), 689-700
- Li, X.S., Wang, Z.L. and Shen, C.K. (1992), "SUMDES - A Nonlinear Procedure for Response Analysis of Horizontally-Layered Sites Subjected to Multi-Directional Earthquake Loading," Department of Civil Engineering, University of California, Davis, California.
- Liao, S.S.C. and Whitman, R.V. (1986), "Overburden Correction Factors for SPT in Sand," Journal of Geotechnical Engineering, ASCE, Vol. 112, No. 3, pp. 373-377.
- Lilhanand, K. and Tseng, W.S. (1988), —Development and Application of Realistic Earthquake Time Histories Compatible with Multiple-Damping Design Spectra,” Proceedings of the 9th Work Conference of Earthquake Engineering, Tokyo-Kyoto, Japan, August 2-9.
- Ling, L.F., (1988), —Back Analysis of Lateral Load Tests on Piles”, M.E. Thesis, Civil Engineering Department, University of Auckland.
- Liu, L. and Dobry, R., (1995), —Effect of Liquefaction on Lateral Response of Piles by Centrifuge Model Tests”, NCEER Report.
- LPILE Plus 5.0 (2006), A Program for the Analysis of Piles and Drilled Shafts Under Lateral Loads, Ensoft, Inc., Austin, TX.
- Luehring, R., Dewey, B., Mejia, L., Stevens, M. and Baez, J., (1998), —Liquefaction Mitigation of Silty Dam Foundation Using Vibro-Stone Columns and Drainage Wicks – A Test Section Case History at Salmon Lake Dam”, Proceedings of the 1998 Annual Conference Association of State Dam Safety Officials, Las Vegas, NV, October 11-14.

- Mace, N., and Martin, G.R. (2000). —An Investigation of Compaction Grouting for Liquefaction Mitigation”, Unpublished Report, Multidisciplinary Center for Earthquake Engineering Research, University at Buffalo.
- Mayne, P.W., Jones, J.S. and Dumas, J.C. (1984). —Ground Response to Dynamic Compaction,” J. of Geot. Eng., ASCE, Vol. 110, No. 6, June, pp. 757-774.
- Makdisi, F.I. and Seed, H.B. (1978), "Simplified Procedure for Estimating Dam and Embankment Earthquake-Induced Deformations," Journal of the Geotechnical Engineering Division, ASCE Vol. 104, No. GT7, pp. 849-867.
- Marcuson, W. F., III, and Bieganousky, W. A. (1977) —SPT and relative density in coarse sands.“ J. Geotech. Engrg. Div., ASCE, 103(11), pp. 1295–1309.
- Marions P. and Hoek E. (2000) —GSA Geologically Friendly Tool for Rock Mass Strength Estimation”. Proceedings International Conference on Geotechnical and Geological Engineering, GeoEng2000, Technomic Publ., 1422-1442, Melbourne.
- Maroney, B.H., (1995), —Large Scale Bridge Abutment Tests to Determine Stiffness and Ultimate Strength under Seismic Loading,” Ph.D Dissertation, University of California, Davis.
- Maroney, B., and Chai, Y. H. (1994). —Bridge abutment stiffness and strength under earthquake loadings.” Proc. of the Second International Workshop on the Seismic Design of Bridges, Queenstown, New Zealand, August 9-12.
- Maroney, B., Kutter, B., Romstad, K., Chai, Y. H., and Vanderbilt, E.(1994). —Interpretation of large scale bridge abutment test results.” Proc. of the Third Caltrans Seismic Research Workshop, Sacramento, June 27-29.
- Martin, G.R. and Qiu, P. (1994). —Effects of Liquefaction on Vulnerability Assessment,” NCEER Highway Project on Seismic Vulnerability of New and Existing Highway Construction, Year One Research Tasks, Technical Research Papers.
- Martin, G. R., and Lam, I., (2000), —Earthquake Resistance Design of Foundations- Retrofit of Existing Foundations”, Proceedings, GeoEng2000, Vol. 1: Invited Paper, Melbourne, Australia, Nov. 19-24, 2000, pp. 1025-1047.
- Martin, J.R., Olgun, C.G., and Eddy, M. (2008) —Unique Site Conditions and Response Analysis Challenges in the Central and Eastern U.S.” presentation prepared for the 2008 Meeting of the Transportation Research Board, Department of Civil and Environmental Engineering, World Institute for Disaster Risk Management, Virginia Polytechnic Institute and State University
- Martin. P.P. (1975)*, "Non-Linear Methods for Dynamic Analysis of Ground Response," Ph.D. Thesis, University of California, Berkeley.
- Matasovic N. (1993) "Seismic Response of Composite Horizontally-Layered Soil Deposits." Ph.D. thesis, Civil Engineering Department, Univ. of California, Los Angeles, CA, 452 p.
- Matasovic, N. and Vucetic, M. (1993), "Cyclic Characterization of Liquefiable Sands," Journal of Geotechnical Engineering, ASCE, Vol. 119, No. 11, pp. 1805-1822.

- Matasovic, N. (2006) D-MOD_2 – “A computer program for seismic response analysis of horizontally layered soil deposits, earthfill dams, and solid waste landfills”, User’s Manual, GeoMotions, LLC, Lacey, Wash., 20 p. plus appendices.
- Matlock, Hudson, (1970), "Correlations for Design of Laterally Loaded Piles in Soft Clay," Proceedings, Second Annual Offshore Technology Conference, Paper No. 1204, Houston, Texas, April 22-24.
- Matlock, H., Ingham, W.B., Allen, E.,K., and Bogard, D., (1980), —“Field Tests of the Lateral-Load Behavior of Pile Groups in Soft Clay,” OTC Proceedings, 1980.
- Mayne, P.W. (2007), —“Cone Penetration Testing, A synthesis of Highway Practice,” NCHRP Synthesis Report No. 368, Transportation Research Board, Washington, D.C., 126 p
- Mayne, P.W. and Rix, G.J. (1993), "Gmax- q_c Relationships for Clays," Geotechnical Testing Journal, ASTM, Vol. 16, No. 1, pp. 54-60.
- Mayne, P.W. and G.J. Rix (1995), —“Correlations Between Shear Wave Velocity and Cone Tip Resistance in Clays,” Soils & Foundations, Vol. 35, No. 2, pp. 107–110.
- Mayne, P.W., Jones, J.S. and Dumas, J.C. (1984), —“Ground Response to Dynamic Compaction”, Journal of Geotechnical Engineering, ASCE, Vol. 110, No. 6, pp. 757-774
- McCauley, M.L., Works, B.W., and Naramore, B.A. (1985). —“Rock Fall Mitigation Report”, Report FHWA/CA/TL-85/12, FHWA, U.S. Department of Transportation.
- MCEER (Multidisciplinary Center for Earthquake Engineering Research) (1999), —“Response of Buried Pipelines Subject to Earthquake Effects”, MCEER Monograph Series No. 3.
- MCEER (Multidisciplinary Center for Earthquake Engineering Research) (2006). —“Seismic Retrofitting Manual for Highway Structures: Part 2- Retaining Walls, Slopes, Tunnels, Culverts and Roadways,” MCEER-0-SP11.
- MCEER (Multidisciplinary Center for Earthquake Engineering Research) (2007),”Modeling of Seismic Wave Scattering on Pile Group and Caissons ”, Technical Report MCEER-07-0017
- McVay, M., Zhang, L., Molnit. T., and Lai, P. (1998), —“Centrifuge Testing of Large Laterally Loaded Pile Groups in Sands,” Journal of Geotechnical and Geoenvironmental Engineering, ASCE, 124(10), October, 1016-1026.
- McVay, M., C. Hays, and M. Hoit. (1996) —“User’s Manual for Florida Pier, Version 5.1”. Department of Civil Engineering, University of Florida (1996).
- Mitchell, J.K., Baxter, C.D.P., and Munson, T.C., (1995), —“Performance of Improved Ground During Earthquakes”, Soil Improvement for Liquefaction Hazards Mitigation, Geotech. Special Pub. No. 49, ASCE, 1-36.
- Moore, I. D. (1989) —“Elastic Buckling of Buried Flexible Tubes- A Review of Theory and Experiment” Journ Geotech Engr, ASCE, Vol. 115, No. 3, Mar., pp 340-358.
- Moulton, Lyle K. (1986). —“Tolerable Movement Criteria for Highway Bridges”, FHWA-TS-85-228.

- Mylonakis, G.; Gazeta, G.; Nikolaou, S. and Chauncey, A. (2002), —Development of Analysis and Design Procedures for Spread Footings”, MCEER-02-0003, October 2.
- NCEER (National Center for Earthquake Engineering Research) (1992). —Case Studies of Liquefaction and Lifeline Performance during Past Earthquakes”, Technical Report NCEER-92-0001, Volume 1, M. Hamada, and T.D. O'Rourke Eds.
- NCEER (National Center for Earthquake Engineering Research) (1996),—Highway Culvert Performance During Earthquakes”, NCEER Technical Report NCEER-96-0015, November.
- NCHRP (National Cooperative Highway Research Program) (2001). —NCHRP Project 12-49: Comprehensive Specification for the Seismic Design of Bridges”, NCHRP Report 472, ATC/MCEER Joint Venture.
- NCHRP (National Cooperative Highway Research Program) (2002), —Recommended Specifications for Large-Span Culverts”, NCHRP Report 473, Transportation Research Board – National Research Council.
- NCHRP (National Cooperative Highway Research Program) (2003). —NCHRP Project 12-49, Recommended LRFD Guidelines for the Seismic Design of Highway Bridges, Part I, Specifications, Part II, Commentary and Appendices, Submitted by MCEER/ATC, Report MCEER/ATC 49, and Liquefaction Study Report, Report MCEER/ATC 49-1.
- NCHRP (National Cooperative Highway Research Program) (2005) —NCHRP 20-07/Task 193-Task 8 Report for Updating Recommended LRFD Guidelines for the Seismic Design of Highway Bridges”, Imbsen and Associates, Sacramento, CA.
- NCHRP (National Cooperative Highway Research Program) (2006), —Rock-Socketed Shafts for Highway Structure Foundations”, NCHRP Synthesis 360, Transportation Research Board.
- NCHRP (National Cooperative Highway Research Program) (2008),” NCHRP Project 12-70, Seismic Analysis and Design of Retaining Walls, Buried Structures, Slopes and Embankments, Recommended Specifications, Commentaries and Example Problems”, NCHRP Report 611, Transportation Research Board, Washington, DC.
- NGDC (National Geodetic Data Center): www.ngdc.gov
- Newark, N. M. (1965), —Effects of Earthquakes on Dams and Embankments”, *Geotechnique*, Vol. 15, No. 2, pp. 139-160
- Newark, N. M. (1968), —Problems in Wave Propagation in Soil and Rock”, *International Symposium on Wave Propagation and Dynamic Properties of Earth Materials*.
- Nogami, T., and Chen, M.L., (1987), —Prediction of Dynamic Lateral Response of Nonlinear Single-Pile by using Winkler Soil Model”, *ASCE Geotechnical Special Publication No. 11*, pp. 39-52.
- NUREG (2001) —Technical Basis for Revision of Regulatory Guidance on Design Ground Motion: Hazard- and Risk-Consistent Ground Motion Spectra Guidelines (2001)” NUREG report CR-6728, prepared for the Nuclear Regulatory Commission by Risk Engineering, Inc., Boulder, Colorado

- Olson, S.M. and Johnson, C.I. (2008), —Analyzing Liquefaction-Induced Lateral Spreads Using Strength Ratios,” J. Geotech. and Geoenviron. Engrg. Volume 134, Issue 8, pp. 1035-1049
- Olson, S. M., and Stark, T. D. (2002), —Liquefied strength ratio from liquefaction flow failure case histories.” Can. Geotech. J., 39, 629–647.
- O’Neill, M.W., and Murchison, Jack M., (1983), —An Evaluation of p-y Relationships in Sands”, A Report to the American Petroleum Institute, (PRAC 82-41-1), University of Houston- University Park, Department of Civil Engineering, Research Report No. GT-DF02-83, May, 1983.
- O’Neill, M.W., and Gazioglu, Sal M., (1984), —An Evaluation of p-y Relationships in Clays, A Report to the American Petroleum Institute”, (PRAC 82-41-2), University of Houston- University Park, Department of Civil Engineering, Research Report No. UHCE-84-3, April, 1984.
- O’Rourke M.J. and Liu, X. (1996), —Continuous Pipeline Subject to Transient PGD: A Comparison of Solutions”, Technical Report NCEER-96-0012.
- O’Rourke, T. D. (1998). —An Overview of Geotechnical and Lifeline Earthquake Engineering.” ASCE Geotechnical Special Publication No. 75—Geotechnical Earthquake Engineering and Soil Dynamics III, Vol. 2.
- O’Rourke T.D. (1999), —An Overview of Geotechnical and Lifeline Earthquake Engineering”, ASCE Geotechnical Special Publication No.75 – Geotechnical Earthquake Engineering and Soil Dynamics III, Vol. 2.
- O’Rourke, T.D., Meyersohn, W.D., Shiba, Y. and Chaudhuri, D. (1994). —Evaluation of Pile Response to Liquefaction-Induced Lateral Spread,” Proceedings, 5th U.S.-Japan Workshop on Earthquake Resistant Design of Lifeline Facilities and Countermeasures Against Soil Liquefaction, Technical Report NCEER-94-0026, National Center for Earthquake Engineering Research, University at Buffalo, pp. 457-478.
- Park, D. and Hashash, Y.M.A. (2003). "Soil damping formulation in nonlinear time domain site response analysis". Journal of Earthquake Engineering
- Park, D., and Hashash, Y. M. A. (2004) —Soil Damping Formulation in Nonlinear Time Domain Site Response Analysis,” Journal of Earthquake Engineering, Vol. 8, No. 2, pp. 249–274.
- Park, R.G. (1983), "Foundations of Structural Geology," Blackie Publishing, Chapman and Hall, New York, New York.
- Peck, R. B., Hendron, A. J., and Mohraz, B. (1972), —State of the Art of Soft Ground Tunnelling”, Proceedings of the Rapid Excavation and Tunnelling Conference, Chicago, IL., Vol. 1.
- PEER (Pacific Earthquake Engineering Research Center) 2005/04, (2005) —Numerical Modeling of the Nonlinear Cyclic Response of Shallow Foundations”, Harden, Chad; Hutchinson, Tara; Martin, G.R., and Kutter, B.L., August, 2005.
- PEER (Pacific Earthquake Engineering Research Center) 2005/14, (2003) —Workshop on Modeling of Nonlinear Cyclic Load Deformation Behavior of Shallow Foundations”, Kutter, B.L.; Martin, G.R., Hutchinson, Tara; Harden, Chad; Gajan, Sivapalan and Phalen, Justin, March, 2003.

- PEER (Pacific Earthquake Engineering Research Center) 2007/04, (2008) —Numerical Models for Analysis and Performance-Based Design of Shallow Foundations Subjected to Seismic Loading”, Gajan, Sivapalan; Hutchinson, Tara; Kutter, B.L.; Raychowdhury, Prishati; Ugalde, Jose, and Stewart, Jonathan P., May, 2008.
- Pender, M.J. (1993), —Seismic Pile Foundation Design and Analysis”, Bulletin of the New Zealand National Society for Earthquake Engineering, Volume 26, Number 1, pp. 49-160
- Penzien, J. (2000), —Seismically Induced Racking of Tunnel Linings,” Earthquake Engineering and Structural Dynamics, pp. 683-691.
- Porbaha, A., Zen, K. and Kobayashi, M. (1999). —Mixing Technology for Liquefaction Mitigation,” Journal of Infrastructure Systems, Vol. 5, No. 1, pp. 21-34.
- Poulos, S.J., Castro, G. and France, W. (1985), "Liquefaction Evaluation Procedure," Journal of Geotechnical Engineering Division, ASCE, Vol. 111, No. 6, pp. 772-792.
- Power, M., et al. (2006), —Seismic Retrofit Manual for Highway Structures: Part II – Retaining Structures, Slopes, Tunnels, Culverts and Roadways,” 2006, MCEER Report: MCEER-06-SP11
- Powers, M. (2004) —Design Ground Motion Library,” Geotechnical Engineering for Transportation Projects, Proceedings of Geo-Trans 2004, Geotechnical Special Publication No. 126, ASCE, pp.778-786.
- Powers, M., Youngs, R., and Chin, C.-C. (2004) —Design Ground Motion Library. Report of PEER-LL Program Task 1F01,” http://peer.berkeley.edu/lifelines/lifelines_pre_2006/final_reports/1F01-FR.pdf, 26 October 2007.
- Priestley, M. J. N., Seible, F., and Calvi, G. M., (1996), —Seismic Design and Retrofit of Bridges”, John Wiley and Son, Inc.
- Priestley, M. J. N., Calvi, G.M., and Kowalsky, M. J., (2007), —Displacement-Based Seismic Design of Structures”, IUSS Press, Pavia, Italy.
- Pryso, R.H. and Egan, J.P. (1981). —Roadway Damage During the San Fernando, California Earthquake of Feb. 9, 1971”, Report No. FHWA/CA/TL-80/17, California Department of Transportation, 184 pp.
- Pyke, R. M. (1979) —Nonlinear Soil Models for Irregular Cyclic Loadings,” Journal of the Geotechnical Engineering Division, Vol. 105, No. 6, pp. 715–726.
- Pyke, R. M. (2000) TESS: —A computer program for nonlinear ground response analyses”, TAGA Engineering Systems and Software, Lafayette, Calif.
- Qiu, P. (1998). —Earthquake-induced Nonlinear Ground Deformation Analyses”, Ph.D. dissertation, University of Southern California, Los Angeles.
- Randall, M.J., Saiidi, M.S., Maragakis, E.M. and Isakovic, T. (1999) —Retainer Design Procedures for Multi-Span Simply-Supported Bridges”, Technical Report MCEER-99-0011, Multidisciplinary Center for Earthquake Engineering Research, University at Buffalo, Buffalo, NY.

- Reese, L.C., Cox, W.R., and Koop, F.D., (1974), —Analysis of Laterally Loaded Piles in Sand,” Proceedings, Sixth Annual Offshore Technology Conference, Vol. 2, Paper No. 2080, Houston, Texas.
- Richards, R. and D. G. Elms (1979). —Seismic Behavior of Gravity Retaining Walls”. J. Geotechnical Eng., ASCE 105(4), 449-464.
- Richardson, G.N., Kavazanjian, E. Jr. and Matasovic, N. (1995). —RQA Subtitle D (258) Seismic Design guidance for Municipal Solid Waste Landfill Facilities”, EPA/600/R-95/051, United States Environmental Protection Agency, Cincinnati, Ohio, 143 p.
- Richter, C.F. (1958), "Elementary Seismology, " W .H. Freeman and Company, San Francisco, California.
- Robertson, P.K., and Wride, C.E., (1998), —Evaluating Cyclic Liquefaction Potential using the Cone Penetration Test,” Canadian Geotechnical Journal, Vol. 35, pp. 442-459.
- Robertson, P.K., and Campanella, R.G., (1983), —Interpretation of Cone Penetration Tests- Part I (Sand),” Canadian Geotechnical Journal, Vol. 20, No. 4, pp. 734-745.
- Robertson, P.K., Campanella, R.G., Gillespie, D., and Greig, J. (1986), —Use of Piezometer Cone Data,” Use of In-Situ Tests in Geotechnical Engineering (GSP 6), American Society of Civil Engineers, Reston, Va., 1986, pp. 1263–1280.
- Rollins, K.M., Gerber, T.M., Lane, J.D. and Ashford. S.A. (2005). "Lateral Resistance of a Full-Scale Pile Group in Liquefied Sand," J. Geotechnical and Geoenvironmental Engrg., ASCE, Vol. 131, No. 1, p. 115-125.
- Rollins, K. M., Weaver, T. J., and Peterson, K. T. (1997). "Statnamic Lateral Load Testing of a Full-Scale Fixed-Head Pile Group," in Proceedings of the National Seismic Conference on Bridges and Highways, Sacramento, California, Federal Highway Administration and California Department of Transportation, July, pp. 267 - 282.
- Romstad, Karl M.; Kutter, Bruce L.; Maroney, Brian H.; Vanderbilt, Eric; Griggs, Matt; Chai, Yuk Hon, (1995), —Experimental measurements of bridge abutment behavior”UCD-STR-95-1, Dept. of Civil and Environmental Engineering, University of California, Davis, 1995-09
- Salgado, R., Boulanger, R.W., and Mitchell, J.V. (1997). —Lateral Stress Effects on CPT Liquefaction Resistance Correlations,” Journal of Geotechnical and Geoenvironmental Engineering, ASCE, August.
- SCEC (Southern California Earthquake Center) (2002). —Recommended Procedures for Implementation of DMG Special Publication 117 Guidelines for Analyzing and Mitigating Landslide Hazards in California,” Southern California Earthquake Center, February.
- SCEC (Southern California Earthquake Center) (1999). —Recommended Procedures for Implementation of DMG Special Publication 117 Guidelines for Analyzing and Mitigating Liquefaction Hazards in California,” Southern California Earthquake Center, March.
- Schnabel, P.B., Lysmer, J. and Seed, H.B. (1972), "SHAKE: A Computer Program for Earthquake Response Analysis of Horizontally Layered Sites," Report No. EERC 72-12, Earthquake Engineering Research Center, University of California, Berkeley, California.

- Schwartz, D.P. and Coppersmith, K.J. (1984). —Fault Behavior and Characteristic Earthquake: Examples from the Wasatch and San Andreas Faults”, J. Geophysical Research, Vol. 89, pp.5681-5698.
- Seed, H.B. (1987). —Design Problems in Soil Liquefaction”, J. Geotechnical Eng., ASCE 113(8), 827-845.
- Seed, H.B. and Lee, K.L. (1966). —Liquefaction of Saturated Sands During Cyclic Loading”, J. Soil Mechanics and foundations Div., ASCE 92(SM6), 105-34.
- Seed, H.B. and Idriss, I.M. (1970), "Soil Moduli and Damping Factors for Dynamic Response Analyses," Report No. EERC 70-10, Earthquake Engineering Research Center, University of California, Berkeley, California, 40 p.
- Seed, H.B., and Idriss, I.M. (1971). —Simplified Procedure for Evaluating Soil Liquefaction Potential,” Journal of the Soil Mechanics, and Foundations Division, American Society of Civil Engineers, Volume 97, Number SM9, September, pp. 1249-1273.
- Seed, H.B. and Peacock, W.H. (1971). —Test procedures for Measuring Soil Liquefaction Characteristics”, J. Soil Mechanics and Foundations Div., ASCE 97(MS8), Proceedings Paper 8330, August, pp.1099-119.
- Seed, H.B. and Silver, M.L. (1972). —Settlement of dry sands during earthquakes.” J. Soil Mech. Found. Div., ASCE, 98(4), 381-397.
- Seed, H.B., Idriss, I.M., Makdisi, F. and Bannerje, N. (1975), "Representation of Irregular Stress Time Histories by Equivalent Uniform Stress Series in Liquefaction Analyses," Report EERC 75-29, College of Engineering, University of California, Berkeley.
- Seed, H.B. and Idriss, I.M. (1982), "Ground Motions and Soil Liquefaction During Earthquakes," Monograph No. 5, Earthquake Engineering Research Institute, Berkeley, California, 134 p.
- Seed, H.B., Idriss, I.M. and Arango, I. (1983), "Evaluation of Liquefaction Potential Using Field Performance Data," Journal of Geotechnical Engineering, ASCE, Vol. 109, No. 3, pp. 458-482.
- Seed, H.B., Wong, R.T., Idriss, I.M. and Tokimatsu, K. (1984), "Moduli and Damping Factors for Dynamic Analyses of Cohesionless Soils," Report No. UCB/EERC-84/14, Earthquake Engineering Research Center, University of California, Berkeley, California.
- Seed, H.B., Tokimatsu, K., Harder, L.F. and Chung, R.M. (1985), "Influence of SPT Procedures in Soil Liquefaction Resistance Evaluations," Journal of Geotechnical Engineering, ASCE, Vol. 111, No. 12, pp. 1425-1445.
- Seed, H.B. and De Alba, P. (1986), "Use of SPT and CPT Tests for Evaluating the Liquefaction Resistance of Sands." In: Use of In-Situ Tests in Geotechnical Engineering, ASCE Geotechnical Special Publication No. 6, pp. 281-302.
- Seed, R.B. and Harder, L.F., Jr. (1990), "SPT-Based Analysis of Cyclic Pore Pressure Generation and Undrained Residual Strength," In: H.B. Seed Memorial Symposium, J.M. Duncan, Editor, Bi-Tech Publishers Ltd., Vancouver, Canada, Vol. 2, pp. 351-376

- Seqad (1997), —Bridge Pile Foundations Under Seismic Loads- Capacity and Design Issues,” Report # 97/10, Job # 97/14, Report by Priestley, M.J., and Seible, Freider, to Earth Mechanics, Inc., Oct. 1997).
- Serventi et al., (2004), Proceedings, Port 2004 Conference, May 23-26, Houston, TX
- Shamsabadi, A., Nordal, S. (2006) —Modeling passive earth pressures on bridge abutments for nonlinear seismic soil-structure interaction using PLAXIS”. PLAXIS Bulletin issue 20.
- Shamsabadi, A., (2007) —Three-Dimensional Nonlinear Seismic Soil-Abutment-Foundation Structure Interaction Analysis of Skewed Bridges.” Ph.D. Dissertation, Department of Civil and Environmental Engineering, University of Southern California (USC) Los Angeles, CA.
- Shamsabadi, A., Rollins, K. M., and Kapuskar, M. (2007). —Nonlinear soil-abutment-bridge structure interaction for seismic performance-based design.” Journal of Geotechnical & Geoenvironmental Eng., ASCE, 133 (6), 707-720.
- Shamsabadi, A., Khalili-Tehrani, P., Stewart, J. P., Yan, L., and Taciroglu, E. (2009). ”Validated Simulation Models for Lateral Response of Bridge Abutments with Typical Backfills,” J. Bridge Eng., ASCE, (in review).
- Silva, W.J. and Lee, K., (1987). —WES RASCAL code for synthesizing earthquake ground motions. State-of-the-art for assessing earthquake hazards in the U.S. Report 24, Miscellaneous Paper S-73-1. U.S. Army Engineers Waterways Experimental Station. Vicksburg, M.S.
- Silva, W., Abrahamson, N. A., Toro, G. R., and Constantino, C. (1997). "Description and Validation of the Stochastic Ground Motion Model." Report Prepared for the Engineering Research and Applications Division Department of Nuclear Energy, Pacific Engineering and Analysis, El Cerrito, CA.
- Silver, M.L. and Seed, H.B. (1971). —Volume Changes in Sands During Cyclic Loading.” J. Soil Mech. Found. Div., ASCE, 97(9), 1171-1182.
- Skempton, A.W. (1986), "Standard Penetration Test Procedures and the Effects in Sands of Overburden Pressure, Relative Density, Particle Size, Ageing and Overconsolidation," Géotechnique, Vol. 36, No. 3, pp. 425-447.
- Smith, D.D. and Duffy, J.D. (1990). —Field Tests and Evaluation of Rockfall Restraining Nets”, Report CA/TL -90/05, Office of Transportation Materials and Research, California Department of Transportation, California.
- Somerville, P.G., N.F. Smith, R.W. Graves, and N.A. Abrahamson (1997). —Modification of Empirical Strong Ground Motion Attenuation Relations to include the Amplitude and Duration Effects of Rupture Directivity”, Seismological Research Letters 68, 199-222.
- Soydemir, C., Zoli, T., Le Plant, K., Kramer, S., Davidson, W. and McCabe, R. (1997). —Seismic Design of Central Artery Bridges Across Charles River in Boston: Geotechnical/Substructure Aspects,” Proc. 2nd Nat. Seismic Conference on Bridges and Highways, FHWA/Caltrans, Sacramento, CA, pp. 1235-1246.

- Stark, T.D., and Olson, S.M., (1995). —Liquefaction Resistance using CPT and Field Case Histories,” *Journal of Geotechnical Engineering, ASCE*, 121(12), pp. 856–869.
- Stevens, J.B. and Audibert, J.M.E., (1979), —ReExamination of p-y Curve Formulations,” *Proceedings, 11th Annual Offshore Technology Conference, Houston, Texas, Paper No. 3402*, pp. 397-403.
- Stewart, J. P., Taciroglu, E. T. , Wallace J. W., Ahlberg E., Lemnitzer, A., Rha, C. S., Khalili-Tehrani, P., Koewn, S., Nigbor, R. L., and Salamanca, A. (2007). —Fullscale cyclic testing of foundation support systems for highway bridges. Part II: abutment backwalls.” *Report No. UCLA-SGEL-2007/02, Structural & Geotechnical Engineering Laboratory, University of California, Los Angeles.*
- Stokoe, K.H., II and Nazarian, S. (1985), "Use of Rayleigh Waves in Liquefaction Studies," *Proc. Session on Measurement and Use of Shear Wave Velocity for Evaluating Soil Dynamic Properties, ASCE National Convention, Denver, Colorado*, pp. 1-17.
- Sun, Golesorkhi, and Seed (1998), —Dynamic Moduli and Damping Ratios for Cohesive Soils”, *Report No. EERC 88-15, University of California, Berkeley.*
- Suzuki, Y., Tokimatsu, K., Taye, Y., and Kubota, Y., (1995a). —Correlation between CPT Data and Dynamic Properties of In Situ Frozen Samples,” *In Proceedings of the 3rd International Conference on Recent Advances in Geotechnical Earthquake Engineering and Soil Dynamics, St. Louis, Mo. Vol. 1. Edited by S.Prakash. University of Missouri-Rolla*, pp. 210–215.
- Suzuki, Y., Tokimatsu, K., Koyamada, K., Taya, Y., and Kubota, Y. (1995b). —Field Correlation of Soil Liquefaction based on CPT Data,” *In Proceedings of the International Symposium on Cone Penetration Testing, CPT '95, Linkoping, Sweden. Vol. 2. SGS. Oct.*, pp. 583–588.
- Tatsuoka, F., Koseki, J. and Tateyama, M. (1995), "Performance of Geogrid-Reinforced Soil Retaining Walls during the Great Honshin-Awaji Earthquake, January 17, 1995," *Proc. 1st International Conference for Earthquake Geotechnical Engineering, Tokyo, Japan, Vol. 1*, pp. 55-62.
- Terashi, M. and Juran, I. (2000). —Ground Improvement- State of the Art,” *In: GeoEng2000: An International Conference on Geotechnical and Geological Engineering, held 19-24 November, 2000, Melbourne, Vol. 1*, pp. 461-519.
- Terashi, M. (2003). —The State of Practice in Deep Mixing Methods,” *In: Grouting and Ground Treatment, Proceedings of the 3rd Intl. Conference, L.F. Johnsen, D.A. Bruce and M.J. Byle, eds., ASCE Geotechnical Special Publication No. 120, Vol. 2*, pp. 25-49.
- Terzaghi, K., (1955), —Evaluation of Coefficients of Subgrade Reaction”, *Geotechnique, Volume 5, Number 4*, pp. 297-326
- Terzaghi, K. and R.B. Peck (1967), "Soil Mechanics in Engineering Practice," 2nd Edition, John Wiley and Sons, New York. The first edition was published in 1948.
- Tokimatsu, K. and Asaka, Y. (1998). —Effects of Liquefaction-Induced Ground Displacements on Pile Performance in the 1995 Hyogoken-Nambu Earthquake,” *Special Issue of Soils and Foundation*, pp. 163-177.
- Tokimatsu, K. and Seed, H.B. (1987). —Evaluation of Settlements in Sands Due to Earthquake Shaking,” *Journal of the Geotechnical Engineering Division, ASCE, Volume 113, Number 8*, pp. 861-878.

- Toro, G.R., N.A. Abrahamson and J.F. Schneider (1997). A Model of Strong Ground Motions from Earthquakes in Central and Eastern North America: Best Estimates and Uncertainties. *Seismological Research Letters*, v.68, no. 1, pp. 41-57
- Trifunac, M.D. and Brady, A.G. (1975), "A Study of the Duration of Strong Earthquake Ground Motion," *Bulletin of the Seismological Society of America*. Vol. 65, pp. 581-626.
- Trifunac, M. D., & Brady, A. G. (1975), "On the correlation of peak acceleration of strong motion with earthquake magnitude, epicentral distance and site conditions". Pages 43–52 of: *Proceedings of the U.S. National Conference on Earthquake Engineering*.
- Toro, G.R., N.A. Abrahamson and J.F. Schneider (1997). "A Model of Strong Ground Motions from Earthquakes in Central and Eastern North America: Best Estimates and Uncertainties". *Seismological Research Letters*, v.68, no. 1, pp. 41-57
- Transportation Research Board (TRB) Special Report 247, "Landslides Investigation and Mitigation" (edited by Turner and Schuster, 1996).
- Transportation Research Board (TRB) (2008). "Seismic Analysis and Design of Retaining Walls, Buried Structures, Slopes and Embankments," NCHRP Report 611, Transportation Research Board.
- USGS (1998a). "Performance of the Built Environment: Lifelines" by Schiff, A.J., in *The Loma Prieta Earthquake Professional Papers*, USGS Professional Paper 1552-B.
- USGS (1998b) "Performance of the Built Environment: Highway Systems" by Yashinsky, M, in *The Loma Prieta Earthquake Professional Papers*, USGS Professional Paper 1552-B.
- USGS (1998c). "Analysis of Earthquake-Reactivated Landslides in the Epicentral Region, Central Santa Cruz Mountains, California" by Cole, William F., Marcum, Dale R., O'Shires, Patrick, and Clark, Bruce R., USGS Professional Paper 1151-C.
- Tsopelas, P. and Constantinou, M.C., (1997) "Study of Elastoplastic Bridge Seismic Isolation System", *Journal of Structural Engineering*, ASCE, 123 (4) pp 489-498.
- Trochalakis, P., Eberhard, M.O., and Stanton, J.F. (1997) "Design of Seismic Restrainers for In-Span Hinges", *Journal of Structural Engineering*, ASCE, Vol. 123, No. 4, pp. 469-478.
- Veletsos, A.S., and Newmark, N.M. (1960) "Effect of Inelastic Behavior on the Response of Simple Systems to Earthquake Motions", *Proceedings of Second World Conference on Earthquake Engineering*, Vol. 2, Japan.
- Vrymoed, J.L. and Calzascia, E.R. (1978), "Simplified Determination of Dynamic Stresses in Earth Dams," in *Proceedings of the Specialty Conference on Earthquake Engineering and Soil Dynamics*, American Society of Civil Engineers, Pasadena, California, June 1978, pp. 991-1006.
- Vucetic, M. (1990) "Normalized Behavior of Clay Under Irregular Cyclic Loading." *Canadian Geotechnical Journal*, Vo. 27, pp. 29–46.
- Vucetic M. and Dobry, R. (1991), "Effect of Soil Plasticity on Cyclic Response," *Journal of Geotechnical Engineering*, ASCE, Vol. 117, No. 1, pp. 89-107.

- Wang, J. (1993), —**S**ismic Design of Tunnels – A Simple State-of-the-Art Design Approach,” Parsons Brinckerhoff Monograph No. 7.
- Wang, S., Kutter, B., Chacko, M.J., Wilson, D.W., and Boulanger, R.W. (1998), —**N**onlinear Seismic Soil-Pile Structure Interaction”, EERI Earthquake Spectra, Volume 14, Number 2, May 1998, pp. 377-395.
- Wells, D.L. and Coppersmith, K.J. (1994). —**E**mpirical Relationships Among Magnitude, Rupture Length, Rupture Area, and Surface Displacement,” Bulletin of the Seismological Society of America, Volume 84, pp. 974-1002.
- Wood, L.A., and Martin, G.M. (1964), —**C**ompressibility of Natural Rubber at Pressures Below 500 kg/cm²”, Rubber Chemistry and Technology, 37, pp 850-85.
- Woods, R.D. (1994), "Geophysical Characterization of Sites," Proc. 12th International Conference on Soil Mechanics and Foundation Engineering, Special Volume Prepared by TC 10, New Delhi, India.
- Wyllie, D.C. and Norrish, N.I. (1996). —**R**ock strength properties and their measurement”, Transportation Research Board, Special Report 247, 372-390.
- Wyss, M. (1979), "Estimating Maximum Expectable Magnitude of Earthquakes from Fault Dimensions," Geology, Vol. 7. pp. 336-340.
- Yan, L., Matasovic, N. and Kavazanjian, E., Jr. (1996), —**S**ismic Response of Rigid Block on Inclined Plane to Vertical and Horizontal Ground Motions Acting Simultaneously”, Proc. 11th ASCE Engineering Mechanics Conference, Fort Lauderdale, Florida, Vol. 2, pp. 1110-1113.
- Youd, T.L. (1993). —**L**iquefaction-Induced Damage to Bridges,” Transportation Research Record No. 14311, National Research Council, National Academy Press, Washington, D.C. 35-41.
- Youd, T.L. (1995). —**L**iquefaction-Induced Lateral Ground Displacement,” State-of-the-Art Paper, Proceedings, Third Intl. Conf. on Recent Advances in Geotechnical Earthquake Engineering and Soil Dynamics, S. Prakash (ed.), St. Louis, MO, April 2-7, Volume II, pp. 911-9253
- Youd, T.L. (1998). —**S**creening Guide for Rapid Assessment of Liquefaction Hazard at Highway Bridge Sites”, Technical Report MCEER-98-0005, Multidisciplinary Center for Earthquake Engineering Research, University at Buffalo.
- Youd, T. L. and C. J. Beckman, (2003). —**P**erformance of Corrugated Metal Pipe (CMP) Culverts during Past Earthquakes.” TCLEE, Monograph 25.
- Youd, T.L. and Perkins, D.M. (1978). —**M**apping of Liquefaction-Induced Ground Failure Potential,” Journal of the Geotechnical Engineering Division, American Society of civil Engineers, Volume 104, Number 4, April, pp. 433-446.
- Youd, T.L. and Idriss, I.M., (1997). —**P**roceedings of the NCEER Workshop on Evaluation of Liquefaction Resistance of Soils”, Salt Lake City, UT, January 5-6, 1996, Technical Report NCEER-97-0022, National Center for Earthquake Engineering Research, University at Buffalo.

- Youd, T.L., Idriss, I.M., Andrus, R.D., Arango, I., Castro, G., Christian, J.T., Dobry, R., Finn, W.D.L., Harder, L.F. Jr., Hynes, M.E., Ishihara, K., Koester, J.P., Liao, S.S.C., Marcuson, W.F., III, Martin, G.R., Mitchell, J.K., Moriwaki, Y., Power, M.S., Robertson, P.K., Seed, R.B., and Stokoe, K.H., II (2001). —Liquefaction Resistance of Soils: Summary Report from the 1996 NCEER and 1998 NCEER/NSF Workshops on Evaluation of Liquefaction Resistance of Soils,” *Journal of Geotechnical Geoenvironmental Engineering*, ASCE, Volume 127, No. 10, pp. 817-833.
- Youngs, R.R. and Coppersmith, K.J. (1985). —Implications of Fault Slip Rates and Earthquake Recurrence Models to Probabilistic Seismic Hazard Estimates”, *Bull. Seism. Soc. Am.*, Vol. 75, No. 4, pp. 939-964.
- Zeghal, M. and Elgamal, A.W. (1994). —Analysis of Site Liquefaction Using Earthquake Records,” *Journal of Geotechnical Engineering*, ASCE, Volume 120, No. 6, pp. 996-1017.